Calmodulin Binding and Activation of Mammalian Nitric Oxide Synthases

by

Donald Eric Spratt

A thesis
presented to the University of Waterloo
in fulfillment of the
thesis requirement for the degree of
Doctor of Philosophy
in
Chemistry

Waterloo, Ontario, Canada, 2008

AUTHOR'S DECLARATION

I hereby declare that I am the sole author of this thesis. This is a true copy of the thesis, including any required final revisions, as accepted by my examiners.

I understand that my thesis may be made electronically available to the public.

Donald E. Spratt

Abstract

Calmodulin (CaM) is a ubiquitous cytosolic Ca^{2+}-binding protein involved in the binding and regulation of more than three-hundred intracellular target proteins. CaM consists of two globular domains joined by a central linker region. In the archetypical model of CaM binding to a target protein, the Ca^{2+}-replete CaM wraps its two domains around a single α-helical target peptide; however, other conformations of CaM bound to target peptides and proteins have recently been discovered. Due to its ability to bind and affect many different intracellular processes, there is significant interest in a better understanding of the structural and conformational basis of CaM's ability to bind and recognize target proteins.

The mammalian nitric oxide synthase (NOS) enzymes are bound and activated by CaM. The NOS enzymes catalyze the production of nitric oxide (•NO), a free radical involved in numerous intercellular processes such as neurotransmission, vasodilation, and immune defense. There are three different isoforms of nitric oxide synthase (NOS) found in mammals – neuronal NOS (nNOS), endothelial NOS (eNOS), and inducible NOS (iNOS). All three enzymes are homodimeric with each monomer consisting of an N-terminal oxygenase domain and a multidomain C-terminal reductase domain. A CaM-binding domain separates the oxygenase and reductase domains. There is a unique opportunity to investigate CaM's control over •NO production by the NOS enzymes since each isoform shows a different mode of activation and control by CaM. At elevated cellular Ca^{2+} concentrations, CaM is able to bind and activate nNOS and eNOS. In contrast, the iNOS isozyme is transcriptionally regulated and binds to CaM in the absence of Ca^{2+}. The focus of this thesis is to better our present understanding of the conformational and structural basis for CaM's ability to bind and activate the three mammalian NOS isozymes with particular emphasis on the interactions between CaM and iNOS.

To further investigate the differences in the association of CaM to the Ca^{2+}-dependent and Ca^{2+}-independent NOS isoforms, a variety of CaM mutants including CaM-troponin C chimeras, CaM EF hand pair proteins, and CaM mutants incapable of binding to Ca^{2+} were employed. The inherent differences in binding and activation observed using these CaM mutants is described. Differences in the binding of the N- and C-terminal domains, as well as the central linker of CaM to peptides corresponding to the CaM-binding domain of each NOS enzyme and holo-NOS enzymes was investigated. The conformation of CaM when bound to NOS peptides and holo-NOS enzymes was also studied using fluorescence (Förster) resonance energy transfer (FRET). A preliminary three-dimensional structural study of Ca^{2+}-replete and Ca^{2+}-deplete CaM in complex with an iNOS CaM-binding domain peptide is also described.

Combining the cumulative results in this thesis, a working model for iNOS's regulation by CaM is proposed. Future suggested experiments are described to further the characterization of CaM binding to the NOS enzymes and other CaM-target proteins. The studies described in this thesis have expanded and improved the present understanding of the CaM-dependent binding and activation of the NOS isozymes, particularly the interactions between CaM and iNOS.

Acknowledgements

I would like to thank my supervisor, Dr. Guy Guillemette, for his friendship, encouragement, and guidance throughout my studies at UW. His support and leadership have been instrumental in my development as a research scientist. I especially enjoyed our "hockey" talks which always seemed to end up with my favourite team, the Toronto Maple Leafs, getting a good-ole roast…ahhh the memories!

I am grateful for the helpful suggestions and advice I have received from the members of my supervisory committee throughout my doctoral studies: Dr. Michael Palmer, Dr. Elizabeth Meiering and Dr. Stephen Seah. I also want to thank Dr. David Spafford and Dr. Ann English, my external examiners, for their unique perspectives and interesting discussions about my work. I would also like to thank Dr. Palmer for the use of his fluorescence equipment and Dr. Thorsten Dieckmann and Dr. Dara Gilbert for their help and guidance with my NMR experiments.

Throughout my 5 years at UW, I've had the priviledge of working and getting to know many different and memorable characters in the G^2 lab: Elena Newman, Geneviève Labbé, Andrea Dupont, Heather Montgomery, Odisho Israel, Yay Duangkham, Erika Murray, Clarence Wang, Jason Yaeck, and Jeremy Bezaire. Thank you for providing a fun and enjoyable lab environment to work in and our amusing discussions on life. I am especially grateful to Valentina Taiakina, whose focused and hard-working attitude was instrumental in helping me complete many experiments for my thesis. To my friends who have been very supportive throughout my studies at UW (you know who you are), thank you. Mom – thanks for proof-reading my thesis. You are a wizard with words.

I'd like to thank my family – my parents, Rick and Diane, for their love and encouragement to pursue my dreams – and my sisters Kim and Vanessa, for smiling and nodding blankly whenever I would bring up my research. Even though all of you would fake being narcoleptic whenever I would mention "calmodulin", I still appreciate you trying to understand what I have been studying for the past 5 years. Finally, my wife, Jillian, whose patience, love and encouragement has been my foundation. I love you and I couldn't have done this without you.

Dedication

To my wife, Jillian
and my family, Rick, Diane, Kim and Vanessa
for your patience, love and support throughout my studies

Table of Contents

AUTHOR'S DECLARATION ..... **ii**
Abstract ..... **iii**
Acknowledgements ..... **v**
Dedication ..... **vi**
Table of Contents ..... **vii**
List of Figures ..... **xiv**
List of Tables ..... **xviii**
List of Abbreviations ..... **xx**
Outline of the Thesis ..... **xxiii**
Chapter 1 Literature Review **1**
1.1 Calmodulin 1
1.1.1 Cellular Calcium 1
1.1.2 EF Hand Motif 3
1.1.3 Characteristics of Calmodulin 5
1.1.4 CaM Binding to Target Peptides and Proteins 8
1.1.5 Solved Structures of CaM bound to Peptides and Enzymes 12
1.1.6 Regulation of CaM binding to target proteins 19
1.2 Nitric Oxide Synthase (NOS) 23
1.2.1 Nitric Oxide 23
1.2.2 Structural characteristics of the Mammalian NOS isozymes 25
1.2.3 Electron transfer within NOS 31
1.2.4 Catalytic mechanism of NOS 34
1.2.5 Regulation of NOS 38
1.2.5.1 Intrinsic regulation of NOS 38
1.2.5.2 Extrinsic regulation of NOS 43
1.2.6 Previous studies on CaM binding to NOS 46
1.2.6.1 CaM binding to NOS CaM-binding domain peptides 46
1.2.6.2 CaM binding to NOS enzymes 49
1.2.6.3 Mutant CaM proteins binding to the cNOS enzymes 50
1.3 Reasons for studying the interaction of NOS with CaM 52

1.4 Research Objectives 53
Chapter 2 Differential Activation of Mammalian Nitric Oxide Synthase Isozymes by Calmodulin-Troponin C Chimeras * 54
2.1 Introduction 54
2.2 Experimental Procedures 58
2.2.1 Cloning of CaM-TnC Chimera 58
2.2.2 Expression of Wild-type CaM 59
2.2.3 Purification of Wild-type CaM 59
2.2.4 CaM-TnC Expression and Purification 61
2.2.5 Electrospray Ionization-Mass Spectrometry of CaM and CaM Proteins 61
2.2.6 eNOS and nNOS Expression 61
2.2.7 eNOS and nNOS Purification 62
2.2.8 iNOS coexpression with wild-type CaM or CaM-TnC Chimeras 65
2.2.9 Purification of iNOS coexpressed with wild-type CaM or CaM-TnC Chimeric Proteins 66
2.2.10 Spectrophotometic Kinetic Assays 67
2.2.10.1 Oxyhemoglobin Capture Assay 68
2.2.10.2 Cytochrome c Reduction Assay 73
2.2.10.3 NADPH Oxidation Assay 76
2.3 Results 78
2.3.1 Protein Expression and Purification 78
2.3.2 cNOS Activation by CaM-TnC Chimeras 80
2.3.3 iNOS Activation by CaM-TnC Chimeras 83
2.4 Discussion 87
2.5 Conclusions 91
Chapter 3 Binding and Activation of Nitric Oxide Synthase Isozymes by Calmodulin EF Hand Pairs * 93
3.1 Introduction 93
3.2 Experimental Procedures 95
3.2.1 CaM Protein Subcloning and Mutagenesis 95
3.2.1.1 pnCaMChlor 95
3.2.1.2 pcCaMKan 95
3.2.1.3 pCaMNNKan and pCaMCCKan 96
3.2.2 Expression and Purification of CaM EF Hand Pair Proteins 96

3.2.3 Expression and Purification of NOS Enzymes 97
3.2.4 Enzyme Kinetics 97
3.2.5 Gel Filtration Studies 97
3.2.6 Native PAGE Studies 98
3.2.7 Aggregation Reversibility for iNOS coexpressed with nCaM 98
3.2.8 CaM Mobility Shift Assay with Synthetic NOS peptides 99
3.3 Results 100
3.3.1 Protein Expression and Purification 100
3.3.2 cNOS Activation by CaM EF Hand Pair Proteins 102
3.3.3 iNOS coexpressed with CaM EF Hand Pair Proteins EDTA Titration Studies 104
3.3.4 iNOS Activation by CaM EF Hand Pair Proteins 107
3.3.5 Enzyme Quaternary Structure 109
3.3.5.1 Gel Filtration Studies on iNOS coexpressed with CaM and nCaM 109
3.3.5.2 Native-PAGE of iNOS coexpressed with nCaM 111
3.3.5.3 Spectropolarimetry of nCaM with Synthetic NOS Peptides 113
3.3.5.4 Gel Mobility Shift Assays of CaM EF Hand Pair Proteins with NOS Peptides 113
3.3.6 Aggregation Reversibility of iNOS coexpressed with nCaM 115
3.4 Discussion 117
3.5 Conclusions 126
Chapter 4 Calcium-deficient Calmodulin Binding and Activation of Neuronal and Inducible Nitric Oxide Synthases * 128
4.1 Introduction 128
4.2 Experimental Procedures 131
4.2.1 Molecular Cloning of CaM_{12}, CaM_{34}, and CaM_{1234} 131
4.2.2 Ca^{2+}-deficient CaM protein Expression and Purification 131
4.2.3 NOS Enzyme Expression and Purification 132
4.2.4 NOS Enzyme Kinetics 134
4.2.4.1 Ferricyanide Reduction Assay 135
4.2.5 CaM Proteins Fluorescent Labeling with Dansyl Chloride 136
4.2.6 Steady-state Fluorescence Measurements 137
4.2.7 Circular Dichroism of Ca^{2+}-deficient CaM Proteins Bound to Synthetic NOS Peptides 138
4.3 Results and Discussion 139

4.3.1 Protein Expression and Purification 140
4.3.2 nNOS Activation by Ca^{2+}-deficient CaM Proteins 142
4.3.3 iNOS Activation by Ca^{2+}-deficient CaM Proteins 142
4.3.4 Ca^{2+}-deficient CaM-NOS Peptide Binding Studies 145
4.3.4.1 Steady-state Fluorescence of Dansyl-labeled CaM Proteins 145
4.3.4.2 Circular Dichroism of Ca^{2+}-deficient CaM Proteins 147
4.4 Conclusions 151
Chapter 5 Differential Binding of Calmodulin Domains to Constitutive and Inducible Nitric Oxide Synthase Enzymes * 152
5.1 Introduction 152
5.2 Experimental Procedures 154
5.2.1 Site-directed Mutagenesis of CaM 154
5.2.2 CaM Protein Expression and Purification 154
5.2.3 CaM Protein Labeling with Acrylodan and Alexa Fluor 546 C_5-maleimide 155
5.2.4 iNOS Peptide Labeling with Dabsyl Chloride 157
5.2.5 NOS Enzyme Expression and Purification 158
5.2.6 Enzyme Kinetics 158
5.2.7 Steady-State Fluorescence 159
5.2.8 Determination of Binding Affinities of CaM-Cys-acr proteins to NOS CaM-binding Domain Peptides 160
5.2.9 FRET Measurements of Alexa-labeled CaM Proteins with Dabsyl-labeled iNOS Peptide 161
5.2.10 Circular Dichroism of nCaM and cCaM bound to synthetic NOS peptides 161
5.3 Results 162
5.3.1 Protein Expression and Purification 162
5.3.2 Characterization of Fluorescently Labeled CaM-Cys Proteins 164
5.3.3 NOS Activation by CaM-Cys and Fluorescently-Labeled CaM Proteins 166
5.3.4 CaM-NOS Peptide Binding Studies 169
5.3.4.1 FRET studies using Alexa-labeled CaM proteins with Dabsyl-labeled iNOS peptide 169
5.3.4.2 Ca^{2+}-Dependent Association of Different Regions of CaM to NOS peptides 171
5.3.4.3 Binding Affinities of CaM-Cys-acr proteins to NOS CaM-binding Domain Peptides 175

5.3.4.4 Effect of nCaM and cCaM on the Secondary Structure of the iNOS peptide 178
5.3.5 CaM-Holo-NOS Enzyme Binding Studies 180
5.3.5.1 Alexa-CaM Binding to Holo-NOS Enzymes using Steady-State Fluorescence 180
5.3.5.2 Displacement of Alexa-CaM from iNOS by the Addition of Excess CaM Proteins .. 183
5.4 Discussion 185
5.5 Conclusions 188
Chapter 6 FRET Conformational Studies of Calmodulin Bound to Nitric Oxide Synthase Enzymes * 190
6.1 Introduction 190
6.1.1 Chapter Overview 194
6.2 Dual-targeted labeling of proteins using cysteine and selenomethionine residues 195
6.2.1 Introduction 195
6.2.2 Experimental Procedures 197
6.2.2.1 Mutagenesis of CaM-L9 197
6.2.2.2 CaM Expression and Selenomethionine Incorporation 198
6.2.2.3 T34SeM CaM-L9 and T34SeM/T110C CaM-L9 Protein Purification 200
6.2.2.4 cNOS Enzyme Kinetics 200
6.2.2.5 Chemical labeling of selenomethionine residues with IAEDANS 200
6.2.2.6 Cysteine labeling of T34SeM/T110C CaM-L9 202
6.2.2.7 Targeted dual labeling of T34SeM/T110C CaM-L9 with maleimide and iodoacetamide derivatives 202
6.2.2.8 Steady-state fluorescence of single and dual labeled CaM-L9 204
6.2.3 Results and Discussion 205
6.2.3.1 CaM-L9 Mutant Protein Expression and Purification 205
6.2.3.2 cNOS Activation by CaM-L9 Mutant Proteins 205
6.2.3.3 Single and Dual Labeling of CaM-L9 Proteins 206
6.2.3.4 Complications with Steady-State Fluorescence using IAEDANS-labeled Selenomethionine containing CaM Proteins 208
6.3 FRET Conformational Analysis of Calmodulin Bound to Nitric Oxide Synthase Peptides and Enzymes 211
6.3.1 Introduction 211
6.3.2 Experimental Procedures 211

6.3.2.1 Mutagenesis of CaM to produce T34C/T110C 211
6.3.2.2 CaM T34C/T110C Expression, Purification and Fluorescent Labeling 212
6.3.2.3 Site-directed Mutagenesis of eNOS, nNOS and iNOS 214
6.3.2.4 Expression and Purification of Heme-free NOS Enzymes 215
6.3.2.5 Steady-State Fluorescence Measurements of Alexa-labeled CaM Proteins with NOS Peptides and Enzymes 216
6.3.2.6 Quin-2 Free Ca^{2+} Concentration Calibration 217
6.3.2.7 Time-Resolved Fluorescence Measurements of Alexa-labeled CaM Proteins with NOS Peptides and Enzymes 219
6.3.2.8 Determination of the Förster Distance (R_O) for Alexa Fluor 546 and DABMI labeled proteins 220
6.3.2.9 FRET distance determination for Alexa Fluor 546/DABMI T34C/T110C CaM with NOS peptides and enzymes 222
6.3.3 Results 224
6.3.3.1 Characterization of Fluorescently Labeled CaM-Cys Proteins 224
6.3.3.2 Steady-State Fluorescence of Alexa-labeled CaM Proteins with NOS Peptides and Enzymes 225
6.3.3.3 Time-resolved measurements for the determination of FRET distances 229
6.3.4 Discussion 247
6.3.5 Conclusions 253
Chapter 7 Preliminary NMR Structural Analysis of Calmodulin Bound to the CaM-binding Domain of Inducible Nitric Oxide Synthase 255
7.1 Introduction 255
7.2 Experimental Procedures 260
7.2.1 ^{13}C and ^{15}N Isotope Incorporation into Wild-type CaM and CaM_{1234} 260
7.2.2 Purification of ^{13}C and ^{15}N isotope labeled wild-type CaM and CaM_{1234} 260
7.2.3 Molecular Cloning of NOS CaM-binding domain peptides 261
7.2.3.1 piNOSpep 261
7.2.3.2 peNOSpep and pnNOSpep 263
7.2.3.3 piNOSCBD-intein, peNOSCBD-intein, and pnNOSCBD-intein 264
7.2.4 Expression of intein-iNOS CaM-binding domain fusion protein 265
7.2.5 Purification of iNOS CaM-binding domain peptide from the intein fusion protein 265
7.2.6 Sample preparation for NMR experiments 267

7.2.7 NMR spectroscopy and data analysis 267
7.3 Results 269
7.3.1 CaM Protein Expression and Purification 269
7.3.2 CaM-iNOS CaM-binding domain peptide purification 270
7.3.3 Preliminary NMR Spectral Analysis 273
7.4 Future Studies 276
Chapter 8 Original Contributions and Recommendations for Future Studies 277
8.1 Original Contributions 277
8.1.1 Working Model of the CaM-dependent regulation of iNOS 281
8.2 Recommendations for Future Studies 285
8.2.1 NMR structural determination of CaM mutants with NOS peptides 285
8.2.2 NMR structural determination of the FMN domains for nNOS and iNOS 286
8.2.3 Characterization of CaM binding and activation of other CaM-dependent target proteins 288
Appendix A – CaM and NOS DNA Sequences 289
Appendix B – Further FRET Analysis of CaM Binding to NOS Peptides and Enzymes 323
Bibliography 325

List of Figures

Figure 1.1 – Mechanisms of Ca^{2+} signaling within the cell. 2
Figure 1.2 – Ca^{2+} co-ordination in a typical Ca^{2+}-binding EF hand. 3
Figure 1.3 – Solved NMR and x-ray crystal structures of CaM in various Ca^{2+}-bound and conformational states. 6
Figure 1.4 – Structural representation of the exposed hydrophobic patches in the (A) N- and (B) C-terminal domains of holo-CaM. 7
Figure 1.5 – Solved structures of CaM bound to various target peptides in an anti-parallel orientation. 15
Figure 1.6 – Solved structures of CaM bound to various target peptides in a parallel orientation. 16
Figure 1.7 – Solved structures of CaM bound to various target peptides and proteins in unique conformations. 18
Figure 1.8 – Chemical structures of CaM antagonist molecules. 20
Figure 1.9 – CaM in complex with various small molecules. 21
Figure 1.10 – NOS-catalysed conversion of L-arginine through the intermediate N^{G}-hydroxy-L-arginine to L-citrulline and •NO. 25
Figure 1.11 – Alignment of NOS enzymes. 26
Figure 1.12 – Chemical structures of cofactors bound to mammalian NOS enzymes. 27
Figure 1.13 – X-ray crystal structures of rat nNOS oxygenase with bound L-arginine 30
Figure 1.14 – X-ray crystal structures of rat nNOS reductase domain. 30
Figure 1.15 – Electron transfer within a NOS dimer. 32
Figure 1.16 – Electron transfer and •NO production controlled by CaM-dependent conformational changes between the NOS cofactors. 33
Figure 1.17 – Proposed catalytic mechanism of the NOS enzymes through two mono-oxygenation reactions. 36
Figure 1.18 – A generalized model of an autohibitory domain and its displacement by Ca^{2+}/CaM. 38
Figure 1.19 – Sequence alignment of the FMN binding region of cytochrome P450 (CYPOR) and the NOS enzymes 39
Figure 1.20 – A proposed three-step model to explain the mechanism that the autoinhibitory insert and CaM use to regulate electron tranfer in the cNOS enzymes. 40
Figure 1.21 – Comparative sequence alignment of the C-terminal tails of the NOS enzymes and cytochrome P450 (CYPOR) 41

Figure 1.22 – Sequence alignment of the CaM-binding domains of the NOS enzymes. 46
Figure 1.23 – Helical wheel diagrams of the CaM-binding domains of the NOS enzymes. 47
Figure 2.1 – Alignment of CaM and cardiac TnC. 55
Figure 2.2 – Alignment of CaM and CaM-TnC chimera proteins. 56
Figure 2.3 – UV-absorbance scan of wild-type CaM 60
Figure 2.4 – UV-visible absorbance scan of (A) nNOS, (B) eNOS, and (C) iNOS coexpressed with wild-type CaM. 65
Figure 2.5 – Spectrophotometric assays employed to monitor electron transfer within the NOS enzymes. 68
Figure 2.6 – Calibration of oxyhemoglobin in a 96 well microtitre plate using serial dilutions. 70
Figure 2.7 – SDS-PAGE of CaM-TnC chimeras. 78
Figure 2.8 – Ability of CaM-TnC chimeras to activate nNOS. 80
Figure 2.9 – Ability of CaM-TnC chimeras to activate eNOS. 81
Figure 2.10 – Ability of coexpressed CaM-TnC chimeras to activate iNOS. 84
Figure 3.1 – Alignment of CaM and EF Hand mutant CaM proteins. 94
Figure 3.2 – 15% SDS-PAGE of purified EF Hand Pair CaM proteins. 100
Figure 3.3 – EDTA titration of iNOS coexpressed with CaM EF Hand Pair Proteins. 105
Figure 3.4 – Gel filration elution profiles of iNOS coexpressed with CaM proteins. 110
Figure 3.5 – 5% Native PAGE studies for iNOS coexpressed with nCaM. 112
Figure 3.6 – Gel Mobility Shift Assay with Synthetic NOS peptides binding to CaM proteins. 114
Figure 3.7 – Aggregation reversibility for iNOS coexpressed with nCaM. 116
Figure 3.8 – Alignment of CaM-binding domain sequences of the three NOS isoforms 123
Figure 3.9 – Structures of nCaM bound to eNOS peptide 124
Figure 4.1 – Schematic representation of CaM_{12}, CaM_{34}, and CaM_{1234}. 130
Figure 4.2 – Gel filration elution profile of iNOS coexpressed with CaM_{12}. 134
Figure 4.3 – Chemical structure of dansyl chloride used to N-terminally label wild-type CaM, CaM_{12}, CaM_{34}, and CaM_{1234} 137
Figure 4.4 – 15% SDS-PAGE of the purified Ca^{2+}-deficient CaM proteins. 140
Figure 4.5 – Ability of wild-type CaM and Ca^{2+}-deficient mutant CaM proteins to activate NOS enzymes. 143
Figure 4.6 – Fluorescence emission spectra of dansyl-CaM proteins in the presence of nNOS and iNOS peptides 146

Figure 4.7 – CD spectra for (A) wild-type CaM, (B) CaM_{1234}, (C) CaM_{12}, and (D) CaM_{34} in the presence and absence of Ca^{2+}. 148
Figure 4.8 – Difference CD spectra for iNOS and nNOS CaM-binding domain peptides in the presence of (A) wild-type CaM, (B) CaM_{1234}, (C) CaM_{12}, and (D) CaM_{34}. 149
Figure 5.1 – Chemical structures of (A) Acrylodan, (B) Alexa Fluor 546 C_5 maleimide, and (C) Dabsyl chloride. 156
Figure 5.2 – X-ray and NMR structures showing the positions of T34, K75 and T110 in A) Holo-CaM, B) Apo-CaM, and C) CaM when bound to eNOS peptide. 162
Figure 5.3 – FRET analysis of (A) CaM-T34C-Alexa and (B) CaM-T110C-Alexa binding to iNOS peptide N-terminally labeled with dabsyl chloride. 170
Figure 5.4 – Steady-state Fluorescence of CaM-Cys-acr proteins binding to synthetic NOS CaM binding domain peptides. 172
Figure 5.5 – Determination of K_{CaM} binding constant for CaM-T110C-acr binding to the eNOS CaM-binding domain peptide using steady-state fluorescence. 176
Figure 5.6 – Effect of Ca^{2+} and EDTA on the secondary structure of (A) nCaM and (B) cCaM bound to synthetic iNOS CaM-binding domain peptide. 179
Figure 5.7 – Steady-state Fluorescence of Alexa Fluor 546 labeled CaM-Cys proteins binding to holo-NOS enzymes. 182
Figure 5.8 – Dissociation of CaM-T110C-Alexa from iNOS coexpressed with nCaM after the addition of excess CaM proteins. 184
Figure 6.1 – X-ray crystal structures showing the positions of T34 and T110 in (A) Holo-CaM compared to CaM when bound to (B & C) the eNOS and (D & E) the nNOS CaM-binding domain peptides. 191
Figure 6.2 – X-ray crystal structures of rat nNOS oxygenase and reductase domains. 193
Figure 6.3 – Reaction schemes involving (A) selenomethionine with iodoacetamide to form selenonium or sulfonium salts, and (B) the cleavage of the selenonium by free thiols. 196
Figure 6.4 – Fluorescent dyes used to selectively label selenomethionine and cysteine residues of T34SeM/T110C CaM-L9. 201
Figure 6.5 – Selective dual labeling of cysteine and selenomethionine residues in T34SeM/T110C CaM-L9. 203
Figure 6.6 – Mass spectrometry of (A) IAEDANS labeled T34SeM CaM-L9 and (B) IAEDANS/DDPM labeled T34SeM/T110C CaM-L9 proteins. 207
Figure 6.7 – Steady-state fluorescence complications with IAEDANS-labeled T34SeM CaM-L9. 208

Figure 6.8 – Chemical structures of (A) Alexa Fluor 546 C_5 maleimide and (B) DABMI used to dual label CaM T34C/T110C. 212
Figure 6.9 – UV-visible absorbance scan of holo-eNOS and eNOS C186A. 216
Figure 6.10 – Structure of the fluorescent Ca^{2+} indicator dye Quin-2. 217
Figure 6.11 – Determination of the K_d of Quin-2 using Ca/EGTA buffers. 219
Figure 6.12 – Emission of Alexa Fluor 546 and absorbance of DABMI-labeled CaM proteins for the determination of spectral overlap interval $J(\lambda)$. 221
Figure 6.13 – Dependence of energy transfer efficiency (E) on the distance (R) between the donor and acceptor dyes. 223
Figure 6.14 – Steady-state FRET measurements using Alexa/DABMI labeled CaM T34C/T110C with synthetic NOS CaM-binding domain peptides. 226
Figure 6.15 – Steady-state FRET measurements using singly labeled CaM-T34C-Alexa (CaM-D) and dual labeled CaM T34C/T110C Alexa/DABMI (CaM-DA) with heme-free cNOS enzymes. 228
Figure 6.16 – Time-resolved fluorescence of (A) Alexa 546-T34C CaM and (B) Alexa 546/DABMI-T34C-T110C CaM. 230
Figure 6.17 – Determined FRET distances for dually-labeled CaM to cNOS peptides and enzymes at varying free Ca^{2+} concentrations. 250
Figure 6.18 – Determined FRET distances for iNOS coexpressed with nCaM with (A) CaM-T34-Alexa CaM and (B) CaM-T110C-Alexa at varying free Ca^{2+} concentrations. 253
Figure 7.1 – Heteronuclear multidimensional NMR experiments typically used for the resonance assignment of proteins. 257
Figure 7.2 – Characteristics of the human iNOS CaM-binding domain expression vector phiNOSCBDKan 263
Figure 7.3 – Gel Mobility Shift Assay of wild-type CaM with synthetic and recombinantly expressed iNOS peptides. 271
Figure 7.4 – 12% SDS-PAGE of intein alone and intein-iNOS peptide time-course expression test in minimal medium. 272
Figure 7.5 – $^{1}H,^{15}N$-HSQC spectra of CaM alone and in complex with iNOS peptide. 274
Figure 8.1 – Working model for CaM-dependent regulation of •NO by iNOS. 283

List of Tables

Table 1.1 – Examples of mammalian proteins that are activated by Ca^{2+}-binding 2

Table 1.2 – Frequency of specific amino acid sequences in the EF hand loops. 4

Table 1.3 – Summary of well-characterized holo-CaM Ca^{2+}-dependent proteins. 10

Table 1.4 – Summary of some Apo-CaM binding proteins. 10

Table 1.5 – •NO-mediated effects in various tissues. 24

Table 1.6 – Summary of the properties and roles of mammalian NOS isozymes 29

Table 1.7 – Residues of CaM shown to be within 4 Å of the eNOS peptide 48

Table 2.1 – Masses of CaM-TnC Chimera proteins [a] 79

Table 3.1 – Masses of CaM EF Hand Pair proteins [a] 101

Table 3.2 – CaM EF Hand Pair Protein Dependent Activation of cNOS Enzymes [a] 102

Table 3.3 – CaM EF Hand Pair Protein Activation of iNOS [a] 107

Table 3.4 – Comparison of eNOS and iNOS CaM-binding domains predicted to aggregate by TANGO with CaM residues that interact with the peptide residues 124

Table 4.1 – Masses of CaM proteins and fluorescently labeled CaM proteins 141

Table 5.1 – Masses of CaM and fluorescently labeled CaM-Cys proteins 163

Table 5.2 – CaM-Cys and fluorescently labeled CaM Dependent Activation of cNOS enzymes [a] 166

Table 5.3 – CaM-Cys and fluorescently labeled CaM Activation of iNOS [a] 168

Table 5.4 – Calculated K_{CaM} affinity constants for acrylodan labeled-CaMs binding to NOS peptides 177

Table 6.1 – Masses and Purification Yield of CaM-L9 mutant proteins 205

Table 6.2 – CaM-L9 Mutant Proteins Dependent Activation of cNOS enzymes [a] 206

Table 6.3 – Masses of Alexa 546 and DABMI labeled CaM-Cys proteins 224

Table 6.4 – Determined FRET distances for Alexa 546/DAB-T34C-T110C CaM alone with increasing free Ca^{2+} concentrations 231

Table 6.5 – Determined FRET distances for Alexa 546/DAB-T34C-T110C CaM in the presence of eNOS peptide with increasing free Ca^{2+} concentrations. 233

Table 6.6 – Determined FRET distances for Alexa 546/DAB-T34C-T110C CaM in the presence of nNOS peptide with increasing free Ca^{2+} concentrations. 235

Table 6.7 – Determined FRET distances for Alexa 546/DAB-T34C-T110C CaM in the presence of iNOS peptide with increasing free Ca^{2+} concentrations 236

Table 6.8 – Determined FRET distances for Alexa 546/DAB-T34C-T110C CaM in the presence of eNOS C186A with increasing free Ca^{2+} concentrations. 238
Table 6.9 – Determined FRET distances for Alexa 546/DAB-T34C-T110C CaM in the presence of nNOS C415A with increasing free Ca^{2+} concentrations. 239
Table 6.10 – Determined FRET distances for CaM-T34C-Alexa 546 in the presence of N-terminally labeled DAB-iNOS peptide with increasing free Ca^{2+} concentrations. 241
Table 6.11 – Determined FRET distances for CaM-T110C-Alexa 546 in the presence of N-terminally labeled DAB-iNOS peptide with increasing free Ca^{2+} concentrations. 242
Table 6.12 – Determined FRET distances for CaM-T34C-Alexa 546 in the presence of iNOS coexpressed with nCaM with increasing free Ca^{2+} concentrations. 244
Table 6.13 – Determined FRET distances for CaM-T110C-Alexa 546 in the presence of iNOS coexpressed with nCaM with increasing free Ca^{2+} concentrations. 245
Table 6.14 – Control time-resolved fluorescence measurements of Alexa 546 labeled CaM proteins with iNOS C200A coexpressed with nCaM. 246
Table 6.15 – Measured distances between T34 and T110 in the solved CaM NMR and x-ray crystal structures. 248
Table 7.1 – Primers used to construct phiNOSCBDKan, prnNOSCBDKan, and peNOSCBDKan .. 262
Table 7.2 – Masses of isotope-labeled wild-type CaM and CaM_{1234} 269
Table 7.3 – Masses of unlabeled iNOS peptide copurified with wild-type CaM. 271

List of Abbreviations

Acrylodan	6-acryloyl-2-dimethylaminonaphtalene
ADP	Adenosine diphosphate
AI	Autoinhibitory domain
δ-ALA	δ-aminolevulinic acid
Alexa Fluor 546	Alexa Fluor 546 C_5-maleimide
AMP	Adenosine monophosphate
Apo-CaM	Ca^{2+}-deplete CaM
APS	Ammonium persulfate
ATP	Adenosine triphosphate
BSA	Bovine serum albumin
Ca^{2+}_c	Cytosolic Ca^{2+}
Ca^{2+}_{ER}	Ca^{2+} stored in the endoplasmic reticulum
Ca^{2+}_o	Extracellular Ca^{2+}
CaM	Calmodulin
CaM_{12}	CaM mutant incapable of binding Ca^{2+} in its N-terminal EF hand pair (aspartate residues 21 and 56 mutated to alanines)
CaM_{34}	CaM mutant incapable of binding Ca^{2+} in its C-terminal EF hand pair (aspartate residues 93 and 131 mutated to alanines)
CaM_{1234}	CaM mutant incapable of binding Ca^{2+} in its N- and C-terminal EF hand pairs (aspartate residues 21, 56, 93, and 131 mutated to alanines)
CaMKI	CaM-dependent protein kinase I
CaMKII	CaM-dependent protein kinase II
CaMKK	CaM-dependent kinase kinase
CaMCC	CaM mutant with two repeats of the C-terminal EF hand pair of CaM (residues 1-8, 82-148, followed by 76-148)
CaMNN	CaM mutant with two repeats of the N-terminal EF hand pair of CaM (residues 1-81, followed by 9-75)
CaM-K75C	CaM where lysine 75 is mutated to a cysteine
CaM-K75C-acr	CaM-K75C labeled with acrylodan
CaM-K75C-Alexa	CaM-K75C labeled with Alexa Fluor 546
CaM-T34C	CaM where threonine 34 is mutated to a cysteine
CaM-T34C-acr	CaM-T34C labeled with acrylodan
CaM-T34C-Alexa	CaM-T34C labeled with Alexa Fluor 546
CaM-T110C	CaM where threonine 110 is mutated to a cysteine
CaM-T110C-acr	CaM-T110C labeled with acrylodan
CaM-T110C-Alexa	CaM-T110C labeled with Alexa Fluor 546
CaM-TnC	CaM-troponin C chimera
CaM-1TnC	CaM mutant with EF hand I exchanged with its cognate in TnC
CaM-2TnC	CaM mutant with EF hand II exchanged with its cognate in TnC
CaM-3TnC	CaM mutant with EF hand III exchanged with its cognate in TnC
CaM-4TnC	CaM mutant with EF hand IV exchanged with its cognate in TnC
CaM-3,4TnC	CaM mutant with EF hands III and IV exchanged with its cognate in TnC
CaN	Calcineurin
CaV1.2 Ca^{2+} channel	Ca^{2+} 1.2 voltage-gated Ca^{2+} channel

cCaM	CaM mutant consisting of the C-terminal EF hand pair and central linker of CaM (residues 76-148)
CD	Circular dichroism
cGMP	Cyclic guanosine monophosphate
cNOS	Constituitive nitric oxide synthase
DABMI	4-dimethylaminophenylazophenyl-4'-maleimide
Dabsyl chloride	4-dimethylaminoazobenzene-4'-sulfonyl chloride
Dansyl chloride	5-dimethylaminonaphthalene-1-sulfonyl chloride
Dansyl-CaM_{12}	Dansyl chloride labeled CaM_{12}
Dansyl-CaM_{34}	Dansyl chloride labeled CaM_{34}
Dansyl-CaM_{1234}	Dansyl chloride labeled CaM_{1234}
Dansyl-wild-type CaM	Dansyl chloried labeled wild-type CaM
DAP kinase I	Death-associated protein kinase I
DAP kinase II	Death-associated protein kinase II
DRP-I kinase	Death-associated related protein kinase I
DTNB	5,5'-dithio-bis(2-nitrobenzoic acid)
DTT	Dithiothreitol
E. coli	*Escherichia coli*
EDTA	Ethylenediaminetetraacetic acid
EGTA	Ethylene glycol-bis(β-aminoethyl ether)-N,N,N',N'-tetraacetic acid
eNOS	Endothelial nitric oxide synthase (NOS III)
eNOS C186A	eNOS with cysteine 186 mutated to an alanine (heme-free)
ESI-MS	Electrospray ionization-mass spectrometry
FAD	Flavin adenine dinucleotide
FeCN	Ferricyanide
FMN	Flavin mononucleotide
FRET	Fluorescence (Förster) resonance energy transfer
H_4B	(6*R*)-5,6,7,8-tetrahydrobiopterin
HbO_4	Oxyhemoglobin
Heme	Iron protoporphyrin IX
Holo-CaM	Ca^{2+}-replete CaM
Hsp90	Heat shock protein 90
IPTG	Isopropyl D-1-thiogalactopyranoside
iNOS	Inducible nitric oxide synthase (NOS II)
iNOS C200A	iNOS with cysteine 200 mutated to an alanine (heme-free)
$Ins(1,4,5)P_3$	Inositol 1,4,5-trisphosphosphate
MARCKS	Myristolylated alanine-rich C kinase substrate
MLCK	Myosin light chain kinase
MQH_2O	Deionized water purified using a Milli-Q system (Millipore)
Myr	Myristoyl group
$NADP^+$	Oxidized nicotinamide adenine dinucleotide phosphate
NADPH	Reduced nicotinamide adenine dinucleotide phosphate
NAP110	NOS-associated protein-110 kDa
nCaM	CaM mutant consisting of the N-terminal EF hand pair of CaM (residues 1-75)
NF-κB	Nuclear factor kappaB
^{15}N-HSQC	^{15}N-Heteronuclear Single Quantum Correlation
NMDA receptor	*N*-methyl-D-aspartate receptor

NMR	Nuclear magnetic resonance
nNOS	Neuronal nitric oxide synthase (NOS I)
nNOS C415A	nNOS with cysteine 415 mutated to an alanine (heme-free)
•NO	Nitric oxide
NOESY	Nuclear Overhauser Effects SpectroscopY
NOHA	N^G-hydroxyl-L-arginine
NOS	Nitric oxide synthase
$•O_2^-$	Superoxide
Olfactory CNG channel	Olfactory cyclic-nucleotide gated channel
$OONO^-$	Peroxynitrite
PCR	Polymerase chain reaction
PIN	Protein inhibitor of NOS
PKG	Protein kinase G
PLC	Phospholipase C
PMSF	Phenylmethylsulphonylfluoride
PSD-95	Post-synaptic density protein-95
QTOF	Quadrupole time-of-flight
ROC	Receptor-operated Ca^{2+} channel
ROS	Reactive oxygen species
RyR	Ryanodine receptor
SDS-PAGE	Sodium dodecyl sulphate polyacrylamide gel electrophoresis
SK K^+ channel	Small conductance Ca^{2+}-activated K^+ channel
SOD	Superoxide dismutase
TEMED	Tetramethylethylenediamine
TFA	Trifluoroacetic acid
TnC	Cardiac troponin C
TOCSY	Total Correlation SpectroscopY
VOC	Voltage-operated Ca^{2+} channel

The three letter and one letter abbreviations for amino acids are used throughout this thesis according to the IUPAC-IUB Combined Commissions in Biochemical Nomenclature (Dixon *et al.*, 1984). Single letter abbreviations are also used for DNA bases.

Outline of the Thesis

This thesis consists of eight chapters with a common focus of studying the binding and activation of mammalian NOS enzymes by CaM. A synopsis for each chapter follows:

Chapter 1 provides a comprehensive review of CaM and its ability to bind to various CaM-dependent target peptides and proteins. CaM binding and activation of NOS and the significance of studying this fascinating and physiologically important protein-protein interaction are also discussed.

Chapter 2 describes the use of CaM-troponin C chimeric proteins to investigate the effect of specific EF hand elements in CaM on the activation of the NOS enzymes using three distinct spectrophotometric assays to monitor electron transfer rates at the various redox centers in the reductase and oxygenase domains of NOS.

Chapter 3 describes the use of CaM EF hand pair proteins to determine the specific domain of CaM responsible for the binding and activation of the NOS enzymes. A particular focus is given to the binding and activation of iNOS with a plausible reason for the strong, irreversible association of CaM to this Ca^{2+}-independent NOS isozyme.

Chapter 4 describes an investigation on the effect of CaM mutant proteins incapable of binding to Ca^{2+} on the association and activation of nNOS and iNOS peptides and enzymes.

Chapter 5 describes the use of fluorescently labeled CaM proteins to monitor the differential binding of the N-domain, C-domain and central linker of CaM to mammalian NOS peptides and enzymes through steady-state fluorescence. The orientation of CaM when bound to iNOS is also determined through the use of FRET.

Chapter 6 contains a combination of various studies with the common focus of monitoring CaM binding to NOS peptides and enzymes using fluorescence. The first study in this chapter focuses on a selective dual labeling methodology to fluorescently label CaM using single cysteine and

selenomethionine residues. The second study involves the monitoring of dynamic conformational changes in CaM when associating to NOS peptides and enzymes using FRET.

Chapter 7 describes the preliminary NMR structural determination of Ca^{2+}-replete and Ca^{2+}-deplete CaM when bound to a peptide corresponding to the canonical CaM-binding domain of iNOS. A summary of the work performed to date as well as future plans for the completion of this study are also included.

Chapter 8 presents the overall conclusions of this doctoral study, contributions of this research to the scientific community, and recommendations for future studies to further the findings presented in this thesis.

Chapter 1
Literature Review

1.1 Calmodulin

1.1.1 Cellular Calcium

Ca^{2+} is an important intracellular secondary messenger that is able to relay information within cells to regulate the activity of numerous physiological processes. An increase of intracellular Ca^{2+} concentration can originate from external sources from outside of the cell or internal Ca^{2+} stores within the cell. For instance, external Ca^{2+} from an external source can include an influx of Ca^{2+} through various channels that span the plasma membrane such as voltage-operated Ca^{2+} channels found in excitable cells (such as muscle cells or neurons) or receptor-operated Ca^{2+} channels (ROCs) which respond to the release of neurotransmitters. Intracellular Ca^{2+} can also be released into the cytosol from internal Ca^{2+} stores found in the endoplasmic or sarcoplasmic reticulum through ryanodine receptor (RyR) Ca^{2+} release channels in response to intracellular secondary messengers, such as inositol 1,4,5-trisphosphate ($Ins(1,4,5)P_3$) generated by phospholipase C (PLC) (Clapham, 1995; Zalk *et al.*, 2007). In response to these small molecule stimuli, the influx of Ca^{2+} into the cytosol typically causes a 100 fold increase in free Ca^{2+} concentrations from approximately 10^{-7} M in a resting cell to 10^{-5} M in an activated cell (Gifford *et al.*, 2007). An overall summary of the regulation of Ca^{2+} release within a cell is shown in Figure 1.1.

Cellular processes regulated by an increase of intracellular Ca^{2+} concentrations include muscle contraction, metabolism, neurotransmission, memory, cell fertilization, cell differentiation, cell proliferation, and cell defense. Cell death can also result if the intracellular concentration of

Ca^{2+} is not properly controlled (Berridge *et al.*, 1998; Berridge *et al.*, 2000). A brief list of proteins that bind to Ca^{2+} within the cell is given in Table 1.1.

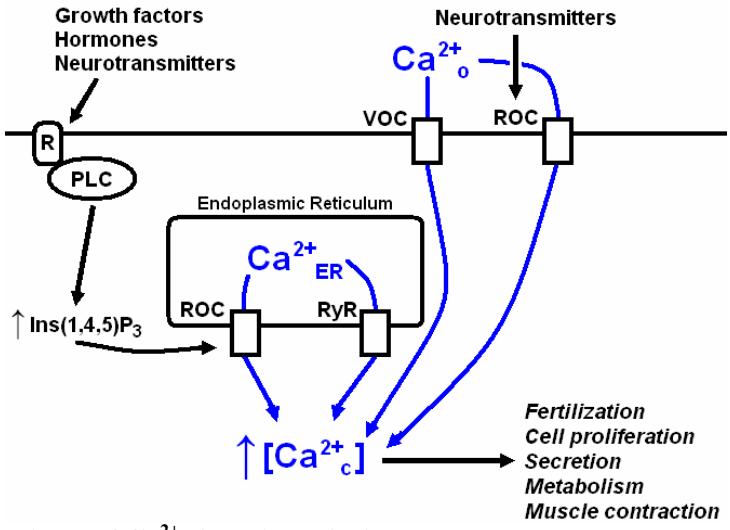

Figure 1.1 – Mechanisms of Ca^{2+} signaling within the cell.
Ca^{2+}_o, Ca^{2+}_c, and Ca^{2+}_{ER} represent Ca^{2+} originating from outside the cell, cytosolic Ca^{2+}, and Ca^{2+} stored in the endoplasmic reticulum, respectively. Voltage-operated and receptor-operated Ca^{2+} channels are labeled as VOC and ROC, respectively. The increased Ca^{2+} concentrations in the cytosol can initiate numerous physiological processes within the cell. This figure is modified from a previous review (Berridge *et al.*, 1998).

Table 1.1 – Examples of mammalian proteins that are activated by Ca^{2+}-binding

Protein	Ca^{2+}-Binding Site	Protein Function
Calmodulin	EF Hand	Ubiquitous modulator of protein kinases and other enzymes
Troponin C	EF Hand	Modulator of muscle contraction
Calretinin, retinin, visinin	EF Hand	Activator of guanylyl cyclase
Calcineurin B	EF Hand	Phosphatase
Calpain	EF Hand	Protease
Inositol phospholipid-specific PLC	EF Hand	Generator of InsP3 and diacylglycerol
α-Actinin	EF Hand	Actin-binding protein
Protein kinase C		Ubiquitous protein kinase
Ca^{2+}-activated K^+ channel		Effector of membrane hyperpolarization
Ryanodine receptor		Effector of intracellular Ca^{2+} release
Na^+/Ca^{2+} exchanger		Effector of the exchange of Ca^{2+} for Na^+ across the plasma membrane
Ca^{2+} ATPase		Pumps Ca^{2+} across membranes
Caldesmon		Regulator of muscle contraction
Parvalbumin	EF Hand	Ca^{2+} buffer
Calbindin	EF Hand	Ca^{2+} buffer
Calsequestrin	EF Hand	Ca^{2+} buffer

Table is a modified summary from a previously published review (Clapham, 1995).

1.1.2 EF Hand Motif

A common Ca^{2+}-binding motif found in many of the proteins listed in Table 1.1 is the EF hand. This motif consists of a helix-loop-helix structural element with the majority of the ligands used to chelate Ca^{2+} located in the loop of the EF hand (Figure 1.2).

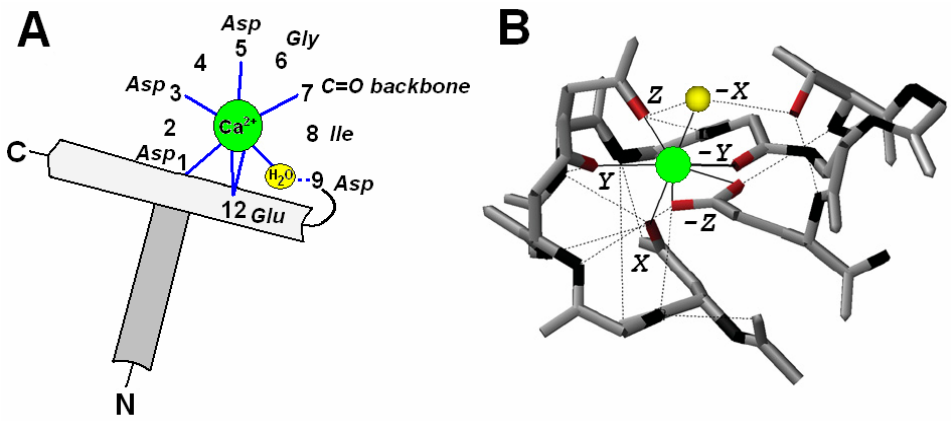

Figure 1.2 – Ca^{2+} co-ordination in a typical Ca^{2+}-binding EF hand.
This figure is shown to clarify the helix-loop-helix EF hand motif and how it is able to chelate a Ca^{2+} ion. **(A)** The entering and exiting helices are shown in dark grey and light grey, respectively. The co-ordinating amino acid sidechains and backbone and water molecule involved in the chelation of Ca^{2+} are shown in blue and yellow, respectively. The most common amino acids found at the critical positions in the EF hand loop (1, 3, 5, 6, 7, 9, and 12) are shown. **(B)** Example of Ca^{2+} co-ordination by the EF hand I of CaM. The pentagonal bipyramidal co-ordination of the Ca^{2+} ion and hydrogen bonding network used to stabilize the ligand co-ordination of Ca^{2+} are represented in solid and dashed lines, respectively. The backbone amide groups, side-chain oxygens, Ca^{2+} ion, and co-ordinating water are shown in black, red, green and yellow, respectively. *X*, *Y*, and *Z* represent the axial positions of the ligands in the pentagonal bipyramdial coordination when bound to Ca^{2+}. This figure was derived from PDB 1EXR (Wilson and Brunger, 2000) and modified from a previous EF hand review (Gifford *et al.*, 2007).

Aspartate and glutamate residues are the most common ligands in this motif, with Asp being more frequent than Glu; this has previously been attributed to a preference in EF hands for less bulky side chains (McPhalen *et al.*, 1991). These amino acid ligands chelate Ca^{2+} with their negatively charged carboxylate groups that can form ionic bonds with the Ca^{2+} cation (Ca–O bonds). The ligands bind to Ca^{2+} in a pentagonal bipyramidal coordination involving seven ligands in total (Figure 1.2). In addition, the EF-loop also contains an extensive hydrogen-bonding network between the chelating residues and the non-chelating residues that offsets the destabilizing repulsion between the

negatively-charged carboxylate sidechains which are in close proximity when coordinated with Ca^{2+} (Gifford *et al.*, 2007). A summary of the amino acids typically found in EF hand loops is shown in Table 1.2.

Table 1.2 – Frequency of specific amino acid sequences in the EF hand loops.

	EF Hand Loop Position [a]											
	1	2	3	4	5	6	7	8	9	10	11	12
Coordinating ligand [b]	*X* sc [c]		*Y* sc		*Z* sc		*-Y* bb		*-X* sc*			*-Z* sc2
Most Common Amino Acid [d]	Asp 100%	Lys 29%	Asp 76%	Gly 56%	Asp 52%	Gly 96%	Thr 23%	Ile 68%	Asp 32%	Phe 23%	Glu 29%	Glu 92%
Frequently Observed Amino Acids [e]		Ala Gln Thr Val Ile Ser Glu Arg	Asn	Lys Arg Asn	Ser Asn		Phe Lys Gln Tyr Glu Arg	Val Leu	Ser Thr Glu Asn Gly Gln	Tyr Ala Thr Leu Glu Lys	Asp Lys Ala Pro Asn	Asp
Calmodulin [f]	1	2	3	4	5	6	7	8	9	10	11	12
EF Hand I	Asp	Lys	Asp	Gly	Asp	Gly	Thr	Ile	Thr	Thr	Lys	Glu
EF Hand II	Asp	Ala	Asp	Gly	Asn	Gly	Thr	Ile	Asp	Phe	Pro	Glu
EF Hand III	Asp	Lys	Asp	Gly	Asn	Gly	Tyr	Ile	Ser	Ala	Ala	Glu
EF Hand IV	Asp	Ile	Asp	Gly	Asp	Gly	Gln	Val	Asn	Tyr	Glu	Glu

Table is modified from a previous EF hand loop review (Gifford *et al.*, 2007).
[a] The position in the EF hand loop for the Ca^{2+} ligands are indicated.
[b] The position in the pentagonal bipyramidal coordination where the *Y* and *Z*-axes are along the plane of the pentagon, while the *X*-axis is in an axial position that is perpendicular to the *Y/Z* plane, based upon a previous structural study (Strynadka and James, 1989).
[c] Codes represent which part of the amino acid at the indicated position is involved in the chelation of the metal ion – side chain (sc) or through the backbone (bb). The asterisk (*) highlights the ligand typically hydrogen-bonded to a water molecule via the side chain of the amino acid at position 9. sc2 denotes the amino acid side chain found at position 12 which uses both of its oxygens in its carboxylate group to chelate the Ca^{2+} ion.
[d] The most common amino acids at each position are highlighted with their corresponding percentages of occurrence in nature.
[e] Amino acids that occur with a frequency greater than 5%.
[f] Amino acids found at the various positions in the four calmodulin EF hand loops. These were added to show the sequence homology of all four EF hand loops in CaM.

Typically, EF hand motifs are found in pairs in nature with their Ca^{2+}-binding being cooperative (Biekofsky and Feeney, 1998). Proteins with EF hand pairs include troponin C, S-100 proteins, and calmodulin.

1.1.3 Characteristics of Calmodulin

Calmodulin (CaM) is a ubiquitous Ca^{2+}-binding protein found in all eukaryotic organisms. Most vertebrates contain three genes that code for CaM (*CAM I*, *CAM II*, and *CAM III*) that are transcribed into approximately 8 different mRNA molecules. Although there are 8 mRNA transcripts that code for CaM, they all produce identical amino acid sequences when translated (Ikura and Ames, 2006). While CaM is identical in all vertebrates, CaM is also expressed in other organisms such as plants, fungi and protozoa (Vetter and Leclerc, 2003). No *CAM* gene has been found in any of the sequenced bacterial genomes, suggesting that this protein is unique to eukaryotes. CaM acts as a signal transducer for many different physiological processes when cellular Ca^{2+} levels increase within a cell (Yamniuk and Vogel, 2004). Due to the manifold and diverse roles of CaM in intracellular signaling, there is significant interest in a better understanding of the structural basis of its recognition of target proteins.

CaM is a 148-amino-acid (16.7 kDa) protein consisting of two globular domains (N- and C-terminal domains) joined by a central linker region giving the protein an overall "dumbbell" shape. There are four functional Ca^{2+}-binding EF hands located in CaM with an EF hand pair located in each of its globular domains. As mentioned in section 1.1.2, CaM's Ca^{2+}-binding EF hands are rich in aspartate and glutamate residues (Table 1.2) giving CaM a low pI of approximately 4. CaM's C-terminal EF hand pair has a 10 fold higher affinity for Ca^{2+} than the N-terminal EF hand pair (Martin *et al.*, 1985). This allows for CaM to have various degrees of saturation with Ca^{2+}, which correspond to different conformations (Jurado *et al.*, 1999). Figure 1.3 shows solved nuclear

magnetic resonance (NMR) spectroscopy and x-ray crystal structures of CaM in its Ca^{2+}-deplete (apo-CaM) and Ca^{2+}-replete (holo-CaM) conformations.

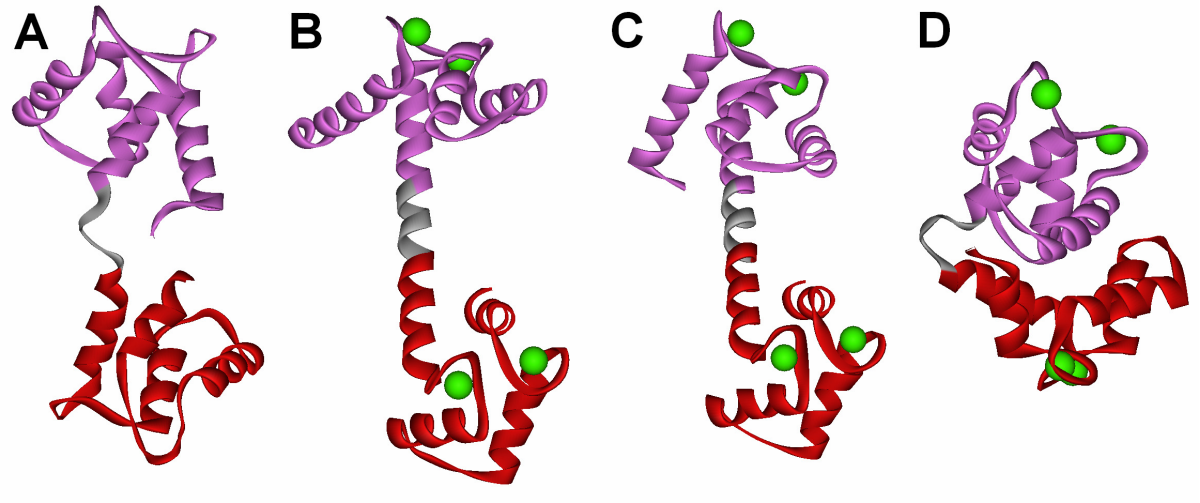

Figure 1.3 – Solved NMR and x-ray crystal structures of CaM in various Ca^{2+}-bound and conformational states.
(A) Apo-CaM (Kuboniwa *et al.*, 1995), **(B)** Holo-CaM (Chattopadhyaya *et al.*, 1992), **(C)** trapped intermediate of holo-CaM (Grabarek, 2005), and **(D)** holo-CaM in a compact conformation (Fallon and Quiocho, 2003). The structure for apo-CaM was solved by NMR, while the other three structures were solved using x-ray crystallography. The N- and C-terminal domains of CaM (N-domain = residues 1-75; C-domain = residues 82-148) are shown in pink and red, respectively. The central linker of CaM (residues 76-81) is shown in grey. Ca^{2+} ions are shown in green. Models were derived from PDB 1CFD (apo-CaM), 1CLL (holo-CaM), 1Y6W (trapped intermediate of holo-CaM) and 1PRW (compact holo-CaM), respectively, and were visualized using ViewerLite 5.0 (Accelrys).

Apo-CaM has a more compact, less flexible conformation than holo-CaM. Holo-CaM structures have demonstrated that this protein can be in an extended state, a compact form, or in a intermediate configuration in between these conformations (Figure 1.3). This is due to the highly flexible nature of CaM's central linker region (residues 76-81), which can be readily unraveled and bent dramatically depending upon the solvent or environment that CaM is exposed to (Slaughter et al., 2005a) as illustrated in the Figure 1.3B and D.

The binding of Ca^{2+} to CaM is cooperative within each lobe of CaM but not between the lobes, meaning that Ca^{2+}-binding to the N- and C-domains is exclusive from one another (Linse *et*

al., 1991; Pedigo and Shea, 1995). The order of Ca^{2+}-binding to CaM has previously been shown to be (1) EF hand III, (2) EF hand IV, (3) EF hand I, and finally (4) EF hand II, with the Ca^{2+} ions dissociating in the reverse order (Kilhoffer *et al.*, 1992). The rate-limiting step for Ca^{2+} dissociation from CaM was also observed to be different between the two domains (EF hands I/II and EF hands III/IV) (Kilhoffer *et al.*, 1992).

CaM contains nine methionines representing 6% of the entire amino acid content of the protein, which is significantly higher than the average methionine content of 1% in known proteomes (Ikura and Ames, 2006). The binding of Ca^{2+} to CaM causes the solvent exposure of large hydrophobic patches in the N- and C-terminal domains which are extremely rich in methionine residues, with four Met residues exposed in each pocket (Bhattacharya *et al.*, 2004; Ikura and Ames, 2006) (Figure 1.4).

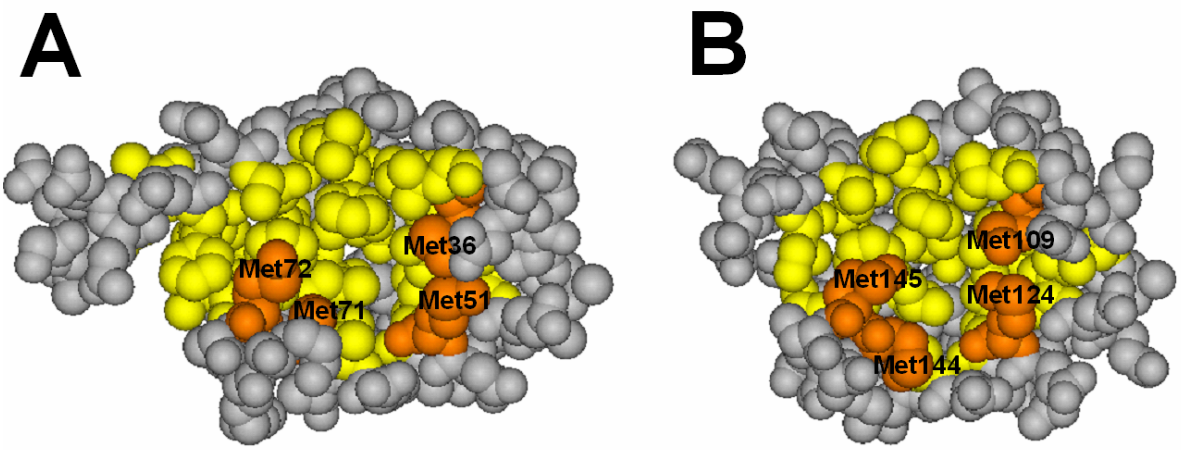

Figure 1.4 – Structural representation of the exposed hydrophobic patches in the (A) N- and (B) C-terminal domains of holo-CaM.
Methionine and surrounding amino acid residues found in the hydrophobic patches of holo-CaM are shown in orange and yellow, respectively. Models were derived from PDB 1CLL (Chattopadhyaya *et al.*, 1992) and were visualized using ViewerLite 5.0 (Accelrys). This figure is based upon a previous CaM review (Ikura and Ames, 2006).

The exposure of these hydrophobic patches helps to explain CaM's ability to bind to its various target proteins. Although each domain has hydrophobic patches exposed to solvent, the physicochemical properties of the N- and C-terminal domains of CaM are markedly different. Comparing the surface binding areas of the N- and C-terminal domains of CaM, the N-terminal domain CaM has 49% hydrophobic and 37% acidic character versus the C-terminal domain of CaM that is 53% hydrophobic and 41% acidic in area (Bhattacharya *et al.*, 2004). These marked differences in hydrophobicity and acidity of the exposed patches can partially explain the specificity for each domain when binding to CaM target proteins. Furthermore, the amino acid side chains (particularly the methionine residues) that interact with target proteins demonstrate innate flexibility which allows these domains to accommodate a variety of amino acid side chains (ie. Trp, Phe, Ile, Leu, Val, and Lys) in the target peptide (Ikura and Ames, 2006). Clearly, the flexibility of the central linker facilitates the orientation of the N- and C-terminal domains of CaM, in combination with the structural plasticity of the methionine amino acids in the CaM hydrophobic patches, allow for the promiscuous nature of CaM binding to its numerous target proteins within the cell.

1.1.4 CaM Binding to Target Peptides and Proteins

Over the past decade, the number of reported target proteins CaM is able to recognize and bind to has risen from approximately 30 to over 300 thanks to the use of protein databases recognizing various CaM binding motifs (Crivici and Ikura, 1995; Ikura and Ames, 2006). CaM's modular characteristic appears to be unique in that the incorporation of a flexible linker between the EF hand pairs causes a large increase in the number of associations and/or interactions CaM can achieve (Ikura and Ames, 2006).

Electrostatics has also been suggested to be in involved in the initial attraction of CaM to its target proteins (Vetter and Leclerc, 2003). The numerous negatively charged residues found in CaM (Glu and Asp), particularly in the central linker region (residues 73-83) and the C-terminal domain

of CaM may form salt bridges with the positively charged residues of the target peptide. These positively charged residues are generally concentrated at either the N- or C-terminus of the CaM-binding domain of a target protein and are implicated in the determination of CaM's orientation when bound to its target protein (Vetter and Leclerc, 2003) (discussed further in section 1.1.5).

Holo-CaM is not the only form of CaM capable of binding to target proteins – apo-CaM is also able to associate to some CaM-target proteins. This contrast between the Ca^{2+}-replete and Ca^{2+}-deplete association of CaM to target proteins adds another level of complexity in studying CaM. The following tables summarize some of the CaM-dependent proteins found in the cell that are bound by holo-CaM (Table 1.3) and apo-CaM (Table 1.4).

Table 1.3 – Summary of well-characterized holo-CaM Ca^{2+}-dependent proteins.

Group	Enzyme or Protein	Putative Function of Enzyme/Protein
Protein kinases	Phosphorylase *b* kinase	Regulate glycogen metabolism
	Myosin light chain kinase	Regulate smooth muscle contraction
	CaM kinase I	Multifunctional
	CaM kinase II	Multifunctional, regulated over 30 enzymes
Phosphoprotein phosphatase	Calcineurin	Metabolic regulation/cell cycle
Second messenger metabolism	Type I adenylate cyclase	Produce cAMP
	cAMP phosphodiesterase	Degrade cAMP
	Constituitive Nitric oxide synthase	Produce nitric oxide
	Ca^{2+}-transport ATPase	Decrease cytosolic Ca^{2+}
	G protein-coupled receptors	Various signaling
Cytoskeletal or muscle	Caldesmon	Inhibit F-actin binding
	MARCKS protein	Inhibit F-actin binding
Metabolism	NAD kinase	Convert NAD to NADP
Other	Microtubules	Inhibit tubulin polymerization

Table is modified from a previously published review (Jurado *et al.*, 1999).

Table 1.4 – Summary of some Apo-CaM binding proteins.

Group	Enzyme or Protein	Putative Function of Enzyme/Protein or Proposed Role*
Enzymes	Phosphorylase *b* kinase	Regulate glycogen metabolism
	Adenylyl cyclase	cAMP production
	Inducible nitric oxide synthase	Produce nitric oxide
	Glutamate decarboxylase	Decarboxylation of glutamate to CO_2 and γ-aminobutyrate
	cGMP-dependent protein kinase	cGMP- and cAMP-dependent phosphorylation
Receptors and ion channels	Inositol 1,4,5-trisphosphate receptor	Inositol 1,4,5-trisphosphate binding
	Sarcoplasmic reticulum Ca^{2+} release channel	Release of Ca^{2+} from the sarcoplasmic reticulum
Cytoskeletal or muscle	Neuromodulin	Reversible CaM storage, regulation of GTP binding to G_{α}, and regulation of phosphatidylinositol metabolism
	Syntrophin	Clustering of Na^{+} channels *
Actin-binding proteins	Myr4	ATP-dependent binding to F-actin
	P190	Actin-activated ATPase

Table is modified from a previously published review (Jurado *et al.*, 1999).

CaM interacts with a variety of peptide sequences within its target enzymes. Typically these CaM recognition sequences are approximately 20 amino acids in length and form a basic, amphipathic α-helical structure with a periodicity of basic residues on one face of the helix and the hydrophobic residues on the opposite side of the helix (Meador *et al.*, 1992; Zhang *et al.*, 1995; Venema *et al.*, 1996; Aoyagi *et al.*, 2003). Although the overall sequences of the peptides that CaM recognizes and binds have very little sequence identity, the positions of several bulky hydrophobic residues are highly conserved. There are three typical recognition motifs used in the classification of CaM-binding domains known as 1-5-8-14 (which include the 1-8-14 motif), 1-5-10, and IQ motifs. The Ca^{2+}-dependent binding of CaM to the 1-5-8-14 motif conforms to the following sequence (FILVW)XXX(FAILVW)XX(FAILVW)XXXXX(FILVW) where any of the underlined hydrophobic residues can occupy sites 1, 5, 8, and 14 while X can represent any amino acid. Examples of CaM-target proteins that have a 1-5-8-14 and 1-8-14 motifs include myosin light chain kinase, calcineurin, and the nitric oxide synthases (Rhoads and Friedberg, 1997). Another Ca^{2+}-dependent CaM-binding motif is the 1-5-10 motif which has a consensus sequence of (FILVW)XXX(FILV)XXXX(FILVW) where any of the underlined hydrophobic residues can occupy sites 1, 5, and 10. Prime examples of CaM-target proteins with 1-5-10 CaM-binding motifs include CaM-dependent kinase I, CaM-dependent kinase II and MARCKS protein (Rhoads and Friedberg, 1997). CaM binds to the IQ motif in a Ca^{2+}-independent manner and the sequence IQXXXRGXXXR (where X denotes any amino acid) defines this motif; however, this overall motif is only loosely adhered to in many cases since the Ile is frequently substituted with a Leu (Jurado *et al.*, 1999). Examples of CaM-target proteins that have IQ motifs are neuromodulin, protein kinase C, p68 RNA helicase and voltage-gated Ca^{2+}-channels (Rhoads and Friedberg, 1997).

1.1.5 Solved Structures of CaM bound to Peptides and Enzymes

The structural basis for CaM's ability to bind to target proteins is of great interest to the research community since CaM plays an important role in inter- and intracellular physiological processes. In 1992, the original structure of CaM bound to a CaM-target peptide from myosin light chain kinase (MLCK) was solved by NMR spectroscopy (Ikura *et al.*, 1992) showing a Ca^{2+}-replete CaM tightly wrapped around the peptide. Soon after this initial structure, an x-ray structure of holo-CaM bound to a peptide from CaM-dependent protein kinase II (CaMKII) was released which also demonstrated CaM wrapping tightly around a target peptide (Meador *et al.*, 1993). These two CaM-target peptide structures suggested a general mechanism for CaM binding to CaM-dependent proteins and enzymes in the cell. When compared to the structure of holo-CaM (Figure 1.3B), it became apparent that CaM's central linker could readily unwind and allow for the optimal orientation of the N- and C-terminal domains of CaM to associate to the basic, amphipathic CaM recognition α-helix.

Since the release of these structures, numerous other CaM-target peptide structures have been solved by using x-ray crystallography and NMR spectroscopy, with most of these structures being released in recent years. These structures predominantly show compact conformations of CaM having either an anti-parallel or parallel orientation when bound to the target peptide. When CaM binds in an anti-parallel fashion, the N-terminal domain of CaM binds closer to the C-terminus of the target peptide, while the C-terminal domain of CaM binds closer to the N-terminus of the peptide. In contrast, when CaM binds to its target protein in a parallel orientation, the N-terminal domain of CaM binds closer to the N-terminus of the target peptide, while the C-terminal domain of CaM closer to the C-terminus of the peptide. Figure 1.5 shows all the solved structures of anti-parallel Ca^{2+}/CaM-target peptide complexes known to date. These CaM-target peptide complexes originate from a wide variety of enzymes including various protein kinases, nitric oxide synthases, ion channels, and receptor proteins. Likewise, Figure 1.6 contains all of the solved structures of

holo-CaM bound to its target peptides in a parallel orientation. These parallel CaM-peptide structures include a voltage-gated Ca^{2+}-channel, myristoylated CAP-23/NAP-22 peptide and CaM-dependent kinase kinase (CaMKK).

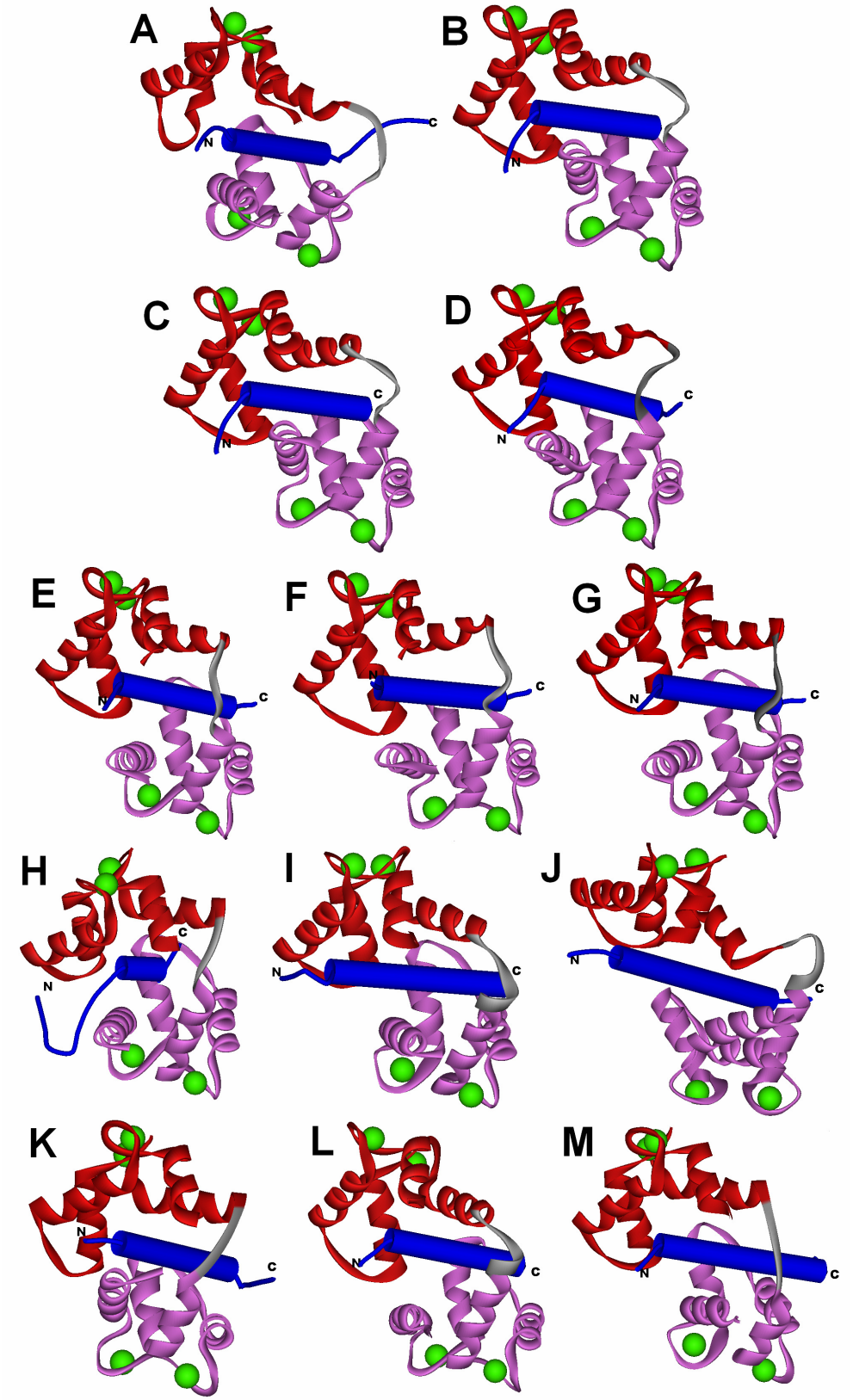
A
B
C
D
E
F
G
H
I
J
K
L
M
N
C

Figure 1.5 – Solved structures of CaM bound to various target peptides in an anti-parallel orientation.

Structures shown represent CaM when bound to peptides derived from **(A)** myosin light chain kinase (MLCK; (Ikura *et al.*, 1992), **(B)** CaM-dependent protein kinase II (CaMKII) (Meador *et al.*, 1993), **(C)** endothelial nitric oxide synthase (eNOS) (Aoyagi *et al.*, 2003), **(D)** neuronal nitric oxide synthase (nNOS) (Ng *et al.* – unpublished, co-ordinates released 2007-12-25), **(E)** death-associated protein kinase I (DAP kinase I) (Kursula *et al.* - unpublished, co-ordinates released 2006-07-04), **(F)** human death-associated protein kinase II (DAP kinase II) (Kursula *et al.* - unpublished, co-ordinates released 2006-03-21), **(G)** death-associated related protein kinase I (DRP-1 kinase) (Kursala *et al.* – unpublished, co-ordinates released 2006-11-14), **(H)** myristoylated alanine-rich C kinase substrate (MARCKS) (Yamauchi *et al.*, 2003), **(I)** CaM-dependent protein kinase I (CaMKI) (Clapperton *et al.*, 2002), **(J)** ryanodine receptor (RyR) (Maximciuc *et al.*, 2006), **(K)** *N*-methyl-D-aspartate receptor (NMDA receptor) (Ataman *et al.*, 2007), **(L)** olfactory cyclic-nucleotide gated channel (olfactory CNG channel) (Contessa *et al.*, 2005), and **(M)** alpha II-spectrin (Simonovic *et al.*, 2006). The colour scheme used is as previous described in Figure 1.3, with the exception that the CaM-target peptides are shown in blue. The N- and C-termini of the target peptides are labeled for clarity purposes. Models were derived from PDB 2BBN (MLCK), 1CDM (CaMKII), 1N1W (eNOS), 2O60 (nNOS), 1YR5 (DAP kinase I), 1WRZ (DAP kinase II), 1ZUZ (DRP-1 kinase), 1IWQ (MARCKS), 1MXE (CaMKI), 1BCX (RyR), 2HQW (NMDA receptor), 1SY9 (olfactory CNG channel), and 2FOT (alpha II-spectrin), respectively. Models were visualized using ViewerLite 5.0 (Accelrys).

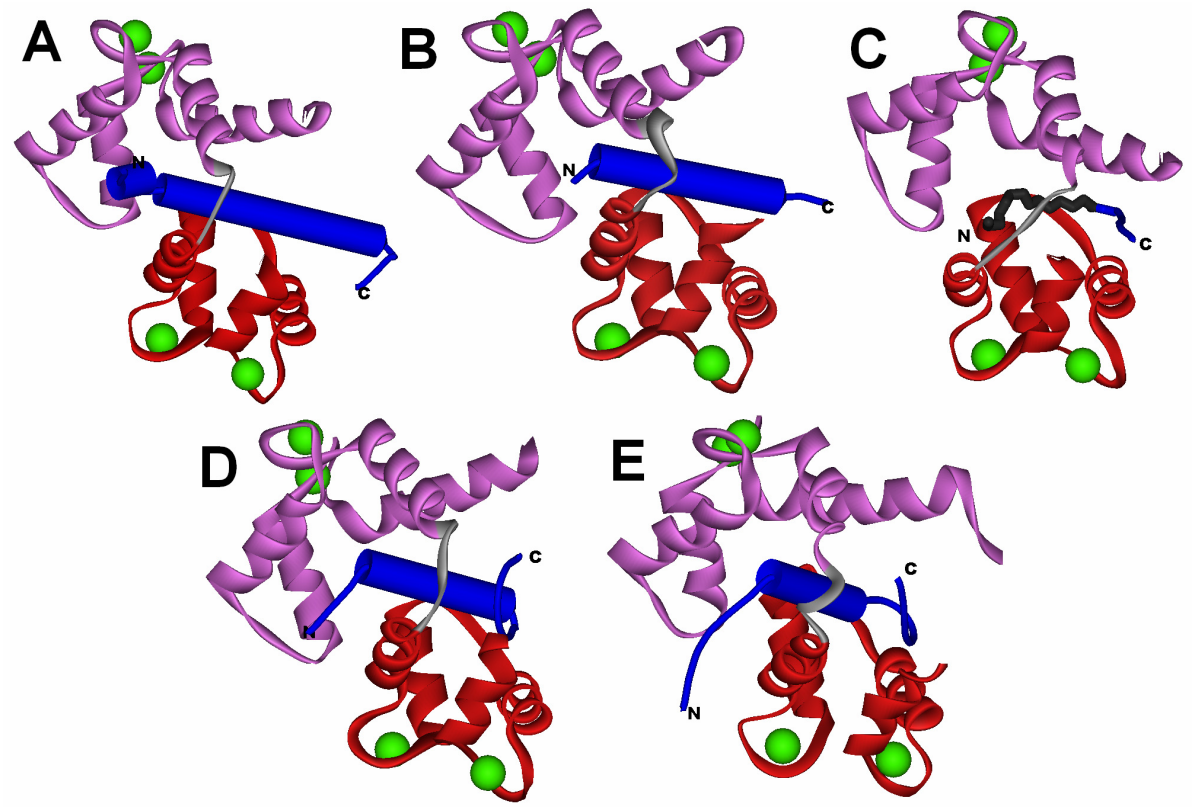

Figure 1.6 – Solved structures of CaM bound to various target peptides in a parallel orientation.
Structures shown represent CaM when bound to peptides derived from **(A & B)** IQ domain of the Ca^{2+} 1.2 voltage-gated Ca^{2+} channel (CaV1.2 Ca^{2+} channel; A – 29 residue peptide solved by x-ray crystallography; B – 22 residue peptide solved by x-ray crystallography) (Fallon and Quiocho, 2003; Van Petegem *et al.*, 2005), **(C)** myristoylated CAP-23/NAP-22 peptide (Matsubara *et al.*, 2004), **(D & E)** CaM-dependent kinase kinase (CaMKK; D – 26 residue peptide solved by x-ray crystallography (Kurokawa *et al.*, 2001); E – 27 residue peptide solved by NMR spectroscopy, (Osawa *et al.*, 1999)). The colour scheme and labels used are as previous described in Figure 1.5 with the exception that the myristoyl group in (C) is shown in dark grey. Models were derived from PDB 2BE6 (A) and 2F3Y (B) (CaV1.2 Ca^{2+} channel), 1L7Z (myristoylated CAP-23/NAP-22), and 1IQ5 (D) and 1CKK (E) (CaMKK), respectively. Models were visualized using ViewerLite 5.0 (Accelrys).

In 1999, the NMR structure of CaM bound to a peptide from the plasma membrane Ca^{2+}-pump was solved, showing that only the C-terminal domain of CaM associated with the target peptide, whereas no association whatsoever occurred with the N-terminal domain of CaM (Elshorst *et al.*, 1999) (Figure 1.7F). This unique structure changed the classic view that CaM always wrapped around its target protein and showed that CaM can take on a variety of other conformations. Similarly, the x-ray crystal structure of CaM in complex with small conductance Ca^{2+}-activated K^+ channel also showed a single domain of CaM associated to the target peptide (Schumacher *et al.*, 2001). In this case, only a Ca^{2+}-replete N-terminal domain of CaM is in complex with the peptide, while the Ca^{2+}-deplete C-terminal domain of CaM does not interact with the peptide at all (Figure 1.7A). Figure 1.7 shows other examples of unique CaM conformations with various target peptides and proteins.

A CaM-target protein structure of particular interest is the unique x-ray crystal structure of CaM in complex with the edema factor of adenylyl cyclase from *Bacillus anthracis* (Figure 1.7E). This structure is unique since it is the first intact protein fragment in complex with CaM ever to be solved (Drum *et al.*, 2002). Another point to note regarding this structure is that CaM does not wrap around its target protein as it typically does (Figure 1.5 and Figure 1.6); instead, the edema factor wraps itself around CaM causing CaM to adopt an extended conformation as well as a decreased affinity for Ca^{2+} in its N-terminal domain, which has since been further corroborated by other x-ray crystal structures (Shen *et al.*, 2005). Another structure of interest is CaM in complex with glutamate decarboxylase solved by NMR (Yap *et al.*, 2003) where CaM wraps around two C-terminal peptides of the enzyme that form a cross-like conformation (Figure 1.7D).

Clearly, the solved structures of CaM-target peptide/protein complexes (Figure 1.3, 1.5, 1.6, and 1.7) demonstrate that CaM's flexibility enables it to take on a variety of conformations when bound to target peptides and proteins ranging from tightly wrapped to extended structures.

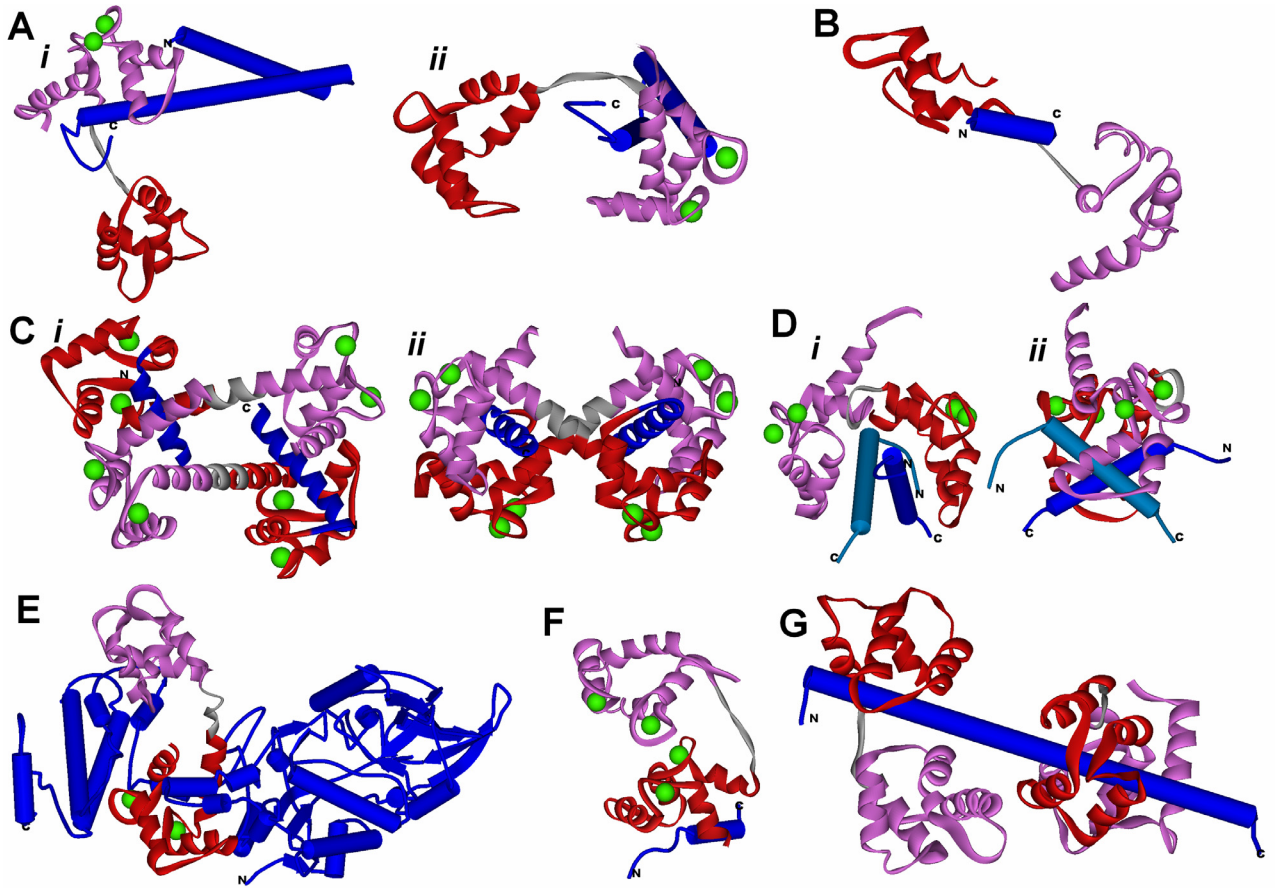

Figure 1.7 – Solved structures of CaM bound to various target peptides and proteins in unique conformations.

Structures shown represent **(A)** holo-CaM bound to the gating domain of the small conductance Ca^{2+}-activated K^+ channel from different perspectives – ***(i)*** sideways and ***(ii)*** down the barrel of the peptide (holo-CaM/SK K^+ channel) (Schumacher *et al.*, 2001), **(B)** apo-CaM bound to the gating domain to the small conductance Ca^{2+}-activated K^+ channel (apo-CaM/SK K^+ channel) (Schumacher *et al.*, 2004), **(C)** fusion protein of CaM with a calcineurin peptide from different perspectives – ***(i)*** sideways and ***(ii)*** on edge (CaM-CaN peptide) (Ye *et al.*, 2006), **(D)** holo-CaM in complex with petunia glutamate decarboxylase from different perspectives – ***(i)*** down the barrel of the peptide and ***(ii)*** sideways (Yap *et al.*, 2003), **(E)** CaM in complex with the edema factor of adenylyl cyclase of *B. anthracis* (Drum *et al.*, 2002), **(F)** holo-CaM in complex with the plasma membrane Ca^{2+}-pump (Elshorst *et al.*, 1999), and **(G)** two apo-CaMs bound to an unconventional myosin V IQ domain (Houdusse *et al.*, 2006). Please note that all of these structures were solved with CaM-target peptides with the exception of (E), which was solved in the presence of the holo-enzyme. The colour scheme and labels used are as previous described in Figure 1.5. Models were derived from PDB 1G4Y (holo-CaM/SK K^+ channel), 1QX7 (apo-CaM/SK K^+ channel), 2F2O (CaM-CaN peptide), 1NWD (Glutamate decarboxylase), 1K93 (edema factor from *B. anthacis*), 1CFF (plasma membrane Ca^{2+} pump), and 2IX7 (apo-CaM/myosin V). Models were visualized using ViewerLite 5.0 (Accelrys).

1.1.6 Regulation of CaM binding to target proteins

An additional feature of CaM that can increase or decrease its affinity of target proteins is posttranslational modifications. Previous studies have demonstrated that CaM can undergo acetylation, trimethylation, carboxymethylation, proteolytic cleavage, methionine oxidation and phosphorylation *in vivo* (Watterson *et al.*, 1980; Murtaugh *et al.*, 1983; Murtaugh *et al.*, 1986; Squier and Bigelow, 2000; Benaim and Villalobo, 2002). These chemical modifications of various residues in CaM have been suggested as a possible mechanism to modulate its activity as a Ca^{2+}-sensor protein in the cell; however, the physiological role for these posttranslational modifications of CaM and their effect on the binding and activation of CaM target enzymes has yet to be determined (Benaim and Villalobo, 2002; Ikura and Ames, 2006).

A recent review discussed the possibility of regulating CaM binding to target proteins at the transcriptional level by studying the promoter and comparing the stabilities and abundance of mRNA transcripts from different CaM genes in rats and humans (ie. *CAM I*, *CAM II*, and *CAM III*) (Kortvely and Gulya, 2004); however, this method of studying CaM's regulation at the transcriptional level is relatively new and requires further studies to determine if this will prove to be an effective method for controlling CaM expression within the cell.

The use of small hydrophobic drug molecules is another method that has been studied to manipulate CaM's association to its target proteins. These drug molecules have been shown to directly bind to CaM and interfere with its ability to associate to target proteins that can lead to altered intracellular processes (Roufogalis *et al.*, 1983). The classic CaM antagonist that has been studied is trifluoperazine (Figure 1.8A), an anti-psychotic drug that has been shown to markedly affect Ca^{2+}/CaM-dependent interactions by binding to the exposed hydrophobic patches in holo-CaM's N- and C-terminal domains. Unfortunately, there is little specificity for this drug in binding to CaM since it has also been shown to interact and inhibit other Ca^{2+}-binding proteins and lipid-

dependent enzymes within the cell (Roufogalis *et al.*, 1983). It was determined experimentally that 4 equivalents of trifluoperazine were capable of binding to CaM by HPLC (Massom *et al.*, 1990) and this finding was later confirmed by x-ray crystallography (Vandonselaar *et al.*, 1994) (Figure 1.9B). Another structure was also solved with trifluoperazine in a 1:1 complex with CaM, demonstrating the variability in the number of molecules that can associate to CaM (Cook *et al.*, 1994) (Figure 1.9A). In both structures of CaM-trifluoperazine, the binding of the drug stimulates CaM to collapse similar to the wrapped conformation of CaM in complex with various target peptides, as previously discussed (section 1.1.5).

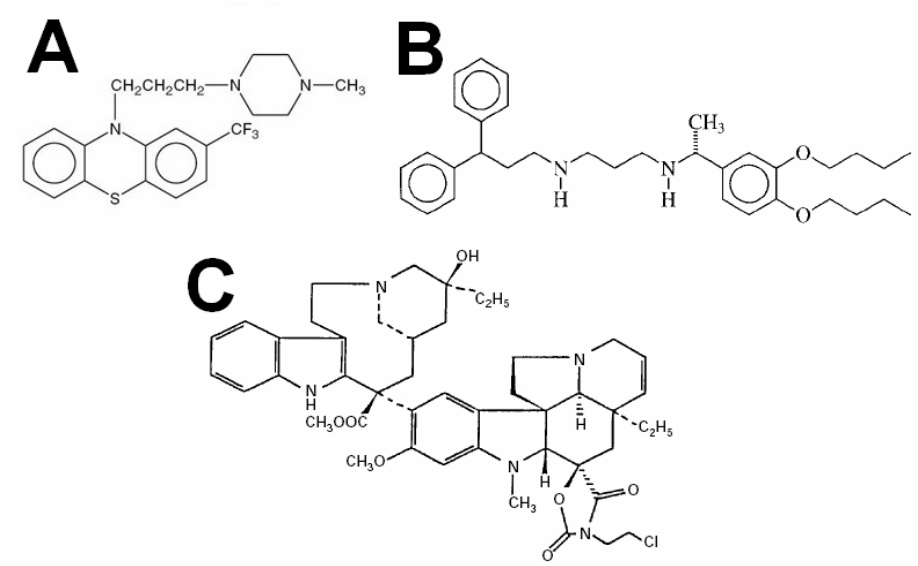

Figure 1.8 – Chemical structures of CaM antagonist molecules.
(A) Trifluoperazine (Massom *et al.*, 1990), **(B)** *N*-(3,3,-diphenylpropyl)-*N*'-[1-*R*-(2,3,4-bis-butoxyphenyl)-ethyl]-propylenediamine, (an arylalkylamine-type CaM antagonist, AAA) (Harmat *et al.*, 2000), and **(C)** 3"-(b-chloroethyl)-2",4"-dioxo-3,5"-spiro-oxazolidino-4-deacetoxy-vinblastine (KAR-2) (Orosz *et al.*, 1997).

Recently, other small molecules that bind to CaM have also been studied. The anti-pyschotic drug, AAA (Figure 1.8B), was shown to have a similar affect on Ca^{2+}/CaM-dependent interactions as trifluorperazine. The anti-tumor drug KAR-2 (Figure 1.8C) was shown to bind to CaM, however, it had very little effect on CaM's ability to bind target proteins (Orosz *et al.*, 1997).

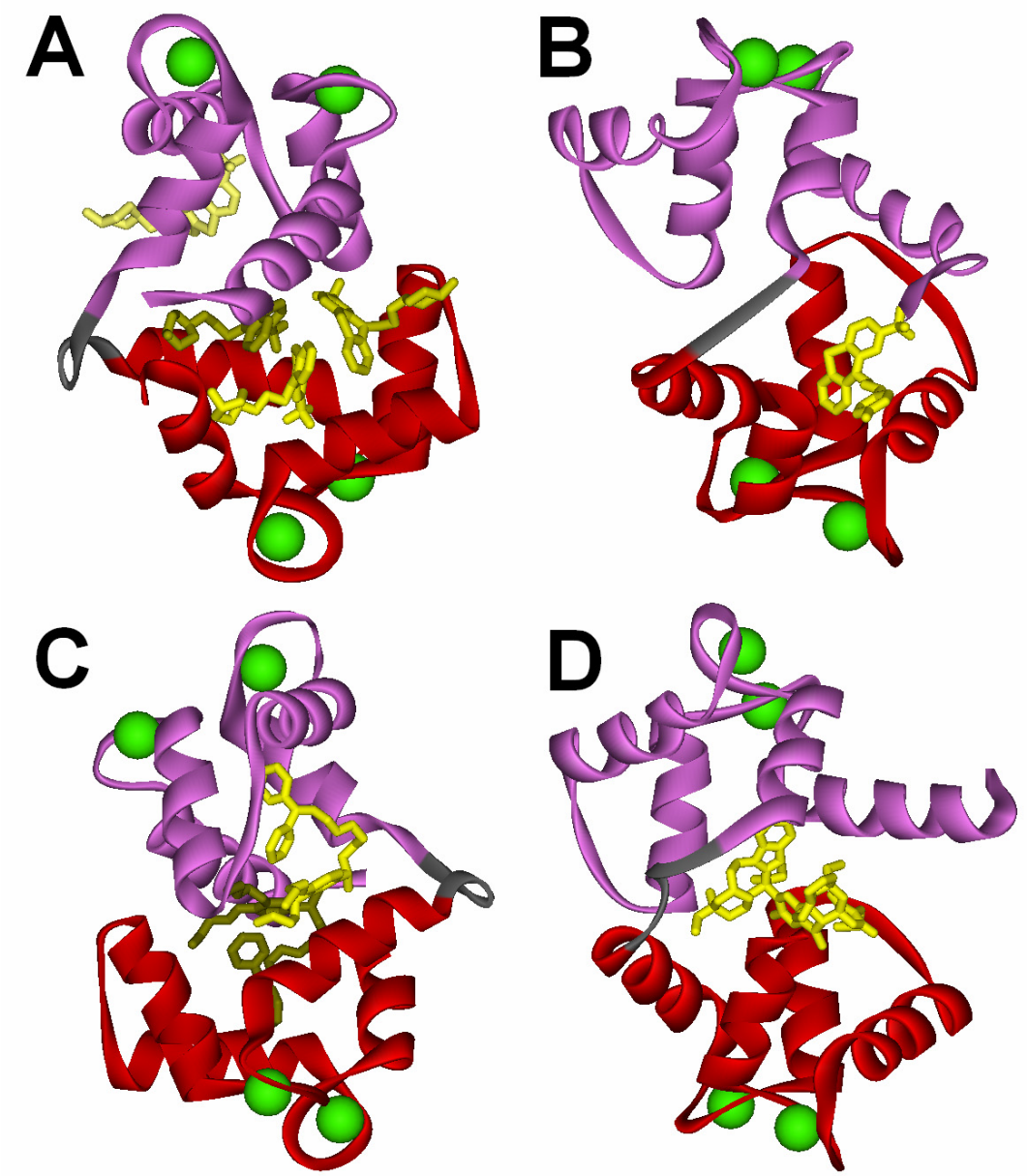

Figure 1.9 – CaM in complex with various small molecules.
Structures shown represent holo-CaM in complex with **(A)** 10-[3-(4-methylpiperazin-1-yl)propyl]-2-(trifluoromethyl)phenothiazine (trifluoperazine, TFP) in a 1:4 complex (Vandonselaar *et al.*, 1994), **(B)** TFP in a 1:1 complex (Cook *et al.*, 1994), **(C)** *N*-(3,3,-diphenylpropyl)-*N'*-[1-*R*-(2,3,4-bis-butoxyphenyl)-ethyl]-propylenediamine (AAA) in a 1:2 complex (Harmat *et al.*, 2000), and **(D)** 3"-(b-chloroethyl)-2",4"-dioxo-3,5"-spiro-oxazolidino-4-deacetoxy-vinblastine (KAR-2) in a 1:1 complex (Horvath *et al.*, 2005). The colour scheme and labels used are as previous described in Figure 1.5 with the exception that the small molecules in complex with CaM are shown in various shades of yellow. Models were derived from PDB 1XA5 (holo-CaM/KAR-2 1:1 complex), 1QIV (holo-CaM/DPD 1:2 complex), 1CTR (holo-CaM/TFP 1:1 complex), and 1LIN (holo-CaM/TFP 1:4 complex). Models were visualized using ViewerLite 5.0 (Accelrys).

Both of these small hydrophobic drug molecules demonstrate a similar mechanism as trifluoperazine on CaM by interacting with the hydrophobic patches in lobes of CaM and causing the protein to collapse around the drug molecule (Harmat *et al.*, 2000; Horvath *et al.*, 2005). Since CaM plays such an important role in many cellular processes, it is actually not an ideal drug target. This method of using drugs to regulate CaM binding to target proteins requires further studies to ensure that these drugs do not affect other essential physiological processes within the cell.

1.2 Nitric Oxide Synthase (NOS)

As mentioned previously, CaM can bind and/or regulate more than 300 intracellular enzymes and proteins. Among these many and varied target enzymes are the mammalian nitric oxide synthase (NOS) isozymes. This section covers the physiological relevance of nitric oxide, as well as the characteristics, mechanism, and regulation of the NOS enzymes. Particular focus is given to the differences in the binding and activation of the NOS enzymes by CaM.

1.2.1 Nitric Oxide

Over the past 15 years, nitric oxide (•NO) has become one of the most studied molecules in biochemistry. The 1998 Nobel Prize in Physiology and Medicine was awarded to Furchgott, Ignarro, and Murad for their studies involving •NO as a cardiovascular signal molecule. A resent search on PubMed (www.ncbi.nlm.nih.gov) shows that over the past 15 years, approximately 88,000 papers have been published on work related to •NO in a wide variety of disciplines.

•NO is a highly reactive diatomic free radical that is biologically active due to its ability to freely diffuse across cellular membranes and interact with intracellular proteins (Snyder and Bredt, 1992). •NO has been found to affect many different processes within mammals including neurotransmission, memory, blood-pressure control, blood clotting, and immune defense (Alderton *et al.*, 2001; Kroncke *et al.*, 2001), with the list continuing to grow. The classic example of •NO-mediated signaling is the activation of soluble guanylyl cyclase in muscle cells surrounding blood vessels. The activation of this enzyme causes an increase of cGMP, an intracellular secondary messenger that activates various cGMP-dependent kinases, including protein kinase G (PKG). PKG is able to phosphorylate the IP_3 receptor (as described in section 1.1.1) which leads to a decrease in intracellular Ca^{2+} levels (Schmidt *et al.*, 1993). The lower Ca^{2+} concentration causes the relaxation

of the smooth muscle cells surrounding the blood vessel and results in vasodilation (Schmidt *et al.*, 1993).

Although •NO is important in many beneficial physiological processes, it can also potentially act as a toxin by reacting with other reactive oxygen species (ROS), such as superoxide ($•O_2^-$) to form peroxynitritre ($OONO^-$). Uncontrolled levels of •NO and $OONO^-$ can alter cellular signaling and cause oxidative damage to lipids, proteins and DNA (Pacher *et al.*, 2007). Table 1.5 gives a summary of some of the beneficial and damaging affects •NO can have on various types of tissue.

Table 1.5 – •NO-mediated effects in various tissues.

Tissue	Messenger/Modulator	Toxin
Blood vessels	Endothelium-derived relaxing factor Anti-thrombotic Inhibition of smooth muscle migration and proliferation	Septic shock Atherosclerosis
Heart	Ischemia Coronary perfusion	Septic shock
Lung	Mucus secretion Immune defense Bronchiociliar motility	Immune complex-induced alveolitis Acute respiratory distress syndrome? Asthma?
Central nervous system	Memory formation Cerebral blood flow and ischemia Synaptogenesis Synaptic plasticity Olfaction	Neurotoxic Migrane
Pancreas	Endocrine/exocrine secretion	β-cell destruction
Gastrointestinal	Blood flow Peristalsis Mucosal protection Exocrine secretion	Mucosal damage Mutagenesis
Immune system	Anti-microbial Anti-tumour	Graft versus host disease Inflammation Septic shock Tissue damage

Table is modified from a previous •NO review (Schmidt and Walter, 1994).

The nitric oxide synthase (NOS, EC 1.14.13.39) enzymes catalyze the production of •NO with L-citrulline as a byproduct through two successive mono-oxygenation reactions requiring reduced nicotinamide adenine dinucleotide phosphate (NADPH) and molecular oxygen (Alderton *et al.*, 2001) (Figure 1.10).

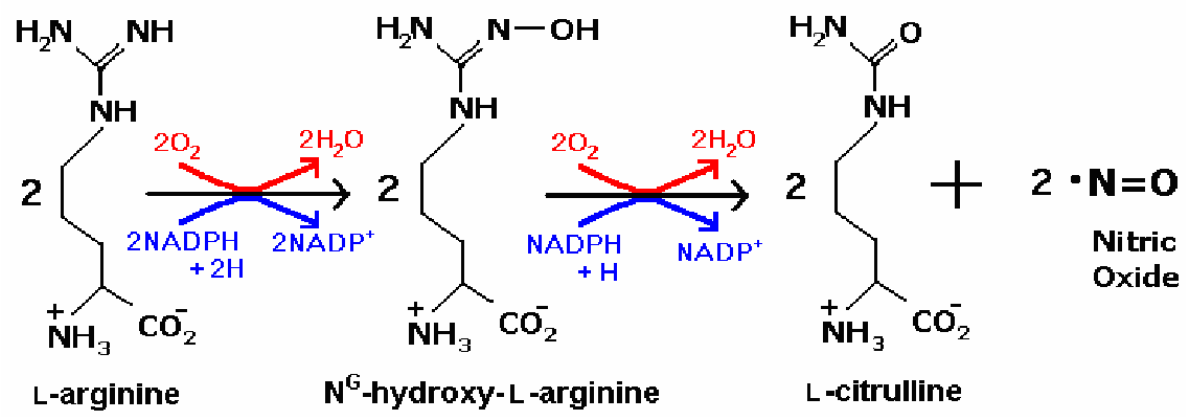

Figure 1.10 – NOS-catalysed conversion of L-arginine through the intermediate N^G-hydroxy-L-arginine to L-citrulline and •NO.
Electrons originating from NADPH and molecular O_2 are required for each of the mono-oxygenation steps. This figure is modified from a previous review (Feldman *et al.*, 1993).

1.2.2 Structural characteristics of the Mammalian NOS isozymes

There are three mammalian NOS isoforms - neuronal NOS (nNOS, NOS I), endothelial NOS (eNOS, NOS III), and inducible NOS (iNOS, NOS II). These three distinct NOS isozymes have been shown to have 51-57% sequence identity in humans (Alderton *et al.*, 2001) and their respective gene locations have been identified. The human nNOS gene is found on chromosome 12q24.2 and extends over 100 kb (Nathan and Xie, 1994). The human eNOS gene is located on chromosome 7q35-7q36 and contains 26 exons over a span of 21 kb (Marsden *et al.*, 1993). The 37 kb gene coding for human iNOS is located on chromosome 17cen-q11.2 and contains 26 exons (Marsden *et al.*, 1994).

The NOS enzymes are homo-dimeric proteins and bind to CaM in a 1:1 ratio when in their active form (Alderton *et al*., 2001). Each NOS monomer contains an N-terminal oxygenase domain and a multidomain C-terminal reductase domain. The oxygenase domain contains binding sites for iron protoporphyrin IX (heme), (6*R*)-5,6,7,8-tetrahydrobiopterin (H_4B), and the substrates L-arginine and molecular oxygen (Roman *et al.*, 2002). The heme iron is penta-coordinated with a cysteine residue that provides the single thiolate axial ligand. This cysteine residue is conserved in all of the NOS enzymes and has been determined to be at positions C186 of bovine eNOS (Chen *et al.*, 1994), C415 of rat nNOS (Richards *et al.*, 1996), and C200 of human iNOS (Cubberley *et al.*, 1997). The reductase domain binds flavin mononucletide (FMN), flavin adenine dinucleotide (FAD), and NADPH (Roman *et al.*, 2002). A CaM-binding domain separates the oxygenase and reductase domains (Figure 1.11). The chemical structures of the four cofactors found in the reductase and oxygenase domains of the mammalian NOS enzymes are shown in Figure 1.12.

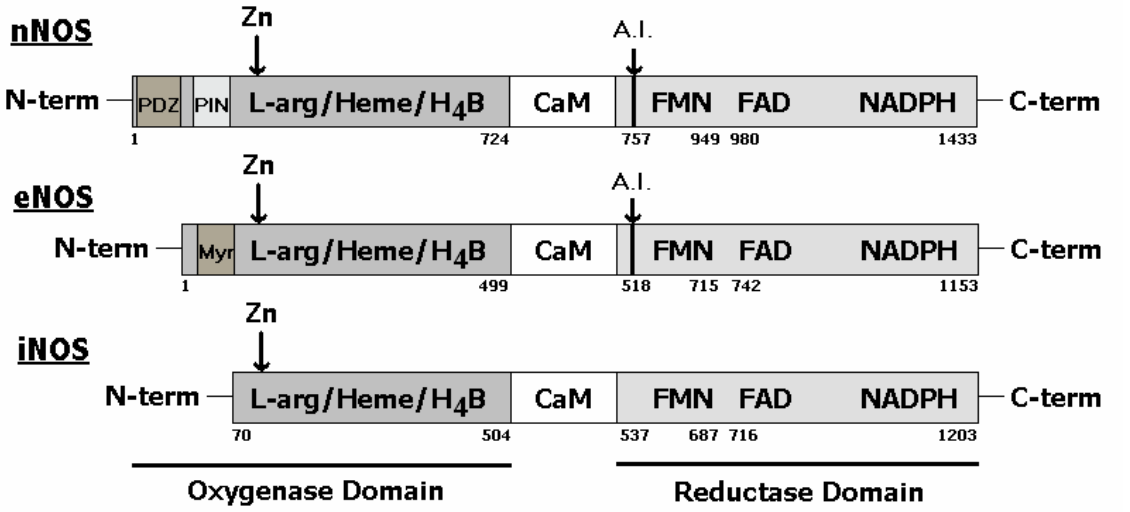

Figure 1.11 – Alignment of NOS enzymes.
The oxygenase and reductase domains are shown in dark grey and light grey, respectively. A CaM-binding domain separates the oxygenase and reductase domains. Numbers represent the amino acid residue at the start and end of the oxygenase, FMN, and FAD/NADPH domains. The myristoylation (Myr) modification site as well as the PDZ, protein inhibitor of NOS (PIN), (6*R*)-5,6,7,8-tetrahydrobiopterin (H_4B), and zinc binding sites are shown. The A.I. represents the auto-inhibitory domains that are exclusive to the nNOS and eNOS enzymes. This figure is modified from a previous review (Alderton *et al.*, 2001).

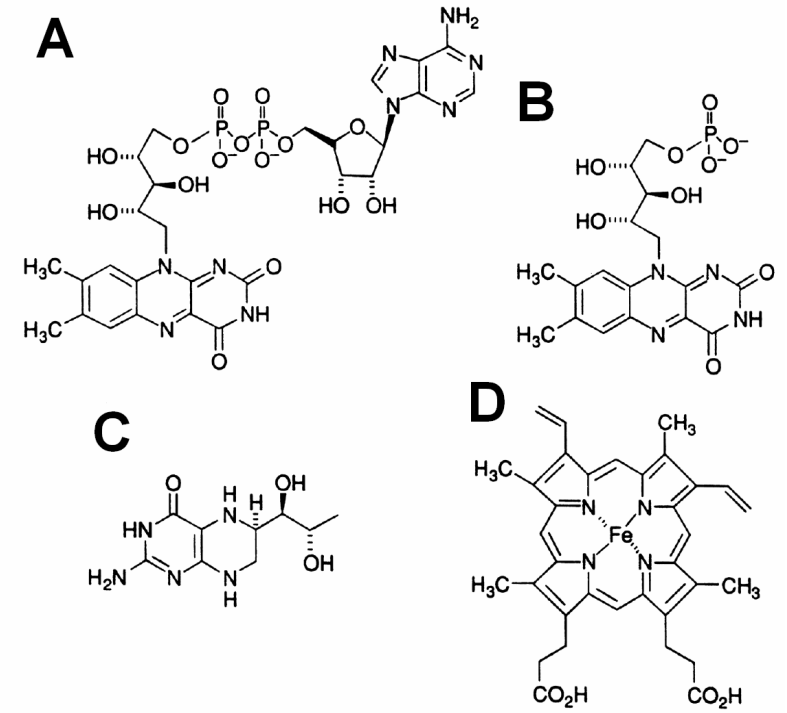

Figure 1.12 – Chemical structures of cofactors bound to mammalian NOS enzymes.
The redox cofactors found in the reductase domain of NOS – **(A)** Flavin adenine dinucleotide (FAD), and **(B)** Flavin mononucleotide (FMN). NOS oxygenase cofactors – **(C)** (6*R*)-5,6,7,8-tetrahydrobiopterin (H_4B), and **(D)** Iron protoporphyrin IX (heme).

The nNOS and eNOS enzymes are constitutively expressed, which is why they are collectively refered to as the constitutive NOS (cNOS) isoforms. Both nNOS and eNOS were initially found to be produced in neuronal and endothelial tissue respectively, but have since been found to be expressed in other tissues throughout the body as well (Ghosh and Salerno, 2003). The molecular weight of rat nNOS and bovine eNOS monomers are 160 kDa and 135 kDa, respectively. The molecular weight difference in the cNOS enzymes can be attributed to the size of their N-termini. The nNOS enzyme contains a unique PDZ domain that interacts with postsynaptic density protein-95 believed to be involved in controlling the localization of nNOS within the cell (Kone, 2000). Another N-terminal binding site exists in nNOS for a protein that inhibits the nNOS enzyme (protein inhibitor of NOS, PIN) by disrupting the production of •NO and $\bullet O_2^-$ (Xia *et al.*, 2006). The

eNOS isozyme has a distinctive myristolation (Myr) N-terminal modification site where a fatty acyl group is posttranslationally attached to allow the enzyme to be associated to the cellular membrane (Figure 1.11). The cNOS enzymes are Ca^{2+}-dependent since their binding and activation are dependent on intracellular Ca^{2+} and CaM concentrations (Roman *et al.*, 2002). •NO produced by nNOS functions as a neurotransmitter, which allows for signalling between distant and adjacent cells (Alderton *et al.*, 2001). •NO operates as a vasodilator when produced by eNOS in blood vessels, allowing for unrestricted blood flow (Snyder and Bredt, 1992).

In contrast to the cNOS enzymes which are constitutively expressed, iNOS is transcriptionally regulated *in vivo* by cytokines in macrophages and binds to CaM at basal levels of Ca^{2+} (Roman *et al*., 2002). Since this enzyme binds to CaM regardless of cellular Ca^{2+} concentrations, this enzyme is classified as Ca^{2+}-independent. The human iNOS monomer has a molecular weight of 125 kDa. To date, iNOS could not be isolated in its CaM-free form. Apparently, the interaction between iNOS and CaM is so strong that CaM is not released once it has associated to iNOS. For this reason, CaM has been classified as a subunit of iNOS (Cho *et al.*, 1992). The properties of the NOS enzymes and some of their roles in diseases are summarized in Table 1.6.

Table 1.6 – Summary of the properties and roles of mammalian NOS isozymes

Structural and Enzymatic Parameters	Active homodimers		
	Ca^{2+}-dependent		Ca^{2+}-independent
	nNOS (NOS I)	eNOS (NOS III)	iNOS (NOS II)
Subunit molecular mass	160 kDa	135 kDa	125 kDa
Inducibility	Constituitive	Constituitive	Inducible
CaM-binding (~ K_d)	~30 x 10^{-9} M	~30 x 10^{-9} M	Subunit-like (<< 30 x 10^{-9} M)
Cofactors	H_4B, FAD, FMN, heme, Zn	H_4B, FAD, FMN, heme, Zn	H_4B, FAD, FMN, heme, Zn
Protein variants	α, β, μ, γ tissue-specific isoforms	—	—
Postranslational modifications	Specific phosphorylation sites present	Myristoylation Palmitoylation Phosphorylation sites present	Specific phosphorylation site present
Sources of superoxide formation	Heme domain, reductase domain	Mainly heme domain	Mainly reductase domain
Major physiological function	Neurotransmission	Vasodilatation	Cytotoxicity
Role in disease	Stroke Muscular dystrophy Ischemia-reperfusion injury	Endothelial dysfunction Hypercholesterolemia Hypertension	Toxic shock Inflammation Autoimmune disease

Table modified from a previously published review (Masters, 2000).

Numerous crystal structures of the three NOS oxygenase domains have been published (Fischmann *et al.*, 1999; Crane *et al.*, 2000; Matter *et al.*, 2005). These x-ray crystal structures have shown that the interface located between the oxygenase domains and a structural zinc ion coordinated by four conserved cysteine residues (two from each monomer) are involved in dimer stability (Figure 1.13). To date, there has only been one solved crystal structure of the reductase domain of nNOS released; it suggests that the reductase domain can also dimerize (Garcin *et al.*, 2004) (Figure 1.14).

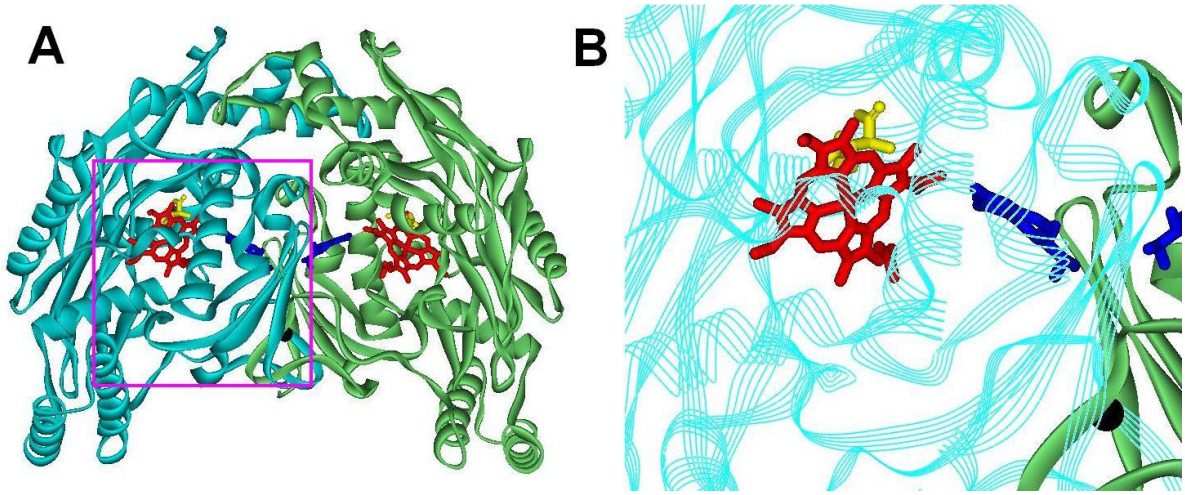

Figure 1.13 – X-ray crystal structures of rat nNOS oxygenase with bound L-arginine.
Each monomer backbone is shown in cyan and green. Heme, H_4B, zinc ion and L-arginine are shown in red, blue, black, and yellow, respectively. **(A)** Solved structure of the rat nNOS oxygenase domain (PDB 1ZVL, (Matter *et al.*, 2005), and **(B)** highlighted region of *panel A* to clarify cofactor locations. Models were visualized using ViewerLite 5.0 (Accelrys).

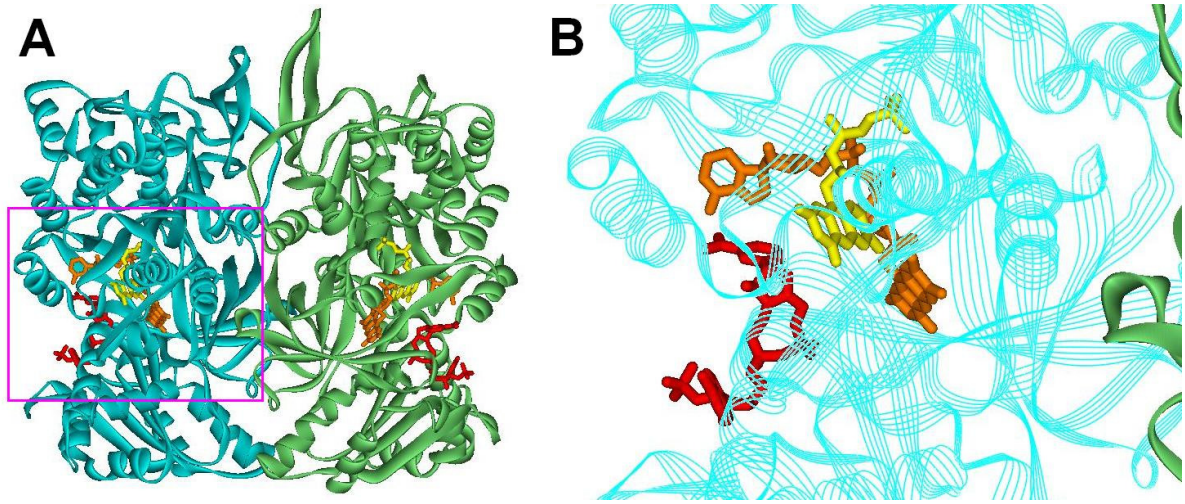

Figure 1.14 – X-ray crystal structures of rat nNOS reductase domain.
Each monomer backbone is shown in cyan and green. $NADP^+$, FAD and FMN are shown in red, orange, and yellow, respectively. **(A)** Solved structure of the rat nNOS reductase domain (PDB 1TLL, (Garcin *et al.*, 2004), and **(B)** highlighted region of *panel A* to clarify cofactor locations. Models were visualized using ViewerLite 5.0 (Accelrys).

While there is no doubt that the oxygenase domains of NOS are dimeric, the question of whether the reductase domain is also involved in the enzyme's dimerization is a point of debate. The dimer observed in the nNOS reductase domain crystal structure could be a crystallization artifact or it could represent another interface or site for NOS dimerization. Future structures of the NOS reductase domains will hopefully clarify if the reductase domain is in fact a monomer or dimer.

1.2.3 Electron transfer within NOS

Electron transfer within the NOS enzymes is dependent on CaM binding. The mechanism of how CaM binding facilitates electron transfer from NADPH to the heme is not fully understood and is not equivalent in all three NOS isoforms (Newman *et al.*, 2004; Spratt *et al.*, 2006). At elevated Ca^{2+} concentrations, CaM binds to the cNOS enzymes and promotes the transfer of electrons originating from NADPH through the reductase domain to the catalytic heme of the adjacent NOS monomer's oxygenase domain (Abu-Soud *et al.*, 1994; Chen *et al.*, 1996; Stevens-Truss *et al.*, 1997; Siddhanta *et al.*, 1998; Sagami *et al.*, 2001; Ghosh and Salerno, 2003). In contrast, electron transfer within the reductase domain of iNOS has previously been determined to be CaM-independent (Newton *et al.*, 1998). Electron transfer from the FMN to the catalytic heme centre in iNOS is generally considered to be CaM-dependent (Siddhanta *et al.*, 1998; Ghosh and Salerno, 2003; Feng *et al.*, 2006).

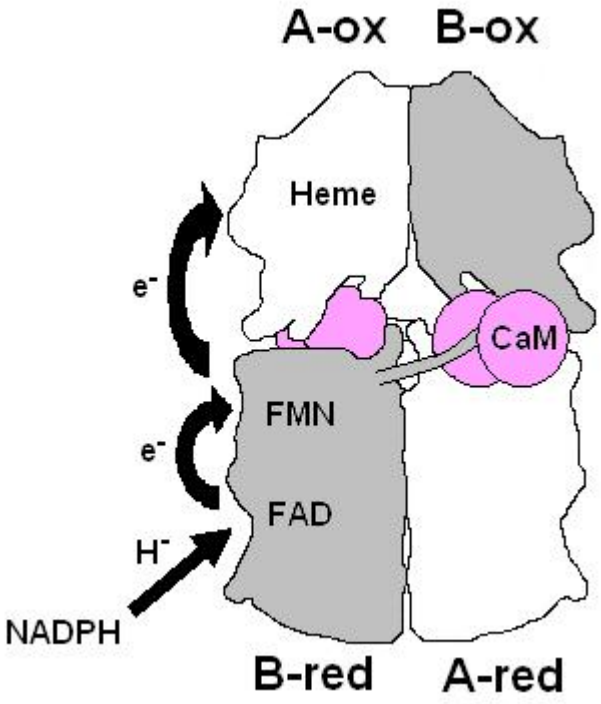

Figure 1.15 – Electron transfer within a NOS dimer.
The NOS monomers are shown in white and grey, respectively. CaM is shown in pink. Electrons are transferred through the reductase domain (NADPH to FAD, FAD to FMN) to the heme in the oxygenase domain of the opposite NOS monomer. This model is derived from the solved crystal structures of the nNOS oxygenase and reductase domains (as shown in Figure 1.13A and Figure 1.14A) from a previously published study (Garcin *et al.*, 2004).

Two explanations for the CaM-dependence of electron transfer in NOS have been proposed: (1) CaM may have the ability to change the redox potential difference between the flavins and the heme of NOS, or (2) CaM is able to cause a structural change in the NOS enzymes, allowing for more efficient electron transfer within the reductase domain and from the reductase to oxygenase domains (Daff *et al.*, 2001). It has been shown that CaM binding to the isolated reductase or oxygenase domains of nNOS does not significantly change the redox potentials of the flavins or heme cofactors (Noble *et al.*, 1999). This finding was later confirmed using full length eNOS and nNOS (Gao *et al.*, 2004). However, a recent study proved that the binding of CaM and $NADP^+$ to the nNOS reductase domain does in fact perturb the redox potential of the flavins (Dunford *et al.*, 2007). In either case,

all of these studies agree that CaM binding is pivotal for efficient electron transfer to occur in NOS. Protein modelling has suggested that the distances between the FAD and FMN cofactors in the reductase domain are too large for efficient electron transfer to take place (Ghosh and Salerno, 2003). Furthermore, these models suggest that the distances between the FMN and heme centres are greater than 25 Å (Ghosh and Salerno, 2003). These distances would be too large for electron transfer to occur from the flavins to the heme; therefore it is probable that a major structural rearrangement is necessary for the NOS enzymes to properly function (Figure 1.16). This suggests that CaM facilitates large conformational changes within NOS by moving the FMN-binding domain, a region within the reductase domain that is suggested to be a highly dynamic and flexible due to a hinge domain, from an electron-accepting position (FAD→FMN) to an electron-donating position (FMN→heme) (Figure 1.16).

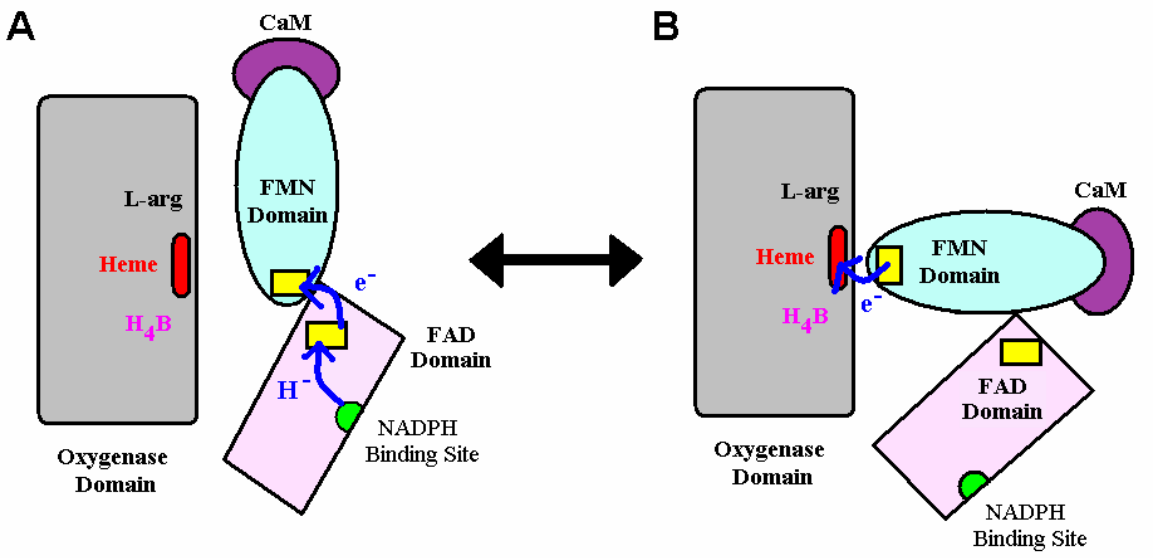

Figure 1.16 – Electron transfer and •NO production controlled by CaM-dependent conformational changes between the NOS cofactors.
(A) Intramolecular electron transfer within the reductase domain, and **(B)** intermolecular electron transfer from the reductase domain to the heme of the oxygenase domain of the adjacent NOS enzyme in the dimer. This model is modified from a previous NOS review (Ghosh and Salerno, 2003).

Another control mechanism for electron transfer in the reductase domain of nNOS is the NADPH conformational lock (Craig *et al.*, 2002; Daff, 2003). Previous studies have suggested that this "locked" conformation occurs after NADPH transfers a hydride to FAD to form $FADH_2$ and a subsequent NADPH molecule binds and is unable to transfer its hydride to reduced $FADH_2$. In order to unlock the reductase domain, the FAD needs to be regenerated to accept another hydride from NADPH and pass electrons through the rest of the NOS enzyme. The large conformational change that CaM induces in the reductase domain of the NOS enzymes (Figure 1.16) allows for the FMN domain to interact with both the FAD to accept electrons and pass the electrons on to the heme during catalysis. The electron transfer from $FADH_2$ to FMN regenerates FAD thereby unlocking the reductase domain (Craig *et al.*, 2002; Daff, 2003). Clearly, these conformational changes caused by CaM are important in stimulating efficient electron transfer with the NOS enzymes.

1.2.4 Catalytic mechanism of NOS

The proposed mechanism for •NO production by NOS involves two successive mono-oxygenation reactions, similar to the cytochrome P450 mono-oxygenase mechanism (Alderton *et al.*, 2001). The first reaction involves the hydroxylation of the guanidino nitrogen of L-arginine to produce the intermediate N^G-hydroxy-L-arginine (NOHA). The second reaction oxidizes NOHA to •NO and L-citrulline (see Figure 1.10).

The NOS and cytochrome P450 enzymes share many common traits including a thiolate-ligated heme prosthetic group (Gorren and Mayer, 2007). Since the mechanism of NOS catalysis is similar to that of cytochrome P450, the structure of the oxygenase domain of the NOS enzymes was originally believed to be similar to other heme containing proteins, such as peroxidases and catalases, which have their heme binding pockets lined predominantly with α-helices (Graham and Peterson, 1999). In contrast, the x-ray crystal structure of iNOS's oxygenase domain demonstrated an overall topology similar to a left-handed baseball catcher's glove with the heme binding-site

located in the palm of the mitt and a large cavity above the heme where O_2 and L-arginine are able to bind (Crane *et al.*, 1997). Another striking difference between the NOS and cytochrome P450 enzymes is the presence of H_4B in the NOS oxygenase domain which has been implicated in NOS dimer stability (Panda *et al.*, 2002).

There have been conflicting reports on the role of H_4B in the catalytic mechanism of NOS. It had previously been postulated that the H_4B is a potential electron donor to the heme and is regenerated by electrons from the reductase domain (Hurshman and Marletta, 2002). However, crystal structures have shown that H_4B is buried within the dimer interface of the enzyme and is supposedly inaccessible to electrons from the reductase domain so that it could not be regenerated after it is oxidized during the mono-oxygenation reactions (Crane *et al.*, 1998; Stuehr, 1999). Although it is generally accepted that the stoichiometry of NADPH oxidation to •NO production is a 3 to 2 ratio (Griffith and Stuehr, 1995), which is in good agreement with FMN acting as the sole electron donor to the heme center, the H_4B cofactor still plays an important role in the mechanism of the NOS enzymes. Recent studies have clarified the direct role H_4B has in the NOS catalytic mechanism. This updated mechanism is shown in Figure 1.17.

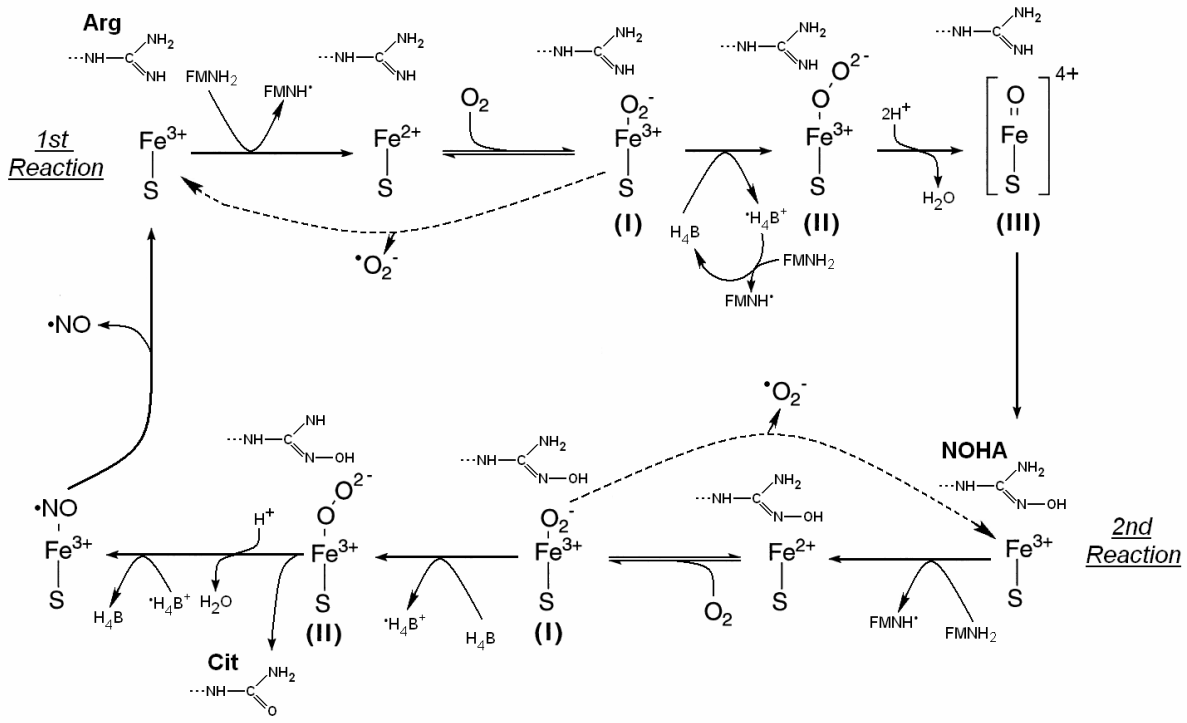

Figure 1.17 – Proposed catalytic mechanism of the NOS enzymes through two mono-oxygenation reactions.
Arg, NOHA, and Cit represent L-arginine, N^G-hydroxy-L-arginine, and L-citruline, respectively. The guanidino-group of L-arginine is shown throughout this mechanism to help clarify the modifications of L-arginine during the two mono-oxygenation reactions. $FMNH_2$, FMNH•, and $•H_4B^+$ represent fully reduced FMN, semi-reduced FMN, and H_4B radical formed during catalysis, respectively. This figure is based upon a recent review (Stuehr *et al.*, 2004) and modified from a previously published NOS review (Stuehr, 1999).

The first mono-oxygenation reaction in the NOS catalytic mechanism involves an electron transfer from the reductase domain to the ferric heme (Fe^{3+}) in the oxygenase domain. This is the slowest step of the reaction and allows for the binding of molecular oxygen and the formation of a ferric-superoxy species (Fe(III)-O_2^-; Species I) (Stuehr, 1999; Stuehr *et al.*, 2004). In order to avoid the release of $•O_2^-$, the input of a second electron from H_4B occurs to generate a ferric-peroxo species (Fe(III)-OO^{2-}; Species II). The formation of a H_4B radical has been supported by numerous studies and H_4B is proposed to be regenerated by another electron from the reductase domain (Hurshman and Marletta, 2002; Hurshman *et al.*, 2003; Stuehr *et al.*, 2004; Gorren and Mayer,

2007). The O—O bond in Species II is subsequently cleaved producing an iron-oxo species (Fe(IV)=O; Species III) and the release of a water molecule (Mansuy and Renaud, 1995). Species III then hydroxylates L-arginine to produce NOHA (Figure 1.17).

The second mono-oxygenation reaction involves the generation of species I, as previously described for the first reaction. Originally, Species II was thought to act as an oxidant and abstract an electron from NOHA to generate a nucleophilic Fe(III)-OO^{2-} species and an NOHA radical. This reactive species was then predicted to react directly with the NOHA radical, generating a tetrahedral intermediate that rearranges to release the products •NO and L-citrulline (Stuehr, 1999). However, recent studies have shown that H_4B is also involved in the second mono-oxygenation reaction of NOHA by donating an electron and subsequently regenerated later in the reaction (Wei *et al.*, 2003a) (Figure 1.17). The first electron transfer from H_4B allows for the formation of Species II, which oxidizes NOHA, causing the subsequent release of citrulline (Wei *et al.*, 2003b). The second electron transfer involves the regeneration of H_4B and the formation of a ferric-•NO product complex (Fe(III) •NO), which then releases •NO, thus completing the NOS catalytic mechanism (Wei *et al.*, 2003b). Another suggested role for H_4B is aiding in the release of •NO from NOS by preventing the formation of a ferrous-•NO complex (Fe(II) •NO) where •NO would be tightly bound (Gorren and Mayer, 2007).

In summary, the NOS enzymes use two different redox cofactors to donate electrons during catalysis – a slow electron transfer from the FMN in the reductase domain and a fast electron transfer from H_4B to avoid the release of $\bullet O_2^-$ and aid in the release of •NO during the second mono-oxygenation reaction (Stuehr *et al.*, 2004).

1.2.5 Regulation of NOS

1.2.5.1 Intrinsic regulation of NOS

Apart from the CaM-dependence of electron transfer within the NOS enzymes, there are numerous other intrinsic structural elements that control •NO production by the NOS enzymes. These include (1) an autoinhibitory domain, (2) a C-terminal tail region, and (3) dimer stability.

1.2.5.1.1 NOS autoinhibitory domains

In general, an autoinhibitory domain is a motif within an enzyme that inhibits the enzyme by blocking and/or interfering with the substrate's ability to bind to the active site (Crivici and Ikura, 1995).

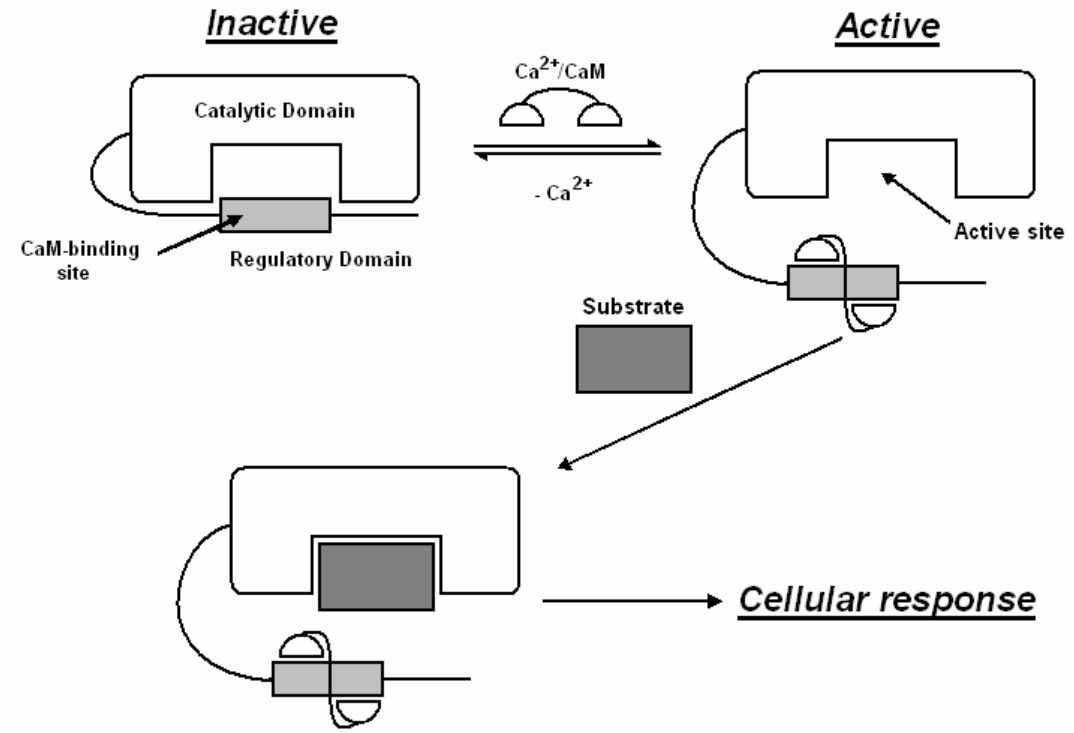

Figure 1.18 – A generalized model of an autohibitory domain and its displacement by Ca^{2+}/CaM.
As Ca^{2+}/CaM binds to the autoinhibitory domain (light grey), the autohibitory domain is displaced allowing the substrate (dark grey) to access and bind to the active site of the enzyme. This figure is modified from a previous CaM review (Crivici and Ikura, 1995).

It is of interest that the Ca^{2+}-dependent nNOS and eNOS isozymes each contain an insert of about 40 amino acids in length in the middle of the FMN-binding subdomains, which is proposed to be an autoinhibitory domain (Salerno *et al.*, 1997) (Figure 1.19).

```
                                                  -FMN Ring (re-face)
CYPOR       AHRYGMRGMS ADPEEYDLAD LSSLPEIDKS LVVFCMATYG EGDPTDNAQD  152
Human nNOS  FKHAFDAKVM SMEEYDIVHL E------HET LVLVVTSTFG NGDPPENGEK  824
Human eNOS  FRKAFDPRVL CMDEYDVVSL E------HET LVLVVTSTFG NGDPPENGES  583
Human iNOS  FTYAFNTKVV CMEQYKANTL E------EEQ LLLVVTSTFG NGDCPSNGQT  601

            -----  ========Location of Regulatory Loop Insert=====
CYPOR       FYDWLQE--- ---------- ---------- ---------- ----------  159
Human nNOS  FGCALMEMRH P-NS--VQEE RKSYKVRFNS VSSYSDSQKS SGDGPDLRDN  873
Human eNOS  FAAALMEMSG PYNSSPRPEQ HKSYKIRFNS ISCSDPLVSS WRRKRKESSN  633
Human iNOS  LKKSLFMMKE ---------- ---------- ---------- ----------  611

            ==    --------FMN Ring (si-face)-------
CYPOR       --TDVDLTGV KFAVFGLGNK TYEHRNAMGK YVDQRLEQLG AQRI  201
Human nNOS  FESAGPLANV RFSVFGLGSR AYPHFCAFGH AVDTLLEELG GERI  917
Human eNOS  TDSAGALGTL RFCVFGLGSR AYPHFCAFAR AVDTRLEELG GERL  677
Human iNOS  -----LGHTF RYAVFGLGSS MYPQFCAFAH DIDPKLSHLG ASQL  650
```

Figure 1.19 – Sequence alignment of the FMN binding region of cytochrome P450 (CYPOR) and the NOS enzymes.
It is important to note that only nNOS and eNOS contain the proposed autoinhibitory inserts in their FMN binding regions. This figure is based upon sequence alignments from two previous studies (Salerno *et al.*, 1997; Garcin *et al.*, 2004).

This inhibitory element is absent in the Ca^{2+}-independent iNOS enzyme (Figure 1.19). Due to its position in the reductase domain of nNOS and eNOS, the autohibitory domain is not close to the active site in the oxygenase domain. Therefore, Salerno and co-workers suggested that the autoinhibitory domain would act by a different mechanism when regulating the activity of the cNOS enzymes than the typical CaM-activated enzymes, as described in Figure 1.18 (Salerno *et al.*, 1997). They demonstrated, through the use of peptides corresponding to the proposed autoinhibitory domain, that these inserts do in fact impair CaM's ability to bind to the cNOS enzymes when Ca^{2+} concentrations are low; however, when Ca^{2+} concentrations increased, Ca^{2+}-replete CaM would be able to induce a conformational change in the autohibitory domain causing it to be displaced from

the CaM-binding domains of nNOS and eNOS (Salerno *et al.*, 1997). This Ca^{2+}/CaM-dependent displacement allows for efficient electron transfer within the cNOS enzymes. Furthermore, the removal of these cNOS autohibitory domains by mutagenesis have been shown to decrease the Ca^{2+}-dependent CaM activation and increase the enzyme activities of nNOS and eNOS at lower Ca^{2+} concentrations (Daff *et al.*, 1999; Nishida and Ortiz de Montellano, 1999; Chen and Wu, 2000; Montgomery *et al.*, 2000). These results further illustrate that these inserts in the cNOS enzymes do not have the properties of the typical autoinhibitory domains found in CaM-activated enzymes. A model describing how the displacement of the autoihibitory domain by Ca^{2+}/CaM might facilitate electron transfer through the reductase domain is shown in Figure 1.20.

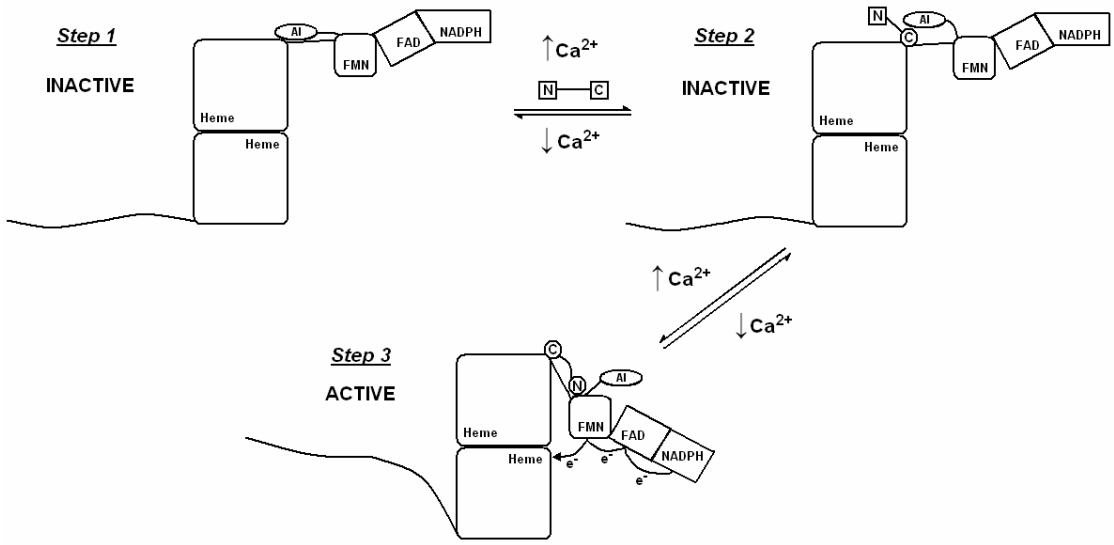

Figure 1.20 – A proposed three-step model to explain the mechanism that the autoinhibitory insert and CaM use to regulate electron tranfer in the cNOS enzymes.
The N- and C-terminal domains of CaM are represented as Ca^{2+}-deplete (squares) and Ca^{2+}-replete (circles). *Step 1* – CaM-free cNOS is inactive and the autoinhibitory domain is docked. The autoinhibitory domain (AI) is shown to dock with the cNOS oxygenase domain at this step, however, the AI may alternatively be docked within the reductase domain. The AI may prevent electron transfer from the FMN to the heme, from FAD to FMN, or a combination of both possible electron steps. *Step 2* – As intracellular Ca^{2+} concentrations increase, the C-terminal domain of CaM becomes Ca^{2+}-replete and is able to bind to the cNOS enzyme however the AI continues to keep the enzyme inactive. *Step 3* – A further increase Ca^{2+} concentration results in the N-terminal lobe of CaM becoming Ca^{2+}-replete and binding to the enzyme causing the displacement of the AI. This causes the promotion of efficient electron transfer with the cNOS enzyme due to the alignment within the reductase domain to allow electron transfer to the oxygenase domain and •NO production. This model is based upon a previous study (Lane and Gross, 2000).

Another possible role for these autoinhibitory domains in the cNOS enzymes is to protect the CaM-binding domains of nNOS and eNOS from proteolysis. The iNOS enzyme protects itself from proteolytic cleavage by calpain (a cysteine protease) by having CaM bound to its CaM-binding domain (Walker *et al.*, 2001). In contrast, the CaM-free cNOS enzymes do not have protection from calpain degradation. nNOS and eNOS have been reported to be susceptible to calpain degradation (Barnes and Gomes, 1995; Laine and de Montellano, 1998) and cNOS mutants lacking the autoinhibitory domain could only be purified when coexpressed with CaM (Montgomery *et al.*, 2000) Therefore, it is conceivable that the autoinhibitory domain not only controls electron transfer within NOS, but it may also prevent proteolysis of the cNOS enzymes in the cell.

1.2.5.1.2 C-terminal tail extension

An additional CaM-modulated regulatory element found in the each of the NOS enzymes is the C-terminal tail extension. This tail extension is not found in cytochrome P450.

```
                              ===============C-terminal tail================
CYPOR       KLMTKGRYSL DVWS------ ---------- ---------- ---------- ------   678
Human nNOS  RMRDDNRYHE DIFGVTLRTY EVTNRLRSES IAFIEESKKD TDEVFSS--- ------  1434
Human eNOS  VLRDQQRYHE DIFGLTLRTQ EVTSRIRTQS FSLQERQLRG AVPWAFDPPG SDTNSP  1202
Human iNOS  QLKSQKRYHE DIFGAVFSYG VKKGNALEEP KGTRL----- ---------- ------  1147
```

Figure 1.21 – Comparative sequence alignment of the C-terminal tails of the NOS enzymes and cytochrome P450 (CYPOR).
The extended C-terminal tail element is found in the cNOS enzymes while it is much shorter in the iNOS isoform. The C-terminal tail is absent in cytochrome P450. This figure is based upon a sequence alignment from a previous study (Garcin *et al.*, 2004).

Previous studies have shown that the removal of the C-terminal tail from the cNOS enzymes resulted in an enzyme with enhanced electron transfer rates through the reductase domain in the absence of CaM; however, the activity of the enzyme was equivalent to wild-type cNOS enzyme in the presence of Ca^{2+}/CaM (Roman *et al.*, 2000a). Similiarly, a truncated C-terminal tail mutant of iNOS

demonstrated a 7-10 fold increase in electron transfer rates in its reductase domain when compared to wild-type iNOS (Roman *et al.*, 2000b). These results suggest that the C-terminal tail extension found in the NOS enzymes is involved in regulating electron transfer through the NOS enzymes.

In a recent study, a mutant of nNOS without its autoinhibitory domain and C-terminal tail extension was produced. It was found that CaM no longer modulates electron transfer through the reductase domain of this nNOS mutant; however, CaM was still required to promote electron transfer from the FMN domain to the heme for •NO production (Roman and Masters, 2006). Clearly, the concerted interactions of the autoinhibitory domain and C-terminal tail extension are involved in the binding and regulation of electron transfer within the cNOS enzymes by CaM.

1.2.5.1.3 •NO-mediated dimer disruption

Biochemical studies have determined that the NOS oxygenase domains display differences in their dimer stability depending on the presence of H_4B and of a zinc ion coordinated by four cysteine residues at the dimer interface (Alderton *et al.*, 2001) (Figure 1.13). Furthermore, it has also been proposed that CaM has an important role in the dimerization of eNOS monomers (Hellermann and Solomonson, 1997). Recent studies have demonstrated that the exposure of eNOS and iNOS to •NO donors or •NO produced by the enzyme itself resulted in the decrease of dimeric NOS enzyme and a correlating increase in NOS monomers (Ravi *et al.*, 2004; Mitchell *et al.*, 2005; Li *et al.*, 2006). The NOS enzymes are only active in their dimeric form and inactivated if this dimer is disrupted. This dimer disruption is the result of *S*-nitrosation of the cysteine residues involved in the co-ordination of the structural zinc ion located at the oxygenase dimer interface. It may act as a mode of feedback inhibition for the NOS enzymes – by *S*-nitrosating its own cysteine residues and causing itself to monomerize, the enzyme can attenuate and control its own •NO production levels *in vivo* (Ravi *et al.*, 2004; Mitchell *et al.*, 2005).

1.2.5.2 Extrinsic regulation of NOS

1.2.5.2.1 Posttranslational modifications of NOS

Posttranslational modifications of the cNOS enzymes, particularly eNOS, have been studied extensively. It has been shown that eNOS can be myristoylated, palmitoylated, acetylated, and phosphorylated in its oxygenase domain. These posttranslational modifications have been implicated in the enzyme's localization in the cell (cytosol, membranes or organelles) but are suggested to have no effect on the •NO production levels, with the exception of phosphorylation (Liu *et al.*, 1997; Michel and Feron, 1997; Hemmens and Mayer, 1998).

Phosphorylation of eNOS-Ser(1177) has been shown to be the most important posttranslational modification required for eNOS activation (Mount *et al.*, 2007). Since Ser(1177) is located in the C-terminal tail extension of eNOS, which is implicated in attenuating electron transfer in the NOS enzymes (see section 1.2.5.1.2), and the phosphorylation of this site allows for an increased electron transfer efficiency in eNOS. Another phosphorylation site has been found in the autoinhibitory region of the flavin mononucleotide (FMN) binding domain of eNOS (Mount *et al.*, 2007). This site (Ser633) has been shown to increase eNOS activity and appears to be important for the maintenance of •NO synthesis rates after initial activation by Ca^{2+}/CaM binding and phosphorylation of Ser(1177) (Michell *et al.*, 2002). A phosphorylation site of interest is eNOS-Thr(497), which is located in the CaM-binding domain of eNOS. This modification is performed by protein kinase C and has been shown to inhibit •NO production by reducing the affinity of eNOS for CaM (Matsubara *et al.*, 2003).

The nNOS enzyme has also been shown to undergo serine or tyrosine phosphorylation in its oxygenase domain, which lowers enzyme activity by two thirds; however, the identity of the modified sites and the mechanism of this inhibition remain unclear (Dawson *et al.*, 1993).

Phosphorylation of Ser(847) in nNOS, which is located in the FMN domain, leads to marked decreases in enzyme activity (Komeima *et al.*, 2000). Clearly, phosphorylation plays a pivotal role in regulating the cNOS enzymes.

The iNOS enzyme has also been shown to be posttranslationally modified. These modifications include an N-terminal palmitoyl group, which influences the localization of iNOS in the cell (Navarro-Lerida *et al.*, 2004). iNOS has also been shown to be phosphorylated by tyrosine kinases but the effect of this modification on iNOS activity remains unclear (Pan *et al.*, 1996). Lastly, iNOS has also been shown to have its rate of turnover in the cell directly regulated by the proteosomal degradation pathway (Musial and Eissa, 2001). In order to control NO synthesis rates in the cell, the turnover of iNOS must be tightly regulated to avoid oxidative stress and damage. Clearly, posttranslational modifications and protein turnover are involved in the extrinsic regulation of iNOS.

1.2.5.2.2 Protein-protein interactions with the NOS enzymes

There are numerous proteins that interact with the NOS enzymes in a variety of roles including activation, inhibition, and trafficking within the cell. Due to the detrimental or beneficial effects mediated by •NO, the cellular localization of nNOS is tightly regulated. The function of the PDZ domain located in the N-terminus of nNOS is to assemble intracellular proteins into multiprotein complexes (Roman *et al.*, 2002). This PDZ element of nNOS has been shown to bind to a wide variety of proteins which is dependent upon the tissue expressing nNOS. For instance, in the brain PSD-95 acts as a "link" protein between nNOS and the NMDA receptor, thereby bringing nNOS in close proximity to the NMDA receptor (Christopherson *et al.*, 1999). Another sequence found in the N-terminus of nNOS is recognized by a protein that is termed PIN, since it acts as a "protein-inhibiting nNOS" by destabilizing the nNOS dimer (Jaffrey and Snyder, 1996).

eNOS has been shown to anchor to caveolae via its N-terminally myristoylate or palmitoyate moieties. Caveolae are characterized as small invaginations found on the surface of epithelial cells and signal transduction cells (Kurzchalia and Parton, 1999). The structural components of caveolae are the integral membrane proteins – caveolin-1, caveolin-2, and caveolin-3. eNOS was shown to be inhibited by its interaction with caveolin-1 and caveolin-3 *in vitro* (Feron *et al.*, 1996). The binding of the molecular chaperone heat shock protein 90 (Hsp90) has been shown to enhance eNOS •NO production (Garcia-Cardena *et al.*, 1998). In these complexes, ATP-dependent conformational changes in Hsp90 uncouple electron transfer from •NO production in eNOS, resulting in the increased formation of $\bullet O_2^-$ (Pritchard *et al.*, 2001).

Similar to eNOS, iNOS also exhibits an interaction with caveolin-1. A previous study demonstrated that caveolin-1 down-regulates iNOS by causing it to colocalize with caveolin-1 in detergent insoluble membrane fractions stearing it towards degradation via the proteasome pathway (Felley-Bosco et al., 2000). NOS-associated protein-110 kDa (NAP110) has been shown to interact with the N-terminal domain of iNOS between residues 1-70 and decreases iNOS activity by 90% (Ratovitski et al., 1999). Furthermore, NAP110 appears to only interact with iNOS monomers and inhibits iNOS homodimerization (Ratovitski et al., 1999).

Regulation of iNOS also occurs at the transcriptional level. The induction of iNOS involves the cooperative interaction of transcription factors and co-regulatory molecules that bind to the iNOS promoter (Zhang et al., 2003). Nuclear factor kappaB (NF-κB), which has been identified as the major trans-activator of the iNOS gene, is able to interact with interferon-γ and histone deacetylase. The interaction between interferon-γ and NF-κB has been shown to physically bend the iNOS promoter resulting in a dramatic increase of iNOS transcription (Saura *et al.*, 1999). Likewise, the interaction between NF-κB with histone deacetylase has been shown to increase iNOS transcription. Hyperacetylation of the iNOS promoter appears to diminish the cytokine induction of iNOS

transcription (Zhang *et al.*, 2003). By recruiting the histone deacetylase enzyme to deacetylate the promoter, NF-κB allows itself to efficiently associate to the iNOS gene's promoter for transcription (Yu *et al.*, 2002). Clearly, the NOS enzymes are extrinsically regulated by a variety of protein-protein interactions in the cell through direct interactions with the NOS enzymes and/or indirectly via transcriptional control.

1.2.6 Previous studies on CaM binding to NOS

Numerous studies have been performed to better understand CaM's binding and activation of the NOS enzymes. The majority of the studies published to date have focused on the Ca^{2+}-dependent cNOS enzymes, while the Ca^{2+}-independent iNOS isoform has been studied very little prior to 2003. The following is a brief summary of previous investigations on the interaction of CaM with the NOS enzymes.

1.2.6.1 CaM binding to NOS CaM-binding domain peptides

The CaM-binding domains of NOS are categorized under the 1-5-8-14 CaM-binding motif, where site 1 is generally an aromatic residue, residues 5 and 8 are hydrophobic, and residue 14 corresponds to a large bulky hydrophobic side chain (section 1.1.4).

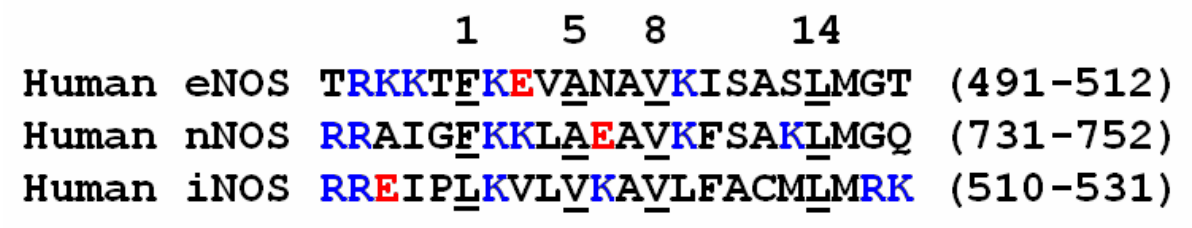

Figure 1.22 – Sequence alignment of the CaM-binding domains of the NOS enzymes.
Acidic and basic residues are shown in red and blue, respectively. Hydrophobic residues found in the 1-5-8-14 CaM-binding motif are underlined. This alignment based upon a previous study (Aoyagi *et al.*, 2003).

The association of CaM to peptides corresponding to the CaM-binding domains of the NOS enzymes has been studied by a variety of biophysical methods including circular dichroism, ^{1}H NMR, and x-ray crystallography. Evidence has shown that when CaM binds to these NOS peptides, this induces an α-helical conformation in the peptide and forms an amphipathic binding surface that is commonly found in CaM-binding sites, as previously described in section 1.1.4 (Zhang *et al.*, 1995; Matsubara *et al.*, 1997; Aoyagi *et al.*, 2003).

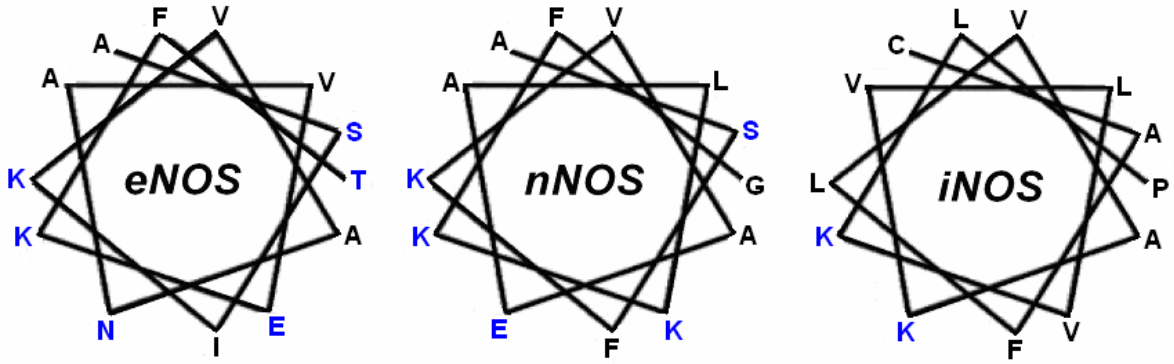

Figure 1.23 – Helical wheel diagrams of the CaM-binding domains of the NOS enzymes. Charged or polar residues (blue) and hydrophobic or non-polar residues (black) are highlighted in the helical wheel diagrams. Note that some of the corresponding charged residues in the cNOS CaM-binding domains are replaced by hydrophobic residues in iNOS. This figure is modified from a previous study (Aoyagi *et al.*, 2003).

As shown in Figure 1.5C and D, the x-ray crystal structures of CaM-eNOS peptide (Aoyagi *et al.*, 2003) and CaM-nNOS peptide (Ng *et al.* – co-ordinates released 2007-12-25) complexes have been solved. Both of these structures demonstrate that CaM wraps tightly around the target peptide in an antiparallel orientation similar to the classic model of MLCK. Analysis of the CaM-eNOS peptide structure demonstrates that CaM binds in an antiparallel orientation, with the majority of the N-terminal residues of CaM associated with the C-terminal residues of the eNOS peptide and the C-terminal domain of CaM interacting mainly with the N-terminal residues of the peptide (Table 1.7).

Table 1.7 – Residues of CaM shown to be within 4 Å of the eNOS peptide

	Alignment of NOS CaM-binding domains			CaM sidechains in contact with eNOS peptide		
Motif 1-5-8-14	Human eNOS	Human nNOS	Human iNOS	N-terminal Domain	C-terminal Domain	Central Linker
	R492	R732	R511	E6, E7*, A10		
	K493	A733	E512		E120*, E123*, E127*	
	K494	I734	I513	E14*		
	T495	G735	P514		M124, E127	
1	**F496**	**F736**	**L515**	**L105, M124, E127*, A128, V136, F141, M144**		
	K497	K737	K516	E7	E127, M144, A147*	
	E498	K738	V517	E7, A10, E11, E14		
	V499	L739	L518	E14	M109, E114, M124	
5	**A500**	**A740**	**V519**		**F92, F141, M144, M145**	
	N501	E741	K520	E11*	M145	
	A502	A742	A521	E11, E14, A15, L18		
8	**V503**	**V743**	**V522**		**V91, F92, L112**	
	K504	K744	L523		S81, E84, I85, A88, M145	
	I505	F745	F524	E11, F12, A15, M72		M76
	S506	S746	A525	A15, L18, F19, L39		
	A507	A747	C526	L39	E87	
	S508	K748	M527	M72, K75	E87	M76
14	**L509**	**L749**	**L528**	**F19, M36, M51, M71, M72, K75**		
	M510	M750	M529	L39, Q41, K75*	E87*	

Residues shown to be involved in hydrogen bonding and ionic interactions are indicated with asterisks. This table is based upon the CaM-eNOS peptide structure (Aoyagi *et al.*, 2003).

Peptides corresponding to the cNOS enzymes have only been shown to bind to Ca^{2+}-replete CaM, whereas the iNOS peptide has been shown to bind to apo-CaM and holo-CaM (Matsubara *et al.*, 1997). Furthermore, the iNOS peptide also adopts an α-helical conformation when bound to apo-CaM (Matsubara *et al.*, 1997).

An interesting study demonstrated that the Ca^{2+}-dependent nNOS can be mutated to mimic the Ca^{2+}-independent iNOS CaM-binding domain. This study involved the mutation of a single glutamate to a lysine residue (E→K at position 6; Figure 1.22) allowed the mutated nNOS peptide to bind to apo-CaM (Censarek *et al.*, 2002). Likewise, the conversion of basic residues in the nNOS

peptide to the corresponding hydrophobic residues in iNOS (K→V, position 3; K→L, position 9; K→M, position 13) resulted in a significant increase in binding affinity for CaM from the micromolar to nanomolar range (Censarek *et al.*, 2002), similar to previously reported K_d values for CaM's affinity for iNOS CaM-binding domain peptides (Anagli *et al.*, 1995; Yuan *et al.*, 1998). Clearly, the CaM-binding domain peptides can act as a good working model for the Ca^{2+}-dependent and Ca^{2+}-independent association of CaM to the NOS enzymes.

1.2.6.2 CaM binding to NOS enzymes

A previous study using ^{125}I-labeled CaM suggested that four sequential steps occur when CaM binds and activates nNOS (Weissman *et al.*, 2002). This model is based upon the knowledge that the C-terminal domain of CaM has a ten fold greater affinity for Ca^{2+} than the N-terminal domain of CaM (Martin *et al.*, 1985). The first step involves the binding of Ca^{2+} to the C-terminal domain of CaM, followed by the Ca^{2+}-replete C-terminal domain of CaM binding to nNOS. Upon an increase of intracellular Ca^{2+} concentrations, the N-terminal domain of CaM binds Ca^{2+}. Finally, the Ca^{2+}-replete N-terminal domain binds to nNOS (Weissman *et al.*, 2002). The binding of the N-terminal domain of CaM to nNOS causes the activation of nNOS by the displacement of the autoinhibitory domain of nNOS. This model also suggests that the deactivation of nNOS is due to the decrease in intracellular Ca^{2+} and occurs in the reverse order of these four steps (Weissman *et al.*, 2002).

Chimeric NOS enzymes have previously been created that combine the CaM-binding domain of iNOS with the residual domains from nNOS (Ruan *et al.*, 1996; Lee and Stull, 1998). These studies demonstrated that the nNOS containing the iNOS CaM-binding domain could be fully activated at lower Ca^{2+} concentrations than wild-type nNOS, and that the designated CaM-binding domain of iNOS is not completely responsible for the Ca^{2+}-independent binding of CaM to iNOS (Lee and Stull, 1998). A subsequent study found that lysine 525 of murine iNOS (position 17), which is located in the FMN domain outside the CaM-binding domain, is involved in iNOS's Ca^{2+}-

independence but did not increase CaM's binding affinity at lower Ca^{2+} levels (Lee *et al.*, 2000). Another study demonstrated using truncated iNOS mutants that residues 484-726, corresponding to the CaM-binding domain and the FMN binding domain of iNOS are responsible iNOS's Ca^{2+}-independence (Ruan *et al.*, 1996). These studies, in conjunction with the NOS peptide studies (section 1.2.6.1), demonstrate the importance of studying the holo-NOS enzymes when determining their Ca^{2+}-dependence as there may be flanking regions in the oxygenase and reductase domains involved in CaM's association to the enzyme.

1.2.6.3 Mutant CaM proteins binding to the cNOS enzymes

A method commonly used to identify specific elements in CaM essential for CaM-dependent enzyme activation is the use of CaM mutant proteins. These mutant proteins have included a variety of single point mutations, the exchange of EF hand motifs within CaM, and truncations of CaM. To date, most of these studies focused solely on the binding and activation of nNOS.

Dr. Antony Persechini and coworkers have produced numerous CaM mutants in the past that were used to study their ability to activate MLCK and nNOS (Persechini *et al.*, 1994; Persechini *et al.*, 1996a; b). These mutants have included single EF hand pairs and duplicated EF hand pairs. Dr. Persechini's studies demonstrated that the N-terminal domain in conjuction with the central linker of CaM is instrumental in the activation of nNOS. Likewise, Dr. Samuel George and coworkers also studied the interaction between nNOS and CaM-troponin C chimeric proteins (i.e. proteins that have single EF hands replaced in CaM with its corresponding EF hand from troponin C) to determine which specific EF hands are responsible for nNOS activation (George *et al.*, 1990; George *et al.*, 1993; Su *et al.*, 1995; Gachhui *et al.*, 1998). These studies demonstrated that helices 2 and 6 of CaM, found in EF hands I (N-domain) and III (C-domain) respectively, act as a latch when associated to nNOS. In this model, helices 2 and 6 are in close proximity to one another and are suggested to control electron transfer from FMN to the heme by interacting with the reductase and/or

the oxygenase domain of nNOS (Su *et al.*, 1995). Recently, another study using oxidized CaM demonstrated that the oxidation of methionine residues in CaM as a result of aging has an inhibitory effect on nNOS activity (Montgomery *et al.*, 2003).

CaM with mutations of glutamate to glutamine residues at position 12 of each EF hand in CaM (-*Z* co-ordination site; Figure 1.2) have been used to study specific Ca^{2+}-binding sites in CaM and its association to nNOS (Stevens-Truss *et al.*, 1997). This study found that CaM EF hand I binding to Ca^{2+} was crucial for nNOS activity. Other CaM mutants deficient in Ca^{2+}-binding within their N- and C-terminal domains have also been produced by mutating conserved aspartate residues at position 1 (*X* co-ordination site; Figure 1.2). These CaM mutants have been used to study the Ca^{2+}-dependent and Ca^{2+}-independent association of CaM to various target proteins such as the inositol 1,4,5-trisphosphate receptor (Sienaert *et al.*, 2002; Kasri *et al.*, 2006), small conductance Ca^{2+}-activated K^+ channels (Lee *et al.*, 2003), and P/Q-type Ca^{2+} channels (DeMaria *et al.*, 2001); however, these mutants have not yet been studied with the NOS enzymes.

While eNOS and nNOS demonstrate similarities in their Ca^{2+}-dependence and regulatory elements (autoinhibitory domain and C-terminal tail), there has been very little reported on the specific elements in CaM that are important for eNOS activation. Likewise, due to the strong association between iNOS and CaM and the necessity of their coexpression to produce active enzyme (Cho *et al.*, 1992), little is known about the interaction between iNOS and CaM.

1.3 Reasons for studying the interaction of NOS with CaM

Over the past seven years, research in our laboratory has been focused on gaining a better understanding of the interaction between the NOS enzymes and CaM. Two facets of the CaM-NOS interaction under study are how CaM is able (1) to bind, and (2) to activate the three isoforms of NOS. It is generally accepted that CaM plays a vital role in controlling electron transfer within the constitutive NOS isoforms. There have been several studies demonstrating that different regions and elements of CaM play an important role in the binding and activation of the cNOS holoenzymes (Persechini *et al.*, 1994; Su *et al.*, 1995; Persechini *et al.*, 1996a; b; Stevens-Truss *et al.*, 1997; Gachhui *et al.*, 1998). The iNOS enzyme can only be purified when coexpressed with CaM, and the two proteins remain tightly associated even after the removal of Ca^{2+}. This has made it difficult to dissect the molecular details of the interaction between the iNOS enzyme and CaM. However, the development of coexpression CaM vectors in our laboratory has allowed for a more thorough investigation of CaM-iNOS specific interactions. This coexpression technique has been utilized throughout the studies reported in this thesis, using some of the aforementioned mutant CaM proteins (section 1.2.6.3) to determine the specific regions of CaM responsible for the Ca^{2+}-independent association of CaM to iNOS (see Chapters 2, 3, and 4).

There is a unique opportunity to investigate CaM control over •NO production by the NOS enzymes since each NOS isoform shows a different mode of activation and control by CaM; however, the underlying mechanism of •NO production remains unclear. The conformations that CaM adopts when bound to the three isoforms of holo-NOS have also not yet been determined.

1.4 Research Objectives

The purpose of this doctoral study was to further elucidate the structure and function of CaM when bound to the three different mammalian NOS isozymes. The overall objectives of this thesis were to:

1. Use CaM mutants to determine the specific elements in CaM responsible for the binding and activation of the NOS enzymes.
2. Determine the conformation of CaM when bound to the NOS CaM-binding domain peptides and holo-NOS enzymes.
3. Determine the three-dimensional structure of CaM in complex with an iNOS CaM-binding domain peptide.

In order to accomplish these objectives, the CaM-NOS interactions were studied using a variety of analytical methods including molecular cloning, protein expression and purification, kinetic spectrophotometric assays, circular dichroism, steady-state and time-resolved fluorescence, fluorescence (Förster) resonance energy transfer (FRET), and nuclear magnetic resonance (NMR) spectroscopy. The results reported in this thesis broaden and clarify our present understanding of the CaM-dependent regulation of the mammalian NOS enzymes.

Chapter 2
Differential Activation of Mammalian Nitric Oxide Synthase Isozymes by Calmodulin-Troponin C Chimeras *

2.1 Introduction

Cardiac troponin C (TnC) is a Ca^{2+}-binding protein whose function is to activate the thin filament cardiac muscle (da Silva *et al.*, 2002). The overall structure of TnC is similar to CaM since both proteins have two globular domains linked by a central helix with each globular domain composed of two EF hands. In particular, the local structures of EF hands I, III and IV of CaM and TnC are closely related. However, the structure of EF hand II of TnC differs from the corresponding region in CaM since helix 4 is redirected significantly when compared to CaM causing a significant difference in the global three-dimensional structure of TnC. Despite their overall structural similarity, TnC has only a 70% sequence similarity with CaM (Figure 2.1). The first EF hand of TnC does not bind Ca^{2+} because of a mutation relative to a CaM-like ancestor so that it can not chelate Ca^{2+} (Su *et al.*, 1995; Gachhui *et al.*, 1998). In addition, TnC has seven more N-terminal and three more central helix residues than CaM. It is noteworthy that TnC is unable to activate CaM dependent enzymes (George *et al.*, 1990; da Silva *et al.*, 2002). The C-terminal domain of CaM binds Ca^{2+} with a higher affinity (K_d = 10^{-6} M) than the N-terminal domain (K_d = 10^{-5} M) (Martin *et al.*, 1985), however, the EF hand

*** The results presented in this chapter have been published as part of:**

Newman, E., **Spratt, D.E.**, Mosher, J., Cheyne, B., Montgomery, H.J., Wilson, D.L., Weinberg, J.B., Smith, S.M., Salerno, J.C., Ghosh, D.K. and Guillemette, J.G. (2004) Differential activation of nitric-oxide synthase isozymes by calmodulin-troponin C chimeras. *J Biol Chem 279*, 33547-33557.

Unless otherwise stated, all of the work reported in this chapter was performed and analysed by the candidate.

IV of TnC binds Ca^{2+} with 1 order of magnitude greater affinity than EF hand IV of CaM (George *et al.*, 1993). Because of their overall structural similarity, domains of CaM have been exchanged for the corresponding domains of TnC to investigate the function of specific regions of the two proteins.

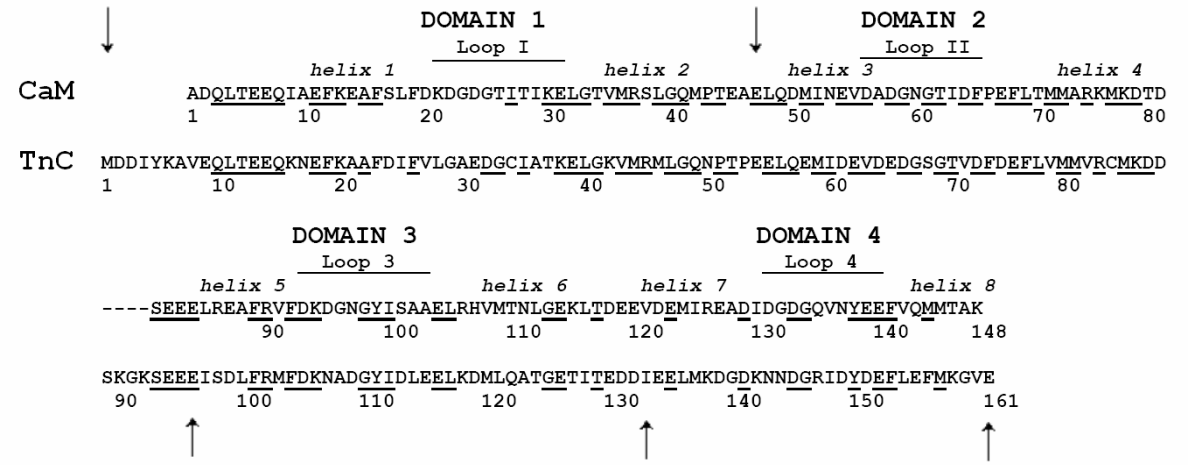

Figure 2.1 – Alignment of CaM and cardiac TnC.
Residue numbers and locations of the four EF hand domains, subdomain loops and helices are as indicated. Amino acids common to both CaM and TnC are underlined. Arrows are shown to indicate the splice points used to originally construct the CaM-TnC chimeras. This figure is based upon previously published studies (Su *et al.*, 1995; Gachhui *et al.*, 1998).

Previous investigations utilized the exchanging of these domains or EF hand motifs between CaM and TnC to find specific regions that affect the activation of CaM-dependent enzymes (George *et al.*, 1993; Su *et al.*, 1995; George *et al.*, 1996; Gachhui *et al.*, 1998; Wang *et al.*, 1998). Chimeras of CaM including each of the four EF hands from TnC have been constructed (e.g. CaM-1TnC contains EF hand I of TnC and EF hands II, III and IV of CaM) (Su *et al.*, 1995; Gachhui *et al.*, 1998).

There is a significant interest in better understanding the structural basis of CaM's ability to interact with a wide variety of target protein, including the NOS isozymes. A previous study on enzyme binding and activation in our laboratory using both nNOS and eNOS demonstrated important differences in the effect that oxidation of CaM methionines has upon the cNOS enzymes

(Montgomery *et al.*, 2003). Moreover, very little was known about the interaction of CaM and activation of the iNOS enzyme at the time of this study.

This study was designed to evaluate the role of the four different CaM EF hands in the activation of the eNOS and iNOS enzymes. Five different CaM-TnC chimeras were used in the investigation: CaM- 1TnC, CaM-2TnC, CaM-3TnC, CaM-4TnC, and CaM-3,4TnC (Figure 2.2).

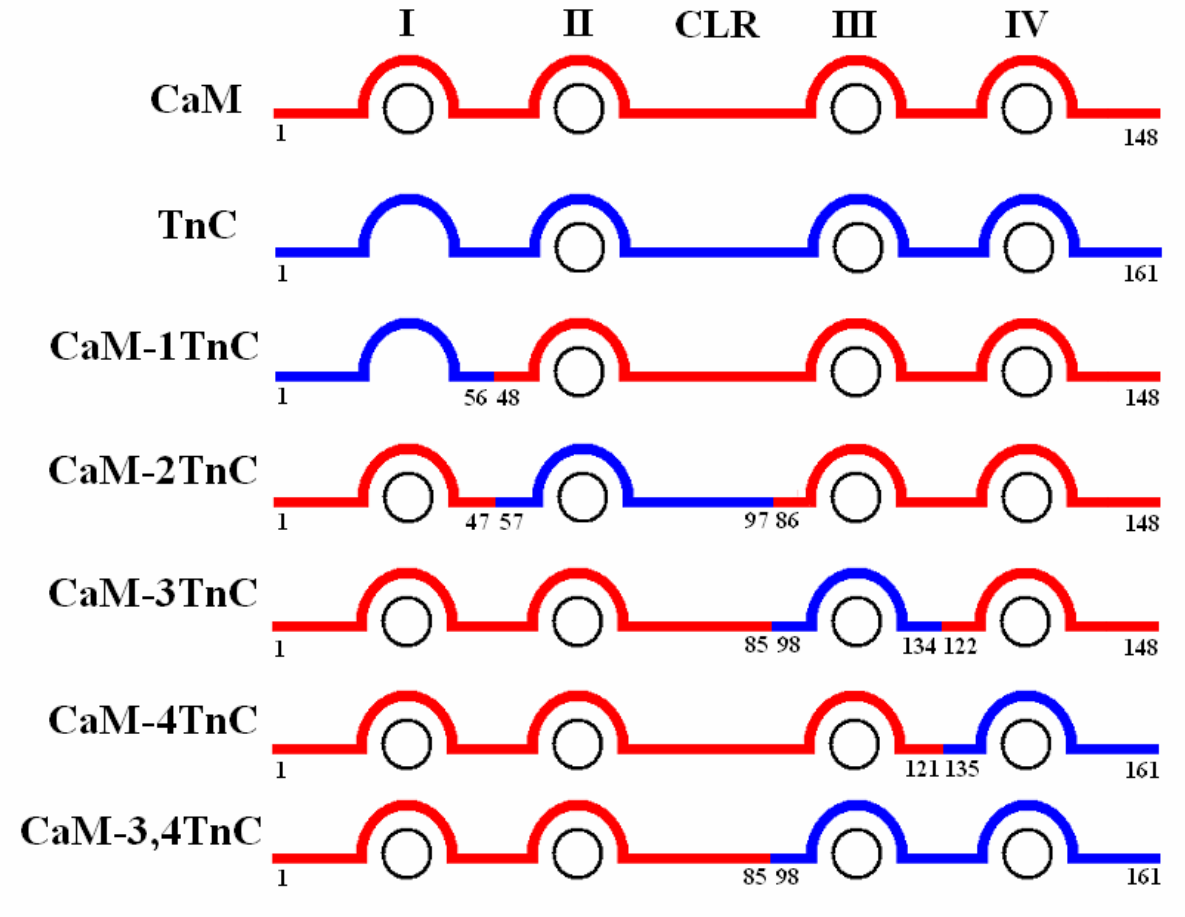

Figure 2.2 – Alignment of CaM and CaM-TnC chimera proteins.
Ca^{2+} ions are represented as circles, CaM and TnC proteins (and fragments) are shown in red and blue, respectively. EF hands and central linker are indicated for clarity purposes.

To assess the role of different CaM regions on aspects of NOS enzymatic function, three distinct activities associated with NOS were studied: 1) electron transfer from NADPH to the reductase

complex (measured by NADPH oxidation); 2) electron transfer from FMN to an acceptor (measured by cytochrome *c* reduction); and 3) electron transfer to the heme (measured by generation of •NO using the oxyhemoglobin capture assay). These biochemical studies with the different CaM-TnC chimeras show marked differences in the binding and activation of iNOS and cNOS enzymes by CaM. Although each of the CaM-TnC chimeras are able to bind to iNOS, EF hands II and III of CaM show Ca^{2+}-dependent activation of the enzyme.

This project was originally designed and started by Mrs. Elena Newman (MSc. 2003, U of Waterloo) with the initial purification and kinetic analyses performed at the conclusion of her thesis. Subsequent to Mrs. Newman's graduation, the candidate completed this study and performed all of the analyses reported in this chapter unless otherwise stated in the experimental procedures section (section 2.2).

2.2 Experimental Procedures

2.2.1 Cloning of CaM-TnC Chimera

The subcloning of CaM-1TnC, CaM-3TnC, CaM-4TnC and CaM-3,4TnC used in this study were performed by Mrs. Elena Newman (MSc. 2003, U of Waterloo), a previous graduate student in our laboratory. The vectors pCaM-1TnCAmp, pCaM-3TnCAmp, pCaM-4TnCAmp and pCaM-3,4TnCAmp were a generous gift from Dr. Dipak Ghosh (Duke University and VA Medical Center, Durham, NC, USA). Their ampicillin resistance necessitated the construction of new vectors for coexpression with iNOS (section 2.2.8). Coding regions for CaM-1TnC, CaM-3TnC, CaM-4TnC and CaM-3,4TnC were subcloned into the kanamycin resistant pET28a vector (Novagen) plasmid using the unique flanking *Nco*I and *Nde*I restriction sites. The resulting vectors, pCaM-1TnCKan, pCaM-3TnCKan, pCaM-4TnCKan and pCaM-3,4TnCKan, were verified by DNA sequencing.

The coding region of CaM-2TnC was cloned into pET28a by Mrs. Elena Newman and the candidate. The vector pCaM-2TnCAmp was a gift from Dr. Ghosh. The coding region of CaM-2TnC was PCR amplified from the pCaM-2TnCAmp plasmid introducing unique flanking *Nco*I and *Nde*I cut sites for subcloning into a vector suitable for coexpression. Primers used were: 2TnCfor 5' GAATACCATGGCAGATCAGCTGACTGAGAAAC 3' and 2TnCrv 5' GGAATTCAAGCTTCATATGTCACTTCGCTGTCATCATTTG 3'. The 475 bp PCR product was blunt end ligated into the *Srf*I site of pPCR-SCRIPT Amp SK (+). The pCaM-2TnCPCRscript vector was subsequently digested with *Nco*I and *Nde*I and subcloned into the kanamycin resistant pET28a vector (Novagen) cut with the same enzymes. The resulting pCaM-2TnCKan vector was verified by sequencing.

2.2.2 Expression of Wild-type CaM

The open reading frame of rat CaM was cloned into the kanamycin resitant pET9d vector (Novagen) by Mrs. Elena Newman (MSc. 2003, U of Waterloo) to produce pET9dCaM. An overnight culture of transformed *E. coli* BL21 (DE3) with pET9dCaM was used to inoculate 2 x 1 L of LB media in 4 L flasks supplemented with 30 μg/ml of kanamycin. These 1 L cultures were grown at 37ºC, 200 rpm to an O.D. at 600 nm of 0.6 – 0.8, induced with 500 μM IPTG and harvested after 3 to 4 hours of protein expression. Cells were harvested by centrifugation at 6000 x g at 4ºC for 5 minutes, flash frozen on dry ice, and subsequently stored at –80ºC.

2.2.3 Purification of Wild-type CaM

Cells were thawed on ice, resuspended in 4 volumes of 50 mM MOPS, 100 mM KCl, 1 mM EDTA, 1 mM DTT, pH 7.5 and lysed by homogenization using an Avestin EmulsiFlex-C5 homogenizer (Ottawa, ON). The lysate was then clarified by centrifugation at 48,000 x g for 30 minutes at 4ºC. A CaM purification protocol previously published was followed (Gopalakrishna and Anderson, 1982) with a few modifications. All of the following steps were carried out at 4ºC in a fridge or on ice. To the clarified supernatant, $CaCl_2$ was added to a concentration of 5 mM in order to saturate CaM with Ca^{2+} and induce the exposure of hydrophobic patches in the N- and C-domains of CaM to allow CaM to interact with the resin. This Ca^{2+}-saturated supernatant was then loaded onto 20 mL of phenyl sepharose 6 fast flow highly-substituted resin (GE Healthcare Bio-Sciences, Baie d'Urfe, PQ) in a 1 cm x 30 cm Econo-column (Bio-Rad Laboratories, Mississauga, ON) equilibrated with Buffer A (50 mM Tris-HCl, 1 mM $CaCl_2$, pH 7.5 @ 4ºC). After the Ca^{2+}-saturated solution was loaded, the resin was washed with 100 mL of Buffer A (5 column volumes). The resin was subsequently washed with 80 mL of Buffer B (4 column volumes of 50 mM Tris-HCl, 500 mM NaCl, 1 mM $CaCl_2$, pH 7.5 @ 4ºC) to remove any non-specific proteins that were interacting with the resin. The resin was finally washed with 50 mL of Buffer A (2.5 column volumes) to remove NaCl from the resin. Wild-type

CaM was then eluted from the phenyl sepharose resin with approximately 30 mL of Buffer C (10 mM Tris-HCl, 10 mM EDTA, pH 7.5 @ 4°C) and 2 mL fractions were collected. Fractions were then scanned from 325 to 250 nm on a Varian Cary UV–visible Spectrophotometer (Varian, Mississauga, ON). Fractions displaying the characteristic absorbance peaks of CaM at 277 nm (for tyrosine residues) and 269, 265, 259, and 253 nm (for phenylalanine residues) were pooled and dialysed overnight against 1 L of Buffer A using 6-8000 MWCO dialysis tubing (VWR International, Mississauga, ON). The normalized absorbance scan of purified wild-type CaM showing peaks at 277, 269, 265, 259, and 253 nm is shown in Figure 2.3.

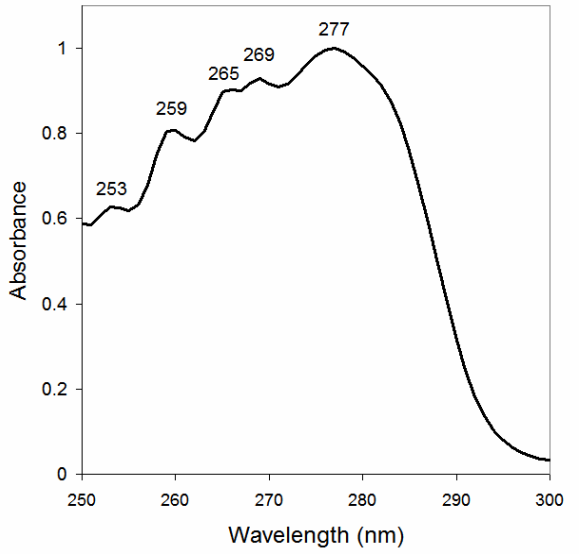

Figure 2.3 – UV-absorbance scan of wild-type CaM
This scan demonstrates the unique absorbance peaks of wild-type CaM found at 277, 269, 265, 259, and 253 nm. Due to the absence of tryptophan residues in CaM, the major peak at 277 nm corresponds to the 2 tyrosine residues located in the C-terminal domain of CaM, while the other peaks represent the numerous phenylalanine residues found throughout CaM depending upon their environment.

Dialysis tubing was prepared by boiling 0.5 L MQH_2O with 200 mg of EDTA and 200 mg sodium bicarbonate for 10 – 20 minutes, followed by extensive rinsing with MQH_2O. Prior to aliquoting the protein for storage, the concentration of CaM was determined using the ε_{277} of 3029 $M^{-1}cm^{-1}$ for CaM

saturated with Ca^{2+} (Gao *et al.*, 1998) or using the Lowry method (Lowry *et al.*, 1951) with wild-type CaM used as the protein standard. The purified wild-type CaM was then aliquoted, flash frozen on dry ice and stored at –80°C.

2.2.4 CaM-TnC Expression and Purification

The CaM-TnC proteins were expressed in *E. coli* BL21(DE3) transformed with pCaM-1TnCKan, pCaM-2TnCKan, pCaM-3TnCKan, pCaM-4TnCKan or pCaM-3,4TnCKan as previously described for wild-type CaM (section 2.2.1). The CaM-TnC proteins were purified using the same procedure used to purify wild-type CaM (section 2.2.3).

2.2.5 Electrospray Ionization-Mass Spectrometry of CaM and CaM Proteins

Electrospray ionization-mass spectrometry (ESI-MS) using a Quadrupole Time-Of-Flight (QTOF) spectrometer (Micromass, Manchester, UK) with an internal standard was then performed on the purified CaM protein to ensure that no posttranslational modifications had occurred. Wild-type CaM was prepared for ESI-MS by transferring the protein into water using a Ym10 centrifugal filter device (Millipore, Billerica, MA, USA) and then diluted using a 1:1 CH_3CN/water solution containing 0.2% formic acid to a concentration of approximately 20 μM. The samples were infused at 10 μl/min. Raw data (m/z) were processed using MaxEnt1 software to yield spectra on a true molecular mass scale.

2.2.6 eNOS and nNOS Expression

Bovine eNOS and rat nNOS were expressed in *E. coli* BL21 (DE3) containing pGroESLChlor co-transformed with peNOShisAmp and pnNOShisAmp. The ampicillin resistant vectors, peNOShisAmp and pnNOShisAmp, contained the coding regions for bovine eNOS or rat nNOS cloned into pCWOri with upstream poly-histidine tags to aid in their purification (section 2.2.7). The original vectors coding for bovine eNOS, rat nNOS, and GroESL were a generous gift from Dr. Betty Sue Masters (University of Texas Health Science Center at San Antonio, San Antonio, TX, USA).

The chloramphenicol resistant pGroESLChlor vector contained the coding regions for GroESL, a molecular chaperone used to help with the proper folding of eNOS and nNOS during protein expression. An overnight culture of transformed *E. coli* BL21 (DE3) with peNOShisAmp and pGroESLChlor or pnNOShisAmp and pGroESLChlor were used to inoculate 3 x 1 L of TB media in 4 L flasks supplemented with 100 μg/ml of ampicillin and 30 μg/ml of chloramphenicol. These 1 L cultures were grown at 37ºC, 200 rpm to an O.D. at 600 nm of 1 – 1.2 and were induced. Induction of these cultures involved the addition of IPTG (500 μM), δ-aminolevulinic acid (δ-ALA, 400 μM; precursor for heme production), ATP (500 μM; for GroESL assembly and activity), ~100 mg of riboflavin (precursor for flavin production) and trace metals (9.6 mg/L $FeSO_4 \bullet 7H_2O$, 2.4 mg/L $MnSO_4 \bullet H_2O$, 2.4 mg/L $AlCl_3 \bullet 6H_2O$, 1.0 mg/L $CoCl_2 \bullet 6H_2O$, 0.5 mg/L $ZnSO_4 \bullet 7H_2O$, 2.4 mg/L $Na_2MoO_4 \bullet 2H_2O$, 0.1 mg/L $CuCl_2 \bullet 2H_2O$, and 0.5 mg/L H_3BO_3). The temperature of the shaker was then lowered to 25^{o}C, 200 rpm. After 40 hours of protein expression, the cells were harvested by centrifugation at 6000 x g at 4^{o}C for 5 minutes, flash frozen on dry ice, and subsequently stored at – 80ºC.

2.2.7 eNOS and nNOS Purification

The overall purification of the NOS enzymes involved the use of ammonium sulfate precipitation, followed by metal chelation chromatography, and finally 2'5' ADP-sepharose chromatography. Cells were thawed on ice, resuspended in 4 volumes of NOS Lysis buffer consisting of 40 mM Tris-HCl, pH 7.5 @ 4^{o}C, 10% glycerol, 1 mM L-arginine, 10 μM H_4B, 3 mM ascorbic acid, 150 mM NaCl, 1 mM PMSF, 4 μg/mL leupeptin, 2 μg/mL aprotinin, 3.5 μg/mL E64, and 0.6 μg/mL peptstatin. The numerous protease inhibitors were added to help decrease the proteolysis of the cNOS enzymes during their purification, as previously reported (Siddhanta *et al.*, 1998). The cells were subsequently lysed by homogenization using an Avestin EmulsiFlex-C5 homogenizer (Ottawa, ON). The lysate was then clarified by centrifugation at 48,000 x g for 30 minutes at 4^{o}C. A purification protocol to

purify eNOS and nNOS that was previously published was followed (Roman *et al.*, 1995) with a few modifications. All of the following steps were carried out at 4°C in a fridge or on ice. To the clarified supernatant, ammonium sulfate was added to 65% (373 mg/mL), stirred for 1 hour, and subsequently centrifuged at 48,000 x g for 30 minutes at 4°C to harvest the precipitated proteins. The ammonium sulfate pellets were then resuspended in a ~100 mL of NOS Pellet buffer (40 mM Tris-HCl, pH 7.5 @ 4°C, 10% glycerol, 1 mM L-arginine, 250 mM NaCl, and 1 mM PMSF). Prior to loading the protein onto 20 mL of Ni^{2+}-chelating resin (Novagen, La Jolla, CA, USA) in a 1 cm x 30 cm Econo-column (Bio-Rad Laboratories, Mississauga, ON), the resin was charged by washing the column with 3 column volumes of 100 mM $NiSO_4$ and equilibrated with 5 column volumes of NOS Pellet buffer. The resuspended ammonium sulfate pellets were then slowly mixed with charged Ni^{2+}-chelating resin equilibrated with NOS Pellet buffer for 1 hour with the addition of an EDTA-free complete protease inhibitor tablet (Roche, Mississauga, ON). The NOS loaded Ni^{2+}-chelating resin was then poured back into the 1 cm x 30 cm Econo-column. The column was subsequently washed with 10 column volumes of NOS Pellet buffer followed by 5 column volumes of 20 mM imidazole in NOS Pellet buffer. The NOS protein was eluted with 200 mM imidazole in NOS Pellet buffer and the most concentrate eluted fraction (~5 mL) was collected.

Prior to loading the protein onto the 2'5' ADP-sepharose resin, the resin was regenerated using three cycles of alternating washes (2 column volumes each wash) with ADP Regeneration Solution 1 (0.1 M Tris-HCl, 0.5 M NaCl, pH 8.5) and ADP Regeneration Solution 2 (0.1 M sodium acetate, 0.5 M NaCl, pH 4.5). Following the regeneration of the column, the 2'5' ADP-sepharose resin was equilibrated with 10 column volumes of ADP Wash buffer (50 mM Tris-HCl, pH 7.5 @ 4°C, 10% glycerol, 100 µM L-arginine, 100 mM NaCl, 1 mM DTT, and 0.1 mM PMSF). The eluted cNOS protein from the metal chelation chromatography column was then diluted with 2 volumes of ADP Wash buffer and loaded onto ~5 mL of 2'5' ADP-sepharose resin (GE Healthcare Bio-Sciences,

Baie d'Urfe, PQ) in a 1 cm x 20 cm Econo-column (Bio-Rad). The loaded resin was then washed with 5 column volumes of ADP Wash buffer, followed by 5 column volumes of ADP Salt Wash buffer (50 mM Tris-HCl, pH 7.5 @ 4°C, 10% glycerol, 100 μM L-arginine, 500 mM NaCl, 1 mM DTT, and 0.1 mM PMSF). The saturated 2' AMP (10 mM) dissolved in ADP Salt Wash buffer (which was warmed at 37°C to help solubilize the 2' AMP) was then used to elute the NOS enzyme and collected in 1-2 mL fractions. Eluted fractions demonstrating the appropriate absorbance peaks between 700 and 300 nm were then pooled and dialyzed at 4°C against 1 L of NOS Dialysis buffer 1 (50 mM Tris-HCl, pH 7.5 @ RT, 10% glycerol, 5 μM L-arginine, 250 mM NaCl, 1 mM DTT, 4 μM H_4B, 3 mM ascorbic acid, and 0.1 mM PMSF) using 6-8000 MWCO dialysis tubing (VWR International, Mississauga, ON). After 3 hours, the NOS sample was transferred into 1 L of NOS Dialysis Buffer 2 (identical to NOS Dialysis Buffer 1 with 100 mM NaCl) and allowed to dialyze overnight at 4°C. Using NOS Dialysis buffer 2 as a baseline, the purified NOS protein was then scanned from 700 to 300 nm and the concentration was determined using the ε_{397} of 72 mM^{-1} cm^{-1} (Stuehr and Ikeda-Saito, 1992). The normalized absorbance scans of purified nNOS and eNOS showing a peak at 397 nm are shown in Figure 2.4.

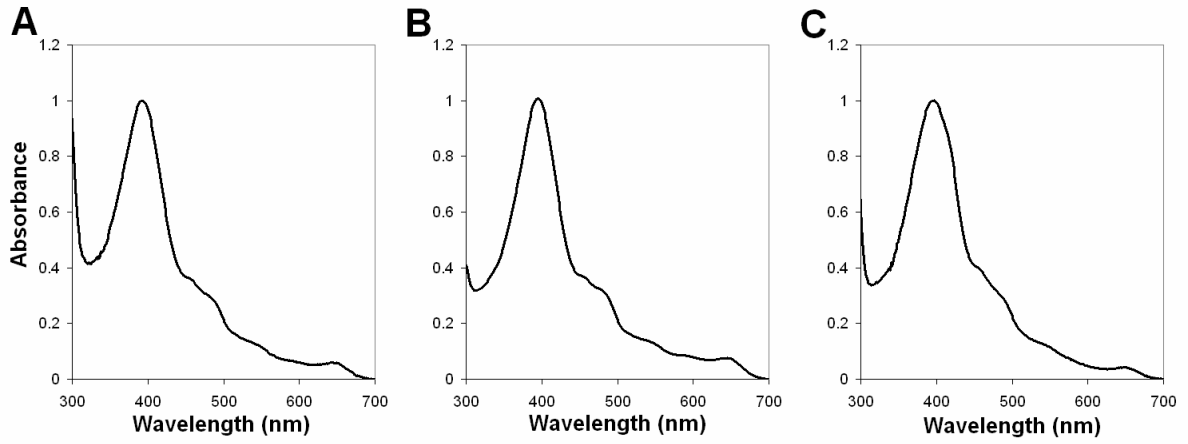

Figure 2.4 – UV-visible absorbance scan of (A) nNOS, (B) eNOS, and (C) iNOS coexpressed with wild-type CaM.
This scan demonstrates the typical absorbance peaks of nNOS, eNOS, and iNOS coexpressed with wild-type CaM at 397 (ferric heme), and 450 and 475 nm (flavins). The absorbance of a pure NOS preparation typically demonstrated a 397 nm / 450 nm ratio of 2.5-3.

If the NOS protein was lower than 2 μM, the NOS protein was concentrated using a Vivaspin 15 ultrafiltration spin column (Sartorius AG Biotechnology, Goettingen, Germany) until the desired concentration was obtained. The purified eNOS and nNOS protein was then aliquoted, flash frozen on dry ice, and subsequently stored at –80^{o}C.

2.2.8 iNOS coexpression with wild-type CaM or CaM-TnC Chimeras

pΔ70iNOShisAmp, a vector coding for human iNOS carrying a deletion of the first 70 amino acids and an N-terminal polyhistidine tail in the ampicillin expression vector pCWOri, was used for the expression of iNOS. This protein will be referred to as iNOS throughout this thesis. The Δ70iNOS was expressed to minimize the proteolysis of iNOS during expression, as well as the numerous rare codons (ie. Arg, AGA/AGG and Pro, CCC) found in the 5' coding region. In order to coexpress iNOS with wild-type CaM and each of the CaM-TnC chimeric proteins, pΔ70iNOShisAmp was co-transformed with a wild-type CaM vector (pCaMChlor) or a CaM-TnC chimera vector (pCaM-1TnCKan, pCaM-2TnC, pCaM-3TnCKan, pCaM-4TnCKan and pCaM-3,4TnCKan) into *E. coli*

BL21 (DE3). For iNOS coexpressed with wild-type CaM, an overnight culture of transformed *E. coli* BL21 (DE3) with pΔ70iNOShisAmp with pCaMChlor was used to inoculate 3 x 1 L of TB media in 4 L flasks supplemented with 100 μg/ml of ampicillin and 30 μg/ml of chloramphenicol. For iNOS coexpressed with CaM-TnC chimeric proteins, BL21 (DE3) pΔ70iNOShisAmp with each of the CaM-TnC chimera vectors were used to inoculate 3 x 1 L of TB media in 4 L flasks supplemented with 100 μg/ml of ampicillin and 30 μg/ml of kanamycin. These 1 L cultures were grown at 37ºC, 200 rpm to an O.D. at 600 nm of 1 – 1.2 and were induced. Induction of these cultures involved the addition of IPTG (500 μM), δ-ALA (400 μM), ~100 mg of riboflavin, and trace metals (as described in section 2.2.6). The temperature of the shaker was then decreased to 25^{o}C, 200 rpm. After 40 hours of protein expression, the cells were harvested by centrifugation at 6000 x g at 4^{o}C for 5 minutes, flash frozen on dry ice, and stored at –80ºC.

2.2.9 Purification of iNOS coexpressed with wild-type CaM or CaM-TnC Chimeric Proteins

The purification of iNOS coexpressed with wild-type CaM followed the same protocol used for eNOS and nNOS (section 2.2.7) with the exception of a 45% ammonium sulfate precipitation (278 mg/mL).

The purification of iNOS coexpressed with CaM-TnC chimeric proteins also followed the protocol used for eNOS and nNOS (section 2.2.7) with the following modifications. 10 mM $CaCl_2$ was added to NOS Lysis, ADP Wash, and ADP Salt Wash buffers in order to stabilize the interaction between the mutant CaM proteins and iNOS. Due to numerous attempted purifications of iNOS coexpressed with mutant CaM proteins, the metal chelation chromatography step was avoided due to the higher susceptibility of NOS being proteolytically cleaved. Following the lysis of the cells and the 45% ammonium sulfate precipitation, the ammonium sulfate pellet was resuspended in ~100 mL of ADP Wash buffer, followed by slow mixing with 2'5' ADP-sepharose resin equilibrated with ADP

Wash buffer for 1 hour with the addition of an EDTA-free complete protease inhibitor tablet (Roche). The NOS loaded 2'5' ADP-sepharose resin was then poured into a 1 cm x 20 cm Econo-column (Bio-Rad). The column was subsequently washed with ADP Wash and ADP Salt Wash buffers. The iNOS protein was then eluted with 2' AMP, scanned and dialysed against NOS Dialysis buffers 1 and 2, as previously described (section 2.2.7). The normalized absorbance scan of purified iNOS coexpressed with wild-type CaM showing a peak at 397 nm is shown in Figure 2.4C.

The concentration of iNOS coexpressed with wild-type CaM or iNOS coexpressed CaM-TnC chimeric proteins were then determined using the ε_{397} of 72 mM^{-1} cm^{-1}, aliquoted, flash frozen on dry ice, and stored at –80^{o}C as previously described (section 2.2.7).

2.2.10 Spectrophotometic Kinetic Assays

Four frequently used kinetic assays employed to measure rates of electron transfer in the NOS enzymes are the NADPH oxidation, ferricyanide reduction, cytochrome *c* oxidation, and oxyhemoglobin capture assay (Figure 2.5). These assays are described in the following sections, with the exception of the ferricyanide assay, which was used exclusively in Chapter 5 (section 4.2.4.1).

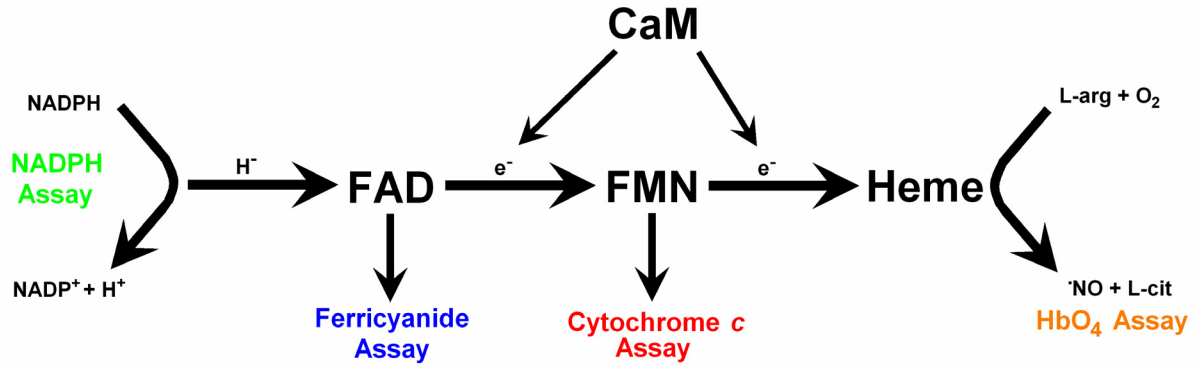

Figure 2.5 – Spectrophotometric assays employed to monitor electron transfer within the NOS enzymes.
(1) *The NADPH assay* measures the oxidation of NADPH to $NADP^+ + H^+$ by monitoring decreases in absorbance at 340 nm. (2) *The ferricyanide assay* measures the hydride transfer to the FAD by monitoring the reduction of Fe(III) to Fe(II) with decreases at 420 nm. (3) *The cytochrome c assay* measures electron transfer through the reductase domain to the FMN by monitoring the reduction of cytochrome *c* with increases at 550 nm. (4) *The oxyhemoglobin (HbO_4) capture assay* measures the production of •NO from L-arginine by monitoring the conversion of oxy to methemoglobin at 401 nm.

2.2.10.1 Oxyhemoglobin Capture Assay

2.2.10.1.1 Oxyhemoglobin Preparation

A 15 mL falcon tube was filled with approximately 5 mL of loosely packed hemoglobin crystals (Sigma) and dissolved in the minimal amount (~2 – 2.5 mL) of 50 mM Tris-HCl, pH 7.5 at room temperature. The total volume of dissolved hemoglobin was approximately 4 – 5 mL and the solution was then kept on ice. Approximately 10 – 20 mg of sodium hydrosulfite was subsequently added to the hemoglobin solution and the tube was inverted several times to thoroughly mix the sample. The hemoglobin solution should turn from a brown to a "cherry" red tinge after the addition of sodium hydrosulfite. Four PD10 gel filtration columns (GE Healthcare) were then equilibrated with Tris buffer which involved washing each column with 25 mL MQH_2O, followed by 25 mL of 50 mM Tris-HCl, pH 7.5 @ RT. One mL of the hemoglobin solution was then loaded onto each PD column. The "ruby" red oxyhemoglobin was then collected and the last few drops were not collected to avoid

contamination with any excess sodium hydrosulfite. The collected oxyhemoglobin was subsequently aliquoted (200 μL), flash frozen on dry ice and stored at –80°C. A spectrophotometric scan was taken from 700 to 350 nm using a 0.2 cm quartz cuvette before and after reduction by sodium hydrosulfite to ensure that the reduction of the hemoglobin was complete. Using the reduced hemoglobin scan, the concentration of oxyhemoglobin in μM was then determined using the following equation:

Equation 2.1 $[HbO_4]\ \mu M = (1.013 \times A_{576} - 0.3269 \times A_{630} - 0.7353 \times A_{560}) \times 100 \times \text{dil. factor} \times 5$

where A_{576}, A_{630}, and A_{560} represent the absorbance value at 576, 630, and 560 nm respectively. The 100 comes from a previous published equation in μM (Hevel and Marletta, 1994), which was based upon the previously solved extinction coefficients of oxyhemoglobin by Benesch and coworkers (Benesch *et al.*, 1973) whose extinction coefficients were expressed in $cm^{-1}M^{-1}$ values. For example, $\varepsilon_{576} = 1.013 \times 10^{-4}\ cm^{-1}M^{-1}$ by Benesch is equivalent to $\varepsilon_{576} = 1.013 * 10^{2}\ cm^{-1}\mu M^{-1}$ published by Hevel. The multiplication factor of 5 was necessary since a 0.2 cm cuvette was used.

2.2.10.1.2 Oxyhemoglobin Calibration

The molar extinction co-efficient for the conversion of oxy- to methemoglobin for the oxyhemoglobin capture assay was calculated based upon a previously used method developed by Dr. Heather Montgomery (PhD. 2004, U of Waterloo) and Dr. Basil Perdicakis (PhD. 2003, U of Waterloo), which was based upon a previously published method (Gross, 1996). Oxyhemoglobin was oxidized to methemoglobin by the addition of potassium ferricyanide ($K_3Fe(CN)_6$). A 12 mM stock solution of $K_3Fe(CN)_6$ was prepared by dissolving 40 mg of $K_3Fe(CN)_6$ in 10 mL of 50 mM Tris-HCl, pH 7.5 @ RT, which was subsequently diluted 1 in 10 with 50 mM Tris-HCl to obtain a 1.2 mM $K_3Fe(CN)_6$ working stock solution. The previously prepared oxyhemoglobin solution was diluted to 40 μM stock solution in 50 mM Tris-HCl, pH 7.5 @ RT to produce the oxyhemoglobin working solution. The methemoglobin working solution was prepared by diluting oxyhemoglobin to 40 μM in the presence

of 0.12 mM $K_3Fe(CN)_6$. 200 µL of the oxyhemoglobin and methemoglobin working solutions were added to 3 wells each on a 96 well microtitre plate (ie. oxy- into wells A1-3, and met in wells A4-6). 100 µL of 50 mM Tris-HCl, pH 7.5 @ RT was then added to rows B-H of columns 1-3, while 50 mM Tris-HCl, 0.12 mM $K_3Fe(CN)_6$, pH 7.5 @ RT was added to rows B-H of columns 4-6 of the microtitre plate in preparation for the serial dilution of oxy- and methemoglobin. Using a milti-channel pipettor, serial dilutions were performed by transferring 100 µL of row A to row B, row B to row C, etc. to row G, where the final 100 µL was removed. Row H was used as the blank. Each dilution was performed in triplicate. Figure 2.6 is shown to help clarify the serial dilution of oxy- and methemoglobin in the microtitre plate.

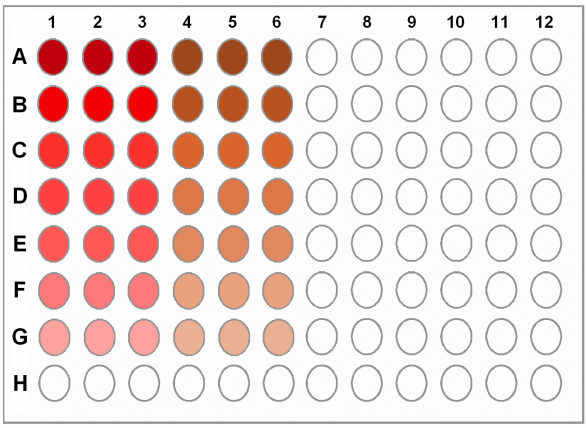

Figure 2.6 – Calibration of oxyhemoglobin in a 96 well microtitre plate using serial dilutions. Columns 1-3 and 4-6 contain oxy- and methemoglobin, respectively. Initially, Row A contained 200 µL of 40 µM oxy- or methemoglobin. Using a multi-channel pipettor, serial dilutions of oxy- and methemoglobin were performed by sequentially transferring 100 µL from Row A into row B, etc. Rows A to G contain 40, 20, 10, 5, 2.5, 1.25 and 0.625 µM oxy- or methemoglobin. The control blanks for the plate are in Row H, as described in section 2.2.10.1.2.

The plate was then read at 401 nm in a SpectraMax 384 Plus 96 well UV-visible spectrophotometer using Soft Max Pro software (Molecular Devices, Sunnyvale, CA). The slopes of OD_{401} versus nanomoles of oxyhemoglobin and OD_{401} versus nanomoles of oxyhemoglobin were calculated using linear regression. The extinction coefficient ($\Delta\varepsilon_{410\ nm\ (met-\ to\ oxyhemoglobin)}$) used in the oxyhemoglobin

assay was determined by taking the difference between the slope of methemoglobin and the slope of oxyhemoglobin. This value ranged from 0.10 to 0.13 $OD_{401\ nm}$ per nanomole of hemoglobin, depending on the oxyhemoglobin preparation (section 2.2.10.1.1).

2.2.10.1.3 Oxyhemoglobin Capture Assay

The spectrophotometric oxyhemoglobin capture assay was used to assess the initial rate of •NO synthesis. This assay was previously developed by Dr. Heather Montgomery and Dr. Basil Perdicakis in our laboratory using 96 well microtitre plates (Perdicakis *et al.*, 2004). This assay involved the use of two separate solutions: (1) the enzyme solution and (2) the substrate solution. The enzyme solution consisted of the NOS enzyme in a 50 mM Tris-HCl, pH 7.5 @ RT buffer with 10 μM FAD, 10 μM FMN, 50 μM H_4B, 500 μM NADPH, 100 μM DTT, 50 U/mL catalase, 100 U/mL superoxide dismutase (SOD), 0.2 mg/mL bovine serum albumin and 10% glycerol. NADPH, DTT, and H_4B were prepared fresh on the day of the assay. H_4B was dissolved in the 20 mM DTT in order to ensure that it was in its reduced form (Hevel and Marletta, 1994; Dawson and Knowles, 1999). The NADPH was added to this solution to react with any L-arginine in the enzyme solution from the dialysis buffer of the NOS. SOD and catalase were added to this solution to react with any reactive oxygen species caused by uncoupled electron transfer in NOS (Hevel and Marletta, 1994). The inclusion of 10% glycerol and 0.2 mg/mL bovine serum albumin (BSA) were to maintain NOS enzyme stability. The substrate solution contained oxyhemoglobin, L-arginine, Tris-HCl, $CaCl_2$ or EDTA (depending on the enzyme being tested), NADPH, BSA, catalase, and SOD.

The assay reactions were performed by adding 10 μL of complete enzyme solution (NOS enzyme, with or without CaM, and enzyme solution), followed by a 2 minute incubation at 25°C. This incubation was included due to the previous finding that the $t_{1/2}$ of ^{125}I CaM binding to nNOS at 23°C was less than 2 minutes (Weissman *et al.*, 2002). Following the incubation, the assay was initiated by the addition of 90 μL of substrate solution to each well containing complete enzyme

solution, for a total of 100 µL per well. The final initiated reaction contained oxyhemoglobin (5 µM), L-arginine (25 µM), Tris-HCl (50 mM, pH 7.5 @ RT), glycerol (1 %), FMN (1 µM), FAD (1 µM), H_4B (5 µM), DTT (1 mM), NADPH (450 µM), BSA (0.18 mg/mL), catalase (50 U/mL), and SOD (100 U/mL). eNOS, nNOS, and iNOS coexpressed with CaM or mutant CaM protein were assayed at 70, 30, and 28.5 nM in 100 µL total well volume in quadruplicate. $CaCl_2$ (200 µM), EDTA (250 µM), and CaM (2 µM) or mutant CaM protein were added to the appropriate samples unless otherwise stated.

After initiation, the microtitre plate was read at 25 – 27°C in a SpectraMax 384 Plus 96 well UV-visible spectrophotometer using Soft Max Pro software (Molecular Devices, Sunnyvale, CA). The reactions were read at 401 nm over 5 minutes at 7 second intervals. Equation 2.2 was used to calculate the activity of the enzyme based upon the rate of absorbance change at 401 nm.

Equation 2.2 $$\text{Activity} = v \times 60\ \text{s} \bullet \text{min}^{-1} / \Delta\varepsilon_{410\ \text{nm (met- to oxyhemoglobin)}} / (\text{well volume} \times [\text{NOS enzyme}]\ \text{in nM} \times \text{NOS molecular weight in g/mol} \times 1000\ \text{mg/g})$$

where *v* represents the slope of the change of absorbance over time in seconds. Activity is expressed as nanomoles of •NO produced per minute per milligram of enzyme (nmol •NO min^{-1} mg^{-1}).

2.2.10.2 Cytochrome c Reduction Assay

2.2.10.2.1 Cytochrome c Preparation

A 15 mL falcon tube was filled with approximately 5 mL of loosely packed horse heart cytochrome *c* crystals (Sigma) and dissolved in the minimal amount (~ 2 – 2.5 mL) of 50 mM Tris-HCl, pH 7.5 at room temperature. The total volume of the dissolved cytochrome *c* was approximately 4 – 5 mL and the solution was then kept on ice. Approximately 10 – 20 mg of bis(dipicolinato)cobaltate (III) was added to the cytochrome *c* solution and the tube was inverted several times to thoroughly mix the sample. The solution should turn from a brown to a redish tinge after the addition of bis(dipicolinato)cobaltate (III). Four PD10 gel filtration columns (GE Healthcare) were then equilibrated with Tris buffer which involved washing each column with 25 mL MQH_2O, followed by 25 mL of 50 mM Tris-HCl, pH 7.5 @ RT. One mL of the cytochrome *c* solution was then loaded onto each PD column. The oxidized cytochrome *c* was then collected. The final few drops were not collected to avoid unwanted contamination with any excess bis(dipicolinato)cobaltate (III). The collected oxidized cytochrome *c* was then aliquoted (200 μL), flash frozen on dry ice and stored at –80^{o}C. A spectrophotometric scan was taken from 700 to 350 nm using a 0.2 cm quartz cuvette before and after oxidation by bis(dipicolinato)cobaltate (III) to ensure that the oxidation of the cytochrome *c* was complete. Using the oxidized cytochrome *c* scan, the concentration of cytochrome *c* in μM was then determined using the ε_{410} of 106.1 $mM^{-1}cm^{-1}$ (Margoliash and Frohwirt, 1959) and the following equation:

Equation 2.3 [Cytochrome *c*] μM = $(A_{410}/\varepsilon_{410})$ x dilution factor x 5 x 1000

where A_{410} represents the absorbance value at 410 nm. The multiplication factor of 5 was necessary since a 0.2 cm cuvette was used. The 1000 converts the solved concentration of cytochrome *c* from mM to μM.

2.2.10.2.2 Cytochrome c Calibration

The calibration of cytochrome *c* was performed in a similar manner to the calibration of oxyhemoglobin (section 2.2.10.1.2) with the exception that 500 μM DTT was used to reduce cytochrome *c* instead of $K_3Fe(CN)_6$. The dilutions of cytochrome *c* were performed in a 96 well microtitre plate, similar to that shown in Figure 2.6, over a concentration range of 20, 40, 60, 80, 100, 120 and 140 μM in the presence (red. cytochrome *c*) or absence (ox. cytochrome *c*) of DTT.

The plate was then read at 550 nm in a SpectraMax 384 Plus 96 well UV-visible spectrophotometer using Soft Max Pro software (Molecular Devices, Sunnyvale, CA). The slopes of OD_{550} versus nanomoles of reduced cytochrome *c* and OD_{550} versus nanomoles of oxidized cytochrome *c* were then calculated using linear regression. The extinction coefficient ($\Delta\varepsilon_{550\ nm\ (reduced\ cyt\ c\text{- to oxidized cyt } c)}$) used in the cytochrome *c* assay was determined by taking the difference between the slope of reduced cytochrome *c* and oxidized cytochrome *c*. Depending on the cytochrome *c* preparation, the extinction coefficient value ranged from 0.047 to 0.050 $OD_{550\ nm}$ per nanomole of cytochrome *c* (section 2.2.10.2.1).

2.2.10.2.3 Cytochrome c Assay

The spectrophotometric NADPH-dependent cytochrome *c* assay was used to assess the initial rate of electron transfer in the NOS reductase domain to the FMN domain. This assay was previously standarized by Dr. Heather Montgomery in our laboratory using 96 well microtitre plates. This assay was performed in a similar manner to the oxyhemoglobin capture assay (section 2.2.10.1.3) with the exception that no DTT or H_4B added. In order to observe the reduction of cytochrome *c* exclusively caused by NOS, DTT and H_4B were not included in this assay because of their ability to reduce cytochrome *c*. This assay involved the use of three separate solutions: (1) the enzyme solution, (2) the cytochrome *c* solution, and (3) the NADPH solution. The enzyme solution consisted of the NOS enzyme in a 50 mM Tris-HCl, pH 7.5 @ RT buffer with 10 μM FAD, 10 μM FMN, 200 μM NADPH,

10 U/mL catalase, 10 U/mL SOD, 0.1 mg/mL BSA and 10% glycerol. NADPH was prepared fresh on the day of the assay. The NADPH was added to this solution to react with any L-arginine in the enzyme solution from the dialysis buffer of the NOS. The cytochrome *c* solution contained cytochrome *c*, Tris-HCl, $CaCl_2$ or EDTA (depending on the enzyme being tested), BSA, catalase, and SOD. The NADPH solution contained only the NADPH used to initiate the assay.

The assay reactions were performed by adding 10 μL of complete enzyme solution (NOS enzyme, with or without CaM, and enzyme solution), followed by a 2 minute incubation at 25°C. Following the incubation, 50 μL of cytochrome *c* solution was added to each well containing the complete enzyme solution, followed by a 30 second incubation. After this brief incubation, the assay was initiated by the addition of 40 μL of NADPH solution to each well, for a total of 100 μL per well. The final initiated reaction contained cytochrome *c* (100 μM), Tris-HCl (50 mM, pH 7.5 @ RT), glycerol (1%), FMN (1 μM), FAD (1 μM), NADPH (200 μM), BSA (0.1 mg/mL), catalase (10 U/mL), and SOD (10 U/mL). eNOS, nNOS, and iNOS coexpressed with CaM or mutant CaM protein were assayed at 50, 5.5, and 5.5 nM in 100 μL total well volume in quadruplicate. $CaCl_2$ (200 μM), EDTA (250 μM), and CaM (2 μM) or mutant CaM protein were added to the appropriate samples unless otherwise stated.

After initiation, the microtitre plate was read at 25 – 27°C in a SpectraMax 384 Plus 96 well UV-visible spectrophotometer using Soft Max Pro software (Molecular Devices, Sunnyvale, CA). The reactions were read at 550 nm over 5 minutes at 7 second intervals. Equation 2.4 was used to calculate the activity of the enzyme based upon the rate of absorbance change at 550 nm.

Equation 2.4 $$\text{Activity} = v * 60\ \text{s} \bullet \text{min}^{-1} / \Delta\varepsilon_{550\ \text{nm (reduced cyt } c\text{- to oxidized cyt } c)} / (\text{well volume} \times [\text{NOS enzyme}]\ \text{in nM} \times \text{NOS molecular weight in g/mol} \times 1000\ \text{mg/g})$$

where *v* represents the slope of the change of absorbance over time in seconds. Activity is expressed as nanomoles of cytochrome *c* reduced per minute per milligram of enzyme (nmol red. cyt *c* min^{-1} mg^{-1}).

2.2.10.3 NADPH Oxidation Assay

The UV-spectrophotometric NADPH assay was used to monitor the initial rate of NADPH oxidation to $NADP^+$ by the reductase domain of the NOS enzymes. This assay, which was previously developed by Dr. Heather Montgomery, utilizes the difference in absorbance at 340 nm of NADPH (absorbant) and $NADP^+$ (non-absorbant) to monitor the rate of NADPH consumption by NOS. This assay was performed in an almost identical manner to the oxyhemoglobin capture assay (section 2.2.10.1.3). This assay involved the use of two separate solutions: (1) the enzyme solution and (2) the NADPH solution. The enzyme solution consisted of the NOS enzyme in a 50 mM Tris-HCl, pH 7.5 @ RT buffer with 10 μM FAD, 10 μM FMN, 50 μM H_4B, 3 mM DTT, 50 U/mL catalase, 100 U/mL SOD, 0.2 mg/mL BSA and 10% glycerol. NADPH, DTT, and H_4B were prepared fresh on the day of the assay, with H_4B was dissolved in the 20 mM DTT, as previously described (section 2.2.10.1.3). The NADPH was added to this solution to react with any L-arginine in the enzyme solution from the dialysis buffer of the NOS. SOD and catalase were added to this solution to react with any reactive oxygen species caused by uncoupled electron transfer in NOS. The NADPH solution contained NADPH, L-arginine, Tris-HCl, $CaCl_2$ or EDTA (depending on the enzyme tested), BSA, catalase, and SOD.

The assay reactions were performed by adding 10 μL of complete enzyme solution (NOS enzyme, with or without CaM, and enzyme solution), followed by a 2 minute incubation at 25°C. Following the incubation, the assay was initiated by the addition of 90 μL of NADPH solution to each well containing complete enzyme solution, for a total of 100 μL per well. The final initiated reaction contained NADPH (500 μM), L-arginine (5 mM), Tris-HCl (50 mM, pH 7.5 @ RT), glycerol (1%),

H_4B (5 μM), DTT (300 μM), BSA (0.2 mg/mL), catalase (50 U/mL), and SOD (100 U/mL). eNOS, nNOS, and iNOS coexpressed with CaM or mutant CaM protein were assayed at 100, 70, and 49 nM in 100 μL total well volume in quadruplicate. $CaCl_2$ (200 μM), EDTA (250 μM), and CaM (2 μM) or mutant CaM protein were added to the appropriate samples unless otherwise stated.

After initiation, the microtitre plate was read at 25 – 27°C in a SpectraMax 384 Plus 96 well UV-visible spectrophotometer using Soft Max Pro software (Molecular Devices, Sunnyvale, CA). The reactions were read at 340 nm over 5 minutes at 7 second intervals. Equation 2.5 was used to calculate the NADPH oxidase activity based upon the rate of absorbance change at 340 nm.

Equation 2.5 Activity = v x 60 s • min^{-1} / $\Delta\varepsilon_{340\ nm\ NADPH\ to\ NADP+)}$ / (well volume x [NOS enzyme] in nM x NOS molecular weight in g/mol x 1000 mg/g)

where v represents the slope of the change of absorbance over time in seconds. The extinction coefficient $\Delta\varepsilon_{340\ nm\ NADPH\ to\ NADP+}$ of -0.0152 OD_{340} per nanomole was used. Activity is expressed as nanomoles of NADPH oxidized per minute per milligram of enzyme (nmol NADPH ox. min^{-1} mg^{-1}).

2.3 Results

2.3.1 Protein Expression and Purification

Each of the expressed and purified CaM-TnC chimeric proteins yielded a high amount of protein ranging from 50 to 80 mg of protein/L of media, depending upon the CaM mutant. Purified CaM-TnC chimeras were then analyzed by SDS-PAGE and were judged to be over 95% homogeneous.

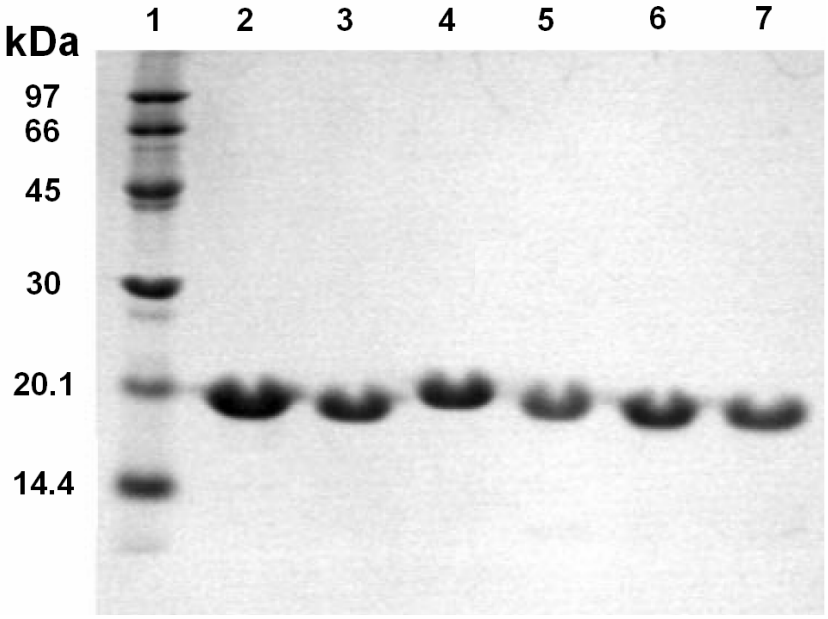

Figure 2.7 – SDS-PAGE of CaM-TnC chimeras.
The purified chimeras were run on a 15% SDS-polyacrylamide gel. Ten µg of each chimeric protein was loaded using buffer containing 5 mM EDTA. *Lane 1*, low molecular mass protein standard (Bio-Rad); *lane 2*, wild-type CaM; *lane 3*, CaM-1TnC; *lane 4*, CaM-2TnC; *lane 5*, CaM-3TnC; *lane 6*, CaM-4TnC; *lane 7*, CaM-3,4TnC.

These CaM-TnC proteins were analyzed in buffers containing EDTA because the chimeras undergo typical shifts toward lower apparent molecular weights when run in a Ca^{2+}-containing loading buffer (results not shown). Electrospray ionization-mass spectrometry was used to further assess the homogeneity of the CaM samples and rule out any modification (Table 2.1).

Table 2.1 – Masses of CaM-TnC Chimera proteins [a]

	Mass (Da) [b]	
CaM proteins	Observed	Theoretical
Wild-type CaM	16706.0	16706 [c]
CaM-1TnC	17795.6	17796
CaM-2TnC	17272.5	17273
CaM-3TnC	16732.3	16732
CaM-4TnC	16893.7	16895
CaM-3,4TnC	16948.3	16941

[a] ESI-MS results from Elena Newman, MSc. – University of Waterloo Thesis (2003)

[b] Masses of deconvoluted ESI-MS spectra were determined with an accuracy of ± 5 Da.

[c] Calculated masses based upon amino acid sequence.

In order to study the effect of the exchanged EF hand motifs in the CaM-TnC chimeric proteins, the iNOS enzyme was coexpressed with wild-type CaM and each of the individual CaM-TnC chimeras. The yield of protein varied depending upon the chimeric protein. iNOS coexpressed with wild-type CaM produced the highest yields of purified iNOS enzyme (5 mg/L media). The yields of iNOS obtained when the enzyme was coexpressed with either CaM-1TnC or CaM-2TnC (1.4 mg/L media) were more than double of the amount of iNOS obtained when coexpressed with CaM-3TnC, CaM-4TnC, or CaM-3,4TnC (0.3 to 0.7 mg/L). When comparing the amounts of iNOS produced when coexpressed with each of the CaM-TnC chimeras, a pattern emerged indicating that the chimeras expressing the C-terminal half of CaM better stabilized the iNOS enzyme. The visible spectra of the iNOS enzymes coexpressed with each of the CaM-TnC chimeras were very similar to wild-type CaM indicating that these enzymes contained proportionate heme and flavins cofactors (results not shown). All of the enzymes were capable of producing •NO based upon the

oxyhemoglobin assay indicating that stable, active enzyme was expressed with each of the mutant chimeric proteins.

2.3.2 cNOS Activation by CaM-TnC Chimeras

After performing the oxyhemoglobin capture, cytochrome *c* reduction, and NADPH oxidation assays, it was apparent that specific residues in EF hands I, III, and IV of CaM are important for nNOS activation. CaM-TnC chimeras containing TnC elements corresponding to any of these EF hands were only capable of activating •NO production from nNOS less than 20% when compared to wild-type CaM (Figure 2.8).

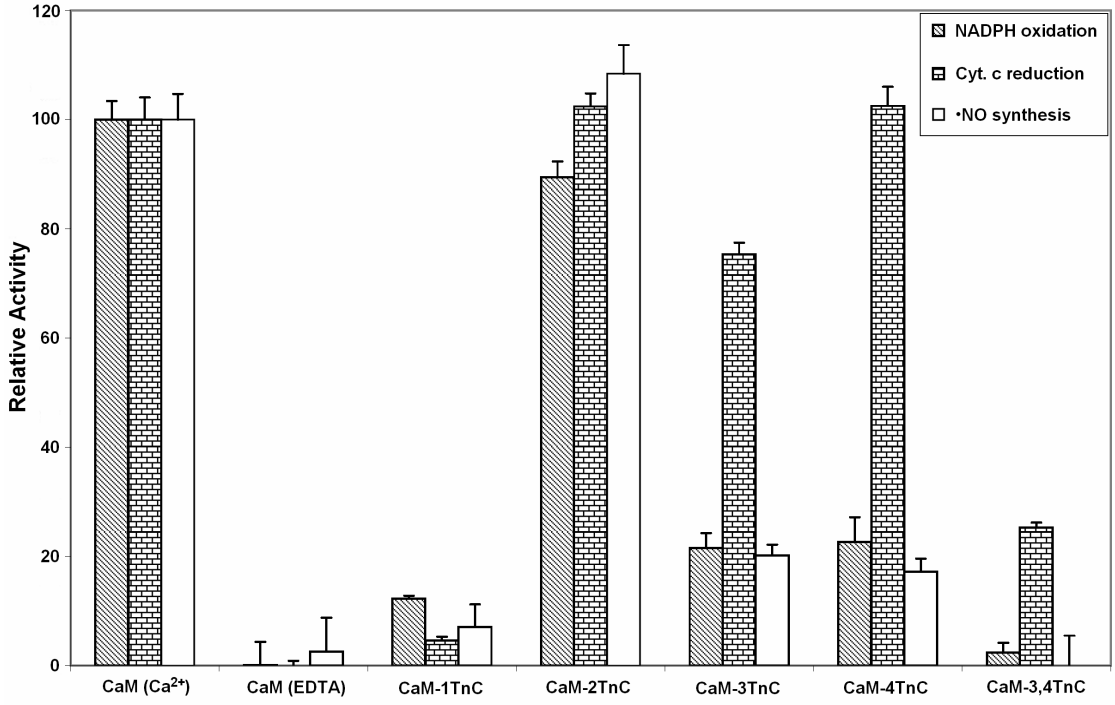

Figure 2.8 – Ability of CaM-TnC chimeras to activate nNOS.
The oxyhemoglobin capture assay, the cytochrome *c* assay, and the NADPH oxidation assay were performed in the presence of either wild-type CaM (2 μM) or CaM-TnC chimeric protein (2 μM) in the presence of either $CaCl_2$ (200 μM) or EDTA (250 μM), as indicated. The activities obtained with nNOS (30 nM) bound to wild-type CaM at 25 °C in the presence of 200 μM $CaCl_2$ were set to 100%. Under these conditions, the activities for nNOS bound to wild-type CaM were 148 min^{-1} for NADPH oxidation, 1163 min^{-1} for cytochrome *c* reduction, and 40 min^{-1} for •NO synthesis. The bar values represent the means ± standard deviation. Each assay was performed in quadruplicate and repeated three or more times.

In contrast, CaM-2TnC, the chimera containing TnC EF hand II, was able to fully activate •NO production by nNOS. Ranking the order the rates of •NO production by nNOS activated by the CaM-TnC chimeras was wild-type CaM ≈ CaM-2TnC >> CaM-3TnC ≈ CaM-4TnC > CaM-1TnC > CaM 3,4 TnC. All of the chimeras were unable to activate •NO production by nNOS in the presence of EDTA. These results are consistent with previous investigations of nNOS activation by CaM-TnC chimeras measured by the L-citrulline formation end point assay (Su *et al.*, 1995) and the oxyhemoglobin capture assay (Gachhui *et al.*, 1998).

This study was the first report on the activation of eNOS by CaM-TnC chimera. Ranking the initial rates of •NO production by eNOS activated by wild-type CaM and CaM-TnC chimera were as follows: wild-type CaM >> CaM-2TnC > CaM-4TnC > CaM-3TnC > CaM-1TnC > CaM-3,4TnC (Figure 2.9).

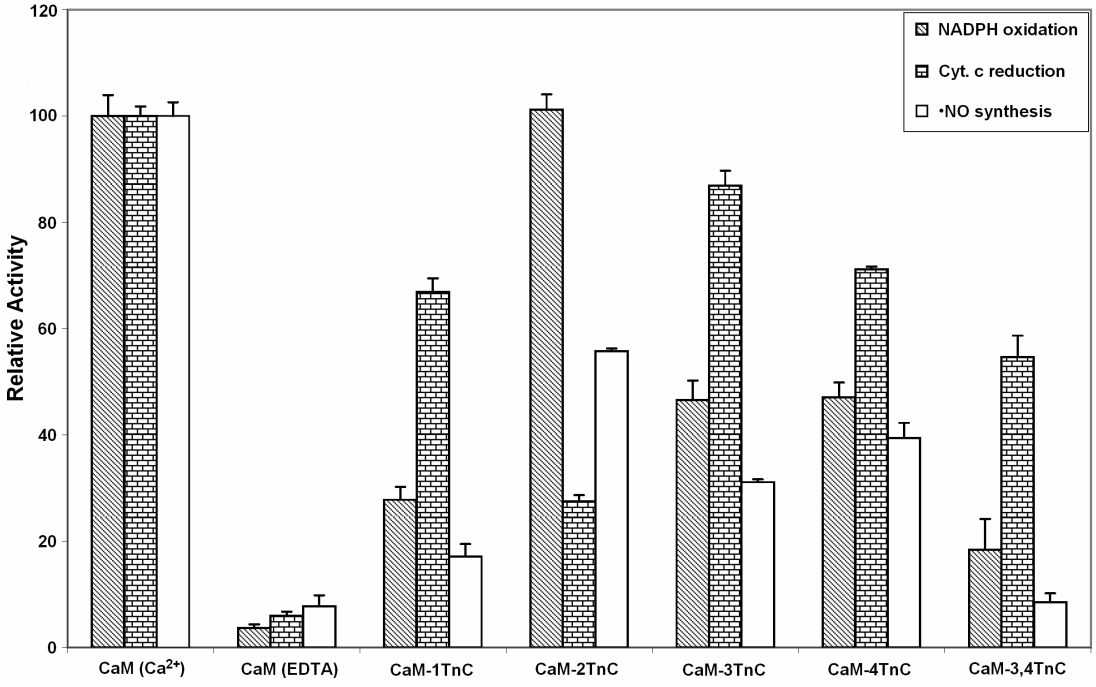

Figure 2.9 – Ability of CaM-TnC chimeras to activate eNOS.
The •NO synthesis, cytochrome *c* reduction, and NADPH oxidation rates were measured as previously described in Figure 2.8. The activities for eNOS (70 nM) bound to wild-type CaM (set to 100%) were 31 min^{-1} for NADPH oxidation, 70 min^{-1} for cytochrome *c* reduction, and 10 min^{-1} for •NO synthesis.

Although the order of activation for the eNOS was similar to that observed for nNOS, it is notable that CaM-2TnC was not able to fully activate the eNOS enzyme. With the exception of CaM-2TnC, all of the chimeras were able to activate •NO production by eNOS to a significantly greater extent than nNOS (Figure 2.9).

The activation of nNOS and eNOS by wild-type CaM resulted in an NADPH consumption to •NO production ratio of more than three instead of the theoretical ratio of 1.5. Similar results for eNOS were previously reported where the researchers reported that the higher relative NADPH consumption was associated with the redox cycling of exogenous unbound flavins added to the reaction buffer of the assay (Vasquez-Vivar *et al.*, 1998). The rate of NADPH oxidation by nNOS activated by either wild-type CaM or the CaM-TnC chimeric proteins showed the same ranking order observed for •NO production, indicating that the observed electron uncoupling from •NO synthesis may be related to the redox cycling of free flavins in the cNOS reductase domain. The observed ratio of NADPH oxidation to •NO synthesis was identical for nNOS activated by both wild-type CaM and CaM-2TnC. These studies demonstrate that wild-type CaM and the CaM-TnC chimeras are able to stimulate nNOS to pass electrons from the flavins in the reductase domain to the heme in the oxygenase domain. Slightly higher ratios of NADPH oxidation to •NO synthesis for the CaM-3TnC and CaM-4TnC chimeras suggest that there is a partial uncoupling of electron transfer from •NO synthesis when using these mutants. NADPH oxidation by eNOS activated by either wild-type CaM or the CaM-TnC chimeric proteins did not show the same ranking order as observed for the production of •NO (Figure 2.9). In each case, eNOS activated by CaM-TnC chimeras showed higher ratios of NADPH consumption to •NO production. This result suggests that eNOS may be more susceptible to electron uncoupling of NADPH oxidation from the production of •NO than nNOS when activated by mutant CaM proteins.

The cytochrome *c* reduction studies demonstrated that each of the chimeras, with the exception of CaM-1TnC, were capable of promoting electron transfer in the reductase domain of nNOS. The reduction rates of cytochrome *c* were markedly higher than the corresponding rates of •NO synthesis for the cNOS enzymes activated by the CaM-3TnC and CaM-4TnC chimeras. The rate of cytochrome *c* reduction by nNOS activated by CaM-2TnC was identical to the rate observed when activated by wild-type CaM. These results demonstrate that EF hands II, III, and IV of TnC are sufficient for the activation of electron transfer within the reductase domain of nNOS. In contrast, specific residues in EF hand I of wild-type CaM appear to be important in order to promote electron transfer through the reductase domain of nNOS since its replacement by its corresponding TnC EF hand results in minimal electron transfer to cytochrome *c*. In contrast, a different trend was observed when investigating the role of the four CaM EF hand domains in the activation of electron transfer within the reductase domain of eNOS. The replacement of either domain 3 or 4 in CaM only slightly diminished the rate of reduction of cytochrome *c*. Furthermore, unlike the result observed with nNOS, the CaM-1TnC chimera still allowed production of about 60% maximal cytochrome *c* reduction by eNOS. In addition, the CaM-2TnC chimera allowed only about 30% maximal cytochrome c reduction rate for eNOS, completely different than that observed for nNOS. The lower rate of production of •NO by eNOS bound to CaM-2TnC in comparison with nNOS can possibly be explained by differences in the interactions between CaM and the reductase domain. This inference can be supported by the observed diminished rate of cytochrome *c* reduction by eNOS activated by CaM-2TnC.

2.3.3 iNOS Activation by CaM-TnC Chimeras

Previous investigations on the CaM-dependent activation of iNOS have been limited and problematic due to the strong binding between the enzyme and CaM. In addition, the sensitivity of iNOS to proteolysis during purification has effectively prevented the isolation of an intact CaM-free iNOS. In

order to circumvent this problem, each of the five CaM-TnC chimeras used in this study were coexpressed separately with the human iNOS enzyme. As previously reported, the coexpression of iNOS with wild-type CaM results in a highly stable complex that shows only a small decrease in activity when treated with EDTA (Venema *et al.*, 1996). The coexpression of iNOS with the different CaM-TnC chimeras provided a unique opportunity to determine the effect of specific regions of CaM that are important for the activation and tight binding of CaM to iNOS.

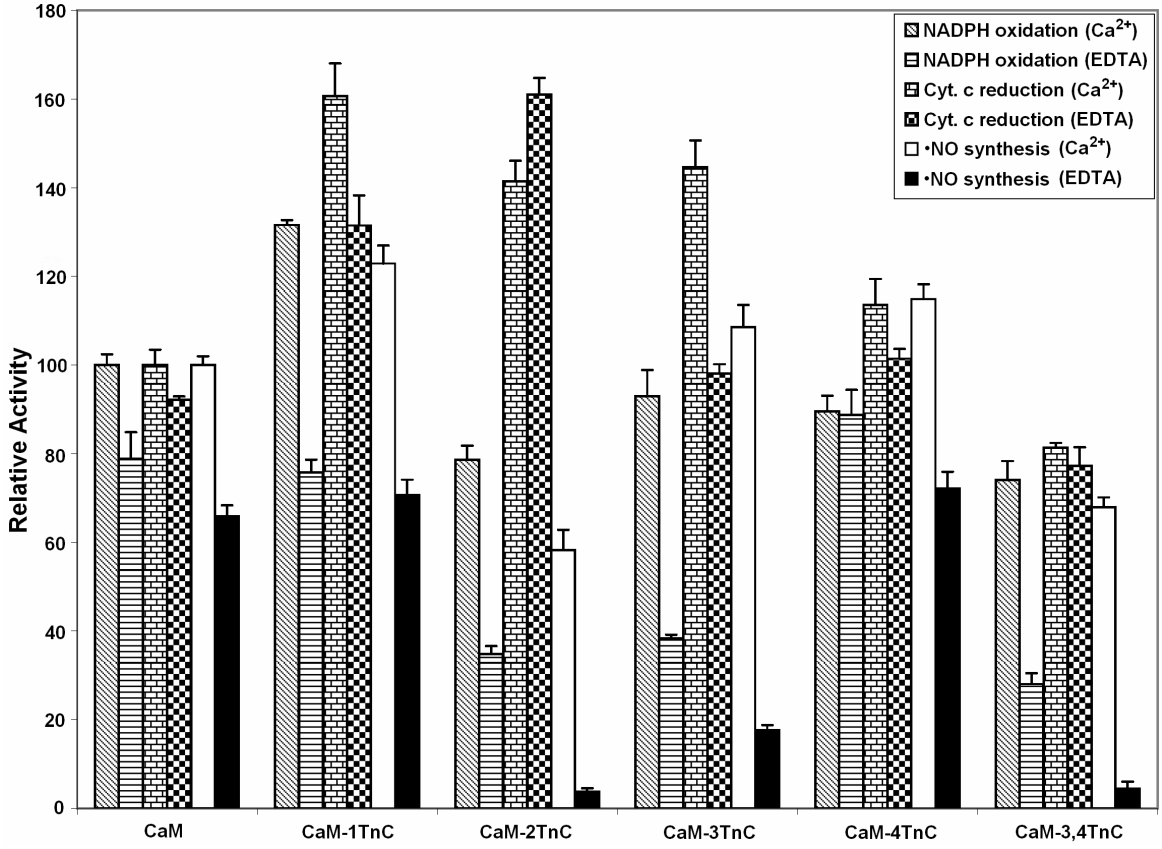

Figure 2.10 – Ability of coexpressed CaM-TnC chimeras to activate iNOS.
The human iNOS enzyme was coexpressed separately with each of the CaM-TnC chimeric proteins. The •NO synthesis, cytochrome *c* reduction, and NADPH oxidation rates were measured as previously described in Figure 2.8 with the exception that no exogenous CaM protein was added to the assays. Each assay was performed in the presence of either $CaCl_2$ (200 μM) or EDTA (250 μM) as indicated. The activities obtained for iNOS coexpressed with wild-type CaM and assayed in the presence of $CaCl_2$ (200 μM) at 25°C were all set to 100%. The rates observed for each assay were 77 min^{-1} (NADPH oxidation, 1395 min^{-1} (cytochrome *c* reduction), and 47 min^{-1} (•NO synthesis). The bar values represent the mean values ± standard deviation. Each assay was performed in quadruplicate and repeated three or more times.

The replacement of CaM EF hands I, III, or IV with their corresponding EF hands in TnC resulted in higher reproducible rates of •NO production ranging from 110 to 123% (Figure 2.10). In contrast, the replacement of EF hand II of CaM (CaM-2TnC) activated iNOS to about 60% maximal velocity. Likewise, the CaM-3,4TnC chimera activated iNOS to about 70% maximal activity. The addition of excess wild-type CaM to each iNOS enzyme coexpressed with CaM-TnC chimeric proteins did not result in any significant change in the activity of the enzyme, indicating that the CaM-binding domain of iNOS were saturated with the mutant CaM-TnC proteins (results not shown).

The addition of 250 μM EDTA to chelate Ca^{2+} resulted in a significant decrease in •NO production by all of the chimeras (Figure 2.10). This Ca^{2+}-dependence was very marked for the iNOS enzyme coexpressed with CaM-2TnC, CaM-3TnC, and CaM-3,4TnC. However, the subsequent addition of excess Ca^{2+} completely reversed the effect of EDTA. These results show that EF hands II and III of CaM contain important elements or residues required for the tight binding of CaM to the iNOS enzyme. In contrast, the addition of EDTA to the iNOS enzymes coexpressed with CaM-1TnC and CaM-4TnC resulted in only a small decrease in enzyme activity that was comparable to that observed for iNOS coexpressed with wild-type CaM. The absence of a Ca^{2+}-dependent activation of iNOS by these two chimeras, CaM-1TnC and CaM-4TnC is consistent with two aspects: (1) the first EF hand of TnC is known not to bind Ca^{2+} and (2) the fourth EF hand of TnC binds Ca^{2+} an order of magnitude stronger than EF hand IV of CaM (George *et al.*, 1993). The addition of excess CaM in the presence of EDTA resulted in over 90% maximal activity for all of the enzymes coexpressed with the CaM-TnC chimeras with the exception of CaM-3,4TnC which only showed 50% activation (results not shown). The mutant CaM-TnC chimeras appear to possibly be displaced by wild-type CaM when incubated in a buffer containing EDTA (discussed in further detail in Chapter 3). These results demonstrate for the first time that there are specific elements in CaM necessary for the tight binding of CaM to iNOS.

A comparison of the CaM-TnC chimeric proteins' ability to activate NADPH oxidation showed similar trends to their activation of •NO synthesis by iNOS (Figure 2.10). The coexpression of wild-type CaM, CaM-1TnC, or CaM-4TnC with iNOS resulted in a stoichiometry of about 1.5 NADPH oxidized per •NO synthesized, even in the presence of excess EDTA. These results indicate that the the iNOS mechanism is more tightly coupled than that found in the cNOS enzymes when using the oxyhemoglobin and NADPH assays. Since the increased levels of NADPH consumption have been associated with the possible redox cycling of exogenous unbound flavins added to the assay buffers (Vasquez-Vivar *et al.*, 1998), the observed difference in electron coupling to •NO production between iNOS and cNOS enzymes may be due to a higher affinity for the FMN in the iNOS enzymes or, alternatively, both having a similar affinity for FMN but iNOS having a much higher rate of •NO production. The iNOS coexpressed with CaM-2TnC, CaM-3TnC, or CaM-3,4TnC also resulted in the proper stoichiometry of 1.5 NADPH molecules consumed per •NO produced, but the addition of EDTA led to a greater than 2-fold increase in the relative rate of NADPH oxidation. EF hands II and III of CaM appear to contain elements necessary to maintain the Ca^{2+}/CaM-dependent coupling of electrons in the iNOS enzyme.

The cytochrome *c* assays were used to monitor electron transfer from the FMN domain in the reductase of iNOS to an exogenous electron acceptor. The iNOS enzymes coexpressed with each of the CaM-TnC chimeric proteins all showed 100% or more greater maximal activity in the presence of both high and low levels of Ca^{2+} (Figure 2.10). These results are consistent with our previous study showing electron transfer from the reductase domain of iNOS enzymes to an artificial electron acceptor is CaM independent (Newton *et al.*, 1998). Most notably, the rates of cytochrome *c* reduction relative to wild-type CaM are over 100% for iNOS enzymes coexpressed with CaM-1TnC, CaM-2TnC, and CaM-3TnC. These increased rates may be due to the replacement of residues in CaM that are not necessary for electron transfer but may normally attenuate the rates of electron

transfer in the reductase domain of iNOS by altering specific interactions between the FAD and FMN or possibly other regions of the enzyme.

2.4 Discussion

The present investigation of CaM interactions with all three NOS isoforms was undertaken to further our understanding of the activation of these enzymes. The binding of CaM to the cNOS enzymes has been shown to affect electron transfer within the reductase domain, whereas the effect of CaM on electron transfer in iNOS is less well understood. In order to study the specific regions of CaM responsible for the activation of the cNOS and iNOS enzymes, CaM-TnC chimeric proteins that have each CaM EF hand replaced with their corresponding EF hands from TnC were employed.

As demonstrated in the results section (section 2.3), the CaM-TnC chimeric proteins showed marked effects on the rates of •NO production and NADPH oxidation of nNOS (Figure 2.8). In contrast, when EF hands III and IV of CaM were exchanged with TnC a small effect on electron transfer rates from NADPH into the reductase domain of nNOS were observed. This is indicative that the lower •NO production rates observed with CaM-3TnC and CaM-4TnC is associated with the reduction of heme by FMN and not within the reductase domain of nNOS. Surprisingly, CaM-2TnC, which contains the replacement of both EF hand II and the central linker of CaM with the corresponding domain in TnC and the largest change of primary sequence of all the CaM-TnC mutants, was able to fully activate nNOS. This interesting result suggests that residues in the C-domain of CaM-3TnC and CaM-4TnC, as well as CaM 1TnC may make important contacts with sequence regions outside the canonical CaM-binding region that may affect electron transfer within nNOS.

Although eNOS displayed a similar activation profile to nNOS with the CaM-TnC chimeras, the activation of eNOS was not equivalent with all the chimeric proteins (Figure 2.9). For instance, the transfer of electrons within the reductase domain of eNOS monitored by the cytochrome *c* assay

was less susceptible to the mutations of CaM than nNOS. Furthermore, although CaM-2TnC was the most potent activator of the five CaM mutants tested, it was only able to activate eNOS to 50% of the maximal activity when compared to wild-type CaM. Likewise, the activation of eNOS by CaM-3TnC and CaM-4TnC was markedly greater when compared to wild-type CaM than what was observed for nNOS. Additionally, CaM-3TnC, CaM-4TnC, and CaM-3,4TnC all promoted electron transfer to cytochrome *c* in eNOS to a greater extent than they activated •NO production. This observation is similar to what was previously observed for nNOS indicating that the less effective activation of •NO production by these chimeric proteins results specifically from a lower rate of FMN to heme electron transfer and not a lower rate of electron transfer within the reductase domain of eNOS. In contrast, CaM-2TnC is less effective in promoting cytochrome *c* reduction in eNOS than in the activation of •NO production suggesting that CaM-2TnC's inability to fully activate •NO production in eNOS may be related to a slower electron transfer rate to the FMN.

The following is the first report on CaM specific interactions in the binding and activation of iNOS. Prior to this study, CaM had to be coexpressed with iNOS to produce a stable and active enzyme. The investigation of the role of different regions of CaM on the activation of iNOS required the development of separate coexpression systems for each of the CaM-TnC chimera proteins. Using these mutant CaM proteins copurified with iNOS, significant differences in the role of CaM in activating iNOS were observed when compared to the cNOS enzymes (Figure 2.10). Coexpression with each of the five CaM-TnC chimeras in the presence or absence of Ca^{2+} showed little or no effect on electron transfer rates into the reductase domain as monitored using the cytochrome *c* assay. These results are consistent with our previous studies using only the reductase domains of both human and mouse iNOS (Newton *et al.*, 1998). In contrast to the result observed for nNOS, CaM-2TnC activated •NO production by iNOS was over 40% less than that observed for iNOS coexpressed with wild-type CaM under Ca^{2+} replete conditions. Although CaM-2TnC activates •NO production to the

same percentage in iNOS and eNOS when compared to the maximal activity with wild-type CaM, it is important to note that CaM-2TnC is the most potently activating chimeric protein of the cNOS enzymes, while it is the least effective in activating iNOS. In contrast, CaM-1TnC is significantly more effective than wild-type CaM in activating •NO production by iNOS, while CaM-3TnC and CaM-4TnC are only slightly more effective; CaM-3,4TnC is more effective than CaM-2TnC but less effective than wild-type CaM (Figure 2.10). Clearly, the results observed for CaM-4TnC indicate that the C-terminal domain of CaM is less important for activating iNOS than in eNOS and nNOS, which is further supported in Chapter 3. Overall, the activation of iNOS indicates that iNOS's requirement for CaM is less stringent than the CaM requirement of eNOS and nNOS and that different regions of CaM that affect the activation of iNOS have a completely different effect on cNOS activation.

The exchange of EF hands II and III, as well as the central linker of CaM with the corresponding TnC motifs, also demonstrated a Ca^{2+}-dependence for CaM-iNOS interactions. The addition of excess EDTA resulted in a significant decrease in •NO production by iNOS coexpressed with CaM-2TnC, CaM-3TnC, or CaM-3,4TnC. This Ca^{2+}-dependent decrease in •NO production was also observed using the NADPH oxidation rates, while no effect was observed for cytochrome *c* reduction rates. This can be explained by the rate-limiting electron transfer occurring between the FMN and heme, since both the NADPH and oxyhemoglobin assays are dependent on electrons being transferred to the heme, while the cytochrome *c* assay only required electrons being transferred through the reductase domain to the FMN. Furthermore, in the presence of EDTA, CaM-2TnC, CaM-3TnC, and CaM-3,4TnC all demonstrated that NADPH was consumed to a greater extent than •NO production indicative that at low Ca^{2+} concentrations, the binding of these chimeras to iNOS caused an increase in electron uncoupling to •NO synthesis. Since CaM-1TnC contains TnC EF hand I which is incapable of binding Ca^{2+} (Su *et al.*, 1995), it was expected that this mutant would be unable to stabilize the strong interactions between CaM and iNOS to the extent of the replaced EF

hand I of CaM. Unexpectedly, CaM-1TnC actually stabilized the interaction and had no adverse effect on enzyme stability and activity. A Ca^{2+}-deplete EF hand I is surprising since the cNOS enzymes and numerous other CaM-dependent proteins require the N-domain of CaM to be Ca^{2+}-replete to bind and activate their target proteins. This Ca^{2+}-independence of EF hand I is further discussed in later chapters (Chapter 3, 5, and 6). On the other hand, the CaM-2TnC and CaM-3TnC results demonstrate that these regions are related to the Ca^{2+}-independent activity of iNOS. All of the single domain replacement chimeras were at least as effective as wild-type CaM in activating electron transfer to cytochrome c; CaM-1TnC, CaM-2TnC, and CaM-3TnC were significantly more effective at promoting electron transfer through the iNOS reductase domain than wild-type CaM. Overall, the results observed for iNOS, eNOS, and nNOS indicate that the requirements for the activation of cytochrome *c* reduction are less stringent than the requirements for the activation of •NO production.

Specific NOS isoform requirements with CaM-1TnC showed that this mutant was completely ineffective in activating cytochrome *c* reduction by nNOS, while CaM-2TnC was less effective than the other chimeras at activating cytochrome *c* reduction in eNOS. These results for both nNOS and eNOS support the previous published studies that demonstrated that CaM can activate reductase domain catalysis by a mechanism other than stimulating electron transfer into the oxygenase domain (Gachhui *et al.*, 1998). Furthermore, these results also show a similar activation profile for eNOS when compared to nNOS, however, the effects of the chimeric proteins on all the electron transfer rates in eNOS are not equivalent. There are still notable differences in the CaM-dependent activation of nNOS and eNOS. Additionally, a marked difference between CaM and TnC is the elongation of the central helix by three additional amino acids (91KGK93, Figure 2.2) in TnC, which is found exclusively in CaM-2TnC and not in wild-type CaM. Previous researchers have proposed that the flexibility of CaM's linker region allows the protein to adjust the orientation of the two globular domains with respect to each other and to the target peptide (Roth *et al.*, 1991; Meador *et al.*, 1993;

Vogel and Zhang, 1995; Ishida and Vogel, 2006). These three additional residues in the linker region of the CaM-2TnC chimera elongate the central helix by about 4.5 Å. However, it is apparent that this elongated helix in CaM-2TnC has no adverse effect on the activation of the cNOS enzymes, meaning that the chimeric protein is capable of making slight adjustments to ensure a proper binding orientation when associated to the cNOS enzymes. In contrast, the effect of CaM-2TnC on the Ca^{2+}/CaM dependence of •NO production by iNOS could be due to a change in the interaction of the linker region of CaM with the enzyme or a subtle conformational change in the relative positions of the globular domains of CaM when bound to iNOS.

2.5 Conclusions

Overall, it is clear that interactions between CaM and the canonical CaM-binding site found between the reductase and oxygenase domains alone are insufficient to account for the activation profiles observed in this study, as previously suggested by other researchers (Ruan *et al.*, 1996; Venema *et al.*, 1996; Ishida and Vogel, 2006). In the cNOS enzymes, regions outside of the CaM-binding domain such as the FMN domain and hinge subdomain, which are involved in positioning the FMN- and FAD-binding domains, are in contact or close proximity with the outside of bound CaM. These regions contain cNOS specific insertions that are associated with CaM control and are thought to be well positioned to interact directly with the exterior of CaM (Salerno *et al.*, 1997). Similarly, regions flanking the canonical CaM-binding domain of iNOS have also been implicated in the Ca^{2+}-independent binding of CaM (Ruan *et al.*, 1996; Venema *et al.*, 1996).

In summary, the results presented in this study show that EF hand I is vital for the CaM-dependent activation of nNOS, which is in agreement with previously published reports (Stevens-Truss *et al.*, 1997; Gachhui *et al.*, 1998). Furthermore, eNOS demonstrated a similar activation profile using CaM-TnC chimeric proteins as nNOS; however, the activation of eNOS was not equivalent, demonstrating that nNOS and eNOS have subtle differences in their regulation by CaM.

Chapter 2: Activation of NOS by CaM-TnC Chimera

In contrast to the results observed for the cNOS enzymes, EF hands II and III were found to be directly related to the Ca^{2+}-dependence of iNOS. This finding was later supported by another group through the use of *Drosophila* CaM that had Ca^{2+}-deficient mutations (Glu→Gln) to study the Ca^{2+}-independence of CaM binding to iNOS (Gribovskaja *et al.*, 2005). Clearly, there are marked differences in the Ca^{2+}-dependent/independent regulation of NOS by CaM that can be correlated to the various interactions that can occur between the NOS enzymes and each of CaM's four EF hands.

Chapter 3
Binding and Activation of Nitric Oxide Synthase Isozymes by Calmodulin EF Hand Pairs *

3.1 Introduction

CaM is a 148 amino acid protein consisting of two globular domains joined by a central linker region. Each domain of CaM contains an EF hand pair. The C-terminal EF hand pair has an affinity for Ca^{2+} (K_d = 10^{-6} M) ten fold greater than the N-terminal EF hand pair (K_d = 10^{-5} M) (Martin *et al.*, 1985). Previous studies involving the exchange of EF hand pairs within CaM have been performed to study specific interactions of CaM domains during their binding and activation with various target proteins, such as the smooth and skeletal myosin light chain kinases, as well as nNOS (Persechini *et al.*, 1996a; b). The present investigation was designed to further assess the role of the two CaM EF hand pairs in the binding and activation of NOS enzymes. To accomplish this study, four different mutant CaM proteins were employed - nCaM, cCaM, CaMNN, and CaMCC. The truncated nCaM construct includes only the N-terminal EF hand pair without the central linker region (residues 1-75), and the complementary cCaM construct includes only the C-terminal EF hand pair including the central linker region (residues 76-148). In addition, CaMNN contains two repeats of the N-terminal EF hand pair (residues 1-81, 9-75), and CaMCC contains two repeats of the C-terminal EF hand pair (residues

*** The results presented in this chapter have been published:**
Spratt, D.E., Newman, E., Mosher, J., Ghosh, D.K., Salerno, J.C., and Guillemette, J.G. (2006) Binding and Activation of Nitric Oxide Synthase Isozymes by Calmodulin EF Hand Pairs. *FEBS Journal 273*, 1759-1771.

Unless otherwise stated, all of the work reported in this chapter was performed and analysed by the candidate.

1-8, 82-148, 76-148). CaMNN and CaMCC EF hand pairs are both connected via the central linker region (residues 76-81). Figure 3.1 shows a schematic representation of the EF hand CaM mutant proteins used in this study.

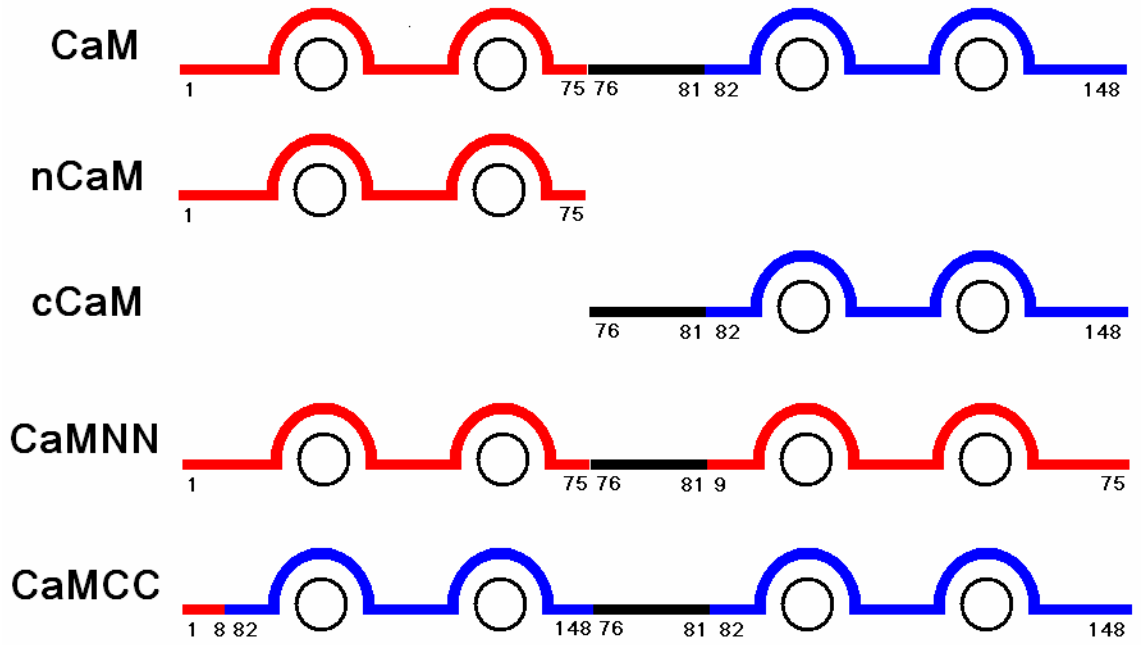

Figure 3.1 – Alignment of CaM and EF Hand mutant CaM proteins.
Ca^{2+} is represented as circles, while the N-terminal and C-terminal domains of CaM are shown in red and blue, respectively. The central linker region of CaM is shown in black.

To date, CaM-iNOS interactions have not been well studied because iNOS could originally only be purified when coexpressed with wild-type CaM (Cho *et al.*, 1992). We previously overcame this problem by coexpressing iNOS with mutant CaM proteins and successfully produced active enzyme (Newman *et al.*, 2004). During our previous study (Chapter 2), CaM-troponin C (CaM-TnC) chimeric proteins were used to probe specific NOS-CaM interactions and we demonstrated that the requirements for iNOS activation were far less stringent than the requirements for cNOS activation (Newman *et al.*, 2004). The primary requirements for iNOS activation were associated with EF hands II and III while the requirements for the cNOS enzymes were associated with EF hand I. The

present study reports on the CaM-dependent activation of mammalian NOS isozymes with a greater focus on CaM-iNOS interactions.

3.2 Experimental Procedures

3.2.1 CaM Protein Subcloning and Mutagenesis

The subcloning and mutagenesis used to produce the CaM EF hand pair mutants used in this study were performed by Mrs. Elena Newman (MSc. 2003, U of Waterloo) and Miss Bo Cheyne (BSc. U of Waterloo, Summer Student), former members in our laboratory. The following subsections (3.2.1.1-3) are summaries on the construction and molecular manipulations employed to produce these CaM mutants.

3.2.1.1 pnCaMChlor

The chloramphenicol resistant CaM expression vector pCaMChlor used in this study was a generous gift from Dr. A. Persechini (University of Missouri-Kansas City, Kansas City, MO, USA). Introduction of a stop codon at residue 76 and a reporter *Xba*I cut site by PCR mutagenesis produced pnCaMChlor, encoding for the N-terminal residues 1-75. The forward and reverse primers were: pC76STF 5' ATGGCGAGGAAGATG*TAA*TCTAGAGACACGGACAGCGAAG 3' and pC76STR 5' CTTCGCTGTCCGTGTCTCTAGA*TTA*CATCTTCCTCGCCAT 3'. The construction of pnCaMChlor was verified by sequencing and used for coexpression with iNOS.

3.2.1.2 pcCaMKan

pcCaMKan, coding for residues 76-148, was used for coexpression with iNOS. The coding region was PCR amplified from the kanamycin resistant pET9dCaM plasmid, consisting of the pET9d vector (Novagen) carrying rat CaM, introducing unique flanking *Nco*I and *EcoR*I sites for subcloning into a vector suitable for coexpression. Primers used were:

cCaMNcoI53 5' CGATGATGGCGAGGACCATGGAGGACACGGACAGCG 3' and cCaMEcoRI35 5' TGCATGATAAAGAAGGAATTCTCACTTAGCCGTCATC 3'. The PCR product was blunt end ligated into the *Srf*I site of pPCR-SCRIPT Amp SK (+). The pcCaMPCRscript vector was subsequently digested with *Nco*I and *EcoR*I and subcloned into the kanamycin resistant pET28a vector (Novagen) cut with the same enzymes and the resulting pcCaMKan vector was verified by sequencing.

3.2.1.3 pCaMNNKan and pCaMCCKan

The vectors pCaMNNAmp and pCaMCCAmp, coding for CaMNN (residues 1-81, followed by 9-75) and CaMCC (residues 1-8, 82-148, 76-81, followed by 82-148), were a generous gift from Dr. Anthony Persechini (Persechini *et al.*, 1996a). Their ampicillin resistance necessitated the construction of new vectors for coexpression with iNOS. Coding regions for CaMNN and CaMCC were subcloned into the kanamycin resistant pET9dCaM plasmid using the unique flanking *Nco*I and *Pst*I restriction sites. The products, pCaMNNKan and pCaMCCKan, were verified by sequencing.

3.2.2 Expression and Purification of CaM EF Hand Pair Proteins

The CaM EF hand pair proteins were expressed and purified by Mrs. Elena Newman and Miss Jennifer Mosher (BSc. U of Waterloo, Summer Student). Overnight cultures of transformed *E. coli* BL21 (DE3) were used to inoculate 1 L of LB media in 4 L flasks supplemented with 30 µg/ml of appropriate antibiotics, kanamycin or chloramphenicol, depending on the CaM mutant (section 3.2.1). 1 L cultures were grown at 37ºC to an O.D. at 600 nm of 0.8 to 1.2, induced with 500 µM IPTG and harvested after 3 hours of expression. Cells were harvested, frozen, and stored at –80ºC. CaM was purified using phenyl sepharose chromatography as previously described (section 2.2.3), frozen in aliquots on dry ice, and stored at –80ºC. ESI-MS was performed on purified proteins using with an internal standard as previously described in section 2.2.5.

3.2.3 Expression and Purification of NOS Enzymes

Rat neuronal and bovine endothelial NOS were expressed in *E. coli* BL21 (DE3) and purified as previously described in sections 2.2.6-7. Human iNOS carrying a deletion of the first 70 amino acids and an N-terminal polyhistidine tail was coexpressed with CaM or a CaM mutant in *E. coli* BL21 (DE3) as previously described (section 2.2.8-9). This protein was coexpressed and purified using ammonium sulfate precipitation, metal chelation chromatography, and 2'5'-ADP affinity chromatography as previously described in section 2.2.9 (Montgomery *et al.*, 2000; Newman *et al.*, 2004). Mrs. Elena Newman and Miss Jennifer Mosher expressed and purified iNOS coexpressed with CaMNN and CaMCC, while the other NOS enzymes used in this study were expressed and purified by the candidate.

3.2.4 Enzyme Kinetics

The initial rate of •NO synthesis was measured using the spectrophotometric oxyhemoglobin assay at 401 nm as previously described in section 2.2.10.1.3. NADPH oxidation by NOS was monitored at 340 nm as previously described in section 2.2.10.3. The NADPH-dependent reduction of cytochrome *c* was monitored at 550 nm as described in section 2.2.10.2.3.

3.2.5 Gel Filtration Studies

The dimerization of iNOS coexpressed with native CaM and nCaM was evaluated by gel filtration on a Superdex 200 HR 10/30 column (Amersham Biosciences), equilibrated with TGND buffer (50 mM Tris-HCl, pH 7.5, 10% glycerol, 0.1 M NaCl, and 1 mM DTT) when observing the effect of basal Ca^{2+} levels, and equilibrated with TGND buffer plus 250 μM EDTA to chelate endogenous Ca^{2+}. The flow rate was maintained at 0.5 mL/min with an AKTApurifier System for Chromatography (Amersham Biosciences) and the temperature was kept constant at 7^{o}C with an electronic wine cooler (Sylvania). Eluted protein and heme were detected at 280 and 398 nm, respectively, using with a

UV-Vis flow-through detector. A gel filtration standard kit (Sigma) containing multiple molecular weight markers was used to calibrate the column.

3.2.6 Native PAGE Studies

Native PAGE was performed as reported by Sigma (Technical Bulletin No. MKR-137, 1986), which is based upon previous experiments by (Hedrick and Smith, 1968) with some modifications. Briefly, the 5% separating gel was prepared as described in the technical bulletin with 5 minutes of deaeration and poured between two glass plates. The stacking gel was prepared by substituting 2 mL of water for the riboflavin solution to the described recipe, as well as the addition of 80 µL 10% APS and 24 µL of TEMED to increase polymerization efficiency, and poured on top of the separating gel using a 10 well comb to prepare the loading wells. The enzyme was incubated in appropriate EDTA concentrations for 5 minutes prior to loading. Sample protein was loaded at 0.25 mg/mL with carbonic anhydrase used as a standard at a concentration of 1 mg/mL. The gel was stained using Coomassie Brilliant Blue R-250 and destained in a 40% methanol, 7% acetic acid solution.

3.2.7 Aggregation Reversibility for iNOS coexpressed with nCaM

Using the spectrophotometric oxyhemoglobin assay, the initial rate of •NO synthesis was measured as previously described (section 2.2.10.1.3) with some slight modifications. iNOS coexpressed with nCaM were assayed at 28.5 nM in a 100 µl total well volume. The enzyme was initially incubated in the presence of EDTA for 15 minutes with all other assay constituents present at concentrations previously reported (Montgomery *et al.*, 2003; Newman *et al.*, 2004). The reaction was initiated by adding oxyhemoglobin and NADPH to the final concentrations of 5 and 450 µM, respectively. 5 mM EDTA, 10 mM $CaCl_2$ and 2 µM wild-type CaM were added to the appropriate samples before incubation or at 0, 2, or 5 minutes after the incubation in EDTA and prior to the initiation of the

assay. iNOS coexpressed with nCaM not incubated in EDTA and initiated without excess Ca^{2+} present was used as the control set at 100%.

3.2.8 CaM Mobility Shift Assay with Synthetic NOS peptides

The NOS CaM-binding domain peptides for bovine eNOS, TRKKT FKEVA NAVKI SASLM (residues 493-512), rat nNOS, KRRAI GFKKL AEAVK FSAKL MGQ (residues 725-747) and human iNOS, RPKRR EIPLK VLVKA VLFAC MLMRK (residues 507-531) were synthesized by SynPeP (SynPeP Corporation, Dublin, CA USA). The ability of CaM and CaM mutant proteins to bind the synthetic NOS peptides was determined from the relative mobility shift of CaM in the presence of each peptide (Erickson-Viitanen and DeGrado, 1987). In a total volume of 15 μL, CaM, CaMNN, and CaMCC (20 μM) were incubated with increasing molar ratios of peptide to CaM protein (0, 0.25, 0.5, 0.75, 1, 1.5, 2, 4, 6, and 8) in binding buffer (100 mM Tris-HCl, pH 7.5, with either 0.2 mM $CaCl_2$ or 1 mM EDTA) at room temperature for 1 hour. nCaM and cCaM (60 μM) were incubated with increasing molar ratios of peptide to CaM protein (0, 0.125, 0.25, 0.375, 0.5, 0.75, 1, 2, 4, and 8) using the same conditions as CaM. After 1 hour, volumes of the samples were halved by the sample loading buffer consisting of 50% glycerol with bromophenol blue as a tracer. The mixtures were then electrophoresed on 15% non-denaturing polyacrylamide gels containing 0.375 M Tris-HCl, pH 8.8, 4 M urea, and either 0.2 mM $CaCl_2$ or 1 mM EDTA. Gels were run at a constant voltage of 100 V in electrode running buffer, which consisted of 25 mM Tris-HCl, pH 8.3, 192 mM glycine, 4 M urea, and either 0.2 mM $CaCl_2$ or 1 mM EDTA. The gels were then stained and visualized using Coomassie Brilliant Blue R-250.

3.3 Results

3.3.1 Protein Expression and Purification

The mutant CaM constructs previously described in section 3.2 expressed well yielding independent expression ranging from 8 to 26 mg protein/L of media depending on the CaM mutant. Purified CaM constructs appeared over 95% homogeneous on 15% SDS-PAGE (Figure 3.2). ESI-MS QTOF confirmed homogeneity and ruled out any posttranslational modification (Table 3.1).

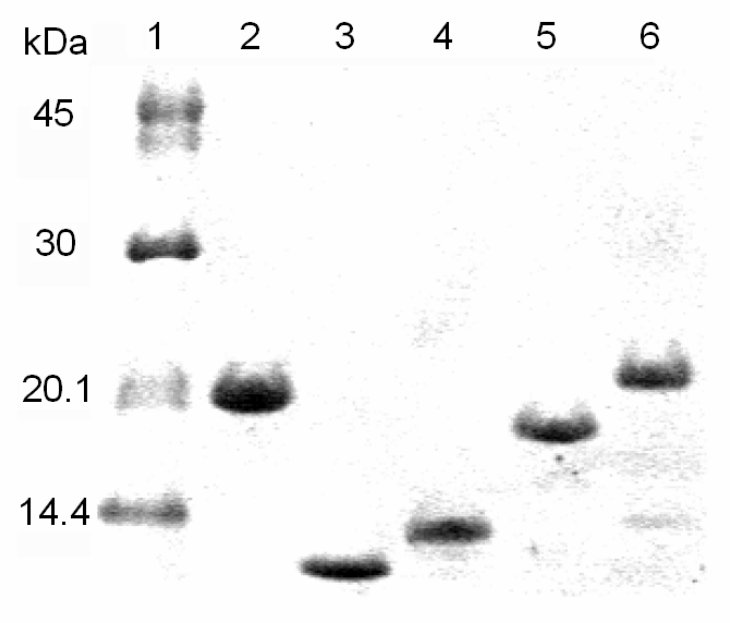

Figure 3.2 – 15% SDS-PAGE of purified EF Hand Pair CaM proteins.
5 µg of each purified CaM protein was loaded in a buffer containing 5 mM EDTA. *Lane 1*, low molecular mass protein standard (GE Healthcare Bio-sciences); *Lane 2*, wild-type CaM; *Lane 3*, nCaM; *Lane 4*, cCaM; *Lane 5*, CaMNN; *Lane 6*, CaMCC.

Table 3.1 – Masses of CaM EF Hand Pair proteins [a]

	Mass (Da) [b]	
CaM proteins	Observed	Theoretical
Wild-type CaM	16706.0	16706 [c]
nCaM	8315.9	8317
cCaM	8408.2	8408
CaMNN	16379.0	16379
CaMCC	17034.0	17034

[a] ESI-MS results from Elena Newman, MSc. – University of Waterloo Thesis

[b] Masses of deconvoluted ESI-MS spectra were determined with an accuracy of ± 5 Da.

[c] Calculated masses based upon amino acid sequence.

The iNOS enzyme was coexpressed with CaM or a mutant CaM construct. Coexpression with wild-type CaM produced the highest yields of purified iNOS (3.2 mg/L of media). Coexpression of iNOS with CaMNN yields were 2 mg/L while coexpression with nCaM gave 0.6 mg/L. Expression of iNOS with cCaM and CaMCC gave the lowest yields of 0.2 mg/L. CaM constructs containing the N-terminal EF hand pair produced higher yields of iNOS, indicating better protection of the CaM binding region than provided by the C-terminal EF pair. Visible spectra of iNOS coexpressed with CaM constructs were indistinguishable from those of iNOS coexpressed with wild-type CaM, indicating proportionate heme and flavin content. All of the CaM constructs showed production of active iNOS by the oxyhemoglobin capture assay, however, the activity of iNOS coexpressed with cCaM was very low.

3.3.2 cNOS Activation by CaM EF Hand Pair Proteins

The nNOS and eNOS enzymes displayed similar but not fully equivalent activation profiles when associated with different CaM mutants. The only CaM construct able to activate •NO production by nNOS was CaMNN; nCaM, cCaM and CaMCC produced little or no activity (Table 1).

Table 3.2 – CaM EF Hand Pair Protein Dependent Activation of cNOS Enzymes [a]

	Neuronal NOS			Endothelial NOS		
CaM protein	NADPH oxidation %	Cyt *c* Reduction %	•NO Production %	NADPH oxidation %	Cyt *c* Reduction %	•NO Production %
CaM	100 ± 2	100 ± 6	100 ± 5	100 ± 4	100 ± 2	100 ± 2
nCaM	6 ± 2	37 ± 3	NAA[b]	5 ± 3	17 ± 1	5 ± 1
cCaM	4 ± 3	NAA	NAA	NAA	NAA	NAA
CaMNN	93 ± 4	90 ± 5	81 ± 3	115 ± 4	111 ± 3	98 ± 4
CaMCC	5 ± 2	NAA	NAA	4 ± 3	43 ± 1	17 ± 3
CaM (EDTA)	6 ± 3	NAA	NAA	NAA	NAA	NAA

[a] The oxyhemoglobin capture assay used to measure the rate of CaM-activated •NO production, the cytochrome *c* assay and the NADPH oxidation assay were performed in the presence of either 2 μM wild-type or mutant CaM protein and either 200 μM $CaCl_2$ or 250 μM EDTA, as indicated. The activities obtained with the respective enzyme bound to wild-type CaM at 25°C in the presence of 200 μM $CaCl_2$ were all set to 100%. The activities for nNOS bound to CaM were 45.5 min^{-1} (•NO synthesis), 142 min^{-1} (NADPH oxidation) and 917.5 min^{-1} (cytochrome *c* reduction). The activities for eNOS bound to CaM were 11 min^{-1} (•NO synthesis), 30 min^{-1} (NADPH oxidation) and 50.7 min^{-1} (cytochrome *c* reduction).

[b] NAA – No apparent activity

These results correlate well with previous reports (Persechini *et al.*, 1994; Persechini *et al.*, 1996a). None of the CaM constructs activated •NO production by nNOS in the presence of 250 μM EDTA, consistent with our previous study of NOS activation by CaM-TnC chimeras (Newman *et al.*, 2004).

CaMNN was also the only CaM construct that produced appreciable •NO production from eNOS. CaMCC activated eNOS to a much smaller extent (20%), while nCaM and cCaM produced little or no activity (Table 3.2). Although the order of activation for eNOS was similar to that of the nNOS enzyme, CaMNN fully activated eNOS but only activated nNOS to about 80% when compared

to wild-type CaM. None of the CaM proteins activated •NO synthesis by eNOS in the presence of EDTA.

The activation of nNOS and eNOS by wild-type CaM resulted in an NADPH consumption to •NO production ratio of more than 3 instead of the theoretical ratio of 1.5. High NADPH consumption rates with eNOS were previously attributed to redox cycling of exogenous unbound flavins added to the reaction buffer of the assay (Vasquez-Vivar *et al.*, 1998). The rate of NADPH oxidation by nNOS activated by wild-type CaM or mutant CaM proteins shows the same degree of enhancement as •NO production. This indicates that any redox cycling requires the reduction of free flavins by the NOS reductase domain. The ratio of NADPH oxidation to •NO synthesis were indistinguishable for nNOS activated by CaM and CaMNN. NADPH oxidation by eNOS activated by either CaM or the mutant CaM proteins did not show the same order as observed for the production of •NO (Table 3.2). The eNOS enzyme showed greater electron uncoupling than nNOS for wild-type CaM and CaMNN. This suggests that eNOS may be more susceptible than nNOS to the uncoupling of electrons from NADPH oxidation to •NO production when activated by mutant CaM proteins, similar to our findings in a previous study (Newman *et al.*, 2004).

Only CaM constructs containing the N-terminal domain of CaM, nCaM and CaMNN, activated cytochrome *c* reduction by nNOS. Constructs lacking the N-terminal domain of CaM, cCaM and CaMCC, produced little or no activation of electron transfer to cytochrome *c*. Specific residues in the N-terminal domain of CaM appear to be required for activation of electron transfer in nNOS.

The activation of electron transfer within the reductase domains of eNOS showed a similar trend to the results obtained for nNOS cytochrome *c* reduction. The details of activation by CaM constructs are not identical; with eNOS, CaMNN is a slightly more potent activator of cytochrome *c* reduction than wild-type CaM, while nCaM produces markedly lower rates of cytochrome *c*

reduction. Notably, CaMCC promoted electron transfer in the reductase domains of eNOS but not nNOS. It appears that specific residues in the N-terminal domain are important for electron transfer in the reductase domains of the cNOS enzymes, and that the central linker region may also play a pivotal role.

3.3.3 iNOS coexpressed with CaM EF Hand Pair Proteins EDTA Titration Studies

In order to determine the concentration of EDTA where •NO production by iNOS coexpressed with CaM and the CaM proteins diminished, the oxyhemoglobin assay was employed to monitor •NO synthesis rates at an enzyme concentration of 28.5 nM with logarithmic increases in EDTA concentrations (Figure 3.3, see Table 3.3 for assay conditions). It is apparent from Figure 3.3A that as EDTA concentrations increase from 0 to 5 mM, activity decreases for iNOS coexpressed with CaM to approximately 50%, however, with the addition of excess CaM under the same conditions, the activity declines but at a much slower rate.

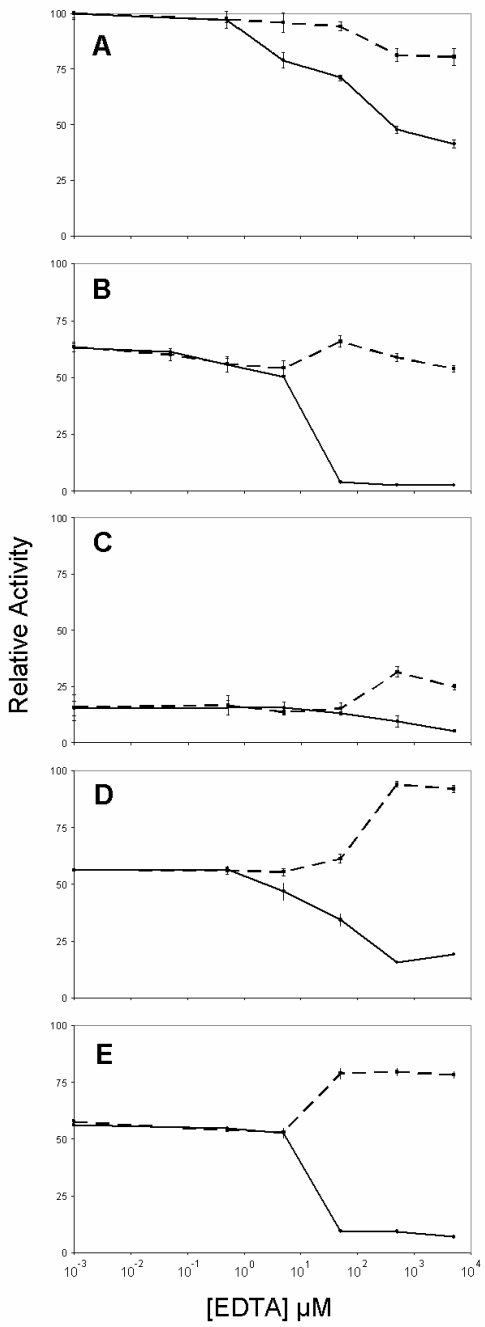

Figure 3.3 – EDTA titration of iNOS coexpressed with CaM EF Hand Pair Proteins.
The oxyhemoglobin capture assay was used to measure the rate of CaM-activated •NO production at an enzyme concentration of 28.5 nM in the presence of EDTA (——) or EDTA with 2 µM CaM (– –), respectively. iNOS coexpressed with wtCaM set at 100% at endogenous Ca^{2+} concentrations. A) iNOS coexpressed with wtCaM, B) iNOS coexpressed with nCaM, C) iNOS coexpressed with cCaM, D) iNOS coexpressed with CaMNN, E) iNOS coexpressed with CaMCC. The bar values represent the mean ± standard deviation.

Conversely, in Figure 3.3B-E, iNOS coexpressed with the CaM mutant proteins titrated with increasing concentrations of EDTA alone showed substantial decreases in activity between 5 and 50 μM. The most noteworthy result was observed for iNOS coexpressed with nCaM which showed 70% maximal activity with basal levels of Ca^{2+} while having no apparent activity in the presence of EDTA above 50 μM (see Figure 3.3B). With the addition of excess CaM to the assay conditions, activity was restored to iNOS coexpressed with nCaM to approximately 70% at EDTA concentrations of 50 μM and above. This result indicates that wild-type CaM is capable of binding to iNOS coexpressed with nCaM in a Ca^{2+} depleted environment. iNOS coexpressed with cCaM displayed a similar trend to the enzyme coexpressed with nCaM, but with a more delayed decrease in activity (see Figure 3.3C). This may be due to the cCaM protein binding more tightly to its Ca^{2+} ions since the C-terminal domain has an order of affinity greater for Ca^{2+} than the N-terminal domain of CaM (Martin *et al.*, 1985). It appears that the cCaM protein is not displaced from the CaM-binding domain of iNOS and the enzyme may be denatured during purification or Ca^{2+} chelation since it cannot be reactivated through the addition of excess CaM.

In Figure 3.3D and E, iNOS coexpressed with CaMNN and CaMCC showed similar trends. They both display a decrease in •NO production rates with increasing concentrations of EDTA to 20% and 10%, respectively, and display marked increases in activity when excess CaM is added to the Ca^{2+} replete environment. They both display enhanced •NO production rates in the presence of higher EDTA concentrations with excess CaM when compared to their respective activities at basal Ca^{2+} levels.

The EDTA concentration of 250 μM was chosen for subsequent assay conditions for iNOS coexpressed with CaM proteins. This is due to there being the greatest difference between the absence and presence of excess CaM for all the iNOS enzymes coexpressed with the CaM proteins.

3.3.4 iNOS Activation by CaM EF Hand Pair Proteins

The coexpression of iNOS with CaM constructs containing the N-terminal domain of CaM, nCaM and CaMNN, resulted in reproducible •NO production rates of approximately 70% in the presence of Ca^{2+} (Table 3.3).

Table 3.3 – CaM EF Hand Pair Protein Activation of iNOS [a]

	NADPH Oxidation		Cyt *c* Reduction		•NO Production		
CaM Protein	%	250 µM EDTA %	%	250 µM EDTA %	%	250 µM EDTA %	500 µM EDTA with 2 µM CaM %
CaM	100 ± 4	96 ± 6	100 ± 2	94 ± 1	100 ± 2	66 ± 2	81 ± 3
nCaM	80 ± 7	28 ± 3	109 ± 3	115 ± 2	71 ± 2	NAA[b]	59 ± 2
cCaM	44 ± 3	20 ± 3	62 ± 1	77 ± 2	12 ± 1	NAA	31 ± 2
CaMNN	48 ± 3	58 ± 3	133 ± 4	133 ± 1	74 ± 7	23 ± 1	94 ± 1
CaMCC	75 ± 1	38 ± 3	69 ± 2	82 ± 3	54 ± 1	7 ± 1	80 ± 2

[a] •NO synthesis, cytochrome *c* reduction and NADPH oxidation rates were measured as described in Table 1 except that no exogenous CaM was added to the assay. Each assay was performed in the presence of either 200 µM $CaCl_2$ or 250 µM EDTA as indicated. The activities obtained for iNOS coexpressed with CaM and assayed in the presence of 200 µM $CaCl_2$ at 25°C were all set to 100% and were 47 min^{-1} (•NO synthesis), 101 min^{-1} (NADPH oxidation) and 1397 min^{-1} (cytochrome *c* reduction).

[b] NAA – No apparent activity

In contrast, CaM proteins consisting of only the C-terminal domains of CaM resulted in reproducible •NO production rates of less than 50%. The addition of excess wild-type CaM to iNOS coexpressed with each of the CaM constructs did not result in any significant change in the activity of the enzyme, indicating that the CaM-binding sites were saturated with mutant CaM proteins and do not exchange rapidly with CaM in solution (results not shown).

The addition of 250 µM EDTA to chelate Ca^{2+} resulted in a significant decrease in the stimulation of •NO production by all of the CaM proteins with the most noteworthy being iNOS

coexpressed with nCaM, which decreased from 70% to no apparent activity (Table 3.3). The iNOS enzyme coexpressed with CaMNN experienced a similar trend, but still retained 25% activity in the presence of EDTA. Little or no activity was observed for iNOS coexpressed with cCaM and CaMCC in the presence of EDTA. These results show that the N-terminal EF hand pair of CaM contains important elements required for the activation of iNOS. Since iNOS coexpressed with CaMNN maintains some activity in the presence of EDTA, in contrast to iNOS coexpressed with only nCaM, the central linker region of CaM may play an important role in the Ca^{2+}-independent binding and activation of iNOS.

Significant levels of •NO synthesis were restored when excess wild-type CaM was added to iNOS coexpressed with any of the four mutant CaM proteins in the presence of EDTA (Table 3.3). These results indicate that a Ca^{2+}-dependent reorganization of the bound mutant can allow for the binding and activation of iNOS by the addition of excess native CaM.

Comparing the stimulation of NADPH oxidation by the CaM constructs showed a pattern comparable to the activation of •NO synthesis by iNOS (Table 3.3). Coexpression of CaM, nCaM, CaMNN and CaMCC with iNOS resulted in a stoichiometry of about 1.5 NADPH oxidized per •NO formed in the presence of Ca^{2+}, while cCaM showed a higher ratio, probably due to electron uncoupling from •NO production. A previous study has reported the production of $•O_2^-$ from the flavin-binding sites of iNOS's reductase domain of iNOS (Xia *et al.*, 1998) which could be a plausible explanation for this observed electron uncoupling from •NO synthesis. In the presence of a large excess of EDTA, only iNOS coexpressed with wild-type CaM maintained tightly coupled electron transfer, whereas iNOS coexpressed with the any of the CaM constructs oxidized more NADPH per •NO produced. These results indicate that •NO production by iNOS coexpressed with CaM and mutant CaM proteins is more tightly coupled than •NO production by cNOS enzymes. This

tendency is especially marked in the presence of Ca^{+2}, but is also evident when Ca^{2+} has been removed with EDTA.

Using the cytochrome *c* assay to monitor electron transfer from the flavins to an exogenous electron acceptor, the iNOS enzymes coexpressed with the CaM proteins, nCaM and CaMNN, reproducibly displayed over 100% of the maximal activity obtained with wild-type CaM in the presence of Ca^{2+} and EDTA. These results are consistent with a previous study in our laboratory showing that electron transfer from the reductase domain of iNOS enzymes to an artificial electron acceptor is CaM independent (Newton *et al.*, 1998).

3.3.5 Enzyme Quaternary Structure

3.3.5.1 Gel Filtration Studies on iNOS coexpressed with CaM and nCaM

Gel filtration studies were performed to investigate the effects of metal ion chelation by EDTA on iNOS dimerization. Using blue dextran (MW 600 kDa), the calibrated column had a void volume of 8.35 mL. The iNOS enzymes were incubated for 5 minutes in the presence of 5 mM EDTA prior to loading the sample onto the gel filtration column equilibrated with buffer containing 250 μM EDTA. The iNOS enzyme coexpressed with wild-type CaM was mainly in the form of a dimer and was not sensitive to Ca^{2+} depletion or the addition of excess CaM (Figure 3.4A-C). The iNOS dimer eluted at a volume of 11.22 mL, corresponding to a molecular weight of ~290 kDa, whereas excess native CaM eluted at 16.0 mL, which represents a protein of less than 30 kDa. As previously reported by many researchers, all of the elution profiles obtained for iNOS coexpressed with CaM contain a contaminating peak apparently representing a proteolytic cleavage fragment (Siddhanta *et al.*, 1998).

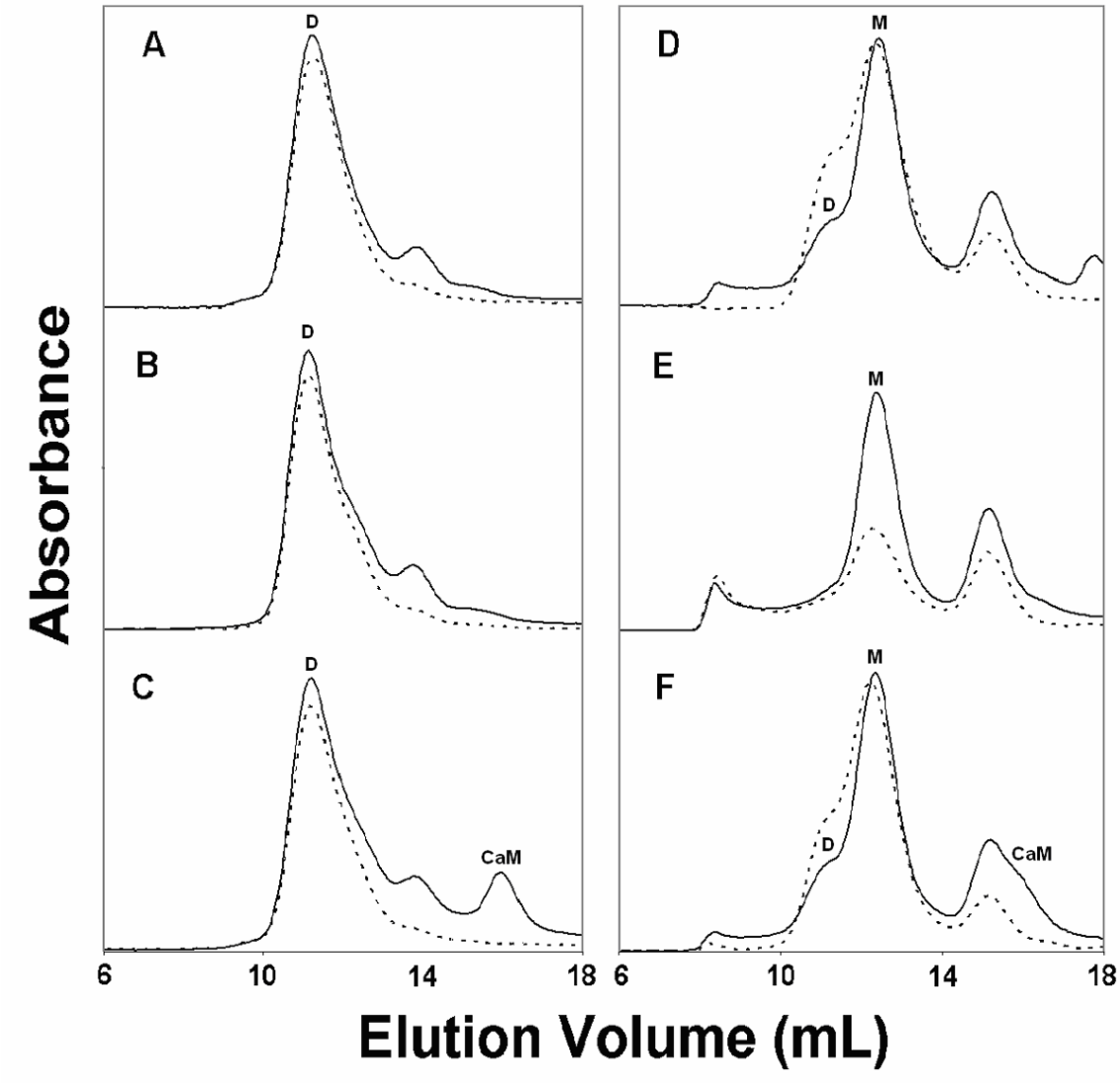

Figure 3.4 – Gel filration elution profiles of iNOS coexpressed with CaM proteins.
Absorbance at 280 and 398 nm are shown as (——) and (- - -), respectively. D, M, and CaM represent NOS dimer, monomer, and excess CaM, respectively. **(A)** 80 µg of purified iNOS coexpressed with CaM was loaded on a Superdex 200 HR 10/30 column equilibrated with 50 mM Tris-HCl, pH 7.5, containing 10% glycerol, 0.1 M NaCl, and 1 mM DTT (TGND Buffer). **(B)** profile of iNOS coexpressed with wild-type CaM incubated with 5 mM EDTA for 5 minutes before loading on the column equilibrated with TGND buffer in the presence of 250 µM EDTA, and **(C)** profile of iNOS coexpressed with wild-type CaM under the same conditions as in *panel B*, with 10 fold excess wild-type CaM added to the 5 minute incubation mixture. **(D)** 25 µg of purified iNOS coexpressed with nCaM in the same conditions as in *panel A*, **(E)** profile of iNOS coexpressed with nCaM under the same conditions as in *panel B*, and **(F)** profile of iNOS coexpressed with nCaM under the same conditions as in *panel C*. Results shown are representative of three similar experiments.

The iNOS enzyme coexpressed with nCaM was used in these experiments because it showed the greatest Ca^{2+} sensitivity of all the iNOS enzymes coexpressed with CaM EF hand pair proteins. In the presence of Ca^{2+}, the elution profile showed the enzyme sample consisted of a mixture of iNOS monomers and dimers (Figure 3.4D). The iNOS monomer eluted at 12.45 mL, corresponding to ~160 kDa. The chelation of Ca^{2+} resulted in the disappearance of the dimer, a substantially decreased enzyme peak and a significant increase in aggregated protein that eluted in the void volume (Figure 3.4E). The increased aggregated protein consists of iNOS since the void volume shows a strong heme absorbance at 398nm. The apparent aggregation of iNOS coexpressed with nCaM in the presence of EDTA accounts for the lost enzyme activity (Table 3.3). Figure 3.4F shows the elution profile for iNOS coexpressed with nCaM treated with EDTA in the presence of excess wild-type CaM. The addition of the excess native CaM appears to prevent the apparent aggregation of the protein. This is likely to occur due to a change in the interaction of nCaM with the enzyme that may expose regions of the protein that are prone to aggregation. These results are fully consistent with the activation properties of the enzyme when excess CaM is added in the absence of Ca^{2+} (Table 3.3).

3.3.5.2 Native-PAGE of iNOS coexpressed with nCaM

Non-denaturing gel electrophoresis of iNOS coexpressed with nCaM indicates that the aggregation of iNOS occurs when pre-incubated with higher concentrations of EDTA (Figure 3.5A). Consistent with the previous result observed with gel filtration, EDTA induced aggregation is diminished when the enzyme is simultaneous incubated with excess wild-type CaM (Figure 3.5B).

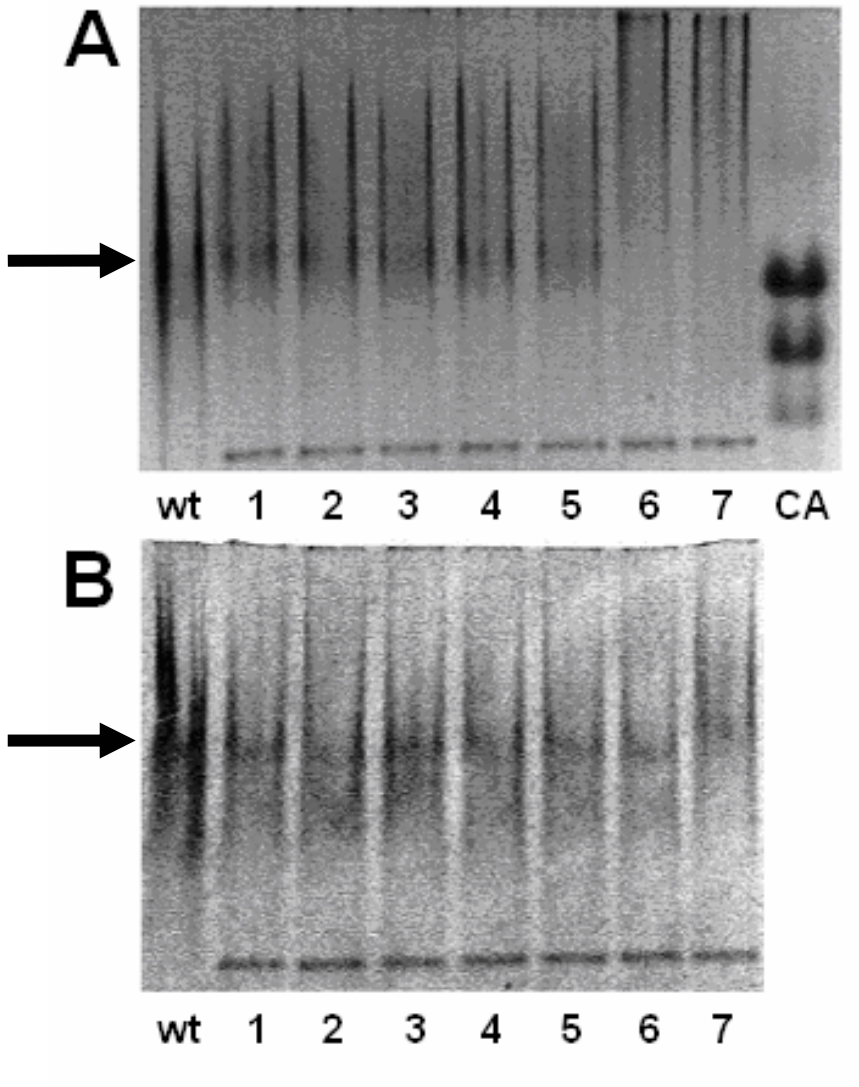

Figure 3.5 – 5% Native PAGE studies for iNOS coexpressed with nCaM.
(A) 0.25 mg/mL in the presence of EDTA alone, **(B)** 0.25 mg/mL in the presence of EDTA and 10 fold excess wild-type CaM. *Lane 1* – [EDTA] = 0 nM; *Lane 2* – [EDTA] = 50 nM; *Lane 3* – [EDTA] = 500 nM; *Lane 4* – [EDTA] = 5 μM; *Lane 5* – [EDTA] = 50 μM; *Lane 6* – [EDTA] = 500 μM; *Lane 7* – [EDTA] = 5 mM. wt and CA represent 0.25 mg/mL iNOS coexpressed with wild-type CaM and 1 mg/mL carbonic anyhydrase, each used as a standard, respectively. Arrows indicate the iNOS coexpressed with wild-type CaM and nCaM.

3.3.5.3 Spectropolarimetry of nCaM with Synthetic NOS Peptides

The structures of synthetic peptides of minimal length derived from the CaM-binding regions of the three mammalian NOS enzymes were studied by circular dichroism (CD) spectroscopy (Note: these results were published with the study described in Chapter 5 – please refer to Figure 5.6 for reference). The iNOS and eNOS peptides alone in solution had predominantly random coil conformations. In the presence of Ca^{2+}, the addition of an equimolar ratio of CaM to either of the peptides resulted in a significant increase in α-helical content. The addition of equal amounts of either iNOS or eNOS peptide to nCaM also resulted in an increase in the α-helical content of both the iNOS and eNOS peptides. As expected, the addition of excess EDTA to eNOS resulted in a mainly random coil structure. Notably, under similar conditions, the iNOS peptide retained some α-helical structure suggesting that the nCaM protein is able to bind to the iNOS peptide in the presence of excess EDTA. Our results show for the first time that while the N-terminal EF hand pair of CaM alone can accommodate the Ca^{2+}-independent binding of wild-type CaM for iNOS, apo-nCaM is not able to activate the enzyme.

3.3.5.4 Gel Mobility Shift Assays of CaM EF Hand Pair Proteins with NOS Peptides

Gel mobility shift assays were performed to investigate the binding of the three NOS peptides to the different CaM constructs. Complex formation between the peptide and CaM construct is monitored by the shift in the mobility of the CaM protein with increasing peptide concentration (Figure 3.6). The mobility of the complexes formed reflects a change in conformation of the protein upon binding to the target peptide in addition to a change in the molecular weight and charge of the complex.

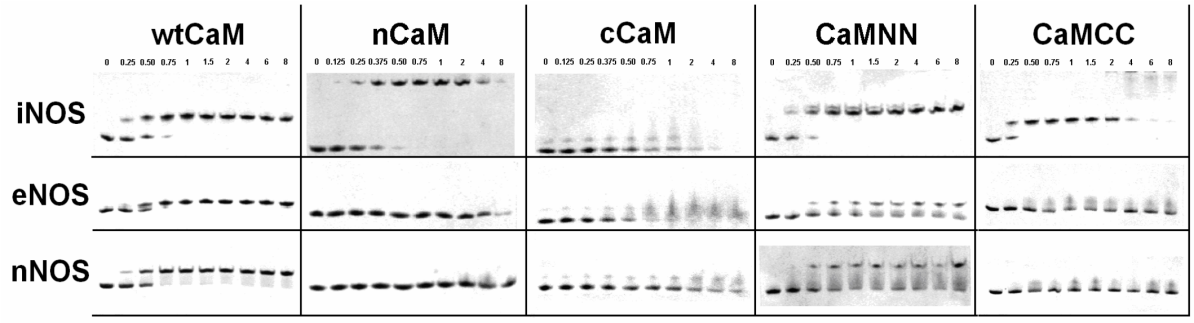

Figure 3.6 – Gel Mobility Shift Assay with Synthetic NOS peptides binding to CaM proteins. CaM, CaMNN, and CaMCC (20 μM) incubated with increasing molar ratios of peptide to CaM of 0, 0.25, 0.5, 0.75, 1, 1.5, 2, 4, 6, and 8 in the presence 0.2 mM $CaCl_2$. The nCaM and cCaM mutants (60 μM) were incubated with molar ratios of 0, 0.125, 0.25, 0.375, 0.5, 0.75, 1, 2, 4, and 8 using the same conditions as described for CaM. The samples were then analyzed by PAGE (15% acrylamide) containing 0.375 M Tris, pH 8.8, 4 M urea, and 0.2 mM $CaCl_2$ and visualized with Coomassie Blue R-250.

Stoichiometric binding in a 1:1 ratio was observed for CaM with all three NOS peptides in the presence of Ca^{2+}. In contrast, nCaM, CaMNN and CaMCC showed strong binding to the iNOS peptide but in a 2:1 protein to peptide ratio. The 2:1 ratio observed for the three CaM constructs indicates that the iNOS peptide can accommodate more than one protein. In contrast, the cCaM protein appears to bind very weakly to the iNOS peptide.

The cCaM and CaMCC constructs seem to only weakly interact with the cNOS peptides resulting in a streaked protein migration (Figure 3.6) while the nCaM protein does not interact at all. Only CaMNN shows binding using this assay but it never goes to completion. These results are consistent with activity assays previous discussed (Table 3.2).

An investigation of complex formation was performed using the apo forms of the CaM constructs incubated with each of the NOS peptides by incubating the samples in the presence of 1 mM EDTA. No mobility shifts were observed for any of the apo-CaM constructs under these conditions (results not shown). The observation of Ca^{2+}-dependent complex formation by CaM incubated with iNOS CaM-binding peptides has been previously reported using this assay (Matsubara

et al., 1997). The shorter iNOS peptides used in these two studies do not bind strongly enough to show complex formation using this assay; however, we did observe proof of binding based on CD analysis, consistent with previously reported studies (Matsubara *et al.*, 1997; Yuan *et al.*, 1998).

3.3.6 Aggregation Reversibility of iNOS coexpressed with nCaM

To determine if the observed aggregation of iNOS coexpressed with nCaM was permanent or reversible, a modified oxyhemoglobin capture assay was employed involving the incubation of the enzyme in EDTA followed by the addition of excess Ca^{2+} prior to the initiation of the assay. When compared to the positive control of iNOS coexpressed with nCaM not incubated in EDTA and initiated without excess Ca^{2+} present, the enzyme when incubated in EDTA alone showed some activity (~20%) while the addition of excess Ca^{2+} to the assay showed an increase in enzyme •NO production rate to approximately 40% (See Figure 3.8) indicative that the aggregation observed is partially reversible. The addition of wild-type CaM to the incubation mixture showed an increase in enzyme activity of approximately 100%.

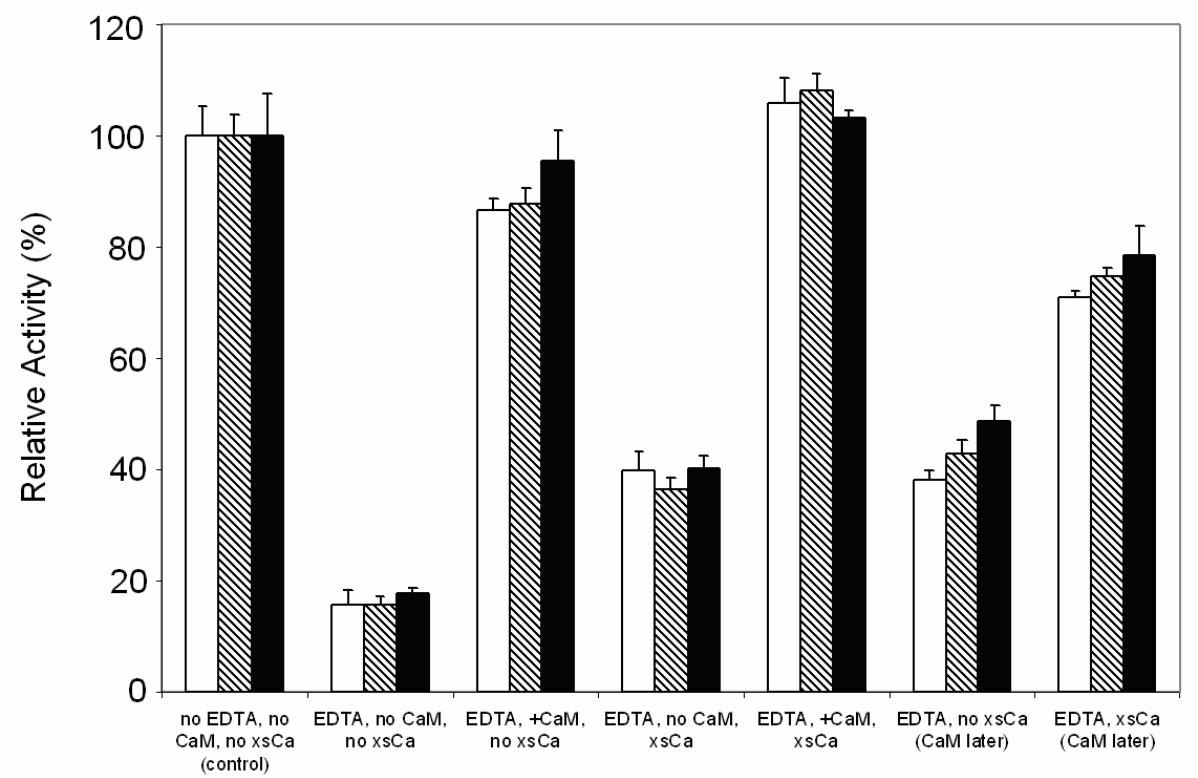

Figure 3.7 – Aggregation reversibility for iNOS coexpressed with nCaM.
After the enzyme was incubated for 15 minutes EDTA, wild-type CaM was added and incubated for at 0 (white), 2 (striped), and 5 minutes (black), respectively. The activities obtained for iNOS coexpressed with nCaM and assayed at 25°C without the addition of EDTA, no excess wild-type CaM or excess Ca^{2+} (xsCa) added after the 15 minute incubation were all set to 100%. The bar values represent the mean ± standard deviation. See Table 3.3 for assay conditions.

3.4 Discussion

The structure of CaM interacting with target peptides derived from sources including myosin light chain kinase, CaM-dependent kinase, and eNOS has been shown to consist of two EF hand pairs linked by a short connector wrapped around a helical target. This model has provided a general mechanism for how CaM binds and activates target proteins (Ikura *et al.*, 1992; Meador *et al.*, 1992; 1993; Aoyagi *et al.*, 2003). However, recent studies have also shown that CaM is able to take on many different conformations when bound to divergent target proteins (Elshorst *et al.*, 1999; Osawa *et al.*, 1999; Schumacher *et al.*, 2001; Drum *et al.*, 2002).

Our previous kinetic study involving all three isoforms of NOS with CaM-TnC chimeras demonstrated that the roles of the four EF hands in the binding and activation of the cNOS and iNOS enzymes are distinct (Chapter 2) (Newman *et al.*, 2004). Replacement of any CaM EF hand by its TnC cognate resulted in significantly decreased •NO synthesis by cNOS; in contrast to the iNOS results, EF hand II was the least sensitive even though it diverges furthest in TnC. These results could be interpreted in terms of the tethered shuttle model where the FMN binding domain is a mobile region of the enzyme and connects the oxygenase domain with the reductase complex (Ghosh and Salerno, 2003). In cNOS, cytochrome *c* reduction required only that the FMN binding domain be released from the reductase complex, but •NO production also required that CaM mediate the interaction of the FMN binding domain with the oxygenase domain.

If CaM is assumed to bind to the NOS enzymes in the closed configuration like MLCK, the N-terminal EF hands bind to the C-terminal end of the target peptide with EF hand II in closest contact with the reductase domain in an antiparallel fashion with the C-terminal EF hands are associated with the N-terminal end of the target peptide. Several possible interactions between CaM EF hand pair proteins and the CaM-binding domains of NOS can occur based upon this classic CaM bound structure. The nCaM protein can be assumed to bind to the N-type recognition site for N-

terminal EF hands, but a minority population of alternative bound species could also exist where a secondary nCaM can bind to the C-type site where the C-domain of CaM usually associates. Likewise, cCaM would also be expected to bind preferentially to recognition sites for the C-terminal EF hand, but a secondary cCaM could also bind to the N-type recognition site.

CaMNN and CaMCC could be bound with either of the two EF hand pairs in position to recognize their preferred targets and with the other pair unassociated with the binding site. However, it is likely that the other EF hand pair often fills the position occupied by the opposite EF hand pair in wild-type CaM. For example, CaMNN would bind with the N-terminal N-type pair associated with the N-type recognition site at the C-terminal end of the target. Meanwhile, the C-terminal N-type pair would weakly associate with the C-domain recognition site at the N-terminal end of the NOS target peptide. Single molecules of CaMNN and CaMCC can in principle occupy the entire CaM-binding site; however, the duplicated CaM EF hand proteins would have a much lower affinity than wild-type CaM.

CaMNN was the only CaM protein that showed appreciable •NO production rates with nNOS and eNOS (Table 3.2), which correlates well with strong binding to the NOS CaM binding domains (Figure 3.6). All other mutant CaM proteins failed to either activate or bind the cNOS enzymes. These results indicate that the N-terminal domain in conjunction with at least the central linker region is required for binding and •NO production by cNOS enzymes. In addition, it is possible that the C-terminal EF hands of CaMNN occupies part of the binding domain usually filled by the C-terminal EF hand pair. The nNOS enzyme is not completely activated when bound to CaMNN, but CaMNN fully activates •NO synthesis by eNOS and reproducibly activates eNOS NADPH oxidation and cytochrome *c* reduction more efficiently than wild-type CaM. CaMCC also slightly activates •NO production (~15%), indicating that eNOS is not as selective for specific elements in the N-terminal CaM domain as nNOS. Our findings correlate well with previous reports of significant differences

between cNOS enzyme activity and electron transfer using mutant CaM proteins and the oxidation of CaM methionine residues (Gachhui *et al.*, 1998; Montgomery *et al.*, 2003; Newman *et al.*, 2004).

Electron transfer through the reductase domains of nNOS to cytochrome *c* was stimulated by constructs that contained the N-terminal EF hand pair of CaM, although CaMNN, with four EF hands and the CaM central linker region, was much more effective than nCaM (Table 3.2). This suggests that interactions between the N-terminal domain of CaM and the reductase domains of nNOS promote the release of the FMN domain from its shielded position in the reductase complex, allowing for efficient electron transfer to an exogenous acceptor. However, in the case of nCaM, electron transfer is partially uncoupled from •NO production, suggesting that the presence of the central linker region of CaM (and perhaps of any C-terminal EF hands) is important in promoting the association of the FMN domain with the oxygenase domain.

Conversely, electron transfer through the reductase domain of eNOS to cytochrome *c* was stimulated by constructs with two EF hand pairs joined by the central linker region, although CaMNN, which contains the N-terminal EF hand pair of CaM, was the most effective. The nCaM protein slightly stimulated cytochrome c reduction. Since both CaMNN and CaMCC are capable of promoting electron transfer to cytochrome *c*, it appears that CaM requirements for the promotion of FMN domain release in eNOS are not as stringent as in nNOS (Newman *et al.*, 2004). Although the patterns of cNOS activation by the mutant CaM constructs are similar, differences in the relative importance of the elements of CaM reveal underlying differences between nNOS and eNOS.

Due to the high susceptibility of iNOS to proteolysis during purification, coupled with the enzyme's strong binding to wild-type CaM, studies on the mechanism of CaM's ability to promote electron transfer within the iNOS homodimer have been limited. As in our previous work (Newman *et al.*, 2004), studies on the role of different EF hand pairs of CaM in iNOS activation necessitated the development of separate coexpression systems for each of the mutant CaM proteins. Our results

using the enzymes bound to the CaM proteins showed significant differences in the role of CaM activating iNOS when contrasted with the cNOS enzymes (compare Table 3.2 and Table 3.3). Similar results were recently reported using a coexpression method consisting of iNOS and different *Drosophila* CaM proteins with mutations in each of the Ca^{2+}-binding sites of CaM (Gribovskaja *et al.*, 2005). Their results further support our earlier findings that EF hands II and III are important for iNOS-CaM activation. Coexpression with each of the CaM proteins did not significantly affect electron transfer through the reductase domains to the cytochrome *c*. These results are consistent with our previous study demonstrating that electron transfer within the reductase domain of iNOS is CaM-independent using only the reductase domains of both human and mouse iNOS (Newton *et al.*, 1998).

In contrast to the results obtained for nNOS and eNOS, we found that nCaM is just as effective in promoting •NO production as CaMNN when bound to iNOS. This result was surprising since nCaM only consists of the N-terminal EF hand pair with no central linker region. The requirement of the N-terminal EF hand pair of CaM for the activation of •NO production by iNOS suggests that this structure is vital in promoting FMN/oxygenase domain interactions (Table 3.3). This result is consistent with our earlier study showing the importance of EF hand II of CaM in binding and activating the iNOS enzyme in the presence and absence of Ca^{2+} (Newman *et al.*, 2004). It is noteworthy that iNOS coexpressed with CaMCC produces •NO at 50% of the rate of iNOS coexpressed with CaM. This may be caused by a tethering effect, in which the central linker region orients the N-terminal domains of CaMCC into a conformation capable of promoting a reduced level of •NO production (Persechini *et al.*, 1996b; a). The addition of excess EDTA to the assays resulted in significant decreases in •NO production rates by iNOS coexpressed with all of the mutant CaM proteins but not with wild-type CaM.

The iNOS enzyme coexpressed with wild-type CaM showed no notable difference in NADPH oxidation rates in the presence of higher and lower concentrations of Ca^{2+}, which was expected since the iNOS enzyme's affinity for CaM is very strong even in the presence of 10 mM EGTA (Venema *et al.*, 1996). Although NADPH oxidation rates for iNOS coexpressed with nCaM, cCaM and CaMCC in the presence of Ca^{2+} and EDTA do not correlate well with the corresponding •NO production rates, the addition of EDTA significantly decreased both NADPH consumption and •NO production stimulated by these constructs (Table 3.3). The very low rates of electron transfer from the FMN to the heme at lower Ca^{2+} concentrations suggest that these CaM constructs are better at promoting FMN domain release than FMN domain/oxygenase association. This trend does not extend to iNOS coexpressed with CaMNN, since there was no significant decrease in NADPH oxidative activity at high or low Ca^{2+} concentrations. This indicates that two EF hand pairs joined by the central linker region in combination with the N-terminal EF hand pair of CaM is sufficient to maintain NADPH oxidation activity in the presence or absence of Ca^{2+}.

iNOS coexpressed with nCaM and CaMNN both displayed reproducibly higher rates of cytochrome *c* reduction in the presence and absence of Ca^{2+} when compared to wild-type CaM (Table 3.3). The increased rates observed with nCaM and CaMNN may indicate that these constructs produce a higher yield of enzyme in which the FMN domain is exposed to cytochrome *c* rather than shielded by interactions with the rest of the reductase complex or the oxygenase domain, suggesting that they are better at promoting the release of the FMN domain towards the oxygenase domain than its reassociation to the reductase domain.

The iNOS enzyme coexpressed with wild-type CaM is a highly stable complex; removal of free Ca^{2+} from the system has little effect on enzyme stability. However, Ca^{2+} chelation does affect •NO production by iNOS through a conformational change within the N-terminal domain of CaM. In contrast, iNOS coexpressed with each of the CaM mutants is less stable than iNOS coexpressed with wild-type CaM. This is apparent from the gel filtration (Figure 3.4) and gel shift assays (Figure 3.6) when comparing iNOS coexpressed with wild-type CaM versus the mutant CaM proteins. In the presence of EDTA, the enzyme coexpressed with mutant CaM protein loses all detectable activity and appears to aggregate. The addition of exogenous CaM to these samples in the presence of EDTA appears to protect the enzyme based on enzyme activity assays (Table 3.3) and apparently maintains the dimeric structure of the enzyme (Figure 3.4F).

The kinetic, gel filtration, and Native PAGE results obtained for iNOS coexpressed with nCaM when incubated in the presence of EDTA indicate that the nCaM has either (1) become displaced by wild-type CaM or (2) iNOS has formed a complex involving both nCaM and wild-type CaM competing for the CaM-binding domain. To test these possibilities, a modified oxyhemoglobin capture assay was performed which involved the prolonged incubation of iNOS coexpressed with nCaM in the presence of EDTA, followed by the subsequent addition of excess Ca^{2+}. This assay was performed to determine if (1) nCaM is still bound or if it is released from the CaM-binding domain and (2) if the aggregation observed by gel filtration and Native PAGE is reversible or irreversible in the presence of Ca^{2+}. The results in Figure 3.7 show that nCaM is still bound to the CaM-binding domain of iNOS and aggregation is partially reversible with the addition of excess Ca^{2+}. CD spectra of nCaM and wild-type CaM bound to synthetic peptide in the presence of EDTA and the subsequent addition of excess Ca^{2+} demonstrated that this partial reversibility of aggregation is also observable for the iNOS CaM-binding domain peptide (results not shown). Both the modified oxyhemoglobin capture assay and CD analysis indicate that the effects of EDTA incubation are partially reversible by

Ca^{2+} addition, suggesting that nCaM rebinds and may not even be fully dissociated. By these criteria, wild-type CaM is more efficient at reversing the EDTA-induced aggregation of iNOS at higher Ca^{2+} concentrations**.** However, it is important to note that this observed aggregation effect may be concentration dependent. The gel filtration, Native-PAGE and spectropolarimetry studies are performed at micromolar concentrations versus nanomolar concentrations used during kinetics; it is conceivable that the 1000 fold lower concentration of iNOS under the assay conditions used may produce significant differences in aggregation behavior.

The statistical mechanics algorithm TANGO predicts the propensity of peptides and proteins to aggregate (Fernandez-Escamilla *et al.*, 2004). Under the conditions used in our experiments, the iNOS CaM-binding peptide has a very high propensity for aggregation (AGG value = 338.19) compared to eNOS (AGG value = 1.00) and nNOS (AGG value = 0). The TANGO results also suggest that the iNOS CaM-binding sequence 'AVLFACML' is particularly susceptible to aggregation (Figure 3.8).

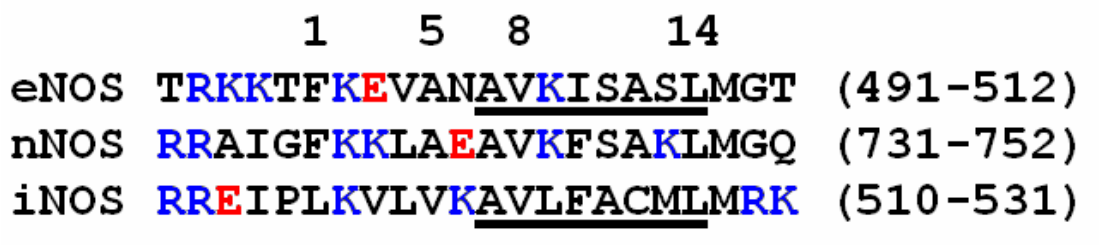

Figure 3.8 – Alignment of CaM-binding domain sequences of the three NOS isoforms.
The amino acids in red and blue represent acidic and basic residues, respectively. The amino acid residues underlined are described in the discussion section (section 3.4).

Based upon the CaM-eNOS peptide structure (Aoyagi *et al.*, 2003), the N-terminal domain residues of CaM would be expected to predominantly interact with this region of the iNOS CaM-binding peptide (Table 3.4).

Table 3.4 – Comparison of eNOS and iNOS CaM-binding domains predicted to aggregate by TANGO with CaM residues that interact with the peptide residues

CaM-Binding Domain		CaM amino acids in contact with eNOS peptide[a,b]		
eNOS	iNOS	N-terminal domain	C-terminal domain	Central Helix
A^{502}	**A^{521}**	Glu^{11}, Glu^{14}, Ala^{15}, Leu^{18}		
V^{503}	**V^{522}**		Val^{91}, Phe^{91}, Leu^{112}	
K^{504}	L^{523}		Ser^{81}, Glu^{84}, Ile^{85}, Ala^{88}, Met^{145}	
I^{505}	F^{524}	Glu^{11}, Phe^{12}, Ala^{15}, Met^{72}		Met^{76}
S^{506}	A^{525}	Ala^{15}, Leu^{18}, Phe^{19}, Leu^{39}		
A^{507}	C^{526}	Leu^{39}	Glu^{87}	
S^{508}	M^{527}	Met^{72}, Lys^{75}	Glu^{84}	Met^{76}
L^{509}	**L^{528}**	Phe^{19}, Met^{36}, Met^{51}, Met^{71}, Met^{72}, Lys^{75}		

[a] Amino acid residues in CaM shown to be within 4 Å of the eNOS CaM-binding peptide reported in (Aoyagi *et al.*, 2003).

[b] Amino acids in bold represent conserved residues in the respective eNOS and iNOS CaM-binding domains.

Using the published co-ordinates for the structure of an eNOS peptide bound to CaM (Aoyagi *et al.*, 2003), a model shown in Figure 3.9 was created consisting of the eNOS peptide bound to only the first 75 residues of CaM to represent the nCaM construct.

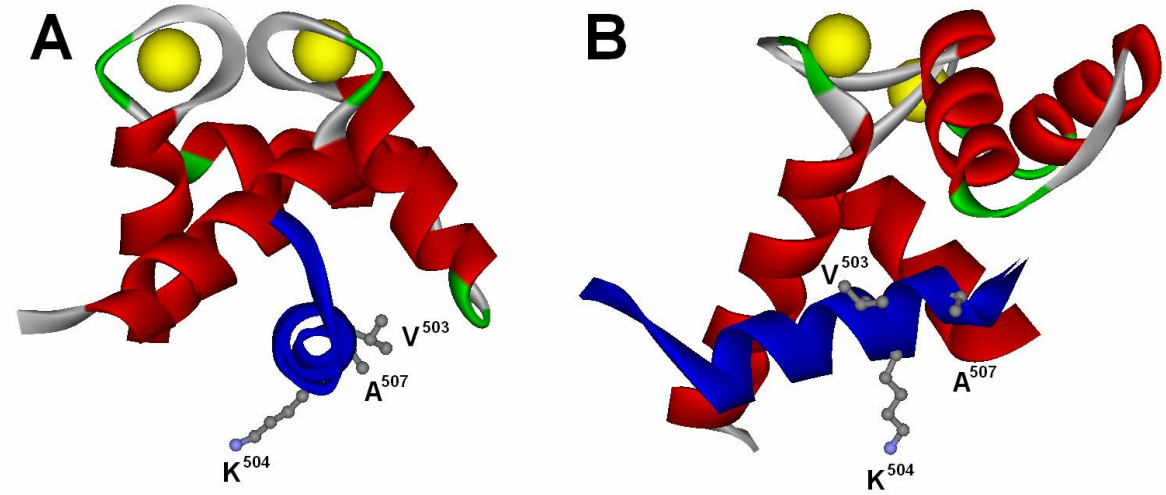

Figure 3.9 – Structures of nCaM bound to eNOS peptide.
(A) Structure from the perspective of looking down the eNOS peptide barrel, and **(B)** a perpendicular representation of *panel A*. Structures are derived from the PDB 1NIW (Aoyagi *et al.*, 2003). CaM residues 4 to 75 peptide backbone, Ca^{2+} ions, and eNOS peptide backbone are shown in red, yellow, and blue, respectively. Peptide residues V^{503}, K^{504}, and A^{507} are shown in grey. Structures were visualized using ViewerLite 5.0 (Accelrys).

Our CD results indicate that the peptide forms a helical structure when bound to nCaM (please refer to Figure 5.6). As shown in Figure 3.9, most of the helical target site including the predicted binding site of the N-terminal EF hand pair of CaM is shielded from solvent. Complete or partial dissociation of nCaM in the presence of EDTA should expose hydrophobic residues in this region. The CaM-binding domain of iNOS has greater hydrophobic character than the cNOS enzymes, which may in part account for the increased affinity of iNOS peptides for CaM in the presence of EDTA.

The model in Figure 3.9 shows that eNOS residue K504 is solvent exposed. The alignment of the CaM-binding sequences in the three NOS isoforms shown in Figure 3.8 indicate that the lysine residue found at this position in both cNOS enzymes is a hydrophobic leucine residue in iNOS. The exposure of a hydrophobic region upon helix formation of the iNOS peptide could account for the tendency of this peptide to aggregation, which can possibly be translated to the observed aggregation of the holo-iNOS enzyme (Figure 3.4 and Figure 3.5). Our gel shift assays indicate that two nCaM molecules bind to each iNOS peptide (Figure 3.6). In the presence of excess peptide, the nCaM protein does not enter the gel and appears to aggregate. At low peptide to CaM ratios, the first nCaM protein must bind to the normal site on the peptide while the second nCaM likely interacts weakly at another site on the peptide further shielding it from the solvent. Upon the addition of excess peptide, the weakly bound nCaM is displaced to bind the freshly added peptide. This displacement exposes the hydrophobic regions of the iNOS peptide including the aforementioned leucine residue resulting in a process that may lead to aggregation.

3.5 Conclusions

Tryptic digestions of CaM have previously been performed to determine which domains of CaM are necessary for target enzyme activation. It has been determined that residues 1-77 and 78-148, each very similar to our constructs for nCaM and cCaM, were unable to activate cAMP phosphodiesterase or calcineurin (Newton *et al.*, 1984), while residues 78-148 were able to fully activate phosphorylase kinase although having a lower affinity than wild-type CaM (Kuznicki *et al.*, 1981).

In a similar study using residues 1-75 of CaM, which is identical to nCaM used in this study, and residues 78-148 of CaM, it was observed that nCaM and the C-terminal domain of CaM are able to activate skeletal myosin light chain kinase (skMLCK) to 20 and 65%, respectively, whereas with gizzard smooth muscle MLCK (gMLCK), the protein was only activated to approximately 10% for each CaM fragment (Persechini *et al.*, 1994). However, when the trypic digests were combined in the assay at higher concentrations (~1000 times more concentrated), skMLCK and gMLCK activity was restored to 85 and 80%, respectively, signifying that the tethering effect of CaM's central helix is not necessary for maximal activity (Persechini *et al.*, 1994). Subsequently, it has also been shown that nNOS is able to be activated in the presence of 5 x 10^6 fold excess nCaM to 50% whereas the C-terminal domain shows no apparent activity. When nNOS was assayed in the presence of nCaM and cCaM, 50% maximal activity was observed, indicating that an intact central helix is required for the full activation of the enzyme (Persechini *et al.*, 1994; Persechini *et al.*, 1996a). Our findings are in good correlation with previously reported literature, where the N-terminal domain in conjunction with the central linker region is required for nNOS activation (Persechini *et al.*, 1996a).

A more recent study tested the possibility that the C-terminal domain of CaM alone is sufficient for the activation of the edema factor of adenylyl cyclase from *Bacillus anthracis* (Drum *et al.*, 2000). They observed no enzyme activity of the exotoxin by the C-terminal domain of CaM,

which indicated that both the N- and C-terminal domains of CaM contributed to activation of the exotoxin.

Our results are novel since the N-terminal domain of CaM alone is sufficient to activate the iNOS isozyme to 70% maximal activity in the presence of Ca^{2+}. Although this is not the first time that a single domain of CaM has been reported to activate its target protein, it is unique in that iNOS is 70% active at stoichiometric concentrations of nCaM.

In addition, our results provide further insight into the requirement of CaM for iNOS expression. Cleavage of iNOS at the CaM-binding site by calpain I in the absence of CaM to protect the enzyme has been reported previously (Walker *et al.*, 2001); however, the aggregation phenomena observed here *in vitro* suggests that in the absence of coexpressed CaM, the iNOS enzyme can aggregate forming inclusion bodies and greatly reducing protein yield. A recent paper reported that mammalian cells may regulate iNOS by removing misfolded and aggregated proteins by a pathway that leads to the formation of aggresomes (Kolodziejska *et al.*, 2005). This may provide a rapid means of clearing the cells of iNOS that would be detrimental to the cell due to its prolonged production of large amounts of •NO. Our finding that displacement of CaM from iNOS leads to aggregation provides a possible mechanism for the regulation of the enzyme. The total intracellular concentration of CaM in the cell appears to be significantly lower than the total concentration of its targets, making it a limiting factor in their regulation (Persechini and Stemmer, 2002). In the dynamic environment of the cell, the network of CaM-dependent signaling pathways may play a role in the cellular regulation of protein processing. Excess production of iNOS in the absence of sufficient quantities of CaM may lead to the aggregation of the enzyme and ultimately its disposal.

Chapter 4
Calcium-deficient Calmodulin Binding and Activation of Neuronal and Inducible Nitric Oxide Synthases *

4.1 Introduction

CaM consists of two globular lobes containing an EF hand pair joined by a central linker region. The C-terminal EF hand pair has a ten fold greater affinity for Ca^{2+} than the N-terminal EF hand pair (Martin *et al.*, 1985). The binding of Ca^{2+} to CaM induces conformational changes in both lobes, leading to a binding state with increased exposure of hydrophobic amino acids that allows for CaM to associate with several target proteins including the NOS isozymes. At elevated Ca^{2+} concentrations, CaM binds to the cNOS enzymes, nNOS and eNOS, making them the Ca^{2+}-dependent NOS enzymes. In contrast, iNOS is transcriptionally regulated *in vivo* by cytokines and binds to CaM at basal levels of Ca^{2+}. Although iNOS is commonly referred to as being Ca^{2+}-independent, we and others have shown that •NO production decreased by about 30% when Ca^{2+} is chelated *in vitro* (Venema *et al.*, 1996; Newman *et al.*, 2004; Spratt *et al.*, 2006).

The question of whether the apo-form of CaM binds to iNOS cannot be simply tested by chelating Ca^{2+} due to the possibility of chelating other divalent metal ions present in the iNOS enzyme or CaM that are potentially essential for enzyme function, such as Fe^{2+}, Zn^{2+}, and Cu^{2+}

*** The results presented in this chapter have been published:**
Spratt, D.E., Taiakina, V., and Guillemette, J.G. (2007) Calcium-deficient Calmodulin Binding and Activation of Neuronal and Inducible Nitric Oxide Synthases. *Biochim Biophys Acta 1774*, 1351-1358.

Unless otherwise stated, all of the work reported in this chapter was performed and analysed by the candidate.

(Demura *et al.*, 1998; Perry and Marletta, 1998; Crane *et al.*, 1999). Additionally, previous studies have demonstrated the effect of various divalent cations on the activation or inhibition of nNOS (Nishimura *et al.*, 1999; Weaver *et al.*, 2002; 2004), which may or may not have an effect on iNOS. Furthermore, the interaction of CaM with its target protein facilitates the tighter binding of Ca^{2+} to CaM (Olwin and Storm, 1985), although exceptions have been reported. For example, the association of CaM with the SK channel results in the locking of the C-terminal lobe of CaM in a Ca^{2+}-free semi-open state (Schumacher *et al.*, 2001). Furthermore, the binding of the edema factor from *B. anthracis* to CaM locks the N-terminal lobe of CaM in a closed conformation regardless of its Ca^{2+} loading state, causing a significant reduction of the N-terminal lobe of CaM's affinity for Ca^{2+} (Shen *et al.*, 2005).

We decided to further investigate the Ca^{2+}-dependent/independent properties of both the binding and activation of iNOS by CaM. To accomplish this, we employed a series of CaM mutants that are defective in Ca^{2+} binding in either the N-terminal lobe (CaM_{12}; CaM D21A and D56A mutations), the C-terminal lobe (CaM_{34}; CaM D93A and D131A), or all four of its Ca^{2+}-binding EF hands (CaM_{1234}; mutations at D21A, D56A, D93A and D131A inclusive). Figure 4.1 shows a schematic representation of these Ca^{2+}-deficient CaM mutants. A previous investigation using single EF hand Ca^{2+}-deficient CaM mutant proteins only studied their effect on the activation of iNOS (Gribovskaja *et al.*, 2005). In order to unequivocally determine whether the binding and activation of iNOS by CaM is Ca^{2+}-independent, we used CaM_{1234} to emulate Ca^{2+}-free CaM. However, as previous studies have demonstrated that the N- and C-terminal lobes of CaM can also be devoid of Ca^{2+} when associated with its target proteins (Schumacher *et al.*, 2001; Shen *et al.*, 2005), we have also used CaM_{12} and CaM_{34} to determine if the Ca^{2+}-independent association of CaM to iNOS is related solely to the Ca^{2+}-free N- or C-terminal lobe of CaM.

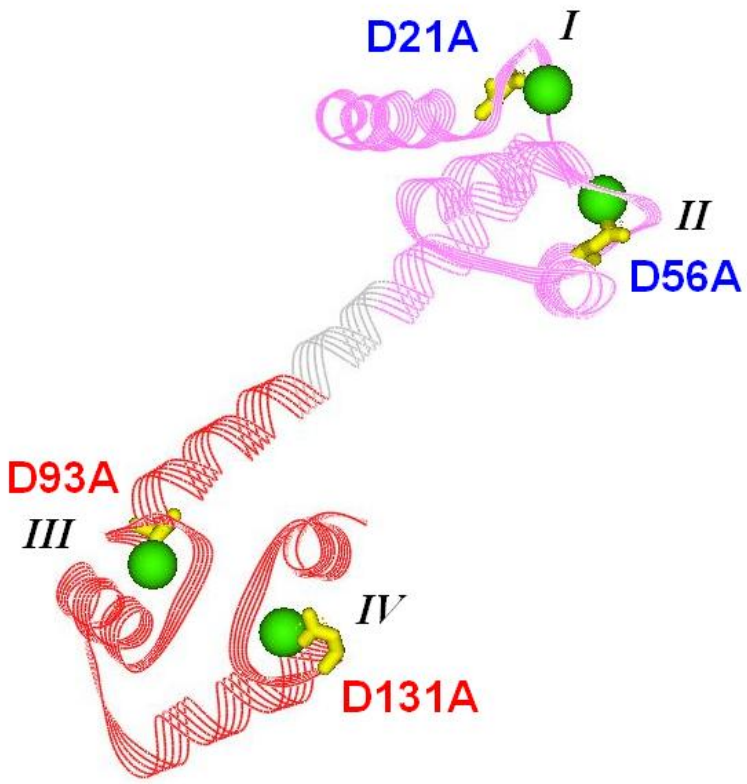

Figure 4.1 – Schematic representation of CaM_{12}, CaM_{34}, and CaM_{1234}.
Mutations at the highly conserved aspartate residues at position 1 in each CaM EF hand (shown in yellow) make the Ca^{2+}-binding motif incapable of binding Ca^{2+}. CaM_{12}, which is unable to bind Ca^{2+} in EF hands I and II (N-domain, mutations D21A and D56A) is labeled in blue. CaM_{34}, which is unable to bind Ca^{2+} in EF hands III and IV (C-domain, mutations D93A and D131A), is labeled in red. CaM_{1234}, which is incapable of binding Ca^{2+} in all four EF hands (both the N- and C-domains, mutations D21A, D56A, D93A, and D131A inclusive), contains all four mutations shown in blue and red. This schematic representation is based upon a previous study (Kilhoffer *et al.*, 1992) and was derived from PDB 1CLL (Chattopadhyaya *et al.*, 1992).

4.2 Experimental Procedures

4.2.1 Molecular Cloning of CaM_{12}, CaM_{34}, and CaM_{1234}

Plasmids coding for CaM_{12}, CaM_{34} and CaM_{1234} were a generous gift from Dr. John Adelman (Oregon Health & Sciences University, Portland, OR, USA) (Lee *et al.*, 2003). The ampicillin resistance of these plasmids necessitated the construction of new vectors for coexpression with iNOS. The cloning of these CaM constructs was performed by the candidate and assisted by Miss Valentina Taiakina (UW Co-op student). The coding regions of each CaM protein were PCR amplified introducing unique flanking *Nco*I and *Sac*I restriction sites for subcloning into a vector suitable for coexpression. The primers used were:

ApoCaMfr 5' AT*TCTAGA*CCATGGCTGACCAACTGACTGAAGAGCAGATCG 3' and ApoCaMrv 5' AT*GTCGAC*GAGCTCTTATCACTTCGCTGTCATCATTTGTAC 3'. The PCR products were subcloned into the kanamycin resistant vector pET28a (Novagen) using the unique *Nco*I and *Sac*I sites. The resulting vectors, $pCaM_{1234}$Kan, $pCaM_{12}$Kan, and $pCaM_{34}$Kan, were verified by DNA sequencing to ensure that no spontaneous mutations had occurred.

4.2.2 Ca^{2+}-deficient CaM protein Expression and Purification

Wild-type CaM was expressed and purified as previously described (sections 2.2.2 and 2.2.3). Overnight cultures of *E. coli* BL21 (DE3) transformed with $pCaM_{1234}$Kan, $pCaM_{12}$Kan, and $pCaM_{34}$Kan were used to inoculate 2 x 1 L of Luria-Bertani media in 4 L flasks supplemented with 30 μg/ml of kanamycin. Cultures were grown at 37ºC, 200 rpm to an OD_{600} of 0.6 to 0.8, induced with 500 μM IPTG and were subsequently harvested after 4 hours of expression, flash frozen on dry ice, and stored at –80ºC. Cells were lysed by five rapid cycles of freeze-thawing between liquid nitrogen and 37°C in a buffer containing 50 mM MOPS, pH 7.5, 100 mM KCl, 1 mM EDTA, 5 mM DTT and 1 mM PMSF. The lysate was clarified by centrifugation at 48,000 g for 30 minutes at 4°C. In order

to remove excess contaminating RNA, the supernatant was treated with NaOH (0.285 M final) heated at 65°C for 15 minutes to allow the RNA complete its self-cleavage. To every 7.5 mL of supernatant, 5 mL of 0.5 M EDTA, 4.5 mL of H_2O, and 0.5 mL of 10 M NaOH was added. This reaction was neutralized with the addition of an equal volume of 1 M HEPES, pH 7.4, which lowered the pH to 8.0. The sample was subsequently heated at 85°C for 10 minutes to precipitate the *E. coli* proteins, as previously described (Salas *et al.*, 2005) and immediately cooled on ice. The sample was then clarified by centrifugation at 48,000 g for 30 minutes at 4°C. Since the larger molecular weight proteins were precipitated by heating, the sample was concentrated with an Amicon YM-10 membrane until the total volume was less than 10 mL, similar to the method previously described to purify CaM_{1234} (Sienaert *et al.*, 2002). The CaM proteins were then exhaustively dialysed against 50 mM Tris, pH 7.5, 1 mM $CaCl_2$, and 1 mM DTT. The purity of the CaM proteins was verified by SDS-PAGE and the final protein concentrations were determined using the *DC* Bio-Rad Protein Assay (Bio-Rad Laboratories, Mississauga, ON) based upon the Lowry method (Lowry *et al.*, 1951). Finally, the CaM proteins were aliquoted, flash frozen on dry ice, and stored at –80°C. Electrospray ionization-mass spectrometry (ESI-MS) was performed on the purified CaM proteins using a Micromass Q-Tof Ultima GLOBAL mass spectrometer (Manchester, U.K.) with an internal standard as previously described in section 2.2.5 (Spratt *et al.*, 2006).

4.2.3 NOS Enzyme Expression and Purification

Rat nNOS was expressed and purified as previously described (Roman *et al.*, 1995) with the exception that the enzyme had an N-terminal polyhistidine tail cloned upstream from its respective start codon. Human iNOS carrying a deletion of the first 70 amino acids and an N-terminal polyhistidine tail was coexpressed with wild-type CaM or CaM mutant protein in *E. coli* BL21 (DE3), as previously described in section 2.2.8. The coexpression and purification of iNOS

coexpressed with these CaM mutant proteins was performed by the candidate and assisted by Miss Valentina Taiakina (UW Co-op student).

Purification of iNOS coexpressed with CaM proteins involved a 45% ammonium sulfate precipitation followed by metal chelation chromatography (section 2.2.9). After elution of the protein with 200 mM imidazole, the samples were dialysed as previously described in section 2.2.9 followed by the use of a Vivaspin 15 ultrafiltration spin column (Sartorius AG Biotechnology, Goettingen, Germany) to concentrate the sample to approximately 2 mL in order to prepare the protein sample for gel filtration. Using a HiLoad 16/60 Superdex 200 prep grade column (GE Healthcare Bio-Sciences, Baie d'Urfe, PQ) equilibrated with 50 mM Tris-HCl, pH 7.5, 10% glycerol, 0.1 M NaCl, and 1 mM DTT, the sample was loaded and 1 mL fractions were collected. The flow rate was maintained at 0.6 mL/min using an AKTApurifier System for Chromatography (GE Healthcare Bio-Sciences) and eluted protein, heme and flavins were monitored at 280 nm, 398 nm, and 450 nm respectively. A gel filtration standard kit (Sigma, Oakville, ON) containing multiple molecular mass markers was used to calibrate the column. Fractions that eluted around 56.6 mL, which corresponds to the dimer of iNOS with CaM bound, were collected and pooled. An example elution profile for iNOS coexpressed with CaM_{12} is shown in Figure 4.2.

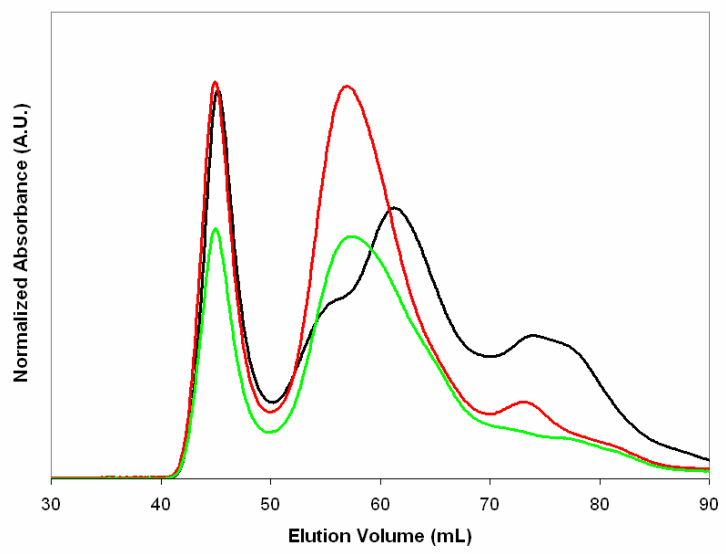

Figure 4.2 – Gel filration elution profile of iNOS coexpressed with CaM_{12}.
Absorbance at 280 (protein; —), 398 (heme; —), and 450 nm (flavins; —) were monitored to track the elution of iNOS coexpressed CaM_{12} the from HiLoad 16/60 Superdex 200 prep grade column. Two milliliters of iNOS coexpressed with CaM_{12} was loaded on to the gel filtration column equilibrated with 50 mM Tris-HCl, pH 7.5, containing 10% glycerol, 0.1 M NaCl, and 1 mM dithiothreitol. Results shown are representative of two similar experiments.

No iNOS monomer was observed using this methodology. The purified iNOS enzymes were subsequently aliquoted, flash frozen on dry ice and stored at -80°C. Flavin content was determined as previously described (Faeder and Siegel, 1973).

4.2.4 NOS Enzyme Kinetics

The NADPH oxidation (section 2.2.10.3), ferricyanide (FeCN) reduction (described in section 4.2.4.1), cytochrome *c* reduction (section 2.2.10.2), and the oxyhemoglobin capture (section 2.2.10.1) assays were performed to monitor electron transfer rates at each redox center of each NOS enzyme, as previously described in Figure 2.5. All of the assays were performed in 96 well microtitre plates in total well volumes of 100 µl at 25°C in a SpectraMax 384 Plus 96 well UV-visible spectrophotometer

using Soft Max Pro software (Molecular Devices, Sunnyvale, CA). 200 μM $CaCl_2$ or 250 μM EDTA, as well as 2 μM wild-type CaM or mutant CaM proteins were added to the appropriate samples.

4.2.4.1 Ferricyanide Reduction Assay

The spectrophotometric NADPH-dependent ferricyanide assay was used to assess the initial rate of electron transfer in the NOS reductase domain to the FAD domain. This assay was performed in a similar manner to the cytochrome *c* reduction assay (section 2.2.10.2) with the exception that no DTT or H_4B was added. Since we want to observe the reduction of ferricyanide exclusively by NOS, DTT and H_4B were not included in this assay because of their ability to reduce ferricyanide. This assay involved the use of three separate solutions: (1) the enzyme solution, (2) the ferricyanide solution, and (3) the NADPH solution. The enzyme solution consisted of the NOS enzyme in a 50 mM Tris-HCl, pH 7.5 @ RT buffer with 10 μM FAD, 10 μM FMN, 200 μM NADPH, 10 U/mL catalase, 10 U/mL SOD, 0.1 mg/mL BSA and 10% glycerol. NADPH was prepared fresh on the day of the assay. The NADPH was added to this solution to react with any L-arginine in the enzyme solution from the dialysis buffer of the NOS. The ferricyanide solution contained ferricyanide (ε_{420} = 1.2 mM^{-1} cm^{-1}), Tris-HCl, $CaCl_2$ or EDTA (depending on the enzyme being tested), BSA, catalase, and SOD. The NADPH solution contained only NADPH used to initiate the assay.

The assay reactions were performed adding 10 μL of complete enzyme solution (NOS enzyme, with or without CaM, and enzyme solution), followed by a 2 minute incubation at 25°C. Following the incubation, 50 μL of ferricyanide solution was added to each well containing the complete enzyme solution, followed by a 30 second incubation. After this brief incubation, the assay was initiated by the addition of 40 μL of NADPH solution to each well, for a total of 100 μL per well. The final initiated reaction contained ferricyanide (1 mM), Tris-HCl (50 mM, pH 7.5 at 25°C), glycerol (1%), FMN (1 μM), FAD (1 μM), NADPH (200 μM), BSA (0.1 mg/mL), catalase (10 U/mL), and SOD (10 U/mL). eNOS, nNOS, and iNOS coexpressed with CaM or mutant CaM

protein were assayed at 50, 5.5, and 5.5 nM in 100 μL total well volume in quadruplicate. $CaCl_2$ (200 μM), EDTA (250 μM), and CaM (2 μM) or mutant CaM protein were added to the appropriate samples unless otherwise stated.

After initiation, the microtitre plate was read at 25 – 27°C in a SpectraMax 384 Plus 96 well UV-visible spectrophotometer using Soft Max Pro software (Molecular Devices, Sunnyvale, CA). The reactions were read at 420 nm over 5 minutes at 7 second intervals. Equation 4.1 was used to calculate the activity of the enzyme based upon the rate of absorbance change at 420 nm.

Equation 4.1 $$\text{Activity} = v \times 60\ \text{s} \bullet \text{min}^{-1} / \Delta\varepsilon_{420\ \text{nm (ox FeCN to red FeCN)}} / (\text{well volume} \times [\text{NOS enzyme}]\ \text{in nM} \times \text{NOS molecular weight in g/mol} \times 1000\ \text{mg/g})$$

where v represents the slope of the change of absorbance over time in seconds. The extinction coefficient $\Delta\varepsilon_{420\ \text{nm ox FeCN to red FeCN}}$ of -0.04882 OD_{340} per nanomole was used. Activity is expressed as nanomoles of ferricyanide reduced per minute per milligram of enzyme (nmol red FeCN min^{-1} mgP^{-1}).

4.2.5 CaM Proteins Fluorescent Labeling with Dansyl Chloride

The CaM proteins were transferred into labeling buffer (0.1 M sodium bicarbonate, pH 7.5 containing 1 mM EDTA) by gel filtration using a Sephadex G-25 PD-10 column (Amersham Biosciences), as described in section 6.2.2.5 (Lang *et al.*, 2005). The concentrations of the CaM proteins were at least 5 mg/mL and the labeling conditions and duration using dansyl chloride (Figure 4.3) were performed as suggested by the manufacturer (Molecular Probes, Eugene, OR, USA).

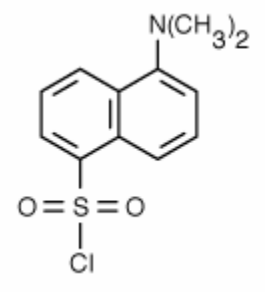

Figure 4.3 – Chemical structure of dansyl chloride used to N-terminally label wild-type CaM, CaM_{12}, CaM_{34}, and CaM_{1234}.
Dansyl chloride (5-dimethylaminonapthalene-1-sulfonyl chloride) was purchased from Molecular Probes.

Excess dansyl chloride was removed by exhaustive dialysis against 50 mM HEPES, 1 mM EDTA, 150 mM NaCl, pH 7.5 to ensure that all non-covalently linked dye was removed from the labeled CaM proteins, as described in section 5.2.3 and other labeling studies (Ottl *et al.*, 1998; Waxham *et al.*, 1998; Spratt *et al.*, 2007b). Labeling yields were determined from absorbance spectra using the ε_{372} of 3,900 $M^{-1}cm^{-1}$ (Molecular Probes) and were compared to actual protein concentrations determined using the Lowry method (Lowry *et al.*, 1951) with wild-type CaM used as the protein standard. Dansyl-labeling versus protein concentration showed that 0.6-0.8 mol of dansyl chloride was incorporated for each mol of CaM protein. ESI-MS (section 2.2.5) was used to confirm successful dansyl-labeling of each CaM protein.

4.2.6 Steady-state Fluorescence Measurements

Fluorescence emission spectra were obtained using a PTI QuantaMaster spectrofluorimeter (London, ON). In an initial volume of 1 mL, a scan of each dansyl-CaM protein (2 μM) was taken in a buffer consisting of 50 mM HEPES, 1 mM EDTA, 150 mM NaCl, pH 7.5. The excitation wavelength for all of the dansyl-labeled CaMs was set at 340 nm and emission was monitored between 400 and 600 nm. Slit widths were set at 2 nm for excitation and 1 nm for emission. The free $[Ca^{2+}]$ was calculated to be <1 nM according to the online algorithm WEBMAXC (Patton *et al.*, 2004). After the first scan,

$CaCl_2$ (0.5 mM final) was added to the cuvette (calculated free [Ca^{2+}] of 0.500 mM), the sample was mixed thoroughly, allowed to incubate for three minutes to reach equilibrium, and scanned. Synthetic rat nNOS or human iNOS CaM-binding domain peptide (10 μM) was subsequently added to the cuvette, the sample was mixed, allowed to incubate, and finally scanned. The NOS CaM-binding domain peptides for rat nNOS (KRRAI GFKKL AEAVK FSAKL MGQ; residues 725–747) and human iNOS (RPKRR EIPLK VLVKA VLFAC MLMRK; residues 507–531) were synthesized by Sigma-Genosys (Oakville, ON). A large blue-shifted emission spectra represents a change in the environment of the dansyl fluorophore due to the CaM protein binding to the NOS peptide. Finally, excess EDTA (5 mM final) was added (calculated free [Ca^{2+}] of 5.8 nM), incubated for three minutes, and a final scan was taken.

4.2.7 Circular Dichroism of Ca^{2+}-deficient CaM Proteins Bound to Synthetic NOS Peptides

CD was performed using a Jasco J-715 CD spectropolarimeter and analyzed using J-715 software (Jasco Inc., Easton, MD, USA) as previously described (Fernando *et al.*, 2002) with some modifications. Samples were measured in a 1 mm quartz cuvette (Hellma, Concord, ON) and kept at 25°C using a Peltier type constant-temperature cell holder (model PFD 3505, Jasco, Easton, MD). Samples consisted of 10 μM wild-type CaM or Ca^{2+}-deficient CaM proteins alone or with equimolar concentrations of synthetic nNOS or iNOS CaM-binding domain peptide. Samples were mixed in 10 mM Tris-HCl buffer (pH 7.5), 150 mM NaCl, containing 200 μM $CaCl_2$ followed by 1 mM EDTA.

4.3 Results and Discussion

Numerous studies have used Ca^{2+} chelators such as EGTA and EDTA to study the Ca^{2+}-dependence of CaM and CaM mutants binding to various CaM-dependent target proteins, including the NOS isozymes (Persechini *et al.*, 1996a; b; Venema *et al.*, 1996; Stevens-Truss *et al.*, 1997; Gachhui *et al.*, 1998; Montgomery *et al.*, 2003; Newman *et al.*, 2004; Gribovskaja *et al.*, 2005; Spratt *et al.*, 2006). Since the interaction of CaM with its target protein myosin light chain kinase (MLCK) facilitates the tighter binding of Ca^{2+} to CaM (Olwin and Storm, 1985), the use of chelators cannot always be used to infer apo-CaM's association to a target protein. Although CaM does bind to the nNOS and iNOS in an antiparallel orientation (Zhang *et al.*, 1995; Spratt *et al.*, 2007b), similar to CaM in complex with MLCK, the tighter binding of Ca^{2+} to the CaM-NOS complex has yet to be proven. In order to determine unequivocally that apo-CaM binds to a Ca^{2+}-independent CaM-target protein, biophysical studies must demonstrate that the protein's association occurs with apo-CaM and not with a CaM variant bound to 1, 2, 3 or 4 Ca^{2+} ions (Jurado *et al.*, 1999). In order to overcome the need of Ca^{2+} chelators, we have coexpressed iNOS with CaM_{12}, $CaM_{34,}$ and CaM_{1234} to investigate Ca^{2+}-free forms of each lobe and the entire CaM protein's abilities to bind and activate iNOS *in vitro*. Furthermore, other divalent cations have previously been shown to have a direct effect on the activity of the NOS enzymes. Perry and Marletta have reported that NOS has the ability to bind to transition metals in a stoichiometric fashion, and have demonstrated that the rate of •NO catalysis is also enhanced by a non-heme iron (Perry and Marletta, 1998). Similarly, Crane and coworkers reported a correlation between the three-dimensional swapping of the N-terminal hook and zinc metal ion release with disulfide formation where they proposed that these may have an impact on iNOS's stability and regulation *in vivo* (Crane et al., 1999). Another study reported that divalent copper ions are capable of activating eNOS activity in crude cell extracts and intact endothelial cells (Demura *et al.*, 1998). Previous studies using nNOS have also demonstrated that the addition of metals such as Ni^{2+}, Ba^{2+},

Mn^{2+}, Pb^{2+}, Sr^{2+}, Cd^{2+}, and Rb^{2+} are able to activate nNOS, whereas Cd^{2+} and combinations of Ca^{2+} with Ni^{2+}, Cd^{2+}, or Mn^{2+} can potently inhibit the enzyme (Nishimura *et al.*, 1999; Weaver *et al.*, 2002; 2004). Our investigation was performed to remove any possible effect that divalent metal chelation has on enzyme activity. The mutant CaM proteins used allowed for the specific investigation of Ca^{2+}-dependent/independent activation and binding of CaM to iNOS.

4.3.1 Protein Expression and Purification

The CaM_{1234}, CaM_{12}, and CaM_{34} constructs previously described (section 4.1) produced good independent expression ranging from 75.3 to 105.8 mg protein/L media, depending on the CaM mutant. Purified CaM constructs appeared over 95% homogeneous on 15% SDS-PAGE and ESI-MS QTOF ruled out posttranslational modification and confirmed homogeneity (Figure 4.4; Table 4.1)

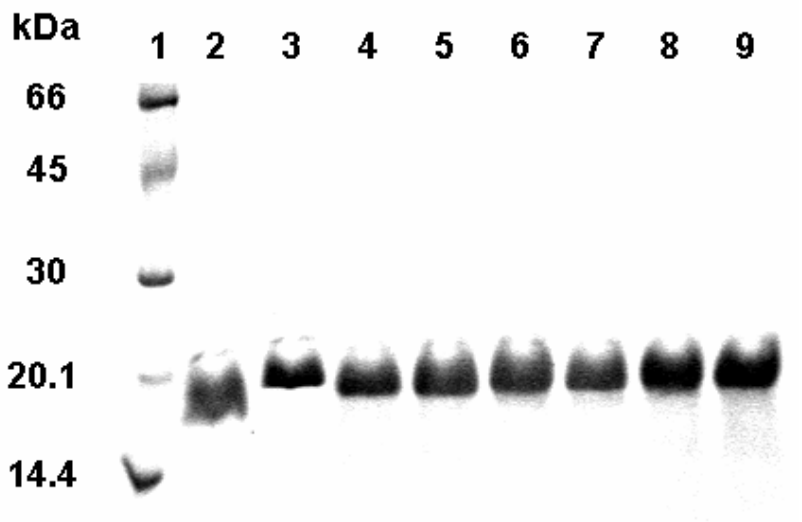

Figure 4.4 – 15% SDS-PAGE of the purified Ca^{2+}-deficient CaM proteins.
A 10 µg sample of each purified CaM protein was loaded onto a standard SDS-PAGE loading buffer containing either 10 mM $CaCl_2$ or EDTA. *Lane 1* – low molecular weight SDS protein marker (GE Healthcare Bio-sciences), *Lanes 2 and 3* – wild-type CaM in the presence of Ca^{2+} and EDTA, respectively, *Lanes 4 and 5* – CaM_{1234} in Ca^{2+} and EDTA, *Lanes 6 and 7* – CaM_{12} in Ca^{2+} and EDTA, *Lanes 8 and 9* – CaM_{34} in Ca^{2+} and EDTA.

Table 4.1 – Masses of CaM proteins and fluorescently labeled CaM proteins

	Mass (Da) [a]	
	Observed	Theoretical
CaM proteins		
Wild-type CaM	16706.0	16706 [b]
CaM_{1234}	16530.0	16530
CaM_{12}	16617.5	16618
CaM_{34}	16617.5	16618
Fluorescent CaM proteins		
Dansyl-wild-type CaM	16936.6	16940 [c]
Dansyl-CaM_{1234}	16762.6	16764
Dansyl-CaM_{12}	16852.0	16853
Dansyl-CaM_{34}	16851.2	16853

[a] Masses of deconvoluted ESI-MS spectra were determined with an accuracy of ± 4 Da.

[b] Calculated masses based upon amino acid sequence.

[c] Expected mass difference with covalently attached dansyl group is 234.3 (Molecular Probes). The manufacturer's MW of the dye is 269.8 Da, which includes a chloride ion that is released upon reaction with the N-terminal amino group.

The iNOS enzyme was coexpressed with CaM or a mutant CaM construct. Coexpression with wild-type CaM produced the highest yields of purified iNOS (4.8 mg/L). Coexpression of iNOS with CaM_{12} yielded 0.4 mg/L while coexpression with CaM_{34} gave 0.5 mg/L. Expression of iNOS with CaM_{1234} gave the lowest yields of 0.2 mg/L. Heme and flavin content of the purified iNOS enzymes coexpressed with CaM_{12} and CaM_{34} constructs were the same as that of iNOS coexpressed with wild-type CaM. In contrast, coexpression of iNOS with CaM_{1234} demonstrated a lower content of flavin to heme (25% when compared to iNOS coexpressed with wild-type CaM), indicative of protein instability during expression or purification. From the relative yields of iNOS enzyme isolated with each of the CaM mutants, it is apparent that some form of Ca^{2+}-dependent change in CaM's structure is required to produce stable and active iNOS enzyme.

4.3.2 nNOS Activation by Ca^{2+}-deficient CaM Proteins

Wild-type CaM was the only CaM protein capable of activating nNOS to produce •NO and reduce cytochrome *c*. CaM_{12}, CaM_{34}, and CaM_{1234} showed little or no activity (Figure 2A). Furthermore, wild-type CaM was unable to bind and activate nNOS in the presence of 250 μM EDTA. These results are consistent with previous reports that Ca^{2+}-replete CaM is required to bind and fully activate nNOS (Stevens-Truss *et al.*, 1997; Newman *et al.*, 2004; Spratt *et al.*, 2006).

4.3.3 iNOS Activation by Ca^{2+}-deficient CaM Proteins

The coexpression of iNOS with CaM_{12} and CaM_{34} constructs resulted in reproducible •NO production rates of approximately 75% and 115%, respectively, in the presence of Ca^{2+} (Figure 4.5A). In contrast, iNOS coexpressed with CaM_{1234} resulted in lower •NO production rates of less than 25% which can be correlated to the lower FMN content of the enzyme. The addition of excess wild-type CaM and mutant CaM proteins to iNOS coexpressed with each of the CaM constructs did not result in any significant change in enzyme activity, indicative that the CaM-binding sites were saturated with mutant CaM proteins and did not exchange rapidly with CaM in solution, identical to our previous studies (Newman *et al.*, 2004; Spratt *et al.*, 2006).

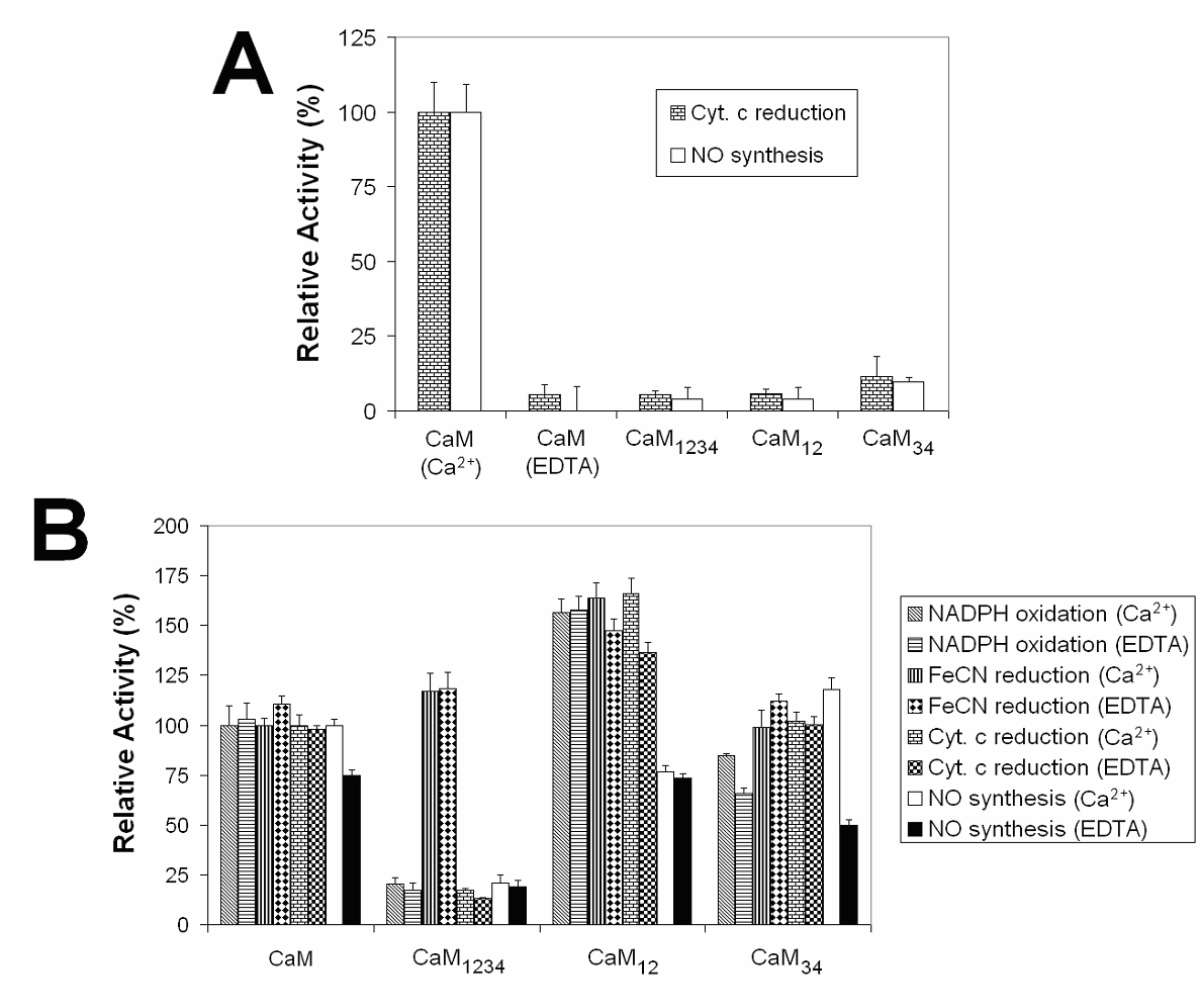

Figure 4.5 – Ability of wild-type CaM and Ca^{2+}-deficient mutant CaM proteins to activate NOS enzymes.

(A) Activation of nNOS by mutant CaM proteins. The oxyhemoglobin capture and cytochrome *c* reduction assays were performed in the presence of either 2 µM wild-type or mutant CaM protein and either 200 µM $CaCl_2$ or 250 µM EDTA, as indicated. The activities obtained with nNOS bound to wild-type CaM at 25°C in the presence of 200 µM $CaCl_2$ were all set to 100%. Under these conditions, the activities for nNOS bound to CaM were 54.5 min^{-1} (•NO synthesis) and 848.5 min^{-1} (cytochrome *c* reduction). **(B)** Activation of iNOS by mutant CaM proteins. The iNOS enzyme was coexpressed separately with each of the CaM proteins and then purified. •NO synthesis, cytochrome *c* reduction, ferricyanide reduction, and NADPH oxidation rates were measured as described in (A) except that no exogenous CaM was added to the assay. Each assay was performed in the presence of either 200 µM $CaCl_2$ or 250 µM EDTA as indicated. The activities obtained for iNOS coexpressed with CaM and assayed in the presence of 200 µM $CaCl_2$ at 25°C were all set to 100% and were 61.7 min^{-1} (•NO synthesis), 978 min^{-1} (cytochrome *c* reduction), 32688 min^{-1} (ferricyanide reduction) and 88.5 min^{-1} (NADPH oxidation). The bar values represent the mean ± standard deviation. Each experiment was performed in quadruplicate and repeated three or more times.

The addition of 250 μM EDTA to chelate Ca^{2+} resulted in a significant decrease in the stimulation of •NO production by wild-type CaM and CaM_{34}. The iNOS enzyme coexpressed with wild-type CaM decreased to 75%, which was consistent with previous studies that demonstrated there is some Ca^{2+}-dependence in iNOS •NO synthesis (Venema *et al.*, 1996; Newman *et al.*, 2004; Spratt *et al.*, 2006). Similarly, iNOS coexpressed with CaM_{34} decreased to 50% in the absence of Ca^{2+} (Figure 4.5B). In contrast, iNOS coexpressed with CaM_{1234} and CaM_{12} showed no Ca^{2+}-dependence in •NO synthesis rates. These results show that a Ca^{2+}-dependent rearrangement of the N-terminal lobe of CaM may be responsible for the partial Ca^{2+}-dependence of iNOS. Furthermore, the observation that the maximal activity of iNOS coexpressed with CaM_{12} is identical in the presence and absence of Ca^{2+} at 75% further supports this result. Consistent with our previous studies, the C-terminal lobe of CaM is responsible for the binding and stability of iNOS, while the N-terminal domain contains the important elements requiring Ca^{2+}-replete conditions for the activation of iNOS (Spratt *et al.*, 2006).

Comparing the stimulation of NADPH oxidation by the CaM constructs showed a pattern comparable to the activation of •NO synthesis by iNOS (Figure 4.5B). Coexpression of wild-type CaM, CaM_{1234}, CaM_{12} and CaM_{34} with iNOS resulted in a stoichiometry of about 1.5 NADPH oxidized per •NO formed in the presence of Ca^{2+}. Likewise, in the presence of a large excess of EDTA, all of the iNOS enzymes maintained tightly coupled electron transfer, with only iNOS coexpressed with wild-type CaM and CaM_{34} showing a slight increase in uncoupling with an NADPH to •NO produced ratio of 2 to 1. The greater uncoupling under Ca^{2+}-depleted conditions of iNOS coexpressed with wild-type CaM and CaM_{34} may again be due to a decreased efficiency of electron transfer due to the aforementioned Ca^{2+}-dependent rearrangement of the N-terminal lobe of CaM. The uncoupled reaction could be the result of the production of $•O_2^-$. Xia and coworkers reported that

iNOS generates $\bullet O_2^-$ mainly at the flavin-binding sites of the reductase domain when the enzyme is treated with heme blockers or L-arginine analogue NOS inhibitors (Xia *et al.*, 1998).

The ferricyanide and cytochrome *c* assays were used to monitor electron transfer from the FAD and FMN, respectively, to an exogenous electron acceptor (Figure 2.5). The coexpressed CaM_{12} with iNOS reproducibly displayed over 140% (FeCN and cyt. *c*) of the maximal activity obtained with wild-type CaM in the presence or absence of Ca^{2+} (Figure 4.5B). Similar to iNOS coexpressed with wild-type CaM, CaM_{34} had approximately 100% activity with little or no variance due to Ca^{2+} concentrations. These findings are consistent with the iNOS reductase domain being CaM-independent (Newton *et al.*, 1998). The iNOS enzymes coexpressed with CaM_{1234} showed slightly higher FeCN reduction rates but much lower rates of reduction for cytochrome *c*. The diminished rate of cytochrome *c* reduction can be attributed to low FMN content of this enzyme when coexpressed with CaM_{1234}.

4.3.4 Ca^{2+}-deficient CaM-NOS Peptide Binding Studies

4.3.4.1 Steady-state Fluorescence of Dansyl-labeled CaM Proteins

The binding of N-terminally labeled wild-type and Ca^{2+}-deficient CaM proteins to synthetic NOS CaM-binding domain peptides was observed using steady-state fluorescence. The addition of Ca^{2+} to the dansyl-labeled wild-type CaM proteins all demonstrated a blue-shifted emission and increased intensity, indicating that wild-type CaM is Ca^{2+}-replete and a structural rearrangement had occurred (Figure 4.6).

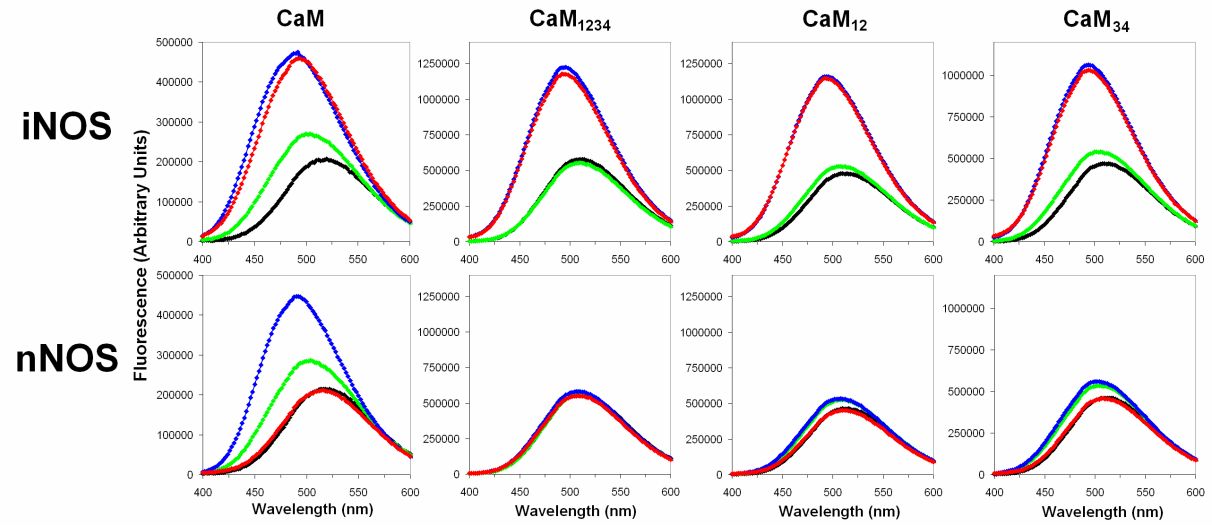

Figure 4.6 – Fluorescence emission spectra of dansyl-CaM proteins in the presence of nNOS and iNOS peptides.
In an initial volume of 1 mL, either dansyl-wild-type CaM, dansyl-CaM_{1234}, dansyl-CaM_{12}, or dansyl-CaM_{34} (2 µM final) was added to 50 mM HEPES, 150 mM NaCl, 1 mM EDTA, pH 7.5 with the emission of each sample observed between 400 and 600 nm (—). The excitation wavelength was set to 340 nm and the excitation and emission slit widths were set at 2 and 1 nm, respectively. $CaCl_2$ (0.5 mM final) was subsequently added and another scan was obtained (—). Wild-type CaM, CaM_{12}, and CaM_{34} showed slight changes in fluorescence while CaM_{1234} showed no effect, representing this protein's inability to bind Ca^{2+}. Synthetic NOS peptide (10 µM) was added, mixed thoroughly, allowed to incubate for 3 minutes to reach equilibrium, and another scan was taken (—). Lastly, EDTA was added to a final concentration of 5 mM, the sample was mixed, and a final scan was taken (—).

As expected, the addition of Ca^{2+} to dansyl-CaM_{1234} resulted in no change in fluorescence since CaM_{1234} is incapable of binding to Ca^{2+}. The addition of the nNOS peptide to dansyl-wild-type CaM caused a large increase in emission intensity and blue-shift, indicative of wild-type CaM's association to the nNOS peptide. Furthermore, the fluorescence increase observed caused by the CaM-nNOS peptide complex was completely reversible with the addition of EDTA, causing the release of the nNOS peptide. Conversely, there was no observed fluorescence change for CaM_{1234}, CaM_{12}, and CaM_{34} when nNOS peptide was added, representing no interaction between the mutant CaM proteins and the nNOS peptide (Figure 4.6). These results are consistent with our kinetic results that

Ca^{2+}-replete CaM is required for its binding to nNOS. In contrast, wild-type CaM as well as each of the declawed CaM proteins are capable of binding to the iNOS CaM-binding domain peptide in a Ca^{2+}-independent manner (Figure 4.6). The addition of excess EDTA had no effect on the association of CaM to the iNOS peptide, showing that unlike nNOS, this process appears to be irreversible. This result, especially with CaM_{1234}, confirms definitively that apo-CaM does in fact associate with iNOS.

4.3.4.2 Circular Dichroism of Ca^{2+}-deficient CaM Proteins

CD was employed to further investigate the Ca^{2+}-deficient CaM proteins ability to bind Ca^{2+} as well as their interaction with the nNOS and iNOS CaM-binding domains peptides. As expected, CaM_{1234} showed no evidence of binding to Ca^{2+} by spectropolarimetry (Figure 4.7), which is in good agreement with our fluorescence result (Figure 4.6). In contrast, CaM_{12} and CaM_{34} showed slight increases in α-helical content; however, the increase in secondary structure was smaller than the Ca^{2+}-dependent changes in wild-type CaM. This result was expected since Ca^{2+} binding to the N- and C-lobes is cooperative, where Ca^{2+}-binding to the C-terminal lobe of CaM effects the N-terminal's affinity for Ca^{2+} by inducing increased α-helicity in the central linker of CaM (Jurado *et al.*, 1999).

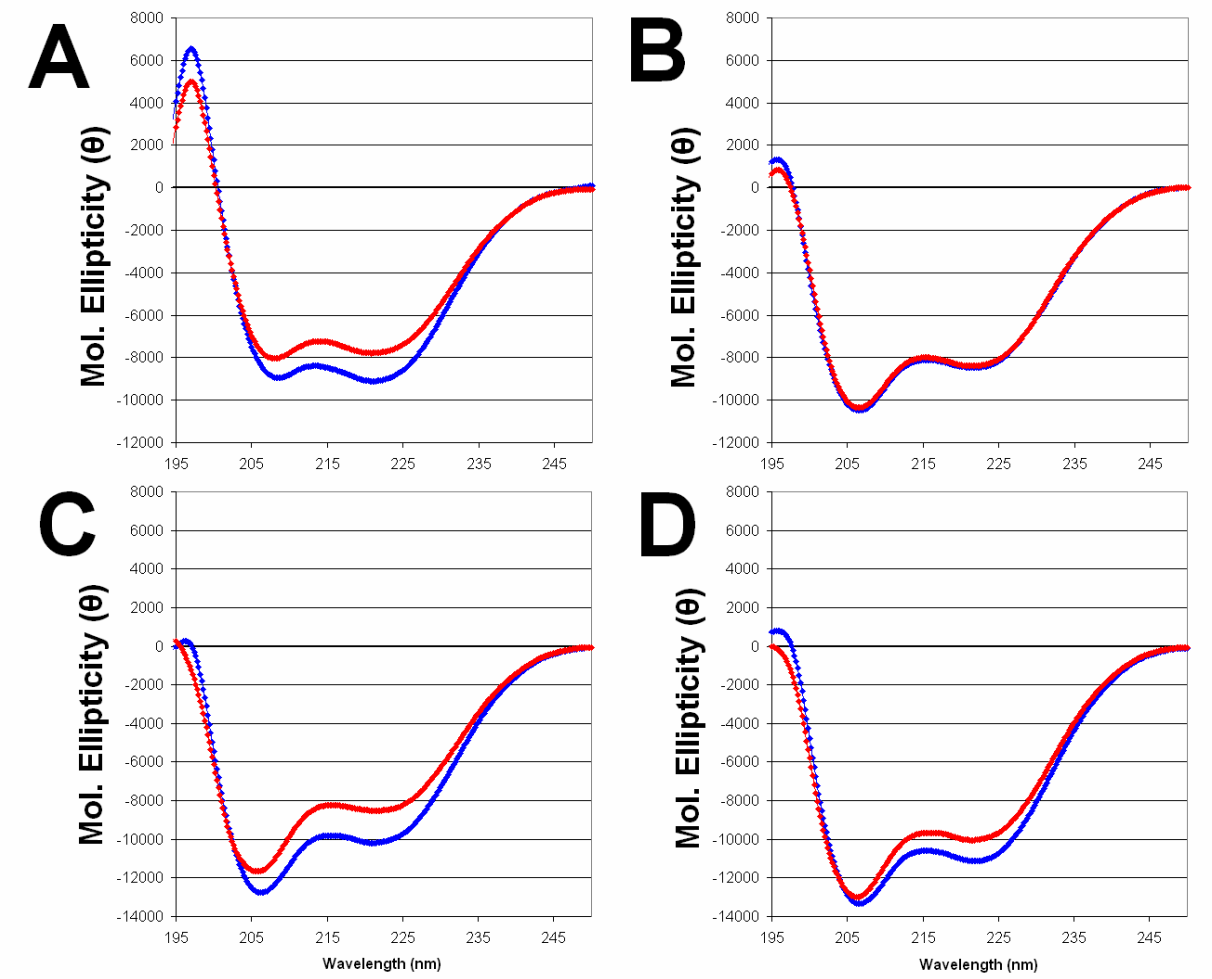

Figure 4.7 – CD spectra for (A) wild-type CaM, (B) CaM_{1234}, (C) CaM_{12}, and (D) CaM_{34} in the presence and absence of Ca^{2+}.
Concentrations of CaM and CaM proteins were 10 μM in 10 mM Tris-HCl, pH 7.5, containing 150 mM NaCl and 200 μM $CaCl_2$ or 1 mM EDTA. CaM protein in the presence of Ca^{2+} or EDTA are shown as (—◆—) and (—◆—), respectively.

Previous investigations have shown that spectropolarimetry is a useful method to monitor the secondary structure of peptides bound to CaM (Matsubara *et al.*, 1997; Yuan *et al.*, 1998; Spratt *et al.*, 2007b). In the absence of CaM proteins, both the nNOS and iNOS peptides showed no secondary structure and were predominantly random coil. The binding of Ca^{2+}-replete wild-type CaM to both the nNOS and iNOS peptide resulted in a large increase in α-helical content for each peptide (Figure 4.8).

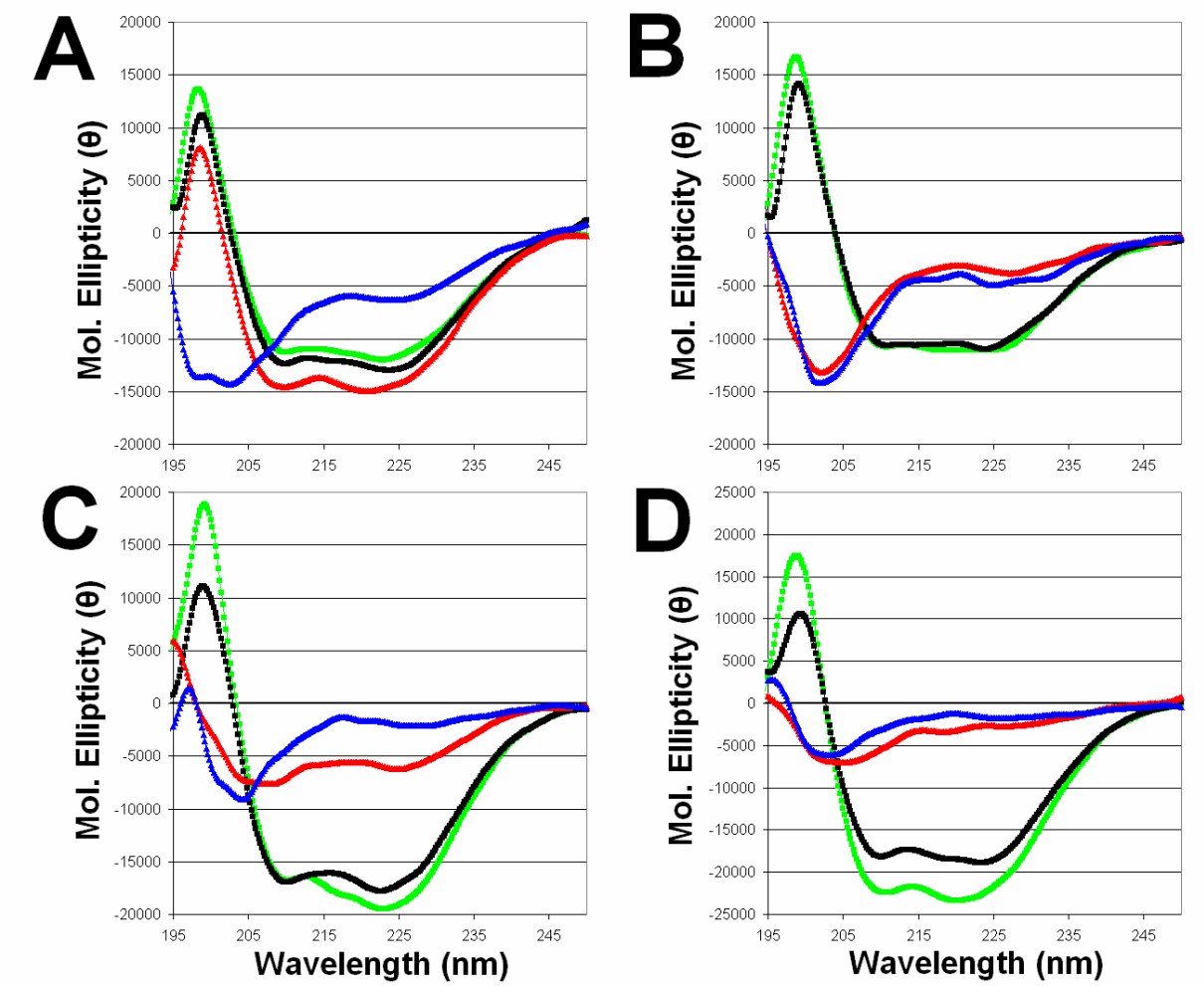

Figure 4.8 – Difference CD spectra for iNOS and nNOS CaM-binding domain peptides in the presence of (A) wild-type CaM, (B) CaM_{1234}, (C) CaM_{12}, and (D) CaM_{34}.
The spectra were calculated by subtracting the spectra for 10 μM CaM alone from the spectra for 10 μM CaM in the presence of 10 μM NOS peptide. Spectra for iNOS peptide in the presence of Ca^{2+} and EDTA are shown as (—■—) and (—■—), respectively. Spectra for nNOS peptide in the presence of Ca^{2+} (—▲—) and EDTA (—▲—) are shown to demonstrate the difference between the Ca^{2+}-dependent nNOS and Ca^{2+}-independent iNOS enzymes. Data is expressed as the mean residue ellipticity (θ) in degree cm^2 $dmol^{-1}$.

The subsequent addition of EDTA caused no change in secondary structure for the wild-type CaM-iNOS peptide complex while the nNOS peptide's secondary structure returned to random coil. These results are consistent with CaM-binding to iNOS being Ca^{2+}-independent and binding to nNOS being Ca^{2+}-dependent.

There was no evidence of association between CaM_{1234} and CaM_{34} with the nNOS peptide as there was no increase in α-helicity. In contrast, all three CaM mutants did show tight Ca^{2+}-independent binding to the iNOS peptide (Figure 4.8), which correlated well to the fluorescent dansyl-CaM results (Figure 4.6). In contrast to CaM_{1234} and CaM_{34}, CaM_{12} did show some Ca^{2+}-dependent association to the nNOS peptide (Figure 4.8). Although this result does not correlate with the dansyl-CaM_{12} binding results (Figure 4.6), it is important to note that the C-terminal lobe is likely the binding domain, while the N-terminal lobe may not be associated to the peptide at all. In a previous model describing sequential CaM binding to nNOS, it was proposed that the C-terminal lobe associates to the CaM-binding domain, followed by the N-terminal lobe (Weissman *et al.*, 2002). Since the C-terminal lobe of CaM_{12} is capable of binding to Ca^{2+}, as evidenced by fluorescence (Figure 4.6) and spectropolarimetry (Figure 4.7), it is conceivable that CaM_{12} would be able to associate to nNOS, however, it would not be able to wrap around the CaM-binding element as it normally would when activating the enzyme.

4.4 Conclusions

Our present results with CaM_{1234}, CaM_{12}, and CaM_{34} demonstrate that our earlier studies using chelators are representative of apo-CaM binding and activation of iNOS (Newman *et al.*, 2004; Spratt *et al.*, 2006) and that using these chelators is a suitable method to observe Ca^{2+}-dependent/independent interactions between CaM and the NOS enzymes. We have shown that apo-CaM is capable of binding and partially activating iNOS in a Ca^{2+}-independent manner, however, Ca^{2+}-replete conditions are required for the full activation of the enzyme. The Ca^{2+}-independence of CaM binding has previously been attributed to favorable van der Waals contacts between the peptide and CaM as well as conformational changes that minimize the exposure of hydrophobic regions of the peptide to solution (Aoyagi *et al.*, 2003). However, other studies have also demonstrated that regions flanking the CaM-binding domain are also responsible for the apparent Ca^{2+}-independent binding of CaM (Ruan *et al.*, 1996; Lee and Stull, 1998; Nishida and Ortiz de Montellano, 1998; Lee *et al.*, 2001). Clearly, a better mechanistic understanding of exactly how CaM both binds and activates the iNOS enzyme continues to be of great interest because of the multiple physiological roles performed by •NO.

Chapter 5
Differential Binding of Calmodulin Domains to Constitutive and Inducible Nitric Oxide Synthase Enzymes *

5.1 Introduction

Interactions between CaM and various CaM target peptides and proteins have previously been measured by fluorescence using single or double cysteine CaM mutants labeled with an appropriate fluorophore. Fortunately, wild-type CaM is devoid of any cysteine residues making a single cysteine substitution a facile method for thiol-specific labeling of CaM for steady-state fluorescence binding studies. For example, previous investigations on CaM-target peptide interactions have involved the fluorescently labeled central linker of CaM to determine CaM's association and dissociation rates from myosin light chain kinase, calcineurin, and CaM kinase II (Torok and Trentham, 1994; Waxham *et al.*, 1998; Quintana *et al.*, 2005). Other examples include single or double cysteine mutations in the N- and C-domains of CaM for fluorescence resonance energy transfer studies (FRET) measurements when binding to a ryanodine receptor peptide and the edema factor of adenylyl cyclase from *Bacillus anthracis* (Drum *et al.*, 2000; Maximciuc *et al.*, 2006). In the archetypical model of CaM binding to a target protein, the Ca^{2+}-replete CaM wraps its two domains around a single α-helical target peptide (Ikura *et al.*, 1992; Meador *et al.*, 1992);

*** The results presented in this chapter have been published:**
Spratt, D.E., Taiakina, V., Palmer, M., and Guillemette, J.G. (2007) Differential Binding of Calmodulin Domains to Constitutive and Inducible Nitric Oxide Synthases. *Biochemistry 46*, 8288-8300.

Unless otherwise stated, all of the work reported in this chapter was performed and analysed by the candidate.

however, other conformations of CaM when bound to target proteins have been discovered (Schumacher *et al.*, 2001; Drum *et al.*, 2002; Yap *et al.*, 2003; Ishida and Vogel, 2006; Ye *et al.*, 2006).

The x-ray structure of CaM bound to the CaM-binding domain of eNOS shows that CaM binds in an anti-parallel fashion with the N-terminal domain of CaM binding to the N-type site closer to the C-terminus, which corresponds to the reductase domain, while the C-terminal domain of CaM binds to the C-type site closer to the N-terminus, corresponding to the oxygenase domain (Aoyagi *et al.*, 2003). In contrast to the cNOS enzymes, iNOS is transcriptionally regulated *in vivo* by cytokines and binds to CaM at basal levels of Ca^{2+}. The Ca^{2+}-independent activity of iNOS appears to result from the concerted interactions of CaM with both the oxygenase and reductase domains in addition to the canonical CaM-binding region (Lee and Stull, 1998). The orientation of CaM when bound to iNOS has previously been proposed to bind in a parallel fashion based on kinetic analysis (Gribovskaja *et al.*, 2005), however, this model has yet to be proven.

There have been several studies demonstrating that the different regions of CaM are important for the binding and activation of the cNOS holoenzymes (Su *et al.*, 1995; Persechini *et al.*, 1996a; b; Stevens-Truss *et al.*, 1997; Gachhui *et al.*, 1998); however, very little has been reported on the binding and activation of the iNOS enzyme by CaM (Newman *et al.*, 2004; Gribovskaja *et al.*, 2005; Spratt *et al.*, 2006). In the present study, we employed three different mutant CaM proteins with single cysteine substitutions found in each region of CaM: CaM-T34C (N-domain), CaM-K75C (central linker), and CaM-T110C (C-domain). These cysteine CaM mutants were fluorescently labeled with acrylodan and Alexa Fluor 546 C_5-maleimide in order to monitor their binding to synthetic NOS CaM-binding domain peptides and the holo-NOS enzymes, respectively. The CaM-binding peptides and holoenzymes of all three mammalian NOS isoforms were utilized since studies involving uncommon CaM-target binding modes require the use of target elements that extend well

outside of the typical CaM binding region of the protein (Ishida and Vogel, 2006). This study was designed to use steady-state fluorescence and CD in the investigation of select regions of CaM when binding to the CaM-binding domain peptides and holo-enzymes of the three mammalian NOS isozymes and to determine the orientation of CaM when bound to iNOS through the use of FRET.

5.2 Experimental Procedures

5.2.1 Site-directed Mutagenesis of CaM

The QuikChange site-directed mutagenesis procedure (Wang and Malcolm, 1999) was used to convert the threonine codons at positions 34 and 110 to cysteines into the kanamycin resistant pET9dCaM plasmid consisting of the pET9d vector (Novagen) carrying rat calmodulin (Spratt *et al.*, 2006). The construction of pCaM-T34C and pCaM-T110C was performed by the candidate and assisted by Miss Valentina Taiakina (UW Co-op student). The forward and reverse primers for the T34C mutation incorporated a unique *Sac*I reporter cut site: wt-T34Cfr 5' CAATAACAACCAAGGAGCTCGGG*TGT*GTGATGCGGTCTC 3' and wt-T34Crv 5' GAGACCGCATCAC*ACA*CCCGAGCTCCTTGGTTGTTATTG 3'. The forward and reverse primers for the T110C mutation involved the removal of a *Pml*I cut site: wt-T110Cfr 5' GCAGAGCTTCGCCACGTTATG*TGT*AACCTTGGAGAGAAG 3' and wt-T110Crv 5' CTTCTCTCCAAGGTT*ACA*CATAACGTGGCGAAGCTCTGC 3'. The resulting pCaM-T34C and pCaM-T110C vectors were confirmed by DNA sequencing. The pCaM-K75C in the ampicillin resistant pET23d vector (Novagen) was a generous gift from Dr. Neal Waxham (University of Texas Medical School at Houston, TX, USA) (Waxham *et al.*, 1998).

5.2.2 CaM Protein Expression and Purification

The expression and purification of CaM-T34C, CaM-K75C, and CaM-T110C was performed by Miss Valentina Taiakina (UW Co-op student). Overnight cultures of *E. coli* BL21 (DE3) transformed with

pCaM-T34C and pCaM-T110C were used to inoculate 2 x 1 L of Luria-Bertani (LB) media in 4 L flasks supplemented with 30 μg/ml of kanamycin. *E. coli* BL21 (DE3) pLysS transformed with pCaM-K75C grown to saturation overnight was used to inoculate 2 x 1 L of LB media supplemented 100 μg/ml of ampicillin and 30 μg/ml chloramphenicol. Cultures were grown at 37ºC, 200 rpm to an OD_{600} of 0.6 to 0.8, induced with 500 μM IPTG and harvested after 4 hours of expression. Cells were harvested by centrifugation, flash frozen on dry ice, and stored at –80ºC. Cells were thawed on ice, resuspended in 4 volumes of 50 mM MOPS, pH 7.5, 100 mM KCl, 1 mM EDTA, 1 mM DTT, and homogenized using an Avestin EmulsiFlex-C5 homogenizer (Ottawa, ON). The CaM proteins were purified using phenyl-sepharose chromatography as previously described in section 2.2.3 with the exception that the dialysis buffer contained 1 mM DTT. The CaM protein concentrations were determined using the ε_{277} of 3029 $M^{-1}cm^{-1}$ (Gao *et al.*, 1998) and were subsequently frozen in aliquots on dry ice and stored at –80°C. Electrospray ionization-mass spectrometry (ESI-MS) was performed on the purified CaM proteins using a Micromass Q-Tof Ultima GLOBAL mass spectrometer (Manchester, U.K.) with an internal standard (Newman *et al.*, 2004; Spratt *et al.*, 2006). The CaM samples were analysed by ESI-MS, as previously described in section 2.2.5.

5.2.3 CaM Protein Labeling with Acrylodan and Alexa Fluor 546 C_5-maleimide

The CaM proteins were transferred into labeling buffer (50 mM Tris-HCl, pH 7.2 containing either 1 mM EDTA or 1 mM $CaCl_2$) by gel filtration using a Sephadex G-25 PD-10 column (Amersham Biosciences) in order to remove the excess reducing agent in the CaM sample, as previously described (Lang *et al.*, 2005). Prior to labeling, the CaM proteins were tested with 5,5'-dithio-bis(2-nitrobenzoic acid) (DTNB; Sigma, Oakville, ON) to ensure that the reactivity of the cysteine sulfhydryl side chains were completely reduced and sufficiently reactive for labeling with acrylodan and Alexa Fluor 546 C_5 maleimide (Figure 5.1; Molecular Probes, Eugene, OR, USA).

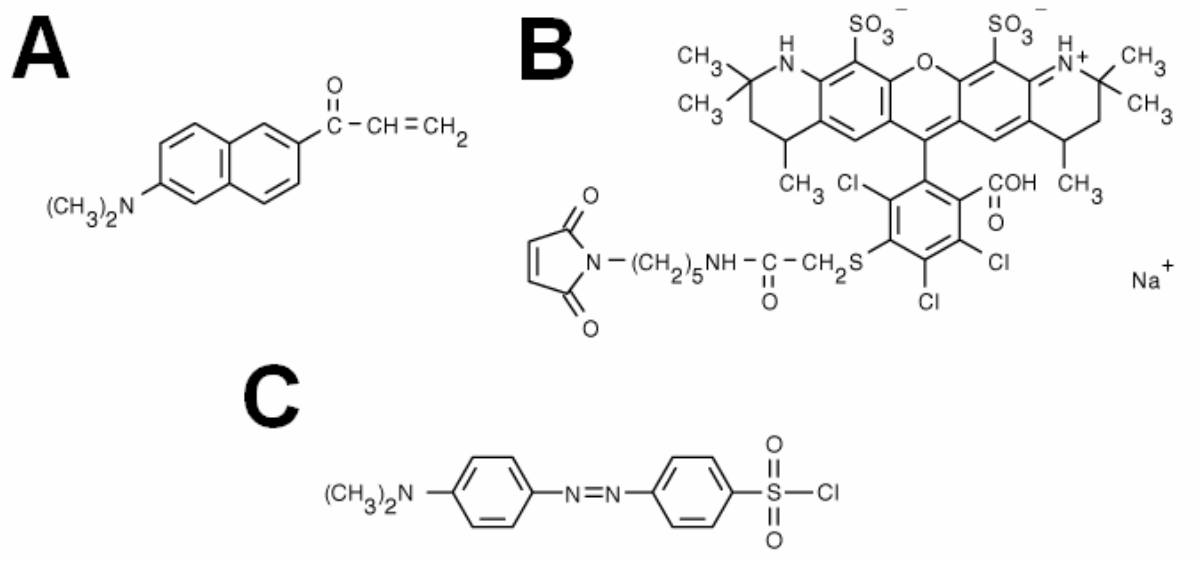

Figure 5.1 – Chemical structures of (A) Acrylodan, (B) Alexa Fluor 546 C_5 maleimide, and (C) Dabsyl chloride.
Acrylodan (6-acryloyl-2-dimethylaminonapthalene) and Alexa Fluor 546 C_5 maleimide were used to thiol specifically label CaM-Cys proteins to monitor the binding of the CaM-Cys proteins to the NOS peptides and holo-enzymes in this study. Dabsyl chloride (4-dimethylaminoazobenzene-4'-sulfonyl chloride) was exclusively used to label the N-terminal primary amine of iNOS peptide to determine the orientation of CaM when bound to iNOS.

Using TNB's ε_{412} of 13,600 $M^{-1}cm^{-1}$, the cysteine residues were determined to be completely reactive in the presence of Ca^{2+} and EDTA. Acrylodan and Alexa Fluor 546 C_5-maleimide were dissolved in *N,N'*-dimethylformamide and 50 mM Tris, pH 7.5, respectively, to a concentration of 20 mM. Either 100 µL of acrylodan or Alexa Fluor 546 solution was added to 1 mL of 100 µM CaM protein (1.67 mg/mL). For acrylodan, the mixture was allowed to react overnight at 10°C with slow mixing, whereas with Alexa Fluor 546, the mixture was mixed slowly and allowed to react for 2 hours at room temperature. The labeling reactions were quenched with the addition of either excess β-mercaptoethanol or dithiothreitol. Excess dye was removed by gel filtration using a PD-10 column pre-equilibrated with 50 mM HEPES, 1 mM EDTA, 150 mM NaCl, pH 7.5. Exhaustive dialysis against 50 mM HEPES, 1 mM EDTA, 150 mM NaCl, pH 7.5 was performed to ensure that all non-

covalently linked dye was removed from the labeled CaM proteins, as previously described in other labeling studies (Ottl *et al.*, 1998; Waxham *et al.*, 1998). Labeling yields were determined from absorbance spectra on a Varian Cary UV–visible Spectrophotometer (Varian, Mississauga, ON). The amount of covalently bound acrylodan was determined using ε_{391} of 20,000 $M^{-1}cm^{-1}$ (Molecular Probes). Covalently linked Alexa Fluor 546 was determined with the ε_{554} of 93,000 $M^{-1}cm^{-1}$ (Molecular Probes). To determine the extent of labeling, the CaM proteins labeled with acrylodan or Alexa Fluor 546 were subjected to ESI-MS to ensure only sulfhydryl-specific labeling.

5.2.4 iNOS Peptide Labeling with Dabsyl Chloride

Two milligrams of lyophilized human iNOS CaM-binding domain peptide, RPKRR EIPLK VLVKA VLFAC MLMRK (residues 507-531 prepared by Sigma Genosys) was dissolved in 1 mL of dabsyl chloride labeling buffer consisting of 0.1 M $NaHCO_3$, pH 7.1. A labeling buffer with a more neutral pH was used to ensure selective labeling of the N-terminus of the peptide as opposed to other primary amines found in the peptide, such as the numerous lysine residues. Dabsyl chloride (Figure 5.1C; Supelco, Bellefonte, PA, USA) was dissolved in *N,N'*-dimethylformamide to a concentration of 25 mM. 100 µL of dabsyl chloride solution was added to 1 mL of iNOS peptide (2 mg/mL) and the mixture was allowed to react for 1.5 hours at 4°C with slow mixing. The reaction mixture was then centrifuged for 5 minutes at 14,000 x g to remove particulate from the sample. Due to the large size of the pellet, the pellet was solubilized in 95% (v/v) H_2O, 5% (v/v) CH_3CN, and 0.1% (v/v) TFA, incubated for 10 minutes at room temperature, and subsequently centrifuged to remove insoluble particles. The presence of peptide in the resolubilized supernatant was confirmed using the *DC* Protein assay (Bio-Rad), based upon the Lowry method (Lowry *et al.*, 1951).

The dabsyl-labeled iNOS peptide was then purified by reverse-phase chromatography on an AKTApurifier System for Chromatography (Amersham Biosciences, Baie d'Urfe, PQ) using a Delta-Pak™ C_{18} HPLC column (2 x 150 mm, 300 Å pore size, 5 µm particle size). The aqueous mobile

phase consisted of 95% (v/v) H_2O, 5% (v/v) CH_3CN, and 0.1% (v/v) TFA while the organic mobile phase containing 95% (v/v) CH_3CN, 5% (v/v) H_2O, and 0.1% (v/v) TFA. After a 2 column volume wash of the column with the aqueous phase, a linear gradient of the organic mobile phase (1.5% / min) was used to elute the labeled peptide from the column. Eluted peptide was detected at 215 and 254 nm while dabsyl chloride was monitored at 466 nm. Unlabeled peptide was eluted at 63% organic mobile phase while the labeled peptide was eluted at 72% organic mobile phase. Isolation of dabsyl-labeled iNOS peptide was confirmed by ESI-MS with only a singly-labeled species observed. The concentration of dabsyl-iNOS peptide was determined using the ε_{466} of 33,000 M^{-1} cm^{-1}.

5.2.5 NOS Enzyme Expression and Purification

Rat neuronal and bovine endothelial NOS were expressed and purified as previously described in sections 2.2.6 and 2.2.7. Human iNOS carrying a deletion of the first 70 amino acids and an N-terminal polyhistidine tail was coexpressed with CaM or nCaM mutant protein in *E. coli* BL21 (DE3), as previously described in sections 2.2.8. Each NOS enzyme was purified using ammonium sulfate precipitation, metal chelation chromatography, and 2'5'-ADP affinity chromatography.

5.2.6 Enzyme Kinetics

The initial rate of •NO synthesis was measured using the spectrophotometric oxyhemoglobin assay as previously described in section 2.2.10.1.3. Assays were performed at 25°C in a SpectraMax 384 Plus 96 well UV-visible spectrophotometer using Soft Max Pro software (Molecular Devices, Sunnyvale, CA). eNOS, nNOS and iNOS coexpressed with CaM or nCaM were assayed at concentrations of 70, 30 and 28.5 nM, respectively in 100 µl total well volumes. 200 µM $CaCl_2$ or 250 µM EDTA as well as 2 µM wild-type CaM, mutant CaM protein, and labeled CaM proteins were added to the appropriate samples.

5.2.7 Steady-State Fluorescence

Fluorescence emission spectra were obtained using a PTI QuantaMaster spectrofluorimeter (London, ON). 100 nM of CaM-T34C-acr, CaM-K75C-acr, or CaM-T110C-acr were used as the fluorescent reporter in the quartz cuvette, similar to a previous study involving calcineurin (Quintana *et al.*, 2005). The excitation wavelength for all of the acrylodan labeled CaMs was set at 375 nm. Slit widths were set at 2 nm for excitation and 2 nm for emission. In a volume of 1 mL, an initial scan was taken with each CaM-Cys-acr protein in a buffer consisting of 50 mM HEPES, 1 mM EDTA, 150 mM NaCl, pH 7.5. After the first scan, synthetic NOS CaM-binding domain peptide (500 nM) was added to the cuvette, the sample was mixed thoroughly, incubated for three minutes to allow the sample to reach equilibrium, and scanned. The calculated free [Ca^{2+}] in this system is <1 nM based on calculations using the online algorithm WEBMAXC (Patton *et al.*, 2004). The NOS CaM-binding domain peptides for human iNOS, RPKRR EIPLK VLVKA VLFAC MLMRK (residues 507-531) was prepared by Sigma Genosys, while bovine eNOS, TRKKT FKEVA NAVKI SASLM (residues 493-512) and rat nNOS, KRRAI GFKKL AEAVK FSAKL MGQ (residues 725-747) were synthesized by SynPeP (SynPeP Corporation, Dublin, CA USA). The sample was then brought to a final free Ca^{2+} concentration calculated to be 0.500 mM, mixed, allowed to incubate for three minutes, and scanned. Finally, excess EDTA (5 mM final) was added (calculated free [Ca^{2+}] of 5.8 nM), incubated for three minutes, and a final scan was taken.

Steady-state fluorescence measurements of CaM-Cys-Alexa Fluor 546 proteins (50 nM) binding to holo-NOS proteins (250 nM) were performed as previously described (see above) with the exception that the excitation wavelength was set at 540 nm with emission monitored between 550 and 700 nm. Fluorescence emission maximum of Alexa labeled CaM was observed at 567 nm, regardless of Ca^{2+} or EDTA presence in the buffer.

5.2.8 Determination of Binding Affinities of CaM-Cys-acr proteins to NOS CaM-binding Domain Peptides

In a starting volume of 1 mL containing CaM-Cys-acr proteins at various concentrations (50, 75, 100, 125, and 150 nM) in a buffer of 50 mM HEPES, 1 mM $CaCl_2$, 150 mM NaCl, pH 7.5, scans were taken between increasing molar ratios of peptide to CaM protein (0, 0.25, 0.5, 0.75, 1, 1.5, 2, and 4). The sample was mixed, incubated for three minutes to reach equilibrium, and scanned between each successive peptide addition. In order to determine the K_{CaM} values for each acrylodan labeled CaM protein when binding to the CaM-binding domain peptides of each NOS isoform, we used a method similar to that previously developed and employed by Dr. Basil Perdicakis (PhD 2003, U of Waterloo) and Dr. Heather Montgomery (PhD 2004, U of Waterloo), former graduate students in our laboratory (Montgomery *et al.*, 2003), with the exception that steady-state fluorescence was used instead of spectrophotometric kinetic analysis. Using the assumption that there is a rapid establishment of equilibrium among all species in the sample, the NOS peptide concentration that results in half-maximal fluorescence of the CaM-NOS peptide complex with depletion of free acrylodan-labeled CaM due to binding with NOS peptide can be described by the following formula (Equation 5.1):

Equation 5.1

$$AC_{50} = 0.5CaM_o + K_{CaM}$$

where AC_{50} is the NOS peptide concentration that results in half-maximal fluorescence signal at a given CaM concentration (nanomolar), CaM_o is the total CaM concentration in the sample (nanomolar), and K_{CaM} is the binding constant in nM, which is determined using the following formula (Equation 5.2):

Equation 5.2

$$K_{CaM} = \frac{[\text{NOS peptide}][\text{CaM}]}{[\text{NOS peptide} \bullet \text{CaM}]}$$

The estimated K_{CaM} for the CaM-Cys-acr proteins binding to the NOS peptides was calculated from the ordinal intercept of the plot of AC_{50} versus NOS peptide concentration, as previously described (Montgomery *et al.*, 2003).

5.2.9 FRET Measurements of Alexa-labeled CaM Proteins with Dabsyl-labeled iNOS Peptide

FRET measurements between dabsyl-labeled iNOS peptide and CaM-T34C-Alexa and CaM-T110C-Alexa were determined in a buffer consisting of 50 mM HEPES, 1 mM $CaCl_2$, 150 mM NaCl, pH 7.5. Using the identical fluorimeter setup as described for steady-state measurements with Alexa-labeled CaMs (see section 5.2.7), an initial scan of 50 nM CaM-T34C-Alexa or CaM-T110C-Alexa alone in a volume of 1 mL was taken. This was followed by the addition of dabsyl-iNOS peptide, the sample was mixed well and incubated for 3 minutes, and a subsequent measurement was taken.

5.2.10 Circular Dichroism of nCaM and cCaM bound to synthetic NOS peptides

CD was performed in a Jasco J-715 CD spectropolarimeter using J-715 analysis software as previously described (section 4.2.7) with some modifications. Samples were measured in a 1 mm quartz cuvette (Hellma, Concord, ON) kept at 25°C using a Peltier type constant-temperature cell holder. Samples consisted of 25 μM nCaM or cCaM alone or equimolar concentrations of CaM protein with synthetic iNOS CaM-binding domain peptide. Samples were mixed in 10 mM Tris-HCl buffer (pH 7.5) containing 150 mM NaCl and 200 μM $CaCl_2$, followed by 1 mM EDTA. Spectra were recorded over a 190-250 nm range with a 1.0 nm band width, 0.2 nm resolution, 100 mdeg sensitivity at a 0.125 s response and a rate of 100 nm/min with a total of 25 accumulations. Data is expressed as the mean residue ellipticity (θ) in degree cm^2 $dmol^{-1}$.

5.3 Results

5.3.1 Protein Expression and Purification

The CaM constructs used in this study have previously been employed in FRET and fluorescence binding studies with CaM target proteins due to their optimal positions in the N- and C-terminal domains (Drum *et al.*, 2000; Allen *et al.*, 2004), as well as the central linker of CaM (Waxham *et al.*, 1998; Quintana *et al.*, 2005) with all three CaM mutants showing no significant effect on enzyme activity. Figure 1 shows the positions of the mutant residues in the reported protein structures of holo-CaM (PDB 1CLL; (Chattopadhyaya *et al.*, 1992), apo-CaM (PDB 1CFD; (Kuboniwa *et al.*, 1995), and CaM in complex with eNOS peptide (PDB 1NIW; (Aoyagi *et al.*, 2003).

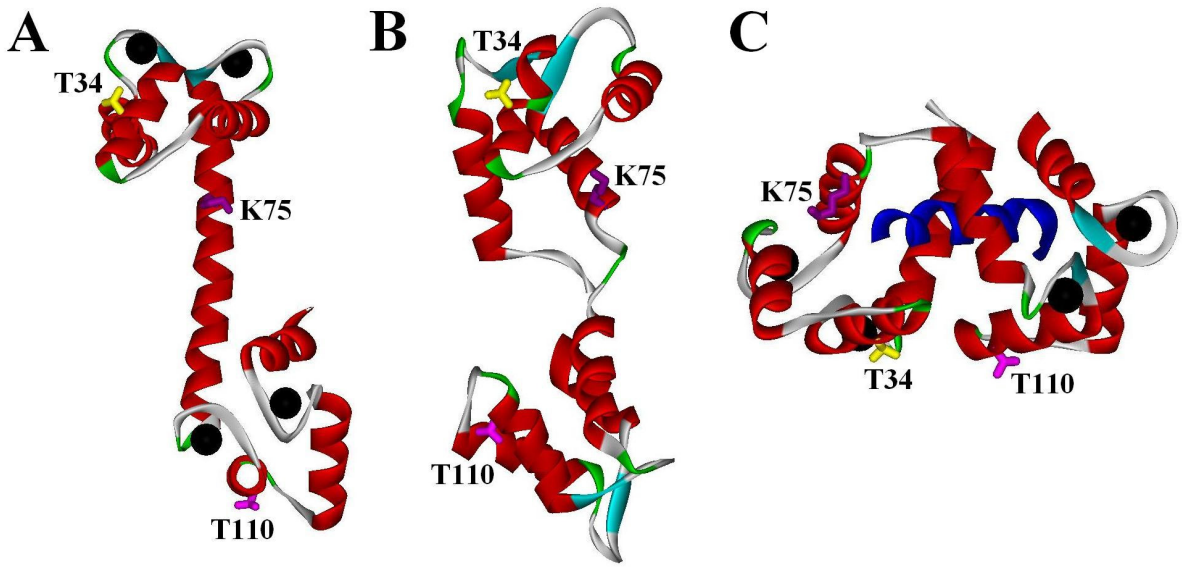

Figure 5.2 – X-ray and NMR structures showing the positions of T34, K75 and T110 in A) Holo-CaM, B) Apo-CaM, and C) CaM when bound to eNOS peptide.
CaM, eNOS peptide, and Ca^{2+} ions are shown in red, blue, and black, respectively. T34, K75, and T110 are shown in yellow, purple, and pink, respectively. Models are derived from PDB 1CLL (Chattopadhyaya et al., 1992), 1CFD (Kuboniwa et al., 1995), and 1NIW (Aoyagi et al., 2003).

When comparing the three structures in Figure 5.2, these residues exhibit varying solvent exposure depending upon the target protein CaM binds to, making these sites optimal for fluorescence binding studies with fluorophores that are highly sensitive to their environment, such as acrylodan (Figure 5.1).

The cysteine CaM proteins were successfully overexpressed in *E. coli*. After purification, we obtained 37.7, 31.0, and 39.3 mg protein/L media of CaM-T34C, CaM-K75C, and CaM-T110C, respectively. ESI-MS QTOF confirmed homogeneity and ruled out any posttranslational modification (Table 5.1).

Table 5.1 – Masses of CaM and fluorescently labeled CaM-Cys proteins

	Mass (Da) [a]	
CaM proteins	Observed	Theoretical [b]
wtCaM	16706.0	16706
CaM T34C	16709.0	16708
CaM K75C	16680.5	16681
CaM T110C	16709.0	16708
CaM T34C-acr (EDTA)	16932.5 [d]	16934 [d]
CaM T34C-Alexa Fluor 546 (EDTA)	17717.5 [e]	17720 [e]
CaM K75C-acr (EDTA)	16905.5	16907
CaM K75C-Alexa Fluor 546 (EDTA)	17690.5	17693
CaM T110C-acr (EDTA)	16932.5	16934
CaM T110C-Alexa Fluor 546 (Ca^{2+})	17717.5	17720

[a] Masses of deconvoluted ESI-MS spectra were determined with an accuracy of ± 3 Da.

[b] Calculated masses pre- and post-labeling with acrylodan.

[c] Condition used to label CaM-Cys protein for 100% single labeling (see section 5.2.3)

[d] Expected mass difference after labeling CaM-Cys proteins with acrylodan is 225.3 Da (Molecular Probes).

[e] Expected mass difference after labeling CaM-Cys proteins with Alexa Fluor 546 C_5 maleimide is 1011.4 Da (Molecular Probes). The manufacturer's MW of the dye is 1034.3, which includes a single counter sodium ion.

5.3.2 Characterization of Fluorescently Labeled CaM-Cys Proteins

The CaM-Cys proteins were tested with DTNB to ensure that the cysteine sulfhydryl side chains were completely reduced and sufficiently reactive for labeling with acrylodan. All of the sulfhydryls in the CaM-Cys proteins were determined to be 100% reactive in the presence of Ca^{2+} and EDTA. This result was confirmed using ESI-MS (Table 5.1).

Previous fluorescent labeling of CaM in our laboratory showed that the cysteine residue in a T110C-CaM mutant exhibited less reactivity in the presence of EDTA (~10%), however, this cysteine residue was 100% reactive in the presence of Ca^{2+} (Lang *et al.*, 2005). This result indicates that Ca^{2+}-binding dictates the solvent exposure of this residue in the C-terminal domain of CaM. In order to determine if the presence of Ca^{2+} would affect the labeling yield of the CaM-Cys mutants that were used in this study, parallel labeling reactions were performed in the presence of 1 mM $CaCl_2$ and 1 mM EDTA. In the reactions containing 1 mM EDTA, only a single-labeled species was obtained with little or no unlabeled CaM-Cys protein observed. Conversely, in the reactions containing 1 mM $CaCl_2$, the majority of the CaM species were singly-labeled with a marked amount of double-labeled CaM (results not shown). This non-specific double labeling of CaM result has also been previously observed using proteins with single selenomethionine residues (Lang *et al.*, 2006). The possible second labeling of CaM has been previously postulated to be the result of non-specific interactions between the dye and the protein (Allen *et al.*, 2004), or possibly due to the exposure of another residue that may display some reactivity towards acrylodan. We exclusively used CaM-Cys-acr labeled in the presence of EDTA because the labeling reactions in the presence of Ca^{2+} showed some undesired double-labeling. Since only single-labeled species were observed by ESI-MS (Table 5.1), the concentrations of CaM-T34C-acr, CaM-K75C-acr, and CaM-T110C-acr were determined spectrophotometrically using the ε_{391} of 20,000 $M^{-1}cm^{-1}$ (Molecular Probes).

Knowing that CaM-T34C and CaM-K75C showed specific labeling in the presence of EDTA with acrylodan, the same labeling conditions were used when labeling these CaM-Cys mutants with Alexa Fluor 546 C_5-maleimide. Inefficient labeling was previously observed with CaM-T110C in the presence of EDTA, whereas 100% labeling was obtained in the presence of Ca^{2+} when labeling with another maleimide dye, *N*-[4-(dimethylamino)-3,5-dinitrophenyl]-maleimide (DDPM) (Lang *et al.*, 2005). Therefore, CaM-T110C was labeled with Alexa Fluor 546 in the presence of Ca^{2+}. Complete and specific labeling was obtained with all of the CaM-Cys proteins and no apparent secondary labeling was confirmed by ESI-MS (Table 5.1). The concentrations of CaM-T34C-Alexa, CaM-K75C-Alexa and CaM-T110C-Alexa were determined using the ε_{554} of 93,000 $M^{-1}cm^{-1}$ (Molecular Probes).

Acrylodan fluorescence was measured exclusively in the presence of the NOS CaM-binding domain peptides. Alexa Fluor 546 C_5-maleimide (Figure 5.1B; Molecular Probes) was used during FRET binding studies using the N-terminally dabsyl-labeled iNOS peptide as well as steady-state fluorescence binding studies with the holo-NOS enzymes due to its far red-shifted excitation and emission spectra. This dye is advantageous due to its ability to be specifically excited in the presence of the absorbent NOS cofactors (heme, FMN, and FAD), which absorb over most of the visible spectrum.

5.3.3 NOS Activation by CaM-Cys and Fluorescently-Labeled CaM Proteins

The oxyhemoglobin capture assay was employed to determine if the CaM-Cys and the fluorescently labeled CaM-Cys proteins were capable of binding and activating the holo-NOS enzymes. The eNOS and nNOS enzymes all exhibited approximately 100% activity in the presence of CaM-T34C, CaM-K75C, and CaM-T110C when compared to wild-type CaM (Table 5.2).

Table 5.2 – CaM-Cys and fluorescently labeled CaM Dependent Activation of cNOS enzymes [a]

CaM protein	Neuronal NOS %	Endothelial NOS %
CaM	100 ± 6	100 ± 1
CaM-T34C	114 ± 7	106 ± 5
CaM-T34C-acrylodan	238 ± 6[b]	87 ± 1
CaM-T34C-Alexa Fluor 546	156 ± 7[c]	104 ± 5
CaM-K75C	113 ± 3	116 ± 2
CaM-K75C-acrylodan	260 ± 7[b]	102 ± 2
CaM-K75C-Alexa Fluor 546	64 ± 4[c]	97 ± 5
CaM-T110C	89 ± 6	97 ± 2
CaM-T110C-acrylodan	157 ± 9[b]	116 ± 1
CaM-T110C-Alexa Fluor 546	185 ± 6[c]	93 ± 6
CaM (EDTA)	NAA[d]	NAA

[a] The oxyhemoglobin capture assay used to measure the rate of CaM-activated •NO production was performed in the presence of either 2 μM wild-type or mutant CaM protein and either 200 μM $CaCl_2$ or 250 μM EDTA, as indicated. The activities obtained with the respective enzyme bound to wild-type CaM at 25°C in the presence of 200 μM $CaCl_2$ were all set to 100%. The activities for nNOS and eNOS bound to CaM were 35.4 and 9.5 min^{-1}, respectively.

[b] Each assay that contained acrylodan labeled-CaM showed markedly greater activity than the equivalent CaM-Cys protein not labeled with acrylodan.

[c] Alexa-CaMs showed increased activity when the N- and C-domains were labeled, but displayed decreased activity when the central linker was labeled.

[d] NAA – No apparent activity

The activation of eNOS by the acrylodan and Alexa Fluor 546 labeled CaM proteins was the same as observed for the unlabeled CaM-Cys proteins (Table 5.2) In contrast, when nNOS was assayed in the presence of the acrylodan-labeled CaM proteins, the •NO production rates were enhanced from

160 (for CaM-T110C-acr) up to 260% (for CaM-T34C-acr) of the rate obtained for wild-type CaM. This observation may be due to acrylodan's highly hydrophobic properties causing a non-specific hydrophobic interaction between the CaM-Cys-acr proteins and nNOS. Similarly, when nNOS was assayed with CaM-T34C-Alexa and CaM-T110C-Alexa, •NO synthesis rates were also enhanced. The nNOS activity in the presence of CaM-K75C-Alexa was decreased to approximately 60%, which may be due to the large Alexa dye disrupting the CaM central linker interaction with nNOS. It is noteworthy that all of the CaM-Cys and labeled CaM-Cys proteins required the presence of Ca^{2+} to activate the cNOS enzymes. Clearly, all of the fluorescently labeled CaM-Cys mutants are able to bind and activate the cNOS enzymes, with nNOS showing marked increases in •NO production rates.

In order to monitor if the labeled and unlabeled CaM-Cys proteins were capable of activating iNOS, we used iNOS coexpressed with nCaM (CaM residues 1-75). In our previous study, we showed that iNOS coexpressed with nCaM displayed no apparent activity in the presence of EDTA; however, with the addition of 2 μM wild-type CaM with EDTA present, activity was maintained (Spratt *et al.*, 2006). This result indicated that a Ca^{2+}-dependent reorganization of the bound truncated nCaM mutant could facilitate its displacement and allow for the binding and activation of iNOS when excess native CaM is added. Significant levels of •NO synthesis were observed when excess CaM-Cys and CaM-Cys-acr mutants were added to iNOS coexpressed with nCaM in the presence of EDTA (Table 5.3).

Table 5.3 – CaM-Cys and fluorescently labeled CaM Activation of iNOS [a]

CaM protein	CaM protein added	Inducible NOS %
iNOSwtCaM (Ca^{2+})	No	100 ± 2
iNOSnCaM (Ca^{2+})	No	64 ± 2
iNOSnCaM (EDTA)	No	NAA [b]
"	CaM	61 ± 4
"	CaM-T34C	60 ± 5
"	CaM-T34C-acrylodan	63 ± 6
"	CaM-T34C-Alexa Fluor 546	21 ± 1
"	CaM-K75C	54 ± 2
"	CaM-K75C-acrylodan	56 ± 2
"	CaM-K75C-Alexa Fluor 546	26 ± 1
"	CaM-T110C	56 ± 4
"	CaM-T110C-acrylodan	85 ± 3
"	CaM-T110C-Alexa Fluor 546	21 ± 2

[a] •NO synthesis rates were measured as described in Table 1 with 2 μM exogenous CaM protein added only to the assays indicated. Each assay was performed in the presence of either 200 μM $CaCl_2$ or 250 μM EDTA as shown. The activity obtained for iNOS coexpressed with CaM and assayed in the presence of 200 μM $CaCl_2$ at 25°C was 50.5 min^{-1} and was set to 100%.

[b] NAA – No apparent activity

All of the mutant CaM proteins displayed identical activation profiles to that of iNOS coexpressed with nCaM with excess wild-type CaM (~60% maximal activation). The only exception was CaM-T110C-acr, which activated the enzyme to 85% maximal activity when compared to iNOS coexpressed with wild-type CaM (Table 5.3). This marked difference between CaM-T110C and its acrylodan-labeled equivalent may be due to a stronger hydrophobic interaction with iNOS, similar to the results previously observed with nNOS (Table 5.2). The Alexa Fluor 546-labeled CaM proteins showed low activation of iNOS (~20%), likely due to steric hindrance by the fluorophore (Table 5.3). Clearly, all of the acrylodan- and Alexa-labeled CaM proteins are capable of activating, and hence, binding to the iNOS enzyme in the absence of Ca^{2+}. The fact that the fluorescently labeled CaM proteins bind and activate the NOS isozymes indicates that the fluorescent binding studies we present

in this study are relevant in describing CaM's association with the various NOS CaM-binding domains.

5.3.4 CaM-NOS Peptide Binding Studies

5.3.4.1 FRET studies using Alexa-labeled CaM proteins with Dabsyl-labeled iNOS peptide

It has previously been shown that CaM binds to the CaM-binding domain of eNOS in an anti-parallel fashion, where the N-terminal domain of CaM binds closer to the C-terminus of the target peptide, classified as the N-type binding site, while the C-terminal domain of CaM binds closer to the N-terminus, corresponding to the C-type binding site (Aoyagi *et al.*, 2003). It has also previously been determined that CaM binds to nNOS in an anti-parallel orientation through NMR (Zhang *et al.*, 1995). Although it has previously been proposed that CaM binds to iNOS in a parallel orientation based upon kinetic data (Gribovskaja *et al.*, 2005), this model has yet to be proven. In order to determine the orientation of CaM when bound to the CaM-binding domain of iNOS we employed FRET to determine relative distances between the N- and C-domains from the N-terminus of an iNOS target peptide. CaM-T34C and CaM-T110C labeled with Alexa Fluor 546 was used as the FRET donor while a synthetic iNOS peptide N-terminally labeled with dabsyl chloride, which is a potent quencher, was used as the FRET acceptor. In essence, the greater the amount of quenching observed represents the Alexa-labeled site on CaM being closer to the N-terminus of the iNOS peptide. Should CaM-T34C-Alexa be quenched to a greater extent than CaM-T110C-Alexa, this would indicate that CaM binds in a parallel manner, however, if the reverse result is observed, this would indicate that CaM binds to iNOS in an anti-parallel fashion.

Our results shown in Figure 5.3 indicate that the fluorescence signal of CaM-T110C-Alexa is quenched to a greater extent than CaM-T34C-Alexa in the presence of dabsyl-iNOS peptide

signifying that when CaM is bound to the iNOS peptide, the C-domain of CaM is closer to the N-terminus of the peptide than the N-domain of CaM.

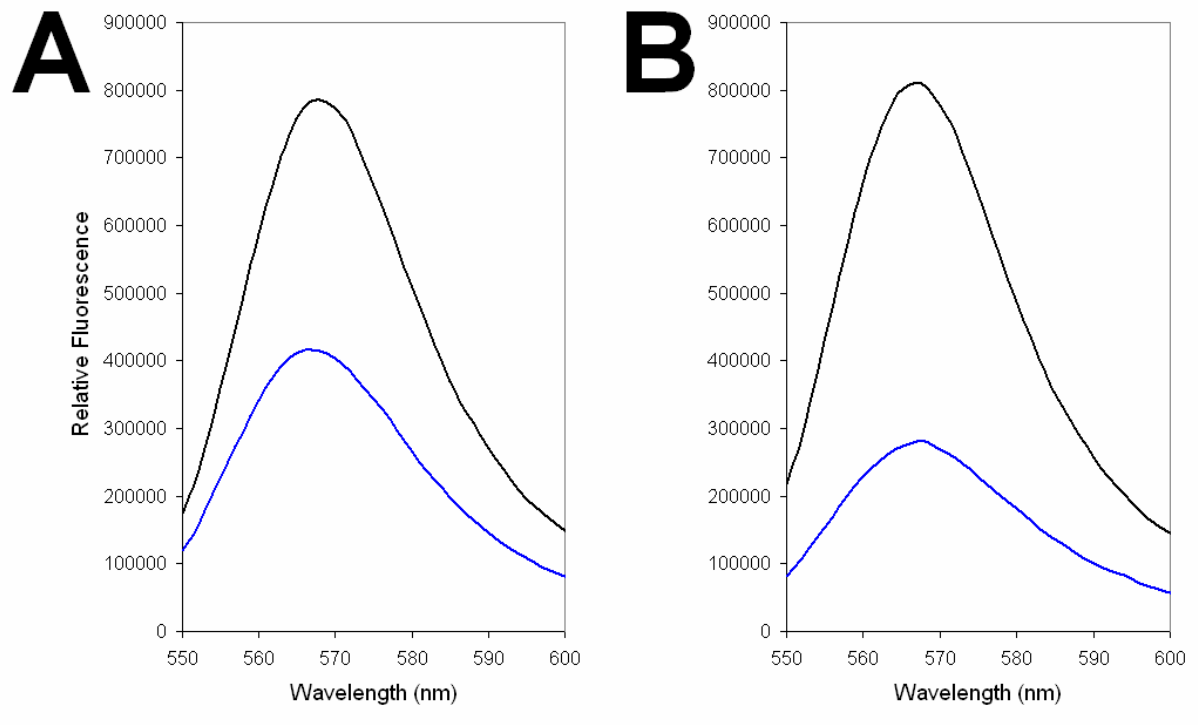

Figure 5.3 – FRET analysis of (A) CaM-T34C-Alexa and (B) CaM-T110C-Alexa binding to iNOS peptide N-terminally labeled with dabsyl chloride.
Alexa-labeled CaMs alone in the presence of Ca^{2+} and in the presence of dabsyl-iNOS peptide are shown as (—) and (—), respectively. The fluorescence signal of CaM-T110C-Alexa is quenched to a greater extent than CaM-T34C-Alexa in the presence of dabsyl-iNOS peptide signifying that when CaM is bound to the iNOS peptide, the C-domain of CaM is closer to the N-terminus of the peptide than the N-domain of CaM. This result suggests that CaM binds to the iNOS CaM-binding domain in an anti-parallel orientation, similar to that already determined for the cNOS enzymes.

These results demonstrate that CaM does in fact bind to the iNOS CaM-binding domain in an anti-parallel orientation, similar to that previously determined for the cNOS enzymes (Zhang *et al.*, 1995; Aoyagi *et al.*, 2003). These FRET results we observed correlate well with the distances between T34 and T110 with the N-terminus of the peptide in the CaM-eNOS structure. This FRET donor-acceptor pair of Alexa Fluor 546 and dabsyl chloride has a theoretical Förster distance value (R_O) of 29 Å

(Molecular Probes), which is optimal for measurements within this CaM-NOS peptide complex, based upon the solved CaM-eNOS structure (Figure 5.2C). The distance between the hydroxyl moiety of T34 in CaM to the N-terminus of the eNOS peptide is 26.3 Å, while the distance between the hydroxyl of T110 to the N-terminus of the eNOS peptide is 19.2 Å. The fluorescence intensity of CaM-T34C-Alexa is approximately 50% when compared to its initial intensity without the dabsyl-iNOS peptide present representing that the fluorescence measurement is approximately equal to the R_0 value of 29 Å. This value is comparable to the measured distance between T34C and the N-terminus of the peptide in the CaM-eNOS structure further supporting our finding that CaM binds to iNOS in an anti-parallel fashion.

5.3.4.2 Ca^{2+}-Dependent Association of Different Regions of CaM to NOS peptides

The binding of acrylodan-labeled CaM proteins to synthetic NOS CaM-binding domain peptides was observed using steady-state fluorescence. The addition of Ca^{2+} to the acrylodan-labeled CaM proteins alone all demonstrated marked changes in fluorescence intensity (Figure 5.4). Emission maxima showed marked blue-shifts in the presence of Ca^{2+} for CaM-T34C-acr and CaM-K75C-acr. CaM-T34C-acr showed fluorescence peaks that shifted from 512 nm (EDTA) to 476 nm (Ca^{2+}). The fluorescence maxima for CaM-K75C-acr were 496 and 484 nm in the presence of EDTA and Ca^{2+}, respectively, and were identical to values previously reported (Waxham *et al.*, 1998; Quintana *et al.*, 2005). In contrast, the emission peak for CaM-T110C-acr at 474 nm in the presence of EDTA moved to 484 nm when Ca^{2+} was added, indicating that acrylodan becomes more solvent exposed when this CaM protein is Ca^{2+}-replete.

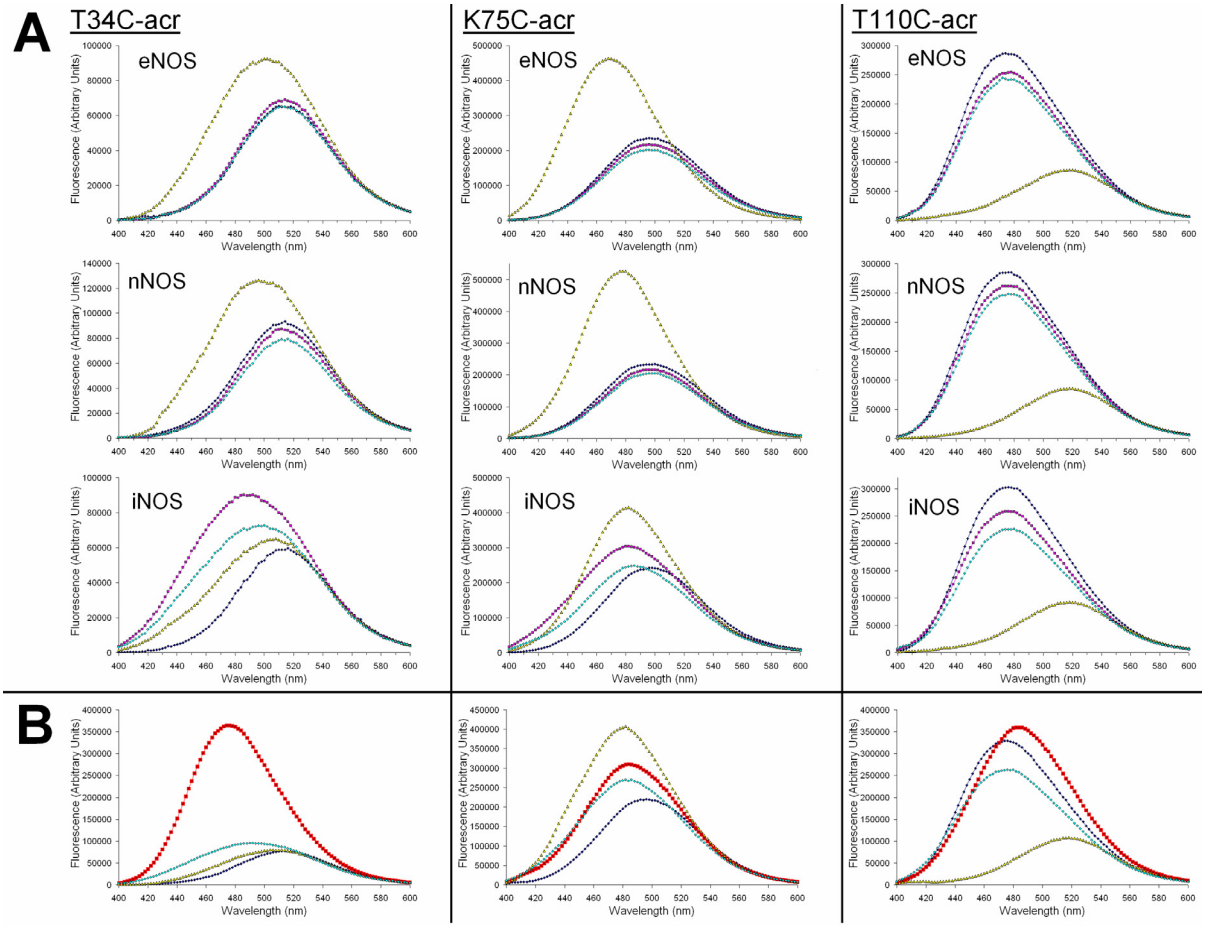

Figure 5.4 – Steady-state Fluorescence of CaM-Cys-acr proteins binding to synthetic NOS CaM binding domain peptides.

(A) In an initial volume of 1 mL, either CaM-T34C-acr, CaM-K75C-acr, and CaM-T110C-acr (100 nM final) was added to 50 mM HEPES, 150 mM NaCl, 1 mM EDTA, pH 7.5 and emission of each sample was observed between 400 and 600 nm (◆). Excitation wavelength was set to 375 nm and the excitation and emission slit widths were set at 2 nm. Synthetic NOS peptide (500 nM) was added, mixed thoroughly, and another scan was taken (■). 1.5 mM $CaCl_2$ (0.5 mM final) was then added and another scan was obtained (▲). In all cases, the addition of Ca^{2+} to the cuvette showed changes in fluorescence emission signal and maxima. Lastly, EDTA was added to a final concentration of 5 mM and an additional scan was taken (●). In between each addition, the sample was allowed to incubate for 3 minutes to reach equilibrium. **(B)** Conditions used were identical as in (A) with the exception that $CaCl_2$ (0.5 mM) was added to the cuvette before the addition of any iNOS peptide. The order of addition to the cuvette was as follows: (1) 100 nM CaM-Cys-acr in 1 mM EDTA (◆), (2) $CaCl_2$ (0.5 mM final, ✕), (3) 500 nM iNOS peptide (▲), and finally (4) EDTA (5 mM final, ●). Samples were incubated for three minutes between each measurement. These measurements were taken to ensure that the fluorescence spectra obtained in (A) for iNOS with each of the CaM-Cys-acr mutants were reproducible regardless of the order of Ca^{2+} or NOS peptide addition.

The addition of the eNOS and nNOS peptides caused little or no change in fluorescence emission of the CaM-T110C-acr protein in the presence of EDTA, signifying minimal or no interaction between the acrylodan labeled CaMs and the cNOS peptides. In contrast, there was ~20% quenching when the iNOS peptide was added, indicative of an association between the peptide and CaM-T110C-acr (Figure 5.4A). The addition of Ca^{2+} resulted in a marked red-shift and a fluorescence intensity decrease of CaM-T110C-acr in the presence of all three NOS peptides, indicating that the fluorophore becomes more solvent exposed upon CaM binding to the NOS peptides (Figure 5.4A). These large Ca^{2+}-dependent changes in acrylodan fluorescence with Ca^{2+} added are indicative of CaM binding to the cNOS peptides, while it represents a large Ca^{2+}-dependent conformational change in the C-domain of CaM when bound to the iNOS peptide. Finally, after the addition of excess EDTA, the acrylodan fluorescence signals closely returned to their original peaks prior to Ca^{2+} addition, signifying the release of the cNOS peptides from the acrylodan-labeled CaM proteins (Figure 5.4A). These results are consistent with the interaction of CaM with eNOS and nNOS being Ca^{2+}-dependent. While these results demonstrate that the C-domain of CaM does interact with the iNOS CaM-binding domain in a Ca^{2+}-independent manner, it is notable that this domain also experiences a large Ca^{2+}-dependent conformational change when it is associated with iNOS.

CaM-T34C-acr showed no change in fluorescence in the presence of EDTA indicating no apparent interaction with the eNOS and nNOS peptides (Figure 5.4A). A marked blue-shift in fluorescence emission was observed with the addition of Ca^{2+}, signifying that CaM-T34C-acr is associating with the cNOS peptides; however, the subsequent addition of EDTA caused the fluorescence signal to return to its original intensity, representing the release of CaM-T34C-acr from the cNOS peptides (Figure 5.4A). These observations further demonstrate that the association of the N-domain of CaM is Ca^{2+}-dependent when binding to the eNOS and nNOS peptides. In contrast,

CaM-T34C-acr showed a blue-shift upon addition of the iNOS peptide in the presence of EDTA (Figure 5.4A) indicating Ca^{2+}-independent binding. The subsequent addition of Ca^{2+} to the CaM-T34C-acr protein showed a slight red-shift in emission, while the final addition of excess EDTA showed small changes in fluorescence intensity, but the spectra never returned to its original peak prior to the addition of iNOS peptide or Ca^{2+} (Figure 5.4A). These changes in fluorescence are indicative of small structural rearrangements in the N-domain of CaM when associated with the iNOS peptide depending on the Ca^{2+} concentration rather than the release of the peptide. This is further exemplified as shown in Figure 5.4B where Ca^{2+} addition to CaM-T34C-acr alone, results in a 5 fold increase in fluorescence with a large blue-shift, indicative of the fluorophore moving to a more hydrophobic environment in a Ca^{2+}-dependent manner. With the subsequent addition of the iNOS peptide, fluorescence is markedly attenuated, which could only result from CaM-T34C-acr's association to the iNOS peptide (Figure 5.4B). Furthermore, the fluorescence spectra after the addition of the iNOS peptide were identical for all of the acrylodan-labeled CaMs binding to the iNOS peptide in the presence of Ca^{2+} (Figure 5.4B) as was observed in Figure 5.4A, where the peptide was added to the cuvette before Ca^{2+}. Taken together, the fluorescence spectra obtained for acrylodan-labeled CaM in the presence of iNOS is reproducible regardless of the order of addition of either Ca^{2+} or the iNOS peptide (Figure 5.4). CaM binding to the iNOS peptide in the absence of Ca^{2+} was observable with CaM-T34C-acr, which is indicative that the Ca^{2+}-independent association previously observed with peptides derived from the CaM-binding domain of iNOS (Anagli *et al.*, 1995; Zoche *et al.*, 1996; Matsubara *et al.*, 1997; Yuan *et al.*, 1998) may be predominantly due to the binding of the Ca^{2+}-depleted N-terminal lobe of CaM.

Fluorescence measurements of CaM's central linker with CaM-K75C-acr showed Ca^{2+}-dependence when binding to the cNOS peptides (Figure 5.4A). This can be related to its position in the central linker of CaM between the two CaM domains that demonstrated a Ca^{2+}-dependent

association to the eNOS and nNOS peptides (Figure 5.4A). In contrast, CaM-K75C-acr showed moderate Ca^{2+}-dependent changes in fluorescence likely due to some structural rearrangement in the presence of the iNOS peptide and EDTA (Figure 5.4). These fluorescent changes are most likely due to the C-terminal Ca^{2+}-dependent conformational changes when associated with the iNOS peptide. In summary, these steady-state fluorescence studies indicate that the N- and C-terminal domains of CaM bind to the iNOS peptide in a Ca^{2+}-independent manner. The N-domain of CaM demonstrated a lower susceptibility to Ca^{2+} concentrations as shown by minimal changes in its conformation, while the C-terminal domain of CaM shows evidence of a Ca^{2+}-dependent rearrangement when associated with the iNOS peptide.

Our steady-state results for acrylodan-labeled CaM proteins binding to cNOS CaM-binding domain peptides are in agreement with the degree of solvent exposure of these residues in the holo- and apo-CaM structures represented in Figure 5.2. For T34, the residue is highly solvent exposed in the apo-CaM structure, almost completely exposed in holo-CaM but more protected from solvent in the CaM-eNOS structure. K75 is relatively solvent exposed in the apo- and holo-CaM structures, whereas, when CaM is bound to eNOS, this residue is more buried. Finally, T110 is relatively buried in the apo- and holo-CaM structures; conversely, T110 is more solvent exposed in the CaM-eNOS crystal structure.

5.3.4.3 Binding Affinities of CaM-Cys-acr proteins to NOS CaM-binding Domain Peptides

The large change in fluorescence intensity upon peptide binding to Ca^{2+}-replete acrylodan-labeled CaM proteins provided a means of determining their binding affinities to each of the NOS CaM-binding domain peptides. Scans were taken between increasing molar ratios of NOS peptide to CaM and repeated for various concentrations for each of CaM-Cys protein labeled with acrylodan. Figure 5.2 shows an example of a titration for CaM-T110C-acr binding to the eNOS peptide. The binding affinities determined for each CaM-Cys-acr protein are shown in Table 5.4.

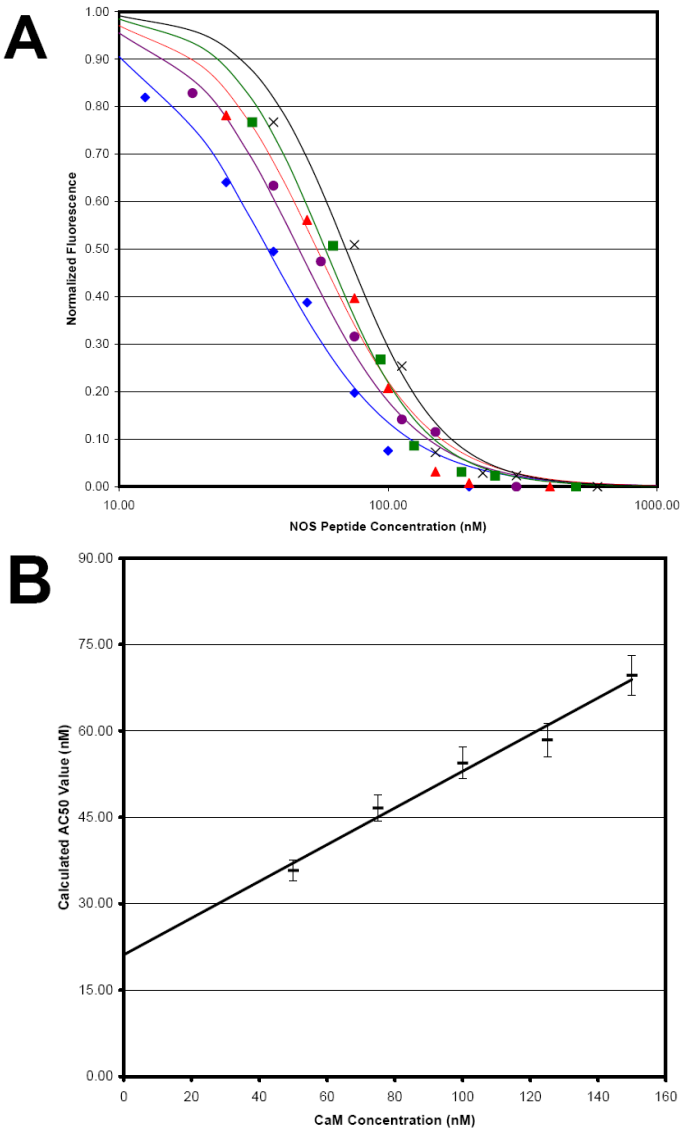

Figure 5.5 – Determination of K_{CaM} binding constant for CaM-T110C-acr binding to the eNOS CaM-binding domain peptide using steady-state fluorescence.
(A) AC_{50} curves of eNOS peptide at CaM-T110C-acr concentrations of 50 nM (◆, 36 nM), 75 nM (●, 47 nM), 100 nM (▲, 54 nM), 125 nM (■, 58 nM), and 150 nM (✕, 70 nM) were determined. The determined AC50 values for each curve are shown in parentheses. **(B)** AC_{50} versus CaM-T110C-acr concentration. The activation constant for CaM binding to nNOS was calculated from the ordinal intercept of panel B as determined by linear regression of the data ($R^2 = 0.98$) and was equal to 21 ± 5 nM, as previously described (Montgomery *et al.*, 2003). All measurements were taken in the presence of 1 mM $CaCl_2$ essentially as described in section 5.2.9 with the exception that incremental increases of NOS peptide were added to saturating concentrations (Molar ratios of 0, 0.25, 0.5, 0.75, 1, 1.5, 2, and 4). Error bars in panel B denote the 95% confidence interval for each point and is representative of collected fluorescence data.

Table 5.4 – Calculated K_{CaM} affinity constants for acrylodan labeled-CaMs binding to NOS peptides

CaM proteins	Affinity (K_{CaM})[a]		
	nNOS peptide (nM)	eNOS peptide (nM)	iNOS peptide (nM)
T34C-acr	4 ± 1	16 ± 4	18 ± 4
K75C-acr	7 ± 2	32 ± 7	4 ± 1
T110C-acr	6 ± 1	21 ± 5	5 ± 1

[a] K_{CaM} values were calculated from the ordinal intercept of AC_{50} versus enzyme concentration as determined by linear regression (Figure 5.5B). The number of data points used in the linear regression for each CaM mutant ranged from four to five. R^2 values were ≥ 0.96. The ± symbol denotes the standard error of the regressed K_{CaM} value.

The affinities of the CaM-Cys-acr proteins for the nNOS peptide are equivalent to previously reported binding studies using the nNOS enzyme and peptide (Vorherr *et al.*, 1993; Zoche *et al.*, 1996; Montgomery *et al.*, 2003). Although the previous reported values were determined using various methods such as kinetic assays, surface plasmon resonance and steady-state fluorescence, our K_{CaM} values are virtually identical. Similarly, the binding affinities obtained for each of the CaM-Cys-acr proteins for the eNOS peptide are comparable to previously reported K_{CaM} values of wild-type CaM for the eNOS enzyme and peptide (Venema *et al.*, 1996; Matsubara *et al.*, 1997; Montgomery *et al.*, 2003). Although our K_{CaM} values are slightly higher than previously reported binding constants, this observation can be accounted for by the addition of a covalently linked non-polar fluorophore which may affect CaM's physicochemical properties slightly when associating with the peptide. However, it is important to note that each of the CaM-Cys-acr proteins are capable of fully activating the eNOS enzyme (Table 5.2) demonstrating that there are no adverse effects to these fluorescent CaM proteins' ability to bind and activate the eNOS isoform.

There have been many varying values reported for CaM's affinity for the iNOS CaM-binding domain peptide; however, all of the K_{CaM} values were in the lower nanomolar concentrations, ranging from <0.1 nM to 4 nM (Anagli *et al.*, 1995; Zoche *et al.*, 1996; Matsubara *et al.*, 1997; Yuan *et al.*, 1998). The affinity constants we determined for the mutant CaM-Cys proteins acrylodan-labeled in the central linker (CaM-K75C-acr) and C-terminal domain (CaM-T110C-acr) are in a similar concentration range as reported in the literature. In contrast, the N-terminal domain mutant of CaM (CaM-T34C-acr) showed a lower affinity than the other regions of CaM (Table 5.4). This observation may be related to the disruption of the stronger interactions between the N-domain of CaM and the N-type site of the iNOS CaM-binding domain, which is discussed in greater detail in the discussion section (section 5.4).

5.3.4.4 Effect of nCaM and cCaM on the Secondary Structure of the iNOS peptide

Using circular dichroism (CD), the interaction between the N- and C-lobes of CaM and the iNOS CaM-binding domain was further investigated. Two previous studies have shown that spectropolarimetry can be used to monitor the secondary structure of peptides that are bound to CaM (Matsubara *et al.*, 1997; Yuan *et al.*, 1998). In order to obtain a CD spectrum for nCaM and cCaM when bound to the iNOS peptide, measurements were taken at 25 μM concentration (Figure 5.6).

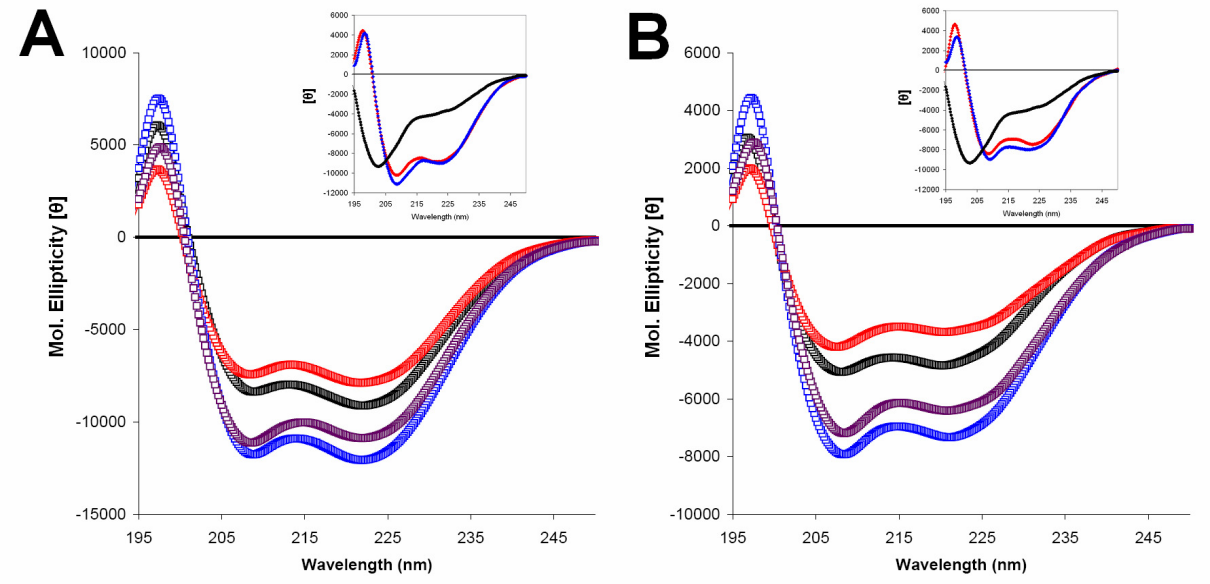

Figure 5.6 – Effect of Ca^{2+} and EDTA on the secondary structure of (A) nCaM and (B) cCaM bound to synthetic iNOS CaM-binding domain peptide.
Spectropolarimetry was performed on 25 µM nCaM (CaM residues 1-75) or cCaM (CaM residues 76-148) with and without 25 µM iNOS peptide. nCaM and cCaM proteins alone in the presence of 200 µM $CaCl_2$ or 1 mM EDTA are shown as (—□—) and (—□—). nCaM or cCaM with iNOS peptide in the presence of 200 µM $CaCl_2$ or 1 mM EDTA are shown as (—□—) and (—□—). The inset figure shows the difference CD spectrum of the CaM proteins with iNOS peptide minus the CaM proteins alone in the presence of 200 µM Ca^{2+} (—◆—) and 1 mM EDTA (—◆—) as well as iNOS peptide alone (—●—) for comparison purposes. The difference CD spectra show that the iNOS peptide retains partial α-helical structure when bound to both nCaM and cCaM in the absence of Ca^{2+}.

In the absence of nCaM or cCaM, the iNOS peptide showed no secondary structure and was predominantly random coil (Figure 5.6 – inset). The binding of either Ca^{2+}-replete nCaM or cCaM to the iNOS peptide resulted in a large increase in α-helical content. Ca^{2+} chelation by EDTA resulted in a decrease in α-helical content of the complex (Figure 5.6). Further analysis of the difference spectra in these experiments shows that the peptide retains some α-helical content when the iNOS peptide is in the presence of either apo-nCaM or apo-cCaM (Figure 5.6 – inset). These results are consistent with published investigations of the binding of holo and apo-CaM to the iNOS CaM-binding peptide (Matsubara *et al.*, 1997; Yuan *et al.*, 1998). It is notable that both lobes can remain bound and induce

α-helical structure upon the peptide under Ca^{2+}-depleted conditions. These results also further support our steady-state fluorescence observations that the interaction of the N- and C-domains of CaM associate to the iNOS peptide in a Ca^{2+}-independent fashion.

5.3.5 CaM-Holo-NOS Enzyme Binding Studies

CaM-binding domain peptides provide a good model for CaM binding to a target protein; however, in order to obtain a true representation of the CaM's interaction with the target protein *in vitro* and *in vivo*, measurements with the target holo-enzyme are required. This is due to other regions outside of the CaM binding element which may or may not affect CaM's association to the target protein (Ishida and Vogel, 2006).

5.3.5.1 Alexa-CaM Binding to Holo-NOS Enzymes using Steady-State Fluorescence

Prior to measuring CaM proteins associating with holo-NOS enzymes, control fluorescence measurements with Alexa-labeled CaM proteins with the NOS peptides were performed. No marked differences in fluorescence were observed, regardless of Ca^{2+} or EDTA presence, indicating that no quenching of the fluorophore emission occurs when bound to the NOS peptides (results not shown).

The CaM-Cys-Alexa proteins, which all emit at 567 nm, all showed a Ca^{2+}-dependent association to the eNOS and nNOS enzymes, as shown by quenching (Figure 5.7), as well as kinetic analysis (Table 5.2). This is apparent from the marked quenching of the fluorophore upon the addition of Ca^{2+} to the cuvette, possibly due to the dye being in close proximity to the heme cofactor since the heme shows broad absorbance over the entire visible spectrum, whereas FMN and FAD absorb very poorly in the 550-700 nm range (Munro and Noble, 1999).

We have previously used gel shift mobility assays to show that peptides coding for the CaM-binding domain of iNOS were capable of binding to two nCaM proteins, which consist of only the N-terminal EF hand pair of CaM (Spratt *et al.*, 2006). This indicated that nCaM was capable of binding

to both the N-type and C-type binding regions of the iNOS CaM-binding peptide. The activity of iNOS coexpressed with nCaM was also shown to be Ca^{2+}-sensitive and the addition of excess wild-type CaM was able to activate the enzyme under Ca^{2+}-depleted conditions (Table 5.1; Chapter 3). This was likely due to the replacement of nCaM from the C-type binding site by the C-terminal domain of wild-type CaM. Since the Alexa-labeled CaM proteins were also capable of activating the iNOS coexpressed with nCaM in the presence of excess EDTA (Table 5.3), we concluded that the labeled-CaMs were binding to the iNOS enzyme in a Ca^{2+}-independent manner. After the addition of iNOS coexpressed with nCaM to the Alexa-labeled CaMs, the samples were incubated for five minutes to allow the mixture to reach equilibrium. In each case, quenching of the fluorophore was observed, indicating CaM associating to iNOS (Figure 5.7). CaM-T110C-Alexa showed the largest quenching effect, which can be attributed to the labeled residue binding directly to the C-type site being closest to the heme containing oxygenase domain. This is in agreement with our FRET studies that show CaM binding to iNOS in an anti-parallel fashion. The CaM-T34C-Alexa and CaM-K75C-Alexa showed smaller but similar trends in quenching (Figure 5.7).

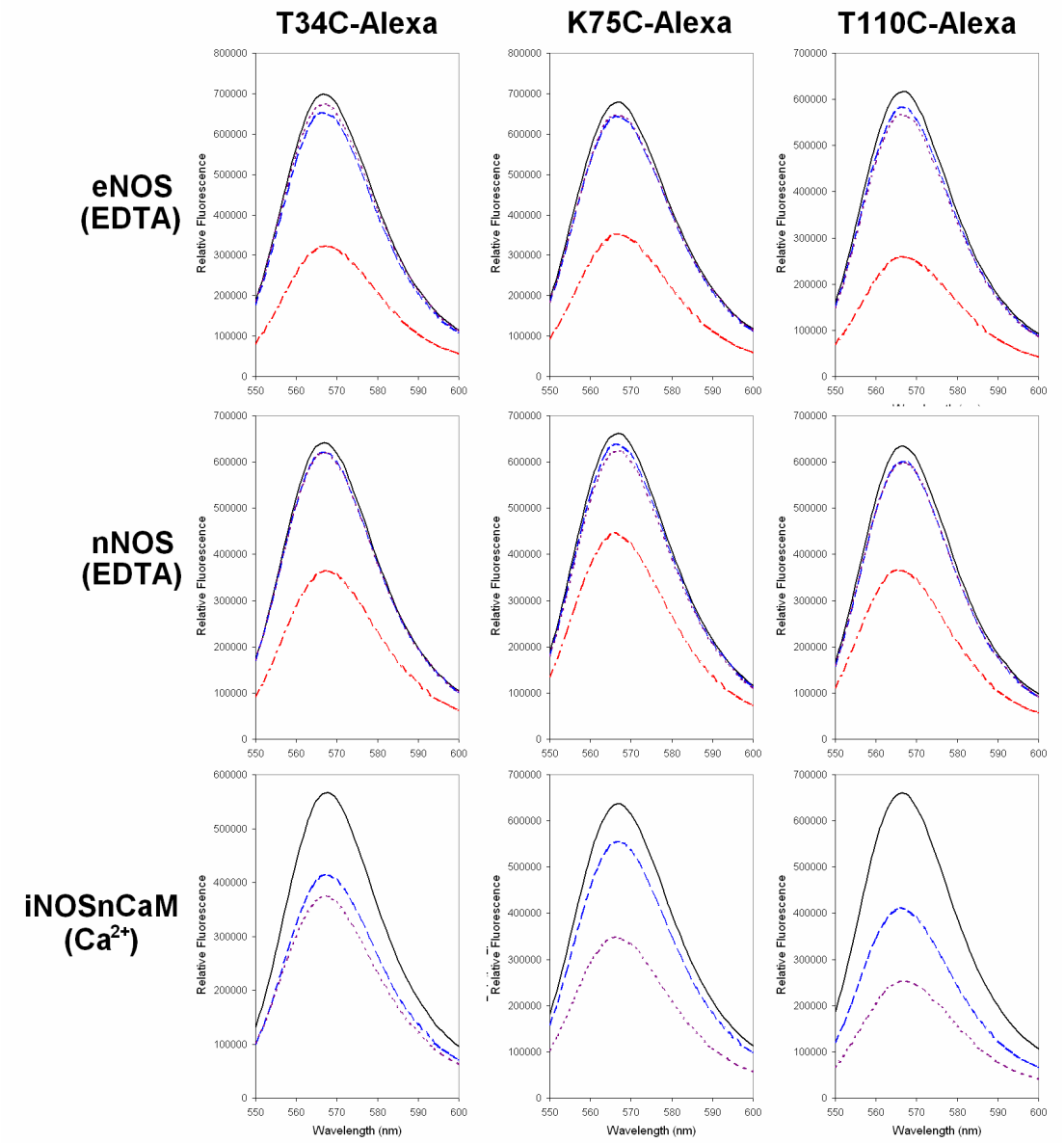

Figure 5.7 – Steady-state Fluorescence of Alexa Fluor 546 labeled CaM-Cys proteins binding to holo-NOS enzymes.

In an initial volume of 1 mL, CaM-T34C-Alexa, CaM-K75C-Alexa, or CaM-T110C-Alexa (50 nM final) was added to 50 mM HEPES, 150 mM NaCl, pH 7.5. The initial scans of eNOS and nNOS contained 1 mM EDTA while scans with iNOS coexpressed with nCaM contained 1 mM $CaCl_2$. The excitation and emission slit widths were set at 2 nm. The excitation wavelength was set to 540 nm and emission of each sample was monitored between 550 and 600 nm (—). Holo-eNOS, nNOS, or iNOS coexpressed with nCaM (250 nM) was then added (— —), followed by 1.5 mM $CaCl_2$ (0.5 mM final) (— – —), and finally 5.5 mM EDTA (5 mM final) (– – – –). In between each successive addition, individual scans were taken. Extra Ca^{2+} was not added to the samples containing iNOS coexpressed with nCaM because its initial scan already contained 1 mM $CaCl_2$.

Upon the addition of EDTA to the cuvette, a greater quenching effect was observed for the CaM proteins labeled at residues 75 and 110, likely due to a Ca^{2+}-dependent conformational change in the C-terminus of the CaM protein that affects its interactions with iNOS (Figure 5.7). In contrast, CaM-T34C-Alexa showed almost no quenching upon the addition of EDTA (Figure 5.7) possibly a result of the N-domain of the labeled CaM failing to displace the coexpressed nCaM that is tightly bound to the N-type binding site of iNOS.

In contrast, we found that Alexa-CaM can displace nCaM from a dabsyl chloride labeled iNOS peptide. Unlike the result we observed with holo-iNOS coexpressed with nCaM where nCaM remains bound to the N-type site of iNOS, both nCaMs that were bound to both the C- and N-type binding sites of the iNOS peptide are able to be completely displaced by CaM-T34C-Alexa and CaM-T110C-Alexa since their FRET measurements were identical to the data presented in Figure 5.3. These results using the iNOS peptide further demonstrate why it is important to use holo-enzymes when monitoring CaM binding to its target proteins because regions outside of the CaM-binding domain affect CaM's association. This is in agreement with a previous study that suggests both the CaM-binding domain and FMN domain of iNOS are required for the iNOS enzyme's Ca^{2+}-independent activity (Ruan *et al.*, 1996).

5.3.5.2 Displacement of Alexa-CaM from iNOS by the Addition of Excess CaM Proteins

Since CaM-T110C-Alexa showed Ca^{2+}-dependent binding and the highest amount of fluorescence quenching when bound to iNOS, we tested if this binding of the C-terminal domain of CaM-T110C-Alexa was permanent or a transient species by the addition of excess CaM proteins under Ca^{2+}-depleted conditions. If the fluorescence signal increases, this would indicate that CaM-T110C-Alexa is released from the iNOS enzyme. Interestingly, fluorescence did increase upon the addition of 100 fold excess (when compared to Alexa-CaM concentration) of wild-type CaM, cCaM, consisting of the

central linker and C-terminal domain of CaM (residues 76-148), and nCaM, consisting of only the N-terminal domain of CaM with no central linker (residues 1-75) (Figure 5.8).

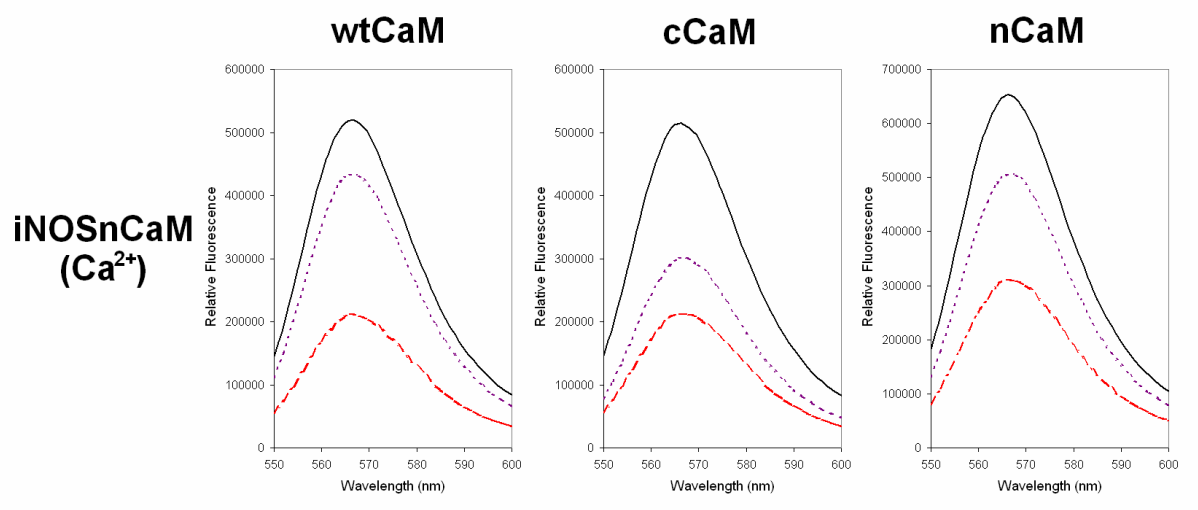

Figure 5.8 – Dissociation of CaM-T110C-Alexa from iNOS coexpressed with nCaM after the addition of excess CaM proteins.
An initial scan of CaM-T110C-Alexa in the presence of 1 mM $CaCl_2$ (▬) was taken, followed by the addition of iNOS coexpressed with nCaM (250 nM) and EDTA to a final concentration of 5 mM (▬ ▬ ▬). Once the sample reached equilibrium, a scan was taken showing the quenched fluorescence due to the Alexa-labeled CaM binding to the iNOS enzyme. 100 fold excess of unlabeled CaM protein was subsequently added and scans were taken every minute until no further fluorescence increase was observed (— — — —). Wild-type CaM, cCaM, and nCaM each took approximately 5 minutes, 15 minutes, and 2 hours, respectively, to reach equilibrium.

This result indicated that the observed apo-CaM-T110C-Alexa association to the C-type binding site of iNOS is a transient species and can be replaced by another CaM protein. Although all of the excess CaM proteins were capable of out-competing CaM-T110C-Alexa, it is notable that the dissociation rates of the Alexa-labeled CaM were not equivalent. Wild-type CaM showed the quickest dissociation in approximately 5 minutes, followed by cCaM in 15 minutes (Figure 5.8). These proteins contain the CaM C-terminal domain that normally interacts with the C-type binding site in the iNOS CaM-binding domain. In contrast, CaM-T110C-Alexa was displaced very slowly by

excess nCaM, taking approximately 2 hours to reach equilibrium (Figure 5.8). This result shows that the N-terminal lobe of CaM is capable of displacing CaM-T110C-Alexa from the C-type site; however, this dissociation is much slower which can be attributed to apo-nCaM having a weak interaction with the C-type binding site. It is also important to note that this transient displacement of CaM-T110C-Alexa was only observed when excess CaM proteins were added to the sample. Chelation of Ca^{2+} alone was not sufficient to displace CaM-T110C-Alexa when bound to holo-iNOS.

5.4 Discussion

The strong Ca^{2+}-independent binding of CaM to iNOS target sequence is quite remarkable but this strong association has also made it difficult to investigate. The solved structures of CaM in complex with peptides representing some of its target sequences have shown that CaM's association is predominantly in an anti-parallel orientation, such as smooth muscle myosin light chain kinase (Ikura *et al.*, 1992; Meador *et al.*, 1992), calcineurin (Ye *et al.*, 2006), alphaII-spectrin (Simonovic *et al.*, 2006), ryanodine receptor (Maximciuc *et al.*, 2006), olfactory cyclic-nucleotide gated channel (Contessa *et al.*, 2005), CaM-dependent protein kinase I (Clapperton *et al.*, 2002), and eNOS (Aoyagi *et al.*, 2003). The exception to these solved anti-parallel CaM target peptide-complexes are the CaM-IQ motifs complexes, which bind in a parallel fashion, such as the voltage-gated 1.2 Ca^{2+} channel (Fallon *et al.*, 2005; Van Petegem *et al.*, 2005). Recently reported structures of CaM bound to larger proteins that encompass its target sequences show the existence of additional novel modes of CaM-binding. Examples of these novel binding modes are CaM in complex with the edema factor of adenylyl cyclase from *B. antracis* (Drum *et al.*, 2002), the Ca^{2+}-activated K^+ channel (Schumacher *et al.*, 2001), plant glutamate decarboxylase (Yap *et al.*, 2003), CaMKK (Kurokawa *et al.*, 2001), CAP-23/NAP-22 (Matsubara *et al.*, 2004), MARCKS (Yamauchi *et al.*, 2003), the plasma membrane Ca^{2+} pump (Elshorst *et al.*, 1999), and a cross-linked calcineurin consisting of two CaMs and two peptides (Ye *et al.*, 2006). The ability of CaM to associate with these many and varied target proteins is not

surprising due to CaM's highly flexible central linker which allows for the N- and C-lobes of CaM to obtain the most favorable conformation in order to bind with its target proteins. Both of the Ca^{2+}-dependent cNOS isoforms have been shown to bind in an anti-parallel fashion (Zhang *et al.*, 1995; Aoyagi *et al.*, 2003). Surprisingly, a recent investigation has proposed that iNOS binds to CaM in a parallel orientation (Gribovskaja *et al.*, 2005). This model would suggest that CaM may bind in a similar process to other Ca^{2+}-independent IQ motifs, such as neuromodulin, however, the CaM binding domain of iNOS does not have any apparent homology to the IQ motifs. If this proposed model were true, it would have important implications for the interactions between CaM and iNOS. For this reason, we designed an experiment to determine the orientation of CaM binding to the iNOS peptide. We have found that CaM binds in an anti-parallel fashion to iNOS, similar to that previously observed for the cNOS enzymes. Since the CaM-binding domains of the NOS enzymes show significant homology (Spratt *et al.*, 2006), our finding that CaM binds to iNOS in an anti-parallel orientation was not surprising.

The use of short synthetic target peptides alone will not provide a full understanding of CaM binding and activation of target proteins (Ishida and Vogel, 2006). Previous observations have indicated there are additional regions outside of the canonical CaM-binding domain that are important for the Ca^{2+}-independent binding of CaM to iNOS (Anagli *et al.*, 1995; Ruan *et al.*, 1996; Venema *et al.*, 1996): To address this situation, we decided to use both an iNOS target peptide as well as the iNOS holoenzyme in our investigation of CaM binding and activation. The Ca^{2+}-independence of CaM for the iNOS has previously been attributed to favourable van der Waals contacts between the peptide and CaM and conformational changes to minimize unfavourable solvent exposure of the hydrophobic regions of the peptide (Aoyagi *et al.*, 2003). The exposure of hydrophobic regions of the iNOS CaM-target peptide upon complex formation has led to problems in aggregation (Matsubara *et al.*, 1997) necessitating our use of a shorter iNOS CaM-target peptide and modified experimental

procedures. A thorough investigation also necessitated the use of holoenzymes in our investigation: This required the purification of iNOS holoenzymes coexpressed in *E. coli* with either CaM of nCaM. We previously demonstrated that iNOS can be coexpressed with the N-terminal domain of CaM alone to produce a stable and active enzyme (Spratt *et al.*, 2006). We further confirmed our previous study by demonstrating that the association of nCaM to the N-type binding site of the iNOS CaM-binding domain is very stable and does not appear to dissociate from holo-iNOS. This finding is supported by our steady-state fluorescence using holo-iNOS enzyme and Alexa-labeled CaMs, as well as our CD data monitoring the association between the iNOS CaM-binding peptide and the N- and C-lobes of CaM.

5.5 Conclusions

A sequential binding model consisting of the ordered binding of the C-terminal lobe to a C-type site followed by the binding of the N-terminal to the N-type site has been proposed for various target proteins including nNOS (Persechini *et al.*, 1994). This mode of CaM association is consistent with the ten-fold higher affinity for Ca^{2+} in the C-lobe than the N-lobe of CaM (Martin *et al.*, 1985) as well as the increased Ca^{2+}-affinity when CaM is bound to its target sequence (Olwin and Storm, 1985). At low basal levels of Ca^{2+}, the C-lobe of CaM is Ca^{2+}-replete and bound to the target sequence. As the cellular concentration increases due to some signaling event, the N-lobe binds to Ca^{2+} allowing for its association with its target sequence leading to activation of the Ca^{2+}/CaM-dependent protein. We investigated the roles of different regions of CaM by using CaM proteins selectively labeled at three different residues. Notably, we showed that both CaM lobes are able to bind to iNOS in a Ca^{2+}-independent process. We were surprised to discover that the C-lobe, and not the N-lobe of CaM, showed the greatest Ca^{2+}-dependent changes in conformation when associated with either the iNOS peptide or the holoenzyme. Our results indicate that the aforementioned sequential model for nNOS (Persechini *et al.*, 1994) does not necessarily apply to the Ca^{2+}-independent iNOS enzyme. This may be the case with iNOS where it has been shown that CaM's association and activation of iNOS is affected by the CaM-binding domain as well as other flanking regions of the enzyme (Anagli *et al.*, 1995; Ruan *et al.*, 1996; Venema *et al.*, 1996).

Our results help to explain how iNOS remains active even under basal levels of Ca^{2+} in the cell. Unlike the cNOS enzymes, the N-terminal lobe of apo-CaM binds to the iNOS enzyme and retains activity, consistent with our previous study (Spratt *et al.*, 2006). In the cell where the number of CaM binding proteins exceeds the amount of CaM present (Persechini and Stemmer, 2002; Tran *et al.*, 2005), the ability of iNOS to rapidly bind to CaM in a Ca^{2+}-independent manner is required to prevent aggregation of the enzyme (Kolodziejska *et al.*, 2005). Although the structural basis for how

these enzymes are bound and activated by CaM is not fully understood, our results further demonstrate that there are marked differences between the Ca^{2+}-dependent and -independent NOS isozymes in terms of their regulation by CaM.

Chapter 6
FRET Conformational Studies of Calmodulin Bound to Nitric Oxide Synthase Enzymes *

6.1 Introduction

The ability of CaM to associate with its various target proteins is due in large part to the inherent flexibility of the central linker separating the N- and C-domains of CaM (Ishida and Vogel, 2006). This flexibility allows CaM to undergo dynamic conformational changes in order to make itself amenable to binding to the various target proteins that CaM can activate, which include the NOS enzymes. Fluorescence (Förster) Resonance Energy Transfer (FRET) has been widely used for studying protein conformation over the past two decades (Heyduk, 2002). FRET is a very versatile method with applications ranging from global conformational studies on native proteins *in vivo* to a single protein molecule. It is a useful tool for the determination of the distance between two different fluorescently labeled residues that are ~10 Å to ~100 Å apart (Heyduk, 2002). Since most biological molecules fall within this distance criterion, it is not surprising that FRET has been used on a variety of proteins, including CaM. CaM has been utilized in numerous FRET studies to determine CaM's conformation when bound to various target proteins due to the ability of CaM to bend its central linker bringing the N- and C-domains of CaM into close proximity of each other. These previous studies involved the use of double cysteine mutations in the N- and C-domains of CaM, specifically at sites T34 and T110C (located in helices 2 and 6 of CaM, respectively), which were fluorescently labeled for FRET measurements when binding to these target proteins. Figure 6.1 shows the positions of T34 and T110 in CaM and demonstrates why these sites in the protein are optimal for FRET measurements.

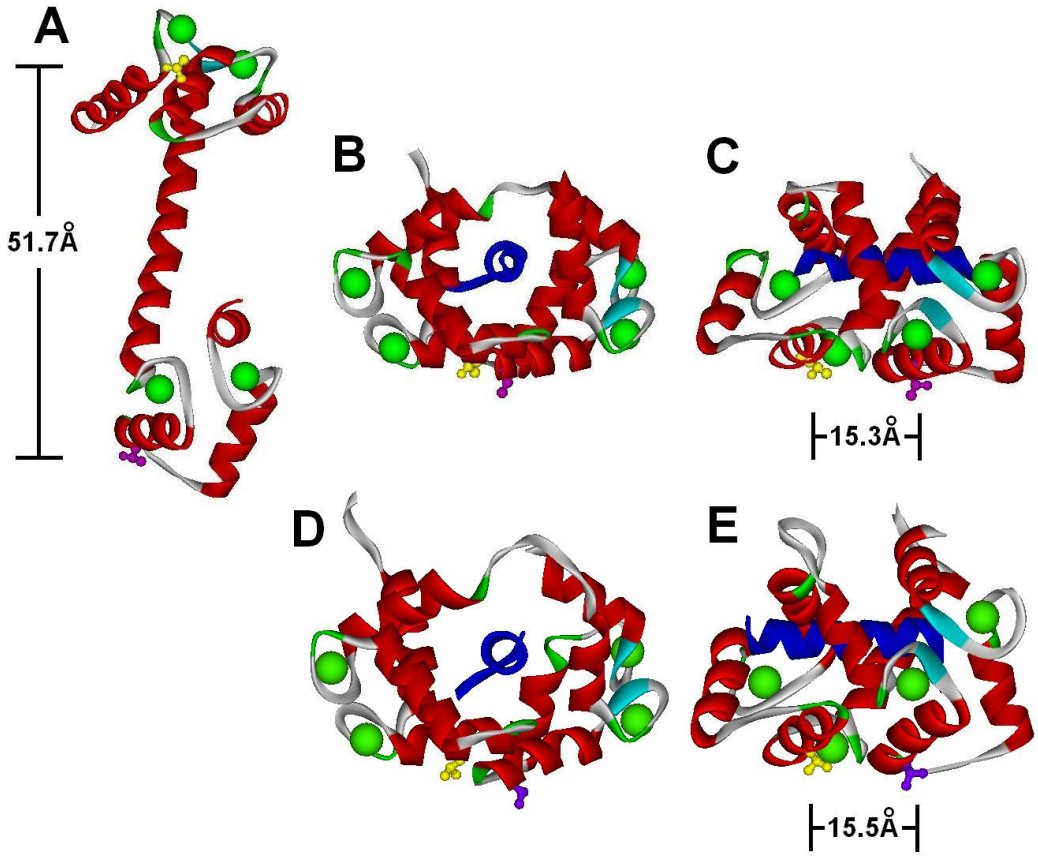

Figure 6.1 – X-ray crystal structures showing the positions of T34 and T110 in (A) Holo-CaM compared to CaM when bound to (B & C) the eNOS and (D & E) the nNOS CaM-binding domain peptides.
CaM, NOS peptide, and Ca^{2+} ions are shown in red, blue, and green, respectively. T34 and T110 residues are shown in yellow and purple, respectively. Models are derived from PDB 1CLL (Chattopadhyaya *et al.*, 1992), 1NIW (Aoyagi *et al.*, 2003), and 2O60 (Ng *et al*. – unpublished, co-ordinates released 2007-12-25). The distances measured between the hydroxyl groups of T34 and T110 are shown to demonstrate that the dynamic conformational change CaM undergoes when bound to the eNOS and nNOS peptides are amenable to FRET measurements.

There are numerous examples in the literature of CaM T34C/T110C being utilized to monitor CaM's conformation, such as CaM bound to a ryanodine receptor peptide, Ca^{2+}/CaM-dependent protein kinase II, human cardiac L-type Ca^{2+}-voltage gated channel (CaV1.2), and the edema factor of adenylyl cyclase from *Bacillus anthracis* (Drum *et al.*, 2000; Torok *et al.*, 2001; Xiong *et al.*, 2005; Maximciuc *et al.*, 2006) or monitoring CaM's conformation when exposed to various organic, viscous, and denaturing solvents (Slaughter *et al.*, 2005a; Slaughter *et al.*, 2005b). Another recent

study employed synthesized *p*-aminophenylalanine derivatives linked with BODIPY fluorophores at the *p*-amino group and introduced these non-natural amino acids into CaM at various sites using the four-base codons GGGU and CGGG in an *E. coli* cell-free translation system (Kajihara *et al.*, 2006).

There is considerable interest in understanding the structural basis of CaM's target protein interactions and diverse regulatory functions. It is well established that CaM is able to interact with its target enzymes in many different conformations, varying from being tightly wrapped when bound to myosin light chain kinase (Ikura *et al.*, 1992), and eNOS (Aoyagi *et al.*, 2003), as determined by NMR and x-ray crystallography, to having an extended structure when bound to the edema factor of adenylyl cyclase from *Bacillus anthacis*, as determined by FRET (Drum *et al.*, 2000) and x-ray crystallography (Drum *et al.*, 2002). The fact that the FRET results of CaM bound to the edema factor were later confirmed by x-ray crystallography validates that the conformation of CaM determined by FRET is representative of a protein's true conformation *in vitro*.

The structure of CaM bound to a peptide corresponding to the CaM-binding domain of eNOS (Aoyagi *et al.*, 2003) and nNOS (PDB 2O60, released 12-25-2007) have been solved and it is known that CaM binds to the NOS enzymes in an anti-parallel orientation (Zhang *et al.*, 1995; Aoyagi *et al.*, 2003; Spratt *et al.*, 2007b). Although the structures and orientation of CaM bound to cNOS peptides have been determined, the conformation of CaM when bound to the holo-NOS enzymes has not been determined. This is due in large part to the size of the NOS enzymes (~124-160 kDa), which would not make it amenable to determine using NMR, as well as the dynamic structural rearrangements that occur within the reductase domain and CaM-binding domains of the NOS enzymes, which would make it difficult to obtain the protein crystals required to perform x-ray crystallography. There are numerous solved crystal structures of the oxygenase domains for each of the NOS isozymes, as well as a solved crystal structure of the nNOS reductase domain without the autoinhibitory domain and

CaM-binding domain being shown in the structure due to their highly flexible nature (Garcin *et al.*, 2004).

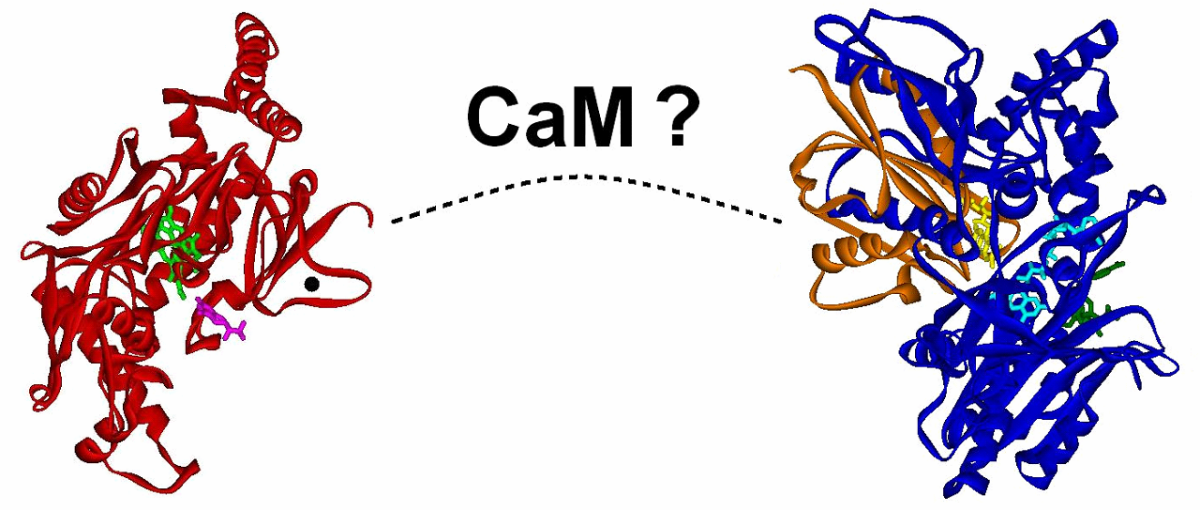

Figure 6.2 – X-ray crystal structures of rat nNOS oxygenase and reductase domains. Oxygenase domain, heme, and H_4B are shown in red, green, and pink, respectively. FMN and FAD/NADPH binding domains of the nNOS reductase domain are shown in orange and blue. FMN, FAD and $NADP^+$ cofactors are shown in yellow, cyan, and dark green, respectively. The structure and conformation of CaM when bound to the holo-NOS enzymes is unknown. Models are derived from PDB 1ZVI (oxygenase) (Matter *et al.*, 2005) and 1TLL (reductase) (Garcin *et al.*, 2004).

Furthermore, determining CaM's conformation when bound to the NOS enzymes may also be affected by flanking regions outside of the putative CaM-binding domain of each NOS isozyme. For instance, regions in the FMN domain of iNOS have been implicated in the Ca^{2+}-independent association of CaM to this enzyme (Ruan *et al.*, 1996). Likewise, the autoinhibitory domain and C-terminal tail in the reductase domains of cNOS enzymes have been shown to be involved in the Ca^{2+}-dependent association of CaM to these enzymes (Roman and Masters, 2006).

The present study was designed to determine the conformation of CaM when bound to all three NOS isoforms. Previous studies in our laboratory have demonstrated differences in CaM binding and activation of the NOS enzymes using CaM-troponin C chimeras, CaM EF hand pair and

Ca^{2+}-deficient mutant CaM proteins (Newman *et al.*, 2004; Spratt *et al.*, 2006; Spratt *et al.*, 2007a). Furthermore, our most recent study demonstrated differences in the Ca^{2+}-dependence of the N- and C-domain when bound to iNOS when compared to the cNOS enzymes using steady-state fluorescence (Spratt *et al.*, 2007b). We anticipate that marked differences will be observed when comparing CaM's conformation bound to the cNOS and iNOS enzymes. These studies will further our understanding of the enzymatic mechanism of the NOS isozymes when bound and activated by CaM.

6.1.1 Chapter Overview

This chapter is in two sections. The first section (section 6.2) discusses work performed in collaboration with Dr. Shenhui Lang (PhD, U of Waterloo) and Dr. Michael Palmer (Associate Professor, U of Waterloo) involving the development of a methodology of dual targeted specific labeling of single cysteine and selenomethionine residues in proteins. The second section (section 6.3) focuses on an alternative method employed to double label CaM with fluorescent dyes and the subsequent FRET analysis of the dual labeled CaM T34C/T110C when bound to NOS peptides and holo-enzymes.

6.2 Dual-targeted labeling of proteins using cysteine and selenomethionine residues

6.2.1 Introduction

The site-selective labeling of CaM has been used extensively to study CaM's ability to interact with target peptides and proteins. Frequently, these studies involved the introduction of a cysteine into the N- or C-domain since CaM does not contain any cysteine residues making this a facile method to site-specifically label CaM with a fluorescent dye. Although there are numerous other residues that can be modified in CaM, such as the numerous lysine residues, it is much more difficult to ensure that site-specific labeling of these residues occur without any unwanted secondary labeling which would make fluorescent binding studies more tedious and difficult to analyze.

Another amino acid residue that has low to moderate frequency in proteins is methionine. Although CaM is methionine rich, containing nine residues out of a total of 148, previous studies in our laboratory have demonstrated that replacement of all nine methionines to leucine has little or no effect on the ability of CaM to bind and activate the cNOS enzymes (Montgomery *et al.*, 2003), as well as making the mutant inert to chemical modification. Previous studies have demonstrated that methionine can be labeled with a varieity of alkylating agents, such as iodoacetate (Gundlach *et al.*, 1959), iodoacetamide derivatives (Zukin *et al.*, 1977; Chung and Lewis, 1986), benzyl bromide (Rogers *et al.*, 1976) or dansylaziridine (Grabarek *et al.*, 1983), which all result in the formation of sulfonium salts (Figure 6.3A).

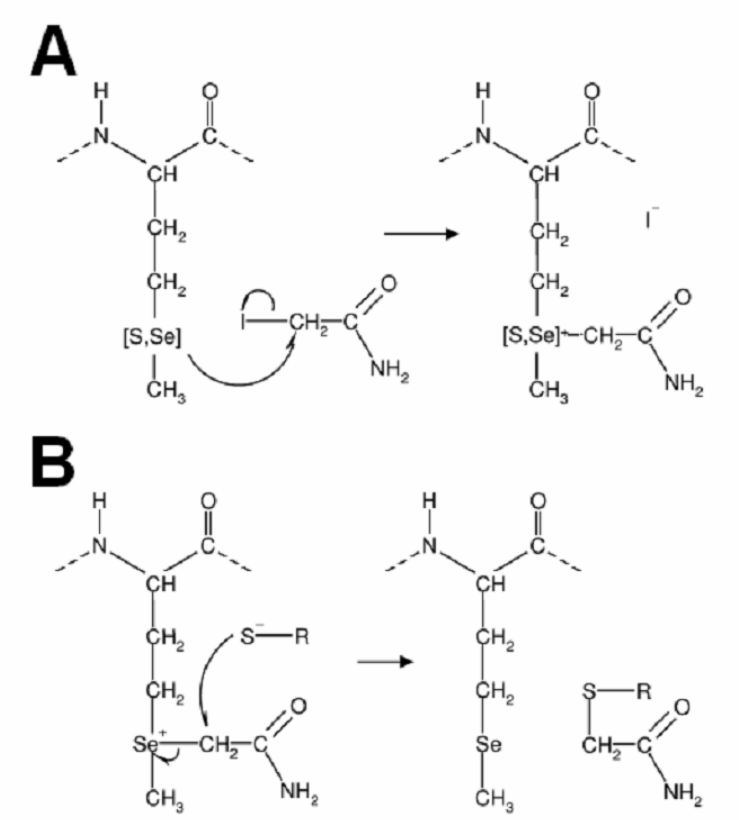

Figure 6.3 – Reaction schemes involving (A) selenomethionine with iodoacetamide to form selenonium or sulfonium salts, and (B) the cleavage of the selenonium by free thiols.

Unfortunately, these alkylation reactions with methionine are relatively inefficient which can account for why their use to modify methionine has not been frequently used as a strategy to site-selective label proteins by the research community.

An alternative to the inefficient labeling of methionine is the use of selenomethionine, an analogue of methionine with selenium substituted for the sulphur in its side chain. Selenomethionine has been used extensively in x-ray crystallography by metabolically incorporating selenomethionine in place of methionine residues to avoid the need for heavy-atom screening, such as mercury or lead; however, previous reports have demonstrated that selenomethionine is capable of being chemically modified (Shepherd and Huber, 1969; Smith and Thompson, 1998). Since selenium is more

nucleophilic than sulfur, Dr. Shenhui Lang (PhD 2003, U of Waterloo) and Dr. Michael Palmer (Associate Professor, U of Waterloo) reasoned that selenomethionine could possibly be a better target for modification with iodoacetamide reagents than methionine. Their preliminary studies confirmed that iodoacetamides react more efficiently with free selenomethionine than methionine. They tested and proved that the site-specific labeling of a single selenomethionine expressed in streptococcal protein CAMP factor could occur.

In collaboration with Dr. Lang and Dr. Palmer, a methodology was developed to site-specifically label selenomethionine residues in proteins for fluorescent studies. In order to further support their studies, the candidate was asked to demonstrate that their technique could also be amenable to fluorescently label other proteins using CaM as a model. This methodology was also expanded upon to include a technique that allows for the dual-labeling of a target protein with single cysteine and selenomethionine residues making the protein amenable for dynamic conformational studies through the use of FRET. Using these approaches to single- and dual-label proteins, we found that metabolically incorporated selenomethionine in proteins provides a facile, highly specific and completely reversible procedure to fluorescently label proteins *in vitro*.

6.2.2 Experimental Procedures

6.2.2.1 Mutagenesis of CaM-L9

The pCaM-L9 vector, consisting of the pET15b ampicillin resistant vector (Novagen) containing a CaM construct with of all nine methionines found in CaM converted to leucines, was a generous gift from Dr. Thomas C. Squier (Pacific Northwest National Laboratory, Richland, WA). The QuikChange site-directed mutagenesis procedure (Wang and Malcolm, 1999) was used to convert a threonine codon at position 34 to a methionine in the methionine-free template pCaM-L9 (Montgomery *et al.*, 2003) to yield the plasmid pT34MCaM-L9. Forward and reverse primers

removed a *Sac*I cut site: T34MLfr2 5' CTACAAAGGAGCTGGGGA*T*GGTGCTGAGATCAC 3' and T34MLrv2 5' GTGATCTCAGCACC*A*TCCCCAGCTCCTTTGTAG 3'. Into the resulting pT34M-CaM-L9 vector, a single cysteine codon was introduced by replacing a threonine codon at position 110, yielding plasmid pT34M-T110C-L9. The forward and reverse primers incorporated a *Pml*I reporter cut site:

T110CLfr 5' GCAGAACTTCGTCACGTGCTGTGCAATCTTGGGGAGAAGCTAAC 3' and T110CLrv 5' GTTAGCTTCTCCCCAAGATTGCACAGCACGTGACGAAGTTCTGC 3'. The successful construction of the pT34MCaM-L9 and pT34M-T110CCaM-L9 vectors was confirmed by DNA sequencing.

6.2.2.2 CaM Expression and Selenomethionine Incorporation

CaM-L9, T34M CaM-L9, T110C CaM-L9, and T34M/T110C CaM-L9 were expressed as previously described (section 2.2.2) with the exception that they were grown in the presence of 100 mg/L ampicillin. Initial attempts to metabolically incorporate selenomethionine into CaM-T34M and CaM-T34M-T110C was performed as previously described (Guerrero *et al.*, 2001) with slight modifications. *E. coli* BL21 (DE3) cells containing either pT34MCaM-L9 and pT34M-T110CCaM-L9 plasmids were grown in 500 mL of LB medium with 100 μg/mL of ampicillin at 200 rpm, 37 °C overnight. Minimal medium was prepared from NH_4Cl (1 g), KH_2PO_4 (3 g), and $Na_2HPO_4{\cdot}7H_2O$ (6 g), dissolved in 0.9 L of deionized water and autoclaved. 20 g glucose, 0.3 g $MgSO_4$, 10 mg $FeCl_3$, and 10 mg thiamine were then dissolved in 100 mL water, the pH was adjusted to 7.4, filter-sterilized, and added to the above solution. L-selenomethionine was added to the minimal medium to a final concentration of 25 mg/L immediately prior to induction. The cells were recovered by centrifugation, washed twice by resuspension and centrifugation with sterilized distilled deionized water, and resuspended in 1 L of selenomethionine minimal medium, yielding an OD_{600} of 0.8 to 1. Protein

expression was induced with 1 mM IPTG for an additional 5 hours at 30°C, 200 rpm. The cells were then harvested by centrifugation and stored at –80°C overnight.

Using this method with *E. coli* BL21 (DE3) (Guerrero *et al.*, 2001) was found to be inefficient at incorporating selenomethionine into CaM (~50%). To ensure that selenomethionine was efficiently incorporated, the methionine-auxotrophic strain *E. coli* strain B834 (DE3) (Novagen) was employed and a modifed version of a previously published protocol was used (Duewel *et al.*, 1997). M9 salts were prepared from $Na_2HPO_4 \cdot 7H_2O$ (12.8 g/L), KH_2PO_4 (3.0 g/L), NaCl (0.5 g/L), and NH_4Cl (1.0 g/L). After adjusting the pH to 7.4 and autoclaving, the 1 L of M9 salts were used to prepare M9 minimal medium by adding filter-sterilized solutions of $MgSO_4$ to 2 mM, $CaCl_2$ to 100 μM, glucose to 4 g/L, and ampicillin to 100 μg/mL.

The B834 (DE3) cells were transfected with pT34MCaM- L9 or pT34M-T110CCaM-L9 and then grown in 20 mL LB medium with 100 mg/mL of ampicillin at 225 rpm, 37°C overnight; 10 mL of the overnight culture was used to inoculate 1 L of M9 minimal medium with 50 mg L-methionine added. The cells were then grown to an OD_{600} of 0.6 to 0.8 at 200 rpm at 37°C, harvested by centrifugation, washed in M9 salts, and finally resuspended in a second liter of M9 minimal medium. The cells were allowed to grow for an additional 30 minutes to exhaust any remaining methionine in the medium. After 30 minutes, 50 mg of L-selenomethionine was added, protein expression was induced with the addition of IPTG (500 μM final concentration), and incubation continued for 5 hours with shaking at 200 rpm, 37 °C. The cells were then harvested by centrifugation, flash frozen on dry ice, and stored at –80 °C. This expression protocol resulted in virtually complete replacement of methionine in CaM-T34M and CaM-T34M/T110C by selenomethionine as judged by mass spectrometry (see Table 6.1). These CaM proteins with selenomethionine incorporated will be referred to as T34SeM CaM-L9 and T34SeM/T110C CaM-L9 throughout this chapter.

6.2.2.3 T34SeM CaM-L9 and T34SeM/T110C CaM-L9 Protein Purification

The CaM mutants were purified as previously described by hydrophobic interaction chromatography on phenyl–Sepharose CL-4B (section 2.2.3). All of the CaM mutants were dialyzed overnight into 50 mM Tris-HCl, 1 mM $CaCl_2$, pH 7.5 with 0.5 mM dithiothreitol.

6.2.2.4 cNOS Enzyme Kinetics

The initial rate of •NO synthesis was measured using the oxyhemoglobin capture assay as previously described (section 2.2.10.1.3). Assays were performed at 25^{o}C in a SpectraMax 384 Plus 96 well UV-visible spectrophotometer using Soft Max Pro software (Molecular Devices, Sunnyvale, CA). eNOS and nNOS were assayed at concentrations of 70 and 30 nM, respectively in 100 µl total well volumes. 200 µM $CaCl_2$ or 250 µM EDTA as well as 2 µM wild-type CaM and mutant CaM protein were added to the appropriate samples.

6.2.2.5 Chemical labeling of selenomethionine residues with IAEDANS

T34SeM CaM-L9 and T34SeM/T110C CaM-L9 was transferred into a labeling buffer consisting of 100 mM sodium acetate, 150 mM NaCl, 1 mM EDTA, pH 5.0 by gel filtration using a Sephadex G-25 PD-10 column (Amersham Biosciences, Baie d'Urfe, PQ) immediately prior to labeling. 5-((((2-iodoacetyl)amino)ethyl)amino)naphthalene-1-sulfonic acid (IAEDANS; Figure 6.4A), purchased from Sigma Aldrich (Oakville, ON), was dissolved in 0.5 M MES buffer, pH 6.0, to a concentration of 100 mM.

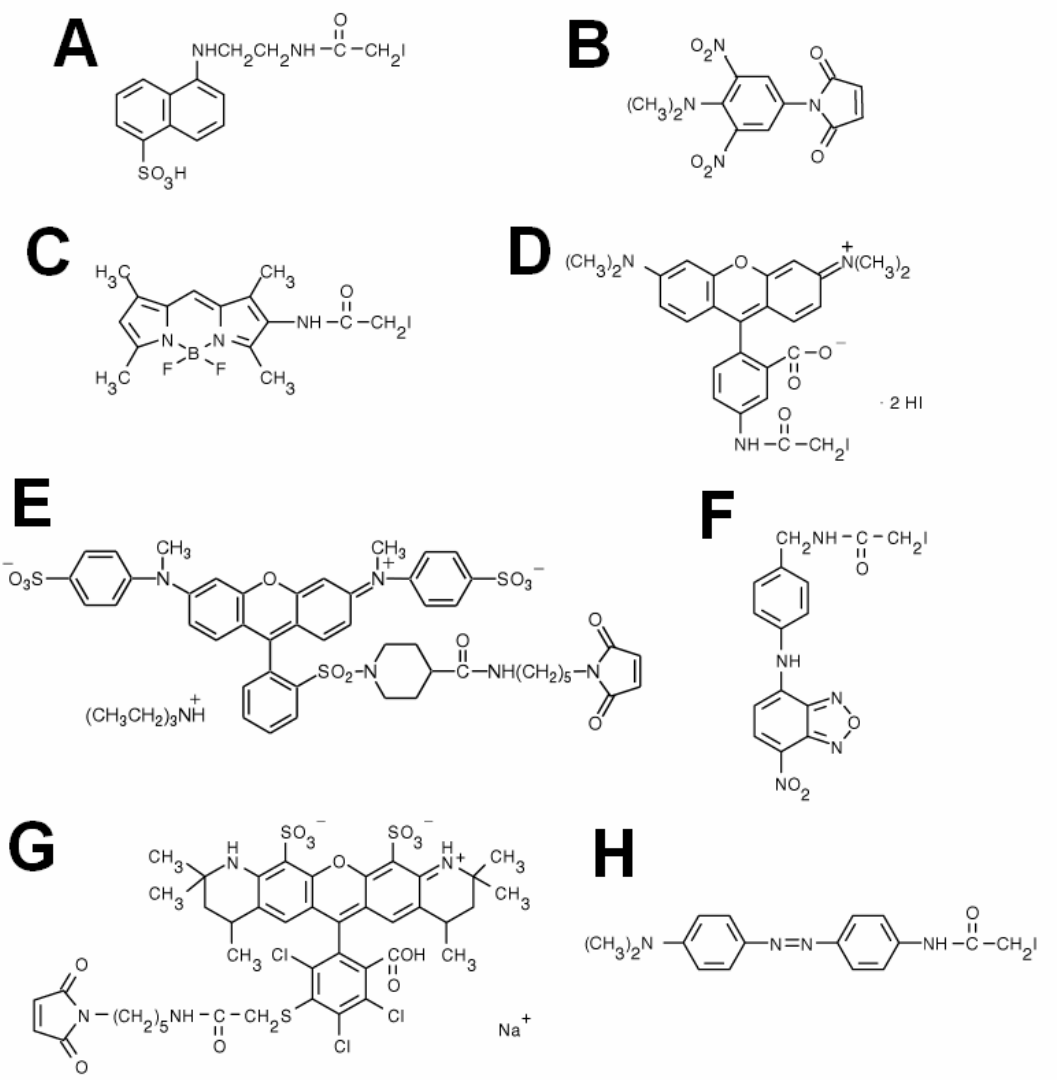

Figure 6.4 – Fluorescent dyes used to selectively label selenomethionine and cysteine residues of T34SeM/T110C CaM-L9.
(A) 1,5-IAEDANS, 5-((((2-iodoacetyl)amino)ethyl)amino) naphthalene-1-sulfonic acid – ε_{336} = 6100 $M^{-1}cm^{-1}$, $em._{max}$ at 490 nm, FW = 434.25; **(B)** DDPM, *N*-(4-Dimethylamino-3,5-dinitrophenyl)maleimide – ε_{443} = 2930 $M^{-1}cm^{-1}$, no emission, FW = 306.23; **(C)** BODIPY 507/545 IA, *N*-(4,4-difluoro-1,3,5,7- tetramethyl-4-bora-3a,4a-diaza-*s*- indacene-2-yl)iodoacetamide – ε_{508} = 69,000 $M^{-1}cm^{-1}$, $em._{max}$ at 543 nm, FW = 431.03; **(D)** 5-TMRIA *single isomer*, tetramethylrhodamine-5-iodoacetamide dihydroiodide – ε_{543} = 89,000 $M^{-1}cm^{-1}$, $em._{max}$ at 567 nm, FW = 825.22; **(E)** QSY 9 C_5 maleimide – ε_{562} = 90,000 $M^{-1}cm^{-1}$, no emission, FW = 1083.30; **(F)** QSY 35 C_5 iodoacetate – ε_{475} = 24,000 $M^{-1}cm^{-1}$, no emission, FW = 453.20; **(G)** Alexa Fluor 546 C_5 maleimide – ε_{554} = 93,000 $M^{-1}cm^{-1}$, $em._{max}$ at 570 nm, FW = 1034.37; **(H)** DABIA, *N*-(4-(4-dimethylaminophenylazo)phenyl)iodoacetamide – ε_{436} = 29,000 $M^{-1}cm^{-1}$, no emission, FW = 408.24.

IAEDANS was added to a final concentration of 10 mM and the labeling reaction was incubated at 25°C for 16 hours. The concentration of T34SeM CaM-L9 used in the labeling reaction was approximately 0.83 mg/mL (49 μM). The labeling reaction was ended and excess dye was removed by gel filtration using another PD-10 column equilibrated with 20 mM HEPES, 150 mM NaCl, 1 mM EDTA, pH 7.0. Labeling yields were determined from absorbance spectra on a Varian Cary UV–visible Spectrophotometer (Varian, Mississauga). For unlabeled CaM saturated with Ca^{2+}, ε_{277} was taken to be 3029 $M^{-1}cm^{-1}$ (Gao *et al.*, 1998). ε_{280} and ε_{336} of IAEDANS were 1060 and 6100 $M^{-1}cm^{-1}$, respectively (Hudson and Weber, 1973). ESI-MS was used to confirm chemical modification of the selenomethionine residue with IAEDANS in T34SeM CaM-L9, as previous described (section 2.2.5).

6.2.2.6 Cysteine labeling of T34SeM/T110C CaM-L9

Cysteine residue of T34SeM/T110C CaM-L9 was labeled with *N*-(4-Dimethylamino-3,5-dinitrophenyl) maleimide (DDPM; Figure 6.4B; Sigma Aldrich) as previously described (section 5.2.3) in a labeling buffer consisting of 50 mM Tris-HCl, 1 mM $CaCl_2$, pH 7.2 by gel filtration using a Sephadex G-25 PD-10 column (Amersham Biosciences). DDPM was dissolved in dimethyl sulfoxide to a working stock concentration of 0.5 mM; the DDPM was added to a final concentration of 30 mM and incubated at 25°C for 2 hours. The reaction was terminated with the addition of excess dithiothreitol followed by the removal of excess label by gel filtration, as previously described (section 6.2.2.5). ε_{280}, ε_{336}, and ε_{443} of DDPM were 9100, 1636, and 2930 $M^{-1}cm^{-1}$ respectively. ESI-MS was used to confirm thiol specific modification of the cysteine residue with DDPM in T34SeM/T110C CaM-L9, as previous described (section 2.2.5).

6.2.2.7 Targeted dual labeling of T34SeM/T110C CaM-L9 with maleimide and iodoacetamide derivatives

The thiol-labeled T34SeM/T110C-DDPM CaM-L9 was subsequently incubated with IAEDANS to derivatize the selenomethionine. The same methodology as previously described to label

selenomethionine residues (section 6.2.2.5) was utilized. A schematic demonstrating the step by step labeling of the cysteine residue followed by the selenomethionine of T34SeM/T110C CaM-L9 is shown in Figure 6.5. ESI-MS was used to verify that dual labeling of T34SeM/T110C CaM-L9 with IAEDANS and DDPM, as previous described (section 2.2.5).

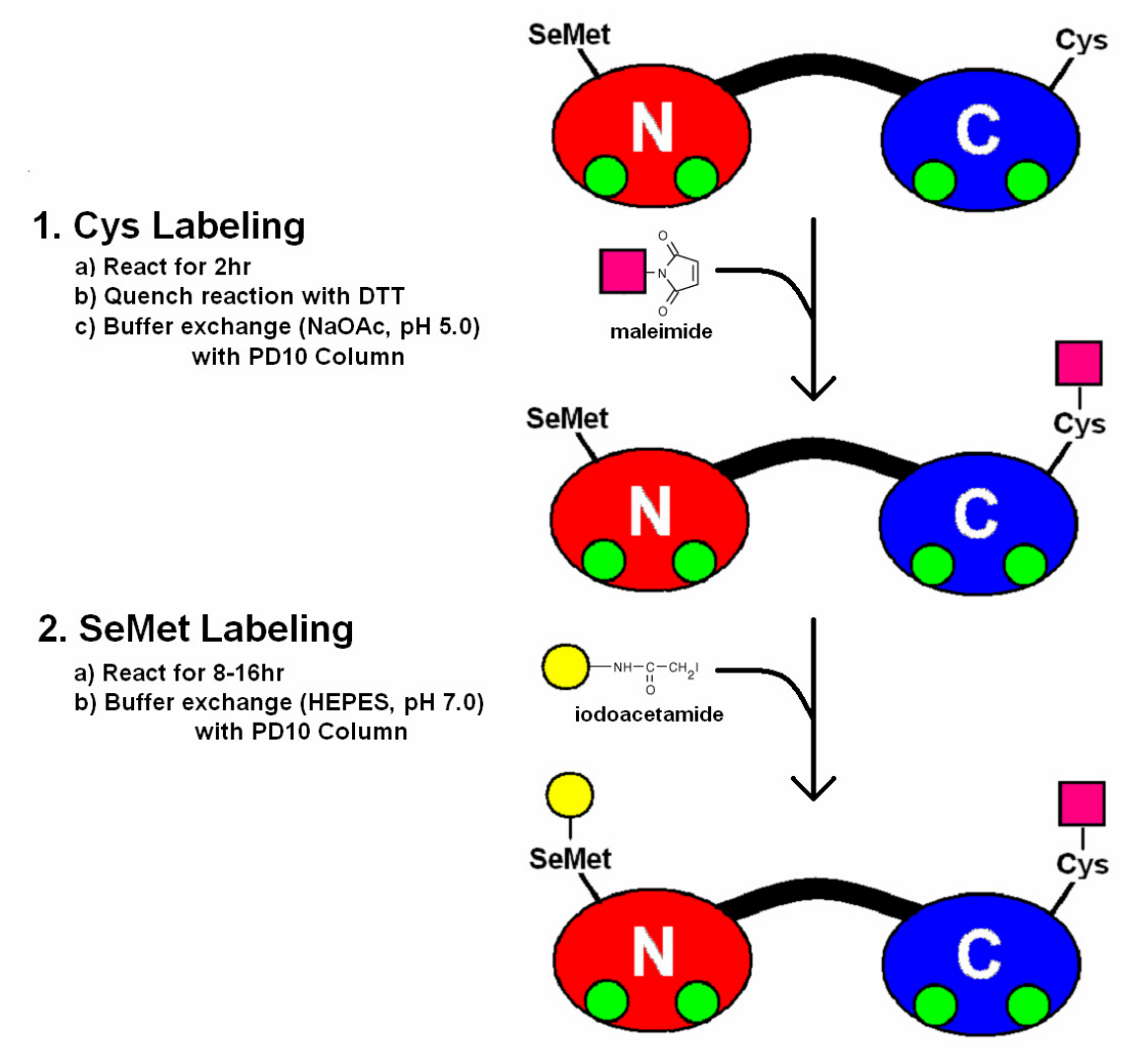

Figure 6.5 – Selective dual labeling of cysteine and selenomethionine residues in T34SeM/T110C CaM-L9.
Ca^{2+}, N- and C-terminal domains of CaM shown in green, red, and blue, respectively. Maleimide and iodoacetamide derivatized fluorophores are shown in pink and yellow. Cysteine labeling occurred in the presence of 1 mM $CaCl_2$, while selenomethionine labeling was exclusively in the presence of 1 mM EDTA. Methodology was used as described in sections 6.2.2.5 and 6.2.2.6.

This methodology was also employed with a variety of red-shifted dyes with the goal of performing FRET measurements with the holo-NOS enzymes. Donor-acceptor pairs that were attempted to be utilized for FRET studies using single selenomethionine (which was reacted exclusively with iodoacetamide derivatives) and cysteine (which was reacted with maleimide or iodoacetamide derivatives) were as follows in sequential order: (1) BODIPY 507/545 IA (Figure 6.4C, donor labeled on T110C – Molecular Probes,) and 5-TMRIA (Figure 6.4D, acceptor labeled on T34SeM – Molecular Probes,); (2) 5-TMRIA (donor labeled on T34SeM) with QSY 35 maleimide (Figure 6.4E, acceptor labeled on T110C – Molecular Probes,); (3) Alexa Fluor 546 C_5 maleimide (Figure 6.4G, donor labeled on T110C – Molecular Probes,) with QSY 9 C_5 maleimide (Acceptor labeled on T110C); (4) Alexa Fluor 546 C_5 maleimide (Donor labeled on T110C) with QSY 35 iodoacetamide (Figure 6.4F, acceptor labeled on T34SeM – Molecular Probes,); and (5) Alexa Fluor 546 C_5 maleimide (donor labeled on T110C) with DABIA (Figure 6.4H, Acceptor on T34SeM – GenoLite Biotek, Portland, OR, USA,).

6.2.2.8 Steady-state fluorescence of single and dual labeled CaM-L9

Fluorescence emission spectra were performed using a PTI QuantaMaster spectrofluorimeter. Fluorescence measurements were performed on IAEDANS labeled T34SeM CaM-L9 and T34SeM/T110C CaM-L9 (2 μM) as previously described (section 4.2.6) with some slight modifications. Excitation was at 336 nm, and emission was measured from 400 to 550 nm.

6.2.3 Results and Discussion

6.2.3.1 CaM-L9 Mutant Protein Expression and Purification

The CaM-L9 proteins were successfully overexpressed in *E. coli* and purified as previously described (sections 2.2.2 and 2.2.3). The yields of each CaM-L9 protein per liter are summarized in Table 6.1. ESI-MS QTOF confirmed homogeneity and ruled out any unwanted posttranslational modification (Table 6.1).

Table 6.1 – Masses and Purification Yield of CaM-L9 mutant proteins

CaM proteins	Mass (Da) [a]		Protein Yield (mgP/L media)
	Observed	Theoretical [b]	
CaM-L9	16544.0	16544	39.6
T34M CaM-L9	16574.5	16574	43.6
T34SeM CaM-L9	16619.0	16621 [c]	23.2
T110C CaM-L9	16546.0	16546	46.0
T34M/T110C CaM-L9	16576.0	16576	48.3
T34SeM/T110C CaM-L9	16620.5	16623 [c]	24.3

[a] Masses of deconvoluted ESI-MS spectra were determined with an accuracy of ± 3 Da.

[b] Calculated masses based upon amino acid sequence of the protein.

[c] Expected mass difference from substituting methionine with selenomethionine is 46.9 Da

6.2.3.2 cNOS Activation by CaM-L9 Mutant Proteins

Prior to the fluorescent labeling of the mutant CaM-L9 proteins, the ability of these proteins to bind and activate the cNOS enzymes was tested using the oxyhemoglobin capture assay. These measurements were taken to ensure that the mutations introduced in the CaM-L9 protein would not impair their ability to bind to the NOS enzymes. All of the proteins demonstrated Ca^{2+}-dependent activation of eNOS and nNOS (Table 6.2) similar to the results previously described in section 5.3.3.

Table 6.2 – CaM-L9 Mutant Proteins Dependent Activation of cNOS enzymes [a]

CaM protein	Neuronal NOS %	Endothelial NOS %
CaM	100 ± 3	100 ± 3
CaM-L9	77 ± 1	78 ± 3
T34M CaM-L9	68 ± 4	71 ± 5
T34SeM CaM-L9	54 ± 2	59 ± 4
T110C CaM-L9	51 ± 3	59 ± 2
T34M/T110C CaM-L9	84 ± 1	56 ± 5
T34SeM/T110C CaM-L9	58 ± 2	67 ± 3
CaM (EDTA)	NAA [b]	NAA [b]

[a] The oxyhemoglobin capture assay used to measure the rate of CaM-activated •NO production was performed in the presence of either 2 μM wild-type or mutant CaM protein and either 200 μM $CaCl_2$ or 250 μM EDTA, as indicated. The activities obtained with the respective enzyme bound to wild-type CaM at 25°C in the presence of 200 μM $CaCl_2$ were all set to 100%.

[b] NAA – No apparent activity

These results demonstrate that all of the mutant CaM-L9 proteins are capable of binding to the cNOS enzymes. These results are in good correlation with previous studies in our laboratory using CaM-L9 and other methionine to leucine mutant CaM proteins (Montgomery *et al.*, 2003).

6.2.3.3 Single and Dual Labeling of CaM-L9 Proteins

As previously described (section 5.3.1), the positions of T34 and T110 in CaM have been used repeatedly by many researchers to monitor the binding of CaM to various target peptides and proteins. While calmodulin contains nine methionine residues, it has been shown that all of these residues can be replaced with leucine without any detrimental effect on its ability to bind and activate its target proteins, such as the cNOS enzymes (Montgomery *et al.*, 2003). A single mutant methionine codon at position 34 was put into the methionine-free CaM mutant, CaM-L9. In contrast to the findings with streptococcal protein CAMP factor and another previous study (Guerrero *et al.*, 2001), quantitative replacement of methionine by selenomethionine required the use of a methionine-

auxotrophic *E. coli* strain B834 (DE3) for expression. Labeling yields of T34SeM CaM-L9 with IAEDANS were similar to those observed for the single selenomethionine mutant of CAMP factor, at approximately 95-100%. These results were confirmed by absorbance and ESI-MS (Figure 6.6).

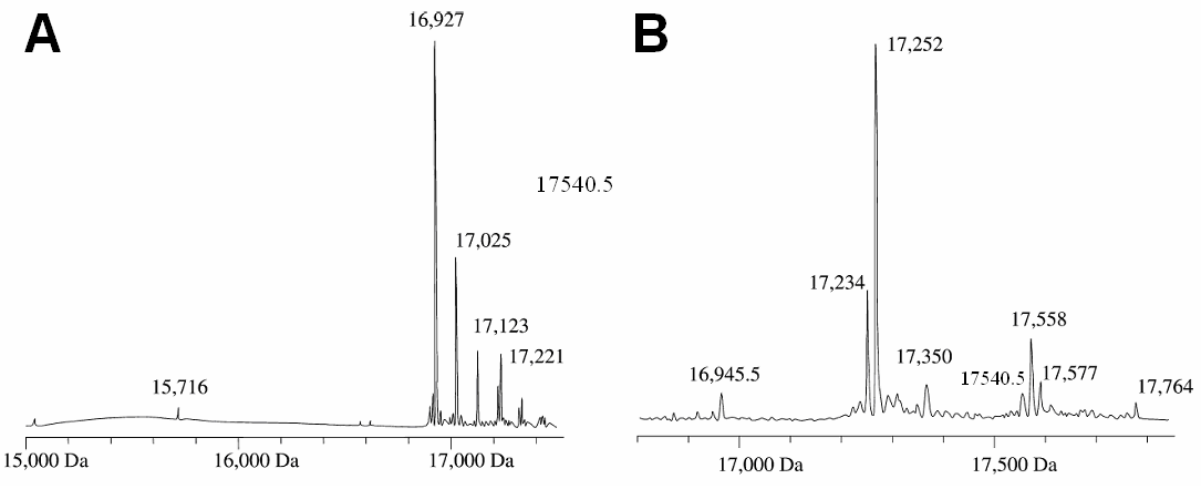

Figure 6.6 – Mass spectrometry of (A) IAEDANS labeled T34SeM CaM-L9 and (B) IAEDANS/DDPM labeled T34SeM/T110C CaM-L9 proteins.
(A) The T34SeM CaM-L9 protein, which contains one residue of selenomethionine but no cysteine, was labeled with IAEDANS (10 mM) for 16 hours. The highest peak at 16,927.0 Da corresponds to the expected singly labeled species. Peaks at higher molecular weight are likely due to phosphate ions associated with the protein. **(B)** The T34SeM/T110C CaM-L9 protein, which contains one residue of selenomethionine and one cysteine, was labeled with DDPM (30mM) for 2 hours, followed by IAEDANS (10 mM) for 16 hours. The 17,234.0 Da peak corresponds to the IAEDANS–DDPM dually-labeled protein. The 17,252.0-Da peak probably corresponds to labeled protein with an ammonium ion adduct. The peak at 17,540.5 Da corresponds to the protein labeled with two AEDANS moieties, with ammonium adduct peaks at 17,558.5 and 17,577 Da.

The use of the red-shifted dyes shown in Figure 6.4 also resulted in the successful dual labeling of T34SeM/T110C CaM-L9. These collective results further support Dr. Lang and Dr. Palmer's finding that selenomethionine residues incorporated into a protein can be specifically and efficiently labeled with iodoacetamide derivatized fluorophores.

6.2.3.4 Complications with Steady-State Fluorescence using IAEDANS-labeled Selenomethionine containing CaM Proteins

Initial steady-state fluorescence measurements with AEDANS-T34SeM CaM-L9 showed some unexpected and complicated results. Successive measurements on the sample showed increasing blue-shifted fluorescence emission spectra (Figure 6.7A).

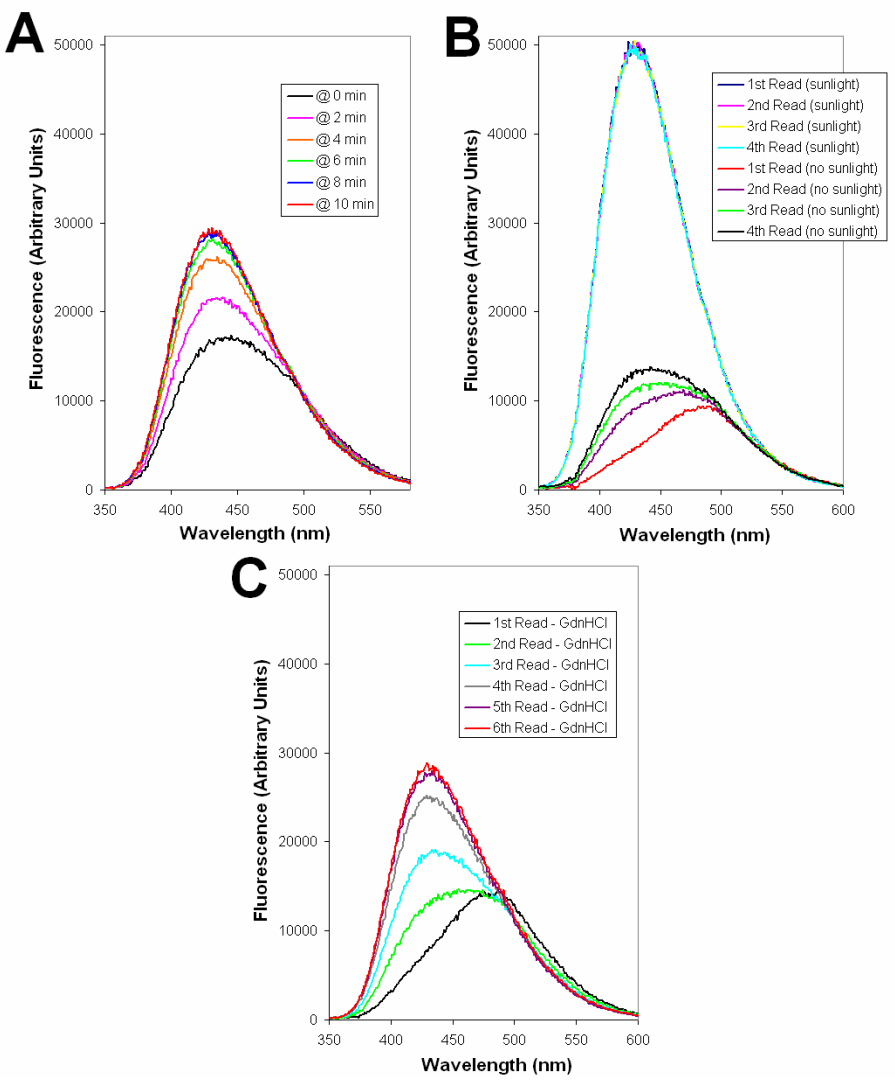

Figure 6.7 – Steady-state fluorescence complications with IAEDANS-labeled T34SeM CaM-L9. **(A)** Time-dependent change in AEDANS-T34SeM CaM-L9 fluorescence. **(B)** Effect of exposure of AEDANS-T34SeM CaM-L9 to direct sunlight. **(C)** Fluorescence of AEDANS-T34SeM CaM-L9 in the presence of 4 M guanidine hydrochloride. Measurements for all of these samples were taken every two minutes until the signal displayed no further change.

This large blue-shift in fluorescence is representative of a significant change in the AEDANS fluorophore's environment, moving from a hydrophilic to a hydrophobic environment. In order to determine if the excitation or light exposure was the cause of this fluorescence change, AEDANS-T34SeM CaM-L9 was treated with (1) direct exposure to sunlight for 30 minutes prior to fluorescence, and (2) treatment with guanidine hydrochloride to unfold the fluorescently labeled protein.

The exposure of AEDANS-T34SeM CaM-L9 to direct sunlight resulted in a five fold increase in fluorescence (Figure 6.7B), correlating well with the fluorophore moving into a hydrophobic environment upon the exposure to light. The control for this sunlight exposure experiment involved incubating the sample for 30 minutes prior to fluorescence measurements in the absence of sunlight. This control demonstrated a similar trend to what was previously observed in Figure 6.7A, with a time-dependent blue-shift in fluorescence.

The treatment of AEDANS-T34SeM CaM-L9 with guanidine hydrochloride was intended to unfold the protein and cause the hydrophilic exposure of the fluorophore to solvent. This control should have remained red-shifted since the fluorophore would be in a hydrophilic environment; however, the repeated measurements of this sample also displayed a blue-shift over time, as previously demonstrated in Figure 6.7A. Dr. Art Szabo (Dean of Science, Wilfrid Laurier University), a fluorescence expert, suggested that these blue-shifted emission spectra were possibly due to the photolysis of selenonium salt (Figure 6.3A) and the subsequent covalent re-attachment or non-covalent interaction of the AEDANS fluorophore at a hydrophobic pocket of CaM.

Another complication with using the selenomethionine labeling method that arose is the thiol-specific cleavage of the selenonium salt (Figure 6.3B). FRET measurements with the dually-labeled T34SeM/T110C CaM-L9 protein were planned to be performed on the holo-NOS enzymes, which are purified in the presence of dithiothreitol, a reducing agent that helps to maintain the stability of the

enzyme. Since the use of free thiols, in combination with the photolysis of the selenonium salt by light, both of which would result in the unwanted release of the fluorophore from the CaM protein and complicated fluorescence analysis, it was decided that an alternative method to dual-label CaM using a double cysteine CaM mutant would be more appropriate (section 6.3).

6.3 FRET Conformational Analysis of Calmodulin Bound to Nitric Oxide Synthase Peptides and Enzymes

6.3.1 Introduction

As previously mentioned (section 6.1), numerous studies have dually-labeled CaM at sites 34 and 110 to determine the conformation of CaM when bound to various target proteins and in different solvents using FRET (Drum *et al.*, 2000; Torok *et al.*, 2001; Slaughter *et al.*, 2005a; Slaughter *et al.*, 2005b; Xiong *et al.*, 2005; Maximciuc *et al.*, 2006). Due to the unforeseen difficulties with the selenomethionine labeling methodology (section 6.2), it was decided that the conventional method of dual-labeling CaM would be adopted. Using thiol-specific dyes to label CaM results in stable covalent linkages between the fluorophores and CaM, allowing for the inclusion of reducing agents, such as dithiothreitol to maintain and stabilize the holo-NOS enzymes during steady-state and time-resolved fluorescence measurements. The present study describes the dual labeling of T34C/T110C CaM mutant protein and its subsequent usage to determine the conformation of CaM when bound to NOS peptides and enzymes using FRET.

6.3.2 Experimental Procedures

6.3.2.1 Mutagenesis of CaM to produce T34C/T110C

The QuikChange site-directed mutagenesis procedure (Wang and Malcolm, 1999) was used to convert the threonine codon at position 34 to a cysteine into the kanamycin resistant pCaM-T110C plasmid consisting of the pET9d vector (Novagen) carrying rat calmodulin with a T110C mutation (section 5.2.1). The construction of pCaM-T34C/T110C was performed by the candidate and assisted by Miss Valentina Taiakina (UW Co-op student). The forward and reverse primers for the T34C

mutation were wt-T34Cfr and wt-T34Crv, as previously described (section 5.2.1). The resulting pCaM-T34C/T110C vector was confirmed by DNA sequencing.

6.3.2.2 CaM T34C/T110C Expression, Purification and Fluorescent Labeling

CaM T34C/T110C was expressed and purified by Miss Valentina Taiakina (UW Co-op student) as previously described (sections 2.2.2 and 2.2.3), with the exception that the dialysis buffer contained 1 mM DTT. The CaM protein concentrations were determined using the ε_{277} of 3029 $M^{-1}cm^{-1}$ for CaM saturated with Ca^{2+} (Gao *et al.*, 1998) and were subsequently frozen in aliquots on dry ice and stored at –80°C.

Labeling of CaM T34C/T110C was performed as previously described (section 5.2.3). The CaM T34C/T110C was transferred into labeling buffer (50 mM Tris-HCl, 1 mM EDTA, pH 7.2) by gel filtration using a Sephadex G-25 PD-10 column (Amersham Biosciences) in order to remove the excess reducing agent in the CaM sample (Lang *et al.*, 2005). Alexa Fluor 546 C_5-maleimide and 4-dimethylaminophenylazophenyl-4'-maleimide (DABMI) were dissolved in 50 mM Tris, pH 7.5 and *N,N'*-dimethylformamide, respectively, to a concentration of 10 mM.

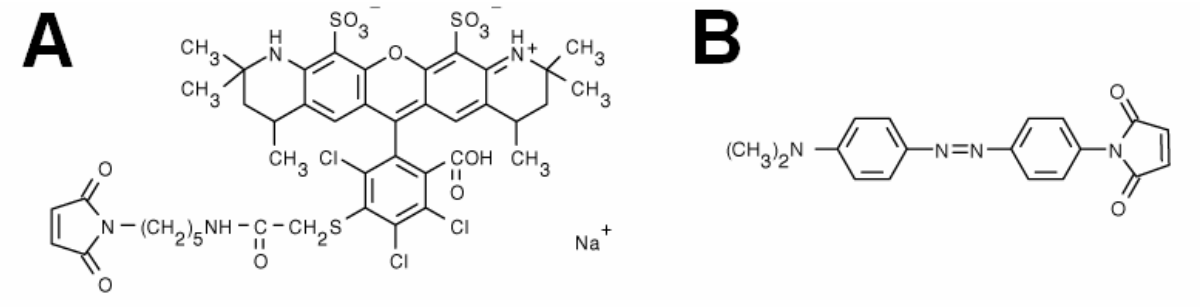

Figure 6.8 – Chemical structures of (A) Alexa Fluor 546 C_5 maleimide and (B) DABMI used to dual label CaM T34C/T110C.
Alexa Fluor 546 (Molecular Probes) and DABMI (4-dimethylaminophenylazophenyl-4'-maleimide; Molecular Probes) were used to thiol specifically label the cysteine residues in CaM T34C/T110C for FRET analysis.

50 µL of Alexa Fluor 546 and DABMI solutions (500 µM final concentration) were added to 1 mL of 100 µM CaM T34C/T110C (1.67 mg/mL). The reaction was mixed slowly and allowed to proceed for 2.5 hours at room temperature. The labeling reaction was subsequently quenched with the addition 10 mM dithiothreitol. Excess dye and dithiothreitol was removed by gel filtration using a PD-10 column pre-equilibrated with 50 mM HEPES, 1 mM EDTA, 150 mM NaCl, pH 7.5. Dialysis against 50 mM HEPES, 1 mM EDTA, 150 mM NaCl, pH 7.5 with two changes of buffer were performed to help remove any remaining non-covalently linked dye from the labeled CaM proteins.

The dually-labeled CaM T34C/T110C was then purified by reverse-phase chromatography on an AKTApurifier System for Chromatography (Amersham Biosciences, Baie d'Urfe, PQ) using a Vydac 214TP C_4 HPLC column (250 x 4.6 mm, 300 Å pore size, 5 µm particle size). The aqueous mobile phase consisted of 95% (v/v) H_2O, 5% (v/v) CH_3CN, and 0.1% (v/v) TFA while the organic mobile phase containing 95% (v/v) CH_3CN, 5% (v/v) H_2O, and 0.1% (v/v) TFA. The column was washed with two column volumes of the aqueous phase followed by a linear gradient of the organic mobile phase (2.5% / min, up to 30%). The dually-labeled CaM proteins (double DABMI, followed by Alexa 546/DABMI, and finally double Alexa 546) were eluted using a linear gradient of the organic mobile phase (0.4 % / min, 30 to 50%). The column was subsequently cleaned with a linear gradient of organic mobile phase (4.2% / min, 50 to 100%). Eluted protein was detected at 278 nm, while DABMI and Alexa Fluor 546 were monitored 467 and 556 nm, respectively. Double-labeled DABMI CaM T34C/T110C eluted at 39.8% organic mobile phase, followed by dually-labeled DABMI/Alexa Fluor 546 CaM at 41.2%, and finally double-labeled Alexa Fluor 546 CaM at 42.3%. Labeling yields were determined from absorbance spectra on a Varian Cary UV–visible Spectrophotometer (Varian, Mississauga, ON). The concentrations of DABMI and Alexa Fluor 546 were determined using the ε_{419} = 34,000 M^{-1} cm^{-1} and the ε_{554} of 93,000 $M^{-1}cm^{-1}$ (both from Molecular

Probes). Isolation of each double- and dually-labeled CaM species was confirmed by ESI-MS (section 2.2.5).

6.3.2.3 Site-directed Mutagenesis of eNOS, nNOS and iNOS

In order to create NOS enzymes incapable of binding to the catalytic heme, the QuikChange site-directed mutagenesis procedure (Wang and Malcolm, 1999) was used to convert the conserved proximal cysteine that acts as a thiolate ligand to the heme to alanines at positions C186 of bovine eNOS (Chen *et al.*, 1994), C415 of rat nNOS (Richards *et al.*, 1996), and C200 of human iNOS (Cubberley *et al.*, 1997), as previously described. The construction of pCWOri-eNOSC186A, pCWOri-nNOSC415A, and pCWOri-iNOSC200A was performed by the candidate and assisted by Miss Valentina Taiakina (UW Co-op student). The ampicillin pCWOri vectors with an N-terminal poly-histidine tag containing the coding regions for bovine eNOS, rat nNOS, and human iNOS carrying a deletion of the first 70 amino acids were used as the templates for mutagenesis. The forward and reverse primers for the C186A mutation of eNOS involved the incorporation of a unique *Xho*I reporter cut site: eNOSC186Afr 5' GGCGCAATGCACCTCGA*GCC*GTGGGCCGCATCCAG 3' and eNOSC186Arv CTGGATGCGGCCCAC*GG*CTCGAGGTGCATTGCGCC 3'. The primers used to produce the C415A mutation in nNOS incorporated a *Xho*I site and removed a *BamH*I site: nNOSC415Afr 5' GGAACGCCTCTCGA*GCC*GTGGGCAG*A*ATCCAGTGGTCCAAGC 3' and nNOSC415Arv 5' GCTTGGACCACTGGAT*T*CTGCCCAC*GG*CTCGAGAGGCGTTCC 3'. Likewise, the iNOS enzyme C200A mutation involved the use of primers adding a unique *Xho*I site and the removal of a *BamH*I site:

iNOSC200Afr 5' CGCAATGCCCCTCGA*GCC*ATTGGGAG*A*ATCCAGTGGTCCAAC 3' and iNOSC200Arv 5' GTTGGACCACTGGA*T*CTCCCAAT*GG*CTCGAGGGGCATTGCG 3'. The resulting plasmids (pCWOri-eNOSC186A, pCWOri-nNOSC415A, and pCWOri-iNOSC200A) were confirmed by DNA sequencing (see Appendix A for primer and vector sequences).

6.3.2.4 Expression and Purification of Heme-free NOS Enzymes

Bovine eNOS C186A and rat nNOS C415A were expressed as previously described (section 2.2.6). Human iNOS C200A was coexpressed with wild-type CaM and nCaM as previously described (section 2.2.8).

The purification of the heme-free eNOS and nNOS enzymes involved precipitation with 45% ammonium sulfate followed by metal chelation chromatography as previously described (section 2.2.7). After elution of the protein with 200 mM imidazole, the samples were dialysed as previously described (section 2.2.7) followed by the use of a Vivaspin 15 ultrafiltration spin column (Sartorius AG Biotechnology, Goettingen, Germany) to concentrate the eNOS and nNOS samples to approximately 2 mL in order to prepare the protein sample for gel filtration. The sample was the loaded on a HiLoad 16/60 Superdex 200 prep grade column (GE Healthcare Bio-Sciences, Baie d'Urfe, PQ) equilibrated with 50 mM Tris-HCl, pH 7.5, 10% glycerol, 0.1 M NaCl, and 1 mM DTT, and 1 mL fractions were collected. The flow rate was maintained at 0.6 mL/min using an AKTApurifier System for Chromatography (GE Healthcare Bio-Sciences) and eluted protein was monitored at 280 nm, while the flavins were monitored at 450 and 480 nm. The nNOS C415A protein that eluted around 54.8 mL, which corresponds to the dimer of nNOS, were collected and pooled. The eNOS C186A protein eluted around 55.6 mL, corresponding to dimeric eNOS, was collected and pooled. The purified heme-free cNOS enzymes were subsequently concentrated using a Vivaspin 15 ultrafiltration spin column and scanned on Varian Cary UV–visible Spectrophotometer. The concentration of the cNOS proteins was determined using ε_{455} of 15,400 $M^{-1}cm^{-1}$ (Newton *et al.*, 1998). Figure 6.9 gives a representative absorbance scan of a heme-free NOS enzyme using eNOS C186A as an example. The proteins were subsequently aliquoted, flash frozen on dry ice and stored at -80^{o}C.

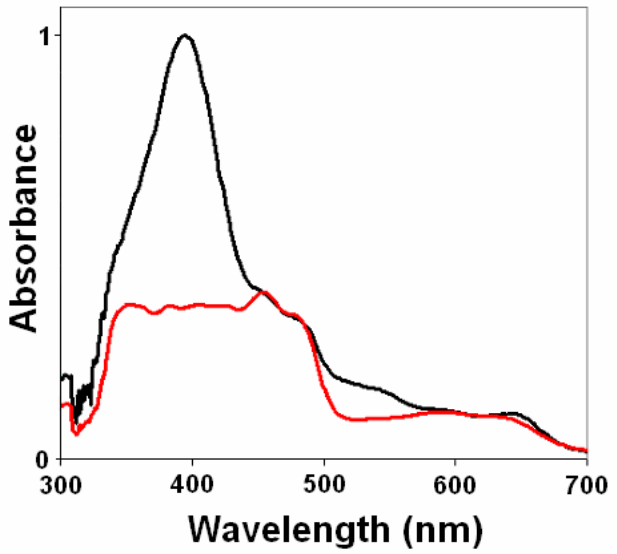

Figure 6.9 – UV-visible absorbance scan of holo-eNOS and eNOS C186A.
These scans demonstrate the spectal differences between the holo-NOS enzymes and heme-free NOS enzymes, using holo-eNOS (—) and heme-free eNOS (—) as an example.

In contrast, iNOS C200A coexpressed with wild-type CaM and nCaM was purified as previously described for iNOS coexpressed with nCaM using ammonium sulfate precipitation, followed by 2'5' ADP Agarose affinity chromatography (sections 2.2.9 and 3.3.3). The concentration of the heme-free iNOS protein was determined using the ε_{455} of 21,000 $M^{-1}cm^{-1}$ (Newton *et al.*, 1998).

6.3.2.5 Steady-State Fluorescence Measurements of Alexa-labeled CaM Proteins with NOS Peptides and Enzymes

Fluorescence emission spectra were obtained using a PTI QuantaMaster spectrofluorimeter. 50 nM CaM-T34C-Alexa Fluor 546 (section 5.2.3) or Alexa Fluor 546/DABMI T34C/T110C CaM were used as the fluorescent reporter in the quartz cuvette. The excitation wavelength for Alexa Fluor 546 labeled CaM was set at 540 nm and emission was monitored between 550 and 700 nm. Slit widths were set at 2 nm for excitation and 1 nm for emission. In an initial volume of 1 mL, a scan was taken with each of CaM protein in a buffer consisting of 50 mM HEPES, 1 mM EDTA, 150 mM NaCl, pH 7.5. After the initial scan, synthetic NOS CaM-binding domain peptide or heme-free cNOS enzyme

(250 nM) was added to the cuvette, the sample was mixed thoroughly, incubated for three minutes to allow the sample to reach equilibrium, and scanned. The NOS CaM-binding domain peptides for human iNOS, RPKRR EIPLK VLVKA VLFAC MLMRK (residues 507-531), bovine eNOS, TRKKT FKEVA NAVKI SASLM (residues 493-512) and rat nNOS, KRRAI GFKKL AEAVK FSAKL MGQ (residues 725-747) were synthesized by Sigma Genosys (Sigma Aldrich, Mississauga, ON). The sample was then brought to a final free Ca^{2+} concentration calculated to be 0.500 mM, mixed, allowed to incubate for three minutes, and scanned. Finally, excess EDTA (5 mM final) was added, incubated for an additional three minutes, and a final scan was taken. The fluorescence emission maximum of CaM-T34C-Alexa and Alexa/DABMI T34C/T110C CaM was observed at 567 nm, regardless of the presence of Ca^{2+} in the buffer.

6.3.2.6 Quin-2 Free Ca^{2+} Concentration Calibration

Quin-2, a fluorescent Ca^{2+} indicator dye developed for the determination of free Ca^{2+} concentrations in solution and cells (Tsien and Pozzan, 1989), was purchased from Molecular Probes (Figure 6.10).

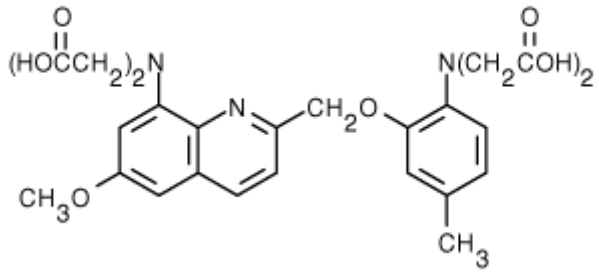

Figure 6.10 – Structure of the fluorescent Ca^{2+} indicator dye Quin-2.
This dye was utilized to determine the free Ca^{2+} concentration in solution during steady-state and time-resolved fluorescence measurements. Quin-2, *N*-(2-((8-(bis(carboxymethyl)amino)-6- methoxy-2-quinolinyl)methoxy)-4- methylphenyl)-*N*-(carboxymethyl)-glycine, ε_{353} = 4000 $M^{-1}cm^{-1}$, em_{max} at 495 nm, FW = 541.51.

Since physiological concentrations of Ca^{2+} in the cell are low, a calibrated Ca^{2+} buffer kit was also purchased from Molecular Probes with two solutions containing 30 mM MOPS, pH 7.2, 100 mM KCl with a 10 mM K_2EGTA buffered solution ("zero" free Ca^{2+}) and a 10 mM Ca/EGTA buffered solution (39 μM free Ca^{2+}) prepared using a previously published method (Tsien and Pozzan, 1989). Steady-state fluorescence measurements were taken in the presence of Quin-2 using the known free Ca^{2+} concentrations of Ca^{2+} at 20°C. For increasing free Ca^{2+} concentrations, these buffers were mixed with increasing ratios of Ca/EGTA to K_2EGTA (ie. 1 mM Ca/EGTA, 2 mM Ca/EGTA, etc.).

The excitation wavelength for Quin-2 was set at 330 nm and emission was monitored between 400 and 600 nm. Excitation and emission slit widths were set at 1 nm and the sample was measured at 20°C. Samples consisted of 1 mL of the mixed Ca/EGTA buffers (ie. 0, 1, 2…9, 10 mM Ca/EGTA) containing 2 μM Quin-2 in a 1 cm quartz cuvette. Once collected, the steady-state fluorescence data was plotted as the log of the $[Ca^{2+}]_{free}$ (x-axis) versus the $\log((F - F_{min})/(F_{max} - F))$ (y-axis). Using this double log plot, the x-intercept was used to determine the K_d for Quin-2 (M), as previously described in a detailed protocol for the Ca^{2+} calibration buffer kit (C-3008, Molecular Probes).

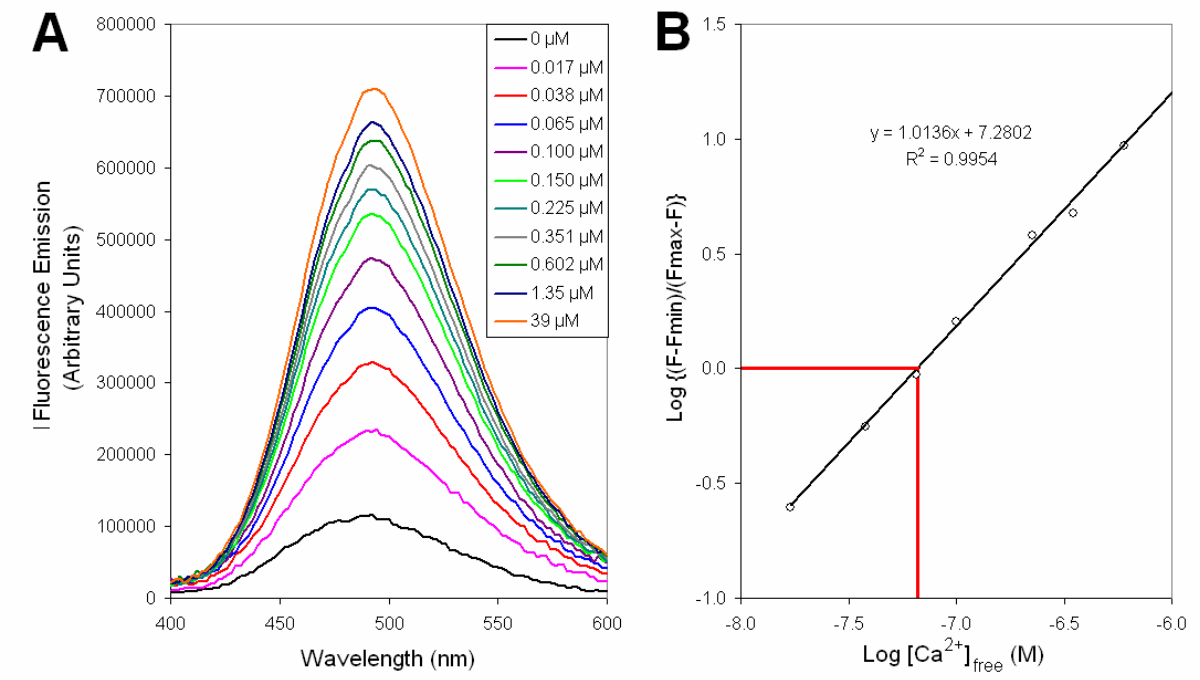

Figure 6.11 – Determination of the K_d of Quin-2 using Ca/EGTA buffers.
(A) Steady-state fluorescence and **(B)** double log plot for the calibration of Quin-2 in 0–10 mM Ca/EGTA buffers. Using the data from A, plot B was derived and the K_d of Quin-2 was determined from the x-intercept (experimental K_d = 66 nM).

The experimentally determined K_d for Quin-2 (66 nM) was in good agreement to the previously published K_d for Quin-2 of 60 nM (Tsien and Pozzan, 1989). Using this curve and K_d, the free Ca^{2+} concentrations were determined for subsequent time-resolved fluorescence measurements.

6.3.2.7 Time-Resolved Fluorescence Measurements of Alexa-labeled CaM Proteins with NOS Peptides and Enzymes

Time-resolved fluorescence was measured using a PicoQuant FluoTime 100 Compact Fluorescence Lifetime Spectrometer (PicoQuant GmbH, Berlin, Germany) using an LED with maximal emission at 500 nm. Settings used on the FluoTime 100 were 50-100% transmittance, intensity 90, and 520 nm bandpass cut-off filter. Samples containing 100 nM CaM-T34C-Alexa (Donor alone) and Alexa/DABMI T34C/T110C CaM (Donor/acceptor) were measured under Ca^{2+}-deplete and -replete

conditions using buffers consisting of 50 mM HEPES, 150 mM NaCl, pH 7.5 with 1 mM EDTA or $CaCl_2$. Using the Ca/EGTA buffer kit (as described in section 6.3.2.6), intermediate Ca^{2+} concentrations were measured over the range of physiological free Ca^{2+} concentrations. These measurements were taken with labeled CaM alone, as well as in the presence of synthetic NOS peptides or heme-free NOS enzymes (500 nM each). Fluorescence decay curves were fit with one or more lifetime components using PicoQuant FluoFit software with the lowest χ^2 value used to determine the best fit of the fluorophore's lifetime.

6.3.2.8 Determination of the Förster Distance (R_O) for Alexa Fluor 546 and DABMI labeled proteins

To determine the Förster distance (R_O), which is defined as the distance where energy transfer between the donor (Alexa Fluor 546) and acceptor (DABMI) is 50%, steady-state fluorescence of singly labeled CaM-Alexa proteins and absorbance of CaM-DAB proteins were measured in the presence of EDTA and Ca^{2+}. Steady-state fluorescence of CaM-T34C-Alexa and CaM-T110C-Alexa was measured on PTI QuantaMaster spectrofluorimeter with excitation set at 475 nm and emission monitored from 350-700 nm. The absorbance of CaM-T34C-DAB and CaM-T110C-DAB was measured from 300-700 nm on an Ultrospec 2100 pro UV/Vis Spectrophotometer (Biochrom Ltd., Cambridge, UK). The R_O value was determined using a macro programmed for Microsoft Excel by Dr. Michael Palmer (Associate Professor, U of Waterloo) entitled "SpectraAnalysis" which allows the user to analyse fluorescence or absorbance spectra in a variety of ways including determining the overlap integral, $J(\lambda)$, an important constant involved in the determination of the R_O value for FRET. Figure 6.12 demonstrates the spectral overlap of Alexa Fluor 546 and DABMI-labeled proteins.

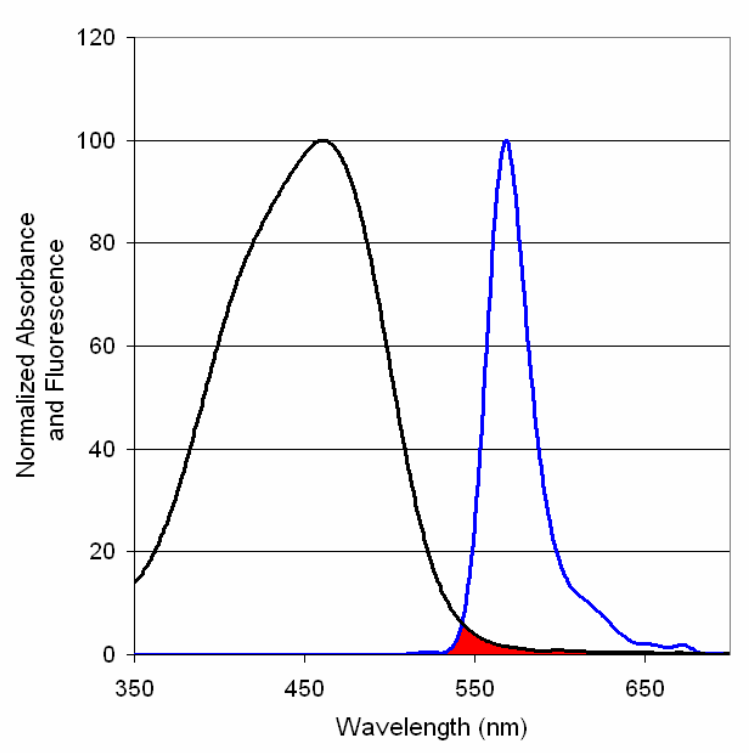

Figure 6.12 – Emission of Alexa Fluor 546 and absorbance of DABMI-labeled CaM proteins for the determination of spectral overlap interval *J*(λ).
The normalized fluorescence emission of CaM-T34C-Alexa and absorbance of CaM-T110C-DAB in the presence of EDTA are shown as (——) and (——), respectively. The overlap interval is highlighted in red.

The overlap integral $J(\lambda)$ is calculated using the following formula:

Equation 6.1

$$J(\lambda) = \int_0^\infty F_D(\lambda)\varepsilon_A(\lambda)\,\lambda^4\,d\lambda$$

where $F_D(\lambda)$ represents the corrected fluorescence intensity of the donor in the wavelength range λ to λ + Δ λ with the area under the curve normalized, $\varepsilon_A(\lambda)$ represents the extinction coefficient of the acceptor at λ, and λ represents the wavelength in nm (Lakowicz, 2006). The overlap integral $J(\lambda)$ is expressed in units of M^{-1} cm^{-1} $(nm)^4$ (Lakowicz, 2006).

The R_O value (in Å) can then be determined using $J(\lambda)$ in the following formula:

Equation 6.2 $$R_O = 0.211[\kappa^2 n^{-4} Q_D J(\lambda)]^{1/6}$$

where κ^2 represents the dipole-dipole coupling orientation factor which is normally assumed to be ⅔; n represents the refractive index of the medium and is normally assumed to be 1.4 for proteins in aqueous solution (Lakowicz, 2006); Q_D represents the quantum yield of the donor and was assumed to be 0.79 for Alexa Fluor 546 (Molecular Probes), which can also be determined as previously described (Van der Meer *et al.*, 1994; Lakowicz, 2006).

6.3.2.9 FRET distance determination for Alexa Fluor 546/DABMI T34C/T110C CaM with NOS peptides and enzymes

Using the fluorescence lifetimes determined using the methodology in section 6.3.2.7, the energy transfer efficiency (E) was determined using the following formula:

Equation 6.3 $$E = 1 - \tau_{DA}/\tau_D$$

where τ_{DA} and τ_D represent the fluorescent lifetimes for donor-acceptor labeled CaM (Alexa Fluor 546/DABMI T34C/T110C CaM) and donor-labeled CaM (CaM-T34C-Alexa), respectively.

Using the energy transfer efficiency (E) values and the R_O value determined in section 6.3.2.8, the FRET distances (R) were finally calculated using the following formula (expressed in Å):

Equation 6.4 $$R = R_O[(1 - E)/E]^{1/6}$$

It is important to note that because energy transfer efficiency (E) is strongly dependent on the distance between the donor and acceptor, FRET distance measurements are only reliable when R is within a factor of 2 of R_O (Lakowicz, 2006). For instance, when $R = 2R_O$, the energy transfer

efficiency would equal 1.54%, where as when $R = 0.5R_O$, then E would equal 98.5%. This phenomenon is demonstrated in Figure 6.13.

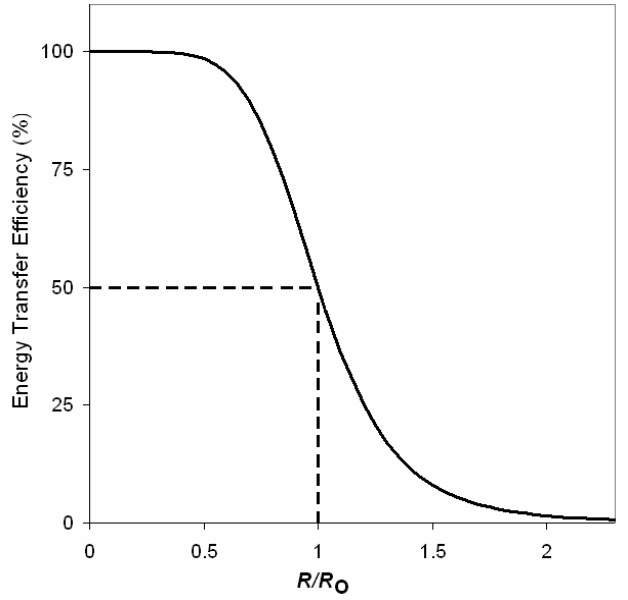

Figure 6.13 – Dependence of energy transfer efficiency (*E*) on the distance (*R*) between the donor and acceptor dyes.
R_O represents the Förster distance, the distance between the donor and acceptor where energy transfer efficiency is 50%.

6.3.3 Results

6.3.3.1 Characterization of Fluorescently Labeled CaM-Cys Proteins

As previously mentioned in Chapter 5, the double cysteine mutants utilized in this study have been used extensively in FRET studies focusing on CaM's conformation alone and in complex with CaM target proteins and peptides (Drum *et al.*, 2000; Torok *et al.*, 2001; Allen *et al.*, 2004; Maximciuc *et al.*, 2006). Their position in helices 2 (T34C) and 6 (T110C) of CaM are in close proximity to each other in the classic wrapped conformation, as seen in the CaM-MLCK complex (Ikura *et al.*, 1992). In contrast, these residues are markedly separated when CaM is in an extended conformation, as seen in holo-CaM (Chattopadhyaya *et al.*, 1992), apo-CaM (Kuboniwa *et al.*, 1995), and CaM in complex with the edema factor from *B. anthracis* (Drum *et al.*, 2002).

The cysteine CaM mutants were successfully overexpressed in *E. coli*. ESI-MS QTOF confirmed homogeneity and ruled out any posttranslational modification (Table 5.1).

Table 6.3 – Masses of Alexa 546 and DABMI labeled CaM-Cys proteins

	Mass (Da) [a]	
CaM proteins	Observed	Theoretical [b]
wtCaM	16706.0	16706
CaM T34C	16709.0	16708
CaM T110C	16709.0	16708
CaM T34C-Alexa Fluor 546	17717.5 [b]	17720 [b]
CaM T110C-Alexa Fluor 546	17717.5	17720
CaM T34C-DABMI	17027.0 [c]	17029 [c]
CaM T110C-DABMI	17027.0	17029
CaM T34C/T110C-Alexa/DABMI	18040.5 [d]	18040 [d]

[a] Masses of deconvoluted ESI-MS spectra were determined with an accuracy of ± 3 Da..
[b] Expected mass difference after labeling CaM-Cys proteins with Alexa Fluor 546 C_5-maleimide is 1011.4 Da (Molecular Probes). The manufacturer's MW of the dye is 1034.3, which includes a single counter sodium ion.
[c] Expected mass difference after labeling CaM-Cys proteins with DABMI is 320.35 Da (Molecular Probes).
[d] Expected mass difference after dual labeling CaM T34C/T110C with Alexa Fluor 546 C_5-maleimide and DABMI is 1331.75 Da (Molecular Probes).

The CaM T34C and T110C proteins were singly labeled with Alexa Fluor 546 and DABMI as previously described in section 5.2.3. Labeling was determined to be complete and was confirmed by ESI-MS (Table 6.3). Protein concentrations were determined using the ε_{419} = 34,000 M^{-1} cm^{-1} and the ε_{554} of 93,000 $M^{-1}cm^{-1}$ for DABMI and Alexa Fluor 546, respectively.

Using the formulas outlined in section 6.3.2.8, the R_O distance was determined to be 31.07 Å in the presence of EDTA and 30.99 Å in the presence of Ca^{2+}. Since both of these values are in good agreement, the assumed R_O used throughout this chapter is 31 Å. This experimentally determined R_O distance correlates well with the theoretical R_O for Alexa Fluor 546 and DABMI of 29 Å (Molecular Probes).

6.3.3.2 Steady-State Fluorescence of Alexa-labeled CaM Proteins with NOS Peptides and Enzymes

Steady-state fluorescence was used to observe if quenching of the Alexa Fluor 546 by DABMI was occurring in the presence of the NOS CaM-binding domain peptides. Quenching of the Alexa Fluor dye represents the dyes being in close proximity to each other, while a lack of quenching would represent the dyes being separated. From the previously published CaM-eNOS (Aoyagi *et al.*, 2003) and CaM-nNOS complexes (Ng *et al*. – unpublished, co-ordinates released 2007-12-25), it is apparent that CaM adopts a tightly wrapped conformation when associated to these peptides and that the T34 and T110 residues are in close proximity to one another. Therefore, it is expected that we should see a marked amount of quenching when the dually-labeled CaM is associated to the cNOS peptides. To date, very little has been reported on the conformation and structure of CaM when associated to iNOS; however, due to the sequence similarity between the cNOS and iNOS CaM-binding domains (Figure 6.14A) and evidence of the iNOS CaM-binding domain becoming α-helical when bound to CaM (Matsubara *et al.*, 1997; Yuan *et al.*, 1998; Spratt *et al.*, 2007a), it is anticipated that CaM will also have a wrapped conformation when bound to the iNOS peptide.

As mentioned previously in section 5.3.5.1, singly-labeled CaM-T34C-Alexa showed no fluorescence changes upon the addition of the NOS peptides regardless of Ca^{2+} or EDTA presence, indicating that no quenching of the fluorophore emission occurs when bound to the NOS peptides. In contrast to the singly-labeled CaM measurements, marked fluorescence changes were observed for dually-labeled Alexa/DABMI CaM in the presence of the NOS peptides, which depended upon the presence of Ca^{2+} (Figure 6.14).

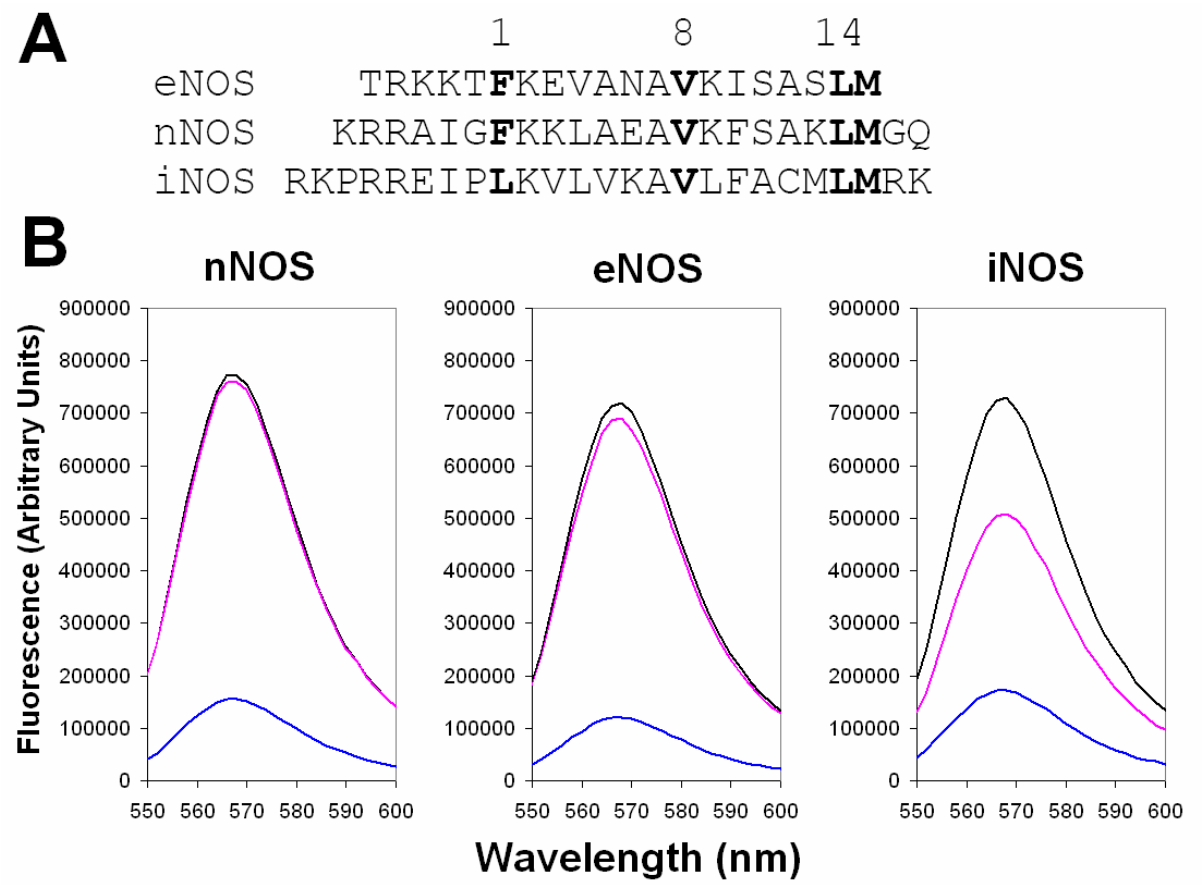

Figure 6.14 – Steady-state FRET measurements using Alexa/DABMI labeled CaM T34C/T110C with synthetic NOS CaM-binding domain peptides.
(A) Alignment of CaM-binding domain peptides for human eNOS, nNOS and iNOS used in this study. **(B)** Steady-state FRET measurements using double labeled CaM T34C/T110C Alexa Fluor 546/DABMI with NOS CaM-binding domain peptides. Measurements shown were in the presence of EDTA (—), Ca^{2+} with NOS peptide (—), and EDTA with NOS peptide (—). Excitation was set at 540 nm and emission was monitored between 550-600 nm.

CaM alone in the presence of EDTA showed little or no quenching, indicating that CaM is in an extended conformation under these conditions. The subsequent addition of Ca^{2+} and NOS peptide resulted in a dramatic fluorescence decrease, indicating that the dyes now are in close proximity to one another, and therefore that CaM wraps around the peptide. The final addition of EDTA to the eNOS and nNOS peptide samples resulted in the return of the fluorescence to its originating intensity. This signifies that CaM releases itself from the peptide and returns to its original extended conformation that also prevails in the absence of NOS peptide. This is in good agreement with previous studies indicating that the interaction between CaM and cNOS peptides is Ca^{2+}-dependent. In contrast, upon addition of EDTA to the CaM-iNOS peptide sample, fluorescence increased slightly but did not return to its original intensity for CaM alone. This shows that CaM is still associated to the iNOS peptide; however, a Ca^{2+}-dependent change in conformation appears to occur as a result of the EDTA addition.

Previous studies have shown that the heme in NOS is a potent quencher of Alexa Fluor 546 and would interfere with FRET measurements (Chapter 5). To avoid this undesired quenching from the heme in the NOS enzymes, the conserved cysteine residue that is axially coordinated to the heme was mutated to an alanine. These cysteine to alanine mutations (nNOS C415A, eNOS C186A, and iNOS 200A) have previously been shown to produce heme-free NOS enzymes (Chen *et al.*, 1994; Richards *et al.*, 1996; Cubberley *et al.*, 1997; Spratt *et al.*, 2006). Furthermore, the oxidized FMN and FAD cofactors in the reductase domain of NOS absorb poorly in the 550-700 nm range (Munro and Noble, 1999).

Similar to the steady-state measurements taken with the NOS peptides, singly labeled CaM-T34C-Alexa and dually-labeled CaM T34C/T110C Alexa/DABMI were measured in the presence of EDTA. This was followed by the addition of Ca^{2+} and heme-free cNOS enzyme, and finally excess EDTA. The singly labeled CaM-T34C-Alexa demonstrated a slight quenching in the presence of

Ca^{2+} and heme-free NOS enzymes (Figure 6.15); however, this quenching was less than what was previously observed with holo-cNOS enzymes in our previous study (Chapter 5) (Spratt *et al.*, 2007b). Although the removal of the heme does not completely stop the quenching of Alexa Fluor 546 fluorescence, it does demonstrate that the removal of the heme can decrease the amount of quenching and minimize its effect in subsequent FRET measurements.

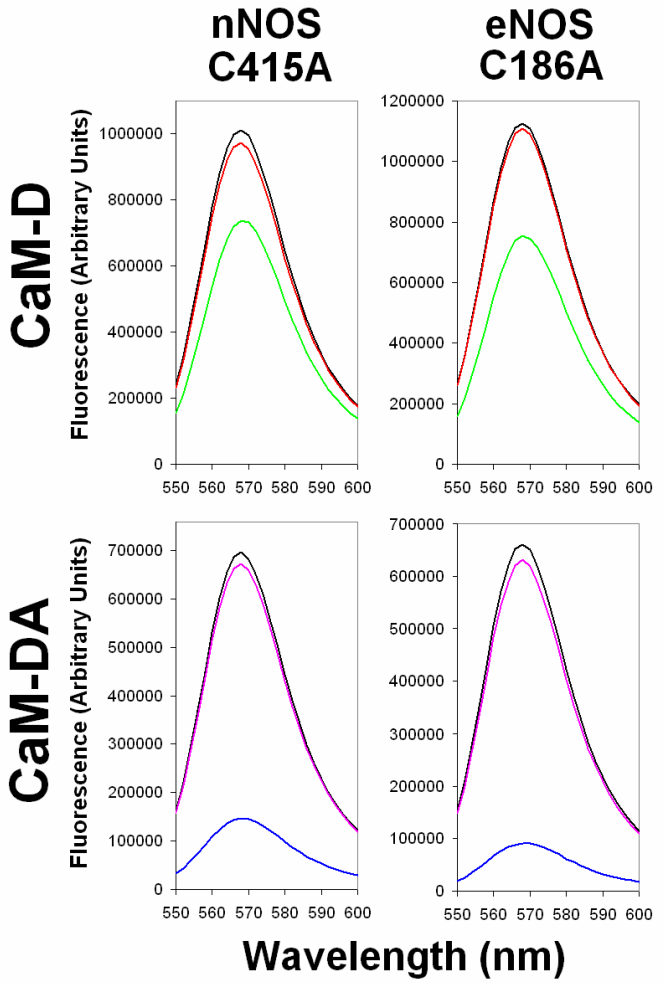

Figure 6.15 – Steady-state FRET measurements using singly labeled CaM-T34C-Alexa (CaM-D) and dual labeled CaM T34C/T110C Alexa/DABMI (CaM-DA) with heme-free cNOS enzymes.
Measurements for CaM-D were in the presence of EDTA alone (—), EDTA with heme-free cNOS (—), and Ca^{2+} with heme-free cNOS (—). Measurements for CaM-DA were in the presence of EDTA alone, EDTA with heme-free cNOS (—), and Ca^{2+} with heme-free cNOS (—). Excitation was set at 540 nm and emission was monitored between 550-600 nm.

Similar to the previous results with the cNOS peptides, there was marked quenching of Alexa Fluor 546 emission in the presence of Ca^{2+} and the heme-free cNOS enzymes. This shows that the dually-labeled CaM also wraps around the cNOS enzymes, similar to that previously observed with the cNOS peptides. The subsequent addition of EDTA also caused the release of CaM from the enzymes further demonstrating the Ca^{2+}-dependent association between the cNOS enzymes and CaM.

Since iNOS cannot be purified without CaM or CaM mutant coexpression and we cannot coexpress dually-labeled fluorescent CaM protein with iNOS, we performed FRET measurements with iNOS coexpressed with the Ca^{2+}-sensitive CaM mutant, nCaM (Chapter 3). This CaM mutant was previously shown to bind to iNOS in a 2:1 ratio (Spratt *et al.*, 2006) and could be displaced from the C-type binding site of the CaM-binding domain by another CaM protein in the presence of EDTA (Spratt *et al.*, 2007b). Although this is a surrogate system and not a true representation of CaM binding to the enzyme, it is the only available method to date that has been shown to have some flux in CaM's association to the iNOS CaM-binding domain. Furthermore, we have also previously shown that nCaM bound to the N-type site of the CaM-binding domain is permanent and cannot be displaced. This is due to the tightly bound nCaM blocking the association of the N-terminal domain of the fluorescently labeled CaM from binding to the N-type site of iNOS's CaM-binding domain (Spratt *et al.*, 2007b). Due to these reasons, performing FRET experiments with the dually-labeled CaM T34C/T110C Alexa/DABMI on iNOS would be difficult to measure and analyse. Therefore, iNOS C200A coexpressed with nCaM is exclusively used as a control for heme-Alexa FRET measurements used later in this chapter (see section 6.3.3.3.5).

6.3.3.3 Time-resolved measurements for the determination of FRET distances

Steady-state fluorescence provides an average of the fluorescent species in a sample. In contrast, time-resolved fluorescence allows for the determination of different conformational species within a sample that can be used to determine FRET distances. Singly-labeled CaM-T34C-Alexa was used as

a control by using the lifetime of the donor alone without the acceptor being present as a reference set at 100%. Any lifetime shorter than the donor alone's lifetime would represent FRET between the donor and the acceptor dyes and could be used to determine the FRET distance between T34 and T110 of CaM in solution.

Fluorescence measurements were taken using dually-labeled CaM T34C/T110C Alexa/DABMI over a range of physiological free Ca^{2+} concentrations (0 to 2 μM) for (1) CaM alone, (2) CaM with NOS CaM-binding domain peptides, and (3) CaM with the heme-free cNOS enzymes. As an example, the time-resolved fluorescence exponential decays determined for CaM-T34C-Alexa and CaM T34C/T110C Alexa/DABMI with nNOS peptide are shown in Figure 6.16.

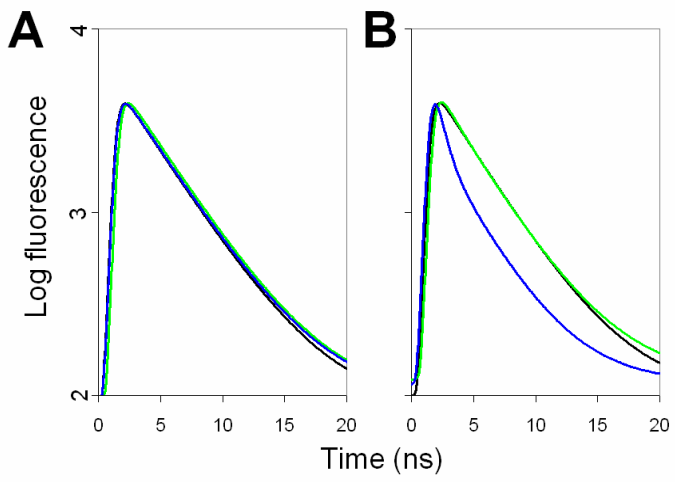

Figure 6.16 – Time-resolved fluorescence of (A) Alexa 546-T34C CaM and (B) Alexa 546/DABMI-T34C-T110C CaM.
Measurements were taken of CaM alone in the presence of EDTA (—) and Ca^{2+} (—), as well as in the presence of Ca^{2+} with nNOS peptide (—). Lifetimes and FRET distances were determined from these fluorescence decay curves by fitting them to multiple exponentials using PicoQuant FluoFit software. The fitting results from the data shown in this figure are summarized in Table 6.6.

6.3.3.3.1 FRET distance determination: Dually-labeled CaM alone

A summary of determined fluorescent lifetimes and FRET distances for dually-labeled CaM T34C/T110C Alexa/DABMI with increasing free Ca^{2+} concentrations is shown in Table 6.4.

Table 6.4 – Determined FRET distances for Alexa 546/DAB-T34C-T110C CaM alone with increasing free Ca^{2+} concentrations.

$[Ca^{2+}]_{free}$ (μM)	R_O[a] (Å)	τ_D[b] (ns) [χ^2]	$\tau_{1(DA)}$ (ns) [χ^2]	A_1[c]	E_1[d]	distance (da_1)[e] (Å)	$\tau_{2(DA)}$ (ns)	A_2	E_2	distance (da_2) (Å)
0	31	4.026 [1.118]	3.861 [1.025]	0.78	0.04	52.43	0.928	0.22	0.77	25.36
0.0156		4.032 [1.066]	3.873 [0.956]	0.82	0.04	52.78	0.993	0.18	0.75	25.73
0.0331		4.028 [1.050]	3.894 [1.080]	0.79	0.03	54.36	0.974	0.21	0.76	25.62
0.0569		4.036 [1.046]	3.859 [1.067]	0.81	0.04	51.81	0.900	0.19	0.78	25.18
0.0878		4.114 [1.103]	3.903 [1.047]	0.75	0.05	50.41	0.949	0.25	0.77	25.36
0.1353		4.099 [0.986]	3.915 [1.078]	0.76	0.04	51.60	0.967	0.24	0.76	25.49
0.1952		4.077 [1.067]	3.896 [1.103]	0.59	0.04	51.70	1.017	0.41	0.75	25.80
0.2913		4.076 [1.119]	3.876 [1.114]	0.52	0.05	50.81	0.974	0.48	0.76	25.56
0.433		4.029 [1.071]	3.809 [1.026]	0.61	0.05	49.86	0.672	0.39	0.83	23.71
0.7801		4.061 [1.105]	3.789 [1.078]	0.67	0.07	48.09	0.765	0.33	0.81	24.30
1.9138		4.046 [1.16]	3.844 [1.083]	0.69	0.05	50.65	0.894	0.31	0.78	25.13

[a] Förster distance (R_O) is the distance where resonance energy transfer is 50% efficient. This value was determined using the methodology described in section 6.3.2.8.

[b] τ_D, $\tau_{1(DA)}$ and $\tau_{2(DA)}$ represent fluorescent lifetimes for donor alone (CaM-T34C-Alexa) and the primary and secondary lifetimes for donor-acceptor (Alexa/DAB labeled CaM), respectively. 2 exponential fits were carried out to minimize χ^2 values using PicoQuant FluoFit software.

[c] RET values were calculated using $E = 1 - (\tau_{DA}/\tau_D)$, where E represents energy transfer efficiency.

[d] A_1 and A_2 represent fractional contribution of fluorescence lifetime decay measurements.

[e] Distance values (da_1 and da_2) were calculated using $R = R_O[(1\text{-}E)/E]^{1/6}$, where R represents the calculated distance between the donor and acceptor (D-A) in Å.

It is apparent from the determined FRET distances that CaM alone is in a predominantly extended conformation (~80%) with a smaller population of CaM being in a compact form (~20%). This extended conformation would be expected to be similar to previously solved NMR structure of apo-CaM where the distance between T34 and T110 is greater than 40 Å (Kuboniwa *et al.*, 1995). Interestingly, as the free Ca^{2+} concentration increased, the relative distances between the Alexa Fluor 546 and DABMI dyes remained the same; however, the fractional contribution of the predominant fluorescent lifetime decreased from 80 – ~60% while the amplitude of the secondary fluorescent decay increased from 20 – ~40% (Table 6.4). This demonstrates that holo-CaM is predominantly in an extended conformation, as previously shown in Figure 6.1A (Chattopadhyaya *et al.*, 1992); however, holo-CaM can also be in a closed and compact form, as previously shown in Figure 1.3D (Fallon and Quiocho, 2003). This ability of holo-CaM to adopt a variety of conformations has been attributed to the flexible central linker region which can unwind readily bringing the N- and C-domains of CaM in close proximity to one another. These results correlate well with a previous FRET study that showed two lifetimes fit the fluorescence decay of a T34C/T110C donor/acceptor labeled CaM, with the predominant species having an amplitude of 75% corresponding to a distance of ~40 Å and the secondary species having an amplitude of 25% and a distance of ~25 Å (Torok et al., 2001). Another study demonstrated at a Ca^{2+} concentration of 150 nM a similar ratio of extended to compact forms (Slaughter *et al.*, 2005a).

FRET distance determination: Dually-labeled CaM with cNOS peptides

Table 6.5 and Table 6.6 provide summaries of the fluorescent lifetimes and determined FRET distances for CaM T34C/T110C Alexa/DABMI in the presence of eNOS and nNOS CaM-binding domain peptides with increasing free Ca^{2+} concentrations.

Table 6.5 – Determined FRET distances for Alexa 546/DAB-T34C-T110C CaM in the presence of eNOS peptide with increasing free Ca^{2+} concentrations.

$[Ca^{2+}]_{free}$ (μM)	R_O [a] (Å)	τ_D [b] (ns) [χ^2]	$\tau_{1(DA)}$ (ns) [χ^2]	A_1 [c]	E_1 [d]	distance (da_1) [e] (Å)	$\tau_{2(DA)}$ (ns)	A_2	E_2	distance (da_2) (Å)
0	31	4.020 [1.095]	3.891 [1.078]	0.78	0.03	54.69	0.969	0.22	0.76	25.61
0.0156		4.034 [1.096]	3.862 [1.075]	0.82	0.04	52.07	1.007	0.18	0.75	25.80
0.0331		4.028 [1.050]	3.839 [0.987]	0.79	0.05	51.21	0.774	0.21	0.81	24.40
0.0569		4.018 [1.114]	3.855 [1.101]	0.81	0.04	52.52	0.836	0.19	0.79	24.81
0.0878		4.100 [1.082]	3.863 [1.101]	0.75	0.06	49.36	0.737	0.25	0.82	24.07
0.1353		4.017 [1.155]	3.846 [1.004]	0.76	0.04	52.08	1.418	0.24	0.65	28.02
0.1952		4.046 [1.051]	3.770 [1.078]	0.59	0.07	47.93	0.754	0.41	0.81	24.25
0.2913		4.077 [1.012]	0.633 [1.124]	0.52	0.84	23.38	3.619	0.48	0.11	43.75
0.433		4.083 [1.065]	0.638 [1.049]	0.61	0.84	23.40	3.356	0.33	0.18	40.00
0.7801		4.059 [1.121]	0.581 [1.107]	0.67	0.86	23.01	3.078	0.33	0.24	37.51
1.9138		4.053 [1.086]	0.600 [1.091]	0.69	0.85	23.16	3.112	0.31	0.23	37.84

[a - e] As previously described in Table 6.4.

Similar to the results observed for CaM alone, there are two lifetimes observed for dually-labeled CaM in the presence of eNOS peptide consisting of an extended species and a compact form. At lower Ca^{2+} concentrations the predominant species in the sample was in an extended conformation greater than 45 Å (~80%) and the compact secondary species of ~25 Å (~20%). As the free Ca^{2+} concentration increased to ~200 nM, a transition was observed with the compact CaM species becoming predominant with the secondary species representing a more extended CaM conformation. Above ~400 nM free Ca^{2+} concentration, measurements demonstrated no significant change in the lifetimes or amplitudes with the predominant species has a distance of ~23 Å (~65%) and the secondary species having a FRET distance of ~38 Å (~35%). These results demonstrate that the association of dually-labeled CaM to the eNOS peptide is Ca^{2+}-dependent and has a FRET distance of 23 Å representing a tightly wrapped conformation, similar to the previously shown in x-ray structure of CaM-bound to the eNOS peptide (Figure 6.1B &C) (Aoyagi *et al.*, 2003).

Similar to the FRET results observed for CaM associating with the eNOS peptide, dually-labeled CaM in the presence of nNOS peptide also showed a similar transition from the extended to wrapped conformation with increasing free Ca^{2+} concentrations. The predominant species had a FRET distance of ~23 Å (~62%) and a secondary species of ~38 Å (~38%), almost identical to the results with the eNOS peptide (Table 6.5). This agrees with the tightly wrapped conformation observed in the recently released CaM-nNOS peptide crystal structure (Figure 6.1D & E) (Ng *et al*. – unpublished, co-ordinates released 2007-12-25).

Table 6.6 – Determined FRET distances for Alexa 546/DAB-T34C-T110C CaM in the presence of nNOS peptide with increasing free Ca^{2+} concentrations.

$[Ca^{2+}]_{free}$ (μM)	R_O [a] (Å)	τ_D [b] (ns) [χ^2]	$\tau_{1(DA)}$ (ns) [χ^2]	A_1 [c]	E_1 [d]	distance (da_1) [e] (Å)	$\tau_{2(DA)}$ (ns)	A_2	E_2	distance (da_2) (Å)
0	31	4.027 [1.036]	3.891 [1.017]	0.87	0.03	54.21	1.160	0.13	0.71	26.66
0.0156		4.012 [1.130]	3.888 [1.013]	0.81	0.03	55.05	0.976	0.19	0.76	25.66
0.0331		4.033 [1.091]	3.902 [1.072]	0.80	0.03	54.58	1.006	0.20	0.75	25.80
0.0569		4.038 [1.120]	3.874 [1.099]	0.80	0.04	52.51	0.876	0.20	0.78	25.03
0.0878		4.044 [1.046]	3.822 [1.040]	0.75	0.05	49.81	0.812	0.25	0.80	24.62
0.1353		4.048 [1.101]	3.759 [1.059]	0.65	0.07	47.54	0.739	0.35	0.82	24.15
0.1952		4.047 [1.151]	3.628 [1.148]	0.52	0.10	44.42	0.685	0.48	0.83	23.78
0.2913		4.078 [1.155]	0.662 [1.076]	0.55	0.84	23.58	3.437	0.45	0.16	41.01
0.433		4.070 [1.064]	0.581 [1.069]	0.62	0.86	22.99	3.253	0.38	0.20	39.03
0.7801		4.074 [1.068]	0.592 [1.19]	0.65	0.85	23.07	3.130	0.35	0.23	37.86
1.9138		4.073 [1.063]	0.623 [1.103]	0.61	0.85	23.31	3.036	0.39	0.25	37.08

[a - e] As previously described in Table 6.4.

6.3.3.3.2 FRET distance determination: Dually-labeled CaM with iNOS peptide

Fluorescence decays and FRET distances determined with increasing free Ca^{2+} concentrations for CaM T34C/T110C Alexa/DABMI in the presence of iNOS CaM-binding domain peptide are summarized in Table 6.7.

Table 6.7 – Determined FRET distances for Alexa 546/DAB-T34C-T110C CaM in the presence of iNOS peptide with increasing free Ca^{2+} concentrations.

$[Ca^{2+}]_{free}$ (μM)	R_O [a] (Å)	τ_D [b] (ns) [χ^2]	$\tau_{1(DA)}$ (ns) [χ^2]	A_1 [c]	E_1 [d]	distance (da_1) [e] (Å)	$\tau_{2(DA)}$ (ns)	A_2	E_2	distance (da_2) (Å)
0	31	4.008 [1.057]	0.598 [1.052]	0.60	0.85	23.19	3.488	0.40	0.13	42.57
0.0156		4.072 [1.072]	0.635 [1.070]	0.57	0.84	23.40	3.310	0.43	0.19	39.60
0.0331		4.087 [1.050]	0.626 [1.118]	0.63	0.85	23.31	3.069	0.37	0.25	37.26
0.0569		4.019 [1.031]	0.646 [1.076]	0.63	0.84	23.54	2.949	0.37	0.27	36.71
0.0878		4.070 [1.069]	0.653 [1.001]	0.67	0.84	23.53	2.983	0.33	0.27	36.68
0.1353		4.045 [1.114]	0.696 [1.080]	0.62	0.83	23.86	2.855	0.38	0.29	35.87
0.1952		4.041 [1.085]	0.711 [1.014]	0.70	0.82	23.97	2.840	0.30	0.30	35.78
0.2913		4.088 [1.059]	0.706 [1.145]	0.67	0.83	23.88	2.839	0.33	0.31	35.55
0.433		4.124 [1.116]	0.729 [1.206]	0.65	0.82	23.99	2.830	0.35	0.31	35.32
0.7801		4.099 [1.082]	0.766 [1.108]	0.67	0.81	24.26	2.949	0.33	0.28	36.27
1.9138		4.140 [1.081]	0.755 [1.101]	0.64	0.82	24.14	2.769	0.36	0.33	34.85

[a - e] As previously described in Table 6.4.

In contrast to the results observed for the cNOS peptides, there was no transition from an extended to compact conformation as the free Ca^{2+} concentration increased. Instead, the predominant species in the sample had a FRET distance of ~24 Å in each measurement and an amplitude of ~65%, consistent with CaM associating to the iNOS peptide in a Ca^{2+}-independent manner. Since the observed FRET distance for CaM bound the iNOS peptide is very similar to that observed with the cNOS peptides at higher Ca^{2+} concentrations (23 Å), it appears to support our previous assumption that CaM binds to

iNOS in a tightly wrapped conformation (section 6.3.3.2). The secondary species in the sample demonstrated a slight decrease in FRET distance as the free Ca^{2+} concentration increased changing from ~40 to ~35 Å at a Ca^{2+} concentration of approximately 50 nM. This slight change in the FRET distance of the secondary species may be related to the Ca^{2+}-dependent conformational change in the C-terminal domain of CaM that we have previously observed using the Ca^{2+}-deficient CaM mutants (Chapter 4). Although the association of this domain is Ca^{2+}-independent (Chapter 4 and Chapter 5), we have also shown that the C-terminal domain appears to have a Ca^{2+}-dependent conformational change that refines the interactions between CaM and the iNOS peptide. Clearly, CaM associates to the iNOS peptide in a Ca^{2+}-independent manner and has a tightly wrapped conformation similar to the Ca^{2+}-dependent cNOS peptides.

6.3.3.3.3 FRET distance determination: Dually-labeled CaM with heme-free cNOS enzymes

Table 6.8 and Table 6.9 summarize the experimentally determined lifetimes and FRET distances for CaM T34C/T110C Alexa/DABMI in the presence of heme-free cNOS enzymes (nNOS C415A and eNOS C186A) with increasing free Ca^{2+} concentrations.

Table 6.8 – Determined FRET distances for Alexa 546/DAB-T34C-T110C CaM in the presence of eNOS C186A with increasing free Ca^{2+} concentrations.

$[Ca^{2+}]_{free}$ (μM)	R_O [a] (Å)	τ_D [b] (ns) [χ^2]	$\tau_{1(DA)}$ (ns) [χ^2]	A_1 [c]	E_1 [d]	distance (da_1) [e] (Å)	$\tau_{2(DA)}$ (ns)	A_2	E_2	distance (da_2) (Å)
0	31	3.952 [1.007]	3.696 [1.125]	0.60	0.06	48.37	0.803	0.40	0.80	24.69
0.0156		4.007 [1.193]	3.707 [1.045]	0.57	0.07	47.14	0.903	0.43	0.77	25.23
0.0331		3.970 [1.121]	3.721 [1.031]	0.55	0.06	48.65	0.988	0.45	0.75	25.79
0.0569		4.036 [1.123]	3.646 [1.106]	0.53	0.10	44.99	0.927	0.47	0.77	25.34
0.0878		3.987 [1.098]	3.633 [1.035]	0.52	0.09	45.70	0.931	0.48	0.77	25.43
0.1353		3.999 [1.039]	0.818 [1.047]	0.51	0.80	24.72	3.540	0.49	0.11	43.57
0.1952		3.957 [1.165]	0.899 [1.074]	0.53	0.77	25.28	3.597	0.47	0.09	45.50
0.2913		3.959 [1.130]	0.759 [1.060]	0.50	0.81	24.39	3.466	0.50	0.12	42.91
0.433		3.996 [1.011]	0.851 [1.061]	0.52	0.79	24.93	3.424	0.48	0.14	41.77
0.7801		3.969 [1.121]	0.781 [1.117]	0.55	0.80	24.52	3.306	0.45	0.17	40.52
1.9138		3.969 [1.159]	0.778 [1.128]	0.58	0.80	24.50	3.242	0.42	0.18	39.77

[a - e] As previously described in Table 6.4.

Table 6.9 – Determined FRET distances for Alexa 546/DAB-T34C-T110C CaM in the presence of nNOS C415A with increasing free Ca^{2+} concentrations.

$[Ca^{2+}]_{free}$ (μM)	R_O [a] (Å)	τ_D [b] (ns) [χ^2]	$\tau_{1(DA)}$ (ns) [χ^2]	A_1 [c]	E_1 [d]	distance (da_1) [e] (Å)	$\tau_{2(DA)}$ (ns)	A_2	E_2	distance (da_2) (Å)
0	31	3.998 [1.123]	3.813 [1.163]	0.63	0.05	50.91	0.995	0.37	0.75	25.79
0.0156	31	4.047 [1.036]	3.734 [1.114]	0.64	0.08	46.86	0.940	0.36	0.77	25.40
0.0331	31	4.019 [0.979]	3.744 [1.105]	0.61	0.07	47.90	0.960	0.39	0.76	25.56
0.0569	31	4.039 [1.084]	3.681 [1.101]	0.56	0.09	45.71	0.938	0.44	0.77	25.40
0.0878	31	4.012 [1.030]	0.933 [1.177]	0.53	0.77	25.41	3.543	0.47	0.12	43.42
0.1353	31	4.007 [1.127]	0.900 [1.100]	0.59	0.78	25.22	3.364	0.41	0.16	40.84
0.1952	31	3.914 [1.054]	0.795 [1.104]	0.60	0.80	24.68	3.117	0.40	0.20	38.91
0.2913	31	3.938 [1.067]	0.784 [1.120]	0.63	0.80	24.58	2.962	0.37	0.25	37.30
0.433	31	3.978 [1.068]	0.721 [1.149]	0.64	0.82	24.11	2.941	0.36	0.26	36.88
0.7801	31	3.914 [1.124]	0.679 [1.077]	0.61	0.83	23.90	2.717	0.39	0.31	35.54
1.9138	31	3.840 [1.085]	0.746 [1.186]	0.64	0.81	24.46	2.795	0.36	0.27	36.52

[a - e] As previously described in Table 6.4.

The FRET distances determined for dually-labeled CaM in the presence of the heme-free cNOS enzymes (~25 Å) are almost identical to the distances observed for CaM with the cNOS peptides (~23 Å) (Tables 6.4, 6.5, 6.8 and 6.9). However, the transition of CaM's conformation from the extended to wrapped conformation with increasing free Ca^{2+} concentrations occurred at a lower Ca^{2+} concentration when compared to the cNOS peptides. Instead, the transition/association of CaM to the eNOS C186A enzyme occurred at ~100 nM free Ca^{2+} concentration (Table 6.8), which is in good

agreement with previous Ca^{2+} titration activation profiles for CaM holo-eNOS (Nishida and Ortiz de Montellano, 1999). Likewise, the transition/association of CaM to nNOS C415A occurred at a lower Ca^{2+} concentration of ~100 nM (Table 6.9), which is lower than the previously reported Ca^{2+} activation concentration for holo-nNOS of 200 nM (Ruan *et al.*, 1996; Nishida and Ortiz de Montellano, 1999).

6.3.3.3.4 FRET distance determination: CaM T34C-Alexa and CaM T110C-Alexa with dabsyl-labeled iNOS peptide

In Chapter 5, we demonstrated that CaM binds to iNOS is in an antiparallel orientation (section 5.3.4.1), similar to that observed in the cNOS enzymes. To further study the subtle Ca^{2+}-dependent conformational change that we previously suggested to occur in the C-terminal domain of CaM when associated to iNOS, FRET measurements were taken using CaM-T34C-Alexa and CaM-T110C-Alexa with N-terminally dabsyl-labeled iNOS peptide (previously described in section 5.2.4) with increasing free Ca^{2+} concentrations.

Tables 6.10 and 6.11 summarize the experimentally determined lifetimes and FRET distances for CaM-T34C-Alexa and CaM-T110C-Alexa in the presence of dabsyl-labeled iNOS peptide with increasing free Ca^{2+} concentrations. The determined FRET distances of ~27 Å for CaM-T34C-Alexa and ~24 Å for CaM-T110C-Alexa showed no fluctuation over the Ca^{2+} titration range. These results show that the N-terminal domain of CaM is further away from the N-terminus of the iNOS peptide than the C-terminal domain of CaM, signifying that CaM does bind to the iNOS peptide in an antiparallel orientation, further supporting our previous finding in Chapter 5. Unfortunately, since the R_O distance is 29 Å, the sensitivity to any subtle conformational changes in the C-terminal domain CaM is limited. If the R_O distance were smaller (eg. ~20 Å), there would be much greater sensitivity since FRET distance determination is the most responsive around its R_O (as previously discussed in section 6.3.2.9).

Table 6.10 – Determined FRET distances for CaM-T34C-Alexa 546 in the presence of N-terminally labeled DAB-iNOS peptide with increasing free Ca^{2+} concentrations.

$[Ca^{2+}]_{free}$ (μM)	R_O [a] (Å)	τ_D [b] (ns) [χ^2]	$\tau_{1(DA)}$ (ns) [χ^2]	A_1 [c]	E_1 [d]	distance (da_1) [e] (Å)	$\tau_{2(DA)}$ (ns)	A_2	E_2	distance (da_2) (Å)
0	31	3.574 [1.192]	1.079 [1.087]	0.61	0.70	26.96	2.775	0.39	0.22	38.15
0.0156		3.346 [1.186]	1.006 [1.130]	0.59	0.70	26.93	2.579	0.41	0.23	37.94
0.0331		3.243 [1.194]	1.043 [1.084]	0.60	0.68	27.37	2.598	0.40	0.20	39.10
0.0569		3.269 [1.191]	0.968 [1.026]	0.61	0.70	26.83	2.601	0.39	0.20	38.88
0.0878		3.169 [1.175]	0.812 [1.111]	0.62	0.74	25.96	2.441	0.38	0.23	37.93
0.1353		3.274 [1.264]	0.892 [1.025]	0.66	0.73	26.32	2.665	0.34	0.19	39.65
0.1952		3.275 [1.283]	0.968 [1.218]	0.67	0.70	26.82	2.691	0.33	0.18	39.99
0.2913		3.099 [1.220]	0.892 [1.154]	0.66	0.71	26.66	2.616	0.34	0.16	41.08
0.433		3.189 [1.182]	0.925 [1.118]	0.65	0.71	26.70	2.654	0.35	0.17	40.48
0.7801		3.301 [1.139]	1.006 [1.103]	0.66	0.70	27.02	2.970	0.34	0.10	44.69
1.9138		3.519 [1.157]	1.017 [1.035]	0.57	0.71	26.68	3.274	0.43	0.07	47.75

[a - e] As previously described in Table 6.4.

Table 6.11 – Determined FRET distances for CaM-T110C-Alexa 546 in the presence of N-terminally labeled DAB-iNOS peptide with increasing free Ca^{2+} concentrations.

$[Ca^{2+}]_{free}$ (μM)	R_O [a] (Å)	τ_D [b] (ns) [χ^2]	$\tau_{1(DA)}$ (ns) [χ^2]	A_1 [c]	E_1 [d]	distance (da_1) [e] (Å)	$\tau_{2(DA)}$ (ns)	A_2	E_2	distance (da_2) (Å)
0	31	2.911 [1.230]	0.551 [1.124]	0.64	0.81	24.33	2.265	0.36	0.22	38.21
0.0156		3.124 [1.259]	0.527 [1.201]	0.67	0.83	23.76	2.237	0.33	0.28	36.17
0.0331		3.234 [1.212]	0.490 [1.170]	0.66	0.85	23.26	2.212	0.34	0.32	35.26
0.0569		3.079 [1.208]	0.571 [1.154]	0.66	0.81	24.22	2.288	0.34	0.26	37.00
0.0878		3.116 [1.231]	0.575 [1.161]	0.67	0.82	24.20	2.279	0.33	0.27	36.63
0.1353		3.005 [1.342]	0.526 [1.142]	0.67	0.82	23.94	2.144	0.33	0.29	36.09
0.1952		2.939 [1.280]	0.530 [1.082]	0.69	0.82	24.09	2.147	0.31	0.27	36.61
0.2913		3.015 [1.170]	0.548 [1.182]	0.70	0.82	24.12	2.187	0.30	0.27	36.45
0.433		2.993 [1.181]	0.501 [1.144]	0.70	0.83	23.73	2.127	0.30	0.29	36.01
0.7801		3.102 [1.237]	0.583 [1.195]	0.71	0.81	24.29	2.304	0.29	0.26	36.99
1.9138		3.130 [1.185]	0.650 [1.248]	0.71	0.79	24.80	2.603	0.29	0.17	40.46

[a - e] As previously described in Table 6.4.

6.3.3.3.5 FRET distance determination: CaM-T34C-Alexa and CaM-T110C-Alexa with iNOS coexpressed with nCaM

FRET measurements were performed to test our hypothesis that two nCaM molecules can bind to iNOS and that the second nCaM associated to the C-type site of iNOS CaM-binding domain can be displaced by another CaM molecule at lower Ca^{2+} concentrations (previously described in Chapter 3 and Chapter 5). This experiment involved the use of iNOS coexpressed with unlabeled nCaM followed by the addition of labeled CaM; the displacement of the second nCaM by the labeled CaM would result in greater fluorescence quenching and a shorter lifetime. Our previous study demonstrated that the heme is a potent quencher of Alexa Fluor 546 fluorescence (Chapter 5); therefore, the association of CaM-T34C-Alexa and CaM-T110C-Alexa to the iNOS enzyme could be monitored by the extent of fluorescence quenching. It is anticipated that as Ca^{2+} concentrations increase, the second nCaM on the C-type site will not be displaced by the Alexa-labeled CaM protein resulting in a slight increase in fluorescence lifetimes.

A summary of determined fluorescent lifetimes and FRET distances for CaM-T34C-Alexa and CaM-T110C-Alexa in the presence of iNOS coexpressed with nCaM and increasing free Ca^{2+} concentrations is shown in Tables 6.12 and 6.13.

Table 6.12 – Determined FRET distances for CaM-T34C-Alexa 546 in the presence of iNOS coexpressed with nCaM with increasing free Ca^{2+} concentrations.

$[Ca^{2+}]_{free}$ (μM)	R_O [a] (Å)	τ_D [b] (ns) [χ^2]	$\tau_{1(DA)}$ (ns) [χ^2]	A_1 [c]	E_1 [d]	distance (da_1) [e] (Å)	$\tau_{2(DA)}$ (ns)	A_2	E_2	distance (da_2) (Å)
0	31	3.856 [1.100]	0.835 [1.184]	0.67	0.78	25.02	3.255	0.33	0.16	41.08
0.0156		3.892 [1.131]	0.787 [1.187]	0.67	0.80	24.66	2.713	0.33	0.30	35.62
0.0331		3.842 [1.085]	0.763 [1.149]	0.66	0.80	24.57	2.629	0.34	0.32	35.27
0.0569		3.783 [1.130]	0.698 [1.165]	0.64	0.82	24.20	2.531	0.36	0.33	34.86
0.0878		3.842 [1.120]	0.779 [1.165]	0.66	0.80	24.68	2.701	0.34	0.30	35.79
0.1353		3.792 [1.087]	0.756 [1.092]	0.66	0.80	24.59	2.664	0.34	0.30	35.77
0.1952		3.826 [1.180]	0.751 [1.142]	0.66	0.80	24.51	2.811	0.34	0.27	36.74
0.2913		3.806 [1.180]	0.765 [1.200]	0.64	0.80	24.63	3.096	0.36	0.19	39.62
0.433		3.796 [1.114]	0.810 [1.157]	0.60	0.79	24.94	3.619	0.40	0.05	51.26
0.7801		3.802 [1.075]	0.799 [1.158]	0.55	0.79	24.86	3.630	0.45	0.05	51.53
1.9138		3.781 [1.123]	0.829 [1.106]	0.61	0.78	25.09	3.594	0.39	0.05	50.74

[a - e] As previously described in Table 6.4.

Table 6.13 – Determined FRET distances for CaM-T110C-Alexa 546 in the presence of iNOS coexpressed with nCaM with increasing free Ca^{2+} concentrations.

$[Ca^{2+}]_{free}$ (μM)	R_O[a] (Å)	τ_D[b] (ns) [χ^2]	$\tau_{1(DA)}$ (ns) [χ^2]	A_1[c]	E_1[d]	distance (da_1)[e] (Å)	$\tau_{2(DA)}$ (ns)	A_2	E_2	distance (da_2) (Å)
0	31	3.775 [1.121]	0.776 [1.139]	0.69	0.79	24.75	3.131	0.31	0.17	40.35
0.0156		3.721 [1.114]	0.724 [1.087]	0.69	0.81	24.46	2.926	0.31	0.21	38.52
0.0331		3.727 [1.111]	0.737 [1.110]	0.69	0.80	24.55	2.713	0.31	0.27	36.53
0.0569		3.717 [1.100]	0.682 [1.087]	0.67	0.82	24.17	2.610	0.33	0.30	35.76
0.0878		3.753 [0.962]	0.677 [1.204]	0.68	0.82	24.09	2.668	0.32	0.29	36.02
0.1353		3.744 [1.113]	0.758 [1.112]	0.70	0.80	24.67	2.766	0.30	0.26	36.86
0.1952		3.759 [1.162]	0.705 [1.083]	0.68	0.81	24.28	2.731	0.32	0.27	36.48
0.2913		3.688 [1.076]	0.738 [1.116]	0.70	0.80	24.61	2.810	0.30	0.24	37.63
0.433		3.686 [1.096]	0.752 [1.190]	0.66	0.80	24.71	3.101	0.34	0.16	40.93
0.7801		3.586 [1.158]	0.788 [1.177]	0.58	0.78	25.10	3.474	0.42	0.03	54.95
1.9138		3.570 [1.038]	0.814 [1.057]	0.63	0.77	25.30	3.471	0.37	0.03	56.08

[a - e] As previously described in Table 6.4.

For both CaM-T34C-Alexa and CaM-T110C-Alexa, the fluorescence of Alexa Fluor 546 was markedly quenched in the presence of iNOS coexpressed with nCaM at all free Ca^{2+} concentrations. The calculated FRET distance was ~24 Å for each, and as previously described in section 6.3.3.3.4, this appears to be at the limit of sensitivity for these FRET dyes. Interestingly, the lifetime of the secondary species for each CaM protein demonstrated a marked increase in amplitude and FRET

distance at free Ca^{2+} concentrations above 400 nM (Figure 6.18). The amplitude increased from ~30 to ~40% for both CaM-T34C-Alexa and CaM-T110C-Alexa representing that this secondary species becomes more pronounced as the free Ca^{2+} concentration increased. Likewise, the FRET distances for CaM-T34C-Alexa and CaM-T110C-Alexa demonstrated a decrease in quenching, indicative of Alexa-labeled CaM not binding to the iNOS enzyme (Tables 6.13 and 6.14). This is significant because it suggests that at a certain Ca^{2+} concentration threshold, the Alexa Fluor dye is no longer quenched as strongly as it was at lower Ca^{2+} levels. Although speculative, this large increase in FRET distance represents a marked change in the distance between the heme and Alexa Fluor 546 dye in the sample which may be the result of the Alexa-labeled CaMs being blocked by the second nCaM at the C-type site of the iNOS CaM-binding domain.

As a control experiment, the heme-free iNOS (iNOS C200A) coexpressed with nCaM was examined to prove that the observed quenching of Alexa Fluor 546 with holo-iNOS coexpressed with nCaM was related solely to the heme (Table 6.14). These results demonstrate that there is no quenching of Alexa Fluor 546 by the heme-free iNOS enzyme coexpressed with nCaM.

Table 6.14 – Control time-resolved fluorescence measurements of Alexa 546 labeled CaM proteins with iNOS C200A coexpressed with nCaM.

Alexa-CaM	$[Ca^{2+}]_{free}$ (μM)	R_O[a] (Å)	τ_D[b] (ns) [χ^2]	$\tau_{1(DA)}$ (ns) [χ^2]	A_1[c]	E_1[d]	distance (da_1)[e] (Å)	$\tau_{2(DA)}$ (ns)	A_2	E_2	distance (da_2) (Å)
T34C	0	31	3.969 [1.136]	3.982 [1.091]	0.68	0.00	CND[f]	0.705	0.32	0.82	24.01
	10		3.991 [1.060]	4.013 [1.055]	0.66	0.00	CND	0.850	0.34	0.79	24.93
T110C	0	31	3.919 [1.079]	3.894 [1.123]	0.67	0.01	71.91	0.702	0.33	0.82	24.05
	10		3.768 [1.070]	3.845 [1.076]	0.67	0.00	CND	0.976	0.33	0.74	26.02

[a - e] As previously described in Table 6.4.
[f] CND – Could not be determined.

6.3.4 Discussion

Although crystal structures of CaM bound to cNOS-target peptides have been solved (Figure 6.1), there have been no reported structures for CaM in complex with an iNOS peptide or any regions outside of the CaM-binding domain for all three NOS enzymes. This has been attributed to a high amount of mobility in various regions of the protein, particularly in the reductase domain making it difficult to form crystals for its structural determination.

The conformational variability of CaM alone and in complex with the target peptides and proteins has been studied extensively by x-ray crystallography and NMR spectroscopy. For instance, the crystal structure of holo-CaM has shown an extended conformation with an intact central linker α-helix (Chattopadhyaya *et al.*, 1992); however, a more recent holo-CaM structure demonstrated a closed, compact conformation with the central linker bent bringing the N- and C-terminal domains into close proximity with each other (Fallon and Quiocho, 2003). The distance between the T34 and T110 hydroxyl groups is ~54 Å in the extended holo-CaM structure and ~17 Å in the compact holo-CaM structure. Such a large conformation change should be detectable by FRET measurements. As mentioned previously, CaM T34C/T110C has been used extensively to monitor conformational changes in CaM alone or in the presence of CaM target peptides and proteins (Drum *et al.*, 2000; Torok *et al.*, 2001; Slaughter *et al.*, 2005a; Slaughter *et al.*, 2005b; Xiong *et al.*, 2005; Maximciuc *et al.*, 2006).

After reviewing all of the released NMR and x-ray crystal structures of CaM alone and CaM-target peptide complexes, two common CaM conformations were found – a wrapped/compact conformation and an extended structure. This is evident from a summary of the distances between CaM residues 34 and 110 (Table 6.15). Most of the distances observed between T34 and T110 demonstrate that CaM is in a compact form, as previously demonstrated in Figure 1.5 and Figure 1.6,

but there are also some examples of extended conformations, as previously shown in Figure 1.3 and Figure 1.7.

In order to determine the conformation of CaM bound to the holo-NOS enzymes, we have used dually-labeled CaM T34C/T110C with the FRET donor-acceptor dyes Alexa Fluor 546 C_5-maleimide and DABMI to determine the conformation of CaM bound to the NOS peptides and holo-NOS enzymes.

Table 6.15 – Measured distances between T34 and T110 in the solved CaM NMR and x-ray crystal structures.

	PDB [a]	Compact Conformation	Distance (Å) [b]	PDB	Extended Conformation	Distance (Å)
CaM	1PRW	compact holo-CaM	17.0	1CFD	apo-CaM	40.3
				1CLL	holo-CaM	54.0
				1Y6W	trapped intermediate of holo-CaM	49.7
CaM-target complex	2O60	Neuronal NOS	15.5	1CFF	Ca^{2+}-pump	33.9
	1NIW	Endothelial NOS	15.3	1G4Y	SK K^+ channel	32.5
	2BBN	Myosin light chain kinase	17.8	1K93	Anthrax edema factor	43.4
	1CDM	CaM-dep protein kinase II	17.8	1NWD	Glutamate decarboxylase	37.6
	1CKK	CaM-dep kinase kinase (NMR)	16.3	2F2O	Calcineurin (fusion) [d]	51.9
	1IQ5	CaM-dep kinase kinase (X-ray)	17.4			52.8
	1IWQ	MARCKS	16.8			
	1L7Z	Myristolated CAP-NAP	15.1			
	1MXE	CaM-dep protein kinase I	14.6			
	1SY9	Olfactory CNG channel	16.1			
	1WRZ	Death associated protein kinase 2	15.7			
	1YR5	Death-associated protein kinase I	16.6			
	1ZUZ	DAPk-related protein kinase I	16.2			
	2BE6	CaV1.2 IQ domain	15.0			
	2FOT	Alpha-II spectrin	13.5			
	2HQW	Glutamate NMDA receptor	16.8			
	2BCX	Ryanodine receptor	24.1			
	2IX7	Apo-CaM with myosin V [c]	20.6			
			19.9			

[a] File downloaded from the Protein Data Bank (PDB).
[b] Measured distance between CaM T34 and T110 hydroxyl groups using ViewerLite 5.0 (Accelrys).
[c] The two values shown for the apo-CaM with myosin V complex represent the two CaM molecules found in the x-ray crystal structure (Houdusse *et al.*, 2006).
[d] The two values shown for the calcineurin structure represent the two CaM-CaN peptide fusion proteins found in the x-ray crystal structure (Ye *et al.*, 2006).

The dually-labeled CaM protein bound to the cNOS peptides and enzymes had almost identical FRET distances demonstrating that CaM assumes a tightly wrapped conformation (Tables 6.5, 6.6, 6.8 and 6.9). Although the FRET distances are not equivalent to the measured distance between T34 and T110 hydroxyl groups in the CaM-eNOS and -nNOS crystal structures, they are still similar.

To clarify the data shown in Tables 6.5, 6.6, 6.8 and 6.9, a summary figure was complied so that the Ca^{2+}-dependence for the association of CaM to the cNOS peptides and enzymes could be compared (Figure 6.17). There is a definite trend in the Ca^{2+}-dependent conformation change of CaM in the presence of the cNOS peptides as free Ca^{2+} concentrations increased (Figure 6.17A and B). This transition at 100-200 nM free Ca^{2+} concentration is in good agreement with the previous reports on the Ca^{2+}-dependent activation of holo-eNOS and holo-nNOS (Nishida and Ortiz de Montellano, 1999; Montgomery *et al.*, 2000).

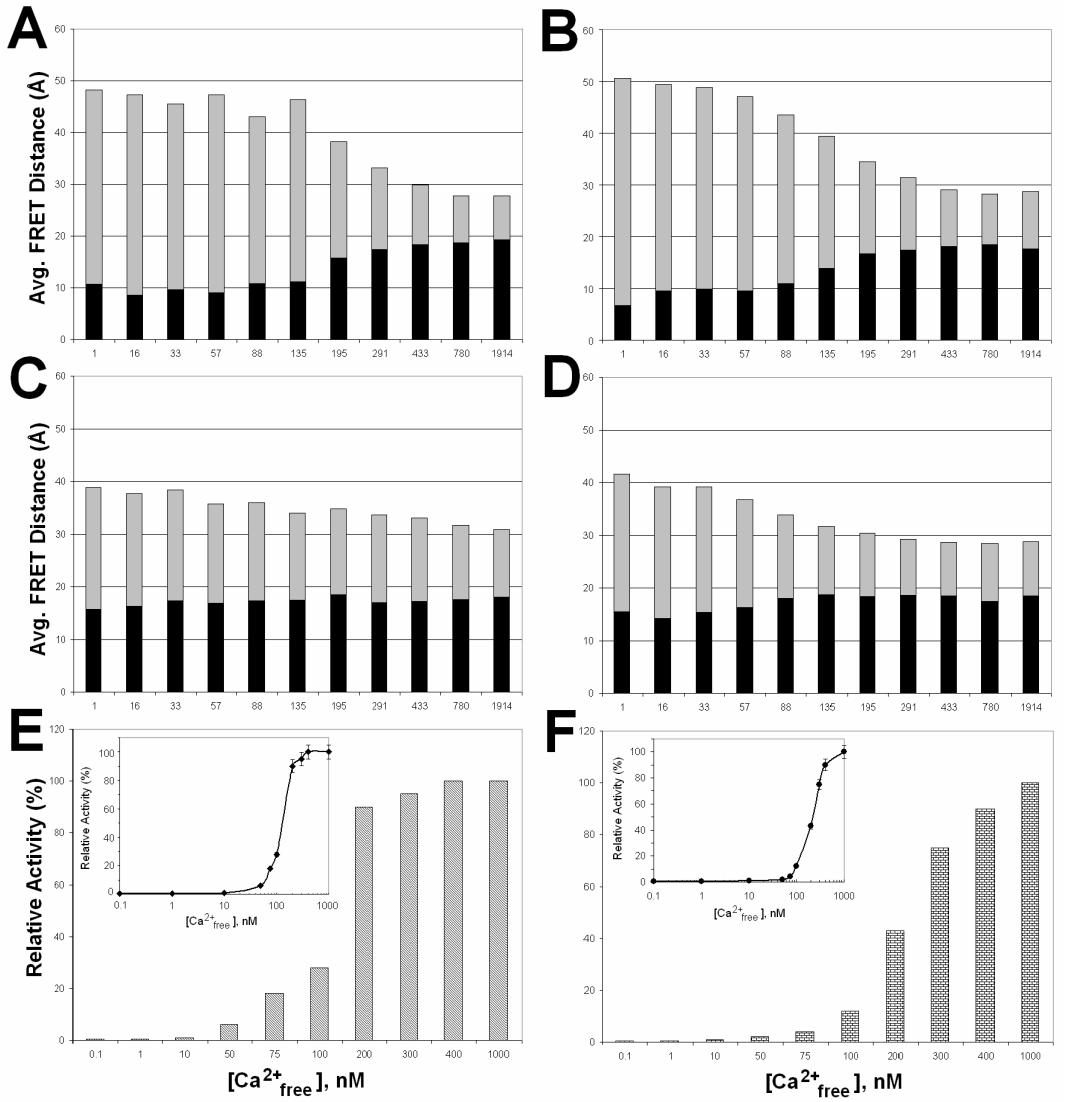

Figure 6.17 – Determined FRET distances for dually-labeled CaM to cNOS peptides and enzymes at varying free Ca^{2+} concentrations.

Averages FRET distances at each Ca^{2+} concentration were determined by using the following formula $(A_1*D_1)+(A_2*D_2)$. This value was then divided into two generalized FRET distance ranges – 20-35 Å (black) and 35 to 50 Å (grey). These average FRET distance values were multiplied by their fractional contribution to the fluorescence decay (A_1 or A_2) and ploted to observe any trends in the FRET distances determined. Data shown is derived from Tables 6.5, 6.6, 6.8 and 6.9. Average FRET distances for dually-labeled CaM with **(A)** eNOS peptide, **(B)** nNOS peptide, **(C)** eNOS C186A (heme-free eNOS), and **(D)** nNOS C415A (heme-free nNOS). The Ca^{2+}-dependent activation of holo-eNOS and holo-nNOS is shown to compare the binding events we observe with the dually-labeled CaM with the known free Ca^{2+} concentrations required for cNOS activation. Ca^{2+}-dependent activation of **(E)** holo-eNOS, and **(F)** holo-nNOS. Panels E and F are derived from a previously published study (Nishida and Ortiz de Montellano, 1999). Inset figures are of the identical cNOS Ca^{2+}-activation data ploted in panels E and F with the free Ca^{2+} concentration plotted on a logarithmic scale.

In contrast, the Ca^{2+}-dependent association of the CaM occurred at a lower free Ca^{2+} concentration for the cNOS enzymes than the cNOS peptides (Figure 6.17). The average FRET distance observed with dually-labeled CaM in the presence of the heme-free cNOS enzymes was ~10 Å shorter than the average FRET distance observed with the cNOS peptides. This may be related to the environment of the Alexa Fluor 546 dye which may be in close proximity to the flavins. This would increase the extent of quenching observed and give the appearance of a shorter FRET distance. The increase in CaM's affinity for the cNOS enzymes at lower Ca^{2+} concentrations may also be related to the various residues found outside of the CaM-binding domain such as the FMN domain itself and possibly the oxygenase domain that have previously been suggested to form contacts with CaM (Ghosh and Salerno, 2003; Newman *et al.*, 2004). Although CaM's conformation may be wrapped at a lower concentration of Ca^{2+} than previously reported (Ruan *et al.*, 1996; Nishida and Ortiz de Montellano, 1999; Montgomery *et al.*, 2000), it is also important to note that these previous studies were determining the Ca^{2+} concentration required for NOS activity. It is possible that CaM has a compact conformation when the Ca^{2+}-replete C-terminal domain of CaM initially binds to the cNOS enzymes; however, as the Ca^{2+} concentration increases, the N-terminal domain of CaM can become Ca^{2+}-replete and fully activate the enzyme. This is in good agreement with a previous model for the activation of the cNOS enzymes by the sequential binding of CaM's C- and N-terminal domains (Lane and Gross, 2000) (previously described in Figure 1.20). Furthermore, since these FRET distances for CaM bound to the cNOS peptides and enzymes are equal, it is fair to say that the solved crystal structures of CaM bound to cNOS CaM-binding domain peptides are a strong working model of CaM's true conformation when bound to the holo-cNOS enzymes. Future structural studies of CaM in complex with the CaM-binding domain and flanking regions in the reductase domain would clarify the true structure of CaM in complex with nNOS and eNOS (discussed further in section 8.2.2).

Interestingly, CaM's conformation when bound to the iNOS peptide appears to be very similar to the cNOS peptides, which is not surprising since the CaM-binding domains for the three mammalian NOS enzymes show a high degree of sequence similarity (Figure 6.14A). As previously mentioned in Chapter 5, the orientation of CaM when bound to the iNOS CaM-binding domain was suggested to be in a parallel fashion (Gribovskaja *et al.*, 2005). In order to test this theory, we used singly labeled N- and C-terminal domains of CaM with an N-terminal dabsyl-labeled iNOS peptide and measured the amount of quenching. Using this method, we were able to deduce that CaM binds to the iNOS CaM-binding domain in an antiparallel orientation similar to the cNOS enzymes (Spratt *et al.*, 2007b). In the same study, we have previously suggested that there is a subtle Ca^{2+}-dependent conformational change in the C-terminal domain of CaM when bound to iNOS while the N-terminal domain was Ca^{2+}-insensitive. In order to further test this slight Ca^{2+}-dependent conformational change in the C-terminal domain of CaM, the same FRET methodology using the N-terminally dabsyl-labeled iNOS peptide with CaM-T34C-Alexa and CaM-T110C-Alexa was used in the presence of increasing free Ca^{2+} concentrations. Unfortunately, we were unable to observe any Ca^{2+}-dependent changes in CaM and we attributed this to the R_O of the FRET donor-acceptor dyes (section 6.3.3.3.4). If another set of FRET donor-acceptor dyes with a shorter R_O were to be used (ie. ~20 Å instead of 31 Å), these FRET measurements would be more sensitive to monitor the subtle Ca^{2+}-dependent conformational changes occurring in the C-terminal domain of CaM when bound to the iNOS CaM-binding domain.

We also tested the displacement of a secondary nCaM from the C-type site of the iNOS CaM-binding domain with fluorescently labeled CaM proteins. Figure 6.18 is another summary figure created to clarify our observations for displacement of the secondary nCaM from iNOS at varying free Ca^{2+} concentrations (Tables 6.13 and 6.14).

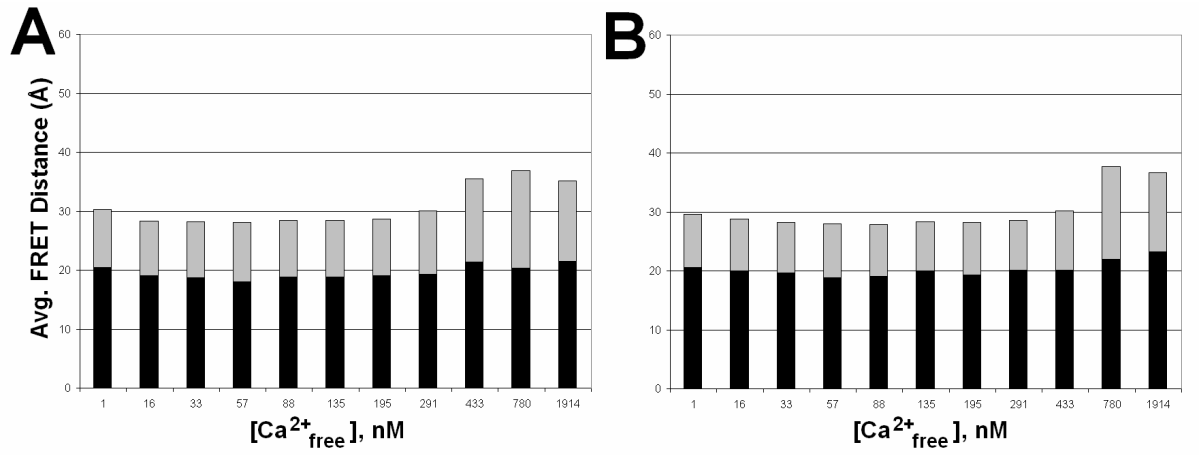

Figure 6.18 – Determined FRET distances for iNOS coexpressed with nCaM with (A) CaM-T34-Alexa CaM and (B) CaM-T110C-Alexa at varying free Ca^{2+} concentrations.
Averages FRET distances at each Ca^{2+} concentration were determined as described in Figure 6.17. Data shown is derived from Tables 6.12 and 6.13.

We found that at free Ca^{2+} concentrations lower than 400 nM, the secondary nCaM could be displaced by Alexa-labeled CaM proteins; however, above this free Ca^{2+} concentration threshold of 400 nM, the nCaM no longer appeared to be displaced.

6.3.5 Conclusions

We have observed the dynamic conformational changes of CaM alone in solution and in association with NOS peptides and enzymes by determining the change in FRET distances between CaM's N- and C-terminal lobes. CaM wraps around all three NOS CaM-binding domain peptides in a compact structure, in agreement with the x-ray structures of CaM-eNOS (Aoyagi *et al.*, 2003) and CaM-nNOS peptide (Ng *et al.* – unpublished). These results test previous models for CaM's association to the cNOS enzymes and clarify the conformation CaM when bound to the holo-enzymes. Past investigations have shown that regions flanking the NOS CaM-binding domain can interact with CaM, such as the autoinhibitory domain and FMN domain itself (Ruan *et al.*, 1996; Venema *et al.*, 1996; Newman *et al.*, 2004; Ishida and Vogel, 2006). For this reason, FRET

measurements were performed with peptides and holo-NOS enzymes to determine if there were any significant differences in CaM's conformation due to these regions outside of the CaM-binding domain. There appears to be no significant difference in the conformation of CaM when bound to the cNOS peptides and holo-cNOS enzymes; however, there does appear to be a variance in the free Ca^{2+} concentration required for CaM to bind to the cNOS enzymes. By determining the conformation and the effect of free Ca^{2+} concentrations on the association of CaM to the three NOS enzymes, we have expanded upon the present understanding of the mechanism CaM uses to bind, and subsequently activate, the NOS enzymes. Future structural studies suggested in Chapter 8 will hopefully expand upon the findings in this investigation.

NOTE: Please see Appendix B for an updated and simplified FRET analysis of Alexa 546/DAB-T34C-T110C CaM in the presence of NOS peptides and enzymes.

Chapter 7
Preliminary NMR Structural Analysis of Calmodulin Bound to the CaM-binding Domain of Inducible Nitric Oxide Synthase

7.1 Introduction

Protein-protein interactions and the dynamic conformational changes that result from the association of two or more proteins play an important role in enzyme catalysis and protein function. In order to gain a better understanding of how proteins change their conformation due to interactions with other proteins, many of the methods previously described, such as circular dichroism (Chapter 4 and 6), fluorescence (Chapter 5) and FRET (Chapter 6), can be used. However, these methods typically give lower structural resolution than the information that can be obtained from nuclear magnetic resonance (NMR) spectroscopy.

NMR spectroscopy is a powerful biophysical technique that can be used to determine the solution three-dimensional structure of proteins in solution at high resolution and to monitor protein-ligand interactions (which include protein-protein, protein-DNA, protein-small molecule complexes) and protein dynamics at the atomic level (Wüthrich, 1986; Jahnke and Widmer, 2004; Carlomagno, 2005). Unlike x-ray crystallography which gives a static representation of a protein structure, NMR spectroscopy is able to monitor the inherent dynamic flexibility in some proteins that would not be amenable to x-ray crystallography (Brunger, 1997; Van Holde *et al.*, 1998). In order to determine the 3D NMR structure of a protein, the sequence specific resonance assignments must first be determined. These are determined using through-bond spin-spin triple resonance heteronuclear NMR experiments (Bax *et al.*, 1994; Kay, 1997) (Figure 7.1).

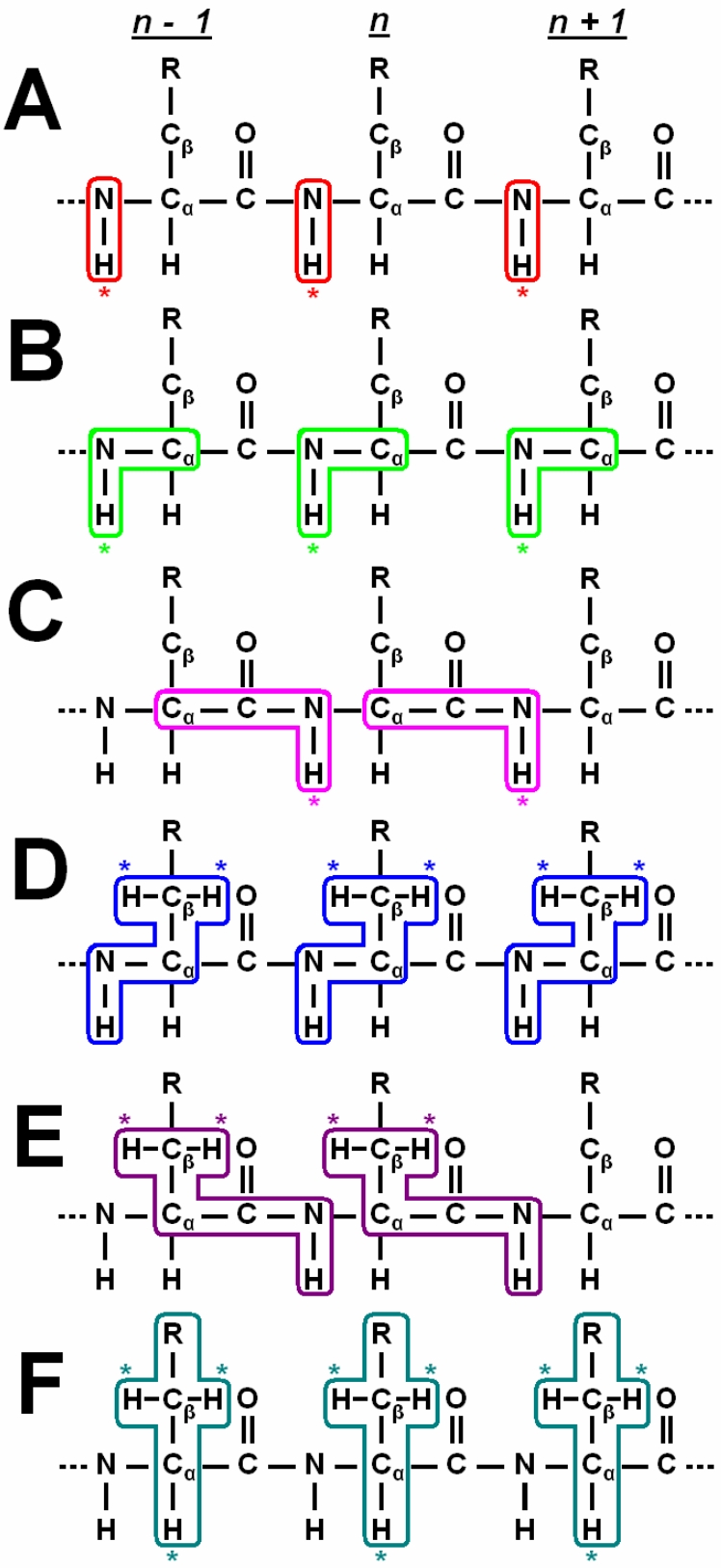
n - 1
n
n + 1
A
B
C
D
E
F

Figure 7.1 – Heteronuclear multidimensional NMR experiments typically used for the resonance assignment of proteins.

These NMR experiments, which send magnetization through bonds in a protein, are used to determine the resonance assignments for each ^{1}H, ^{13}C, and ^{15}N in a protein. Asterisks represent the initial atom that is magnetized for each experiment. **(A)** ^{15}N-heteronuclear single quantum correlation (^{15}N-HSQC – shown in red) – 2D experiment which shows a single cross-peak for amide groups (^{15}N—^{1}H) in a protein. **(B)** HNCA (shown in green) – 3D experiment with magnetization starting at an amide proton (^{15}N—^{1}H), which is then transferred through the ^{15}N to the $^{13}C_{\alpha}$, and finally transferred back to the originating ^{15}N—^{1}H. **(C)** HN(CO)CA (shown in pink) - 3D experiment with magnetization starting at an amide proton, which is then transferred through the ^{15}N and ^{13}C=O to the $^{13}C_{\alpha}$, and finally transferred back to the originating amide proton. **(D)** CBCANH (shown in blue) - 3D experiment with magnetization starting at protons attached to a $^{13}C_{\beta}$, which is then transferred through the $^{13}C_{\alpha}$ to the ^{15}N—^{1}H. **(E)** CBCA(CO)NH (shown in purple) - 3D experiment with magnetization starting at protons attached to a $^{13}C_{\beta}$, which is then transferred through $^{13}C_{\alpha}$ and ^{13}C=O to the ^{15}N—^{1}H. **(F)** 3D-TOtal Correlation SpectroscopY (TOCSY – shown in cyan) – 3D experiment with magnetization starting at protons attached to ^{13}C found in the sidechains of the protein. HNCA, HN(CO)CA, CBCANH and CBCA(CO)NH are useful NMR experiments to assign the resonance peaks for nuclei in the peptide backbone, while TOCSY is used to assign sidechain resonance peaks for each residue in the protein (Van Holde *et al.*, 1998; Cavanagh *et al.*, 2007).

Following the determination of the resonance assignments of all the ^{1}H, ^{13}C, and ^{15}N atoms in the protein, distance constraints can then be determined using through-space nuclear Overhauser effect spectroscopy (NOESY) (Cavanagh *et al.*, 2007). NOSEY experiments give NOE cross-peaks that arise from dipole-dipole spin interactions of nuclei that are distant in a protein's primary sequence but are in close proximity (~5 Å) in the protein's folded structure (Van Holde *et al.*, 1998). NOE experiments also give information on the local secondary structure in a protein – for instance, an α-helix has strong sequential $C_{\alpha}H$/NH cross-peaks between residues *i* and *i* + 3, whereas β-sheets have strong $C_{\alpha}H$/NH cross-peaks between residues *i* and *i* + 1 (Van Holde *et al.*, 1998). These local secondary structures and NOE distances determined from the NOESY experiments are then used as conformational constraints when solving the 3D structure of a protein using computational molecular dynamics (Cavanagh *et al.*, 2007).

Most of the published structures of CaM alone and bound to target peptides have been determined using x-ray crystallography. However, there are also numerous NMR structural studies on holo-CaM (Ikura *et al.*, 1990), apo-CaM (Kuboniwa *et al.*, 1995), and truncated CaM mutants, such as Ca^{2+}-replete and -deplete nCaM and cCaM (Finn *et al.*, 1995; Ishida *et al.*, 2000; Chou *et al.*, 2001) and the recently published structure of a CaM mutant consisting of only EF hands II and III (Lakowski *et al.*, 2007). There is also precedent for using NMR to study CaM's 3D structure when associated to CaM-target peptides. These structures include holo-CaM bound to CaM-binding domain peptides derived from CaM-dependent kinase kinase (Osawa *et al.*, 1999), olfactory CNG channel (Contessa *et al.*, 2005), glutamate decarboylase (Yap *et al.*, 2003), plasma membrane Ca^{2+} pump (Elshorst *et al.*, 1999), and myosin light chain kinase (Ikura *et al.*, 1992). To date, there is no reported NMR structure of CaM when bound to any of the NOS CaM-binding domains. The conformational dynamics of CaM alone and in complex with target peptides have also been studied

by NMR (Barbato *et al.*, 1992; Torok *et al.*, 1992; Tjandra *et al.*, 1995; Lee *et al.*, 2002; Chang *et al.*, 2003; Prabhu *et al.*, 2003).

Although numerous x-ray structures of the oxygenase and reductase domains of the NOS enzymes have been solved (Figure 6.2), the structure of the holo-NOS enzymes in complex with CaM has not been determined. This is due in large part to the inherent flexibility and dynamic nature of the NOS CaM-binding domains. The x-ray structures of holo-CaM bound to peptides corresponding to the CaM-binding domains of eNOS (Aoyagi *et al.*, 2003) and nNOS (Ng *et al.* – co-ordinates released 12-25-2007) have also been determined (Figure 1.5 C & D), however, the high resolution 3D structure of CaM bound to the CaM-binding domain of iNOS has not yet been determined. The solved structure of a CaM-iNOS peptide complex would be of great interest due to the important role iNOS-derived •NO has in various physiological processes within the cell.

This chapter describes the development of expression systems for ^{15}N and ^{13}C isotopic labeling of CaM and an iNOS peptide for the resonance assignments and NOESY experiments which will be used to solve the 3D structure a CaM-iNOS peptide complex. The NMR analysis of holo-CaM bound to an iNOS CaM-binding domain peptide is well underway in collaboration with Dr. Thorsten Dieckmann (Associate Professor, U of Waterloo) and Dr. Dara Gilbert (U of Waterloo). Conventional through-bond spin-spin and through-space NOESY triple resonance NMR experiments (Figure 7.1) are presently being used to make resonance assignments (Sattler *et al.*, 1999) and to assign NOE interactions in the CaM-iNOS peptide complex. It is important to note that the solved CaM-iNOS peptide structure will only be a working model for CaM binding to iNOS, since regions flanking the CaM-binding domain have been implicated in the Ca^{2+}-independent association of CaM to iNOS (Ruan *et al.*, 1996). These studies will determine and clarify the underlying structural differences in the binding, and ultimately the activation, of the Ca^{2+}-dependent cNOS and the Ca^{2+}-independent iNOS enzymes by CaM.

7.2 Experimental Procedures

7.2.1 ^{13}C and ^{15}N Isotope Incorporation into Wild-type CaM and CaM_{1234}

E. coli BL21 (DE3) were transfected with pET9dCaM (section 2.2.2) or $pCaM_{1234}Kan$ (section 4.2.1) and grown in 50 mL LB medium with 30 mg/mL of kanamycin at 225 rpm, 37°C to an OD_{600} of 0.8-1.0. Once the cells reached the optimal density, 4 mL of the starter culture was harvested by centrifugation at 6000 x g for 7 minutes in a sterile 50 mL Oakridge tube. The cells were then resuspended in 5 mL of sterile complete NMR minimal medium. Complete NMR minimal medium was prepared as previously described (Markley and Kainosho, 1993) by autoclaving 1 L of $Na_2HPO_4•7H_2O$ (12.8 g/L), KH_2PO_4 (3.0 g/L), and NaCl (0.5 g/L) and allowing it to cool to room temperature, followed by the addition of media additives, which included: NH_4Cl or $^{15}NH_4Cl$ (1.0 g/L), glucose or U-$^{13}C_6$-glucose (2.0 g/L), $MgSO_4$ (2 mM), $CaCl_2$ (100 μM), thiamine (0.05 mg/L) and kanamycin (30 mg/L). Depending upon which isotope was to be incorporated, glucose and/or NH_4Cl was substituted with U-$^{13}C_6$-glucose or $^{15}NH_4Cl$. This liter of complete NMR minimal medium was then inoculated with the resuspended cells and the cells were grown to an OD_{600} of 0.8-1.0 at 200 rpm, 37°C (approximately 10-12 hours). Protein expression was then induced with the addition of IPTG (500 μM final concentration), and induction continued for 5 hours with shaking at 200 rpm, 37 °C. The cells were then harvested by centrifugation, flash frozen on dry ice, and stored at –80°C.

7.2.2 Purification of ^{13}C and ^{15}N isotope labeled wild-type CaM and CaM_{1234}

^{13}C-^{15}N wild-type CaM and ^{15}N wild-type CaM were purified as previously described by hydrophobic interaction chromatography on phenyl–Sepharose CL-4B (section 2.2.3). ^{15}N CaM_{1234} was purified as previous described (section 4.2.2). The sample was subsequently concentrated to ~ 2 mL using a Vivaspin 15 ultrafiltration spin column (Sartorius AG Biotechnology, Goettingen, Germany) and

filtered through a 0.45 μm filter to remove any particulate material. The sample was then subjected to gel filtration using a HiLoad 16/60 Superdex 75 prep grade column (GE Healthcare Bio-Sciences, Baie d'Urfe, PQ) equilibrated with 50 mM Tris-HCl, pH 7.5, and 150 mM NaCl, and 1 mM DTT. The flow rate was maintained at 1.0 mL/min using an AKTApurifier System for Chromatography (GE Healthcare Bio-Sciences) and eluted protein was monitored at 278 and 254 nm. A gel filtration standard kit (Sigma, Oakville, ON) containing multiple molecular mass markers was used to calibrate the column. The purified ^{13}C-^{15}N wild-type CaM, ^{15}N wild-type CaM and ^{15}N CaM_{1234} were finally dialyzed overnight into 50 mM Tris-HCl, 1 mM $CaCl_2$, pH 7.5 with 0.5 mM DTT (to prevent any unwanted oxidation of methionine residues found in CaM). The proteins were then aliquoted, flash frozen on dry ice, and stored at –80^{o}C. The purified CaM proteins were analyzed by ESI-MS using a Micromass Q-Tof Ultima GLOBAL mass spectrometer (Manchester, U.K.) with an internal standard as previously described in section 2.2.5.

7.2.3 Molecular Cloning of NOS CaM-binding domain peptides

7.2.3.1 piNOSpep

The cloning of the CaM-binding domain of human iNOS (residues 507-531; RPKRR EIPLK VLVKA VLFAC MLMRK) involved the use of three pairs of single-stranded complementary oligonucleotides using a similar methodology to a previously published study (Bisaglia *et al.*, 2005). These primers were designed to have complementary sticky ends for the facile ligation of the 5' and 3' ends of the open-reading frame (eg. for *Nco*I which recognizes and cuts C/CATGG, the 5' end of the first primer was 5' CATGG). The primers used to construct the CaM-binding domain of iNOS are summarized in Table 7.1 and a schematic depiction of this cloning methodology is shown in Figure 7.2. This construction also involved the incorporation of a 10-histidine tag followed by a thrombin cleavage site (LVPR/GS) upstream from the open-reading frame for the future cleavage and

removal of the poly-histidine-tag. The primers were synthesized by Sigma-Genosys (Mississauga, ON) and were 5' phosphorylated to aid in the efficiency of the ligation reaction.

Table 7.1 – Primers used to construct phiNOSCBDKan, prnNOSCBDKan, and peNOSCBDKan

Primer	Sequences
iCBDp1fr	5' CATGGGCAGCAGCCATCATCATCATCACCATCATCATCATCACAGCAGCGGCCTGGTACCGCGGGGCAGCCA 3'
iCBDp2fr	5' TATGCGCCCCAAGCGCCGCGAGATCCCCCTTAAGGTTCTTGTTAAGGCC 3'
iCBDp3fr	5' GTTCTTTTCGCCTGCATGCTTATGCGCAAGTAATAGGGATCCGAATTCA 3'
iCBDp1rv	5' CCGCGGTACCAGGCCGCTGCTGTGATGATGATGATGGTGATGATGATGATGGCTGCTGCC 3'
iCBDp2rv	5' CAAGAACCTTAAGGGGGATCTCGCGGCGCTTGGGGCGCATATGGCTGCC 3'
iCBDp3rv	5' AGCTTGAATTCGGATCCCTATTACTTGCGCATAAGCATGCAGGCGAAAAGAACGGCCTTAA 3'
nCBDfr	5' TATGAAACGGCGCGCCATTGGGTTTAAAAAGCTAGCCGAGGCCGTTAAATTTTCCGCCAAGTTGATGGGGCA GTAATAGGGATCCGAATTCA 3'
nCBDrv	5' AGCTTGAATTCGGATCCCTATTACTGCCCCATCAACTTGGCGGAAAATTTAACGGCCTCGGCTAGCTTTTTAAA CCCAATGGCGCGCCGTTTCA 3'
eCBDfr	5' TATGACGCGTAAGAAAACTTTTAAAGAGGTGGCCAACGCCGTGAAGATATCGGCTAGCCTTATGTAATAGGGA TCCGAATTCA 3'
eCBDrv	5' AGCTTGAATTCGGATCCCTATTACATAAGGCTAGCCGATATCTTCACGGCGTTGGCCACCTCTTTAAAAG TTTTCTTACGCGTCA 3'

In preparation for the ligation of these primers, the six primers (iCBDp1fr, iCBDp2fr, iCBDp3fr, iCBDp1rv, iCBDp2rv, and iCBDp3rv) were mixed in equal portions, heated to 95^{o}C for 10 minutes and allowed to cool slowly to room temperature to facilitate annealing of the overlapping sequences. The annealed DNA was then cloned into the kanamycin resistant pET28a (Novagen) plasmid using the unique flanking *Nco*I and *Hind*III restriction sites. The resulting vector, piNOSpep, was verified by DNA sequencing (UW Molecular Biology Core Facility).

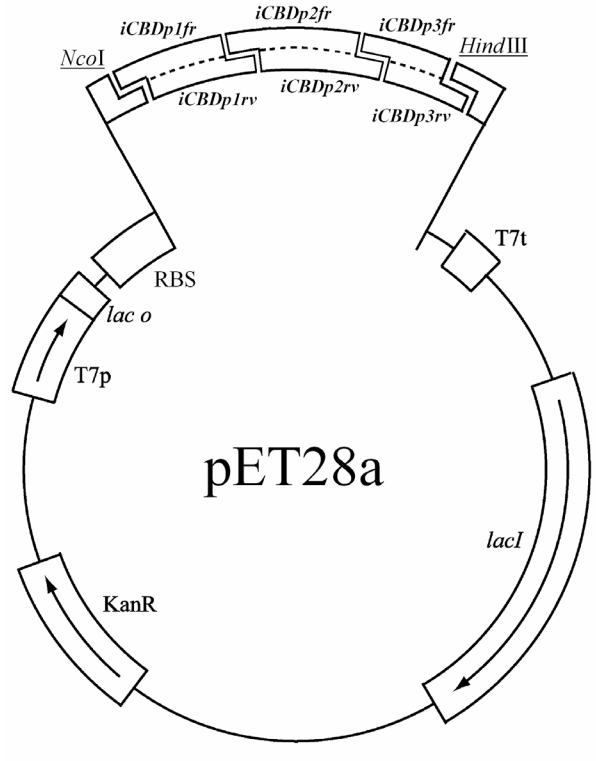

Figure 7.2 – Characteristics of the human iNOS CaM-binding domain expression vector phiNOSCBDKan
Arrows indicate the transcriptional orientation of the corresponding genes and promoters. The human iNOS CaM-binding domain sequence was cloned between the unique *Nco*I and *Hind*III sites found in the multiple cloning site of pET28a (Novagen). Abreviations used are: KanR, kanamycin-resistance determinant; *lac o*, lac operator sequence; *lacI*, gene coding for the lac repressor; T7p, T7 promoter; T7t, T7 terminator; RBS, ribosomal binding site.

7.2.3.2 peNOSpep and pnNOSpep

Using piNOSpep as the parent vector, the CaM-binding domains of bovine eNOS (residues 493-512; TRKKT FKEVA NAVKI SASLM) and rat nNOS (residues 725-747; KRRAI GFKKL AEAVK FSAKL MGQ) were cloned using a similar methodology as described above (section 7.2.3.1) but using a single pair of primers corresponding to the eNOS and nNOS CaM-binding domains, were used with complementary sticky ends for the 5' *Nde*I and 3' *Hind*III restriction sites (eg. for *Nde*I CA/TATG, 5' end of the primer was 5' TATG). The primers used to construct the eNOS and nNOS

CaM-binding domain expression vectors are shown in Table 7.1. The resulting vectors, peNOSpep and pnNOSpep, were verified by DNA sequencing.

7.2.3.3 piNOSCBD-intein, peNOSCBD-intein, and pnNOSCBD-intein

Difficulties were experienced when expressing the iNOS CaM-binding domain peptide using the expression vector piNOSpep in *E. coli* BL21 (DE3). These difficulties included dramatic cell density decreases upon induction and the grey to black cell dicolouration, most likely due to the aggregation of the over-expressed hydrophobic iNOS peptide (see section 3.4 for further discussion). Furthermore, since only one aromatic residue (Phe) is found in these peptides, it was difficult to monitor all three NOS peptides by absorbance during their purification. In order to circumvent these problems, the coding regions for iNOS, eNOS and nNOS CaM-binding domains were subcloned into pTYB12 (New England Biolabs, Markham, ON), an ampicillin resistant vector coding for a chitin-binding domain-intein fusion protein with a multiple cloning site downstream at its 3' end. The coding regions for the three NOS CaM-binding domains were amplified by PCR, introducing unique flanking *Nde*I and *Hind*III restriction sites for subcloning into pTYB12. The primers used were iCBDp1fr (Table 7.1) and NOSCBDrv 5' ATAA*CTGCAG*CCCGGGAAAACAGCATTCCAGG 3'. The coding regions of each CaM protein were then subcloned into the pTYB12 vector using the unique *Nde*I and *Pst*I restriction sites. The resulting vectors, piNOSCBD-intein, peNOSCBD-intein, and pnNOSCBD-intein, were verified by DNA sequencing to ensure that no spontaneous mutations had occurred. Although the peNOSCBD-intein and pnNOSCBD-intein vectors will not be mentioned again in this chapter, they will be discussed in Chapter 8 where future experiments and conclusions are discussed.

7.2.4 Expression of intein-iNOS CaM-binding domain fusion protein

An overnight culture of *E. coli* ER2566 (DE3) transfected with piNOSCBD-intein (section 7.2.3.3) was used to inoculate 2 x 1 L of LB media in 4 L flasks supplemented with 100 µg/ml of ampicillin. These 1 L cultures were grown at 37ºC, 200 rpm to an $O.D_{600}$ of 0.6 – 0.8, induced with 500 µM IPTG and harvested after 6 hours of expression. Cells were harvested by centrifugation at 6000 x g at 4°C for 5 minutes, flash frozen on dry ice, and subsequently stored at –80ºC.

In preparation for future ^{15}N isotope incorporation, a minimal medium expression test of the intein-iNOS CaM-binding domain fusion protein was performed in complete NMR minimal medium as previously described for wild-type CaM and CaM_{1234} (section 7.2.1) with the following modifications: (1) Cells were grown in the presence of 100 mg/L of ampicillin, (2) the incubator temperature was lowered to 22°C immediately after induction with 500 µM IPTG which has previously been shown to be the optimal temperature for intein-fusion protein expression (New England Biolabs, Pickering, ON), and (3) the cells were harvested 6 hours after induction.

7.2.5 Purification of iNOS CaM-binding domain peptide from the intein fusion protein

The following purification was performed by the candidate with the assistance of Yay Duangkham (MSc. student, U of Waterloo). Cells were thawed on ice, resuspended in 4 volumes of Lysis Buffer (20 mM HEPES, 500 mM NaCl, 1 mM EDTA, 0.1% Tween 20, pH 7.0) and lysed by homogenization using an Avestin EmulsiFlex-C5 homogenizer (Ottawa, ON). The lysate was then clarified by centrifugation at 48,000 x g for 30 minutes at 4°C. All of the following steps were carried out at 4°C in a refrigerator or on ice. 10 mL of chitin beads (New England Biolabs) in a 1 cm x 30 cm Econo-column (Bio-Rad Laboratories, Mississauga, ON) was equilibrated with High Salt Wash Buffer (20 mM HEPES, 500 mM NaCl, 1 mM $CaCl_2$, pH 7.0) prior to loading the clarified supernatent. The clarified supernatant was then loaded onto the column at a flow rate of 0.5 mL/min

to allow for the chitin-binding domain of the fusion protein to associate to the resin. After the sample was loaded, the resin was washed with 80 mL of High Salt Wash Buffer (8 column volumes) at a rate of 2 mL/min. The resin was subsequently washed with 40 mL of Low Salt Wash Buffer (4 column volumes of 20 mM HEPES, 150 mM NaCl, 1 mM $CaCl_2$, pH 7.0), which removes any proteins that interact weakly with the resin. 15 mg of wild-type CaM in 5 mL (3 mg/mL) was then loaded onto the resin at 0.5 mL/min to bind and protect the iNOS CaM-binding domain from aggregation. The addition of wild-type CaM yields a stable complex with the iNOS CaM-binding domain and makes it easier to monitor the elution of this CaM-NOS peptide complex by absorbance later in the purification. Furthermore, this method allows for the addition of unlabeled wild-type CaM with ^{15}N-iNOS CaM-binding domain peptide for future NMR studies exclusively on the iNOS peptide. The resin was finally washed with 140 mL of Low Salt Wash Buffer (14 column volumes) at 2 mL/min to finish removing any non-specific interactions with the resin and excess CaM that did not associate to the intein-iNOS peptide fusion protein. Finally, the column was quickly flushed with 35 mL of Cleavage Buffer (3.5 column volumes of 20 mM HEPES, 500 mM NaCl, 1 mM $CaCl_2$, 50 mM DTT, pH 8.5) and incubated for 40 hours at room temperature to induce the intein thiol-dependent cleavage and release the CaM-iNOS peptide complex. DTT, the higher pH and temperature were used to increase the efficiency of intein cleavage to mimic the conditions routinely used by the manufacturer (New England Biolabs). After the 40 hour incubation, the CaM-iNOS peptide complex was then eluted from the column with cleavage buffer without DTT.

The sample was then concentrated to ~1 mL using a Vivaspin 15 ultrafiltration spin column and filtered through a 0.45 μm filter to remove any particulate material prior to loading the sample onto a HiLoad 16/60 Superdex 75 prep grade gel filtration column, as previously described for ^{15}N wild-type CaM (section 7.2.2). Fractions containing CaM-iNOS peptide were pooled, aliquoted, flash frozen on dry ice, and stored at –80°C. The CaM-iNOS peptide complex was then sent for ESI-MS

analysis as previously described (section 2.2.5) to confirm purification of wild-type CaM and the presence of the iNOS CaM-binding domain peptide. The purified CaM was also run on a gel shift mobility assay as previously described (section 3.2.8) to confirm that the CaM-iNOS peptide complex was formed.

7.2.6 Sample preparation for NMR experiments

^{15}N-^{13}C-labeled, ^{15}N-labeled and unlabeled wild-type CaM samples were prepared for NMR measurements by transferring the proteins into an NMR buffer consisting of 100 KCl, 10 mM $CaCl_2$, 0.2 mM NaN_3 and 91%/9% ^2H_2O at pH 6.0 using a Ym10 centrifugal filter device (Millipore, Billerica, MA, USA). This NMR buffer has previously used in another CaM-target peptide complex NMR study (Yap *et al.*, 2003). Two wild-type CaM-iNOS peptide samples with different combinations of isotope labeling were used during the NMR experiments. Sample A consisted of ^{15}N-labeled wild-type CaM in complex with unlabeled iNOS peptide, while Sample B consisted of ^{15}N-^{13}C-labeled wild-type CaM in complex with unlabeled iNOS peptide. All NMR samples contained at least 1.0 mM wild-type CaM and 1.2 mM human iNOS peptide (to ensure complex saturation) in a total volume of 500 µL. Lyophilized iNOS peptide (synthesized by Sigma-Genosys) was added to the CaM solution in small titrating increments until complex saturation was observed by complete peak changes observed in the ^{15}N-HSQC spectrum.

7.2.7 NMR spectroscopy and data analysis

All NMR data were acquired at 25^{o}C on Bruker 600 and 700 MHz spectrometers equipped with ^{1}H/^{13}C/^{15}N triple-resonance probes with XYZ-gradients (Bruker, Billerica, MA, USA). In order to determine resonance assignments for isotopically labeled wild-type CaM in complex with unlabeled iNOS peptide, the following set of experiments were conducted. The amide cross-peaks were obtained from an ^{15}N-HSQC experiment (Muhandiram and Kay, 1994). Using the previously

published resonance assignments of holo-CaM alone as a reference (accession code bmr547 in the Biological Magnetic Resonance Data Bank, Ikura *et al*., 1990), the initial assignment of the amide protons in the CaM-iNOS complex in the ^{15}N-HSQC spectrum was performed. To assign the amide protons that could not initially be resolved in the ^{15}N-HSQC spectum, the peptide backbone resonances were assigned using standard 3D NMR measurements, which included HNCA, HN(CO)CA, CBCANH, and CBCA(CO)NH experiments using sample B (Grzesiek and Bax, 1992; Muhandiram and Kay, 1994). Side-chain resonance assignments were obtained from a HCCH-TOCSY spectrum of sample B (Bax *et al.*, 1990). Data were analyzed using Computer Aided Resonance Assignment (CARA), a free downloadable program from www.nmr.ch (Keller, 2004).

7.3 Results

7.3.1 CaM Protein Expression and Purification

Each of the expressed and purified ^{15}N-labeled wild-type CaM, ^{15}N-^{13}C wild-type CaM, and ^{15}N CaM_{1234} proteins produced high yields of 40.1, 37.9, and 22.7 mg/L, respectively. These purified CaM proteins were judged to be over 95% homogeneous by SDS-PAGE (results not shown). Likewise, ESI-MS was used to further assess the homogeneity and proved that the expression and purification protocol used (sections 7.2.1 and 7.2.2) resulted in virtually complete isotope incorporation for ^{13}C-^{15}N wild-type CaM, ^{15}N wild-type CaM and ^{15}N CaM_{1234} (Table 7.2).

Table 7.2 – Masses of isotope-labeled wild-type CaM and CaM_{1234}

	Mass (Da) [a]	
CaM proteins	Observed	Theoretical [b]
Wild-type CaM [c]	16706.0	16706
^{15}N wild-type CaM [d]	16891.5	16894
^{15}N-^{13}C wild-type CaM [e]	17592.0	17608
CaM_{1234} [f]	16530.0	16530
^{15}N CaM_{1234} [g]	16713.5	16718

[a] Masses of deconvoluted ESI-MS spectra were determined with an accuracy of ± 5 Da.

[b] Calculated masses based upon amino acid sequence.

[c] Mass of wild-type CaM as previously determined in Table 2.1.

[d] Expected mass difference with ^{15}N isotope labeled wild-type CaM is 188 Da.

[e] Expected mass difference with ^{15}N-^{13}C isotope labeled CaM is 902 Da. The large discrepancy in the mass is due to the use of 99% $^{13}C_6$-glucose.

[f] Mass of CaM_{1234} as previously determined, see Table 4.1.

[g] Expected mass difference with ^{15}N isotope labeled CaM_{1234} is 188 Da.

7.3.2 CaM-iNOS CaM-binding domain peptide purification

The iNOS CaM-binding domain peptide alone was difficult to purify due to its propensity to aggregate. This aggregation was overcome by the binding of wild-type CaM to the intein-iNOS peptide fusion protein on the column. Since CaM is highly hydrophilic with a pI of ~4, it not only is able to protect the peptide from aggregation during purification, but it also ensured that the CaM-peptide complex will remain in solution throughout purification. Furthermore, this method allows for the copurification of the isotopically labeled iNOS peptide in complex with unlabeled wild-type CaM. This complex can then be used in future NMR experiments to determine the resonance assignments and NOE interactions of the iNOS peptide when bound to CaM.

The expressed and copurified CaM-iNOS peptide complex produced a yield of 0.5 mg/L. ESI-MS was used to assess the homogeneity and confirm that the copurification with wild-type CaM was successful (Table 7.3). Subsequent to the ESI-MS result, the copurified CaM-iNOS peptide complex was tested using a gel shift mobility assay (section 3.2.8) to ensure that the purified complex was pure, saturated and demonstrated the expected mobility shift when compared to wild-type CaM alone (Figure 7.3).

Table 7.3 – Masses of unlabeled iNOS peptide copurified with wild-type CaM.

Proteins/Peptides	Mass (Da) [a] Observed	Theoretical [b]
iNOS peptide (from intein-fusion protein) [c]	3391.9	3393
Wild-type CaM (copurified)	16704.5	16706
iNOS peptide (synthesized by Synpep) [d]	2995.5	2997
iNOS peptide (synthesized by Sigma Genosys) [e]	2995.5	2997

[a] Masses of deconvoluted ESI-MS spectra were determined with an accuracy of ± 4 Da.

[b] Calculated masses based upon amino acid sequence.

[c] Expected mass of intein-fusion protein derived iNOS peptide with addition N-terminal residues AGHM.

[d & e] Synthesized iNOS peptides used to saturate ^{15}N wild-type CaM and ^{15}N-^{13}C wild-type CaM for NMR experiments, respectively. These measurements were taken to ensure the identity of the peptides after a report that an investigation of Synpep for illegally falsifying their peptide analyses was published. The correct mass was observed signifying that the peptide synthesized by Synpep was correct.

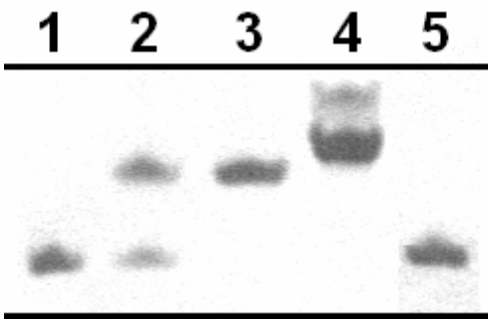

Figure 7.3 – Gel Mobility Shift Assay of wild-type CaM with synthetic and recombinantly expressed iNOS peptides.
Wild-type CaM (20 μM) was incubated with synthetic iNOS peptide in the presence 0.2 mM $CaCl_2$. CaM-iNOS peptide derived from intein-iNOS peptide fusion protein was loaded without any additional peptide added. The samples were then analyzed by PAGE (15% acrylamide) containing 0.375 M Tris, pH 8.8, 4 M urea, and 0.2 mM $CaCl_2$ and visualized with Coomassie Blue R-250. *Lanes 1* & *5* – wild-type CaM alone; *Lane 2* – wild-type CaM with 0.5 molar equivalents of synthetic iNOS peptide; *Lane 3* – wild-type CaM with 2 molar equivalents of synthetic iNOS peptide; *Lane 4* – wild-CaM copurified with iNOS peptide derived from intein-iNOS peptide fusion protein.

The iNOS-peptide from the intein-fusion protein demonstrates a greater mobility shift which can be attributed to the extra histidine residue derived from the cleaved intein fusion protein at the N-terminus of the peptide (additional N-terminal of AG*H*M; Figure 7.3). Clearly, a pure, saturated CaM-iNOS peptide complex is purified using the purification methodology described in section 7.2.5.

Furthermore, expression tests using the intein-iNOS peptide in NMR minimal medium demonstrate that the fusion protein expresses well after 6 hours of induction (Figure 7.4).

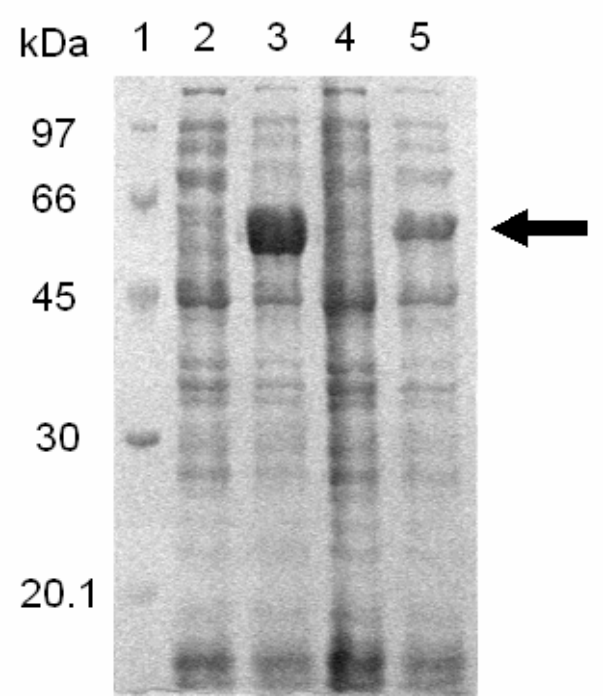

Figure 7.4 – 12% SDS-PAGE of intein alone and intein-iNOS peptide time-course expression test in minimal medium.
Protein was loaded in a standard SDS-loading buffer. Samples consisted of ER 2566 (DE3) *E. coli* transformed with pTYB12 (intein alone) or piNOSpep-intein (intein-iNOS peptide) before and after 6 hours induction with 500 μM IPTG. *Lane 1*, low molecular mass protein standard (GE Healthcare Bio-sciences); *Lane 2*, intein alone at t = 0; *Lane 3*, intein alone at t = 6 hours; *Lane 4*, intein-iNOS peptide at t = 0; *Lane 5*, intein-iNOS peptide at t = 6 hours. Expected size of intein alone and intein-iNOS peptide fusion protein are 60.4 and 61.8 kDa, respectively.

These results for the purification of unlabeled CaM-iNOS peptide complex and expression tests for iNOS-peptide in complete NMR minimal medium demonstrate that the future purification of ^{15}N-labeled iNOS peptide from the intein-fusion protein for NMR experiments should be feasible.

7.3.3 Preliminary NMR Spectral Analysis

^{15}N wild-type CaM was titrated with lyophilized synthetic iNOS peptide until the CaM-iNOS sample was saturated with iNOS peptide. The disappearance and corresponding appearance of resonance peaks during iNOS peptide titration demonstrated the formation of the CaM-iNOS peptide complex. Analysis of the ^{15}N-HSQC of ^{15}N wild-type CaM complexed with iNOS peptide demonstrated marked chemical shift perturbations in the NMR spectra when compared to ^{15}N wild-type CaM. As described in section 7.2.7, the initial assignment of the amide protons in the CaM-iNOS complex in the ^{15}N-HSQC spectrum was performed and compared to the previously published resonance assignments of holo-CaM alone as a reference spectrum (Ikura *et al.*, 1990).

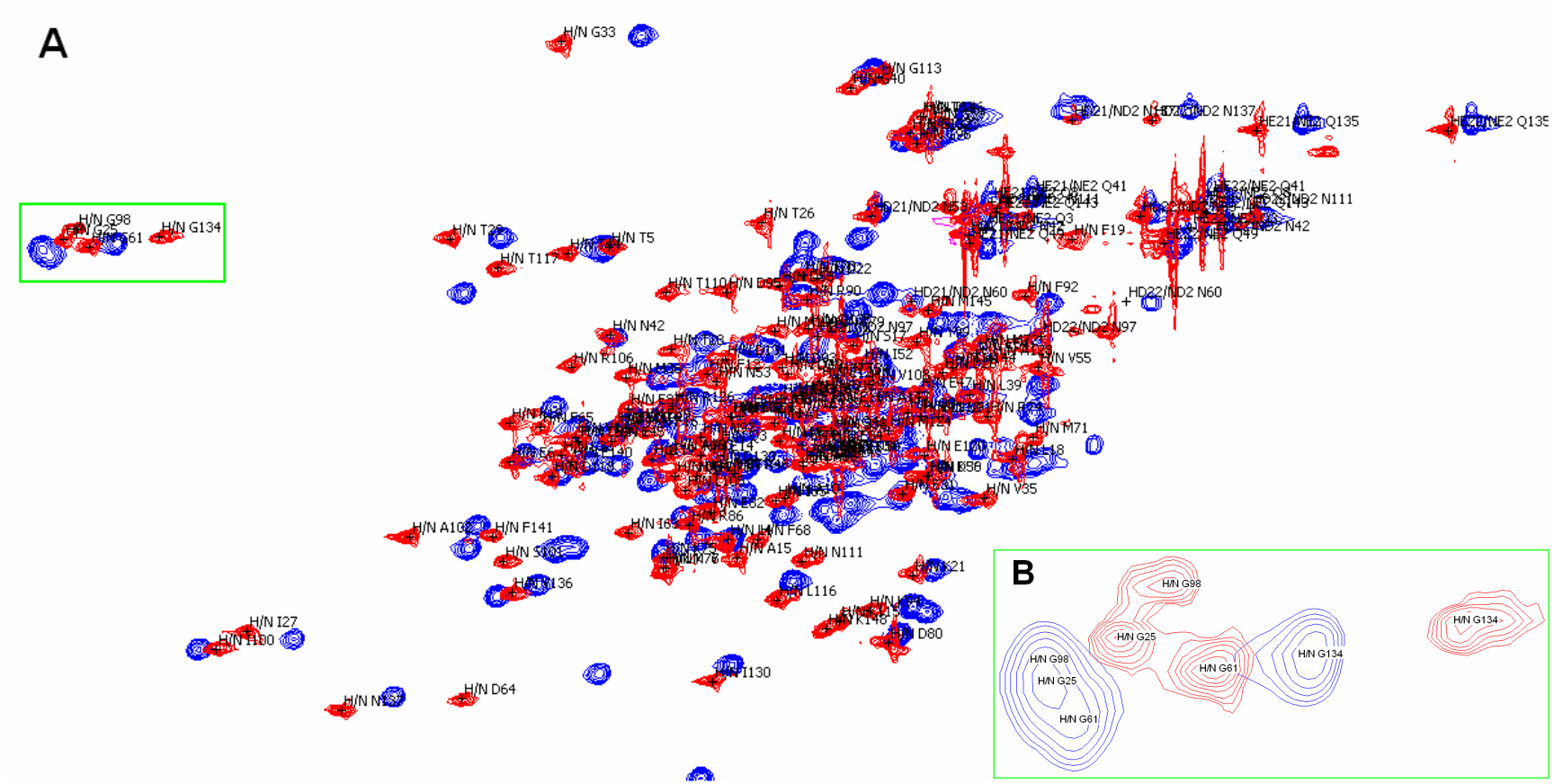

Figure 7.5 – $^{1}H,^{15}N$-HSQC spectra of CaM alone and in complex with iNOS peptide.
(A) Spectra from CaM alone and in complex with iNOS peptide are shown in blue and red, respectively. Residues are labeled with preliminary resonance assignments for the CaM-iNOS peptide complex. These assignments are only preliminary and need to be further refined using other types of 3D NMR experiments. **(B)** Magnification of highlighted region *panel A* (green) is shown to demonstrate the chemical shift perturbations observed for wild-type CaM residues G25, G61, G98, and G134 when alone (blue) and bound to iNOS peptide (red).

The 3D-HNCA, 3D-HN(CO)CA, 3D-CBCANH, and 3D-CBCA(CO)NH experiments have been acquired and appear to be of good quality with many cross-peaks. This will enable the next stage of peptide backbone resonance assignments for CaM in complex with iNOS peptide. A future 3D-HCCH-TOCSY is planned to complete the resonance assignments for sidechains in CaM. 3D-NOESY experiments will then be performed to obtain through-space distance constraints for pairs of protons and localized secondary structure in CaM from chemical shifts and peptide backbone NOE interactions. Finally, ^{13}C-^{12}C half filter experiments are also planned to determine interactions between ^{13}C-labeled side chains of CaM in close proximity to unlabeled sidechains of the iNOS peptide. The tertiary structure calculation of CaM in complex with the iNOS peptide will involve using distance restraints obtained from ^{13}C and ^{15}N-NOESY experiments and standard computational molecular dynamic algorithms (Cavanagh *et al.*, 2007).

7.4 Future Studies

The experiments described in this chapter provide the ground work and establish the feasibility of the structural determination of a holo-CaM-iNOS peptide complex. As mentioned in section 7.3.3, numerous 3D NMR experiments have been performed or are planned to complete the resonance assignments of CaM in complex with an iNOS peptide. The purification of ^{15}N-labeled iNOS peptide with unlabeled wild-type is also planned (see section 7.3.2) in order to obtain more detailed 3D structural information on the peptide when bound to CaM. The detailed 3D NMR solution structure of CaM bound to iNOS that will be solved in the future from this study will be compared with the known crystal structures of CaM bound to eNOS (Aoyagi *et al.*, 2003) and the recently released structure of CaM bound to nNOS (Ng *et al*., co-ordinates released 12-15-2007). It is anticipated that the inherent structural differences in the association of CaM to Ca^{2+}-dependent cNOS enzymes and Ca^{2+}-independent iNOS will be determined.

Furthermore, the Ca^{2+}-independent association of CaM with the CaM-binding domain of iNOS is of great interest due to the diverse and manifold physiological roles iNOS-derived •NO plays in the cell. In order to discern if any major structural differences are present in holo- and apo-CaM when bound to the iNOS peptide, future NMR experiments using CaM_{1234} to mimic apo-CaM (Chapter 4) are planned. To date, only ^{15}N-labeled CaM_{1234} has been expressed and purified; however, the expression and purification of ^{13}C-^{15}N CaM_{1234} is also planned. In addition, the copurification of ^{15}N-isotopically labeled iNOS peptide from the intein-iNOS peptide fusion protein with unlabeled CaM_{1234} is also planned for the detailed 3D solution structure of the iNOS peptide in complex with apo-CaM.

These NMR structural studies of holo- and apo-CaM in complex with an iNOS CaM-binding domain peptide will provide a better understanding of the Ca^{2+}-independent binding and mechanistic control of iNOS by CaM.

Chapter 8
Original Contributions and Recommendations for Future Studies

8.1 Original Contributions

Differential activation of NOS isozymes by CaM-TnC chimeras (Chapter 2).

Using CaM-TnC chimeric proteins, we determined that EF hand I was critical for cNOS activation. The iNOS enzyme was coexpressed with each CaM-TnC to test their effect on iNOS activity. In contrast to the results observed for the cNOS enzymes, EF hands II and III were found to contain important elements required for the Ca^{2+}-independence of the enzyme. This study was novel in that we were the first to ever report on specific elements in CaM required for the activation of iNOS. Prior to this study, iNOS could only be produced in the presence of wild-type CaM (Cho *et al.*, 1992); The development of this coexpression methodology to produce iNOS bound to mutant forms of CaM was a significant milestone in studying CaM-iNOS interactions.

Binding and activation of NOS isozymes by CaM EF hand pairs (Chapter 3).

In this study, four different mutant CaM proteins were used to investigate the role of the two CaM EF hand pairs in the binding and activation of the mammalian NOS enzymes. Our results show that the N-terminal EF hand pair in conjunction with the central linker region is required for cNOS enzyme binding and activation, whereas the N-terminal EF hand pair of CaM (nCaM) contains important binding and activating elements for iNOS. This is novel since prior to this study, iNOS could only be produced with CaM or CaM mutants having all four EF hands present. In our gel filtration studies, we demonstrated under Ca^{2+}-deplete conditions that the addition of excess CaM is able to protect

iNOS against aggregation. We also found that two nCaMs could associate to the iNOS CaM-binding domain simultaneously using gel mobility shift assays. From these data, we proposed a model explaining why the iNOS enzyme must be coexpressed with wild-type CaM *in vitro* due its propensity to aggregate when residues of the highly hydrophobic CaM-binding domain are exposed to an aqueous environment.

Ca^{2+}-deficient CaM binding and activation of neuronal and inducible NOS (Chapter 4).

We used CaM mutants deficient in Ca^{2+}-binding with mutations in the N-lobe (CaM_{12}), the C-lobe (CaM_{34}), or both lobes of CaM (CaM_{1234}) to determine their effect on the binding and activation of the Ca^{2+}-dependent nNOS and Ca^{2+}-independent iNOS isoforms. Four different kinetic assays were employed to monitor the effect of these CaM mutants on electron transfer rates in NOS. The CaM mutants were unable to activate nNOS, however, our CD results demonstrated that the Ca^{2+}-replete C-terminal lobe of CaM is capable of binding to the nNOS peptide. A future experiment is recommended to expand upon this particular finding of the C-terminal binding to nNOS without activation (described in section 8.2.1). The results from this study also proved for the first time without the use of chelators that apo-CaM is capable of binding to iNOS peptides and holoenzymes. We also found that the activation of iNOS by the N-terminal domain of CaM was Ca^{2+}-independent, whereas activation by the C-terminal domain of CaM was Ca^{2+}-dependent.

Differential binding of CaM domains to constituitive and inducible NOS (Chapter 5).

In order to investigate the binding of specific regions in CaM to NOS peptides and enzymes, we developed a methodology to selectively label specific residues in the N-terminal lobe, C-terminal lobe, or linker region of the protein with fluorescent dyes. We used an N-terminally labeled an iNOS

CaM-binding domain peptide with dabsyl chloride in order to perform FRET studies between Alexa-labeled residues in the N- and C-terminal domains of CaM and determined that CaM binds to iNOS in an antiparallel orientation. Steady-state fluorescence and circular dichroism studies show that both the N- and C-terminal EF hand pairs of CaM bind to the CaM-binding domain peptide of iNOS in a Ca^{2+}-independent manner; however, only the C-terminal domain showed large Ca^{2+}-dependent conformational changes when associated with the target sequence. Steady-state fluorescence showed that Alexa-labeled CaM proteins are capable of binding to holo-iNOS coexpressed with nCaM. The nCaM protein binds to both the N- and C-type sites of the iNOS CaM-binding domain with nCaM bound at the C-type site being able to be displaced with the addition of excess CaM. Noteably, the nCaM bound to the N-type site demonstrated that its association is Ca^{2+}-independent and is markedly more stable than its association to the C-type site. These results were novel since no one had previously shown that the association of CaM to iNOS is not permanent. It is likely that the N-terminal lobe of CaM binding to the iNOS CaM-binding domain is Ca^{2+}-independent whereas the C-terminal lobe of CaM demonstrated a Ca^{2+}-dependent conformational change when bound to iNOS. This variation of the Ca^{2+}-dependent/independent association of the N- and C-terminal domains of CaM contrasts to the previously proposed model of CaM's sequential association to the nNOS enzyme (Weissman *et al.*, 2002). This investigation provided further insight into why iNOS remains active even under basal levels of Ca^{2+} in the cell.

FRET conformational studies of CaM bound to NOS enzymes (Chapter 6).

This study was first to use FRET in monitoring the dynamic conformational changes in CaM when associated to NOS peptide and enzymes in the presence of increasing free Ca^{2+} concentrations. We found that CaM has a wrapped conformation when bound to the iNOS and cNOS peptides similar to the previously solved x-ray crystal structures of the CaM-eNOS and CaM-nNOS peptide complexes.

Furthermore, the conformation of CaM bound to the both full-length eNOS and nNOS is identical to its conformation bound to the NOS peptides signifying that the crystal structures of CaM bound to the cNOS peptides are a good working model. Future recommended experiments to further the findings of CaM's conformation bound to the holo-NOS enzymes are described in section 8.2.2.

Preliminary NMR structural determination of CaM bound to the CaM-binding domain of iNOS (Chapter 7).

The 3D structure of a CaM-iNOS peptide complex is currently being studied and will hopefully be completed in the coming year. A method to isotopically label the iNOS peptide bound to unlabeled CaM was developed which has never been reported before. This novel methodology allowed us to overcome the difficulty with the aggregation properties of the iNOS CaM-binding domain. The NMR structural determination of holo- and apo-CaM in complex with an iNOS CaM-binding domain peptide will be of great interest to the NOS research community and provide a better understanding of the Ca^{2+}-independent binding and mechanistic control of iNOS by CaM. This study will also serve as a foundation for future NMR CaM-NOS interaction studies that are recommended in sections 8.2.1 and 8.2.2.

8.1.1 Working Model of the CaM-dependent regulation of iNOS

By combining the cumulative results in this thesis, a working model for the CaM-dependent regulation of iNOS is proposed (Figure 8.1). This model builds on the previous model proposed by Garcin and coworkers for the Ca^{2+}-dependent activation of the cNOS enzymes (Figure 1.15) (Garcin *et al.*, 2004). Since previous studies have shown that electron transfer in the reductase domain of iNOS is CaM-independent (Newton *et al.*, 1998), the only point of electron transfer that appears to be affected directly by CaM is the FMN to heme electron transfer step.

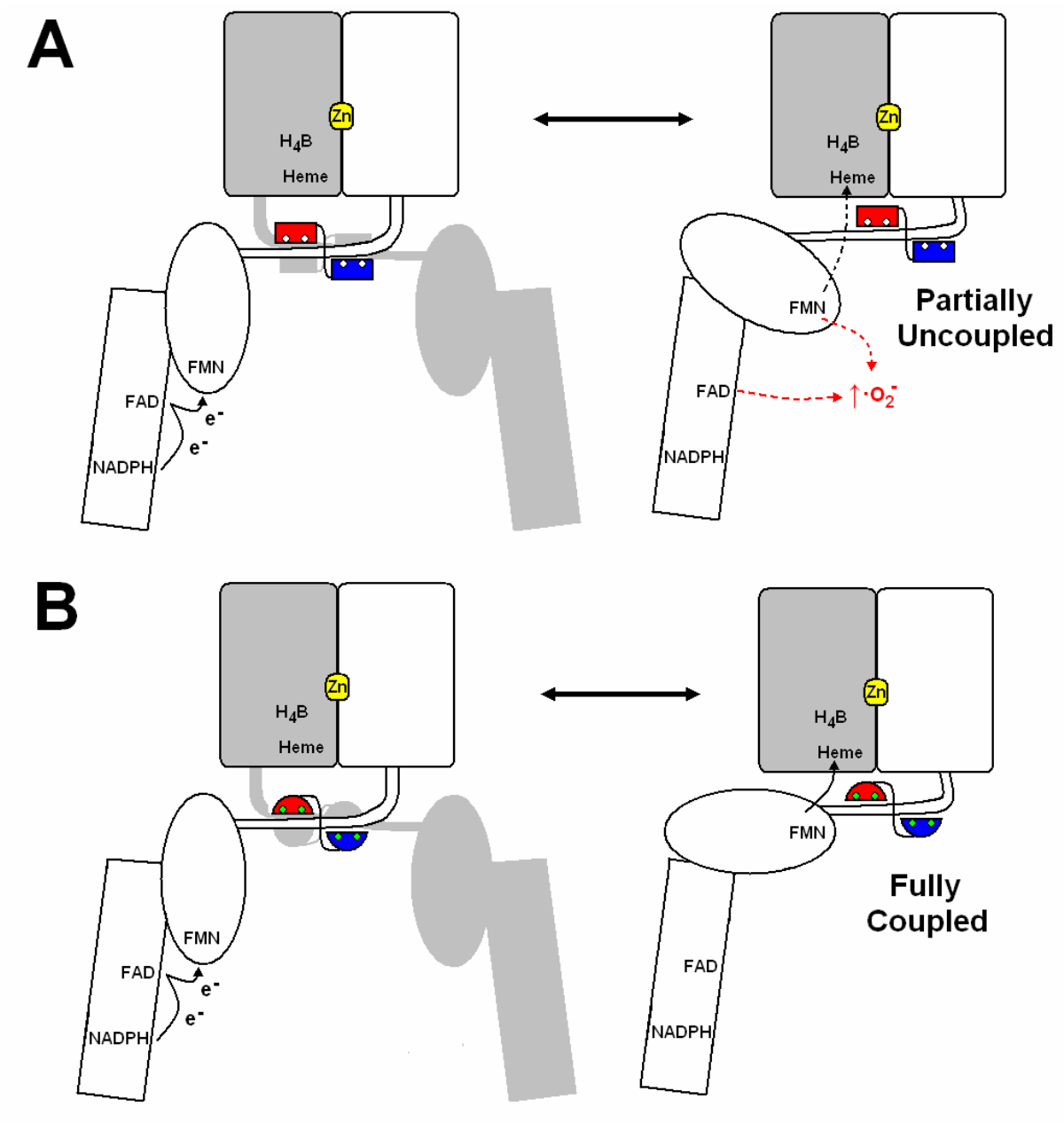
A
Zn
H_4B
Heme
FMN
FAD
NADPH
e-
e-
Zn
H_4B
Heme
FMN
FAD
NADPH
O_2^-
Partially
Uncoupled
B
Zn
H_4B
Heme
FMN
FAD
NADPH
e-
e-
Zn
H_4B
Heme
FMN
FAD
NADPH
Fully
Coupled

Figure 8.1 – Working model for CaM-dependent regulation of •NO by iNOS.

This model is based upon a previous study (Garcin *et al.*, 2004) with the exception that the reductase domain is not shown as a dimer (for explanation, please see section 1.2.2). Each monomer of NOS is shown in white and grey, respectively. The structural zinc at the dimer interface of the oxygenase domain is shown in yellow. The N- and C-terminal domains of CaM are shown in red and blue respectively. Ca^{2+}-deplete and Ca^{2+}-replete EF hands of CaM are shown as white and green circles. Based upon our previous study, CaM binds in an antiparallel fashion (Chapter 5). The N-terminal domain of CaM binds closer the reductase domain and interacts directly with the FMN domain. The C-terminal domain of CaM binds closer to the oxygenase domain. Our studies have shown that the N-terminal domain of CaM contains important binding and activating elements for iNOS (Chapter 3). At basal Ca^{2+} concentrations, this CaM domain is Ca^{2+}-deplete and binds very tightly to the N-type site of the iNOS CaM-binding domain. The N-terminal domain of CaM does not appear to have any Ca^{2+}-dependent affect on electron transfer rates within iNOS, as previously shown in Chapters 4 and 5. **(A)** Apo-CaM is able to bind to the iNOS enzyme. The reductase domain of iNOS is CaM-independent and is able to transfer electrons efficiently from NADPH through the reductase domain to the FMN (Newton *et al.*, 1998). After electrons are transferred to the FMN, a CaM-dependent conformational change in the FMN domain occurs, where the FMN domain moves from an electron accepting position to an electron donating position. The electrons from $FMNH_2$ are able to transferred to the catalytic heme of the other NOS monomer; however, this structural change in the reductase domain is not perfect (~70% when compared to Ca^{2+}-replete CaM) and electrons are able to be uncoupled from •NO production to produce $•O_2^-$. $•O_2^-$ production has previously been linked to electron uncoupling from the flavins in the reductase domain of iNOS (Xia *et al.*, 1998). This uncoupling, which results in an NADPH oxidized to •NO produced ratio greater than 2:1, and lower •NO production rates by iNOS has been attributed to the Ca^{2+}-deplete C-terminal lobe of CaM, as previously described in Chapters 4 and 5. **(B)** An increase in free Ca^{2+} concentration causes the C-terminal domain of CaM to become Ca^{2+}-replete. This directly affects the CaM-dependent conformational change in the FMN domain to dock perfectly with the oxygenase domain so that it can pass its electons efficiently to the catalytic heme. This results in the reductase domain derived electrons being tightly coupled to •NO production with an NADPH oxidation to •NO produced ratio of 1.5:1. Although it is still unclear if the N-terminal domain of CaM is Ca^{2+}-deplete or Ca^{2+}-replete in the fully active form iNOS, it is clear that Ca^{2+} binding to CaM is required for electrons to be fully coupled to •NO synthesis.

Although this model is simplistic in describing the effect of the various domains of CaM on electron transfer with iNOS, it does demonstrate the importance of Ca^{2+} binding to the C-terminal domain of CaM to promote efficient electron transfer from the FMN domain to the heme for •NO synthesis. The completion of the NMR structural study of Ca^{2+}-replete and Ca^{2+}-deplete CaM bound to an iNOS CaM-binding domain peptide (Chapter 7) will determine the specific interactions that are occurring between CaM and the iNOS CaM-binding domain. Since nCaM alone is able to bind and activate iNOS, and the N-terminal domain of CaM binds closest to the FMN domain of iNOS, an experiment is suggested. This experiment would involve the structural determination of CaM in complex with an extended iNOS CaM-binding domain-FMN domain construct (section 8.2.2). This investigation would help refine the working CaM-iNOS model since important contacts between CaM and regions flanking the CaM-binding domain have been implicated in the Ca^{2+}-independence of iNOS (Ruan *et al.*, 1996). This study may also provide information on the dynamic properties of the FMN domain with varying free Ca^{2+} concentrations, as previously described in Chapter 6. Clearly, a better understanding of how CaM binds and activates the iNOS enzyme continues to be of great interest due to the diverse physiological roles performed by •NO and this working model is a progressive step in clarifying this enzyme's mechanism.

8.2 Recommendations for Future Studies

The following is a summary of recommended experiments to expand upon the findings presented in this thesis. These suggested experiments would test current models and clarify the mechanism of CaM binding and activation of the NOS enzymes.

8.2.1 NMR structural determination of CaM mutants with NOS peptides

As previously described in Chapter 7, intein-fusion protein expression systems for all three NOS CaM-binding domains have been created. These vectors can be used to produce ^{15}N and ^{13}C isotope labeled peptides for future NMR studies with various CaM mutants that have been described throughout this thesis. There are several combinations of CaM mutant proteins bound to NOS CaM-binding domain peptides that can possibly be investigated by NMR spectroscopy. Once the NMR structure of CaM bound to the iNOS peptide has been determined, the assigned resonance peaks for the CaM-iNOS peptide complex can act as a reference spectrum for these future studies.

A CaM mutant of particular interest would be CaM_{12}, which is incapable of binding Ca^{2+} in its N-terminal domain (Chapter 4). Using circular dichroism, it was demonstrated that this mutant could bind to the nNOS CaM-binding domain peptide (section 4.3.4.2). In a previous model, it was proposed that the Ca^{2+}-replete C-terminal domain of CaM can bind to the cNOS enzymes first, and following a subsequent increase in cytosolic Ca^{2+} concentrations, the N-terminal domain of CaM is then able to bind and activate the enzyme (Weissman *et al.*, 2002). In order to test this model as well as observe a possible intermediate species in the binding and activation of the cNOS enzymes, the 3D structural determination of CaM_{12} in complex with the CaM-binding domains of nNOS and/or eNOS is suggested. The elucidation of this intermediate structure would also be of general interest to the CaM research community since this sequential mode of CaM binding and activation has been suggested to occur in other Ca^{2+}-dependent CaM-target proteins such as the plasma Ca^{2+}-ATPase

(Sun and Squier, 2000), CaM-dependent protein kinase II (Torok *et al.*, 2001), and MLCK (Persechini *et al.*, 1994; Bayley *et al.*, 1996).

8.2.2 NMR structural determination of the FMN domains for nNOS and iNOS

The FMN domain of the NOS reductase domain plays a pivotal role in electron transfer within the NOS enzymes; however, the detailed 3D structure of the FMN domain in complex with CaM has yet to be determined. It has been suggested that the FMN domain of the NOS enzymes are highly dynamic and undergo a large conformational change when bound to CaM (section 1.2.3; Figure 8.1). The cNOS enzymes also contain a putative autoinhibitory element in their FMN domains that have also been suggested to undergo a conformational change upon CaM binding to the enzyme (section 1.2.5.1.1). Although the crystal structure of nNOS's reductase domain has previously been solved (Garcin *et al.*, 2004), this crystal structure did not contain the CaM-binding domain or show the autoinhibitory element, important regulatory regions that control electron transfer within the NOS enzyme. These regulatory regions have been suggested to be highly dynamic making their structural determination difficult using x-ray crystallography. As mentioned previously, NMR spectroscopy is able to observe the intrinsic flexibility in some proteins and would be able to monitor the movement of these regulatory elements in nNOS. This would be a ground-breaking study and of great interest to the NOS research community if the underlying structural and mechanistic basis for the autoinhibitory element in regulating electron transfer within the cNOS enzymes was determined. Furthermore, this structure would expand upon the solved crystal structures of CaM bound to the CaM-binding domain peptides of eNOS (Aoyagi *et al.*, 2003) and nNOS (Ng *et al.* – unpublished) by determining other contacts between CaM and the cNOS enzymes that have previously been suggested to occur with the reductase domain or possibly the autoinhibitory domain itself (Newman *et al.*, 2004; Spratt *et al.*, 2006).

In order to determine the structure of the nNOS FMN domain in the presence and absence of CaM, constructs have previously been created that include the CaM-binding domain and autohibitory domain of nNOS based upon a previous study (Garnaud *et al.*, 2004). This nNOS construct (nNOSFMNCaM) has been demonstrated to produce stable soluble protein that is FMN replete; however, sufficient yields when expressed in minimal media from NMR measurements may become an obstacle. Optimization of expression in minimal medium will have to be performed to maximize ^{15}N and ^{13}C isotope incorporation and may require subcloning of this construct into a more suitable expression vector containing a T7-promoter. Once stable protein has been produced, the 3D NMR structure could be determined in the presence and absence of CaM. Particular focus should be given to the conformational changes that occur in the FMN domain upon CaM binding in the CaM-binding domain and the autoinhibitory domain. The effect of free Ca^{2+} concentration could also be studied using Ca^{2+}/EGTA buffers (Chapter 6) to determine the effect of Ca^{2+} on the nNOSFMNCaM protein.

Unlike the cNOS enzymes, iNOS does not contain an autohibitory element. Since regions in iNOS's FMN domain flanking the CaM-binding domain have also been implicated in the Ca^{2+}-independent association of CaM to iNOS (Ruan *et al.*, 1996), it would be advantageous to determine the structure of iNOS's FMN domain. A construct coding for the FMN domain of iNOS in conjunction with its CaM-binding domain has been cloned by the candidate. This construct is based upon the sequence alignment of the aforementioned nNOSFMNCaM construct that produces soluble protein (Garnaud *et al.*, 2004). Using the soon-to-be solved 3D NMR structure of CaM bound to the iNOS CaM-binding domain peptide as a starting point (Chapter 7), the iNOSFMNCaM construct could be solved using standard triple resonance NMR spectroscopic techniques. By solving the structure of both the nNOS and iNOS FMN domains in complex with CaM, a detailed comparison of the differences between their FMN domains can be performed that will help to further clarify the regulatory differences between the Ca^{2+}-dependent and Ca^{2+}-independent NOS enzymes.

8.2.3 Characterization of CaM binding and activation of other CaM-dependent target proteins

Numerous CaM mutant proteins have been created to elucidate the specific elements or regions in CaM required for the binding and activation of the NOS enzymes. These various mutant CaM proteins, which include CaM-troponin C chimera (Chapter 2), CaM EF hand pair mutants (Chapter 3), Ca^{2+}-deficient CaM mutants (Chapter 4), and numerous other CaM with point mutations, have been instrumental in expanding our knowledge on the interactions that occur between CaM and NOS. Clearly, with this large repertoire of CaM mutants and experience studying protein-protein interactions involving CaM, it is conceivable that studying another CaM-dependent target protein of physiological interest would be a logical progression. For example, the x-ray crystal structures of CaM associated to the CaM-binding domains of death-associated protein kinases have recently been solved (Kursula *et al.* - unpublished). These kinases are linked to a variety of cell death-related signaling pathways (Bialik and Kimchi, 2006); however the detailed affect of CaM and its various regions on the activation of these important kinases has not yet been determined. With over 300 proteins and enzymes in the cell suggested to be CaM-dependent (Ikura and Ames, 2006), there is a multitude of possible CaM-target enzymes that can be studied in the future.

Appendix A – CaM and NOS DNA Sequences

Sequences of CaM and NOS Vectors used in this thesis
(in order of appearance in this Appendix):

pCaMChlor - Wild-type CaM in pACMIP
pET9dCaM - Wild-type CaM in pET9d
pCaM-1TnCKan – CaM-1TnC in pET28a
pCaM-2TnCKan – CaM-2TnC in pET28a
pCaM-3TnCKan - CaM-3TnC in pET28a
pCaM-4TnCKan – CaM-4TnC in pET28a
pCaM-3,4TnCKan – CaM-3,4TnC in pET28a
pnCaMChlor – nCaM in pCaMChlor
pcCaMKan – cCaM in pET28a
pCaMNNKan – CaMNN cloned in pET9dCaM
pCaMCCKan – CaMCC cloned in pET9dCaM
pCaM-L9 – CaM-L9 in pET15b
pT34MCaM-L9 – T34M CaM-L9 in pCaM-L9
pT110CCaM-L9 – T110C CaM-L9 in pCaM-L9
pT34M-T110CCaM-L9 – T34M/T110C CaM-L9 in pT34MCaM-L9
pCaM-T34C – CaM-T34C in pET9dCaM
pCaM-T110C – CaM-T110C in pET9dCaM
pCaM-T34C/T110C - CaM T34C/T110C in pCaM-T110C
pCaM$_{1234}$Kan – CaM$_{1234}$ in pET28a
pCaM$_{12}$Kan – CaM$_{12}$ in pET28a
pCaM$_{34}$Kan – CaM$_{34}$ in pET28a
piNOSpep – iNOS CaM-binding domain with N-terminal polyhistidine tag in pET28a
pnNOSpep – nNOS CaM-binding domain with N-terminal polyhistidine tag in pET28a
peNOSpep – eNOS CaM-binding domain with N-terminal polyhistidine tag in pET28a
piNOSCBD-intein – iNOS CaM-binding domain-intein fusion protein in pTYB12
pnNOSCBD-intein – nNOS CaM-binding domain-intein fusion protein in pTYB12
peNOSCBD-intein – eNOS CaM-binding domain-intein fusion protein in pTYB12
pΔ70iNOShisAmp – Human Δ70iNOS with N-terminal polyhistidine tag in pCWOri
pnNOShisAmp – Rat nNOS with N-terminal polyhistidine tag in pCWOri
peNOShisAmp – Bovine NOS with N-terminal polyhistidine tag in pCWOri
pCWOri-iNOSC200A – Human Δ70iNOS C200A with N-terminal polyhistidine tag in pCWOri
pCWOri-nNOSC415A – Rat nNOS C415A with N-terminal polyhistidine tag in pCWOri
pCWOri-eNOSC186A – Bovine eNOS C186A with N-terminal polyhistidine tag in pCWOri

pCaMChlor - Wild-type CaM in pACMIP – cloned between *Nco*I and *Pst*I

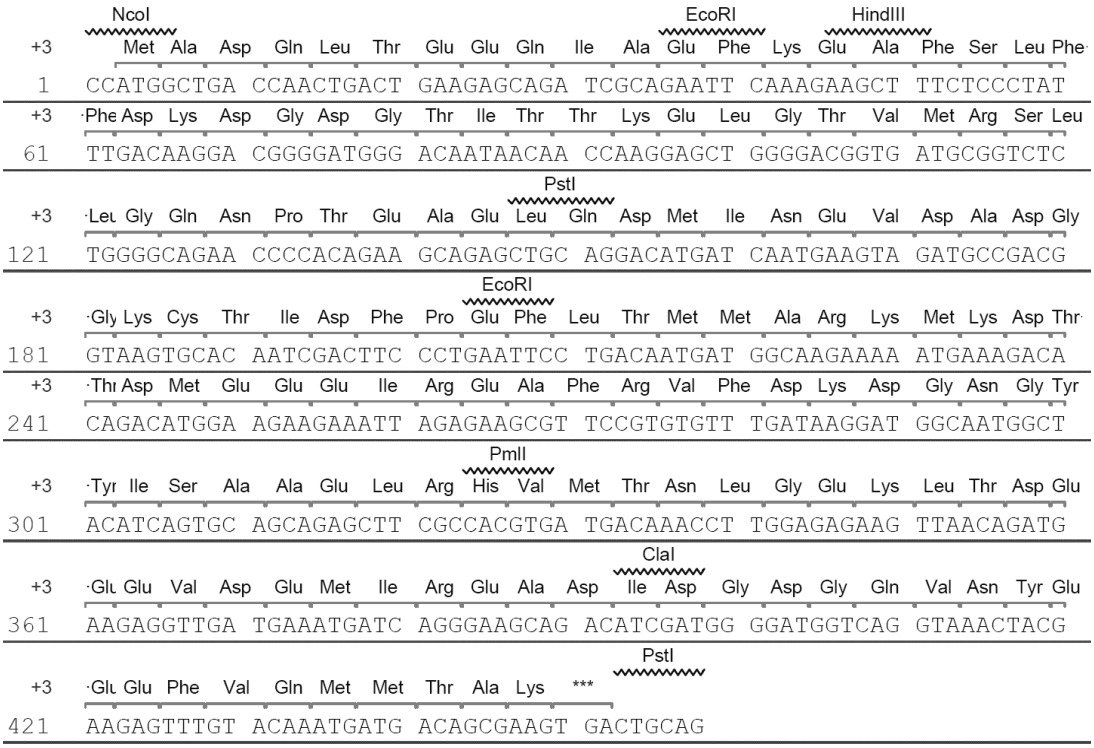

pET9dCaM - Wild-type CaM in pET9d – cloned between *Nco*I and *Bam*HI

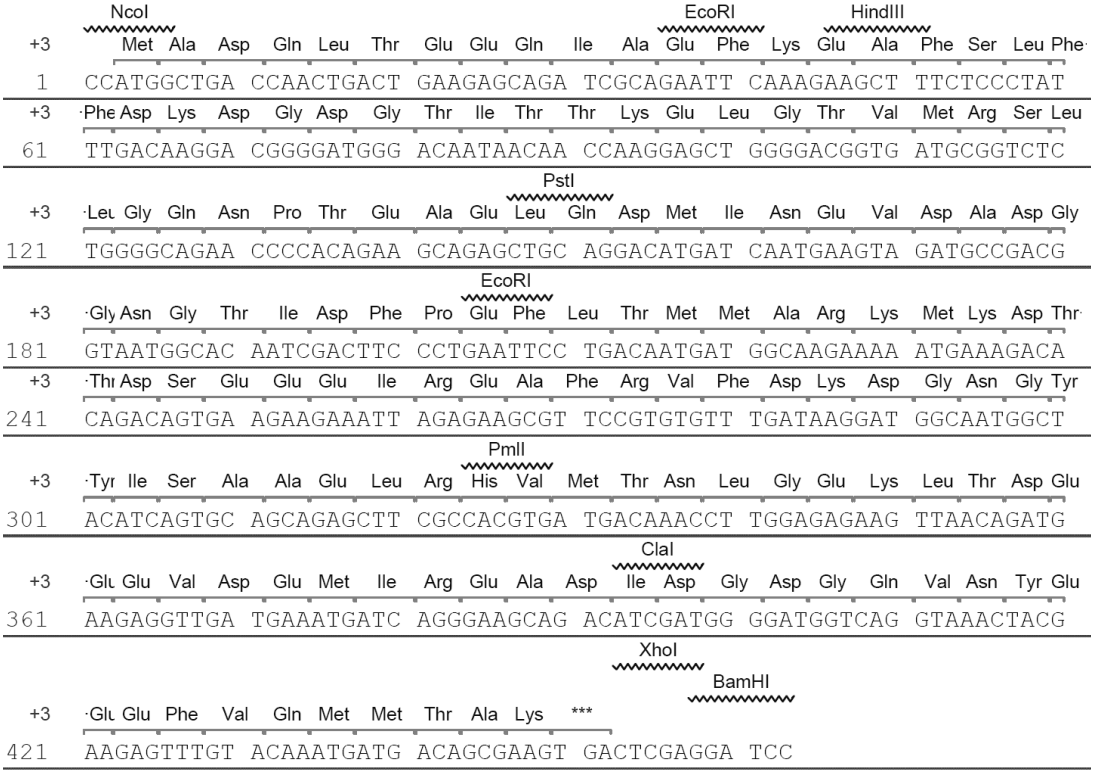

pCaM-1TnCKan – CaM-1TnC in pET28a – cloned between *Nco*I and *Nde*I

Note: **NNN** represents ~800 extra bp that were required for cloning of this construct

pCaM-2TnCKan – CaM-2TnC in pET28a – cloned between *Nco*I and *Nde*I

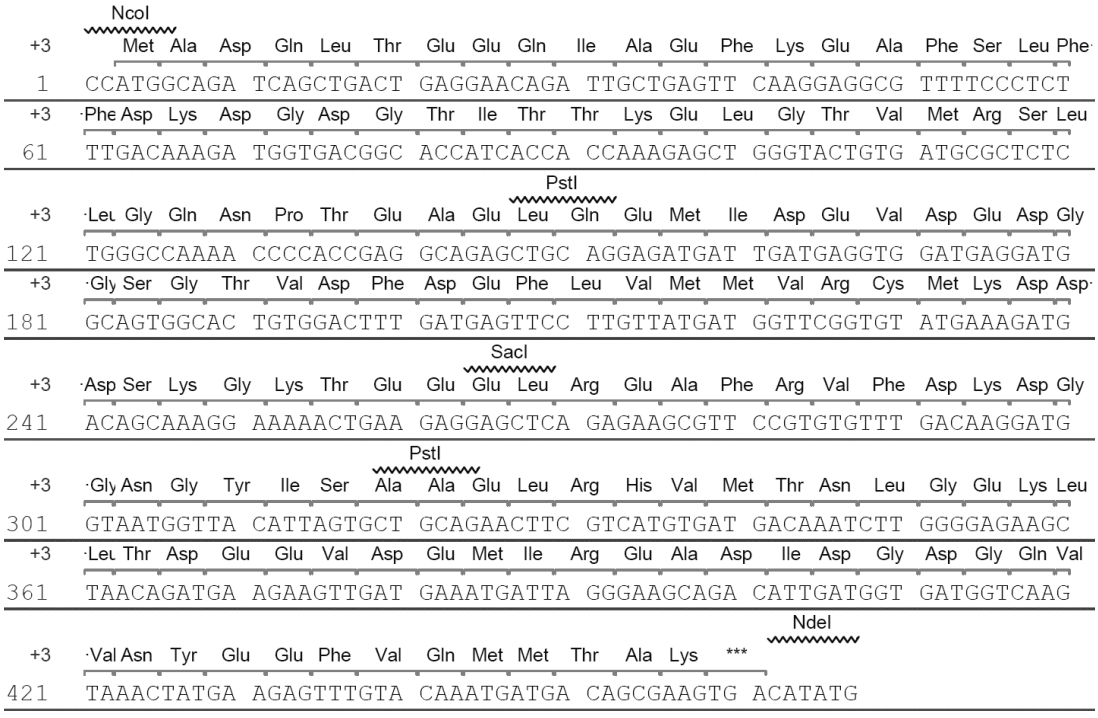

pCaM-3TnCKan - CaM-3TnC in pET28a – cloned between *Nco*I and *Nde*I

Note: **NNN** represents ~800 extra bp that were required for cloning of this construct

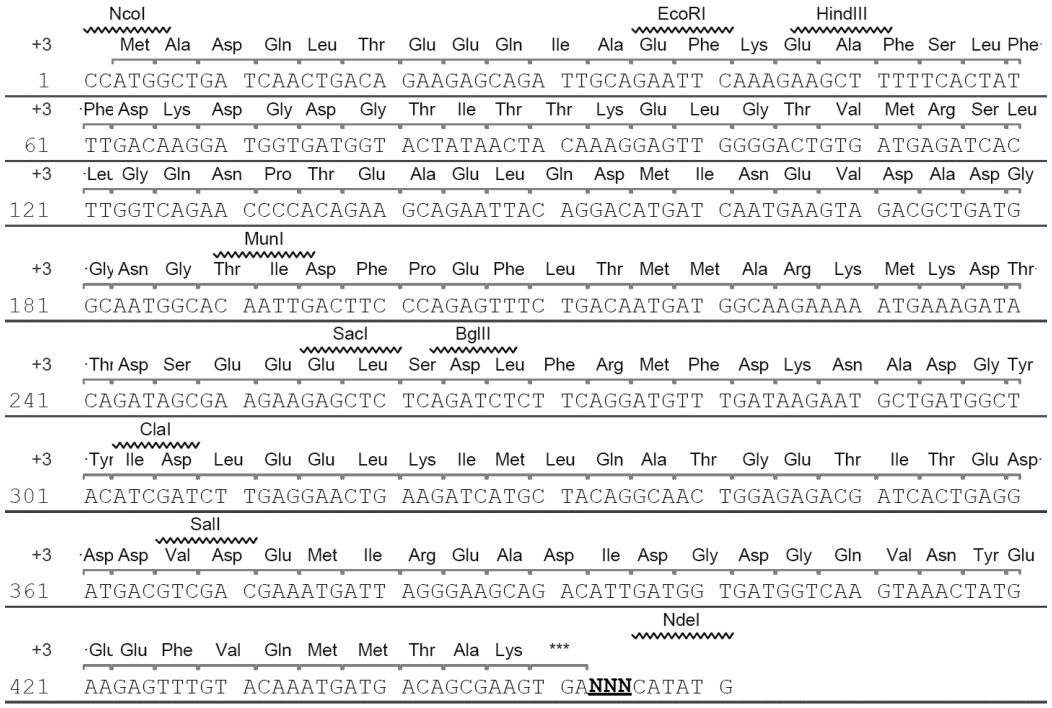

pCaM-4TnCKan – CaM-4TnC in pET28a – cloned between *Nco*I and *Nde*I

Note: **NNN** represents ~400 extra bp that were required for cloning of this construct

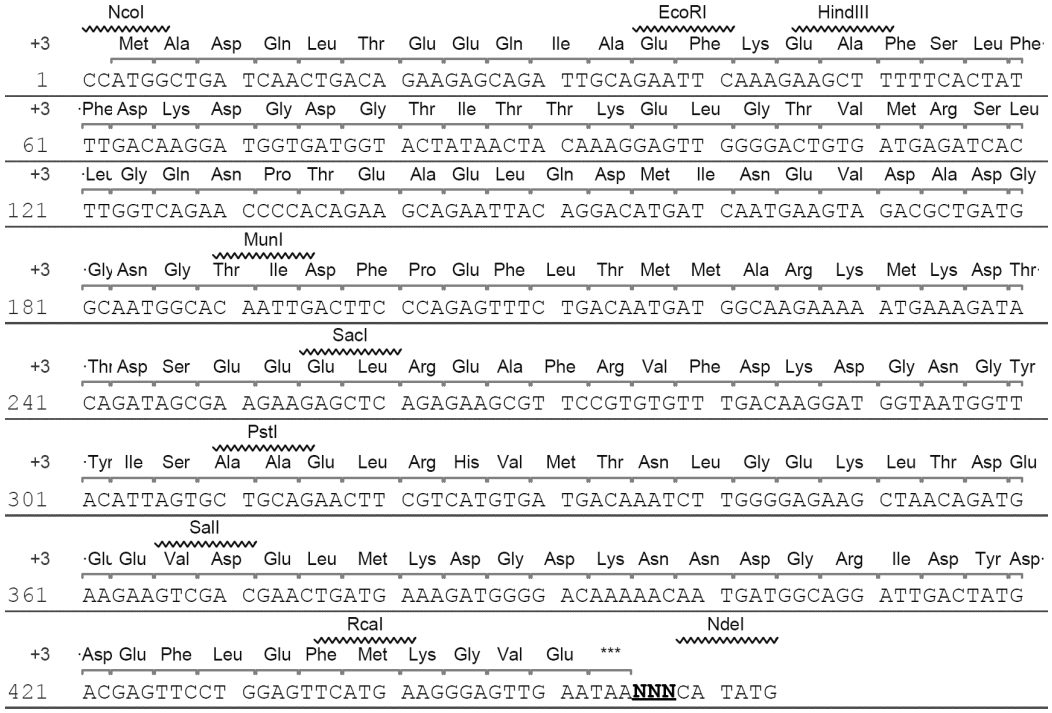

pCaM-3,4TnCKan – CaM-3,4TnC in pET28a – cloned between *Nco*I and *Nde*I

Note: **NNN** represents ~400 extra bp that were required for cloning of this construct

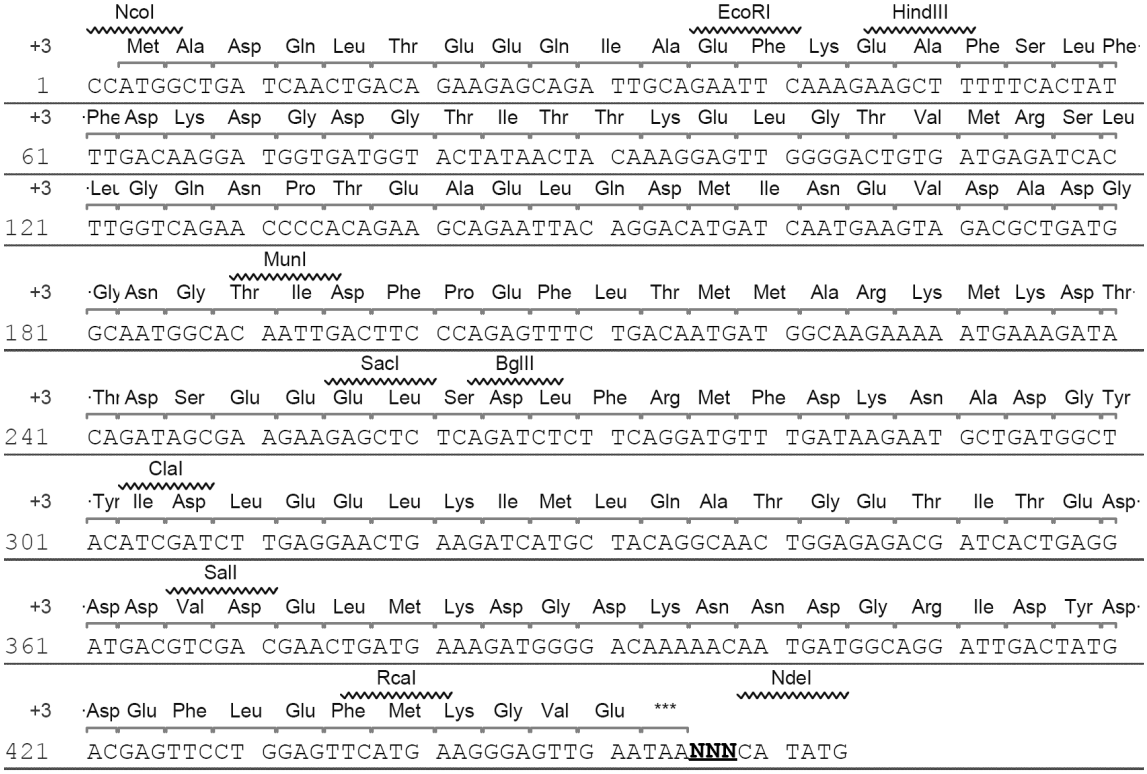

pnCaMChlor – nCaM in pCaMChlor – produced by incorporating stop codon at 76 by mutagenesis (*Xba*I reporter site)

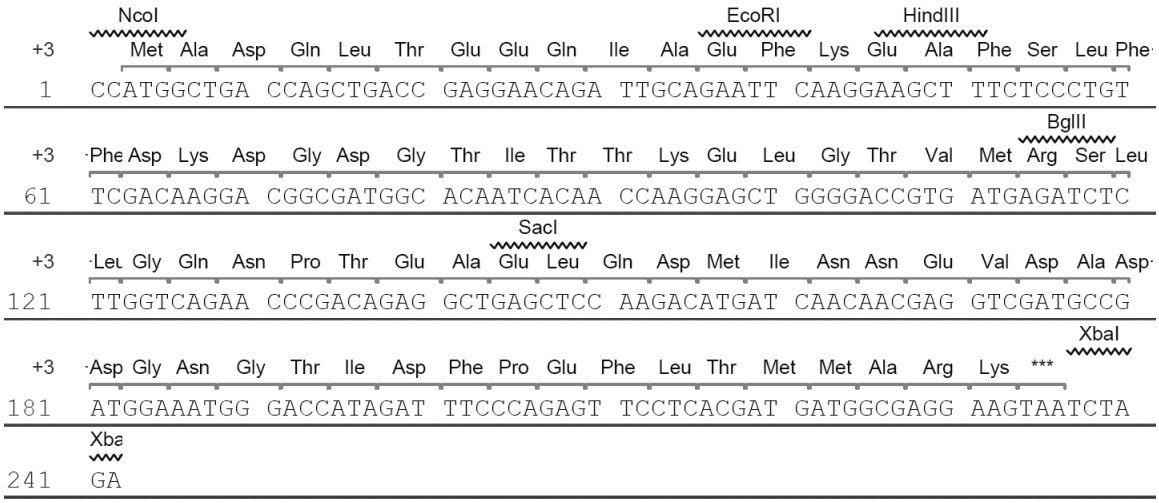

Appendix A – CaM and NOS DNA Sequences

pcCaMKan – cCaM in pET28a – cloned between *Nco*I and *Eco*RI

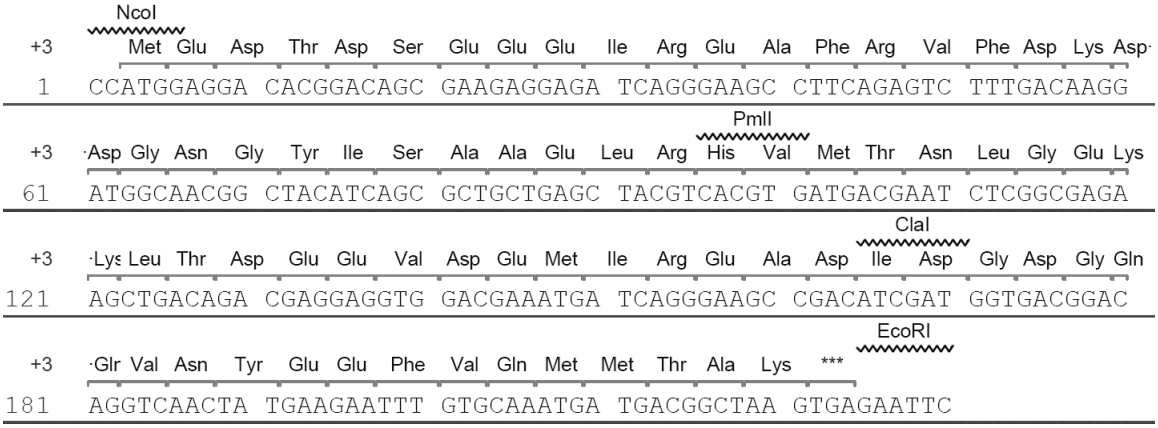

pCaMNNKan – CaMNN cloned in pCaMKan – cloned between *Nco*I and *Pst*I

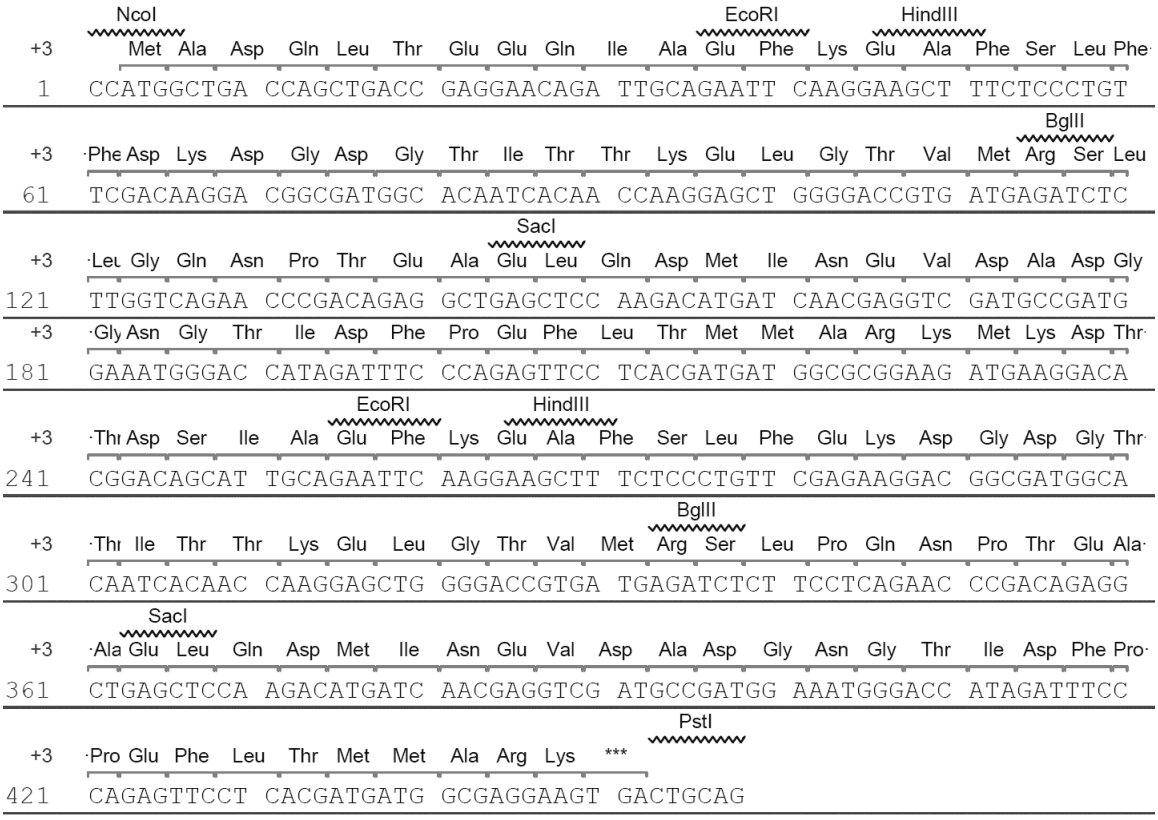

pCaMCCKan – CaMCC cloned in pCaMKan – cloned between *Nco*I and *Pst*I

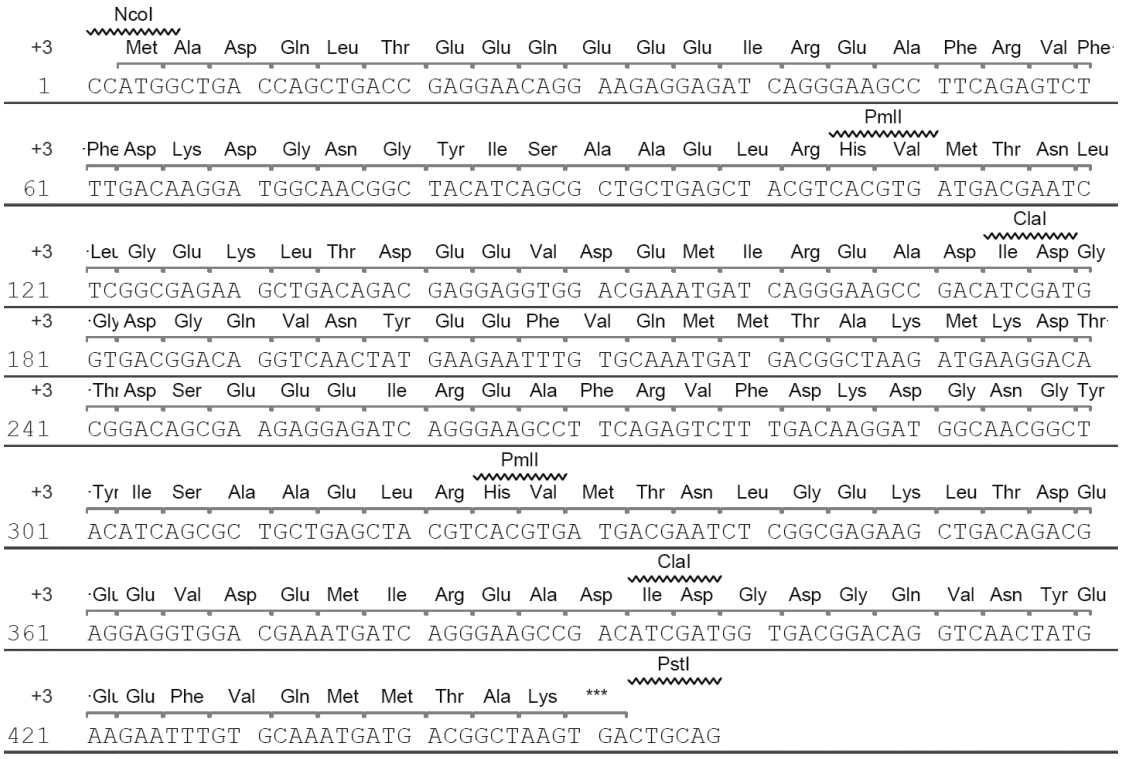

pCaM-L9 – CaM-L9 in pET15b (Amp^r) – cloned between *Nco*I and *Bam*HI

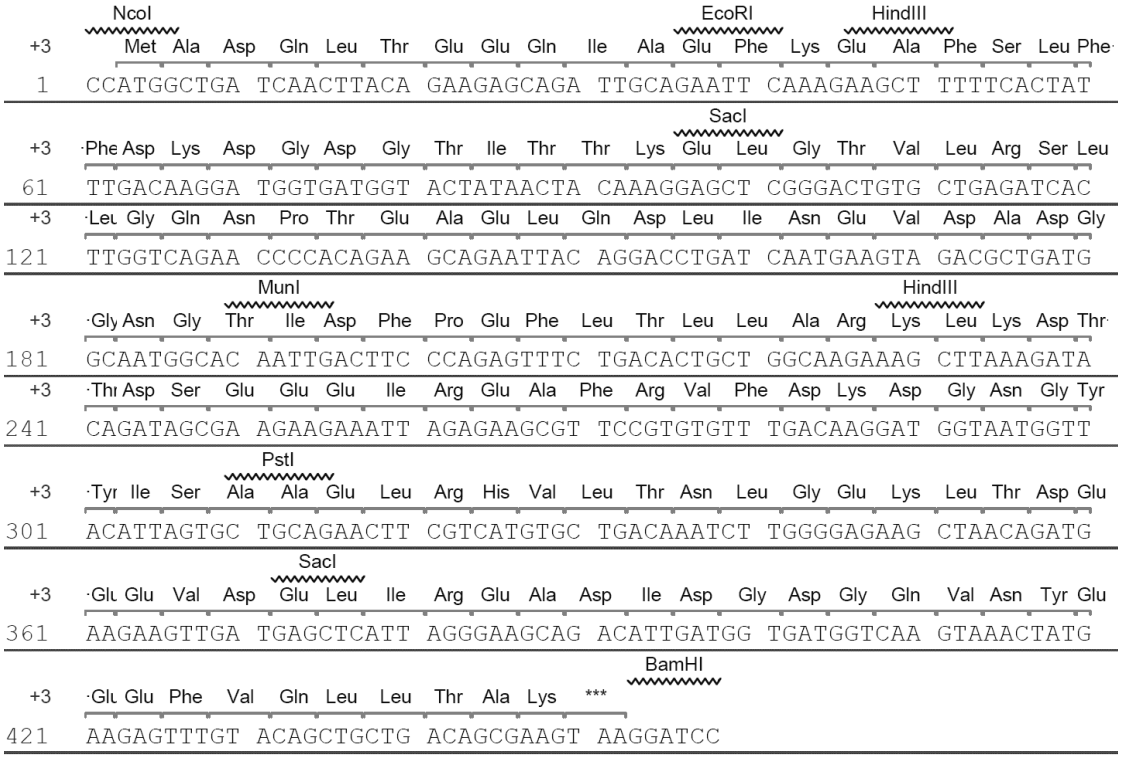

Appendix A – CaM and NOS DNA Sequences

pT34MCaM-L9 – T34M CaM-L9 in pCaM-L9 – produced by incorporating Met at codon 34 by mutagenesis (removal of *Sac*I reporter site)

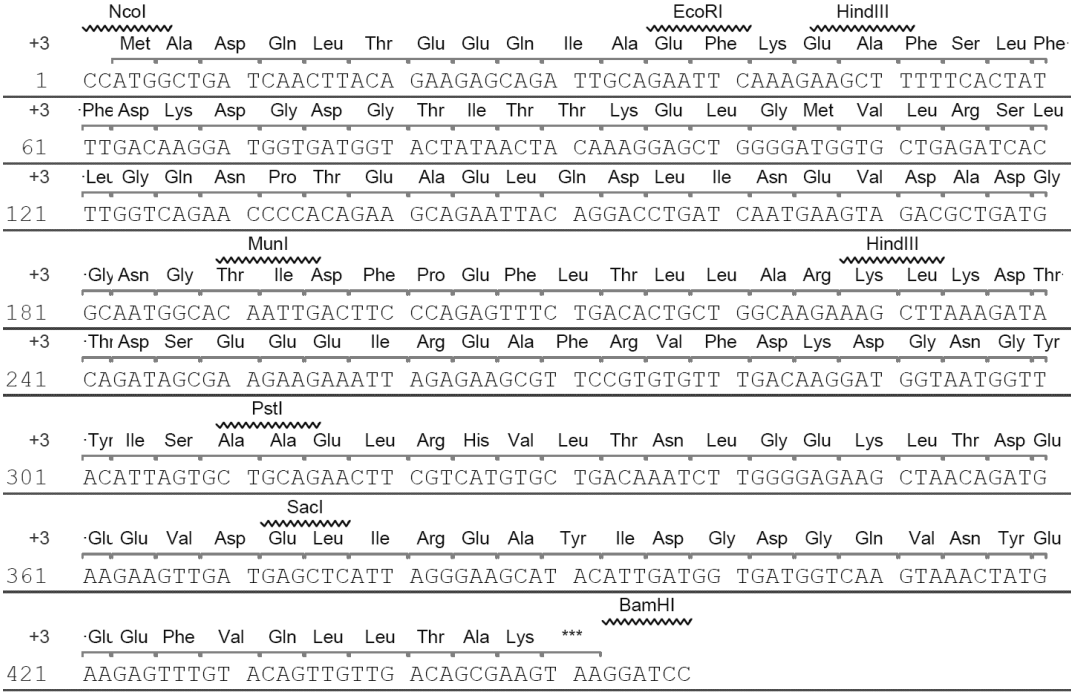

pT110CCaM-L9 – T110C CaM-L9 in pCaM-L9 – produced by incorporating Cys at codon 110 by mutagenesis (*Pml*I reporter site)

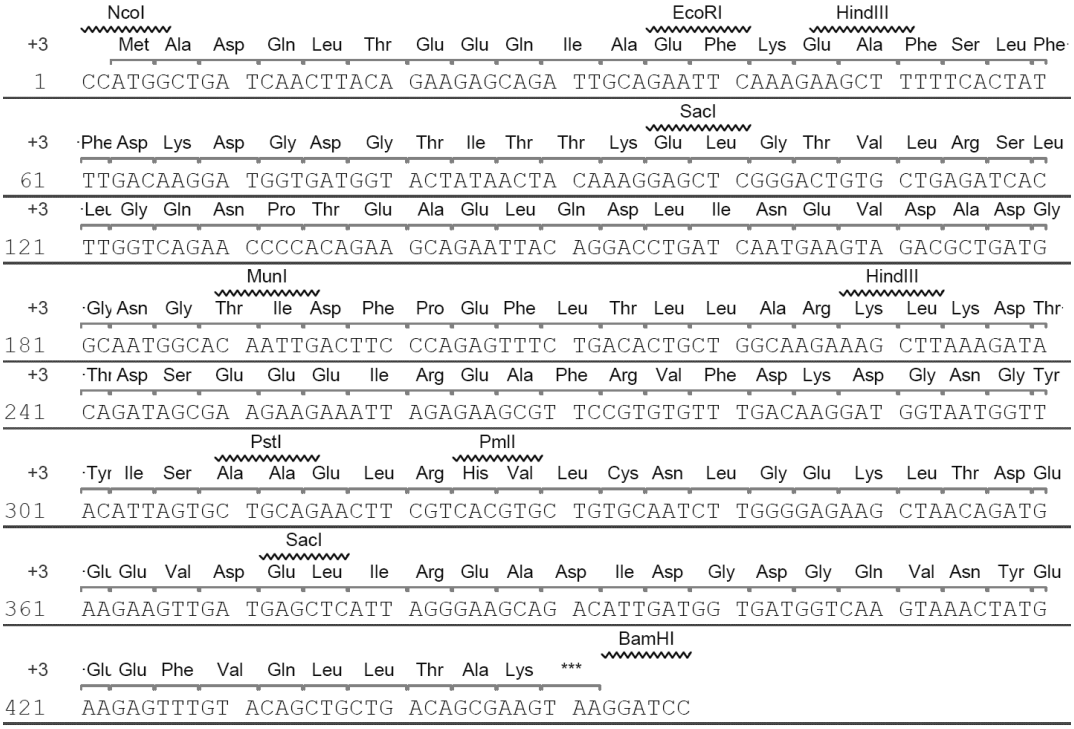

pT34M-T110CCaM-L9 – T34M/T110C CaM-L9 in pT34MCaM-L9 – produced by incorporating Cys at codon 110 by mutagenesis (*Pml*I reporter site)

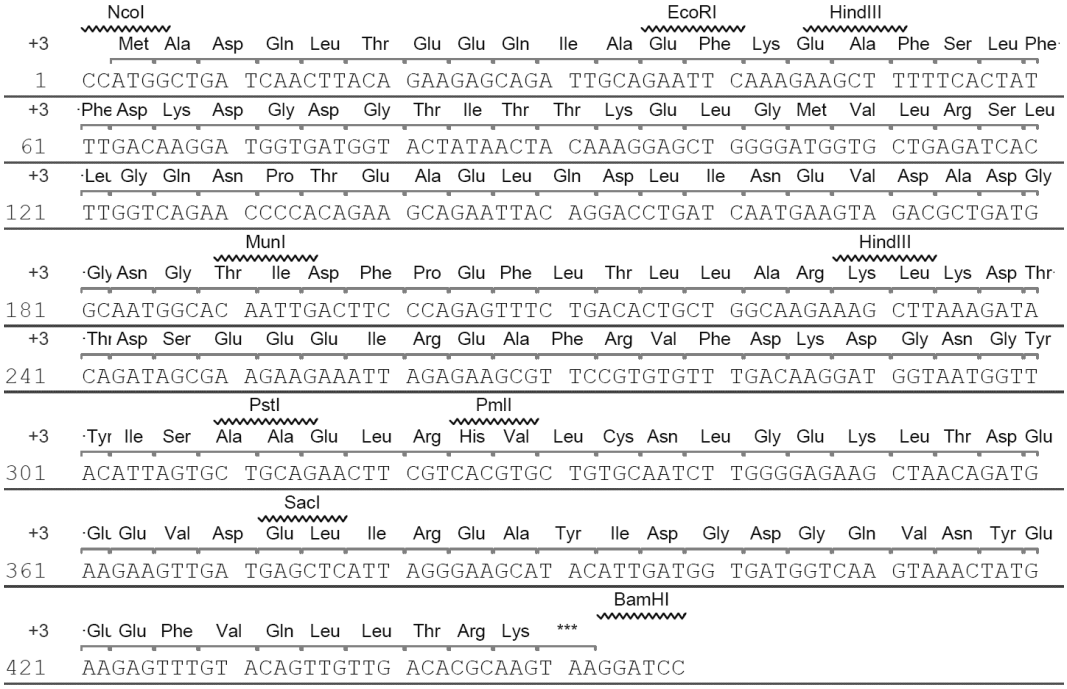

pCaM-T34C – CaM-T34C in pET9dCaM – produced by incorporating Cys at codon 34 by mutagenesis (*Sac*I reporter site)

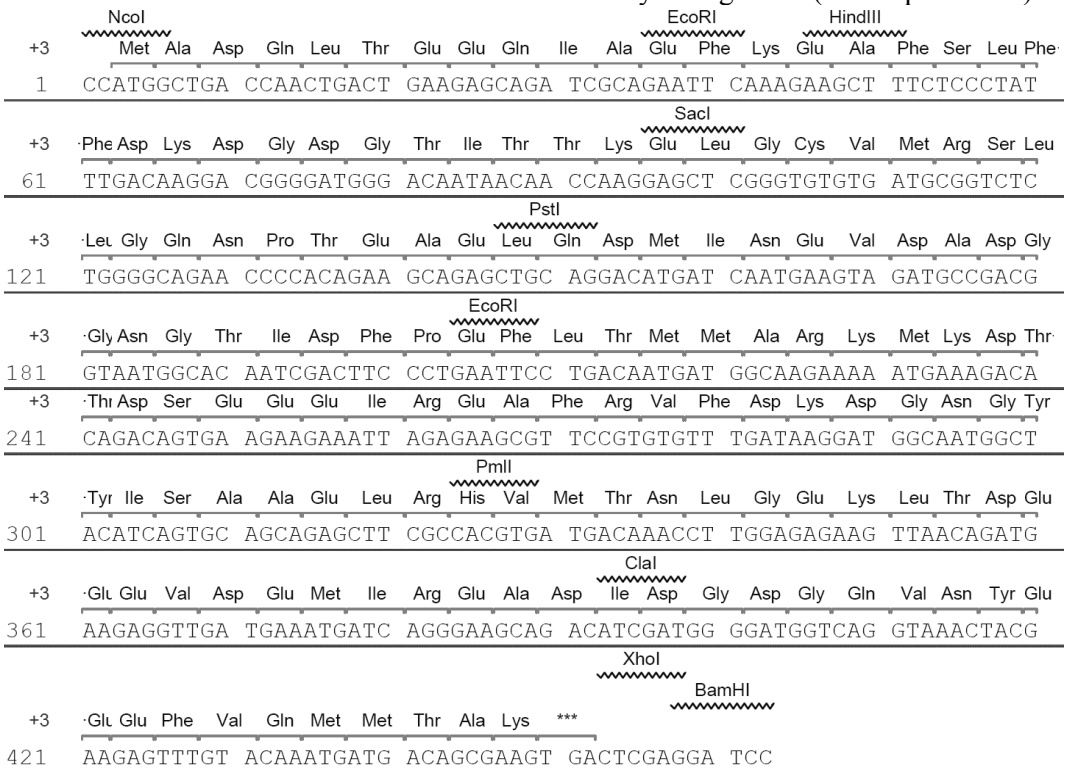

pCaM-T110C – CaM-T110C in pET9dCaM – produced by incorporating Cys at codon 110 by mutagenesis (removal of *Pml*I reporter site)

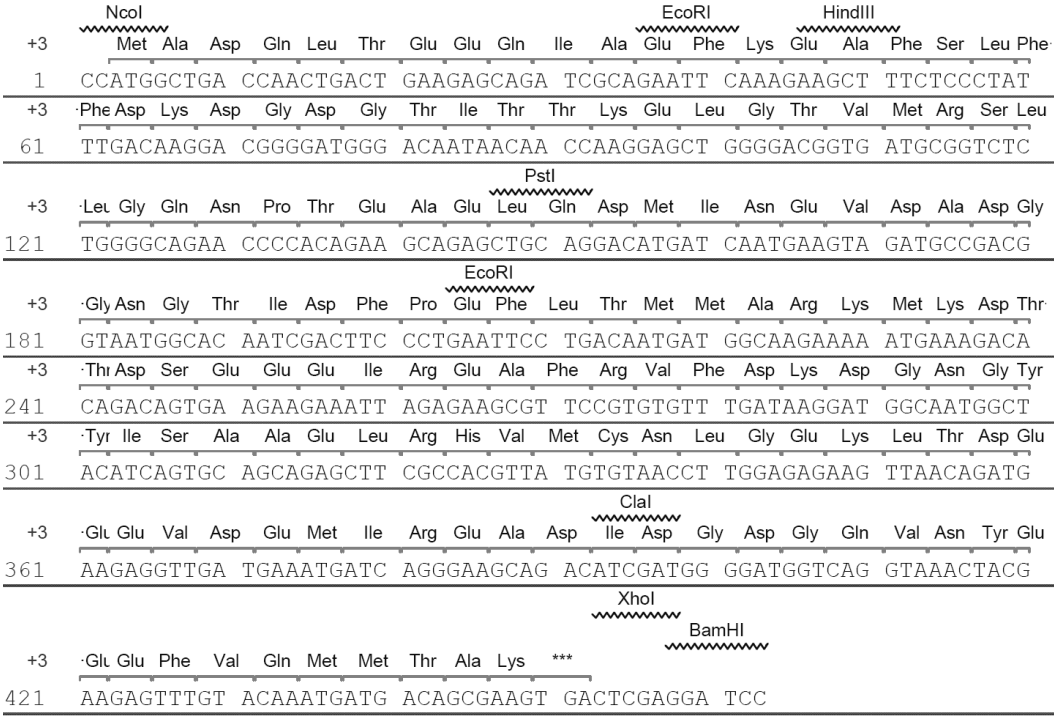

pCaM-T34C/T110C - CaM T34C/T110C in pCaM-T110C – produced by incorporating Cys at codon 34 by mutagenesis (*Sac*I reporter site)

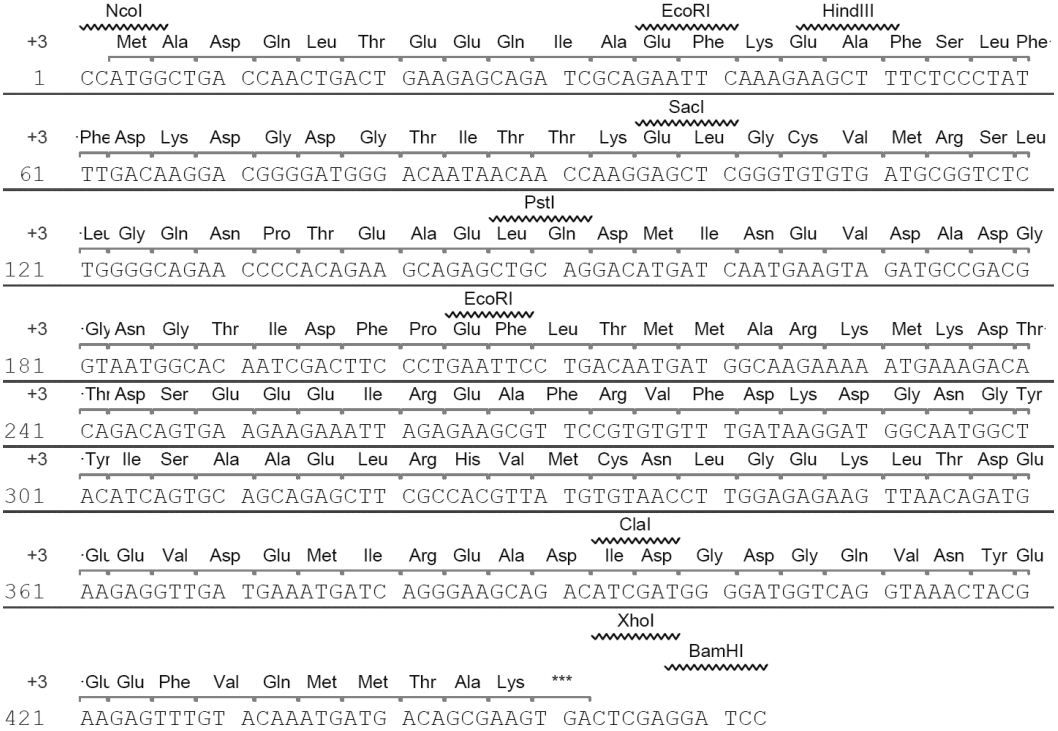

pCaM$_{1234}$Kan – CaM$_{1234}$ in pET28a – cloned between *Nco*I and *Sac*I

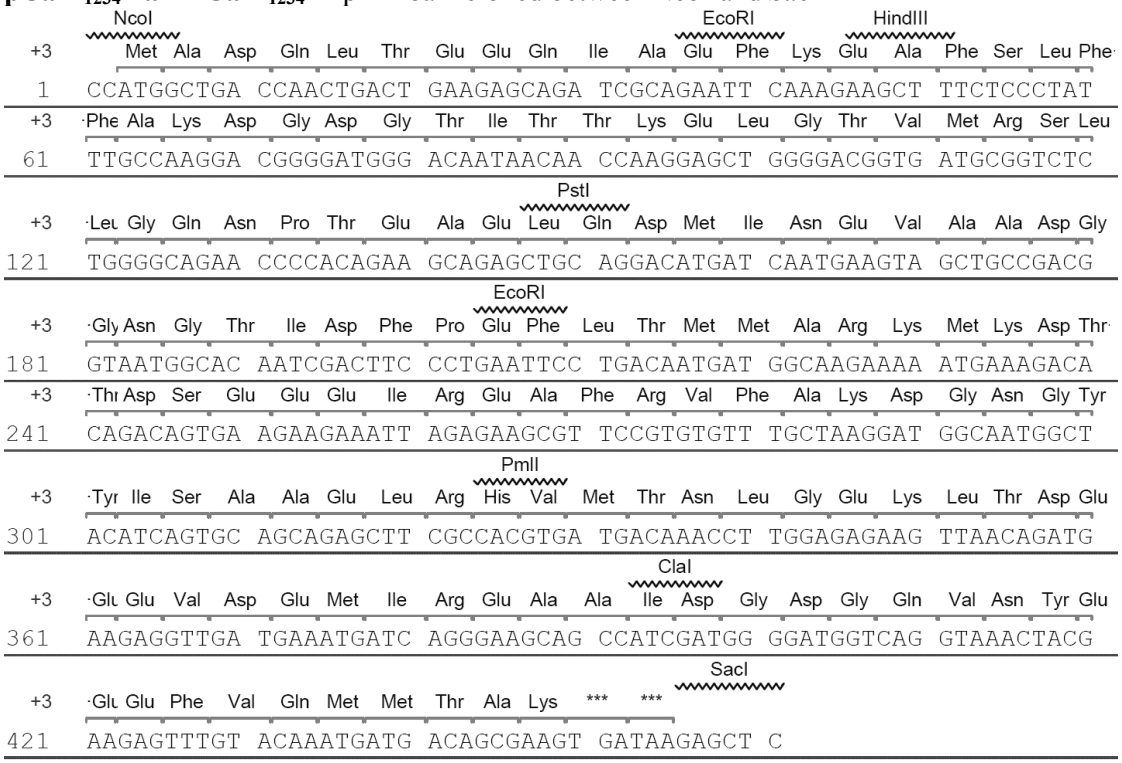

pCaM$_{12}$Kan – CaM$_{12}$ in pET28a – cloned between *Nco*I and *Sac*I

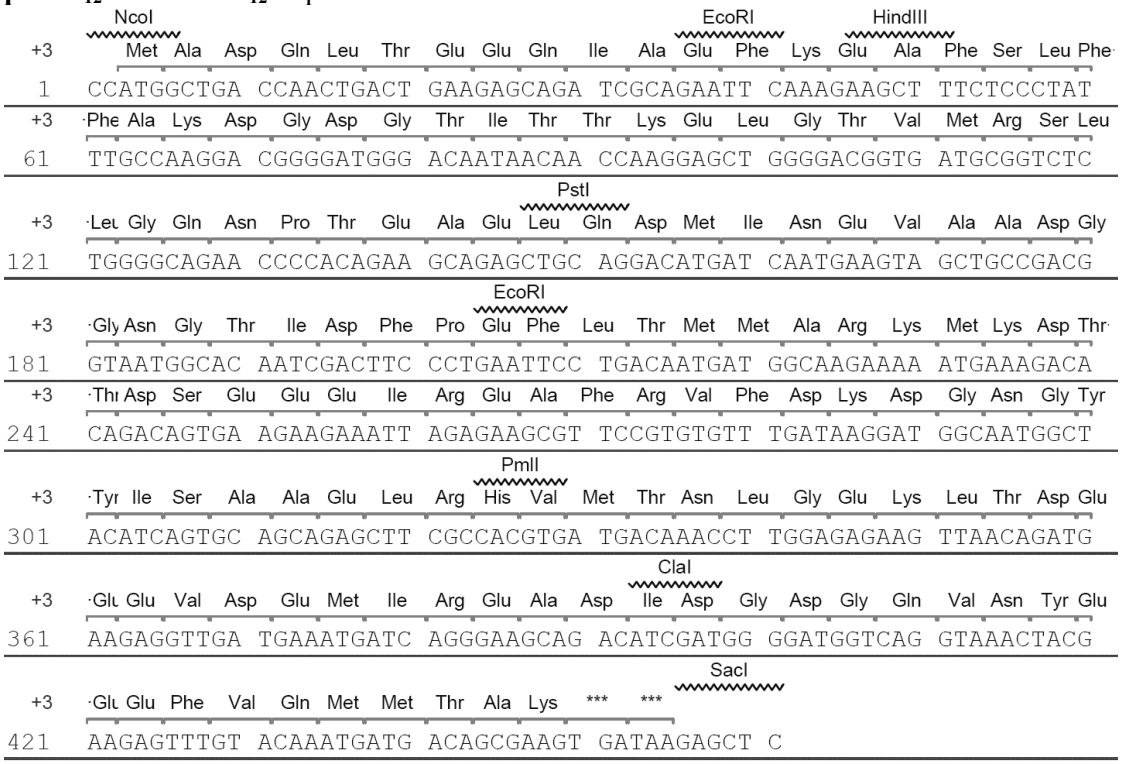

Appendix A – CaM and NOS DNA Sequences

pCaM$_{34}$Kan – CaM$_{34}$ in pET28a – cloned between *Nco*I and *Sac*I

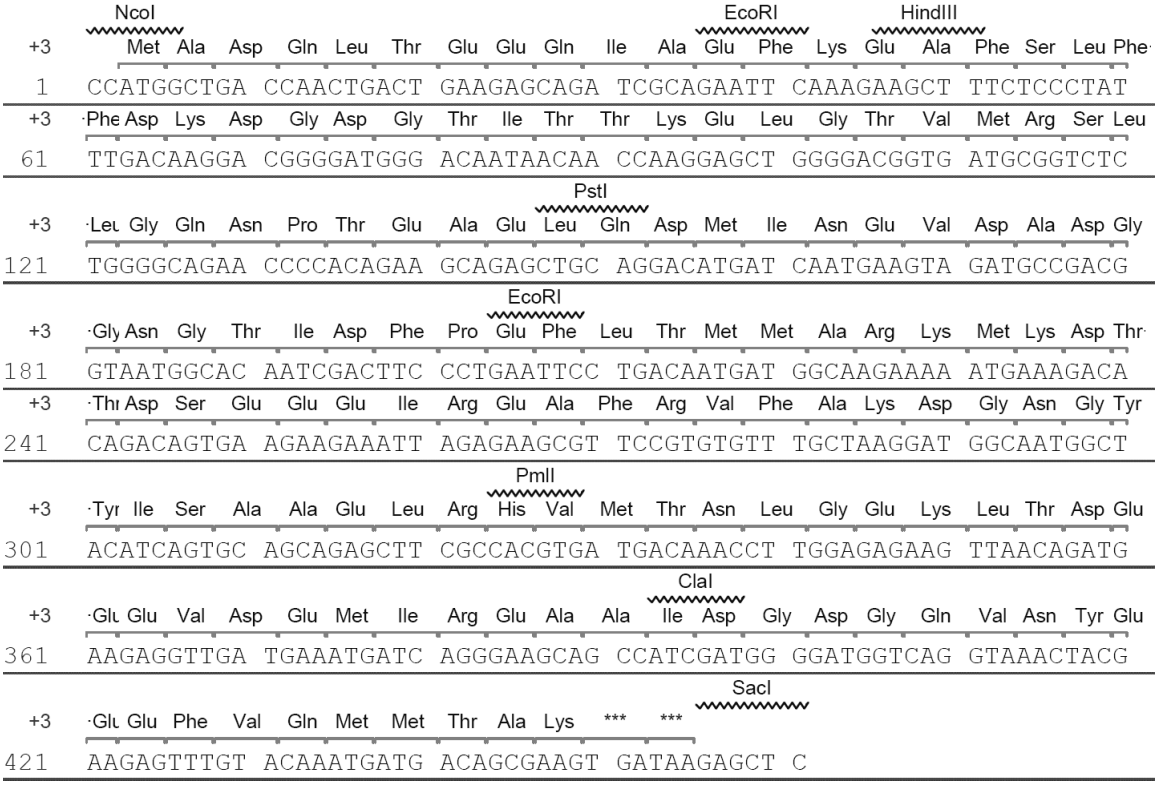

piNOSpep – iNOS CaM-binding domain with N-terminal polyhistidine tag in pET28a (Kan^r) – cloned between *Nco*I and *Bam*HI

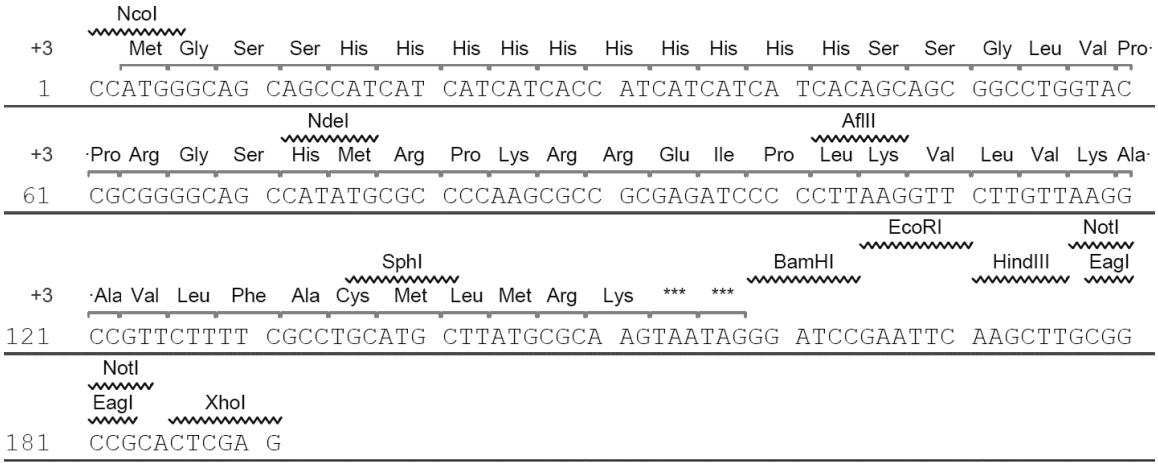

pnNOSpep – nNOS CaM-binding domain with N-terminal polyhistidine tag in pET28a (Kan^r) – cloned between *Nco*I and *Bam*HI

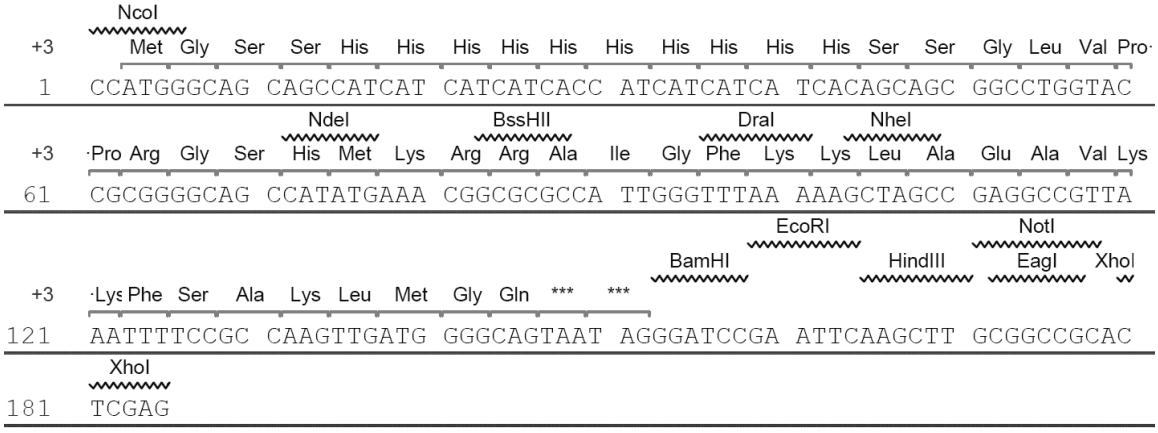

peNOSpep – eNOS CaM-binding domain with N-terminal polyhistidine tag in pET28a (Kan^r) – cloned between *Nco*I and *Bam*HI

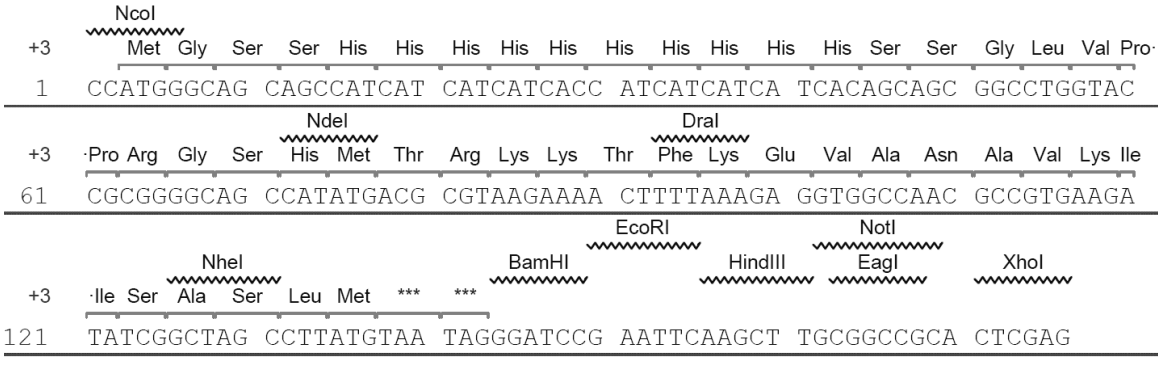

piNOSCBD-intein – iNOS CaM-binding domain-intein fusion protein in pTYB12 (Amp^r)
– cloned between *Nde*I and *Pst*I

Note: **NNN** represents ~1200 extra bp that were required for cloning of this construct

```
+1    Met Lys Ile Glu Glu Gly Lys Leu Val Ile Gly Ser Leu Glu Gly Cys Phe Ala Lys Gly
1     ATGAAAATCG AAGAAGGTAA ACTGGTAATC GGTTCCCTGG AGGGTTGCTT TGCCAAGGGT
+1    Thr Asn Val Leu Met Ala Asp Gly Ser Ile Glu Cys Ile Glu Asn Ile Glu Val Gly Asn
61    ACCAATGTTT TAATGGCGGA TGGGTCTATT GAATGTATTG AAAACATTGA GGTTGGTAAT
+1    Lys Val Met Gly Lys Asp Gly Arg Pro Arg Glu Val Ile Lys Leu Pro Arg Gly Arg Glu
121   AAGGTCATGG GTAAAGATGG CAGACCTCGT GAGGTAATTA AATTGCCCAG AGGAAGAGAA
+1    Thr Met Tyr Ser Val Val Gln Lys Ser Gln His Arg Ala His Lys Ser Asp Ser Ser Arg
181   ACTATGTACA GCGTCGTGCA GAAAAGTCAG CACAGAGCCC ACAAAAGTGA CTCAAGTCGT
+1    Glu Val Pro Glu Leu Leu Lys Phe Thr Cys Asn Ala Thr His Glu Leu Val Val Arg Thr
241   GAAGTGCCAG AATTACTCAA GTTTACGTGT AATGCGACCC ATGAGTTGGT TGTTAGAACA
+1    Pro Arg Ser Val Arg Arg Leu Ser Arg Thr Ile Lys Gly Val Glu Tyr Phe Glu Val Ile
301   CCTCGTAGTG TCCGCCGTTT GTCTCGTACC ATTAAGGGTG TCGAATATTT TGAAGTTATT
+1    Thr Phe Glu Met Gly Gln Lys Lys Ala Pro Asp Gly Arg Ile Val Glu Leu Val Lys Glu
361   ACTTTTGAGA TGGGCCAAAA GAAAGCCCCC GACGGTAGAA TTGTTGAGCT TGTCAAGGAA
+1    Val Ser Lys Ser Tyr Pro Ile Ser Glu Gly Pro Glu Arg Ala Asn Glu Leu Val Glu Ser
421   GTTTCAAAGA GCTACCCAAT ATCTGAGGGG CCTGAGAGAG CCAACGAATT AGTAGAATCC
                                HindIII                                   BglII
+1    Tyr Arg Lys Ala Ser Asn Lys Ala Tyr Phe Glu Trp Thr Ile Glu Ala Arg Asp Leu Ser
481   TATAGAAAGG CTTCAAATAA AGCTTATTTT GAGTGGACTA TTGAGGCCAG AGATCTTTCT
+1    Leu Leu Gly Ser His Val Arg Lys Ala Thr Tyr Gln Thr Tyr Ala Pro Ile Leu Tyr Glu
541   CTGTTGGGTT CCCATGTTCG TAAAGCTACC TACCAGACTT ACGCTCCAAT TCTTTATGAG
+1    Asn Asp His Phe Phe Asp Tyr Met Gln Lys Ser Lys Phe His Leu Thr Ile Glu Gly Pro
601   AATGACCACT TTTTCGACTA CATGCAAAAA AGTAAGTTTC ATCTCACCAT TGAAGGTCCA
+1    Lys Val Leu Ala Tyr Leu Leu Gly Leu Trp Ile Gly Asp Gly Leu Ser Asp Arg Ala Thr
661   AAAGTACTTG CTTATTTACT TGGTTTATGG ATTGGTGATG GATTGTCTGA CAGGGCAACT
+1    Phe Ser Val Asp Ser Arg Asp Thr Ser Leu Met Glu Arg Val Thr Glu Tyr Ala Glu Lys
721   TTTTCGGTTG ATTCCAGAGA TACTTCTTTG ATGGAACGTG TTACTGAATA TGCTGAAAAG
+1    Leu Asn Leu Cys Ala Glu Tyr Lys Asp Arg Lys Glu Pro Gln Val Ala Lys Thr Val Asn
781   TTGAATTTGT GCGCCGAGTA TAAGGACAGA AAAGAACCAC AAGTTGCCAA AACTGTTAAT
                                    NheI
+1    Leu Tyr Ser Lys Val Val Arg Gly Ala Ser Thr Asn Pro Gly Val Ser Ala Trp Gln Val
841   TTGTACTCTA AAGTTGTCAG AGGTGCTAGC ACAAATCCTG GTGTATCCGC TTGGCAGGTC
                                  MunI
+1    Asn Thr Ala Tyr Thr Ala Gly Gln Leu Val Thr Tyr Asn Gly Lys Thr Tyr Lys Cys Leu
901   AACACAGCTT ATACTGCGGG ACAATTGGTC ACATATAACG GCAAGACGTA TAAATGTTTG
+1    Gln Pro His Thr Ser Leu Ala Gly Trp Glu Pro Ser Asn Val Pro Ala Leu Trp Gln Leu
961   CAGCCCCACA CCTCCTTGGC AGGATGGGAA CCATCCAACG TTCCTGCCTT GTGGCAGCTT
                NcoI
+1    Gln Gly Gly His Gly Gly Ile Arg Asn Asn Leu Asn Thr Glu Asn Pro Leu Trp Asp Ala
1021  CAAGGTGGCC ATGGTGGTAT TCGCAATAAT CTTAATACTG AGAATCCATT ATGGGACGCT
+1    Ile Val Gly Leu Gly Phe Leu Lys Asp Gly Val Lys Asn Ile Pro Ser Phe Leu Ser Thr
1081  ATTGTTGGCT TAGGATTCTT GAAGGACGGT GTCAAAAATA TTCCTTCTTT CTTGTCTACG
+1    Asp Asn Ile Gly Thr Arg Glu Thr Phe Leu Ala Gly Leu Ile Asp Ser Asp Gly Tyr Val
1141  GACAATATCG GTACTCGTGA AACATTTCTT GCTGGTCTAA TTGATTCTGA TGGCTATGTT
+1    Thr Asp Glu His Gly Ile Lys Ala Thr Ile Lys Thr Ile His Thr Ser Val Arg Asp Gly
1201  ACTGATGAGC ATGGTATTAA AGCAACAATA AAGACAATTC ATACTTCTGT CAGAGATGGT
```

piNOSCBD-intein (con't - 2)

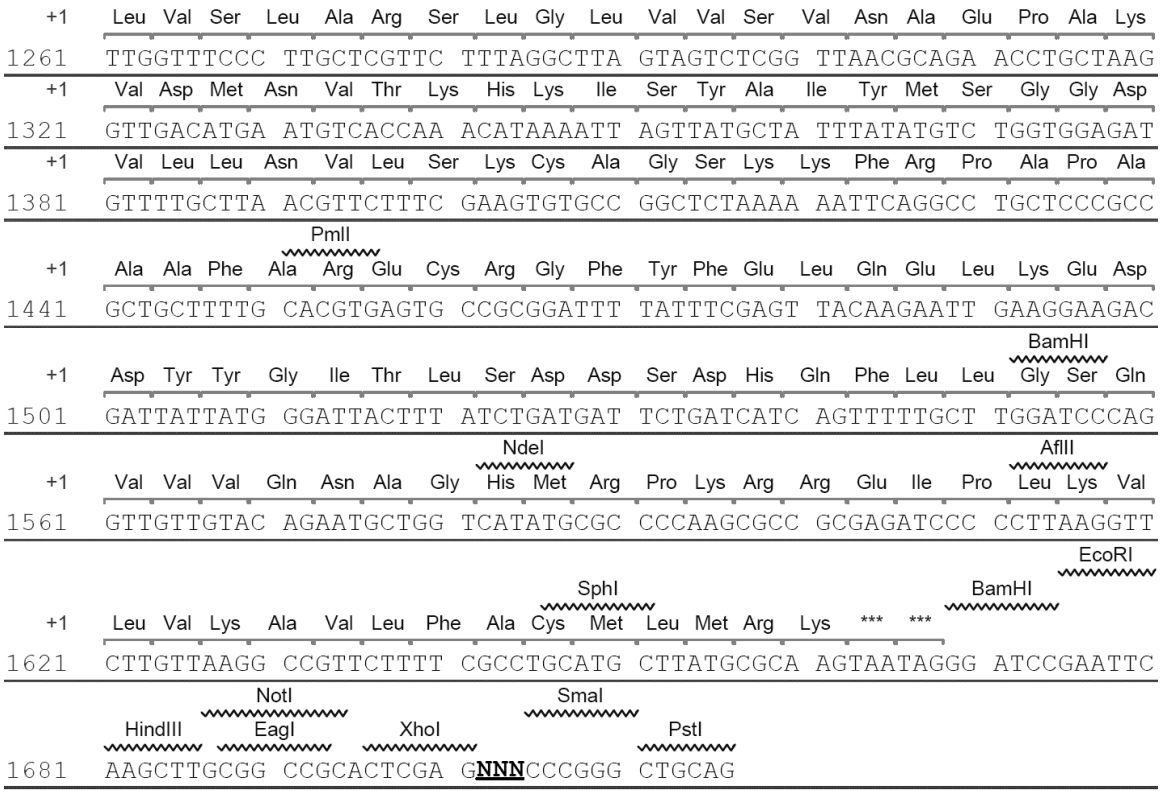

pnNOSCBD-intein – nNOS CaM-binding domain-intein fusion protein in pTYB12 (Amp^r)
– cloned between *Nde*I and *Pst*I

Note: **NNN** represents ~1200 extra bp that were required for cloning of this construct

```
+1    Met Lys Ile Glu Glu Gly Lys Leu Val Ile Gly Ser Leu Glu Gly Cys Phe Ala Lys Gly
1     ATGAAAATCG AAGAAGGTAA ACTGGTAATC GGTTCCCTGG AGGGTTGCTT TGCCAAGGGT
+1    Thr Asn Val Leu Met Ala Asp Gly Ser Ile Glu Cys Ile Glu Asn Ile Glu Val Gly Asn
61    ACCAATGTTT TAATGGCGGA TGGGTCTATT GAATGTATTG AAAACATTGA GGTTGGTAAT
+1    Lys Val Met Gly Lys Asp Gly Arg Pro Arg Glu Val Ile Lys Leu Pro Arg Gly Arg Glu
121   AAGGTCATGG GTAAAGATGG CAGACCTCGT GAGGTAATTA AATTGCCCAG AGGAAGAGAA
+1    Thr Met Tyr Ser Val Val Gln Lys Ser Gln His Arg Ala His Lys Ser Asp Ser Ser Arg
181   ACTATGTACA GCGTCGTGCA GAAAAGTCAG CACAGAGCCC ACAAAAGTGA CTCAAGTCGT
+1    Glu Val Pro Glu Leu Leu Lys Phe Thr Cys Asn Ala Thr His Glu Leu Val Val Arg Thr
241   GAAGTGCCAG AATTACTCAA GTTTACGTGT AATGCGACCC ATGAGTTGGT TGTTAGAACA
+1    Pro Arg Ser Val Arg Arg Leu Ser Arg Thr Ile Lys Gly Val Glu Tyr Phe Glu Val Ile
301   CCTCGTAGTG TCCGCCGTTT GTCTCGTACC ATTAAGGGTG TCGAATATTT TGAAGTTATT
+1    Thr Phe Glu Met Gly Gln Lys Lys Ala Pro Asp Gly Arg Ile Val Glu Leu Val Lys Glu
361   ACTTTTGAGA TGGGCCAAAA GAAAGCCCCC GACGGTAGAA TTGTTGAGCT TGTCAAGGAA
+1    Val Ser Lys Ser Tyr Pro Ile Ser Glu Gly Pro Glu Arg Ala Asn Glu Leu Val Glu Ser
421   GTTTCAAAGA GCTACCCAAT ATCTGAGGGG CCTGAGAGAG CCAACGAATT AGTAGAATCC
                                HindIII                                   BglII
+1    Tyr Arg Lys Ala Ser Asn Lys Ala Tyr Phe Glu Trp Thr Ile Glu Ala Arg Asp Leu Ser
481   TATAGAAAGG CTTCAAATAA AGCTTATTTT GAGTGGACTA TTGAGGCCAG AGATCTTTCT
+1    Leu Leu Gly Ser His Val Arg Lys Ala Thr Tyr Gln Thr Tyr Ala Pro Ile Leu Tyr Glu
541   CTGTTGGGTT CCCATGTTCG TAAAGCTACC TACCAGACTT ACGCTCCAAT TCTTTATGAG
+1    Asn Asp His Phe Phe Asp Tyr Met Gln Lys Ser Lys Phe His Leu Thr Ile Glu Gly Pro
601   AATGACCACT TTTTCGACTA CATGCAAAAA AGTAAGTTTC ATCTCACCAT TGAAGGTCCA
+1    Lys Val Leu Ala Tyr Leu Leu Gly Leu Trp Ile Gly Asp Gly Leu Ser Asp Arg Ala Thr
661   AAAGTACTTG CTTATTTACT TGGTTTATGG ATTGGTGATG GATTGTCTGA CAGGGCAACT
+1    Phe Ser Val Asp Ser Arg Asp Thr Ser Leu Met Glu Arg Val Thr Glu Tyr Ala Glu Lys
721   TTTTCGGTTG ATTCCAGAGA TACTTCTTTG ATGGAACGTG TTACTGAATA TGCTGAAAAG
+1    Leu Asn Leu Cys Ala Glu Tyr Lys Asp Arg Lys Glu Pro Gln Val Ala Lys Thr Val Asn
781   TTGAATTTGT GCGCCGAGTA TAAGGACAGA AAAGAACCAC AAGTTGCCAA AACTGTTAAT
                                    NheI
+1    Leu Tyr Ser Lys Val Val Arg Gly Ala Ser Thr Asn Pro Gly Val Ser Ala Trp Gln Val
841   TTGTACTCTA AAGTTGTCAG AGGTGCTAGC ACAAATCCTG GTGTATCCGC TTGGCAGGTC
                                  MunI
+1    Asn Thr Ala Tyr Thr Ala Gly Gln Leu Val Thr Tyr Asn Gly Lys Thr Tyr Lys Cys Leu
901   AACACAGCTT ATACTGCGGG ACAATTGGTC ACATATAACG GCAAGACGTA TAAATGTTTG
+1    Gln Pro His Thr Ser Leu Ala Gly Trp Glu Pro Ser Asn Val Pro Ala Leu Trp Gln Leu
961   CAGCCCCACA CCTCCTTGGC AGGATGGGAA CCATCCAACG TTCCTGCCTT GTGGCAGCTT
                NcoI
+1    Gln Gly Gly His Gly Gly Ile Arg Asn Asn Leu Asn Thr Glu Asn Pro Leu Trp Asp Ala
1021  CAAGGTGGCC ATGGTGGTAT TCGCAATAAT CTTAATACTG AGAATCCATT ATGGGACGCT
+1    Ile Val Gly Leu Gly Phe Leu Lys Asp Gly Val Lys Asn Ile Pro Ser Phe Leu Ser Thr
1081  ATTGTTGGCT TAGGATTCTT GAAGGACGGT GTCAAAAATA TTCCTTCTTT CTTGTCTACG
+1    Asp Asn Ile Gly Thr Arg Glu Thr Phe Leu Ala Gly Leu Ile Asp Ser Asp Gly Tyr Val
1141  GACAATATCG GTACTCGTGA AACATTTCTT GCTGGTCTAA TTGATTCTGA TGGCTATGTT
+1    Thr Asp Glu His Gly Ile Lys Ala Thr Ile Lys Thr Ile His Thr Ser Val Arg Asp Gly
1201  ACTGATGAGC ATGGTATTAA AGCAACAATA AAGACAATTC ATACTTCTGT CAGAGATGGT
```

pnNOSCBD-intein (con't - 2)

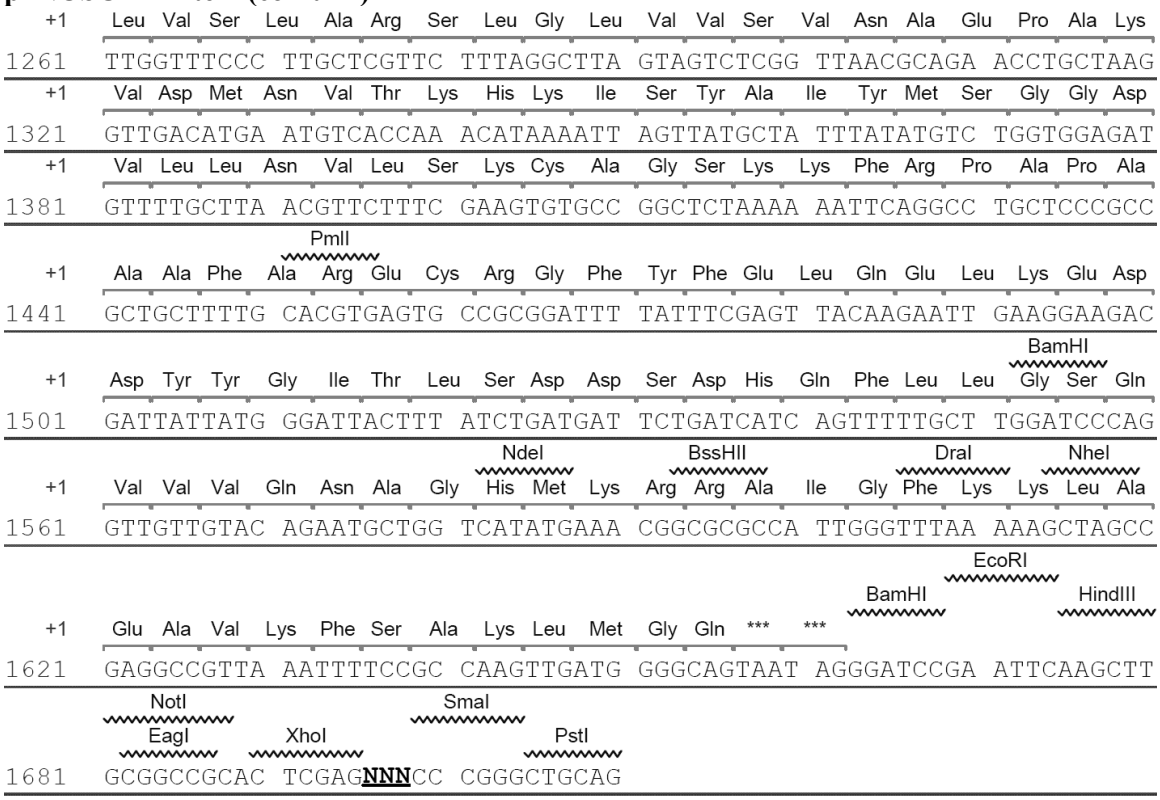

peNOSCBD-intein – eNOS CaM-binding domain-intein fusion protein in pTYB12 (Amp^r)
– cloned between *Nde*I and *Pst*I

Note: **NNN** represents ~1200 extra bp that were required for cloning of this construct

```
+1    Met Lys Ile Glu Glu Gly Lys Leu Val Ile Gly Ser Leu Glu Gly Cys Phe Ala Lys Gly
1     ATGAAAATCG AAGAAGGTAA ACTGGTAATC GGTTCCCTGG AGGGTTGCTT TGCCAAGGGT
+1    Thr Asn Val Leu Met Ala Asp Gly Ser Ile Glu Cys Ile Glu Asn Ile Glu Val Gly Asn
61    ACCAATGTTT TAATGGCGGA TGGGTCTATT GAATGTATTG AAAACATTGA GGTTGGTAAT
+1    Lys Val Met Gly Lys Asp Gly Arg Pro Arg Glu Val Ile Lys Leu Pro Arg Gly Arg Glu
121   AAGGTCATGG GTAAAGATGG CAGACCTCGT GAGGTAATTA AATTGCCCAG AGGAAGAGAA
+1    Thr Met Tyr Ser Val Val Gln Lys Ser Gln His Arg Ala His Lys Ser Asp Ser Ser Arg
181   ACTATGTACA GCGTCGTGCA GAAAAGTCAG CACAGAGCCC ACAAAAGTGA CTCAAGTCGT
+1    Glu Val Pro Glu Leu Leu Lys Phe Thr Cys Asn Ala Thr His Glu Leu Val Val Arg Thr
241   GAAGTGCCAG AATTACTCAA GTTTACGTGT AATGCGACCC ATGAGTTGGT TGTTAGAACA
+1    Pro Arg Ser Val Arg Arg Leu Ser Arg Thr Ile Lys Gly Val Glu Tyr Phe Glu Val Ile
301   CCTCGTAGTG TCCGCCGTTT GTCTCGTACC ATTAAGGGTG TCGAATATTT TGAAGTTATT
+1    Thr Phe Glu Met Gly Gln Lys Lys Ala Pro Asp Gly Arg Ile Val Glu Leu Val Lys Glu
361   ACTTTTGAGA TGGGCCAAAA GAAAGCCCCC GACGGTAGAA TTGTTGAGCT TGTCAAGGAA
+1    Val Ser Lys Ser Tyr Pro Ile Ser Glu Gly Pro Glu Arg Ala Asn Glu Leu Val Glu Ser
421   GTTTCAAAGA GCTACCCAAT ATCTGAGGGG CCTGAGAGAG CCAACGAATT AGTAGAATCC
                                HindIII                                   BglII
+1    Tyr Arg Lys Ala Ser Asn Lys Ala Tyr Phe Glu Trp Thr Ile Glu Ala Arg Asp Leu Ser
481   TATAGAAAGG CTTCAAATAA AGCTTATTTT GAGTGGACTA TTGAGGCCAG AGATCTTTCT
+1    Leu Leu Gly Ser His Val Arg Lys Ala Thr Tyr Gln Thr Tyr Ala Pro Ile Leu Tyr Glu
541   CTGTTGGGTT CCCATGTTCG TAAAGCTACC TACCAGACTT ACGCTCCAAT TCTTTATGAG
+1    Asn Asp His Phe Phe Asp Tyr Met Gln Lys Ser Lys Phe His Leu Thr Ile Glu Gly Pro
601   AATGACCACT TTTTCGACTA CATGCAAAAA AGTAAGTTTC ATCTCACCAT TGAAGGTCCA
+1    Lys Val Leu Ala Tyr Leu Leu Gly Leu Trp Ile Gly Asp Gly Leu Ser Asp Arg Ala Thr
661   AAAGTACTTG CTTATTTACT TGGTTTATGG ATTGGTGATG GATTGTCTGA CAGGGCAACT
+1    Phe Ser Val Asp Ser Arg Asp Thr Ser Leu Met Glu Arg Val Thr Glu Tyr Ala Glu Lys
721   TTTTCGGTTG ATTCCAGAGA TACTTCTTTG ATGGAACGTG TTACTGAATA TGCTGAAAAG
+1    Leu Asn Leu Cys Ala Glu Tyr Lys Asp Arg Lys Glu Pro Gln Val Ala Lys Thr Val Asn
781   TTGAATTTGT GCGCCGAGTA TAAGGACAGA AAAGAACCAC AAGTTGCCAA AACTGTTAAT
                                    NheI
+1    Leu Tyr Ser Lys Val Val Arg Gly Ala Ser Thr Asn Pro Gly Val Ser Ala Trp Gln Val
841   TTGTACTCTA AAGTTGTCAG AGGTGCTAGC ACAAATCCTG GTGTATCCGC TTGGCAGGTC
                                  MunI
+1    Asn Thr Ala Tyr Thr Ala Gly Gln Leu Val Thr Tyr Asn Gly Lys Thr Tyr Lys Cys Leu
901   AACACAGCTT ATACTGCGGG ACAATTGGTC ACATATAACG GCAAGACGTA TAAATGTTTG
+1    Gln Pro His Thr Ser Leu Ala Gly Trp Glu Pro Ser Asn Val Pro Ala Leu Trp Gln Leu
961   CAGCCCCACA CCTCCTTGGC AGGATGGGAA CCATCCAACG TTCCTGCCTT GTGGCAGCTT
                NcoI
+1    Gln Gly Gly His Gly Gly Ile Arg Asn Asn Leu Asn Thr Glu Asn Pro Leu Trp Asp Ala
1021  CAAGGTGGCC ATGGTGGTAT TCGCAATAAT CTTAATACTG AGAATCCATT ATGGGACGCT
+1    Ile Val Gly Leu Gly Phe Leu Lys Asp Gly Val Lys Asn Ile Pro Ser Phe Leu Ser Thr
1081  ATTGTTGGCT TAGGATTCTT GAAGGACGGT GTCAAAAATA TTCCTTCTTT CTTGTCTACG
+1    Asp Asn Ile Gly Thr Arg Glu Thr Phe Leu Ala Gly Leu Ile Asp Ser Asp Gly Tyr Val
1141  GACAATATCG GTACTCGTGA AACATTTCTT GCTGGTCTAA TTGATTCTGA TGGCTATGTT
+1    Thr Asp Glu His Gly Ile Lys Ala Thr Ile Lys Thr Ile His Thr Ser Val Arg Asp Gly
1201  ACTGATGAGC ATGGTATTAA AGCAACAATA AAGACAATTC ATACTTCTGT CAGAGATGGT
```

peNOSCBD-intein (con't - 2)

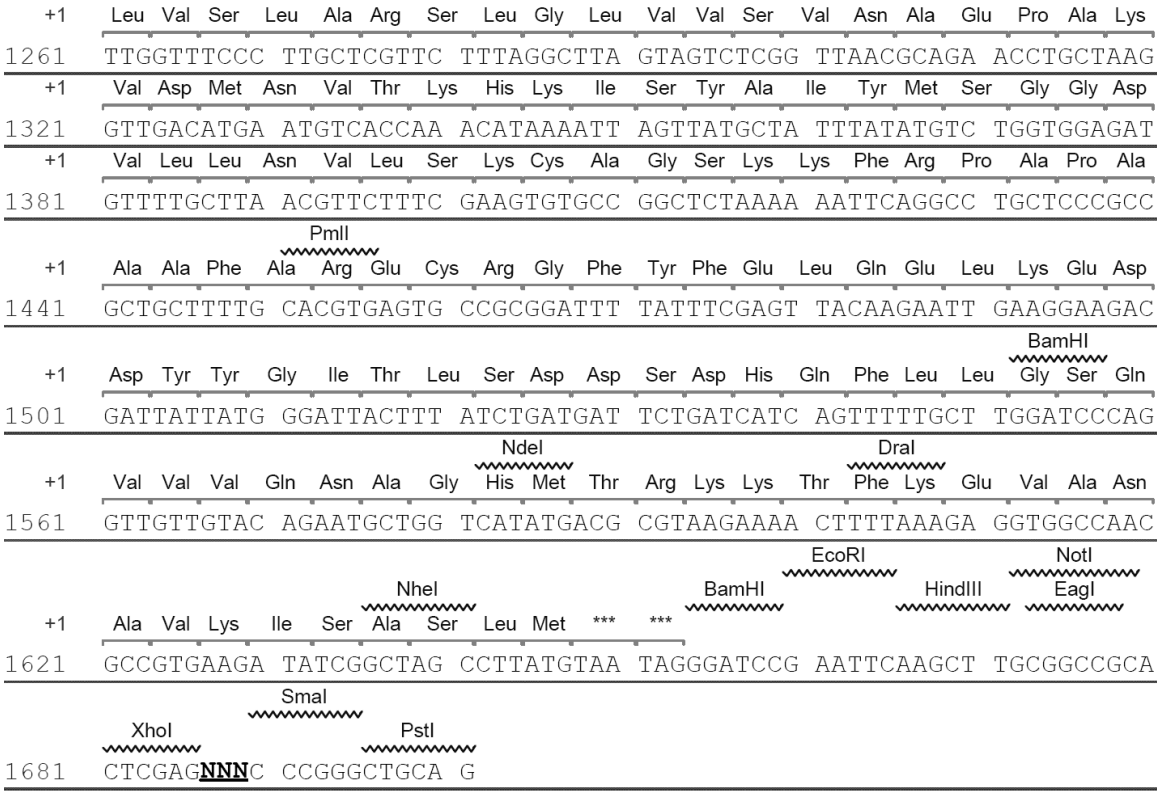

Appendix A – CaM and NOS DNA Sequences

Primers used for NOS Sequencing:

The following primers were used to sequence the entire open reading frames of the NOS enzymes in pCWOri before and after mutagenesis at intervals of ~500 bp (Section 6.3.2.3).

For Human iNOS:

pCWOri-fr	5' TCGGCTCGTATAATGTGTGG 3'
505iNOSfr	5' TTCACCATAAGGCCAAAGGG 3'
1000iNOSfr	5' TCCGCTATGCTGGCTACCAG 3'
1550iNOSfr	5' GAATGAATACCGGTCCCGTG 3'
2002iNOSfr	5' CTGGCAATGGAGAGAAACTG 3'
2501iNOSfr	5' GAACTACCTGCCGGGGGAGC 3'
3069iNOSfr	5' GACCCAGTGCCCTGCTTTGTGC 3'
3496iNOSfr	5' AGCTGGTGGCTGCCAAGCTG 3'

For Rat nNOS:

pCWOri-fr	5’ TCGGCTCGTATAATGTGTGG 3’
432nNOSrv	5’ CCATTACCCAGACCTGTGAC 3’
303nNOSfr	5’ GGGCTTCACTACACATCTGG 3’
778nNOSfr	5’ ATGACCTGTGGGGGAAGGAC 3’
1334nNOSfr	5’ ATGTCAAGTATGCCACCAAC 3’
1820nNOSfr	5’ TGGAGGAAGTAGCCAAGAAG 3’
2422nNOSfr	5’ ACCTTTGGCAATGGAGACCC 3’
2945nNOSfr	5’ AAGGTCTTTCCAATGTTCAC 3’
3411nNOSfr	5’ GTGGAAGTGGGGCAAGAACC 3’
3903nNOSfr	5’ CAAGGGCGTCTTCAGAGAGC 3’
4200nNOSfr	5’ AACGTATGAAGTGACCAACC 3’

For Bovine eNOS:

pCWOri-fr	5’ TCGGCTCGTATAATGTGTGG 3’
93eNOSrv	5’ CCGAACACCAGCTCACTCTC 3’
292eNOSfr	5’ GACCTCCACCCGCTGAGCAG 3’
777eNOSfr	5’ AACATGCTGCTGGAAATCGG 3’
1295eNOSfr	5’ GAGAATGGAGAGAGTTTTGC 3’
1762eNOSfr	5’ GGGACCACATAGGCATCTGC 3’
2263eNOSfr	5’ GATTTTGGCAGGAGAGGCTG 3’
2364eNOSfr	5’ TGCCCGCCCCGCTGCTCCTC 3’
2690eNOSfr	5’ GAGAGGGGCTGTCATTCCAC 3’

NOTE: For clarify purposes, the sites where these primers anneal are shown in the following NOS sequences.

pΔ70iNOShisAmp – Human Δ70iNOS with N-terminal polyhistidine tag in pCWOri
– cloned between *Nde*I and *Hind*III

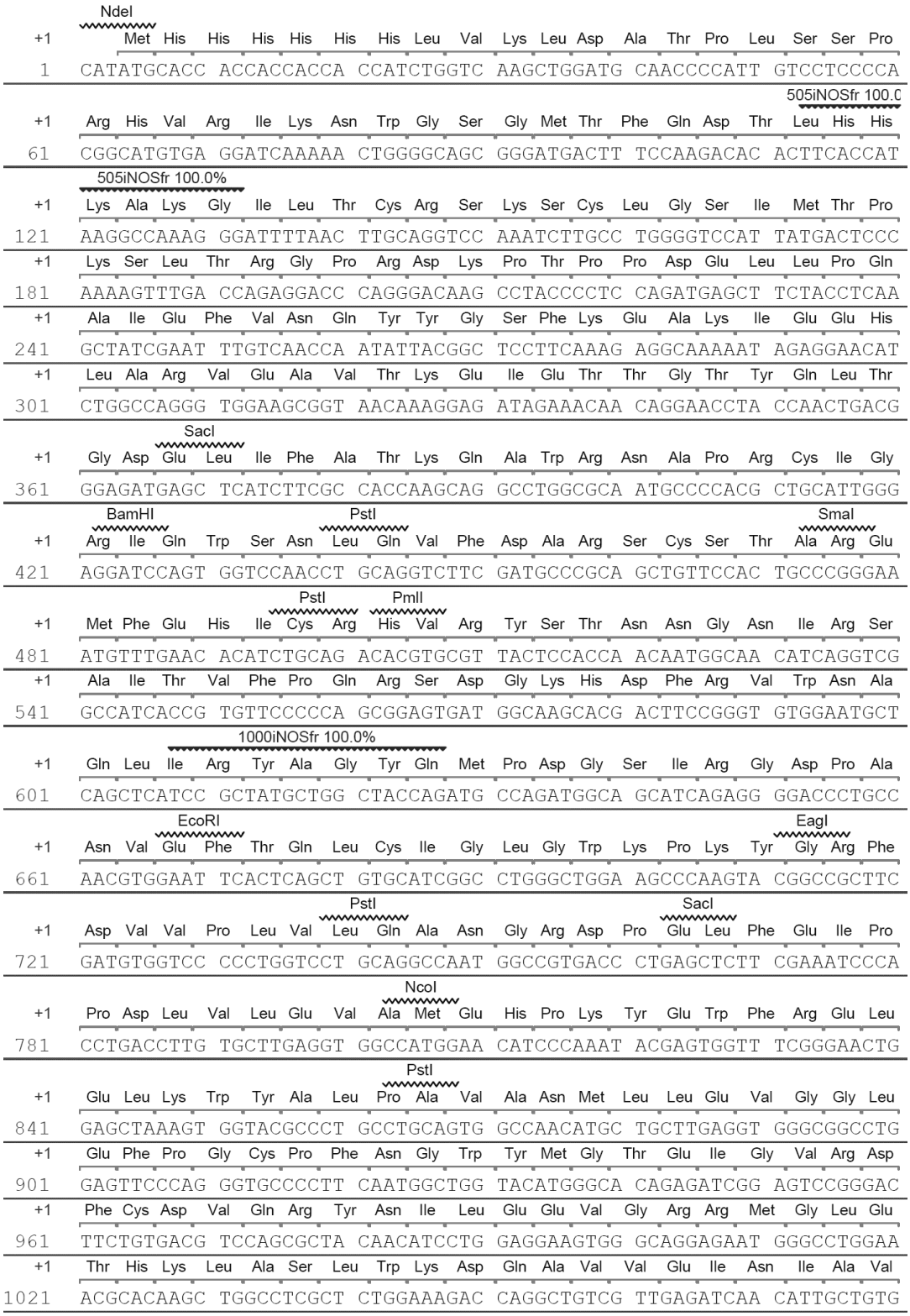

pΔ70iNOShisAmp (con't - 2)

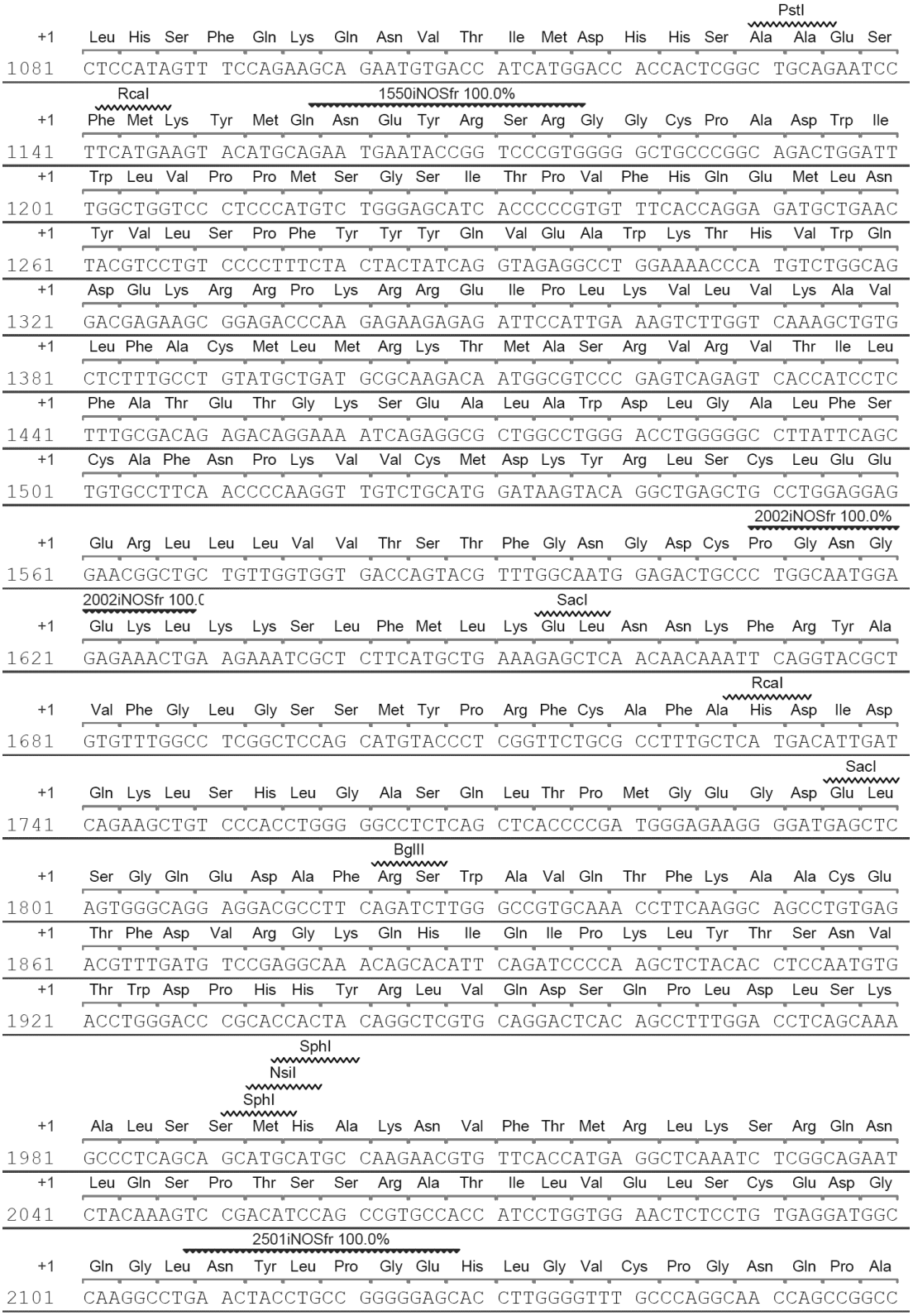

pΔ70iNOShisAmp (con't - 3)

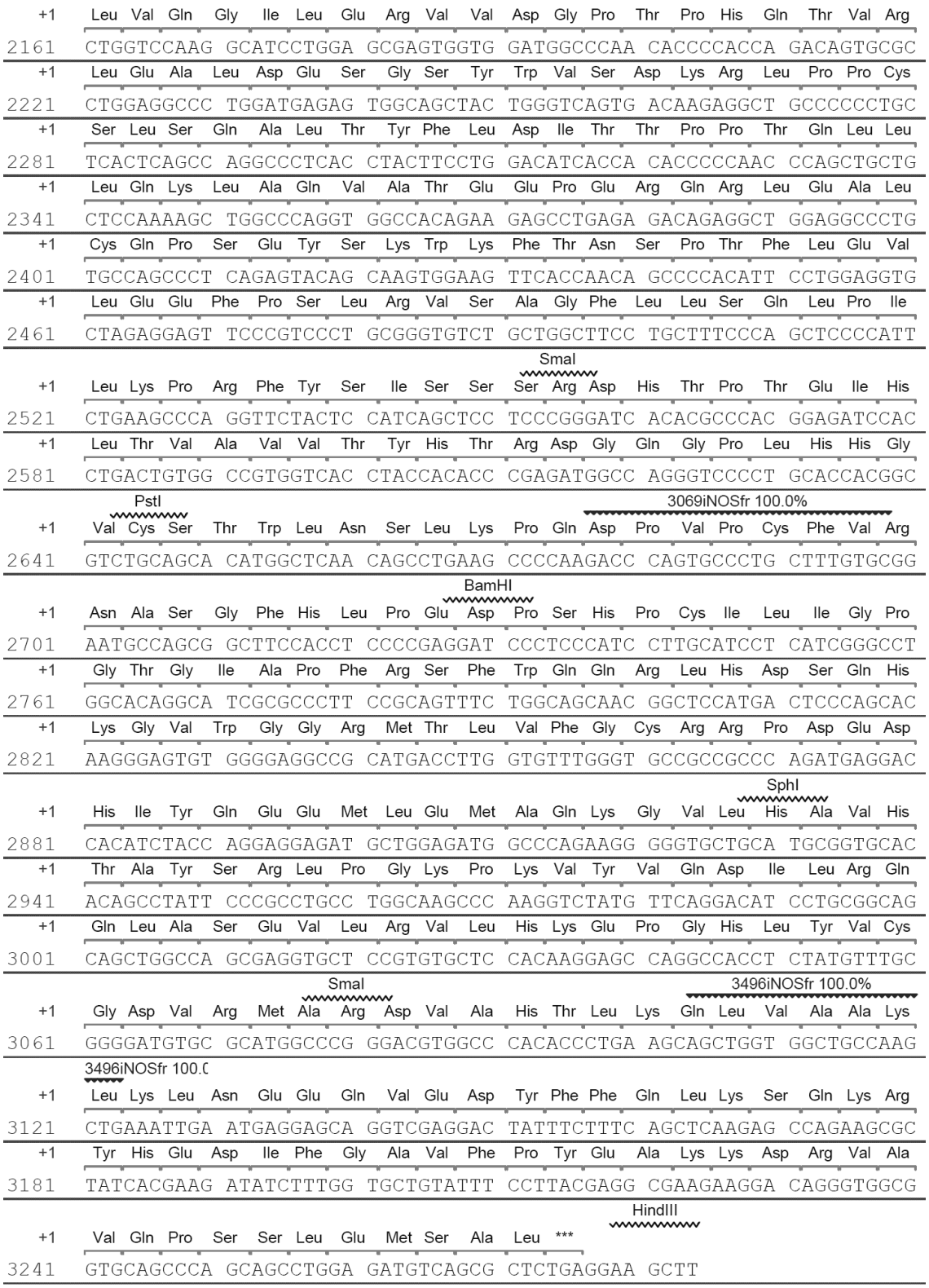

Appendix A – CaM and NOS DNA Sequences

pnNOShisAmp – Rat nNOS with N-terminal polyhistidine tag in pCWOri

– cloned between *Nde*I and *Bam*HI

Note: Mutations relative to Pubmed sequence: I269V and P959A (found in human nNOS) and F1014S

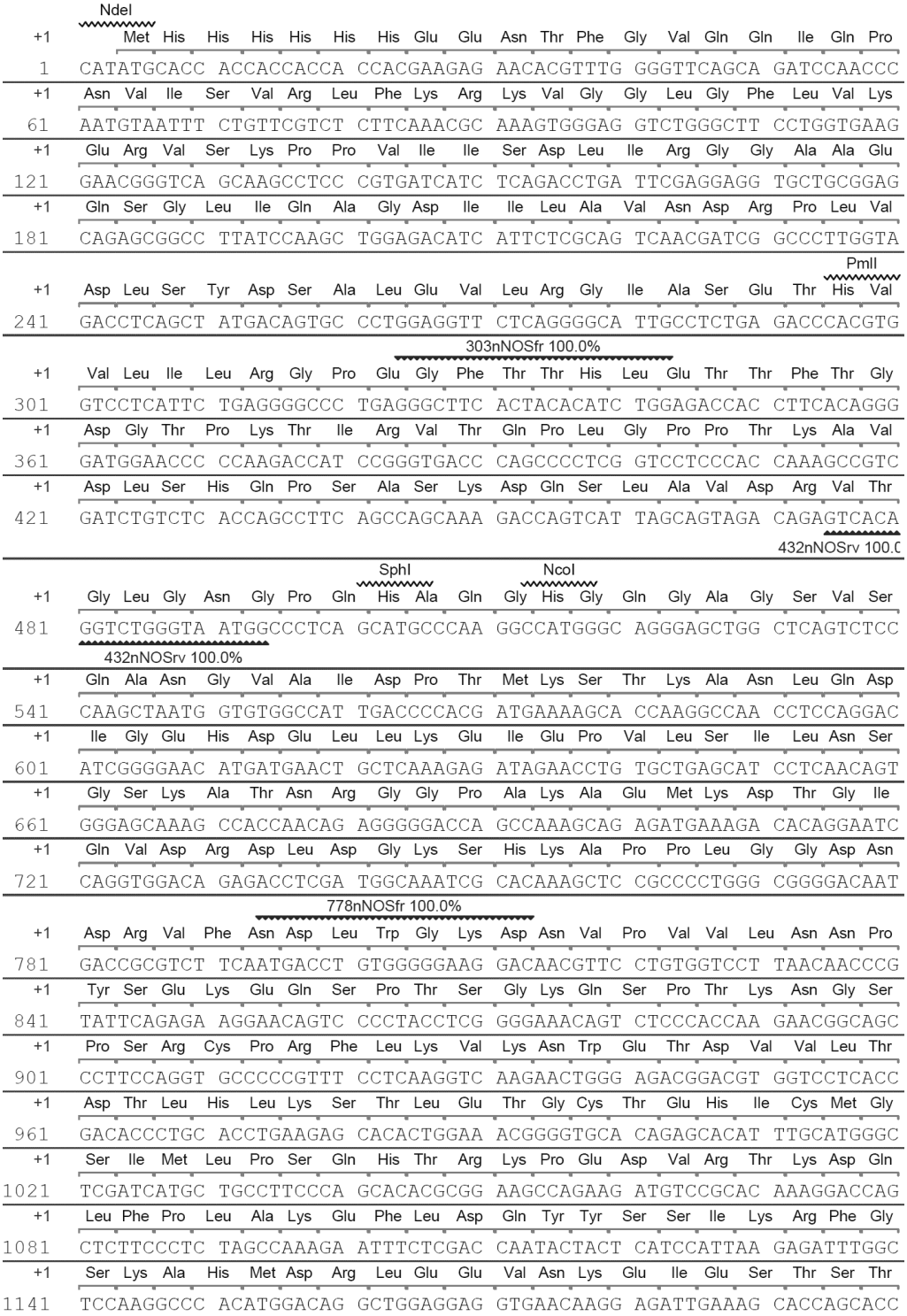

pnNOShisAmp (con't - 2)

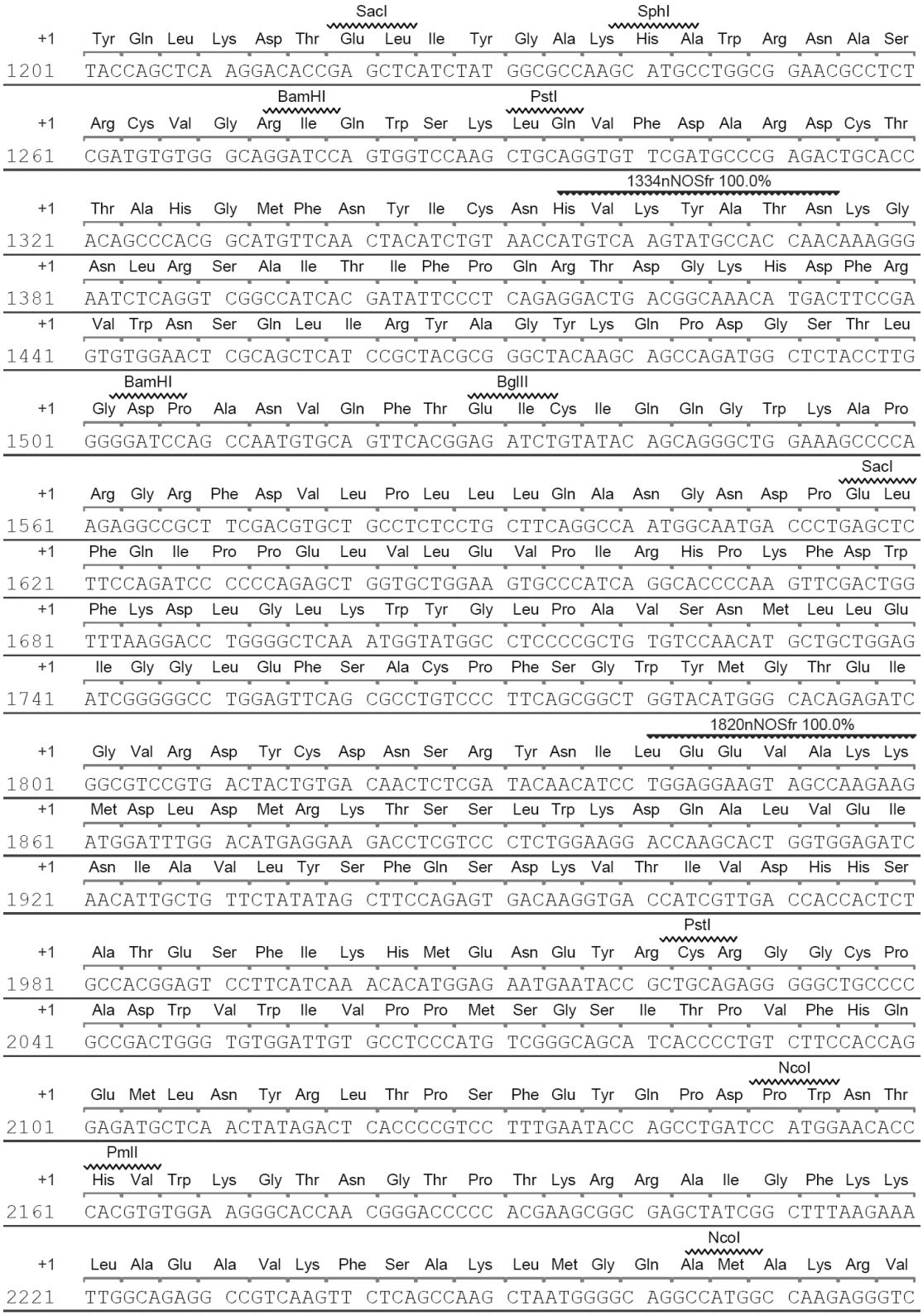

pnNOShisAmp (con't - 3)

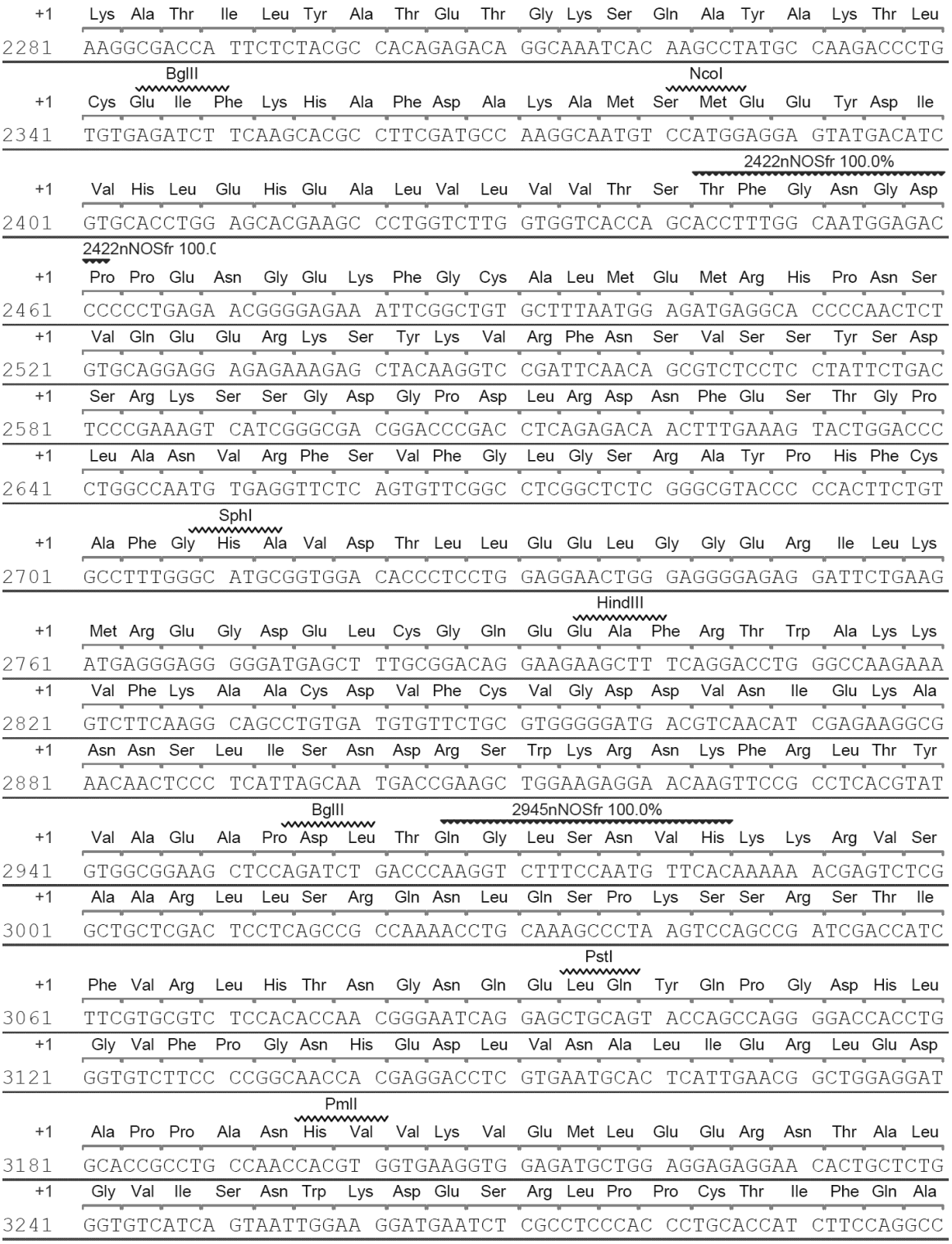

pnNOShisAmp (con't - 4)

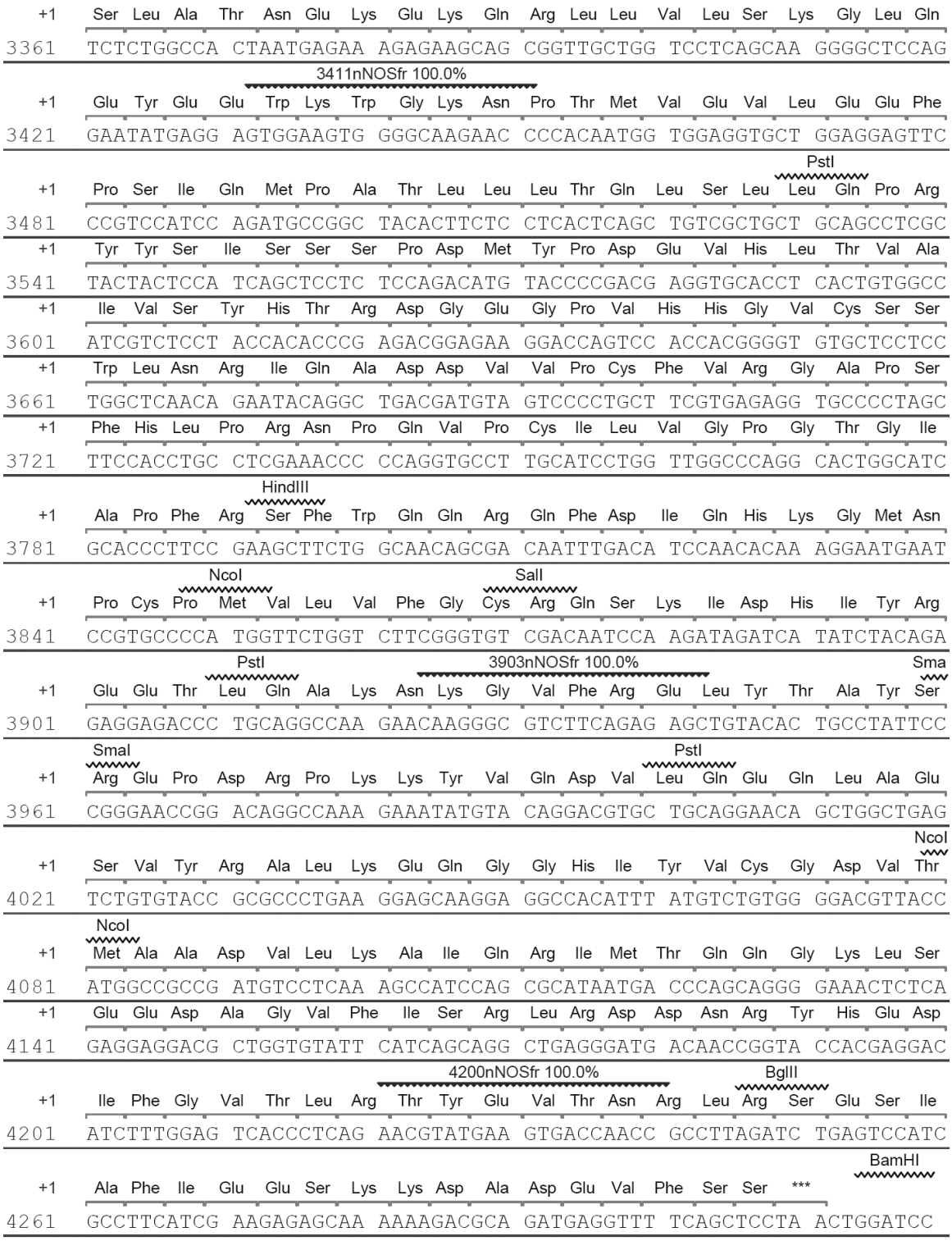

peNOShisAmp – Bovine NOS with N-terminal polyhistidine tag in pCWOri

– cloned between *Nde*I and *Eco*RI with upstream polyhistidine tag

Note: Mutations relative to Pubmed sequence: C109R and T750A

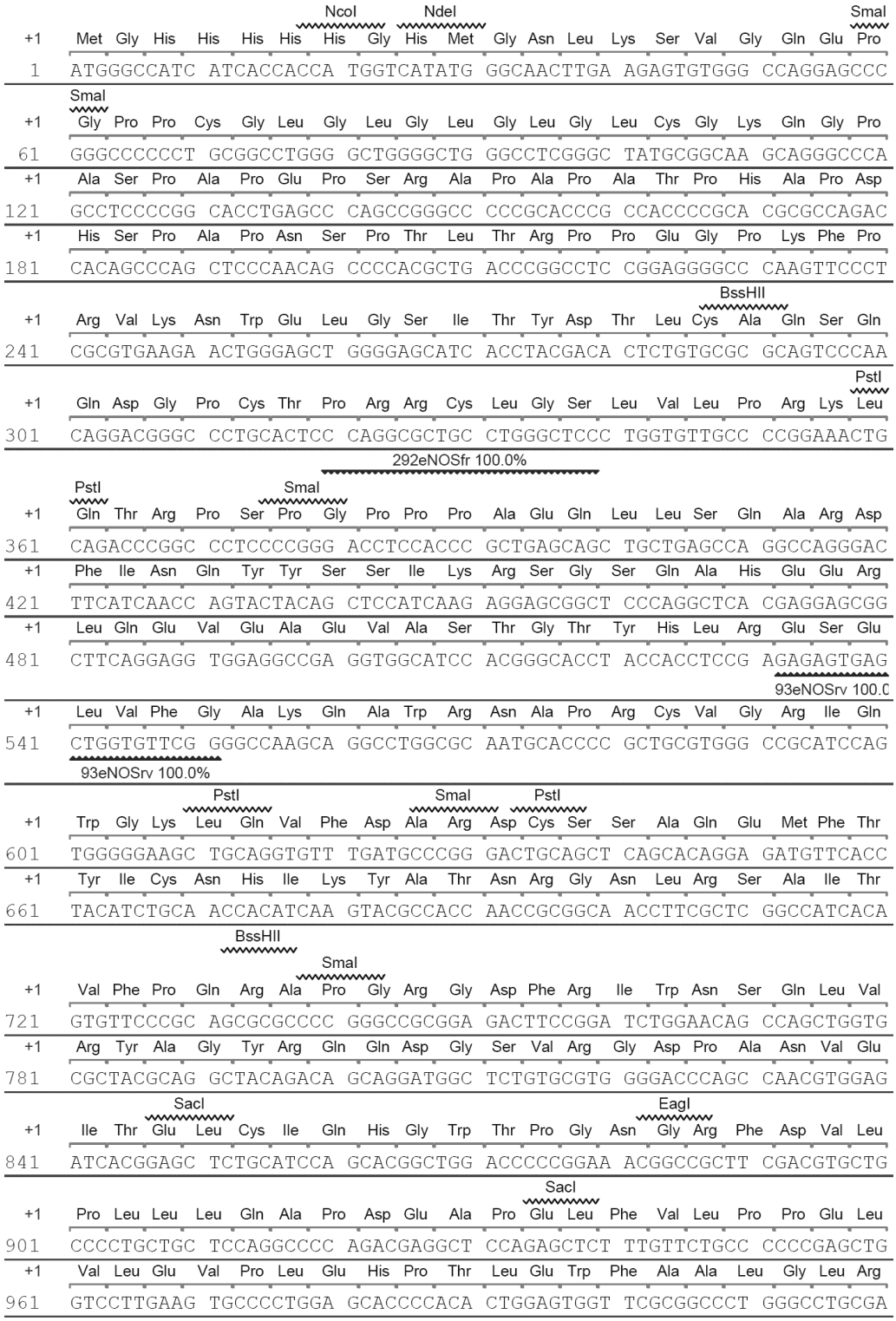

peNOShisAmp (con't - 2)

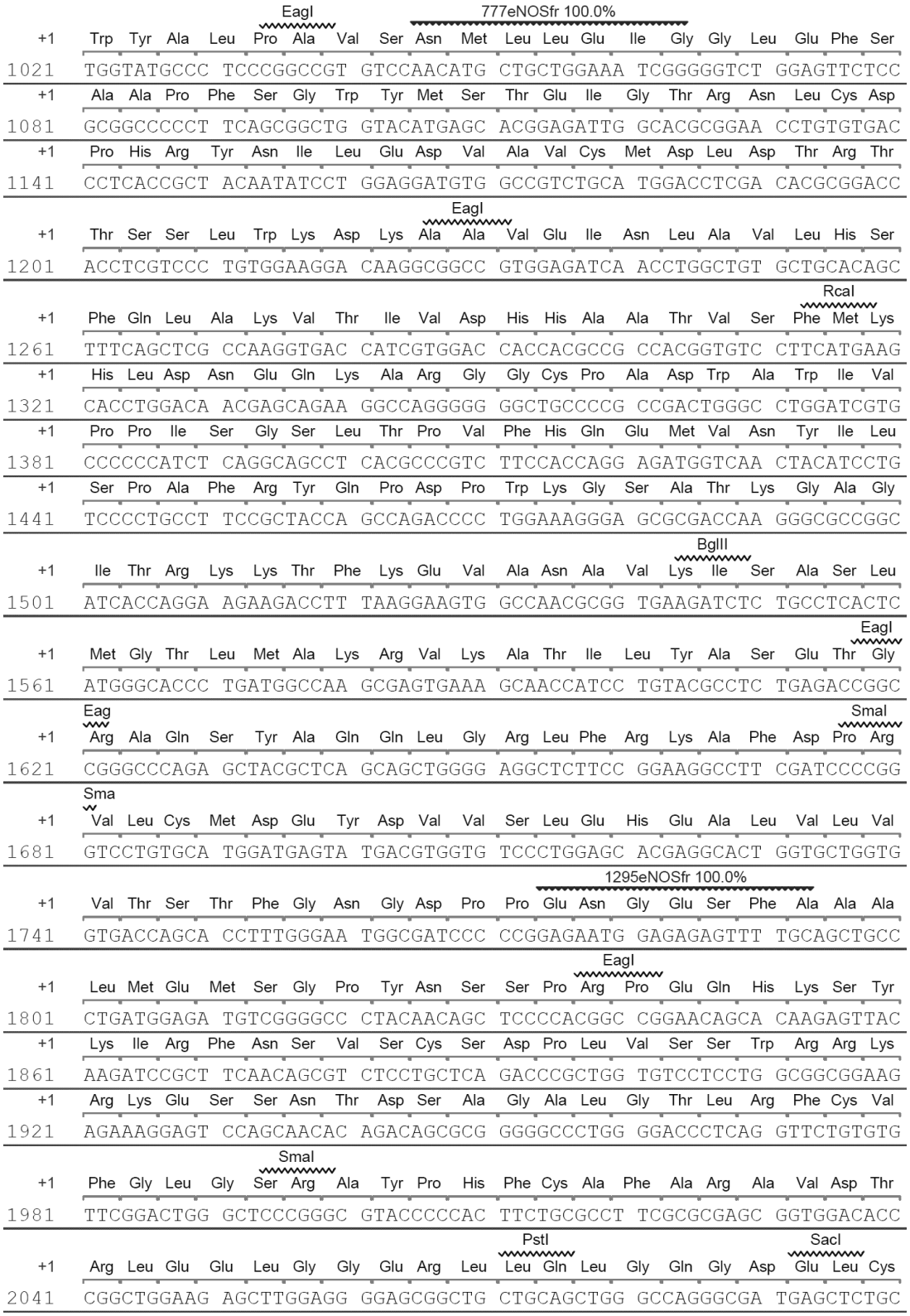

peNOShisAmp (con't - 3)

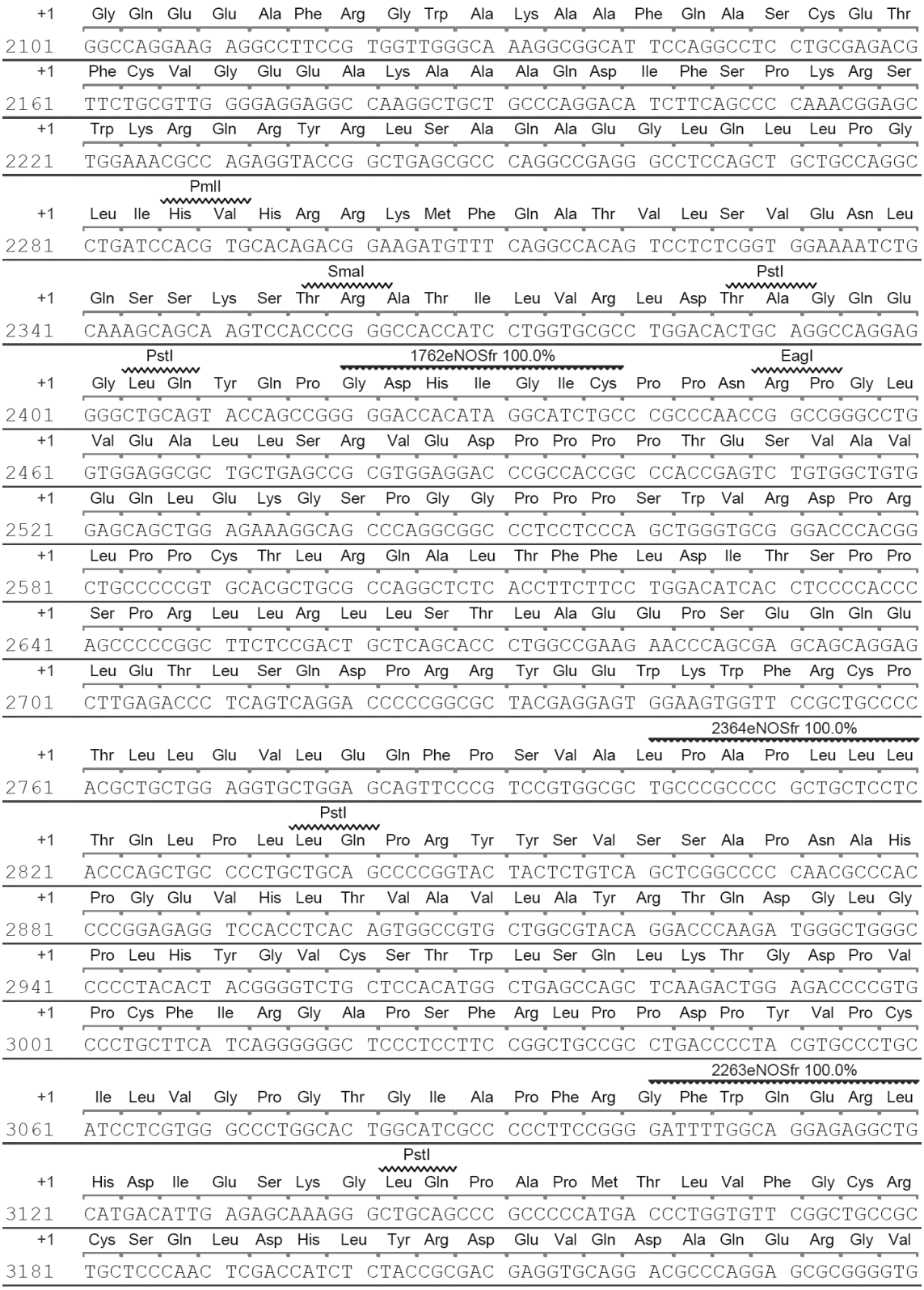

peNOShisAmp (con't - 4)

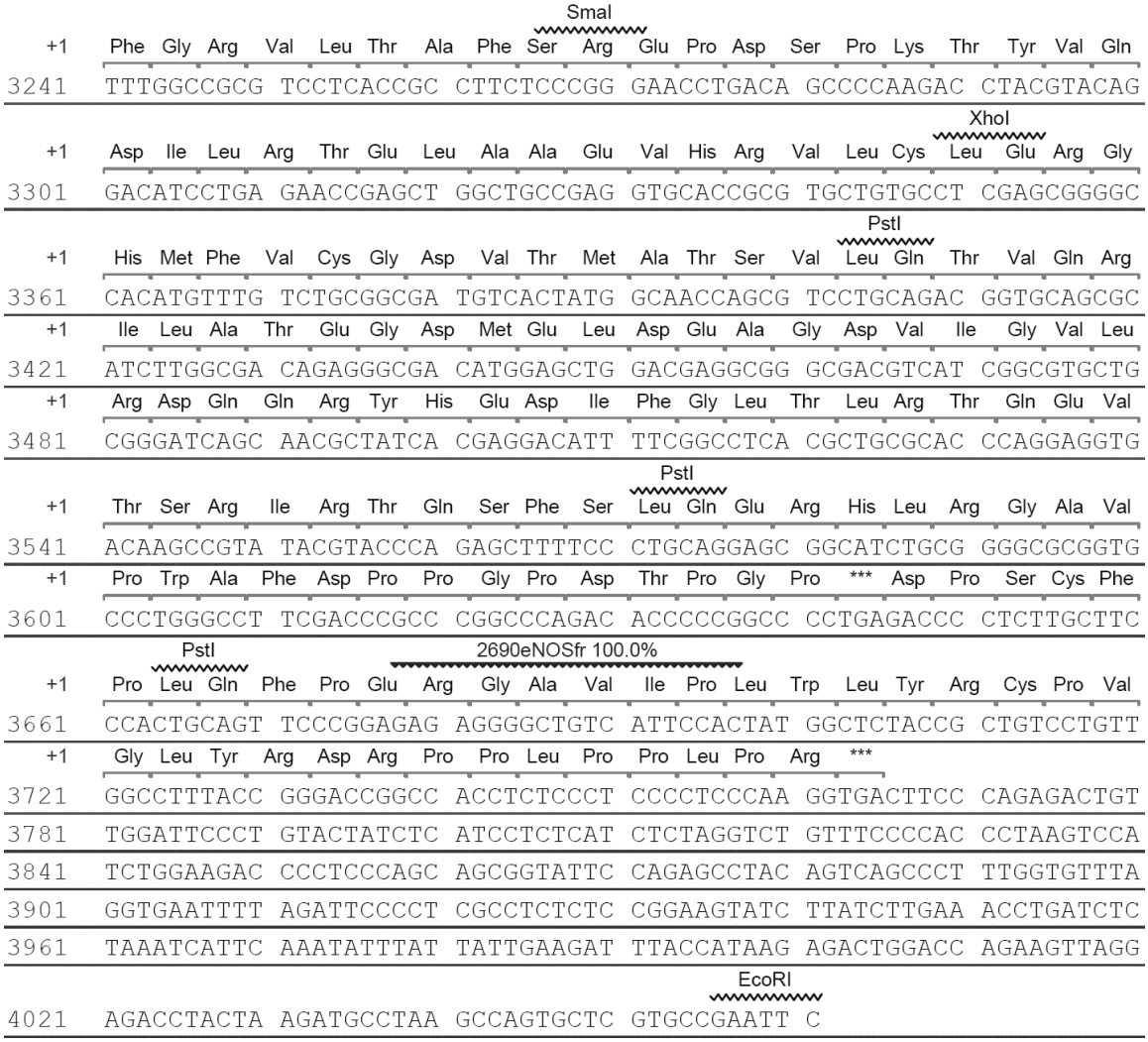

pCWOri-iNOSC200A – Human Δ70iNOS C200A with N-terminal polyhistidine tag in pΔ70iNOShisAmp – produced by incorporating Ala at codon 200 by mutagenesis (*Xho*I reporter site)

Note: Only showing region of iNOS with mutation – rest of sequence shown in pΔ70iNOShisAmp

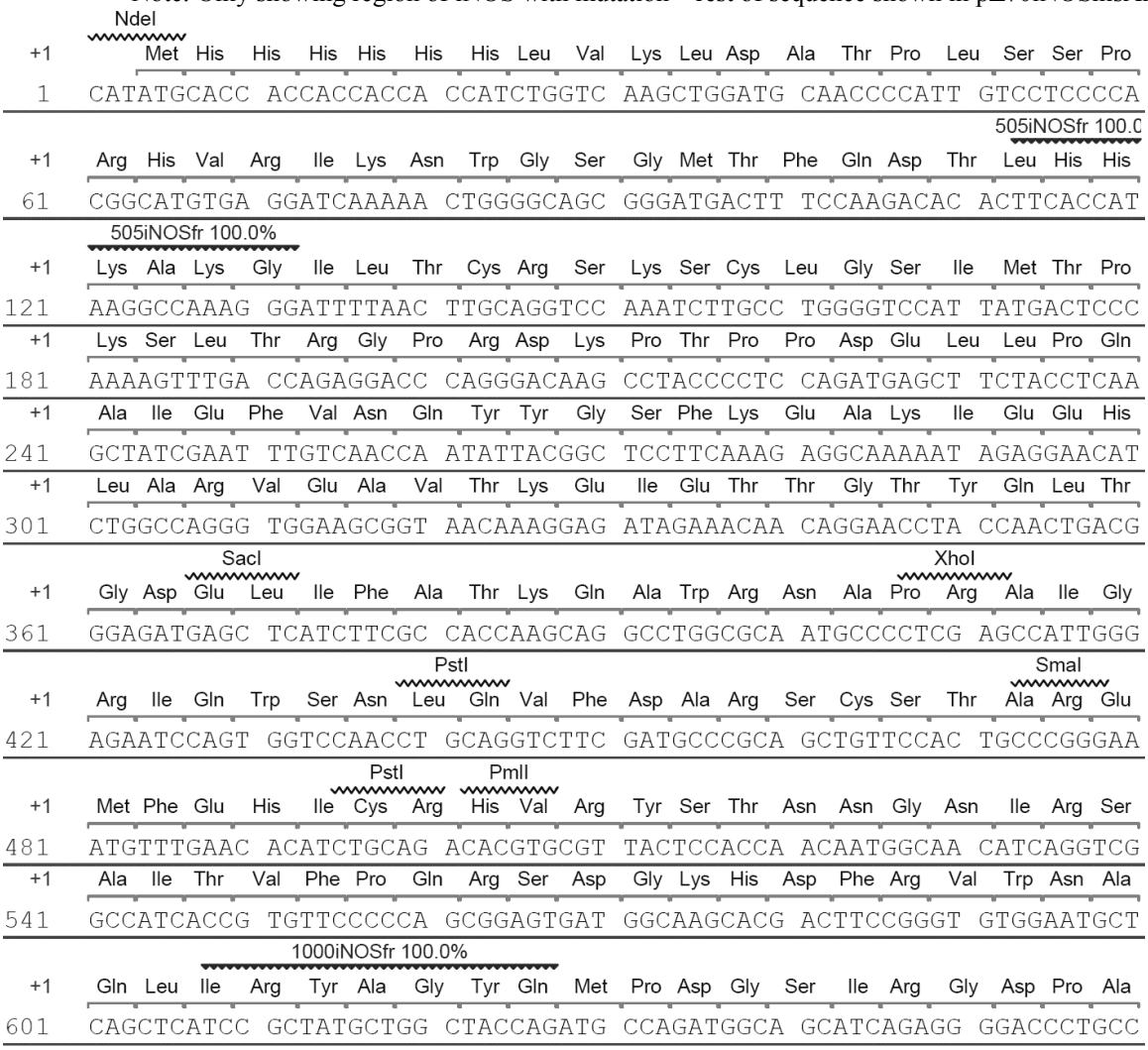

pCWOri-nNOSC415A – Rat nNOS C415A with N-terminal polyhistidine tag in pnNOShisAmp – produced by incorporating Ala at codon 415 by mutagenesis (*Xho*I reporter site)

Note: Only showing region of nNOS with mutation – rest of sequence shown in pnNOShisAmp

778nNOSfr 100.0%

```
+1    Asp Arg Val Phe Asn Asp Leu Trp Gly Lys Asp Asn Val Pro Val Val Leu Asn Asn Pro
781   GACCGCGTCT TCAATGACCT GTGGGGGAAG GACAACGTTC CTGTGGTCCT TAACAACCCG
+1    Tyr Ser Glu Lys Glu Gln Ser Pro Thr Ser Gly Lys Gln Ser Pro Thr Lys Asn Gly Ser
841   TATTCAGAGA AGGAACAGTC CCCTACCTCG GGGAAACAGT CTCCCACCAA GAACGGCAGC
+1    Pro Ser Arg Cys Pro Arg Phe Leu Lys Val Lys Asn Trp Glu Thr Asp Val Val Leu Thr
901   CCTTCCAGGT GCCCCCGTTT CCTCAAGGTC AAGAACTGGG AGACGGACGT GGTCCTCACC
+1    Asp Thr Leu His Leu Lys Ser Thr Leu Glu Thr Gly Cys Thr Glu His Ile Cys Met Gly
961   GACACCCTGC ACCTGAAGAG CACACTGGAA ACGGGGTGCA CAGAGCACAT TTGCATGGGC
+1    Ser Ile Met Leu Pro Ser Gln His Thr Arg Lys Pro Glu Asp Val Arg Thr Lys Asp Gln
1021  TCGATCATGC TGCCTTCCCA GCACACGCGG AAGCCAGAAG ATGTCCGCAC AAAGGACCAG
+1    Leu Phe Pro Leu Ala Lys Glu Phe Leu Asp Gln Tyr Tyr Ser Ser Ile Lys Arg Phe Gly
1081  CTCTTCCCTC TAGCCAAAGA ATTTCTCGAC CAATACTACT CATCCATTAA GAGATTTGGC
+1    Ser Lys Ala His Met Asp Arg Leu Glu Glu Val Asn Lys Glu Ile Glu Ser Thr Ser Thr
1141  TCCAAGGCCC ACATGGACAG GCTGGAGGAG GTGAACAAGG AGATTGAAAG CACCAGCACC
```

SacI, SphI, XhoI

```
+1    Tyr Gln Leu Lys Asp Thr Glu Leu Ile Tyr Gly Ala Lys His Ala Trp Arg Asn Ala Ser
1201  TACCAGCTCA AGGACACCGA GCTCATCTAT GGCGCCAAGC ATGCCTGGCG GAACGCCTCT
```

XhoI, PstI

```
+1    Arg Ala Val Gly Arg Ile Gln Trp Ser Lys Leu Gln Val Phe Asp Ala Arg Asp Cys Thr
1261  CGAGCCGTGG GCAGAATCCA GTGGTCCAAG CTGCAGGTGT TCGATGCCCG AGACTGCACC
```

1334nNOSfr 100.0%

```
+1    Thr Ala His Gly Met Phe Asn Tyr Ile Cys Asn His Val Lys Tyr Ala Thr Asn Lys Gly
1321  ACAGCCCACG GCATGTTCAA CTACATCTGT AACCATGTCA AGTATGCCAC CAACAAAGGG
```

pCWOri-eNOSC186A – Bovine eNOS C186A with N-terminal polyhistidine tag in peNOShisAmp – produced by incorporating Ala at codon 186 by mutagenesis (*Xho*I reporter site)

Note: Only showing region of eNOS with mutation – rest of sequence shown in peNOShisAmp

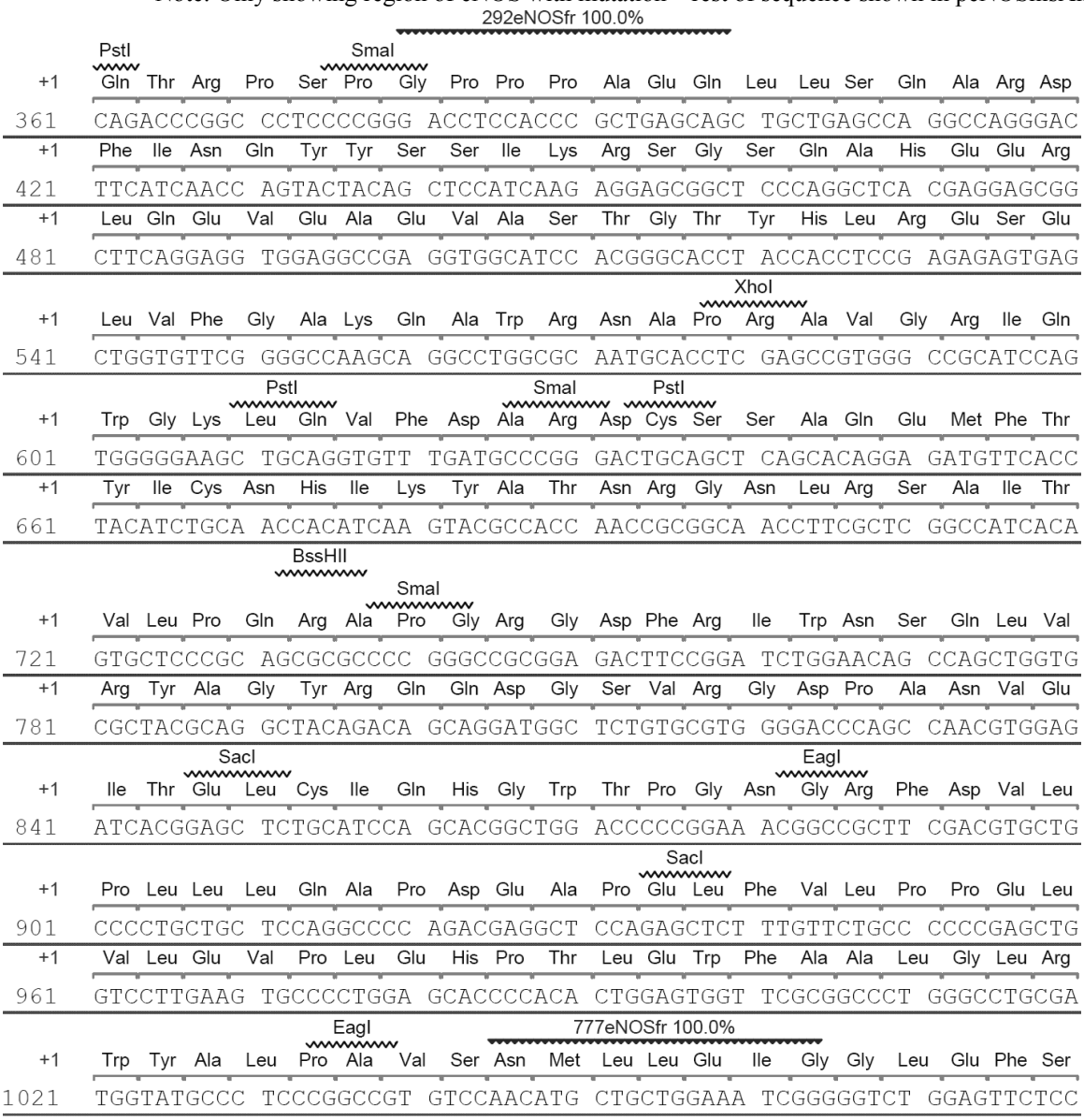

Appendix B – Further FRET Analysis of CaM Binding to NOS Peptides and Enzymes

Upon further analysis of the FRET data tables in Chapter 6 (Tables 6.4-14), it became apparent that two general fluorescence species were observed – a longer lifetime, corresponding to an extended CaM conformation (~4 ns), and a shorter lifetime, representing a compact structure of CaM in complex with the NOS peptides and enzymes (~0.8 ns). In collaboration with Dr. Michael Palmer, all of the collected time-resolved fluorescence raw data was re-fitted using these two lifetimes and the fractional contribution of the longer (~4 ns) and shorter (~0.8 ns) lifetime components were determined. Since the longer lifetime was at the limit of FRET distance analysis, we focused specifically on the shorter lifetime component and plotted the change in its contribution to the fluorescent decay in relation to the free Ca^{2+} concentration (Figure B-1).

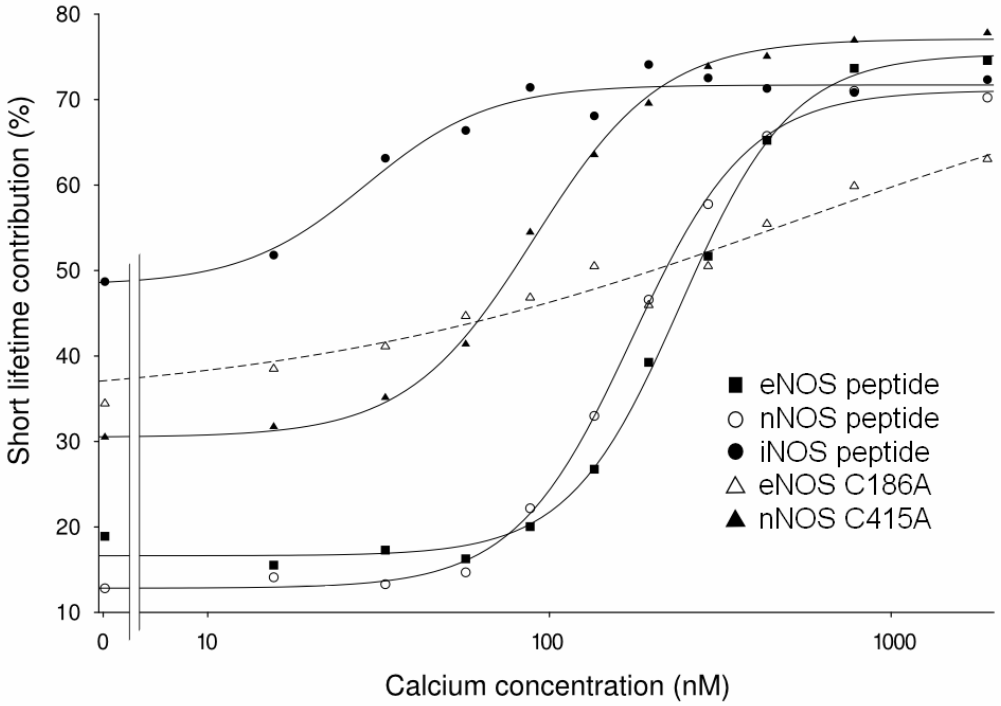

Figure B-1 – Assocition of Alexa 546/DAB-T34C-T110C CaM to NOS peptides and enzymes with increasing free Ca^{2+} concentrations. The short lifetime contribution increase represents CaM associating to the peptides and enzymes in a wrapped conformation.

Appendix B – Further FRET Analysis of CaM-NOS

Although Figure B-1 is quite different than Figure 6.17, the new figure clearly demonstrates that there is a Ca^{2+}-dependence on the fractional contribution of the shorter lifetime in all of the FRET measurements with NOS peptides and enzymes. It is apparent that the eNOS and nNOS peptides require a higher free Ca^{2+} concentration for their association with CaM (K_{Ca} ~ 250 nM), whereas eNOS C186A and nNOS C415A require lower free Ca^{2+} concentrations (K_{Ca} ~ 100 nM). As discussed in Chapter 6, this can be attributed to the regions flanking the CaM-binding domain of eNOS and nNOS that are involved in the recruitment of CaM such as the FMN domain. Interestingly, the iNOS peptide appears to have some Ca^{2+}-dependence in its binding, however, this occurs at very low free Ca^{2+} concentrations (< 30 nM). This is good agreement with the activation and fluorescence studies presented throughout this thesis.

Future measurements to further clarify the findings presented here would include:

1. Perform more measurements using Alexa 546/DAB-T34C-T110C CaM with eNOS C186A at free Ca^{2+} extremes (< 100 nM and > 2 uM) to have more data points to better fit the data (see Figure B-1).
2. Perform more FRET measurements using Alexa 546/DAB-T34C-T110C CaM with iNOS peptide at very low free Ca^{2+} concentrations to further confirm the observed Ca^{2+}-dependence shown in Figure B-1.

Bibliography

Abu-Soud, H.M., Yoho, L.L. and Stuehr, D.J. (1994) Calmodulin controls neuronal nitric-oxide synthase by a dual mechanism. Activation of intra- and interdomain electron transfer. *J Biol Chem 269*, 32047-50.

Alderton, W.K., Cooper, C.E. and Knowles, R.G. (2001) Nitric oxide synthases: structure, function and inhibition. *Biochem J 357*, 593-615.

Allen, M.W., Urbauer, R.J., Zaidi, A., Williams, T.D., Urbauer, J.L. and Johnson, C.K. (2004) Fluorescence labeling, purification, and immobilization of a double cysteine mutant calmodulin fusion protein for single-molecule experiments. *Anal Biochem 325*, 273-84.

Anagli, J., Hofmann, F., Quadroni, M., Vorherr, T. and Carafoli, E. (1995) The calmodulin-binding domain of the inducible (macrophage) nitric oxide synthase. *Eur J Biochem 233*, 701-8.

Aoyagi, M., Arvai, A.S., Tainer, J.A. and Getzoff, E.D. (2003) Structural basis for endothelial nitric oxide synthase binding to calmodulin. *EMBO J 22*, 766-75.

Ataman, Z.A., Gakhar, L., Sorensen, B.R., Hell, J.W. and Shea, M.A. (2007) The NMDA Receptor NR1 C1 Region Bound to Calmodulin: Structural Insights into Functional Differences between Homologous Domains. *Structure 15*, 1603-17.

Barbato, G., Ikura, M., Kay, L.E., Pastor, R.W. and Bax, A. (1992) Backbone dynamics of calmodulin studied by 15N relaxation using inverse detected two-dimensional NMR spectroscopy: the central helix is flexible. *Biochemistry 31*, 5269-78.

Barnes, J.A. and Gomes, A.V. (1995) PEST sequences in calmodulin-binding proteins. *Mol Cell Biochem 149-150*, 17-27.

Bax, A., Clore, G.M. and Gronenborn, A.M. (1990) $^{1}H–^{1}H$ correlation via isotropic mixing of ^{13}C magnetization, a new three-dimensional approach for assigning ^{1}H and ^{13}C spectra of ^{13}C-enriched proteins. *J Magn Reson 88*, 425-431.

Bax, A., Vuister, G.W., Grzesiek, S., Delaglio, F., Wang, A.C., Tschudin, R. and Zhu, G. (1994) Measurement of homo- and heteronuclear J couplings from quantitative J correlation. *Methods Enzymol 239*, 79-105.

Bayley, P.M., Findlay, W.A. and Martin, S.R. (1996) Target recognition by calmodulin: dissecting the kinetics and affinity of interaction using short peptide sequences. *Protein Sci 5*, 1215-28.

Benaim, G. and Villalobo, A. (2002) Phosphorylation of calmodulin. Functional implications. *Eur J Biochem 269*, 3619-31.

Benesch, R.E., Benesch, R. and Yung, S. (1973) Equations for the spectrophotometric analysis of hemoglobin mixtures. *Anal Biochem 55*, 245-8.

Bibliography

Berridge, M.J., Bootman, M.D. and Lipp, P. (1998) Calcium--a life and death signal. *Nature 395*, 645-8.

Berridge, M.J., Lipp, P. and Bootman, M.D. (2000) The versatility and universality of calcium signalling. *Nat Rev Mol Cell Biol 1*, 11-21.

Bhattacharya, S., Bunick, C.G. and Chazin, W.J. (2004) Target selectivity in EF-hand calcium binding proteins. *Biochim Biophys Acta 1742*, 69-79.

Bialik, S. and Kimchi, A. (2006) The death-associated protein kinases: structure, function, and beyond. *Annu Rev Biochem 75*, 189-210.

Biekofsky, R.R. and Feeney, J. (1998) Cooperative cyclic interactions involved in metal binding to pairs of sites in EF-hand proteins. *FEBS Lett 439*, 101-6.

Bisaglia, M., Trolio, A., Tessari, I., Bubacco, L., Mammi, S. and Bergantino, E. (2005) Cloning, expression, purification, and spectroscopic analysis of the fragment 57-102 of human alpha-synuclein. *Protein Expr Purif 39*, 90-6.

Brunger, A.T. (1997) X-ray crystallography and NMR reveal complementary views of structure and dynamics. *Nat Struct Biol 4 Suppl*, 862-5.

Carlomagno, T. (2005) Ligand-target interactions: what can we learn from NMR? *Annu Rev Biophys Biomol Struct 34*, 245-66.

Cavanagh, J., Fairbrother, W.J., Palmer, A.G., Rance, M. and Skelton, N.J. (2007). Protein NMR spectroscopy: principles and practice. Elsevier Academic Press, New York, NY, USA.

Censarek, P., Beyermann, M. and Koch, K.W. (2002) Target recognition of apocalmodulin by nitric oxide synthase I peptides. *Biochemistry 41*, 8598-604.

Chang, S.L., Szabo, A. and Tjandra, N. (2003) Temperature dependence of domain motions of calmodulin probed by NMR relaxation at multiple fields. *J Am Chem Soc 125*, 11379-84.

Chattopadhyaya, R., Meador, W.E., Means, A.R. and Quiocho, F.A. (1992) Calmodulin structure refined at 1.7 A resolution. *J Mol Biol 228*, 1177-92.

Chen, P.F., Tsai, A.L., Berka, V. and Wu, K.K. (1996) Endothelial nitric-oxide synthase. Evidence for bidomain structure and successful reconstitution of catalytic activity from two separate domains generated by a baculovirus expression system. *J Biol Chem 271*, 14631-5.

Chen, P.F., Tsai, A.L. and Wu, K.K. (1994) Cysteine 184 of endothelial nitric oxide synthase is involved in heme coordination and catalytic activity. *J Biol Chem 269*, 25062-6.

Chen, P.F. and Wu, K.K. (2000) Characterization of the roles of the 594-645 region in human endothelial nitric-oxide synthase in regulating calmodulin binding and electron transfer. *J Biol Chem 275*, 13155-63.

Cho, H.J., Xie, Q.W., Calaycay, J., Mumford, R.A., Swiderek, K.M., Lee, T.D. and Nathan, C. (1992) Calmodulin is a subunit of nitric oxide synthase from macrophages. *J Exp Med 176*, 599-604.

Chou, J.J., Li, S., Klee, C.B. and Bax, A. (2001) Solution structure of Ca(2+)-calmodulin reveals flexible hand-like properties of its domains. *Nat Struct Biol 8*, 990-7.

Christopherson, K.S., Hillier, B.J., Lim, W.A. and Bredt, D.S. (1999) PSD-95 assembles a ternary complex with the N-methyl-D-aspartic acid receptor and a bivalent neuronal NO synthase PDZ domain. *J Biol Chem 274*, 27467-73.

Chung, D.G. and Lewis, P.N. (1986) Internal architecture of the core nucleosome: fluorescence energy transfer studies at methionine-84 of histone H4. *Biochemistry 25*, 5036-42.

Clapham, D.E. (1995) Calcium signaling. *Cell 80*, 259-268.

Clapperton, J.A., Martin, S.R., Smerdon, S.J., Gamblin, S.J. and Bayley, P.M. (2002) Structure of the complex of calmodulin with the target sequence of calmodulin-dependent protein kinase I: studies of the kinase activation mechanism. *Biochemistry 41*, 14669-79.

Contessa, G.M., Orsale, M., Melino, S., Torre, V., Paci, M., Desideri, A. and Cicero, D.O. (2005) Structure of calmodulin complexed with an olfactory CNG channel fragment and role of the central linker: residual dipolar couplings to evaluate calmodulin binding modes outside the kinase family. *J Biomol NMR 31*, 185-99.

Cook, W.J., Walter, L.J. and Walter, M.R. (1994) Drug binding by calmodulin: crystal structure of a calmodulin-trifluoperazine complex. *Biochemistry 33*, 15259-65.

Craig, D.H., Chapman, S.K. and Daff, S. (2002) Calmodulin activates electron transfer through neuronal nitric-oxide synthase reductase domain by releasing an NADPH-dependent conformational lock. *J Biol Chem 277*, 33987-94.

Crane, B.R., Arvai, A.S., Gachhui, R., Wu, C., Ghosh, D.K., Getzoff, E.D., Stuehr, D.J. and Tainer, J.A. (1997) The structure of nitric oxide synthase oxygenase domain and inhibitor complexes. *Science 278*, 425-31.

Crane, B.R., Arvai, A.S., Ghosh, D.K., Wu, C., Getzoff, E.D., Stuehr, D.J. and Tainer, J.A. (1998) Structure of nitric oxide synthase oxygenase dimer with pterin and substrate. *Science 279*, 2121-6.

Crane, B.R., Arvai, A.S., Ghosh, S., Getzoff, E.D., Stuehr, D.J. and Tainer, J.A. (2000) Structures of the N(omega)-hydroxy-L-arginine complex of inducible nitric oxide synthase oxygenase dimer with active and inactive pterins. *Biochemistry 39*, 4608-21.

Crane, B.R., Rosenfeld, R.J., Arvai, A.S., Ghosh, D.K., Ghosh, S., Tainer, J.A., Stuehr, D.J. and Getzoff, E.D. (1999) N-terminal domain swapping and metal ion binding in nitric oxide synthase dimerization. *Embo J 18*, 6271-81.

Crivici, A. and Ikura, M. (1995) Molecular and structural basis of target recognition by calmodulin. *Annu Rev Biophys Biomol Struct 24*, 85-116.

Cubberley, R.R., Alderton, W.K., Boyhan, A., Charles, I.G., Lowe, P.N. and Old, R.W. (1997) Cysteine-200 of human inducible nitric oxide synthase is essential for dimerization of haem domains and for binding of haem, nitroarginine and tetrahydrobiopterin. *Biochem J 323 (Pt 1)*, 141-6.

Da Silva, E.F., Oliveira, V.H., Sorenson, M.M., Barrabin, H. and Scofano, H.M. (2002) Converting troponin C into calmodulin: effects of mutations in the central helix and of changes in temperature. *Int J Biochem Cell Biol 34*, 657-67.

Daff, S. (2003) Calmodulin-dependent regulation of mammalian nitric oxide synthase. *Biochem Soc Trans 31*, 502-5.

Daff, S., Noble, M.A., Craig, D.H., Rivers, S.L., Chapman, S.K., Munro, A.W., Fujiwara, S., Rozhkova, E., Sagami, I. and Shimizu, T. (2001) Control of electron transfer in neuronal NO synthase. *Biochem Soc Trans 29*, 147-52.

Daff, S., Sagami, I. and Shimizu, T. (1999) The 42-amino acid insert in the FMN domain of neuronal nitric-oxide synthase exerts control over Ca(2+)/calmodulin-dependent electron transfer. *J Biol Chem 274*, 30589-95.

Dawson, J. and Knowles, R.G. (1999) A microtiter-plate assay of nitric oxide synthase activity. *Mol Biotechnol 12*, 275-9.

Dawson, T.M., Steiner, J.P., Dawson, V.L., Dinerman, J.L., Uhl, G.R. and Snyder, S.H. (1993) Immunosuppressant FK506 enhances phosphorylation of nitric oxide synthase and protects against glutamate neurotoxicity. *Proc Natl Acad Sci U S A 90*, 9808-12.

Demaria, C.D., Soong, T.W., Alseikhan, B.A., Alvania, R.S. and Yue, D.T. (2001) Calmodulin bifurcates the local Ca2+ signal that modulates P/Q-type Ca2+ channels. *Nature 411*, 484-9.

Demura, Y., Ameshima, S., Ishizaki, T., Okamura, S., Miyamori, I. and Matsukawa, S. (1998) The activation of eNOS by copper ion (Cu2+) in human pulmonary arterial endothelial cells (HPAEC). *Free Radic Biol Med 25*, 314-20.

Dixon, H.B.F., Cornish-Bowden, A., Liebecq, C., Loening, K.L., Moss, G.P., Reedijk, J., Velick, S.F. and Vliegenthart, J.F.G. (1984) IUPAC-IUB Joint Commission on Biochemical Nomenclature (JCBN). Nomenclature and symbolism for amino acids and peptides. Recommendations 1983. *Eur J Biochem 138*, 9-37.

Drum, C.L., Yan, S.Z., Bard, J., Shen, Y.Q., Lu, D., Soelaiman, S., Grabarek, Z., Bohm, A. and Tang, W.J. (2002) Structural basis for the activation of anthrax adenylyl cyclase exotoxin by calmodulin. *Nature 415*, 396-402.

Drum, C.L., Yan, S.Z., Sarac, R., Mabuchi, Y., Beckingham, K., Bohm, A., Grabarek, Z. and Tang, W.J. (2000) An extended conformation of calmodulin induces interactions between the

structural domains of adenylyl cyclase from Bacillus anthracis to promote catalysis. *J Biol Chem 275*, 36334-40.

Duewel, H., Daub, E., Robinson, V. and Honek, J.F. (1997) Incorporation of trifluoromethionine into a phage lysozyme: implications and a new marker for use in protein 19F NMR. *Biochemistry 36*, 3404-16.

Dunford, A.J., Rigby, S.E., Hay, S., Munro, A.W. and Scrutton, N.S. (2007) Conformational and thermodynamic control of electron transfer in neuronal nitric oxide synthase. *Biochemistry 46*, 5018-29.

Elshorst, B., Hennig, M., Forsterling, H., Diener, A., Maurer, M., Schulte, P., Schwalbe, H., Griesinger, C., Krebs, J., Schmid, H., Vorherr, T. and Carafoli, E. (1999) NMR solution structure of a complex of calmodulin with a binding peptide of the Ca2+ pump. *Biochemistry 38*, 12320-32.

Erickson-Viitanen, S. and Degrado, W.F. (1987) Recognition and characterization of calmodulin-binding sequences in peptides and proteins. *Methods Enzymol 139*, 455-78.

Faeder, E.J. and Siegel, L.M. (1973) A rapid micromethod for determination of FMN and FAD in mixtures. *Anal Biochem 53*, 332-6.

Fallon, J.L., Halling, D.B., Hamilton, S.L. and Quiocho, F.A. (2005) Structure of calmodulin bound to the hydrophobic IQ domain of the cardiac Ca(v)1.2 calcium channel. *Structure 13*, 1881-6.

Fallon, J.L. and Quiocho, F.A. (2003) A closed compact structure of native Ca(2+)-calmodulin. *Structure 11*, 1303-7.

Feldman, P.L., Griffith, O.W. and Stuehr, D.J. (1993) The surprising life of nitric oxide. *Chem Eng News 71*,

Felley-Bosco, E., Bender, F.C., Courjault-Gautier, F., Bron, C. and Quest, A.F. (2000) Caveolin-1 down-regulates inducible nitric oxide synthase via the proteasome pathway in human colon carcinoma cells. *Proc Natl Acad Sci U S A 97*, 14334-9.

Feng, C., Thomas, C., Holliday, M.A., Tollin, G., Salerno, J.C., Ghosh, D.K. and Enemark, J.H. (2006) Direct measurement by laser flash photolysis of intramolecular electron transfer in a two-domain construct of murine inducible nitric oxide synthase. *J Am Chem Soc 128*, 3808-11.

Fernandez-Escamilla, A.M., Rousseau, F., Schymkowitz, J. and Serrano, L. (2004) Prediction of sequence-dependent and mutational effects on the aggregation of peptides and proteins. *Nat Biotechnol 22*, 1302-6.

Fernando, P., Abdulle, R., Mohindra, A., Guillemette, J.G. and Heikkila, J.J. (2002) Mutation or deletion of the C-terminal tail affects the function and structure of Xenopus laevis small heat shock protein, hsp30. *Comp Biochem Physiol B Biochem Mol Biol 133*, 95-103.

Feron, O., Belhassen, L., Kobzik, L., Smith, T.W., Kelly, R.A. and Michel, T. (1996) Endothelial nitric oxide synthase targeting to caveolae. Specific interactions with caveolin isoforms in cardiac myocytes and endothelial cells. *J Biol Chem 271*, 22810-4.

Finn, B.E., Evenas, J., Drakenberg, T., Waltho, J.P., Thulin, E. and Forsen, S. (1995) Calcium-induced structural changes and domain autonomy in calmodulin. *Nat Struct Biol 2*, 777-83.

Fischmann, T.O., Hruza, A., Niu, X.D., Fossetta, J.D., Lunn, C.A., Dolphin, E., Prongay, A.J., Reichert, P., Lundell, D.J., Narula, S.K. and Weber, P.C. (1999) Structural characterization of nitric oxide synthase isoforms reveals striking active-site conservation. *Nat Struct Biol 6*, 233-42.

Gachhui, R., Abu-Soud, H.M., Ghosha, D.K., Presta, A., Blazing, M.A., Mayer, B., George, S.E. and Stuehr, D.J. (1998) Neuronal nitric-oxide synthase interaction with calmodulin-troponin C chimeras. *J Biol Chem 273*, 5451-4.

Gao, J., Yin, D., Yao, Y., Williams, T.D. and Squier, T.C. (1998) Progressive decline in the ability of calmodulin isolated from aged brain to activate the plasma membrane Ca-ATPase. *Biochemistry 37*, 9536-48.

Gao, Y.T., Smith, S.M., Weinberg, J.B., Montgomery, H.J., Newman, E., Guillemette, J.G., Ghosh, D.K., Roman, L.J., Martasek, P. and Salerno, J.C. (2004) Thermodynamics of oxidation-reduction reactions in mammalian nitric-oxide synthase isoforms. *J Biol Chem 279*, 18759-66.

Garcia-Cardena, G., Fan, R., Shah, V., Sorrentino, R., Cirino, G., Papapetropoulos, A. and Sessa, W.C. (1998) Dynamic activation of endothelial nitric oxide synthase by Hsp90. *Nature 392*, 821-4.

Garcin, E.D., Bruns, C.M., Lloyd, S.J., Hosfield, D.J., Tiso, M., Gachhui, R., Stuehr, D.J., Tainer, J.A. and Getzoff, E.D. (2004) Structural basis for isozyme-specific regulation of electron transfer in nitric-oxide synthase. *J Biol Chem 279*, 37918-27.

Garnaud, P.E., Koetsier, M., Ost, T.W. and Daff, S. (2004) Redox properties of the isolated flavin mononucleotide- and flavin adenine dinucleotide-binding domains of neuronal nitric oxide synthase. *Biochemistry 43*, 11035-44.

George, S.E., Su, Z., Fan, D. and Means, A.R. (1993) Calmodulin-cardiac troponin C chimeras. Effects of domain exchange on calcium binding and enzyme activation. *J Biol Chem 268*, 25213-20.

George, S.E., Su, Z., Fan, D., Wang, S. and Johnson, J.D. (1996) The fourth EF-hand of calmodulin and its helix-loop-helix components: impact on calcium binding and enzyme activation. *Biochemistry 35*, 8307-13.

George, S.E., Vanberkum, M.F., Ono, T., Cook, R., Hanley, R.M., Putkey, J.A. and Means, A.R. (1990) Chimeric calmodulin-cardiac troponin C proteins differentially activate calmodulin target enzymes. *J Biol Chem 265*, 9228-35.

Ghosh, D.K. and Salerno, J.C. (2003) Nitric oxide synthases: domain structure and alignment in enzyme function and control. *Front Biosci 8*, d193-209.

Gifford, J.L., Walsh, M.P. and Vogel, H.J. (2007) Structures and metal-ion-binding properties of the Ca2+-binding helix-loop-helix EF-hand motifs. *Biochem J 405*, 199-221.

Gopalakrishna, R. and Anderson, W.B. (1982) Ca2+-induced hydrophobic site on calmodulin: application for purification of calmodulin by phenyl-Sepharose affinity chromatography. *Biochem Biophys Res Commun 104*, 830-6.

Gorren, A.C. and Mayer, B. (2007) Nitric-oxide synthase: a cytochrome P450 family foster child. *Biochim Biophys Acta 1770*, 432-45.

Grabarek, Z. (2005) Structure of a trapped intermediate of calmodulin: calcium regulation of EF-hand proteins from a new perspective. *J Mol Biol 346*, 1351-66.

Grabarek, Z., Grabarek, J., Leavis, P.C. and Gergely, J. (1983) Cooperative binding to the Ca2+-specific sites of troponin C in regulated actin and actomyosin. *J Biol Chem 258*, 14098-102.

Graham, S.E. and Peterson, J.A. (1999) How similar are P450s and what can their differences teach us? *Arch Biochem Biophys 369*, 24-9.

Gribovskaja, I., Brownlow, K.C., Dennis, S.J., Rosko, A.J., Marletta, M.A. and Stevens-Truss, R. (2005) Calcium-binding sites of calmodulin and electron transfer by inducible nitric oxide synthase. *Biochemistry 44*, 7593-601.

Griffith, O.W. and Stuehr, D.J. (1995) Nitric oxide synthases: properties and catalytic mechanism. *Annu Rev Physiol 57*, 707-36.

Gross, S.S. (1996) Microtiter plate assay for determining kinetics of nitric oxide synthesis. *Methods Enzymol 268*, 159-68.

Grzesiek, S. and Bax, A. (1992) Correlating backbone amide and side chain resonances in larger proteins by multiple relayed triple resonance NMR. *J Am Chem Soc 114*, 6291-6293.

Guerrero, S.A., Hecht, H.J., Hofmann, B., Biebl, H. and Singh, M. (2001) Production of selenomethionine-labelled proteins using simplified culture conditions and generally applicable host/vector systems. *Appl Microbiol Biotechnol 56*, 718-23.

Gundlach, H.G., Moore, S. and Stein, W.H. (1959) The reaction of iodoacetate with methionine. *J Biol Chem 234*, 1761-4.

Harmat, V., Bocskei, Z., Naray-Szabo, G., Bata, I., Csutor, A.S., Hermecz, I., Aranyi, P., Szabo, B., Liliom, K., Vertessy, B.G. and Ovadi, J. (2000) A new potent calmodulin antagonist with arylalkylamine structure: crystallographic, spectroscopic and functional studies. *J Mol Biol 297*, 747-55.

Hedrick, J.L. and Smith, A.J. (1968) Size and charge isomer separation and estimation of molecular weights of proteins by disc gel electrophoresis. *Arch Biochem Biophys 126*, 155-64.

Hellermann, G.R. and Solomonson, L.P. (1997) Calmodulin promotes dimerization of the oxygenase domain of human endothelial nitric-oxide synthase. *J Biol Chem 272*, 12030-4.

Hemmens, B. and Mayer, B. (1998) Enzymology of nitric oxide synthases. *Methods Mol Biol 100*, 1-32.

Hevel, J.M. and Marletta, M.A. (1994) Nitric-oxide synthase assays. *Methods Enzymol 233*, 250-8.

Heyduk, T. (2002) Measuring protein conformational changes by FRET/LRET. *Curr Opin Biotechnol 13*, 292-6.

Horvath, I., Harmat, V., Perczel, A., Palfi, V., Nyitray, L., Nagy, A., Hlavanda, E., Naray-Szabo, G. and Ovadi, J. (2005) The structure of the complex of calmodulin with KAR-2: a novel mode of binding explains the unique pharmacology of the drug. *J Biol Chem 280*, 8266-74.

Houdusse, A., Gaucher, J.F., Krementsova, E., Mui, S., Trybus, K.M. and Cohen, C. (2006) Crystal structure of apo-calmodulin bound to the first two IQ motifs of myosin V reveals essential recognition features. *Proc Natl Acad Sci U S A 103*, 19326-31.

Hudson, E.N. and Weber, G. (1973) Synthesis and characterization of two fluorescent sulfhydryl reagents. *Biochemistry 12*, 4154-61.

Hurshman, A.R., Krebs, C., Edmondson, D.E. and Marletta, M.A. (2003) Ability of tetrahydrobiopterin analogues to support catalysis by inducible nitric oxide synthase: formation of a pterin radical is required for enzyme activity. *Biochemistry 42*, 13287-303.

Hurshman, A.R. and Marletta, M.A. (2002) Reactions catalyzed by the heme domain of inducible nitric oxide synthase: evidence for the involvement of tetrahydrobiopterin in electron transfer. *Biochemistry 41*, 3439-56.

Ikura, M. and Ames, J.B. (2006) Genetic polymorphism and protein conformational plasticity in the calmodulin superfamily: two ways to promote multifunctionality. *Proc Natl Acad Sci U S A 103*, 1159-64.

Ikura, M., Clore, G.M., Gronenborn, A.M., Zhu, G., Klee, C.B. and Bax, A. (1992) Solution structure of a calmodulin-target peptide complex by multidimensional NMR. *Science 256*, 632-8.

Ikura, M., Kay, L.E. and Bax, A. (1990) A novel approach for sequential assignment of 1H, 13C, and 15N spectra of proteins: heteronuclear triple-resonance three-dimensional NMR spectroscopy. Application to calmodulin. *Biochemistry 29*, 4659-67.

Ishida, H., Takahashi, K., Nakashima, K., Kumaki, Y., Nakata, M., Hikichi, K. and Yazawa, M. (2000) Solution structures of the N-terminal domain of yeast calmodulin: Ca2+-dependent conformational change and its functional implication. *Biochemistry 39*, 13660-8.

Ishida, H. and Vogel, H.J. (2006) Protein-peptide interaction studies demonstrate the versatility of calmodulin target protein binding. *Protein Pept Lett 13*, 455-65.

Jaffrey, S.R. and Snyder, S.H. (1996) PIN: an associated protein inhibitor of neuronal nitric oxide synthase. *Science 274*, 774-7.

Jahnke, W. and Widmer, H. (2004) Protein NMR in biomedical research. *Cell Mol Life Sci 61*, 580-99.

Jurado, L.A., Chockalingam, P.S. and Jarrett, H.W. (1999) Apocalmodulin. *Physiol Rev 79*, 661-82.

Kajihara, D., Abe, R., Iijima, I., Komiyama, C., Sisido, M. and Hohsaka, T. (2006) FRET analysis of protein conformational change through position-specific incorporation of fluorescent amino acids. *Nat Methods 3*, 923-9.

Kasri, N.N., Torok, K., Galione, A., Garnham, C., Callewaert, G., Missiaen, L., Parys, J.B. and De Smedt, H. (2006) Endogenously bound calmodulin is essential for the function of the inositol 1,4,5-trisphosphate receptor. *J Biol Chem 281*, 8332-8.

Kay, L.E. (1997) NMR methods for the study of protein structure and dynamics. *Biochem Cell Biol 75*, 1-15.

Keller, R. (2004). The Computer Aided Resonance Assignment Tutorial, 1st Ed., CANTINA Verlag.

Kilhoffer, M.C., Kubina, M., Travers, F. and Haiech, J. (1992) Use of engineered proteins with internal tryptophan reporter groups and pertubation techniques to probe the mechanism of ligand-protein interactions: investigation of the mechanism of calcium binding to calmodulin. *Biochemistry 31*, 8098-106.

Kolodziejska, K.E., Burns, A.R., Moore, R.H., Stenoien, D.L. and Eissa, N.T. (2005) Regulation of inducible nitric oxide synthase by aggresome formation. *Proc Natl Acad Sci U S A 102*, 4854-9.

Komeima, K., Hayashi, Y., Naito, Y. and Watanabe, Y. (2000) Inhibition of neuronal nitric-oxide synthase by calcium/ calmodulin-dependent protein kinase IIalpha through Ser847 phosphorylation in NG108-15 neuronal cells. *J Biol Chem 275*, 28139-43.

Kone, B.C. (2000) Protein-protein interactions controlling nitric oxide synthases. *Acta Physiol Scand 168*, 27-31.

Kortvely, E. and Gulya, K. (2004) Calmodulin, and various ways to regulate its activity. *Life Sci 74*, 1065-70.

Kroncke, K.D., Fehsel, K., Suschek, C. and Kolb-Bachofen, V. (2001) Inducible nitric oxide synthase-derived nitric oxide in gene regulation, cell death and cell survival. *Int Immunopharmacol 1*, 1407-20.

Kuboniwa, H., Tjandra, N., Grzesiek, S., Ren, H., Klee, C.B. and Bax, A. (1995) Solution structure of calcium-free calmodulin. *Nat Struct Biol 2*, 768-76.

Kurokawa, H., Osawa, M., Kurihara, H., Katayama, N., Tokumitsu, H., Swindells, M.B., Kainosho, M. and Ikura, M. (2001) Target-induced conformational adaptation of calmodulin revealed by the crystal structure of a complex with nematode Ca(2+)/calmodulin-dependent kinase kinase peptide. *J Mol Biol 312*, 59-68.

Kurzchalia, T.V. and Parton, R.G. (1999) Membrane microdomains and caveolae. *Curr Opin Cell Biol 11*, 424-31.

Kuznicki, J., Grabarek, Z., Brzeska, H., Drabikowski, W. and Cohen, P. (1981) Stimulation of enzyme activities by fragments of calmodulin. *FEBS Lett 130*, 141-5.

Laine, R. and De Montellano, P.R. (1998) Neuronal nitric oxide synthase isoforms alpha and mu are closely related calpain-sensitive proteins. *Mol Pharmacol 54*, 305-12.

Lakowicz, J.R. (2006). Principles of fluorescence spectroscopy. Springer, New York, NY, USA.

Lakowski, T.M., Lee, G.M., Okon, M., Reid, R.E. and Mcintosh, L.P. (2007) Calcium-induced folding of a fragment of calmodulin composed of EF-hands 2 and 3. *Protein Sci 16*, 1119-32.

Lane, P. and Gross, S.S. (2000) The autoinhibitory control element and calmodulin conspire to provide physiological modulation of endothelial and neuronal nitric oxide synthase activity. *Acta Physiol Scand 168*, 53-63.

Lang, S., Spratt, D.E., Guillemette, J.G. and Palmer, M. (2005) Dual-targeted labeling of proteins using cysteine and selenomethionine residues. *Anal Biochem 342*, 271-9.

Lang, S., Spratt, D.E., Guillemette, J.G. and Palmer, M. (2006) Selective labeling of selenomethionine residues in proteins with a fluorescent derivative of benzyl bromide. *Anal Biochem 359*, 253-8.

Lee, A.L., Sharp, K.A., Kranz, J.K., Song, X.J. and Wand, A.J. (2002) Temperature dependence of the internal dynamics of a calmodulin-peptide complex. *Biochemistry 41*, 13814-25.

Lee, S.J., Beckingham, K. and Stull, J.T. (2000) Mutations at lysine 525 of inducible nitric-oxide synthase affect its Ca2+-independent activity. *J Biol Chem 275*, 36067-72.

Lee, S.J., Beckingham, K. and Stull, J.T. (2001) Ca2+-independent activity of nitric oxide synthase. *Biochem Biophys Res Commun 284*, 526-30.

Lee, S.J. and Stull, J.T. (1998) Calmodulin-dependent regulation of inducible and neuronal nitric-oxide synthase. *J Biol Chem 273*, 27430-7.

Lee, W.S., Ngo-Anh, T.J., Bruening-Wright, A., Maylie, J. and Adelman, J.P. (2003) Small conductance Ca2+-activated K+ channels and calmodulin: cell surface expression and gating. *J Biol Chem 278*, 25940-6.

Li, D., Hayden, E.Y., Panda, K., Stuehr, D.J., Deng, H., Rousseau, D.L. and Yeh, S.R. (2006) Regulation of the monomer-dimer equilibrium in inducible nitric-oxide synthase by nitric oxide. *J Biol Chem 281*, 8197-204.

Linse, S., Helmersson, A. and Forsen, S. (1991) Calcium binding to calmodulin and its globular domains. *J Biol Chem 266*, 8050-4.

Liu, J., Hughes, T.E. and Sessa, W.C. (1997) The first 35 amino acids and fatty acylation sites determine the molecular targeting of endothelial nitric oxide synthase into the Golgi region of cells: a green fluorescent protein study. *J Cell Biol 137*, 1525-35.

Lowry, O.H., Rosebrough, N.J., Farr, A.L. and Randall, R.J. (1951) Protein measurement with the Folin phenol reagent. *J Biol Chem 193*, 265-75.

Mansuy, D. and Renaud, J. (1995) Heme-thiolate proteins different from cytochromes P450 catalyzing monooxygenations. Cytochrome P450: structure, mechanism, and biochemistry. P. R. Ortiz De Montellano ed., Plenum Press. New York, NY, USA.

Margoliash, E. and Frohwirt, N. (1959) Spectrum of horse-heart cytochrome c. *Biochem J 71*, 570-2.

Markley, J.L. and Kainosho, M. (1993) Stable isotope labeling and resonance assignments in larger proteins NMR of Macromolecules: A Practical Approach. G. C. K. Roberts ed., Oxford University Press. Oxford, UK**:** 101–152.

Marsden, P.A., Heng, H.H., Duff, C.L., Shi, X.M., Tsui, L.C. and Hall, A.V. (1994) Localization of the human gene for inducible nitric oxide synthase (NOS2) to chromosome 17q11.2-q12. *Genomics 19*, 183-5.

Marsden, P.A., Heng, H.H., Scherer, S.W., Stewart, R.J., Hall, A.V., Shi, X.M., Tsui, L.C. and Schappert, K.T. (1993) Structure and chromosomal localization of the human constitutive endothelial nitric oxide synthase gene. *J Biol Chem 268*, 17478-88.

Martin, S.R., Andersson Teleman, A., Bayley, P.M., Drakenberg, T. and Forsen, S. (1985) Kinetics of calcium dissociation from calmodulin and its tryptic fragments. A stopped-flow fluorescence study using Quin 2 reveals a two-domain structure. *Eur J Biochem 151*, 543-50.

Massom, L., Lee, H. and Jarrett, H.W. (1990) Trifluoperazine binding to porcine brain calmodulin and skeletal muscle troponin C. *Biochemistry 29*, 671-81.

Masters, B.S. (2000) Structural variations to accommodate functional themes of the isoforms of NO synthases. Nitric oxide: biology and pathobiology. L. I. Ignarro ed., Academic Press. New York, NY, USA**:** 91-104.

Matsubara, M., Hayashi, N., Jing, T. and Titani, K. (2003) Regulation of endothelial nitric oxide synthase by protein kinase C. *J Biochem 133*, 773-81.

Matsubara, M., Hayashi, N., Titani, K. and Taniguchi, H. (1997) Circular dichroism and 1H NMR studies on the structures of peptides derived from the calmodulin-binding domains of inducible and endothelial nitric-oxide synthase in solution and in complex with calmodulin. Nascent alpha-helical structures are stabilized by calmodulin both in the presence and absence of Ca2+. *J Biol Chem 272*, 23050-6.

Matsubara, M., Nakatsu, T., Kato, H. and Taniguchi, H. (2004) Crystal structure of a myristoylated CAP-23/NAP-22 N-terminal domain complexed with Ca2+/calmodulin. *Embo J 23*, 712-8.

Matter, H., Kumar, H.S., Fedorov, R., Frey, A., Kotsonis, P., Hartmann, E., Frohlich, L.G., Reif, A., Pfleiderer, W., Scheurer, P., Ghosh, D.K., Schlichting, I. and Schmidt, H.H. (2005) Structural analysis of isoform-specific inhibitors targeting the tetrahydrobiopterin binding site of human nitric oxide synthases. *J Med Chem 48*, 4783-92.

Maximciuc, A.A., Putkey, J.A., Shamoo, Y. and Mackenzie, K.R. (2006) Complex of calmodulin with a ryanodine receptor target reveals a novel, flexible binding mode. *Structure 14*, 1547-56.

Mcphalen, C.A., Strynadka, N.C. and James, M.N. (1991) Calcium-binding sites in proteins: a structural perspective. *Adv Protein Chem 42*, 77-144.

Meador, W.E., Means, A.R. and Quiocho, F.A. (1992) Target enzyme recognition by calmodulin: 2.4 A structure of a calmodulin-peptide complex. *Science 257*, 1251-5.

Meador, W.E., Means, A.R. and Quiocho, F.A. (1993) Modulation of calmodulin plasticity in molecular recognition on the basis of x-ray structures. *Science 262*, 1718-21.

Michel, T. and Feron, O. (1997) Nitric oxide synthases: which, where, how, and why? *J Clin Invest 100*, 2146-52.

Michell, B.J., Harris, M.B., Chen, Z.P., Ju, H., Venema, V.J., Blackstone, M.A., Huang, W., Venema, R.C. and Kemp, B.E. (2002) Identification of regulatory sites of phosphorylation of the bovine endothelial nitric-oxide synthase at serine 617 and serine 635. *J Biol Chem 277*, 42344-51.

Mitchell, D.A., Erwin, P.A., Michel, T. and Marletta, M.A. (2005) S-Nitrosation and regulation of inducible nitric oxide synthase. *Biochemistry 44*, 4636-47.

Montgomery, H.J., Bartlett, R., Perdicakis, B., Jervis, E., Squier, T.C. and Guillemette, J.G. (2003) Activation of constitutive nitric oxide synthases by oxidized calmodulin mutants. *Biochemistry 42*, 7759-68.

Montgomery, H.J., Romanov, V. and Guillemette, J.G. (2000) Removal of a putative inhibitory element reduces the calcium-dependent calmodulin activation of neuronal nitric-oxide synthase. *J Biol Chem 275*, 5052-8.

Mount, P.F., Kemp, B.E. and Power, D.A. (2007) Regulation of endothelial and myocardial NO synthesis by multi-site eNOS phosphorylation. *J Mol Cell Cardiol 42*, 271-279.

Muhandiram, D.R. and Kay, L.E. (1994) Gradient-enhanced triple-resonance three-dimensional NMR experiments with improved sensitivity. *J Mag Res Series B 103*, 203-216.

Munro, A.W. and Noble, M.A. (1999) Fluorescence analysis of flavoproteins. *Methods Mol Biol 131*, 25-48.

Murtaugh, T.J., Rowe, P.M., Vincent, P.L., Wright, L.S. and Siegel, F.L. (1983) Posttranslational modification of calmodulin. *Methods Enzymol 102*, 158-70.

Murtaugh, T.J., Wright, L.S. and Siegel, F.L. (1986) Posttranslational modification of calmodulin in rat brain and pituitary. *J Neurochem 47*, 164-72.

Musial, A. and Eissa, N.T. (2001) Inducible nitric-oxide synthase is regulated by the proteasome degradation pathway. *J Biol Chem 276*, 24268-73.

Nathan, C. and Xie, Q.W. (1994) Regulation of biosynthesis of nitric oxide. *J Biol Chem 269*, 13725-8.

Navarro-Lerida, I., Corvi, M.M., Barrientos, A.A., Gavilanes, F., Berthiaume, L.G. and Rodriguez-Crespo, I. (2004) Palmitoylation of inducible nitric-oxide synthase at Cys-3 is required for proper intracellular traffic and nitric oxide synthesis. *J Biol Chem 279*, 55682-9.

Newman, E., Spratt, D.E., Mosher, J., Cheyne, B., Montgomery, H.J., Wilson, D.L., Weinberg, J.B., Smith, S.M., Salerno, J.C., Ghosh, D.K. and Guillemette, J.G. (2004) Differential activation of nitric-oxide synthase isozymes by calmodulin-troponin C chimeras. *J Biol Chem 279*, 33547-57.

Newton, D.C., Montgomery, H.J. and Guillemette, J.G. (1998) The reductase domain of the human inducible nitric oxide synthase is fully active in the absence of bound calmodulin. *Arch Biochem Biophys 359*, 249-57.

Newton, D.L., Oldewurtel, M.D., Krinks, M.H., Shiloach, J. and Klee, C.B. (1984) Agonist and antagonist properties of calmodulin fragments. *J Biol Chem 259*, 4419-26.

Nishida, C.R. and Ortiz De Montellano, P.R. (1998) Electron transfer and catalytic activity of nitric oxide synthases. Chimeric constructs of the neuronal, inducible, and endothelial isoforms. *J Biol Chem 273*, 5566-71.

Nishida, C.R. and Ortiz De Montellano, P.R. (1999) Autoinhibition of endothelial nitric-oxide synthase. Identification of an electron transfer control element. *J Biol Chem 274*, 14692-8.

Nishimura, J.S., Narayanasami, R., Miller, R.T., Roman, L.J., Panda, S. and Masters, B.S. (1999) The stimulatory effects of Hofmeister ions on the activities of neuronal nitric-oxide synthase. Apparent substrate inhibition by l-arginine is overcome in the presence of protein-destabilizing agents. *J Biol Chem 274*, 5399-406.

Noble, M.A., Munro, A.W., Rivers, S.L., Robledo, L., Daff, S.N., Yellowlees, L.J., Shimizu, T., Sagami, I., Guillemette, J.G. and Chapman, S.K. (1999) Potentiometric analysis of the flavin cofactors of neuronal nitric oxide synthase. *Biochemistry 38*, 16413-8.

Olwin, B.B. and Storm, D.R. (1985) Calcium binding to complexes of calmodulin and calmodulin binding proteins. *Biochemistry 24*, 8081-6.

Orosz, F., Vertessy, B.G., Salerno, C., Crifo, C., Capuozzo, E. and Ovadi, J. (1997) The interaction of a new anti-tumour drug, KAR-2 with calmodulin. *Br J Pharmacol 121*, 955-62.

Osawa, M., Tokumitsu, H., Swindells, M.B., Kurihara, H., Orita, M., Shibanuma, T., Furuya, T. and Ikura, M. (1999) A novel target recognition revealed by calmodulin in complex with Ca2+-calmodulin-dependent kinase kinase. *Nat Struct Biol 6*, 819-24.

Ottl, J., Gabriel, D. and Marriott, G. (1998) Preparation and photoactivation of caged fluorophores and caged proteins using a new class of heterobifunctional, photocleavable cross-linking reagents. *Bioconjug Chem 9*, 143-51.

Pacher, P., Beckman, J.S. and Liaudet, L. (2007) Nitric oxide and peroxynitrite in health and disease. *Physiol Rev 87*, 315-424.

Pan, J., Burgher, K.L., Szczepanik, A.M. and Ringheim, G.E. (1996) Tyrosine phosphorylation of inducible nitric oxide synthase: implications for potential post-translational regulation. *Biochem J 314 (Pt 3)*, 889-94.

Panda, K., Rosenfeld, R.J., Ghosh, S., Meade, A.L., Getzoff, E.D. and Stuehr, D.J. (2002) Distinct dimer interaction and regulation in nitric-oxide synthase types I, II, and III. *J Biol Chem 277*, 31020-30.

Patton, C., Thompson, S. and Epel, D. (2004) Some precautions in using chelators to buffer metals in biological solutions. *Cell Calcium 35*, 427-31.

Pedigo, S. and Shea, M.A. (1995) Discontinuous equilibrium titrations of cooperative calcium binding to calmodulin monitored by 1-D 1H-nuclear magnetic resonance spectroscopy. *Biochemistry 34*, 10676-89.

Perdicakis, B., Montgomery, H.J., Guillemette, J.G. and Jervis, E. (2004) Validation and characterization of uninhibited enzyme kinetics performed in multiwell plates. *Anal Biochem 332*, 122-36.

Perry, J.M. and Marletta, M.A. (1998) Effects of transition metals on nitric oxide synthase catalysis. *Proc Natl Acad Sci U S A 95*, 11101-6.

Persechini, A., Gansz, K.J. and Paresi, R.J. (1996a) Activation of myosin light chain kinase and nitric oxide synthase activities by engineered calmodulins with duplicated or exchanged EF hand pairs. *Biochemistry 35*, 224-8.

Persechini, A., Gansz, K.J. and Paresi, R.J. (1996b) A role in enzyme activation for the N-terminal leader sequence in calmodulin. *J Biol Chem 271*, 19279-82.

Persechini, A., Mcmillan, K. and Leakey, P. (1994) Activation of myosin light chain kinase and nitric oxide synthase activities by calmodulin fragments. *J Biol Chem 269*, 16148-54.

Persechini, A. and Stemmer, P.M. (2002) Calmodulin is a limiting factor in the cell. *Trends Cardiovasc Med 12*, 32-7.

Prabhu, N.V., Lee, A.L., Wand, A.J. and Sharp, K.A. (2003) Dynamics and entropy of a calmodulin-peptide complex studied by NMR and molecular dynamics. *Biochemistry 42*, 562-70.

Pritchard, K.A., Jr., Ackerman, A.W., Gross, E.R., Stepp, D.W., Shi, Y., Fontana, J.T., Baker, J.E. and Sessa, W.C. (2001) Heat shock protein 90 mediates the balance of nitric oxide and superoxide anion from endothelial nitric-oxide synthase. *J Biol Chem 276*, 17621-4.

Quintana, A.R., Wang, D., Forbes, J.E. and Waxham, M.N. (2005) Kinetics of calmodulin binding to calcineurin. *Biochem Biophys Res Commun 334*, 674-80.

Ratovitski, E.A., Bao, C., Quick, R.A., Mcmillan, A., Kozlovsky, C. and Lowenstein, C.J. (1999) An inducible nitric-oxide synthase (NOS)-associated protein inhibits NOS dimerization and activity. *J Biol Chem 274*, 30250-7.

Ravi, K., Brennan, L.A., Levic, S., Ross, P.A. and Black, S.M. (2004) S-nitrosylation of endothelial nitric oxide synthase is associated with monomerization and decreased enzyme activity. *Proc Natl Acad Sci U S A 101*, 2619-24.

Rhoads, A.R. and Friedberg, F. (1997) Sequence motifs for calmodulin recognition. *Faseb J 11*, 331-40.

Richards, M.K., Clague, M.J. and Marletta, M.A. (1996) Characterization of C415 mutants of neuronal nitric oxide synthase. *Biochemistry 35*, 7772-80.

Rogers, G.A., Shaltiel, N. and Boyer, P.D. (1976) Facile alkylation of methionine by benzyl bromide and demonstration of fumarase inactivation accompanied by alkylation of a methionine residue. *J Biol Chem 251*, 5711-7.

Roman, L.J., Martasek, P. and Masters, B.S. (2002) Intrinsic and extrinsic modulation of nitric oxide synthase activity. *Chem Rev 102*, 1179-90.

Roman, L.J., Martasek, P., Miller, R.T., Harris, D.E., De La Garza, M.A., Shea, T.M., Kim, J.J. and Masters, B.S. (2000a) The C termini of constitutive nitric-oxide synthases control electron flow through the flavin and heme domains and affect modulation by calmodulin. *J Biol Chem 275*, 29225-32.

Roman, L.J. and Masters, B.S. (2006) Electron transfer by neuronal nitric-oxide synthase is regulated by concerted interaction of calmodulin and two intrinsic regulatory elements. *J Biol Chem 281*, 23111-8.

Roman, L.J., Miller, R.T., De La Garza, M.A., Kim, J.J. and Siler Masters, B.S. (2000b) The C terminus of mouse macrophage inducible nitric-oxide synthase attenuates electron flow through the flavin domain. *J Biol Chem 275*, 21914-9.

Roman, L.J., Sheta, E.A., Martasek, P., Gross, S.S., Liu, Q. and Masters, B.S. (1995) High-level expression of functional rat neuronal nitric oxide synthase in Escherichia coli. *Proc Natl Acad Sci U S A 92*, 8428-32.

Roth, S.M., Schneider, D.M., Strobel, L.A., Vanberkum, M.F., Means, A.R. and Wand, A.J. (1991) Structure of the smooth muscle myosin light-chain kinase calmodulin-binding domain peptide bound to calmodulin. *Biochemistry 30*, 10078-84.

Roufogalis, B.D., Minocherhomjee, A.M. and Al-Jobore, A. (1983) Pharmacological antagonism of calmodulin. *Can J Biochem Cell Biol 61*, 927-33.

Ruan, J., Xie, Q., Hutchinson, N., Cho, H., Wolfe, G.C. and Nathan, C. (1996) Inducible nitric oxide synthase requires both the canonical calmodulin-binding domain and additional sequences in order to bind calmodulin and produce nitric oxide in the absence of free Ca2+. *J Biol Chem 271*, 22679-86.

Sagami, I., Daff, S. and Shimizu, T. (2001) Intra-subunit and inter-subunit electron transfer in neuronal nitric-oxide synthase: effect of calmodulin on heterodimer catalysis. *J Biol Chem 276*, 30036-42.

Salas, V., Sanchez-Torres, J., Cusido-Hita, D.M., Garcia-Marchan, Y., Sojo, F., Benaim, G. and Villalobo, A. (2005) Characterisation of tyrosine-phosphorylation-defective calmodulin mutants. *Protein Expr Purif 41*, 384-92.

Salerno, J.C., Harris, D.E., Irizarry, K., Patel, B., Morales, A.J., Smith, S.M., Martasek, P., Roman, L.J., Masters, B.S., Jones, C.L., Weissman, B.A., Lane, P., Liu, Q. and Gross, S.S. (1997) An autoinhibitory control element defines calcium-regulated isoforms of nitric oxide synthase. *J Biol Chem 272*, 29769-77.

Sattler, M., Schleucher, J. and Griesinger, C. (1999) Heteronuclear multidimensional NMR experiments for the structure determination of proteins in solution employing pulsed field gradients. *Prog NMR Spectrosc 34*, 93-158.

Saura, M., Zaragoza, C., Bao, C., Mcmillan, A. and Lowenstein, C.J. (1999) Interaction of interferon regulatory factor-1 and nuclear factor kappaB during activation of inducible nitric oxide synthase transcription. *J Mol Biol 289*, 459-71.

Schmidt, H.H., Lohmann, S.M. and Walter, U. (1993) The nitric oxide and cGMP signal transduction system: regulation and mechanism of action. *Biochim Biophys Acta 1178*, 153-75.

Schmidt, H.H. and Walter, U. (1994) NO at work. *Cell 78*, 919-25.

Schumacher, M.A., Crum, M. and Miller, M.C. (2004) Crystal structures of apocalmodulin and an apocalmodulin/SK potassium channel gating domain complex. *Structure 12*, 849-60.

Schumacher, M.A., Rivard, A.F., Bachinger, H.P. and Adelman, J.P. (2001) Structure of the gating domain of a Ca2+-activated K+ channel complexed with Ca2+/calmodulin. *Nature 410*, 1120-4.

Shen, Y., Zhukovskaya, N.L., Guo, Q., Florian, J. and Tang, W.J. (2005) Calcium-independent calmodulin binding and two-metal-ion catalytic mechanism of anthrax edema factor. *Embo J 24*, 929-41.

Shepherd, L. and Huber, R.E. (1969) Some chemical and biochemical properties of selenomethionine. *Can J Biochem 47*, 877-81.

Siddhanta, U., Presta, A., Fan, B., Wolan, D., Rousseau, D.L. and Stuehr, D.J. (1998) Domain swapping in inducible nitric-oxide synthase. Electron transfer occurs between flavin and heme groups located on adjacent subunits in the dimer. *J Biol Chem 273*, 18950-8.

Sienaert, I., Nadif Kasri, N., Vanlingen, S., Parys, J.B., Callewaert, G., Missiaen, L. and De Smedt, H. (2002) Localization and function of a calmodulin-apocalmodulin-binding domain in the N-terminal part of the type 1 inositol 1,4,5-trisphosphate receptor. *Biochem J 365*, 269-77.

Simonovic, M., Zhang, Z., Cianci, C.D., Steitz, T.A. and Morrow, J.S. (2006) Structure of the calmodulin alphaII-spectrin complex provides insight into the regulation of cell plasticity. *J Biol Chem 281*, 34333-40.

Slaughter, B.D., Unruh, J.R., Allen, M.W., Bieber Urbauer, R.J. and Johnson, C.K. (2005a) Conformational substates of calmodulin revealed by single-pair fluorescence resonance energy transfer: influence of solution conditions and oxidative modification. *Biochemistry 44*, 3694-707.

Slaughter, B.D., Unruh, J.R., Price, E.S., Huynh, J.L., Bieber Urbauer, R.J. and Johnson, C.K. (2005b) Sampling unfolding intermediates in calmodulin by single-molecule spectroscopy. *J Am Chem Soc 127*, 12107-14.

Smith, J.L. and Thompson, A. (1998) Reactivity of selenomethionine--dents in the magic bullet? *Structure 6*, 815-9.

Snyder, S.H. and Bredt, D.S. (1992) Biological roles of nitric oxide. *Sci Am 266*, 68-71, 74-7.

Spratt, D.E., Newman, E., Mosher, J., Ghosh, D.K., Salerno, J.C. and Guillemette, J.G. (2006) Binding and activation of nitric oxide synthase isozymes by calmodulin EF hand pairs. *Febs J 273*, 1759-71.

Spratt, D.E., Taiakina, V. and Guillemette, J.G. (2007a) Calcium-deficient calmodulin binding and activation of neuronal and inducible nitric oxide synthases. *Biochim Biophys Acta 1774*, 1351-8.

Spratt, D.E., Taiakina, V., Palmer, M. and Guillemette, J.G. (2007b) Differential binding of calmodulin domains to constitutive and inducible nitric oxide synthase enzymes. *Biochemistry 46*, 8288-300.

Squier, T.C. and Bigelow, D.J. (2000) Protein oxidation and age-dependent alterations in calcium homeostasis. *Front Biosci 5*, D504-26.

Stevens-Truss, R., Beckingham, K. and Marletta, M.A. (1997) Calcium binding sites of calmodulin and electron transfer by neuronal nitric oxide synthase. *Biochemistry 36*, 12337-45.

Strynadka, N.C. and James, M.N. (1989) Crystal structures of the helix-loop-helix calcium-binding proteins. *Annu Rev Biochem 58*, 951-98.

Stuehr, D.J. (1999) Mammalian nitric oxide synthases. *Biochim Biophys Acta 1411*, 217-30.

Stuehr, D.J. and Ikeda-Saito, M. (1992) Spectral characterization of brain and macrophage nitric oxide synthases. Cytochrome P-450-like hemeproteins that contain a flavin semiquinone radical. *J Biol Chem 267*, 20547-50.

Stuehr, D.J., Santolini, J., Wang, Z.Q., Wei, C.C. and Adak, S. (2004) Update on mechanism and catalytic regulation in the NO synthases. *J Biol Chem 279*, 36167-70.

Su, Z., Blazing, M.A., Fan, D. and George, S.E. (1995) The calmodulin-nitric oxide synthase interaction. Critical role of the calmodulin latch domain in enzyme activation. *J Biol Chem 270*, 29117-22.

Sun, H. and Squier, T.C. (2000) Ordered and cooperative binding of opposing globular domains of calmodulin to the plasma membrane Ca-ATPase. *J Biol Chem 275*, 1731-8.

Tjandra, N., Kuboniwa, H., Ren, H. and Bax, A. (1995) Rotational dynamics of calcium-free calmodulin studied by 15N-NMR relaxation measurements. *Eur J Biochem 230*, 1014-24.

Torok, K., Lane, A.N., Martin, S.R., Janot, J.M. and Bayley, P.M. (1992) Effects of calcium binding on the internal dynamic properties of bovine brain calmodulin, studied by NMR and optical spectroscopy. *Biochemistry 31*, 3452-62.

Torok, K. and Trentham, D.R. (1994) Mechanism of 2-chloro-(epsilon-amino-Lys75)-[6-[4-(N,N-diethylamino)phenyl]-1,3,5-triazin-4-yl]calmodulin interactions with smooth muscle myosin light chain kinase and derived peptides. *Biochemistry 33*, 12807-20.

Torok, K., Tzortzopoulos, A., Grabarek, Z., Best, S.L. and Thorogate, R. (2001) Dual effect of ATP in the activation mechanism of brain Ca(2+)/calmodulin-dependent protein kinase II by Ca(2+)/calmodulin. *Biochemistry 40*, 14878-90.

Tran, Q.K., Black, D.J. and Persechini, A. (2005) Dominant affectors in the calmodulin network shape the time courses of target responses in the cell. *Cell Calcium 37*, 541-53.

Tsien, R. and Pozzan, T. (1989) Measurement of cytosolic free Ca2+ with quin2. *Methods Enzymol 172*, 230-62.

Van Der Meer, B.W., Coker, G. and Chen, S.Y.S. (1994). Resonance energy transfer : theory and data. VCH, New York, NY, USA.

Van Holde, K.E., Johnson, W.C. and Ho, P.S. (1998). Principles of physical biochemistry. Prentice Hall, Upper Saddle River, NJ, USA.

Van Petegem, F., Chatelain, F.C. and Minor, D.L., Jr. (2005) Insights into voltage-gated calcium channel regulation from the structure of the CaV1.2 IQ domain-Ca2+/calmodulin complex. *Nat Struct Mol Biol 12*, 1108-15.

Vandonselaar, M., Hickie, R.A., Quail, J.W. and Delbaere, L.T. (1994) Trifluoperazine-induced conformational change in Ca(2+)-calmodulin. *Nat Struct Biol 1*, 795-801.

Vasquez-Vivar, J., Kalyanaraman, B., Martasek, P., Hogg, N., Masters, B.S., Karoui, H., Tordo, P. and Pritchard, K.A., Jr. (1998) Superoxide generation by endothelial nitric oxide synthase: the influence of cofactors. *Proc Natl Acad Sci U S A 95*, 9220-5.

Venema, R.C., Sayegh, H.S., Kent, J.D. and Harrison, D.G. (1996) Identification, characterization, and comparison of the calmodulin-binding domains of the endothelial and inducible nitric oxide synthases. *J Biol Chem 271*, 6435-40.

Vetter, S.W. and Leclerc, E. (2003) Novel aspects of calmodulin target recognition and activation. *Eur J Biochem 270*, 404-14.

Vogel, H.J. and Zhang, M. (1995) Protein engineering and NMR studies of calmodulin. *Mol Cell Biochem 149-150*, 3-15.

Vorherr, T., Knopfel, L., Hofmann, F., Mollner, S., Pfeuffer, T. and Carafoli, E. (1993) The calmodulin binding domain of nitric oxide synthase and adenylyl cyclase. *Biochemistry 32*, 6081-8.

Walker, G., Pfeilschifter, J., Otten, U. and Kunz, D. (2001) Proteolytic cleavage of inducible nitric oxide synthase (iNOS) by calpain I. *Biochim Biophys Acta 1568*, 216-24.

Wang, S., George, S.E., Davis, J.P. and Johnson, J.D. (1998) Structural determinants of Ca2+ exchange and affinity in the C terminal of cardiac troponin C. *Biochemistry 37*, 14539-44.

Wang, W. and Malcolm, B.A. (1999) Two-stage PCR protocol allowing introduction of multiple mutations, deletions and insertions using QuikChange Site-Directed Mutagenesis. *Biotechniques 26*, 680-2.

Watterson, D.M., Sharief, F. and Vanaman, T.C. (1980) The complete amino acid sequence of the Ca2+-dependent modulator protein (calmodulin) of bovine brain. *J Biol Chem 255*, 962-75.

Waxham, M.N., Tsai, A.L. and Putkey, J.A. (1998) A mechanism for calmodulin (CaM) trapping by CaM-kinase II defined by a family of CaM-binding peptides. *J Biol Chem 273*, 17579-84.

Weaver, J., Porasuphatana, S., Tsai, P., Cao, G.L., Budzichowski, T.A., Roman, L.J. and Rosen, G.M. (2002) The activation of neuronal nitric-oxide synthase by various divalent cations. *J Pharmacol Exp Ther 302*, 781-6.

Weaver, J., Porasuphatana, S., Tsai, P., Cao, G.L., Budzichowski, T.A., Roman, L.J. and Rosen, G.M. (2004) The effect of divalent cations on neuronal nitric oxide synthase activity. *Toxicol Sci 81*, 325-31.

Wei, C.C., Crane, B.R. and Stuehr, D.J. (2003a) Tetrahydrobiopterin radical enzymology. *Chem Rev 103*, 2365-83.

Wei, C.C., Wang, Z.Q., Hemann, C., Hille, R. and Stuehr, D.J. (2003b) A tetrahydrobiopterin radical forms and then becomes reduced during Nomega-hydroxyarginine oxidation by nitric-oxide synthase. *J Biol Chem 278*, 46668-73.

Weissman, B.A., Jones, C.L., Liu, Q. and Gross, S.S. (2002) Activation and inactivation of neuronal nitric oxide synthase: characterization of Ca(2+)-dependent [125I]Calmodulin binding. *Eur J Pharmacol 435*, 9-18.

Wilson, M.A. and Brunger, A.T. (2000) The 1.0 A crystal structure of Ca(2+)-bound calmodulin: an analysis of disorder and implications for functionally relevant plasticity. *J Mol Biol 301*, 1237-56.

Wüthrich, K. (1986). NMR of proteins and nucleic acids. Wiley, Toronto, ON.

Xia, Y., Berlowitz, C.O. and Zweier, J.L. (2006) PIN inhibits nitric oxide and superoxide production from purified neuronal nitric oxide synthase. *Biochim Biophys Acta 1760*, 1445-9.

Xia, Y., Roman, L.J., Masters, B.S. and Zweier, J.L. (1998) Inducible nitric-oxide synthase generates superoxide from the reductase domain. *J Biol Chem 273*, 22635-9.

Xiong, L., Kleerekoper, Q.K., He, R., Putkey, J.A. and Hamilton, S.L. (2005) Sites on calmodulin that interact with the C-terminal tail of Cav1.2 channel. *J Biol Chem 280*, 7070-9.

Yamauchi, E., Nakatsu, T., Matsubara, M., Kato, H. and Taniguchi, H. (2003) Crystal structure of a MARCKS peptide containing the calmodulin-binding domain in complex with Ca2+-calmodulin. *Nat Struct Biol 10*, 226-31.

Yamniuk, A.P. and Vogel, H.J. (2004) Calmodulin's flexibility allows for promiscuity in its interactions with target proteins and peptides. *Mol Biotechnol 27*, 33-57.

Yap, K.L., Yuan, T., Mal, T.K., Vogel, H.J. and Ikura, M. (2003) Structural basis for simultaneous binding of two carboxy-terminal peptides of plant glutamate decarboxylase to calmodulin. *J Mol Biol 328*, 193-204.

Ye, Q., Li, X., Wong, A., Wei, Q. and Jia, Z. (2006) Structure of calmodulin bound to a calcineurin peptide: a new way of making an old binding mode. *Biochemistry 45*, 738-45.

Yu, Z., Zhang, W. and Kone, B.C. (2002) Histone deacetylases augment cytokine induction of the iNOS gene. *J Am Soc Nephrol 13*, 2009-17.

Yuan, T., Vogel, H.J., Sutherland, C. and Walsh, M.P. (1998) Characterization of the Ca2+ -dependent and -independent interactions between calmodulin and its binding domain of inducible nitric oxide synthase. *FEBS Lett 431*, 210-4.

Zalk, R., Lehnart, S.E. and Marks, A.R. (2007) Modulation of the ryanodine receptor and intracellular calcium. *Annu Rev Biochem 76*, 367-85.

Zhang, M., Yuan, T., Aramini, J.M. and Vogel, H.J. (1995) Interaction of calmodulin with its binding domain of rat cerebellar nitric oxide synthase. A multinuclear NMR study. *J Biol Chem 270*, 20901-7.

Zhang, W., Kuncewicz, T., Yu, Z.Y., Zou, L., Xu, X. and Kone, B.C. (2003) Protein-protein interactions involving inducible nitric oxide synthase. *Acta Physiol Scand 179*, 137-42.

Zoche, M., Bienert, M., Beyermann, M. and Koch, K.W. (1996) Distinct molecular recognition of calmodulin-binding sites in the neuronal and macrophage nitric oxide synthases: a surface plasmon resonance study. *Biochemistry 35*, 8742-7.

Zukin, R.S., Hartig, P.R. and Koshland, D.E., Jr. (1977) Use of a distant reporter group as evidence for a conformational change in a sensory receptor. *Proc Natl Acad Sci U S A 74*, 1932-6.